RELAY IN THE LOOP TEST PROCEDURES FOR ADAPTIVE OVERCURRENT PROTECTION

by

EMILIO C. PIESCIOROVSKY

E.E., National Technological University, Argentina, 1998
M.MKTG., National University of La Plata, Argentina, 2001
M.S.E.E., Kansas State University, United States of America, 2009

AN ABSTRACT OF A DISSERTATION

submitted in partial fulfillment of the requirements for the degree

DOCTOR OF PHILOSOPHY

Department of Electrical and Computer Engineering
College of Engineering

KANSAS STATE UNIVERSITY
Manhattan, Kansas

2015

Abstract

Microgrids with distributed generators have changed how protection and control systems are designed. Protection systems in conventional U.S. distribution systems are radial with the assumption that current flows always from the utility source to the end user. However, in a microgrid with distributed generators, currents along power lines do not always flow in one direction. Therefore, protection systems must be adapted to different circuit paths depending on distributed generator sites in the microgrid and maximum fuse ampere ratings on busses.

Adaptive overcurrent protection focuses on objectives and constraints based on operation, maximum load demand, equipment, and utility service limitations. Adaptive overcurrent protection was designed to protect the power lines and bus feeders of the microgrid with distributed generators by coordinating fuses and relays in the microgrid. Adaptive overcurrent protection was based on the relay setting group and protection logic methods. Non-real-time simulator (NRTS) and real-time simulator (RTS) experiments were performed with computer-based simulators. Tests with two relays in the loop proved that primary relays tripped faster than backup relays for selectivity coordination in the adaptive overcurrent protection system. Relay test results from tripping and non-tripping tests showed that adaptive inverse time overcurrent protection achieved selectivity, speed, and reliability.

The RTS and NRTS with two relays in the loop techniques were described and compared in this work. The author was the first graduate student to implement real-time simulation with two relays in the loop at the Burns & McDonnell - K-State Smart Grid Laboratory. The RTS experimental circuit and project are detailed in this work so other graduate students can apply this technique with relays in the loop in smart grid research areas such as phasor measurement units, adaptive protection, communication, and cyber security applications.

RELAY IN THE LOOP TEST PROCEDURES FOR ADAPTIVE OVERCURRENT PROTECTION

by

EMILIO C. PIESCIOROVSKY

E.E., National Technological University, Argentina, 1998
M.MKTG., National University of La Plata, Argentina, 2001
M.S.E.E., Kansas State University, United States of America, 2009

A DISSERTATION

submitted in partial fulfillment of the requirements for the degree

DOCTOR OF PHILOSOPHY

Department of Electrical and Computer Engineering
College of Engineering

KANSAS STATE UNIVERSITY
Manhattan, Kansas

2015

Approved by:

Co-Major Professor
Dr. Noel N. Schulz

Approved by:

Co-Major Professor
Dr. Anil Pahwa

Abstract

Microgrids with distributed generators have changed how protection and control systems are designed. Protection systems in conventional U.S. distribution systems are radial with the assumption that current flows always from the utility source to the end user. However, in a microgrid with distributed generators, currents along power lines do not always flow in one direction. Therefore, protection systems must be adapted to different circuit paths depending on distributed generator sites in the microgrid and maximum fuse ampere ratings on busses.

Adaptive overcurrent protection focuses on objectives and constraints based on operation, maximum load demand, equipment, and utility service limitations. Adaptive overcurrent protection was designed to protect the power lines and bus feeders of the microgrid with distributed generators by coordinating fuses and relays in the microgrid. Adaptive overcurrent protection was based on the relay setting group and protection logic methods. Non-real-time simulator (NRTS) and real-time simulator (RTS) experiments were performed with computer-based simulators. Tests with two relays in the loop proved that primary relays tripped faster than backup relays for selectivity coordination in the adaptive overcurrent protection system. Relay test results from tripping and non-tripping tests showed that adaptive inverse time overcurrent protection achieved selectivity, speed, and reliability.

The RTS and NRTS with two relays in the loop techniques were described and compared in this work. The author was the first graduate student to implement real-time simulation with two relays in the loop at the Burns & McDonnell - K-State Smart Grid Laboratory. The RTS experimental circuit and project are detailed in this work so other graduate students can apply this technique with relays in the loop in smart grid research areas such as phasor measurement units, adaptive protection, communication, and cyber security applications.

Table of Contents

List of Figures

List of Tables

Acknowledgements

I would like to express my sincere appreciation and gratitude to Dr. Noel N. Schulz from the Department of Electrical and Computer Engineering. She was my major advisor and provided great support, guidance, and care throughout my PhD program. Dr. Schulz is the associate dean for Research and Graduate Programs at the College of Engineering and director of the Burns & McDonnell – K-State Smart Grid Laboratory. She gave me the opportunity to work with her and build and run the Smart Grid Laboratory. In the Smart Grid Laboratory, I gained great experience and knowledge that allowed me to improve my background as a researcher, teacher, and electrical engineer. I would like to thank the Electrical Power Affiliates Program for the operational support of the Smart Grid Laboratory. A special thanks to Burns & McDonnell for being the main sponsor of the Burns & McDonnell – K-State Smart Grid Laboratory where I performed my research activities.

I would like to express my gratitude to Dr. Anil Pahwa from the Department of Electrical and Computer Engineering. He was my co-advisor, and he opened the first door at Kansas State University for me when I arrived in Manhattan, Kansas, with my wife. I will never forget him as a professor and human being that gave me the first opportunity at Kansas State University.

Also, I would like to thank to my lovely wife, Dr. Maria S. Ferrer. She was a great emotional support, especially when I had to be away from her for a couple of months to finish my research at Kansas State University. She was my companion in this academic journey that started as a personal dream and transformed into a reality.

Emilio C. Piesciorovsky

Manhattan, Kansas, 2015

Dedication

I would like to dedicate this thesis to my lovely parents, Wanda R. Kublinski and Dr. Emilio F. Piesciorovsky, who gave me my first education at home, based on moral, responsibility, and respect principles for other human beings.

Chapter 1 - Introduction

Diesel generators have been the primary choice for distributed generator application in distribution systems for utilities in the United States [1]. Distributed generation refers to the production of electricity near the consumption. The concept of distributed generation has received widespread attention in the power industry because the use of distributed generators has changed how power distribution systems are designed, operated, and maintained [2]. Distributed generators are typically utilized as backup generators in case the utility source is not available because of equipment (utility source, breakers and/or power lines) failure or maintenance operations. Conventional distribution systems in the United States are radial with an inherent assumption that power flow always occurs from the utility source to the end user [2]. Distributed generation must implement protection, control and communication system that could be integrated into the utility source and bus feeders. Application of distributed generators in radial systems requires that protection systems control breakers in various circuit paths formed by breakers, fuses, and relays that require an adaptive overcurrent protection system fitted in those circuit paths. In this research, proposed adaptive overcurrent protection was tested by two relay in the loop techniques. Non-real-time simulator (NRTS) and real-time simulator (RTS) experiments were performed using SEL-AMS [3] and OP5600 [4] computer-based simulators, respectively, with two SEL-451 relays [5] in the loop.

1.1 Research application

Distributed generators located at various places in the microgrid require protective relays in order to change their protection and control settings. For example, when distributed generators are placed at no identical sites, power system improves because of the resulting increased number of circuit paths to feed users in case of equipment (utility source, breakers and/or power

lines) failure or maintenance operations. In certain circuit paths with distributed generators, currents along power lines could flow in different directions depending on what type of distributed generator was connected to end users. Figure 1.1 shows the Utility (A) and distributed generator (B) circuit paths. In these two microgrid modes, red arrows indicate current directions along the power lines, feeder fuses, utility source, and distributed generator branches.

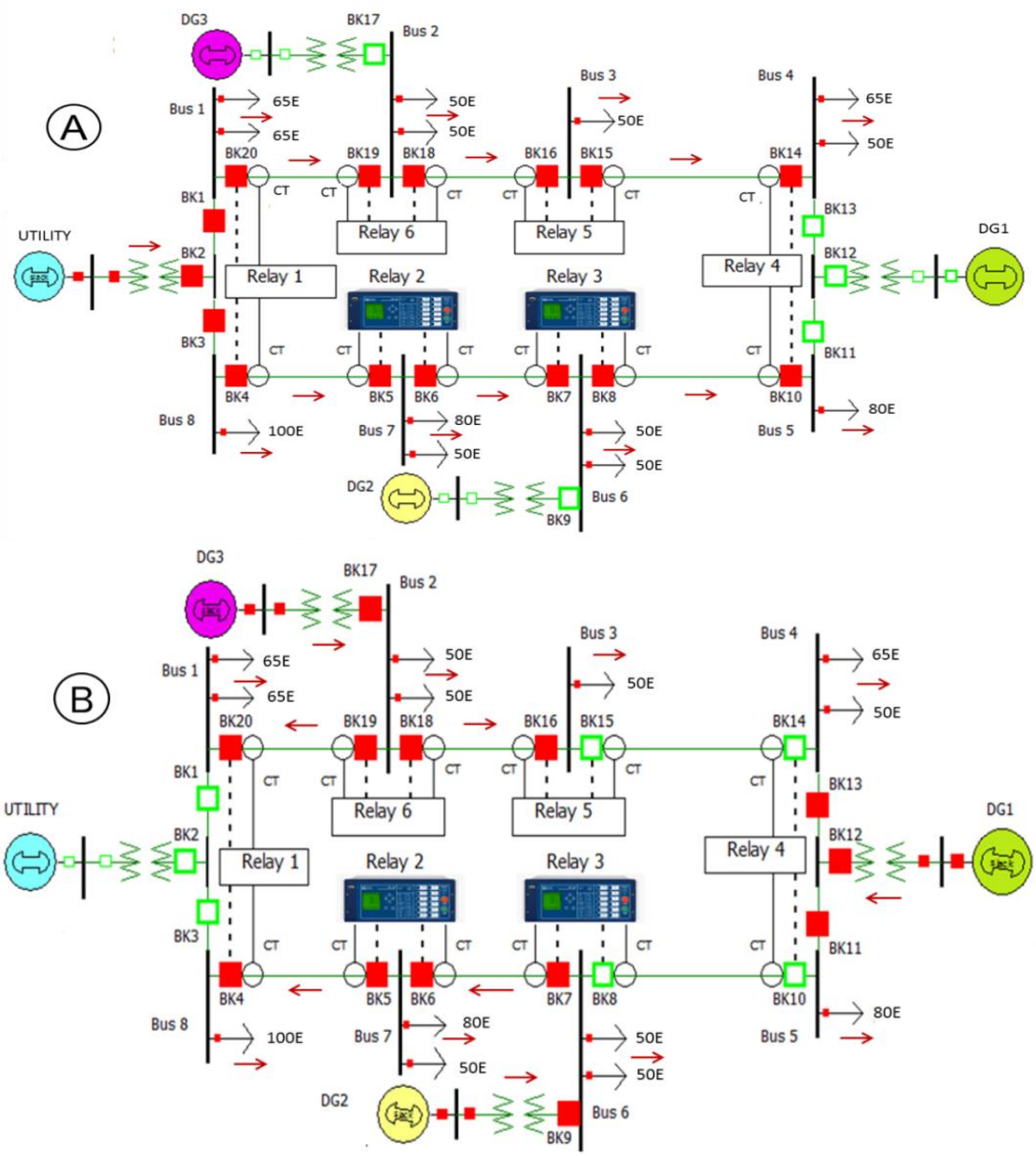

Figure 1.1: Utility (A) and distributed generator (B) modes

In a microgrid with distributed generators, diesel generators can be connected at islanding modes. Islanding refers to the condition in which a distributed generator feeds a location when the utility source is not available (blackout). In islanding applications, the absent utility source is disconnected from the grid, and the distributed generators are connected to local circuits. In Utility (A) mode, the circuit path was formed by the utility source and two branches. These two branches were formed by Busses 1 to 4 and 5 to 8. However, in distributed generator (B) mode, the DG1, DG2, and DG3 distributed generators were connected to islanding applications. As shown in Figure 1.1, protection and control settings of Relays 2 and 3 had to be adapted to specific circuit paths because currents did not flow always in identical direction. Feeder fuses coordinated with Relays 2 and 3 differ in circuits shown in Figure 1.1. In Figure 1.1 (A), Relays 2 and 3 are coordinated with 50E and 80E fuses, respectively. However, in Figure 1.1 (B), Relays 2 and 3 are coordinated with 100E and 80E fuses, respectively. In addition, as shown in circuits of Figure 1.1, Relays 2 and 3 must not trip always the same breakers at fault overcurrent. In Figure 1.1 (A), Relays 2 and 3 must trip "BK6" and "BK8" breakers, respectively, at fault overcurrent. However, in Figure 1.1 (B), Relays 2 and 3 must trip "BK5" and "BK7" breakers, respectively. Application of distributed generators in a microgrid requires adaptive overcurrent protection that selects inverse time overcurrent settings of relays based on maximum ampere rating fuses on busses and expected tripped breakers at fault overcurrents for circuit paths in the microgrid.

1.2 Adaptive overcurrent protection

In this dissertation, adaptive overcurrent protection is defined for circuit paths in the microgrid based on calculation of inverse time overcurrent settings and relay's breaker protection logic for circuit paths by grouping identical inverse time overcurrent settings and protection logic

gates into relay setting groups. Protection logic gates ("AND" or "ZERO") depended on initial breaker states of relay and expected tripped and not-tripped relay breakers at fault overcurrents for the circuit paths. Microgrid circuits (test modes) were selected based on microgrid constraints (operation, maximum load demand, equipment and utility service limitations). Adaptive overcurrent protection was formed by six relays, but verified by RTS and NRTS with two relays in the loop. This research focused on circuit paths for Relays 2 and 3 in the microgrid. Power flow and fault analysis were performed for circuit paths in order to collect current magnitudes on the relay's breakers. In order to find maximum and minimum fault currents in power lines, fault analysis was performed at line-to-line (LL), three-phase balanced (3PB), single-line-to ground (SLG), and double-line-to ground (DLG) faults. Power lines of the microgrid were defined as protection areas in circuit paths. Based on circuit paths and fault locations, expected tripped and non-tripped relay breakers were selected, and maximum ampere rating fuses on busses for circuit paths were chosen in order to calculate inverse time overcurrent settings of relays.

Inverse time-current curve models of relays and fuses were created based on manufacturer literature [5, 6]. Inverse time overcurrent elements of the relays were set by U3 (very inverse) time-current curve, and time dial settings (TDS) and secondary overcurrent pickups (Ip) were calculated. For all circuit paths of Relays 2 and 3, inverse time-current curves of the relay's overcurrent elements and maximum ampere rating fuses were plotted for each branch of circuit paths. Selectivity coordination between upstream (backup) and downstream (primary) protective devices was verified in time-current logarithmic plots. Maximum load and fault currents were plotted, verifying that calculated inverse time overcurrent settings did not trip and did trip the relay's breakers, respectively. Coordination time intervals (CTIs) between

backup and primary protection devices at maximum fault currents were calculated, verifying that calculated CTIs were not less than the minimum CTI. The RTS experiment was set without a breaker operation time in order to validate the RTS experiment with minimum CTI between backup and primary relays (without breaker operation time) based on IEEE Std. 242-2001 [7]. "AND" and "ZERO" protection logic gates were created in order to trip and not trip the relay's breakers, respectively, at fault overcurrents. Although the breaker nearest to the fault location tripped, other breakers feeding the bus loads did not trip. In addition, breakers inside the protection areas cleared fault overcurrents more quickly than breakers outside the protection areas. Primary relays tripped faster than backup relays.

1.3 Relay in the loop techniques

Electrical engineers commonly verify relay settings with relay test systems before placing relays in substations. In this research, two relay in the loop techniques were applied in order to verify adaptive overcurrent protection. Equipment and software of the Burns & McDonnell - K-State Smart Grid Laboratory [8] were integrated into this research. This author built and operated the K-State Smart Grid Laboratory (2011-14) in order to apply NRTS and RTS with relays in the loop. Protective relays are devices that make decisions in power systems and have protection, control, measurement, and communication functions. By exploring new relay applications in the Burns & McDonnell - K-State Smart Grid Laboratory [8], control and protection power systems were studied in real-time simulation scenarios. Figure 1.2 shows control (A) and equipment (B) areas used in this research.

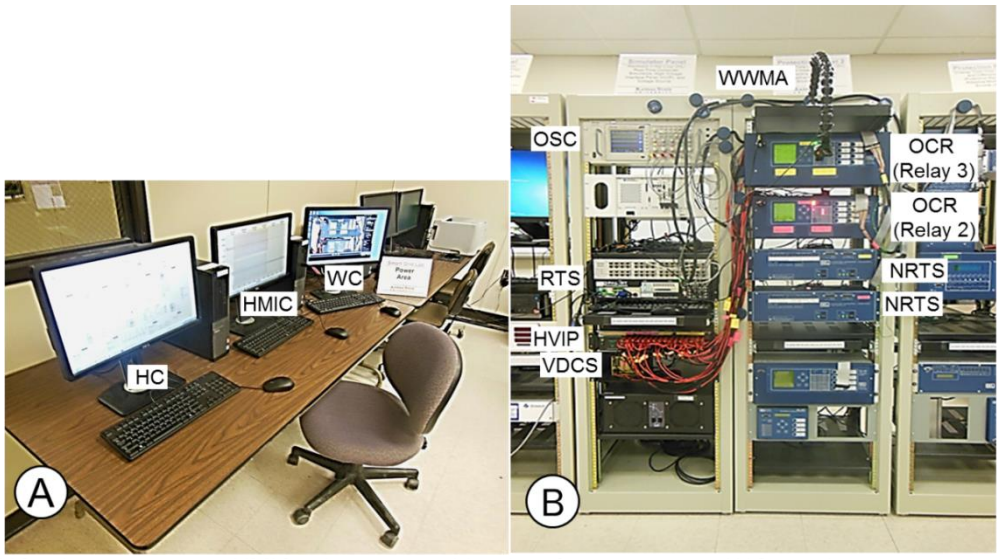

HC = host computer, HMIC = human machine interface computer, WC = webcam computer, OCR = Overcurrent relay (SEL 451), HVIP = high voltage interface panel, NRTS = non-real time simulator (SEL-AMS), RTS = real time simulator (OP5600), OSC = oscilloscope, WWMA = webcam with magnetic arm, VDCS = voltage source (125 Vdc)

Figure 1.2: Control (A) and equipment (B) areas in the NRTS and RTS experiment

Adaptive overcurrent protection for the microgrid with distributed generation was verified with an NRTS and RTS with two SEL-451 relays [5] in the loop. In the NRTS experiment, relay settings were verified by individual experimental circuits; each relay was connected to a specific SEL-AMS [3]. Therefore, Relays 2 and 3 were not synchronized in time. Results were collected individually from each relay test, and the performance of both relays working together as primary and backup protections was observed. In addition, the NRTS experiment was not a real-time simulation because secondary currents and voltages of the pre-fault, fault, and post-fault states had to be calculated in order to set the NRTS before running the relay tests. In the RTS experiment, relay settings were verified with a common experimental circuit for both relays. The microgrid with distributed generators was simulated in real-time. Therefore, Relays 2 and 3 were synchronized in time, and relay test results were collected from both relays working together. In the RTS experiment, the primary relay was observed to trip more quickly than the backup relay for circuit paths of the microgrid.

1.4 Research impact

Current distribution power systems have more fuses than protective relays because fuses are less expensive than protective relays. Application of fuses in conventional radial power systems (utility source - end users) is very common. Although fuses are a metallic strip that melts and opens an electric circuit if the current exceeds a safety level, protective relays are microprocessors that select various safety levels in order to open an electrical circuit at fault overcurrent. In addition, although fuses only have protection functions, protective relays have protection, communication, control, and measurement functions. Because application of distributed generators in distribution power systems has increased during the last decade [1], fuses must be integrated with protective relays in order to create adaptive overcurrent protections for microgrids with distributed generators. In this research, a protection and control system was developed in order to protect power lines and feeder busses of a microgrid with distributed generators based on adaptive inverse time overcurrent protection.

In order to include a topic of interest for the utility industry, the research impact of this application was verified with three original equipment manufacturers (OEMs) of protective relays before initiating work. Results of the research impact questionnaire submitted to ten engineers in protection power system areas are presented in Figure 1.3. The questionnaire is included in Table A.1 of Appendix A. As shown in Figure 1.3 (A), no engineers were aware of fuses that can communicate with relays in a power distribution system; therefore, feeder fuses that communicate with relays could be an innovative application. For example, integration of power line wireless sensors with fuses could create hybrid smart fuses that communicate fuse ampere rating, currents, and on-off line states to relays. As shown in Figure 1.3 (B), 90% of engineers thought that relays could be integrated to fuses with communication in a real distribution system. As shown in Figure 1.3 (C), 50% and 40% of engineers thought that fuse-

relay adaptive protection could improve selectivity in an original distribution system with fuses "Some" and "A lot", respectively. As shown in Figure 1.3 (D), 50% and 30% of engineers thought that fuse-relay adaptive protection provides innovation to a distribution system "A lot" and "Some", respectively.

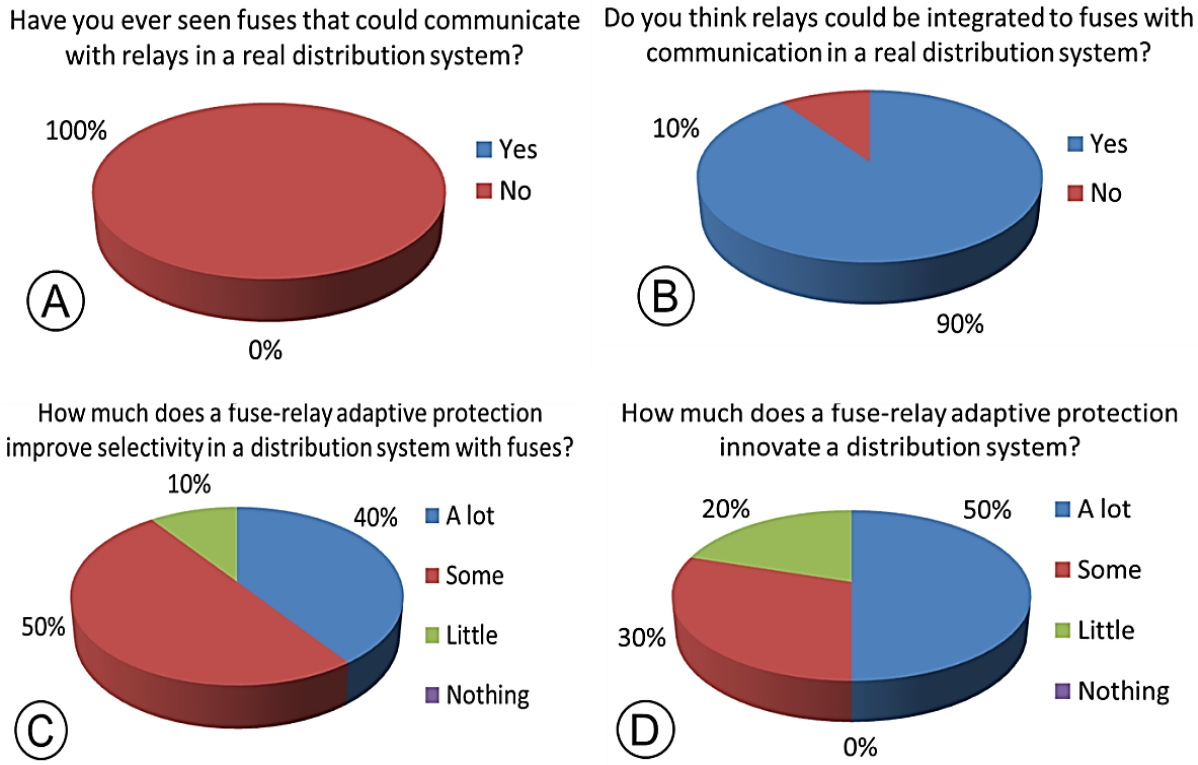

Figure 1.3: Research impact questionnaire

Adaptive overcurrent protection that integrates fuses with relays in a real distribution system results in an innovative application. In the NRTS experiment, relay setting groups with inverse time overcurrent settings were selected manually. However, in the RTS experiment, relay setting groups with inverse time overcurrent settings were selected from the host computer that simulated the power system through the relay's control outputs.

Another impact of this research is related to application of OP5600 (real-time simulator) with two relays in the loop. This author was the first graduate student to implement real-time simulation with two relays in the loop by integrating relay digital and analog signals with

OP5600 [4] at Burns & McDonnell - K-State Smart Grid Laboratory [8]. The RTS experimental circuit and project is fully explained in this dissertation so that other graduate students can apply this technique in research areas such as phasor measurement units, adaptive protection systems, and communication and cyber security applications.

1.5 Research

The work presented in this dissertation describes steps to design an adaptive overcurrent protection in a microgrid with distributed generators focused on relay setting groups, inverse time overcurrent element, and protection logics. In addition, relay in the loop techniques based on RTS and NRTS to verify adaptive overcurrent protection are described. Adaptive overcurrent protection was developed in order to protect power lines and feeders in distribution power systems represented by a microgrid with distributed generators, integrating feeder fuses, and protective relays for circuit paths in the microgrid. The process to establish adaptive overcurrent protection was systematically described, and RTS and NRTS experiments were developed in order to verify settings of Relays 2 and 3 located at line and distributed generator busses, respectively. Relays 2 and 3 were tested at maximum load (pre-fault state) and fault currents (fault states). Also, selectivity coordination between backup and primary protective relays was verified measuring CTIs at maximum fault currents for circuit paths of Relays 2 and 3 in the microgrid.

Chapter 2 reviews literature of various adaptive overcurrent protection methods and relay in the loop techniques in order to verify relay settings. Adaptive overcurrent protection algorithms from the literature review are described and compared to the adaptive overcurrent protection system. Types of relay test systems based on computer-based simulators with relays in the loop are also described and compared. In this research, the RTS and NRTS with relays in the

loop were applied in order to verify adaptive overcurrent protection. RTS and NRTS used the OP5600 [4] and SEL-AMS [3] systems, respectively. In this research, RTS OP5600 [4] was configured in order to operate as a real-time relay test system.

Chapter 3 describes the equipment and circuit of the microgrid and the single-line-diagram and equipment of the microgrid with distributed generators. The microgrid was formed by the utility source and three distributed generators. The microgrid with distributed generators had two main feeders formed by three power lines on each main feeder. These two main branches were formed by Busses 1 to 4 and 5 to 8, corresponding to 650-632-671-680 nodes of IEEE 13-Node test feeder [9]. Medium voltage (MV) fuses were selected for load feeders. The chapter also describes the steps to create the power lines, transformers, generators, and loads of the microgrid with the Power World® software [10] in order to prepare the microgrid to run the power flow and fault analysis.

Chapter 4 presents adaptive overcurrent protection based on relay setting groups and protection logics, and creation of adaptive overcurrent protection is systematically described. Microgrid circuits (test modes) were selected based on microgrid constraints (operation, maximum load demand, equipment and utility service limitations). Circuit paths were selected for Relay 2 and 3 busses in the microgrid circuits (test modes), and power flow and fault analysis were performed in order to collect current magnitudes on the relay's breakers. In the microgrid, power lines were defined as protection areas for circuit paths. Fault locations and expected tripped and non-tripped relay breakers were selected, and maximum ampere rating fuses on busses were selected in order to calculate inverse time overcurrent settings of relays. Inverse time-current curve models of relays and fuses were created in order to plot inverse time-current curves of protection devices. For all circuit paths of Relays 2 and 3, inverse time-current curves

of the relay's overcurrent elements and maximum ampere rating fuses were plotted for each branch of circuit paths. Maximum load and fault currents were plotted, verifying that calculated inverse time overcurrent element settings did and did not trip relay breakers, respectively. CTIs between backup and primary protection devices at maximum fault currents were calculated, verifying that calculated CTIs were not less than the minimum CTI. Protection logics of the relay's control outputs were created to trip or not trip relay breakers at fault overcurrents. In adaptive overcurrent protection, setting groups of Relays 2 and 3 were selected by grouping identical inverse time overcurrent settings and protection logic gates of relay breakers for circuit paths in the microgrid.

Chapter 5 describes how Relays 2 and 3 were set before running the NRTS and RTS experiments. Relays 2 and 3 contained four and six setting groups, respectively, and each relay had to control two breakers. Inverse time overcurrent elements of setting groups for Relays 2 and 3 were set with AcSELerator Quickset® software [11]. The Global, Breaker monitor, Groups, Outputs, Front panel, and Report options were set, and the setting groups were established for adaptive overcurrent protection.

Chapter 6 describes RTS and NRTS experimental circuits for testing Relays 2 and 3 in adaptive overcurrent protection of the microgrid with distributed generators. Hardware and software of experimental circuits are also described. SEL-AMS [3] and OP5600 [4] were connected for the NRTS and RTS experiments, respectively. The low level test interface (LLTI), mainboard input voltages, and control inputs and outputs are described for Relays 2 and 3 based on the SEL-451 relay instruction manual [5]. Analog and digital signals applied to experimental circuits are described based on the SEL-AMS instruction manual [3] and OP5600 user guide [4]. High voltage interface panel (HVIP) circuits between control inputs of Relays 2 and 3 and digital

outputs of OP5600 are also described. NRTS and RTS experiments were segregated into subcircuits: (1) current and voltage measurement, (2) breaker trip, (3) breaker state pole, (4) setting group, and (5) breaker record event circuits. Diagrams of subcircuits were compared for NRTS and RTS experiments.

Chapter 7 describes test steps to run non-real-time simulation with relays in the loop. In the NRTS experiment, tripping and non-tripping tests were run for adaptive overcurrent protection of the microgrid with distributed generators. NRTS simulated the trip coil and auxiliary contacts of the breakers and pre-fault, fault, and post-fault states. The calculation (1), preparation (2), execution (3), and collection (4) steps for tripping and non-tripping tests are also described. Relays 2 and 3 were verified during tripping and non-tripping tests. In the collection phase of tripping tests, measured relay times were collected in order to estimate the fault state time for non-tripping tests, and then tripping tests were run before non-tripping tests. Tripping and non-tripping tests for Relays 2 and 3 were run with SEL-5401® software [12]. In the NRTS experiment, tripping and non-tripping tests were run individually for each relay.

Chapter 8 presents NRTS experiment results for Relays 2 and 3. The NRTS experiment was segregated into tripping tests, including backup protection tests, and non-tripping tests. Tripped breaker states, and measured relay and fault clearing time values were collected during tripping tests. In the tripping tests, the fault state time was greater than the expected fault clearing time required if relays tripped. However, in the non-tripping tests, the fault state time was less than the relay time required if relays did not trip. Percent error values of Relays 2 and 3 were calculated for measured and theoretical relay times of tripping tests. Measured CTIs between backup and primary relays were estimated using measured relay times collected during the tripping tests.

Chapter 9 describes how the project model was built for adaptive overcurrent protection of the microgrid. The project model was created with RT-LAB® software [13] integrated with libraries from Matlab®/Simulink® software [14]. The project model was run with the real-time simulator OP5600 [4] with two SEL-451 relays [5] in the loop. In the RTS experiment, the project model was built before running real-time tests. The project model was formed by the SM_Network (master) and SC_console subsystems. The SM_Network (master) subsystem simulated the microgrid and recorded test results after real-time simulation. However, the SC_console subsystem triggered the external control signal for the fault block and supervised the real-time test during execution of the RTS experiment.

Chapter 10 presents test steps to run real-time simulation with relays in the loop, including steps to run tripping and non-tripping relay tests. The edition (1), preparation (2), compilation (3), execution (4), and collection (5) phases to run real-time simulations are also described. In the RTS experiment, tripping and non-tripping tests were run for Relays 2 and 3. In the tripping tests, relays tripped for an overcurrent fault situation, collecting the Matlab® and relay record event files from the host and human machine interface (HMI) computers, respectively. However, in the non-tripping tests, only Matlab® files were collected because relays did not save the record events if relays did not trip.

Chapter 11 presents results of the RTS experiment. The RTS experiment was segregated into tripping and non-tripping tests; backup protection tests were included in the tripping tests. Setting groups, A-B-C line currents, trip signals, and breaker states of Relays 2 and 3 were collected in the tripping and non-tripping tests. In tripping tests, real-time simulation was stopped at a time greater than the sum of pre-fault and fault clearing times in order to observe if relays tripped. However, non-tripping tests were stopped at a time less than the sum of pre-fault

and relay times in order to observe if relays did not trip. Relays 2 and 3 were tested in the loop with OP5600 [4]. Analysis of the relay's record events was performed, and A-B-C line currents of tripped breaker and digital variables of the protection logic gate ("AND") were plotted. Percent error values of Relays 2 and 3 were calculated by measured and theoretical relay times for tripping tests. Measured CTIs between primary and backup relays were collected for backup tests in order to verify protection coordination scenarios.

Chapter 12 presents conclusions about inverse time overcurrent adaptive protection for microgrid with distributed generators and comparison of relay in the loop techniques used in this research. Selectivity, speed, and reliability were achieved in adaptive overcurrent protection and verified with collected results of tripping and non-tripping relay tests. Selectivity was validated by collecting breaker state sequences of Relays 2 and 3 for tripping and non-tripping tests. Speed was validated by collecting measured fault clearing times of Relays 2 and 3 for tripping tests. In addition, the speed of protection logic gate ("AND") to trip relay breakers generated the trip signal without delay, confirming non-delay in protection logic applied in adaptive inverse time overcurrent protection. Reliability was validated by performing backup relay tests in order to disconnect the LLTI of primary relays (simulating a failure in current transformers of primary relays) and observe whether or not backup relays tripped, thereby validating reliability of the protection system. In this research, adaptive overcurrent protection was verified by testing Relays 2 and 3 with NRTS and RTS experiments. NRTS and RTS experiments were performed with SEL-AMS [3] and OP5600 [4] as NRTS and RTS, respectively. Conclusions were drawn from the application of these two relay in the loop techniques to test Relays 2 and 3.

Chapter 2 - Literature review

Adaptive overcurrent protection has attracted the attention of electrical engineers because it improves the selectivity and reliability of protection and control systems in power systems in which circuit paths could be available based on circuit breaker states. Adaptive overcurrent protection topics have increased in relevancy because of application of distributed generators in utility distribution power systems. This chapter introduces literature contributions and topics of interest related to adaptive overcurrent protection, such as microgrid and distributed generators, experimental methods to validate adaptive overcurrent protections, wireless power line sensors, hybrid smart fuses, and technical-economical evaluation (reliability, selectivity, speed, and cost) of protection systems.

2.1 Microgrid and distributed generators

A microgrid, a small electric power system connected to the utility grid through a point of common coupling. uses on-site distributed generators to supply all or portions of local demands. Key features of microgrid operation include logical islanding from the utility grid and the ability to be self-controlled in island mode. When a fault is at a distribution network, local microgrids can enhance power system reliability by switching to island mode as local distributed generators continue to supply microgrid loads [15]. However, integration of distributed generators in radial distribution systems regarding selectivity and coordination of existing overcurrent protection schemes must be studied in order to implement adaptive protection in a microgrid with distributed generators [16]. The amount of distributed generation connected to distribution networks currently creates challenges for traditional protection of distribution networks due to bidirectional power flows, and fault current contribution of distributed generators [17]. Typically, a relay system is designed to achieve the highest levels of speed, reliability,

selectivity, simplicity, and cost-efficiency [18]. Oudalov et al, 2014 [19] presented an application of a protection solution for a microgrid with distributed generators. This application was based on automatic adaptive protection that changes protection settings according to microgrid configurations. Gupta et al, 2013 [20] presented a critical review of existing adaptive protection schemes, technical challenges, and advancement regarding suitability for operating in a smart grid scenario. The conventional overcurrent protection scheme faces selectivity and sensitivity issues in grid and microgrid faults because the fault current levels could differ for the same relay. Adaptive protection is the most promise technique in microgrid configurations. However, feasibility, reliability, and cost benefits are associated with implementation of adaptive microgrid protection schemes.

2.2. Adaptive multifunction and overcurrent protections

Types of adaptive protection systems for a microgrid with distributed generators could be segregated into multifunction (overcurrent, distance, and differential protections) and overcurrent (directional, instantaneous, and/or inverse time overcurrent) protection groups. In adaptive protection systems of a microgrid with distributed generators, the overcurrent protection group has more publications than the multifunction protection group because overcurrent protection is used more often in distribution systems than distance and differential protections.

Publications related to the multifunction protection group for adaptive protection systems in a microgrid with distributed generators are listed below:

Ramaswamy et al, 2011[21] proposed a genetic algorithm, or optimization technique, in order to achieve microgrid objectives and constraints, such as voltage control, grid reconfiguration, and adaptive overcurrent and distance protection. The presence of distributed generators in smart grids introduces factors that require additional consideration for solving the

multi-objective optimization. This publication enlisted objectives and constraints for voltage control, grid reconfiguration, and protection applications that require additional consideration for solving multi-objective optimization.

Abdulhadi et al, 2011 [22] presented an adaptive protection architecture for smart grid applications which reflected the utility and functional requirements at various life cycle stages of a scheme. These life cycle stages demonstrated the physical mapping of the architecture's adaptive functionality in a prototype scheme, thereby facilitating the integration of modern digital substations and the integration of de-risking schemes and self-contained modules suitable for reuse of the smart grid.

Sham et al, 2011 [23] proposed the design and development of a new adaptive distance relaying scheme in order to overcome the adverse effects of the static synchronous compensator (STATCOM). Because conventional relays cannot provide reliable protection in midpoint STATCOM application, this new adaptive distance relaying scheme was designed and developed to mitigate the adverse effects of STATCOM in transmission lines.

Islam et al, 2012 [24] suggested a microgrid protection and safety concept with a central control and monitoring unit in which a multifunctional intelligent digital relay was used. Central control and monitoring infrastructure was used as an adaptive relay setting strategy for the microgrid, and protection strategies were investigated for adaptive safety protection in grid-connected and islanded modes at various types of faults.

Ojaghi et al, 2013 [25] suggested a full adaptive technique to set all overcurrent relays in high voltage substations which can be used online with no need to employ a communication infrastructure. This technique was based on an appropriate equivalent circuit of the power grid in the substation, online estimation of the equivalent circuit parameters, and application of the

equivalent circuit in order to estimate required short-circuit currents. The full adaptive technique was used to set overcurrent relays of a typical 230/20-kV substation connected to a sample 9-bus grid, and a function to initially remove faults along the line was created by setting the overcurrent relay of a power line as backup for its distance relay. If the distance relay failed to punctually remove fault, the overcurrent relay operated in order to resolve the problem. This coordination between relays was studied by solving overcurrent settings for two critical points, at the beginning of the first and second zones of the distance relay.

Laaksonen et al, 2014 [26] emphasized focus on design aspects of the adaptive multifunction protection system, addressing issues such as selection of alternative setting groups, components, and system architecture; system configuration; and programmed logic. The adaptive multifunction protection system was based on a centralized controller that ran real-time analysis of data received from field intelligent electronic devices and communicated with them via International Electrotechnical Commission (IEC) 61850 communications. The adaptive protection and microgrid control system was developed and installed at Hailuoto Island in Finland.

Relevant publications regarding the overcurrent protection group for adaptive protection systems in a microgrid with distributed generators are listed below:

Laway et al, 1993 [27] presented an adaptive protection algorithm applied to setting and coordinating directional overcurrent relays in an interconnected power system. The algorithm was developed to set and coordinates relays in an online mode; therefore, relays self-adaptively responded to changing conditions, operational or structural, of the power system.

Sachdev et al, 1995 [28] presented a topology detection technique suitable for use in adaptive directional overcurrent relaying applications. While the substation control computer at

each substation determined topology of the substation, the central control computer determined system wide topology from information supplied by the substation control computer. The technique was applied to three networks, and three operating states of each network were used for the tests. Execution times required to identify topology of the selected systems for various states were monitored and found to be acceptable for implementing the proposed technique in the developed adaptive protection scheme.

Zhang et al, 2008 [29] presented a setting group method as a solution to the adaptive overcurrent protection scheme in a shipboard power system. Use of setting groups of relays and a simple logic applied by directional overcurrent protection relay allowed comparison of the magnitude of the relay input current to the threshold value (pickup current setting) in order to verify the fault status in the power system. When the input current exceeded the pickup value, a trip signal was sent to the circuit breakers.

Mahat et al, 2011 [30] proposed an adaptive protection system that updated trip characteristics of relays when distribution system conditions were urged to change into grid, island, and losing generator modes. This adaptive protection overcame challenges of overcurrent protection in distribution systems with distributed generation. Relay trip characteristics were updated by detecting operating states (grid connected or island) and the faulted section. The adaptive protection also proposed a faulted section detection using time overcurrent characteristics of directional overcurrent relays. Simulation results showed that the operating state and faulted section could be correctly identified and protection system settings could be updated to more quicly clear the faults.

Liu et al, 2012 [31] proposed a novel adaptive protection method that measured only local information rather than use of the communication in order to adapt protection settings to

the change of grid-connected or islanded modes, network topology (radial or meshed), and disconnection of distributed generators. Directional overcurrent relays were adopted in the distributed system to shorten the tripping time in order to maintain the distributed generator connection. Relay settings were calculated offline and modified online according to state detection, including islanding detection, power flow detection, and fault section detection.

Matic-Cuka et al, 2012 [32] presented a new Hierarchically Coordinated Protection (HCP) approach to mitigate effects of increased grid complexities. The proposed approach utilized local and wide area measurements and relied on three HCP framework levels: fault anticipation and prediction, adaptive fault detection, and overcurrent relay operation correction in case of unwanted tripping. The HCP offered intelligence to directional overcurrent relays at all voltage levels and using information and statistics from the systems, such as weather, lightning, animal and bird migration patterns, and component outage history, to enhance protection system tripping dependability and security.

Khederzadeh, 2012 [33] presented a setting group method as a solution to numerical relays in order to adapt their settings to the microgrid status. Settings for inverse time overcurrent relays were calculated offline and saved in the relays, and settings were automatically changed to the associated group of settings. Status of the microgrid was transferred by a communication link typically available in a microgrid to the relays.

Buque et al, 2012 [34] developed an adaptive overcurrent relaying scheme for a microgrid using intelligent inverse time overcurrent relay models that detect the mode of operation of the microgrid. Results showed that the relaying scheme adjusted its setting by sensing the mode of operation of the microgrid with practically no delay time.

Montoya et al, 2013 [35] suggested a methodology to set up overcurrent directional protection. Adaptability was achieved through a self-adaptive algorithm that allowed the operator to change the setup of any overcurrent devices remotely. This method for the coordination of inverse time overcurrent characteristics using an adaptive scheme was validated through two co-simulation techniques.

Rones et al, 2013 [36] presented an adaptive overcurrent protection of overhead distribution feeder system using inverse time overcurrent relay, recloser, and sectionalizer. The impact of distribution generator on radial overhead distribution feeder system with overcurrent relay, recloser, and sectionalizer was evaluated for distributed generation conformed by wind farms.

Jafari et al, 2013 [37] proposed a protection scheme to avoid changing the setting of protective devices for various operating conditions. Traditional distribution networks have radial and unidirectional topology, so the protection system of these networks was based on time and current coordination of inverse time overcurrent protection devices affected by distributed generators. This protection scheme was based on a self-adaptive method for a microgrid in which under reach fault currents were detected and compensated by relays to adapt overcurrent protection scheme.

Singh, 2013 [38] presented an adaptive overcurrent protection coordination approach that restored directional and inverse time overcurrent relay coordination according to changing fault current contribution from distributed generation sources. A microgrid model was simulated and relay settings were optimized with help of a robust and fast covariance mean evolution strategy based on optimization of the algorithm.

Mishra et al, 2014 [39] presented an approach that utilized local and wide area measurements and relied on fault anticipation and prediction, adaptive fault detection, and relay operation correction for unwanted tripping. This proposed scheme provided time flexibility to protect the system in order to adjust biasing between dependability and security for each disturbance, thereby reducing the missed operation rate of relay. The main contribution of this paper was implementation of adaptive relaying using variable time setting multiplier or dial setting for inverse time overcurrent relays depending on severity of short circuit, fault impedance, and fault location.

2.3 Adaptive overcurrent protections

Overcurrent is the most popular protection function used in microgrids with distributed generators. Overcurrent protections can be classified as instantaneous (50), inverse time-current (51), and overcurrent directional (67) protections [40]. In a microgrid with distributed generators, application of adaptive overcurrent protections could be presented for radial and non-radial power systems. Protective devices used in a distribution power system integrated to a microgrid could include relays, fuses, and/or reclosers. Methods to validate adaptive overcurrent protection systems are based on use of software programs and/or computer-based simulations which can be developed for non-real-time and real-time simulators with or without hardware-in-the-loop (HIL). Table 2.1 shows a comparison of relevant literature based on publication years, protective devices, power systems, overcurrent protection, and experimental methods for adaptive overcurrent protection studies in microgrid with distributed generators.

Table 2.1: Adaptive overcurrent protection literature review

References	Protective devices			Power system		Overcurrent protection[(1)]			Experimental methods (simulations)				
	Relay	Fuse	Recloser	Radial	Non-radial	50	51	67	Computer software	NRTS with HIL	RTS without HIL	RTS with HIL	HIL [No of relays]
Laway *et al*, 1993 [27]	X				X		X	X	X				0
Sachdev *et al*, 1995 [28]	X				X			X	X				0
Zhang *et al*, 2008 [29]	X				X			X	X		X	X	1
Mahat *et al*, 2011 [30]	X			X	X		X	X	X				0
Liu *et al*, 2012 [31]	X			X	X	X	X	X	X				0
Matic-Cuka *et al*, 2012[32]	X				X			X	X				0
Khederzadeh 2012 [33]	X			X			X			X			2
Buque *et al*, 2012 [34]	X			X			X		X				0
Montoya *et al*, 2013 [35]	X			X	X		X	X	X		X		0
Rones *et al*, 2013 [36]	X	X	X	X			X		X				0
Jafari *et al*, 2013 [37]	X			X			X		X				0
Singh, 2013 [38]	X			X	X		X	X	X				0
Mishra *et al*, 2014 [39]	X				X		X	X	X				0

[(1)]Instantaneous (50), inverse time (51), and directional (67) overcurrent protections based on IEEE Std. C37.2-2008 [40], NRTS: non-real-time simulation, RTS: real-time simulation, HIL: Hardware-in-the-loop

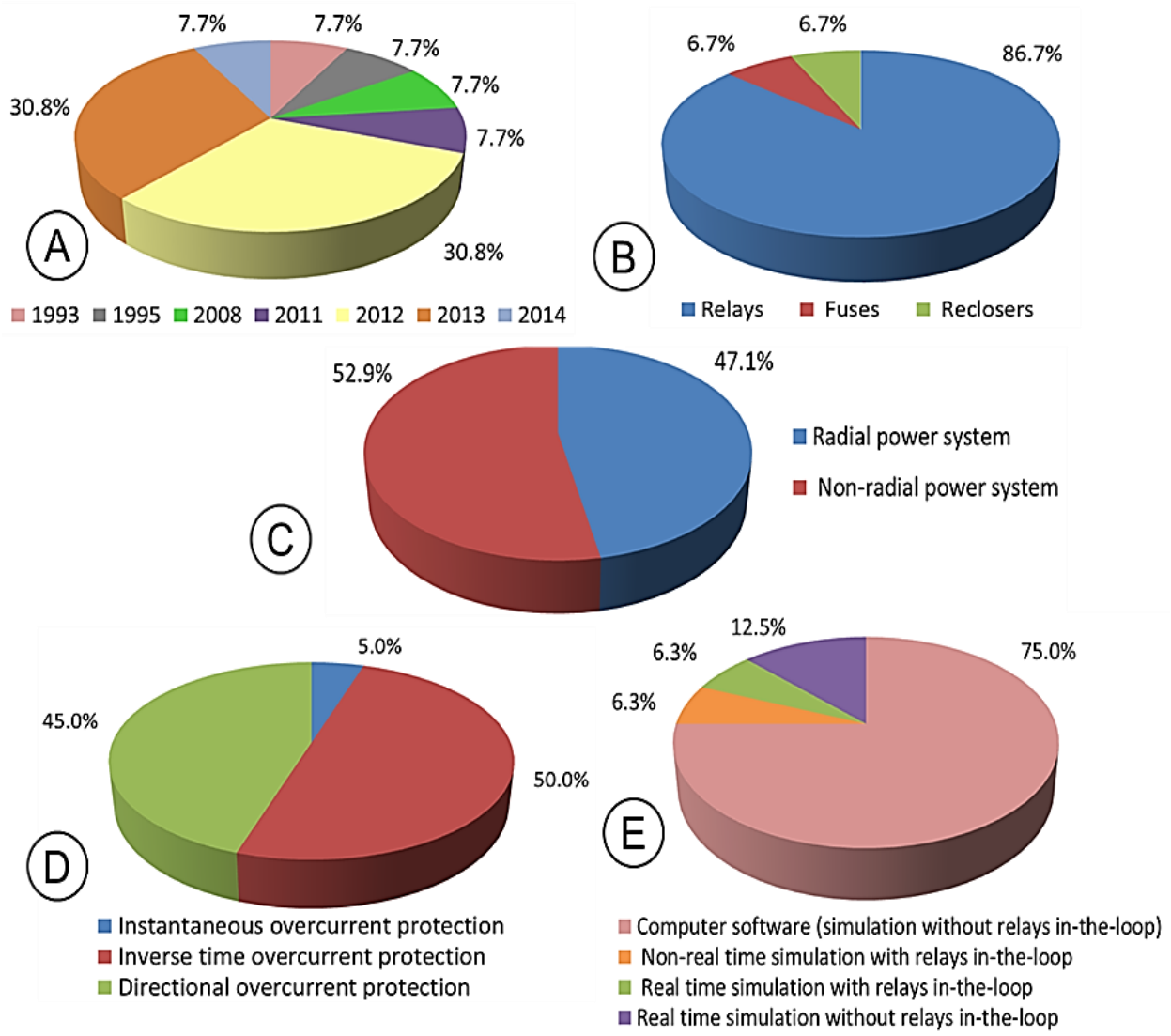

Figure 2.1: Publication years (A), protective devices (B), power systems (C), overcurrent protection (D), and experimental methods (E) for adaptive overcurrent protection studies in microgrid with distributed generators collected from relevant literature review

Figure 2.1 illustrates information collected from Table 2.1 with most relevant publications regarding adaptive overcurrent protection in microgrid with distributed generators since 1993. More than 70% of reports were published between 2011 and 2014 (Figure 2.1 (A)). Relays are the most popular protective devices in the analysis and study of adaptive overcurrent protection in a microgrid with distributed generators due to protection, control, communication, and measurement functions of relays (Figure 2.1 (B)). However, in the proposed research,

adaptive overcurrent protections had to be integrated into conventional radial power systems in which fuses were the most frequently used protective devices and power line sensors were used at fuse locations. Relays and fuses could comprise adaptive overcurrent protection that integrates the microgrid with conventional radial power systems protected with fuses.

Microgrids with distributed generators are required in order to study adaptive overcurrent protection in radial and non-radial power systems (Figure 2.1 (C)). Application of distributed generators connected in parallel to other distributed generators and/or utility sources allow power to flow from the utility source to the end user, from the distributed generator to the end user, and from the distributed generator to the utility grid. In the proposed research, adaptive overcurrent protection was based on a microgrid application with constraints (operation, maximum load demand, equipment, and utility service limitations). Objectives and constraints to develop algorithms in adaptive overcurrent protections are crucial in order to solve control problems [21].

Directional and inverse time overcurrent protections typically are used more often than instantaneous overcurrent protection (Figure 2.1 (D)). Although directional overcurrent protection is related to application of adaptive overcurrent protections in a radial power system, inverse time overcurrent protection is related to coordination of relays and/or fuses with inverse time-current curves. In the proposed research, adaptive overcurrent protection was based on integration of inverse time overcurrent relays and fuses in power lines and feeders, respectively. Relays were coordinated to other relays and fuses, selecting maximum ampere rating fuses on busses in the microgrid.

Computer software is the most common tool for studying adaptive overcurrent protections in a microgrid with distributed generators (Figure 2.1 (E)). However, the real-time simulator with relays in the loop is the most recommended technique to study adaptive

overcurrent protections because relays are connected in a real-time environment that allows integration of HIL. In the proposed research, adaptive overcurrent protection was verified with a real-time and non-real-time simulator with two relays in the loop.

2.4 Experimental methods to validate adaptive overcurrent protections

A microgrid can operate as a radial or non-radial power system in which currents no always flow in identical directions. The microgrid can use protective relays, reclosers, and/or fuses. Methods to validate the adaptive overcurrent protection system can be developed based on computer software, non-real-time, and real-time simulators. Non-real-time and real-time simulators allow installation of relays in the loop, and relay in the loop techniques are essential for verification of the adaptive overcurrent protection system with a relay application. In Table 2.1, adaptive overcurrent protection schemes presented in the literature review were simulated by the following experimental methods:

Laway et al, 1993 [27] validated an adaptive directional and inverse time overcurrent protection for a non-radial power system, testing an adaptive overcurrent algorithm with a computer program.

Sachdev et al, 1995 [28] demonstrated an adaptive protection scheme, testing three networks with computer software simulation. Execution times required to identify topology of the selected systems for various states were monitored during the tests.

Zhang et al, 2008 [29] simulated a shipboard power system for a shipboard and adaptive overcurrent protection using various techniques. The protective device was thoroughly modeled with Matlab® Simulink® [41] software and then downloaded to a DSpace® [42] controller board that was interfaced with a real-time simulator in order to perform corresponding HIL tests. Results of these HIL tests were compared to similar tests using an SEL351-S relay [43].

Mahat et al, 2011 [30] and Liu et al, 2012 [31] simulated the same distribution system in Denmark. The verification method was implemented with DigSILENT® PowerFactory [44] and Matlab® Simulink® [41] software.

Matic-Cuka et al, 2012 [32] developed the IEEE 39-bus New England test system in order to perform the proposed HCP scheme for transmission applications with a computer software simulation.

Khederzadeh, 2012 [33] presented a setting group method as a solution for numerical relays in order to adapt their settings to the microgrid status. In order to validate this setting group method, various settings for the overcurrent relays were calculated offline and saved in the relays. Settings were automatically changed to the associated group of settings.

Buque et al, 2012 [34] developed an adaptive relaying scheme for a microgrid that could detect the mode of operation in the microgrid. Matlab® Simulink® [41] software was used to simulate the relay and power system models.

Montoya et al, 2013 [35] proposed an adaptive protection scheme to coordinate overcurrent relays. This scheme was validated through two co-simulation techniques: real-time simulation and HIL simulations. These techniques required integration of a power system analysis toolbox called PSAT® [45] and LabVIEW™ [46] software. Results of real-time and HIL simulations were compared and validated with the offline ETAP® [47] software.

Rones et al, 2013 [36] developed and evaluated an adaptive overcurrent feeder protection scheme and an adaptive recloser and sectionalizers feeder protection scheme in order to vanquish the impact of wind turbines as distributed generators. Distribution system conductor sizing and protection coordination studies were performed with a Power System Computer Aided software called PSCAD® [48] and Matlab® Simulink® [41] software package for simulations.

Jafari et al, 2013 [37] presented a self-adaptive method for the smart microgrid that compensated the underreached fault current detected by the relay system. The microgrid test system is part of the Himmerlands Elforsyning distribution network in Aalborg, Denmark, that was simulated with PSCAD ® [48] software.

Singh, 2013 [38] presented an adaptive overcurrent protection coordination approach that restored overcurrent relay coordination based on changing fault current contribution from distributed generation sources. The microgrid model was simulated with Matlab® Simulink® [41] software.

Mishra et al, 2014 [39] proposed adaptive protections that analyzed adaptability of the relay based on a fuzzy inference system in which the action and response time of the relay were considered by taking the short circuit current, fault impedance, and location of the fault from the end as inputs. The microgrid was based on an IEEE14 bus system simulated by ETAP® [47] software in order to calculate fault currents, and the fuzzy inference system was simulated using Matlab® Simulink® [41] software.

In the proposed research, adaptive overcurrent protection was based on overcurrent relays applied in a nonconventional radial power system with the assumption that power always flows from the utility source to end user or distributed generator to end user. However, depending on the selected circuit path, the distributed generator could be located at various sites of the microgrid, thereby allowing power to flow along power lines in not always the identical direction. In the proposed research, inverse time-current curves of relays and fuses were coordinated in adaptive overcurrent protection, and the assumption was made that adaptive overcurrent protection was created in order to protect the power lines and feeders. Depending on circuit paths in the microgrid and maximum ampere rating fuses on busses, inverse time

overcurrent settings of relays were calculated. Although 75% of adaptive overcurrent protection studies shown in Figure 2.1 were validated by software and computer programs, the proposed research was verified with relay in the loop techniques. Verification of the adaptive overcurrent system was based on two relay test methods: the non-real-time simulator and real-time simulator with relays in the loop. Real relays were advantageously applied during verification; therefore, logic functions inside relays were applied in order to implement the adaptive overcurrent algorithm. Wiring connections of relays were also performed in order to create the real circuit of this adaptive overcurrent protection system simulated with a non-real-time and real-time power system.

2.5 Algorithms of adaptive overcurrent protection

Design of an adaptive protection system requires a method for detecting all circuit topologies along the power system. In this research, the topology detection technique was based on identification of circuit topologies in power systems, and the adaptive relay system was based on the fact that power system status can change. Therefore, relay settings were modified based on power system modifications [18]. Protective relays along the power system provide a continuous service, detecting failures or abnormalities inside control protection areas. Protective relay tasks are accomplished by opening breakers in the protection area in order to isolate the fault, thereby avoiding excessive damage to equipment or possible collapse of the power system. Protection systems are designed to achieve the highest level of speed, reliability, selectivity, simplicity, and cost-efficiency. Current application of adaptive relaying techniques in protection systems is more feasible than previous application because current protective relays are programmable devices with extensive logic, memory, data transfer, communication, and reporting capabilities. Therefore, relays are protective devices to develop adaptive relay

techniques in power systems. Adaptive overcurrent algorithms systematically describe the process to set relays as adaptive overcurrent protections. From Table 2.1, published algorithms of adaptive overcurrent protection were plotted and compared as flow charts [27, 30, 34, 35, and 38].

Figure 2.2 shows the algorithm for adaptive coordination of directional overcurrent relays described by Laway et al, 1993 [27]. The flow chart of the algorithm can be explained with descriptions of the following phases: (1) topology processor, (2) load flow program, (3) adaptive selection of pickup overcurrent, (4) fault analysis program, (5) primary/ backup relay pairs, (6) optimal relay setting, and (7) communication of the settings to the relays [27].

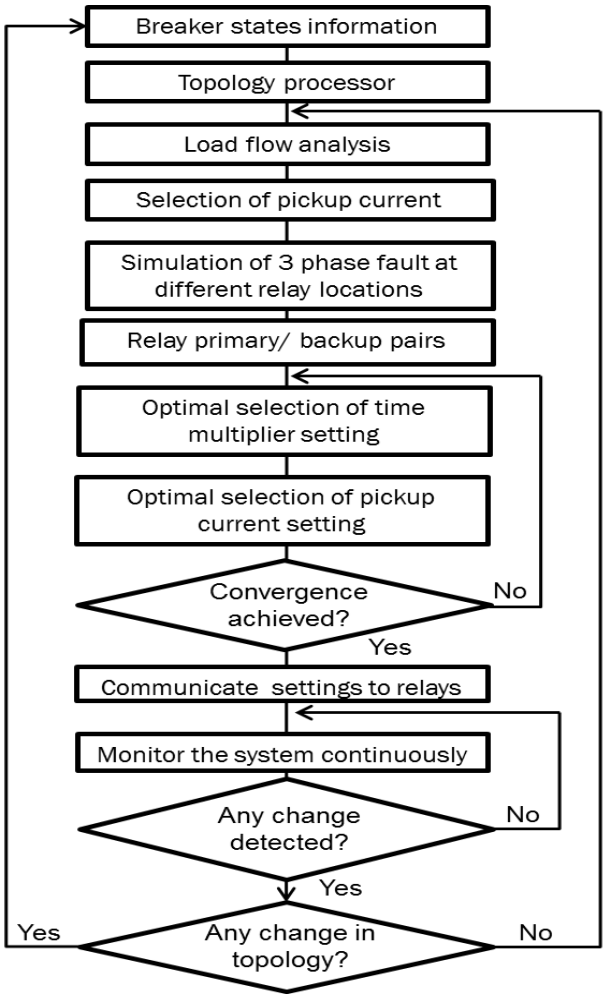

Figure 2.2: Adaptive coordination of directional overcurrent relays [27]

Figure 2.3 shows the algorithm for the adaptive setting of relays presented by Mahat et al, 2011 [30]. The flow chart describes an adaptive overcurrent algorithm that allows the distribution generation system to operate in islanded or grid mode. In this algorithm, current measurements were needed in order to update down-stream relay settings, and voltage and frequency measurements were needed in order to change directional relay settings for islanding and grid connected conditions, according to Mahat et al, 2011 [30] and Liu et al, 2012 [31].

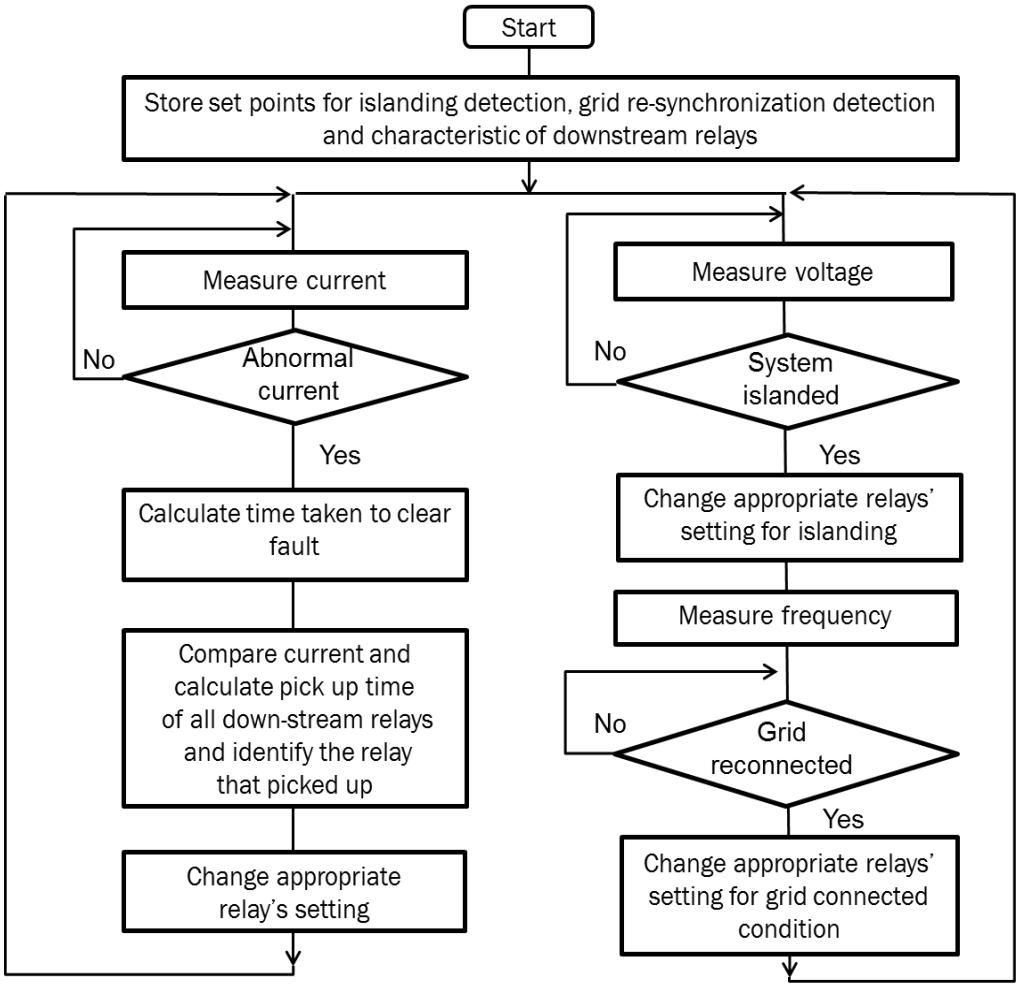

Figure 2.3: Flow chart for adaptive setting for relays [30]

Figure 2.4 shows the algorithm of adaptive relaying scheme presented by Buque et al, 2012 [34]. The adaptive overcurrent relay model was designed according to the IEC standard equation for normal inverse definite minimum time. The adaptive overcurrent relaying scheme

automatically selects the pickup current setting of the relays after setting the operation mode in the microgrid. Based on initial relay parameters (current transformer ratios, time multiplier, and plug setting) and the root mean square (RMS), current values are determined in order to calculate the operating time of relays. If the secondary current is smaller than the pickup current, operating time of relays is re-calculated. However, if the secondary current is higher than the pickup current, the calculated trip time is sent to the circuit breaker [34].

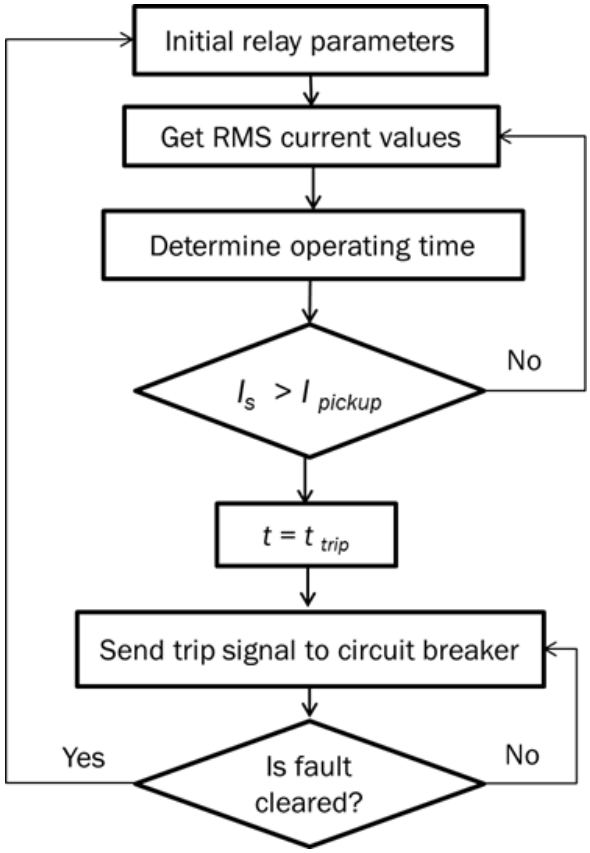

Figure 2.4: Flow diagram of adaptive relaying scheme [34]

Figure 2.5 shows the algorithm of the adaptive protection methodology presented by Montoya et al, 2013 [35]. This methodology makes an initial configuration of overcurrent protective devices when the utility is the only power source of the radial distribution network. Then the methodology checks the state of the distributed generators and power flow analysis to determine if changes have occurred. If so, power flow validation is performed in order to

reconfigure all overcurrent protective devices according to estimation parameters. Parameters that allow adaptive behavior are well-known by the utility. These parameters include line current flow along the breaker, symmetric fault current, and inverse time overcurrent settings (pickup current and time dial setting parameters) of protective devices [35]. Inverse time overcurrent settings were established according to the American National Standards Institute (ANSI) or IEC.

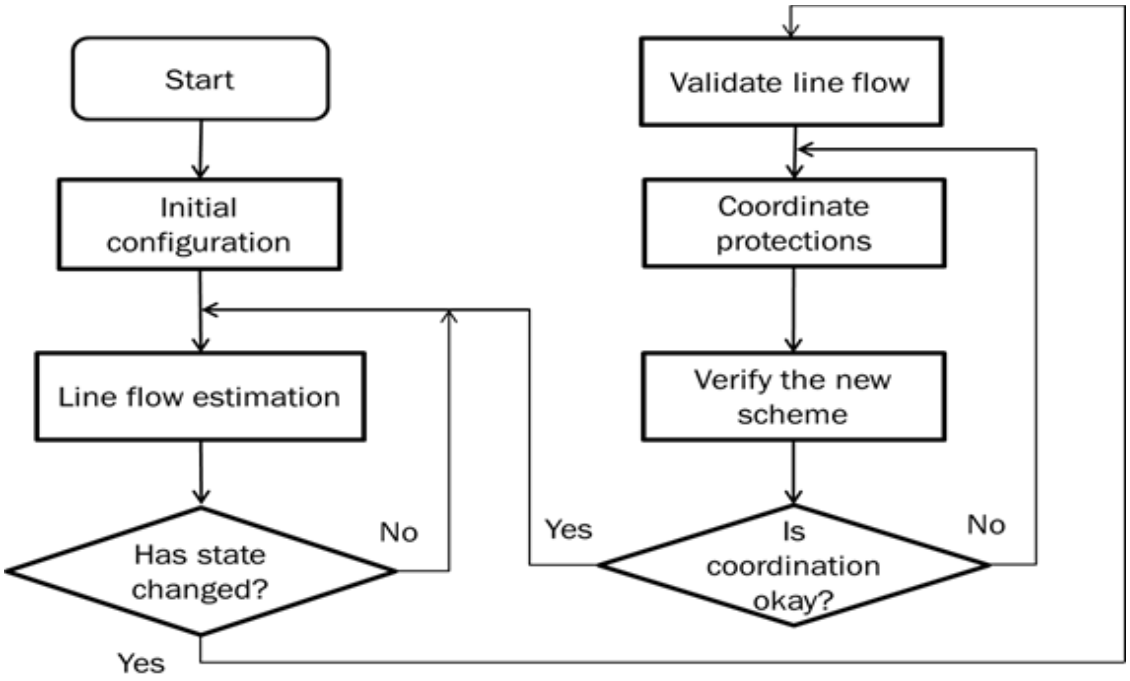

Figure 2.5: Adaptive protection methodology [35]

Figure 2.6 shows the algorithm of adaptive overcurrent protection presented by Singh, 2013 [38]. The flow chart in Figure 2.6 is based on an adaptive protection system for a distributed generation source in the power distribution system and an expert adaptive overcurrent protection coordination approach that restores overcurrent relay coordination according to the changing fault current contribution from distributed generation sources. Relay settings are optimized with the help of a robust and fast covariance mean evolution strategy based on an optimization algorithm [38].

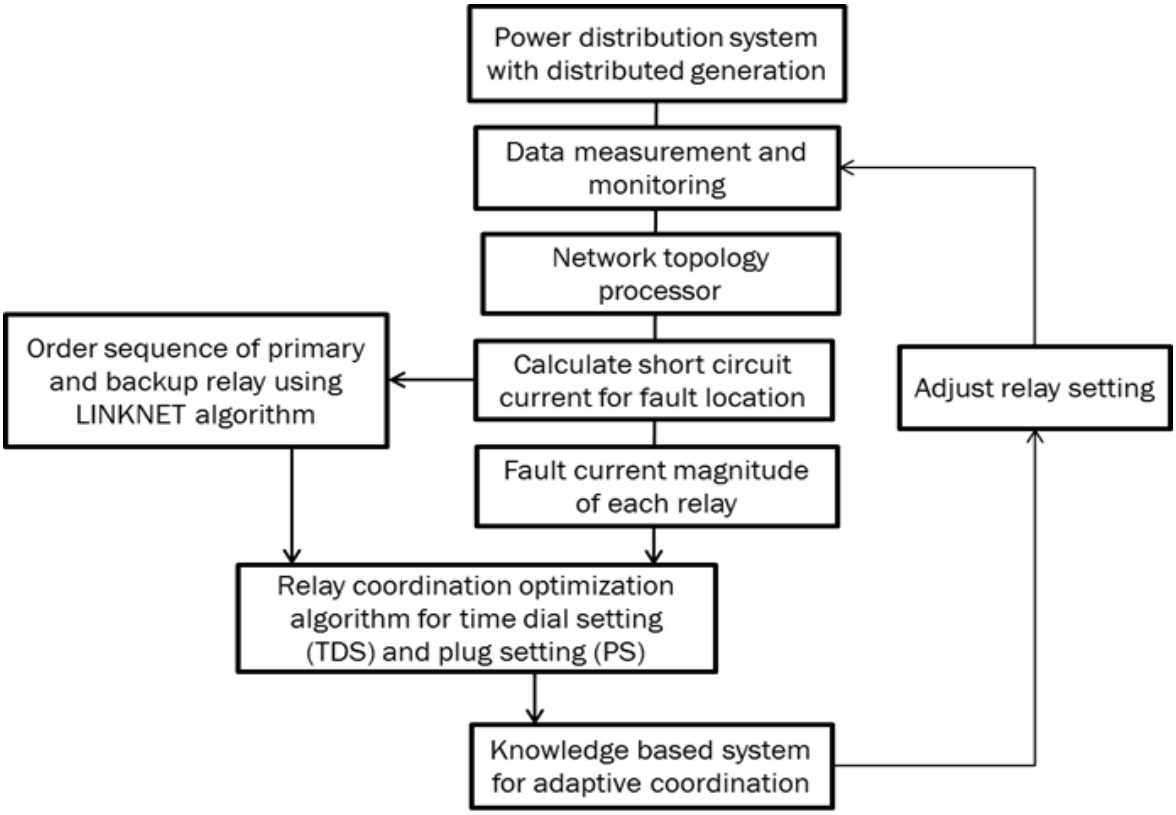

Figure 2.6: Adaptive overcurrent relay coordination algorithm [38]

Flow charts steps defined in Figures 2.2 to 2.6 were useful tools for developing the algorithm in the proposed research. The proposed adaptive overcurrent algorithm was based on non-conventional radial distribution formed by distributed generators at various locations in the microgrid that allowed currents in power lines no always flow in identical direction. In order to develop algorithms in adaptive protection, the presence of objectives and constraints is required to solve control problems [21]. Ramaswamy et al, 2011 [21] listed voltage control, grid reconfiguration, and adaptive protection objectives and constraints. Mantawy et al, 2003 [49] listed voltage control objectives and constraints for optimization in adaptive overcurrent protection. Distribution grid reconfiguration is defined as altering the topological structure of distribution feeders by changing open/closed states of breakers so that the objective function is minimized and constraints are met. Objectives and constraints in grid reconfiguration are listed

by De Oliveira et al, 2004 [50], Mendoza et al, 2006 [51], Enacheanu et al, 2008 [52], and Hong et al, 2005 [53]. According to Damborg et al, 2000 [54], "Adaptive protection is a protection philosophy which permits and seeks to make adjustment to various protection functions in order to make them more attuned to prevailing power system conditions." The need for adaptive protection arises because rapid switching actions, including islanding, load shedding, and generator tripping, are beneficial for maintaining synchronism in unstable situations. Damborg et al, 2000 [54], Bittencourt et al, 2009 [55], Chattopadhyay et al, 1991 [56], So et al, 1997 [57], and Ghanbarian et al, 2008 [58] listed adaptive protection objectives and constraints.

In this proposed research, voltage control, grid reconfiguration, and adaptive protection constraints and objectives were added to the adaptive overcurrent protection algorithm. In addition, the proposed adaptive overcurrent algorithm was based on coordinating fuses-relays and relays-relays compared to only relays-relays in the algorithms shown in Figures 2.2 to 2.6. Table 2.2 shows a comparison of adaptive overcurrent protection algorithms from the literature review versus proposed research.

Table 2.2: Adaptive overcurrent protection algorithms from literature review versus proposed research

Characteristics of adaptive overcurrent protection algorithms				Figure 2.2 Laway et al, 1993 [27]	Figure 2.3 Mahat *et al*, 2011 [30]	Figure 2.4 Buque *et al*, 2012 [34]	Figure 2.5 Montoya *et al*, 2013 [35]	Figure 2.6 Singh, 2013 [38]	Proposed research
Objectives and Constraints	**Voltage control**	**Busses**	Bus voltage service limit range in microgrid		X				X
		Transformers	Tap changer limits of transformers						X
	Grid reconfiguration	**Grid mode**	Utility source feed loads	X	X	X	X		X
		Island mode	Distributed generators feed loads	X	X	X	X		X
		Emergency mode	Utility source and distributed generators feed loads						
		Loads	Maximum load demand scenario						X
		Distributed generators	No parallel connection of distributed generators						X
			Maximum prime real and reactive power						X
		Stability	Frequency measurements		X				
	Adaptive protection	**Setting verification**	Maximum load current (relays do no trip)						X
			Minimum fault current (relays trip)	X	X	X	X	X	X
			Maximum fault current (relays trip)	X	X	X	X	X	X
			Selectivity coordination	X	X	X	X	X	X
			Minimum coordination time interval	X	X	X	X	X	X
		Overcurrent protection	Instantaneous overcurrent protection						
			Inverse time overcurrent protection	X	X	X	X	X	X
			Directional overcurrent protection	X	X		X	X	X[(1)]
		Protection devices	Relays	X	X	X	X	X	X
			Fuses						X
			Reclosers						
		Protection areas	Power lines	X	X	X	X	X	X
			Bus feeders						X

[(1)]Based on creating protection logic gates (AND, ZERO) for circuit paths in microgrid

2.6 Wireless power line sensors and hybrid smart fuses

Today's digital society requires efficient fault management and load monitoring of electrical distribution networks. Processing data requirements from the distribution network by installing no wireless sensors at different locations, such as incoming and outgoing power lines of secondary substations, requires a substantial cabling effort. Wireless sensors are promising technical and economical product alternatives for smart grid projects [59]. As utilities attempt to implement personalized concepts of the smart grid, the need for accurate sensor data and utilization of that data in individual smart grid implementations is essential [60]. Leon et al, 2007 [61] presents application of wireless sensor network technology to detect mechanical failures in transmission lines, obtain a complete physical and electrical picture of the power system in real-time, diagnose imminent and permanent faults, and determine appropriate control measures that could be automatically suggested to system operators.

An application based on integration of equipment in order to create smart grid network architectures that are not commercially available in the market was developed by Salvadori et al, 2013 [62]. In this application, the smart grid network is denominated by hybrid smart grid network architecture [62]. The hybrid network architecture for monitoring, diagnosis, and supervisory control applied to smart grids consists of wireless sensor network, power line communications, and a controller area network based on easy/low cost implementation. This hybrid network architecture has simple set up implementation of redundant routines. Hybrid network architecture was implanted in one underground electric substation power distribution, characterized as an extremely hostile environment for supervisory control applications. The main challenge of the hybrid network architecture was to establish a communication system installed inside the substation [62].

In this proposed research, adaptive overcurrent protection system must communicate in order to implement the relay setting group changes. The communication link between the relays and power system was needed to select the setting groups of the relays in the adaptive overcurrent protection system, based on the maximum fuse ampere rating on bus feeders, and circuit paths based on breakers states in the microgrid. In this research, the real relay interface was implemented using two SEL 451 relays [5] in the loop with an OP5600 [4] real-time simulator.

Although "fuse-relay" communication is not implemented with real fuses, the literature review revealed a need to find answers related to "fuse-relay" communication. Initially, the concepts of a smart fuse that could implement a "fuse-relay" communication was selected as an option to integrate radial and non-radial power systems; therefore, information about smart fuses in distribution systems was collected. Design, development, and application of a smart fuse in medium voltage distribution system were presented by Radhakrishnanand et al, 1994 [63], but no smart fuse product or vendor was found in the market. In addition, in response to the research questionnaire, all colleagues stated that they had never encountered fuses that could communicate with relays in a real distribution system. Therefore, the concept of a hybrid smart fuse was developed by integrating a fuse with a power line sensor, LineWatchTM [64], for medium voltage power distribution system. As a result, "fuse communication" could be implemented by adding a power line sensor at each fuse at bus feeders in order to collect the fuse location (feeder and bus names), ampere ratings, measured currents, and states (blow out or closed). If a fuse is blown or closed, power line sensors could measure current along the power line. Information collected from the power line sensor could be received by relays in order to make decisions regarding relay settings. Although the hybrid smart fuse was not implemented in

this research, communication between relays and microgrid to change setting groups of relays based on selected circuit path and maximum fuse ampere ratings was implemented by a real-time simulator with two relays in the loop.

2.7 Relay in the loop techniques

A literature review on relay test techniques, apparatus, modes, and applications was developed in IEEE Xplore. Sachdev et al, 2000 [65] presented relay test systems for testing numerical relays. This publication was useful to understand relay in the loop test techniques. Testing techniques were based on the nature of output data for testing relays, including analog test sets based on the simulation of outputs of analog waveform generators to test relays (1), digital-analog test sets based on the simulation of disturbances and usage of outputs of simulations to test relays (2), and data-recorder test sets based on the application of disturbance data recorded by relays and data-recorders (3).

The test apparatus used to test relays included the relay test set (1), real-time playback digital simulator (2), and real-time digital simulator (3). The relay test set was the most economical alternative and was able to simulate fundamental frequency and transient waveforms while quantifying data from the simulation after running the test. The relay test set consisted of a computer (laptop or PC) and a test set. In this case, computer-generated numerical data were converted to analog form by digital/output converters. The real-time playback digital simulator was similar to the relay test set except that functions performed in the computer and test set were integrated into one device. The real-time digital simulator was based on a target computer that generated a signal source created by a real-time operating system and completed the simulation for each time step within the step. Time steps to provide simulations were in the order of 50 microseconds [65]. The target computer sent data to the tested relay/s and the relay/s received

data in real-time output from the target computer. The real-time digital simulator used instantaneous values instead of stored waveforms to perform simulations. The real-time digital simulator simulated the entire power system in order to perform relay tests.

Relay tests are typically performed in four modes: (1) open-loop, (2) closed-loop, (3) semi-closed loop, and (4) end-to-end. Open-loop tests do not consider power system response after a relay tripping for a fault situation. Open-loop tests are used to verify the relay when a fault is in its primary zone of protection. In addition, open-loop tests are used to check operating boundaries of the relays. A relay test set and real-time playback digital simulator test apparatus can be used to perform open-loop tests [65]. Closed-loop tests consider power system response after a relay trip for a fault, and a breaker is opened. The application of closed-loop tests is important when the relay operation impact must measure possible disturbances in the power system. The necessity of sensing the power system after clearing the fault made of the closed-loop test an important tool to verify relay speed and power system response. Real-time digital simulator test apparatus are typically used to perform closed-loop tests [65]. The real-time digital simulator for closed-loop is a useful tool to test protection and control systems in a large-scale power system [66]. The type of relay test depends on the size of the power system that must be simulated. Real-time simulator and real-time playback digital simulator test apparatus can simulate limited power systems and model a typical power line with equivalent power sources at each end. However, real-time digital simulator test apparatus can model complex power systems [65]. A relay test apparatus matrix based on cost, test mode, simulator types, and power system size is shown in Figure 2.7. In this matrix, the SEL-AMS [3] is indicated as a relay test set, the FREJA 300 [67] is indicated as a real-time playback digital simulator, and the OP5600 [4] is indicated as a real-time digital simulator.

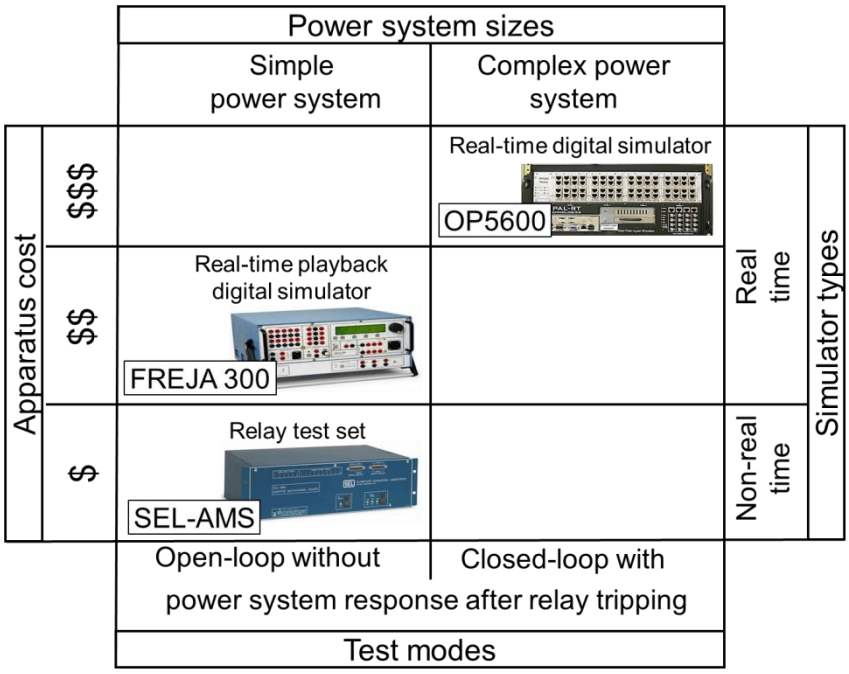

Figure 2.7: Relay test apparatus matrix: SEL-AMS relay test system [3], FREJA 300 relay test system [67], and OP5600 real-time simulator [4]

The SEL-AMS [3] is the commercial relay test system manufactured by Schweitzer Engineering Laboratories (SEL) to test SEL relays. However, OP5600 [4] is a real-time simulator adapted to work as a real-time digital simulator test apparatus. OP5600 real-time simulator uses RT-LAB® [13] software to integrate host and target (OP5600) computers and Matlab® Simulink® [41] software to simulate the power system. Results of a relay test using OP5600 [5] real-time simulator and FREJA 300 [67] relay test system validated OP5600 as a relay in the loop test technique [68]. In addition, an overcurrent relay model was validated for real-time simulation without and with HIL; validation was done using the overcurrent protection feature from the SEL-487E [69] relay. Event reports generated by the SEL-487E [69] relay during HIL testing were compared to results obtained from stand-alone testing and software model in order to validate the overcurrent relay model [70]. Almas et al, 2013 [68] and 2012 [70] performed real-time tests with one relay in the loop.

The first fully digital real-time power system simulator was introduced more than 20 years ago. Prior to this time, real-time simulations were performed using scaled down analogue models of actual power system components; however, many difficulties and inaccuracies were inherent in this approach. Moreover, operating and purchase costs of real-time simulators were so high that many organizations could not afford the acquisition and maintenance of such expensive tools. The introduction of real-time digital simulators contributed significantly to the power industry [71]. Modeling accuracy and flexibility of the real-time digital simulator have improved because operating and purchase costs have decreased significantly, and the real-time digital simulator has gained widespread acceptance among equipment manufacturers, electrical utilities, and engineering colleges in academic and research areas [72].

In this research, SEL-AMS [3] and OP5600 [4] were used as non-real and real-time simulators, respectively. Based on the test apparatus used in this work, non-real-time and real-time simulators allowed simulations of limited and complex power systems, respectively. SEL-AMS [3] and OP5600 [4] were used to verify relay setting groups for adaptive overcurrent protection. SEL-AMS [3] was a valid relay test system for this research because the proposed adaptive protection system was based on a radial power system in which circuit paths could be converted to an equivalent one-power-source circuit for each test. In addition, the application of non-real-time and real-time simulators with relays in the loop allowed comparison of relay times by double verification. In the proposed research, the real-time simulator was connected to two relays in the loop that allowed verification of selectivity coordination between primary and backup relays, demonstrating that primary relays tripped faster than backup relays.

2.8 Reliability, selectivity, speed, and cost

Design of a new protection system for a distribution system requires the study of variables such as reliability (security, and dependability), selectivity, and cost in order to define an appropriate technical and economical solution [73]. Based on IEEE Standard C37.100-1992 [74], reliability, security, selectivity, and dependability of a relay or relay system (protection system) are indicated in Table 2.3.

Table 2.3: Reliability (security and dependability) and selectivity, IEEE Std. C37.100-1992 [74]

1. Reliability	**1.a Security**	**1.b Dependability**
A measure of the degree of certainty that the relay, or relay system, will perform correctly.	That facet of reliability that relates to the degree of certainty that a relay or relay system will operate correctly.	The facet of reliability that relates to the degree of certainty that a relay or relay system will operate correctly.
2. Selectivity		
A general term describing the interrelated performance of relays and breakers and other protective devices; complete selectivity is obtained when a minimum amount of equipment is removed from service for isolation of a fault or other abnormality.		

Although protective relays should quickly detect all system abnormalities, other considerations may detract from this primary objective. In general, a relay system is designed to achieve the highest level of speed, reliability, selectivity, simplicity, and cost-efficiency [18]. In power distribution systems, utilities have utilized fuses instead of protective relays because fuses are less expensive than protective relays. However, cost of protective relays has decreased in the last years, and protective relays allow creation of protection systems with higher reliability than fuses. In addition, use of backup and primary protective devices and adaptive overcurrent protection systems based on relay applications allows creation of protection systems with a high selectivity for microgrid with distributed generators. Application of a protection system for a microgrid with distributed generators using fuses (with wireless line sensors) and relays with communication could be an acceptable technical-commercial solution to increase reliability and

selectivity at low equipment cost. Protection of power lines and feeders in a microgrid with distributed generators could be implemented using fuse-relay communication.

Protective relays are more reliable than fuses because current-time curves on protective relays are based on microprocessors. However, current-time curves on fuses are represented by minimum melting and clearing time curves that depend on fuse thermal models. Application of backup and primary protective devices to protect power lines and feeders improves selectivity because when primary protection fails, backup protection could clear the fault currents. Also, adaptive overcurrent protection systems improve selectivity because relay settings could be fit to various circuit paths of the microgrid and maximum ampere rating of fuses on feeders. Fuses require a drop-out fuse switch in order to place fuses in power lines or feeders. However, overcurrent relays are more expensive than fuses, and overcurrent relay applications require circuit breakers, Vdc external sources, current transformers (CTs), and communication devices. Table 2.4 shows comparison of four protection systems (A, B, C, and D) in order to evaluate reliability, selectivity, speed, and equipment cost of protection systems. Utilities most often use cases A and B for protection systems to protect power lines and feeders in a radial distribution system. Use of relay communication (Case C) increases reliability and selectivity for the protection system, but cost also increases because relays require breakers to control circuits, Vdc external sources to feed trip and control circuits, CTs to measure line currents, and communication devices to connect relays to a control center computer.

Case D was proposed in this research. Selectivity was better than in Cases A and B because communication was implemented in order to select setting groups of relays based on maximum ampere fuse rating located in feeder busses and fuse states (blow out or closed). Case

D was also more reliable than Case A because relays instead of fuses were used to protect power lines and feeders.

Cases A and B could have some speed issues because if a maximum ampere rating fuse on a feeders blew out, overcurrent settings of protective devices in power lines could not be adapted to the new active maximum ampere rating fuse on feeders. However, Cases C and D demonstrated significant speed because they contained relay and power system communication, thus allowing adaptation of overcurrent settings of relays in power lines to actual maximum ampere rating fuses on feeders.

Cases B, C, and D could be used in the design of an adaptive overcurrent protection system, but only Cases C and D integrated power lines and feeders into adaptive overcurrent protection. Case B integrated only power lines into adaptive overcurrent protection, and relay overcurrent settings were selected based only on circuit paths of the microgrid. Therefore, if a fuse blew out, relay overcurrent settings could not be adapted to a new maximum ampere rating fuse. Case D demonstrated more economic advantages than Case C because no circuit breakers, CTs, or relays were required on feeders. In this research, adaptive overcurrent protection for power lines and feeders with selective coordination was based on calculation and selection of relay setting groups based on maximum fuse ampere ratings on bus feeders and circuit paths in the microgrid.

Table 2.4: Protection and control systems for microgrid in a distribution power system

Cases	Protective devices in protection areas		Communication		Protection, communication, and control equipment in protection areas		Conclusions				
	Power lines	Feeders	Relay	Fuse	Power lines	Feeders	Reliability	Selectivity	Speed	Equipment Cost	Observations
A	Fuses	Fuses	No	No	Drop-out fuse switches, fuses	Drop-out fuse switches, fuses	Little	Little	Some	Little	No application of adaptive overcurrent protection
B	Relays	Fuses	Yes	No	Overcurrent relays, breakers, CTs, Vdc external sources[(2)], comm. devices	Drop-out fuse switches, fuses	Some	Some	Some	Some	Power line adaptive overcurrent protection
C	Relays	Relays	Yes	No	Overcurrent relays, breakers, CTs, Vdc external sources[(2)], comm. devices	Overcurrent relays, breakers, CTs, Vdc external sources[(2)], comm. devices	A lot	A lot	A lot	A lot	Power line and feeder adaptive overcurrent protection
D	Relays	Fuses[(1)]	Yes	Yes	Overcurrent relays, breakers, CTs, Vdc external sources[(2)], comm. devices	Drop-out fuse switches, fuses, power line sensors, comm. devices	Some	A lot	A lot	Some	Power line and feeder adaptive overcurrent protection

CTs: current transformers, [(1)] Fuses with wireless line sensors to detect fuse states (blow out or closed) and maximum ampere fuse rating, [(2)]Vdc external sources to feed trip and control circuits

2.9 Chapter summary

This chapter introduced contributions reported in the literature related to adaptive overcurrent protection and topics such as microgrid and distributed generators, experimental methods to validate adaptive overcurrent protections, wireless power line sensors and hybrid smart fuses, and technical-economical evaluation (reliability, selectivity, speed, and cost) of protection systems. The literature review was segregated into multifunction (overcurrent, distance, and differential protections) and overcurrent (directional, instantaneous, and/or inverse time overcurrent) protection groups.

The literature review focused on microgrid and distributed generators and descriptions of microgrid operations such as grid-connected and islanded modes and adaptability were developed. The review highlighted the necessity of implementing adaptive protection and control systems in the microgrid with distributed generators, where feasibility, reliability, and cost benefit issues are concerns associated with implementation of adaptive microgrid protection schemes. Relevant literature to adaptive overcurrent protection in microgrid with distributed generators was compared by publication year, protective devices, power systems, overcurrent protection, and experimental methods. Published algorithms of adaptive overcurrent protections were plotted as flow charts [27, 30, 34, 35, and 38] and compared to this research.

A literature review of smart fuses was also conducted in the chapter, and the concept of a hybrid smart fuse was developed by integrating a fuse with a power line sensor for medium voltage applications with communication for distribution system applications. A literature review of relay test techniques, apparatus, modes, and applications was done in IEEE Xplorer. A relay test apparatus comparison based on apparatus cost, test modes (open and closed-loop), types of simulations (non-real-time and real-time simulation), and power system sizes (simple and

complex power system) was done between relay test set, real-time playback digital, and real-time digital simulators.

The primary objective of the literature review was to find parameters that must be considered in order to design a new relay or relay system (protection system) for a distribution power system. Four protection systems were compared based on reliability (security and dependability), selectivity, and cost in order to define an appropriate technical-economical solution for this research.

Chapter 3 - Microgrid

This chapter presents a single-line diagram of the microgrid, explains equipment of the microgrid with distributed generators, and describes utilization of Power World® software to apply the per-unit method [10]. Per-unit impedances of power lines, distribution and utility transformers, utility source, and distributed generators were estimated based on equal voltage areas of the microgrid. Steps to create power lines, transformers, generators, and microgrid loads with Power World® software [10] are described in order to prepare the microgrid to run power flow and fault analysis.

3.1 Microgrid

For this study, the circuit of the microgrid with distributed generators was based on a distribution system with two main feeders formed by three power lines on each main feeder. The two main branches were formed by the 1-2-3-4 and 5-6-7-8 busses that corresponded to the 650-632-671-680 nodes of the IEEE 13 node test feeder [9]. The microgrid had three distributed generators and one utility source. When no failures were presented in the microgrid (normal operation), the microgrid was connected to the utility substation. In the event of a failure in the utility substation and/or microgrid power lines, distributed generators were connected as auxiliary generators in island modes; therefore, the distributed generators were not connected in parallel with other microgrid generators. Figure 3.1 shows a single-line diagram of the microgrid with distributed generators. The per-unit method [75] was applied using Power World® software [10], and 100 MVA was set as the base power of the new system. In the microgrid, line-to-line voltages of the 1 (7.2 kV), 2 (115 kV), and 3 (0.48 kV) areas were limited by utility and distribution transformers. Impedances of areas were named impedances of the old system, and base impedances were named impedances of the new system (S_{base} = 100 MVA).

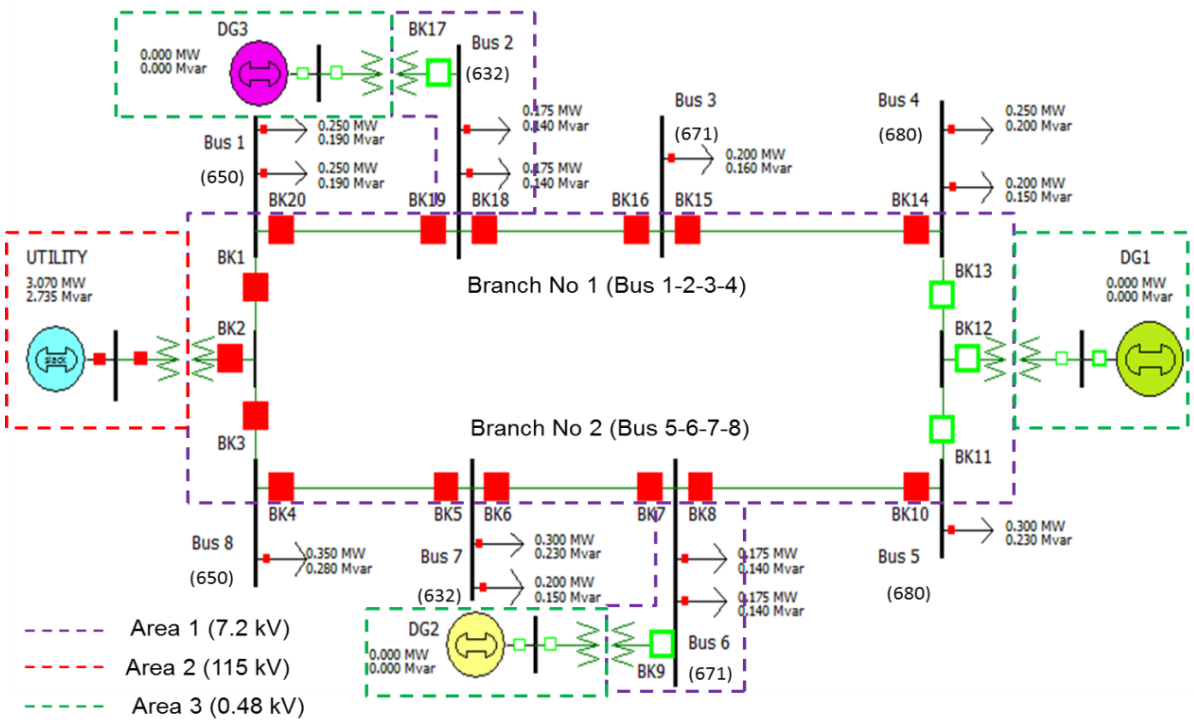

Figure 3.1: Microgrid with distributed generators using Power World® software [10]

In Figure 3.1, the violet, red, and green dashed lines represent Areas 1 (7.2 kV), 2 (115 kV), and 3 (0.48 kV), respectively. Table 3.1 indicates the areas, equipment, line-to-line voltage of areas, total power of areas, and impedances of the old and new systems.

Table 3.1: Areas and equipment in the microgrid (S_{base} = 100 MVA)

Areas	**Equipment**	**Line-to-line voltage of area V_{area} [kV]**	**Total power of area S_{area} [MVA]**	**Impedances [Ω]**	
				Old system $Z_{old} = V^2_{area} / S_{area}$	**New system $Z_{new} = V^2_{area} / S_{base}$**
1	Power lines	7.2	100	0.5184	0.5184
	Utility transformer		5	10.368	
	Distribution transformer		2.5	20.736	
2	Utility source	115	1500	1013.916	132.25
3	Distributed generators	0.48	2.281	0.101	0.002304

In order to create the microgrid shown in Figure 3.1, Power World® software [10] was opened, and the "File" menu and "New Case" option were selected. The "Options" menu and "Simulator Options" were selected, and then the "General" setting for the power flow solution window was set at 100 MVA as assumed base total power. Figure 3.2 shows the steps to create a new case and set per-unit base total power using Power World® software [10].

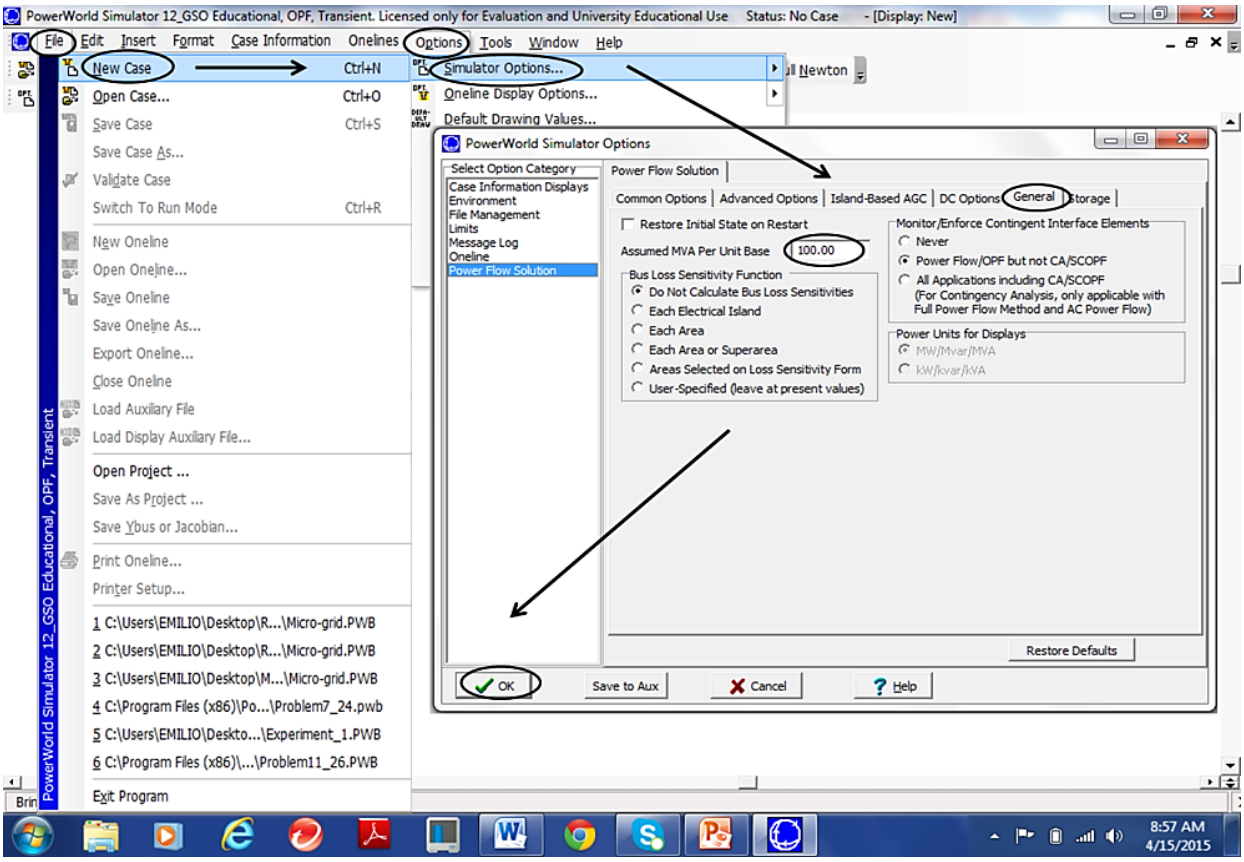

Figure 3.2: Opening new case and setting per-unit base total power using Power World® software [10]

Positive, negative, and zero sequence impedances per-unit for the power lines, distribution and utility transformers, utility source, and distributed generators were converted to a new system (Sbase = 100 MVA) for Areas 1 (7.2 kV), 2 (115 kV), and 3 (0.48 kV) and set using Power World® software [10].

3.2 Area 1 (7.2 kV)

Per-unit impedances of the power lines and utility and distribution transformers were estimated in Area 1 (7.2 kV). Total power of the power lines and utility and distribution transformers were 100, 5, and 2.5 MVA, respectively. Positive, negative, and zero sequence impedances per-unit in the new system, based on 100 MVA, were estimated to create the power lines and utility and distribution transformers using Power World ® software [10].

3.2.1 Power lines

In the power lines of the microgrid, characteristics of the overhead conductor, presented as Configuration 601 for the IEEE 13 node test feeder [9], were considered. Table 3.2 shows characteristics of the overhead conductor for Configuration 601 in Figure 3.3.

Table 3.2: Characteristics of the overhead conductor for Configuration 601

Cable	Size [AWG]	Type	Resistance [Ω/mile] (1)	Diameter [inches]	GMR [feet] (2)	Ampacity [Amps] (3)	Phasing	ID
Phase	556,5	ACSR	0.186	0.927	0.0311	730	BACN	500
Neutral	4/0	ACSR	0.592	0.56	0.0081	340		

ACSR: Aluminum Conductor Steel Reinforced, (1) 60 Hz resistance at 50 °C, (2) Geometric Mean Radius, (3) Ampacity at 50 °C

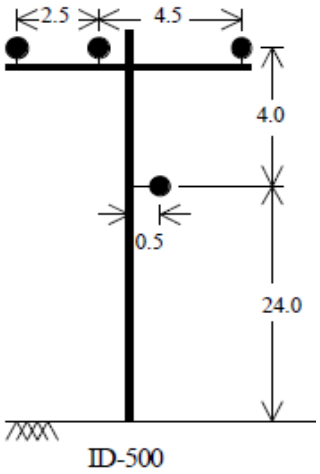

Figure 3.3: Power line of 601Configuration [9]

Three-phase balanced loads were considered in the microgrid because the Power World® software [10] allowed simulation of only a three-phase balanced power system during power flow analysis. In addition, neutral cables of the power lines for Configuration 601 were neglected in the microgrid. Table 3.3 shows positive, negative, and zero sequence impedances in ohms per mile for the overhead conductor of Configuration 601 collected from IEEE 13 node test feeder [9].

Table 3.3: Sequence impedances per mile for overhead conductor of Configuration 601

Impedances	**Real Part [Ω/mile]**	**Imaginary Part [Ω/mile]**
Positive sequence [$z_{L1} = r_{L1} + j\,x_{L1}$]	0.3375	j 1.0478
Negative sequence [$z_{L2} = r_{L2} + j\,x_{L2}$]	0.3414	j 1.0348
Zero sequence [$z_{L0} = r_{L0} + j\,x_{L0}$]	0.3465	j 1.0179

In the microgrid, power lines 1-2, 2-3, 7-8, and 6-7 had lengths of 6000 ft, but power lines 3-4 and 5-6 had lengths of 3000 ft. Original lengths of power lines on the IEEE 13 node test feeder were multiplied by 3 in the microgrid. Table 3.4 shows lengths of power lines in the microgrid.

Table 3.4: Lengths of power lines in the microgrid

IEEE 13 Node Test Feeder		**Microgrid**		
Initial Node	**End Node**	**Initial Node**	**End Node**	**Length, ft. (miles)**
650	632	Bus 1	Bus 2	6000 (1.136)
		Bus 8	Bus 7	
632	671	Bus 2	Bus 3	6000 (1.136)
		Bus 7	Bus 6	
671	680	Bus 3	Bus 4	3000 (0.568)
		Bus 6	Bus 5	

When positive and negative sequence impedances of a transmission line were set using Power World® software [10], only positive and zero sequence impedances per-unit were available. Using the identical values for positive and negative sequence impedances per-unit,

positive and zero sequence impedances per mile and power line lengths from Tables 3.3 and 3.4, respectively, were collected in order to calculate positive and zero sequence impedances per-unit. The positive sequence reactance of a breaker was *j* 0.0005 per-unit based on the Power World® presentation [76]. Because the power lines had two breakers, reactance of *j* 0.001 per-unit was added to the positive sequence reactance. Positive sequence impedances of the power lines per-unit were estimated using Equation (3.1).

$$Z_{L1\,pu} = \frac{z_{L1} \times l}{Z_{L\,new}} = \left[\frac{r_{L1} \times l}{V_{L\,area}^2 / S_{base}} \right] + j \left[\frac{x_{L1} \times l}{V_{L\,area}^2 / S_{base}} + 0.001 \right] \tag{3.1}$$

where $Z_{L1\,pu}$ is positive sequence impedance of the power line per-unit, z_{L1} is positive sequence impedance of the power line in ohms per mile, $Z_{L\,new}$ is base impedance of the new system of the power line in ohms, l is length of the power line in miles, $V_{L\,area}$ is area line-to-line voltage of the power line in kV, S_{base} is base total power of the new system in MVA, $r_{L\,1}$ is positive sequence resistance of the power line in ohms per mile, and $x_{L\,1}$ is positive sequence reactance of the power line in ohms per mile.

The zero sequence impedance of power lines per-unit were estimated using Equation (3.2).

$$Z_{L0\,pu} = \frac{z_{L0} \times l}{Z_{L\,new}} = \left[\frac{r_{L0} \times l}{V_{L\,area}^2 / S_{base}} \right] + j \left[\frac{x_{L0} \times l}{V_{L\,area}^2 / S_{base}} \right] \tag{3.2}$$

where $Z_{L0\,pu}$ is zero sequence impedance of the power line per-unit, z_{L0} is zero sequence impedance of the power line in ohms per mile, $Z_{L\,new}$ is base impedance of the new system of the power line in ohms, l is length of the power line in miles, $V_{L\,area}$ is area line-to-line voltage of the power line in kV, S_{base} is base total power of the new system in MVA, r_{L0} is zero sequence

resistance of the power line in ohms per mile, and x_{L0} is zero sequence reactance of the power line in ohms per mile.

Power line resistances and reactances for positive and zero sequence impedances per-unit were estimated using Equations (3.1) and (3.2), respectively. As shown in Table 3.1, line-to-line voltage of power lines for Area 1 was 7.2 kV, and the base total power of the new system was 100 MVA. Positive, negative, and zero resistances and reactances in ohms per mile were collected from Table 3.3, and lengths of power lines were collected from Table 3.4. As shown in Table 3.5, positive and zero sequence resistances and reactances per-unit of power lines in the microgrid were calculated using Equations (3.1) and (3.2), respectively.

Table 3.5: Positive and zero sequence resistances and reactances of power lines in p.u.

Power lines of the microgrid	**Positive sequence impedance** $[Z_{L1\,pu} = R_{L1\,pu} + j\,X_{L1\,pu}]$		**Zero sequence impedance** $[Z_{L0\,pu} = R_{L0\,pu} + j\,X_{L0\,pu}]$	
	Resistance $R_{L1\,pu}$ **[pu]**	**Reactance** $j\,X_{L1\,pu}$ **[pu]**	**Resistance** $R_{L0\,pu}$ **[pu]**	**Reactance** $j\,X_{L0\,pu}$ **[pu]**
1-2, 2-3, 7-8, 6-7	0.700	2.301	0.800	2.201
3-4, 5-6	0.400	1.101	0.400	1.101

Resistances and reactances of power lines were rounded to 1 digit before summing breaker reactances of j 0.001

Power World® software [10] in the "Edit Mode" was used to insert Busses 1, 2, 3, 4, 5, 6, 7, and 8 into the microgrid, and busses of power lines were set at line-to-ground voltage of 4.16 kV. Once all busses were installed, the power lines were connected to 4.16 kV busses of the microgrid. Figure 3.4 illustrates the steps to insert power lines into the microgrid.

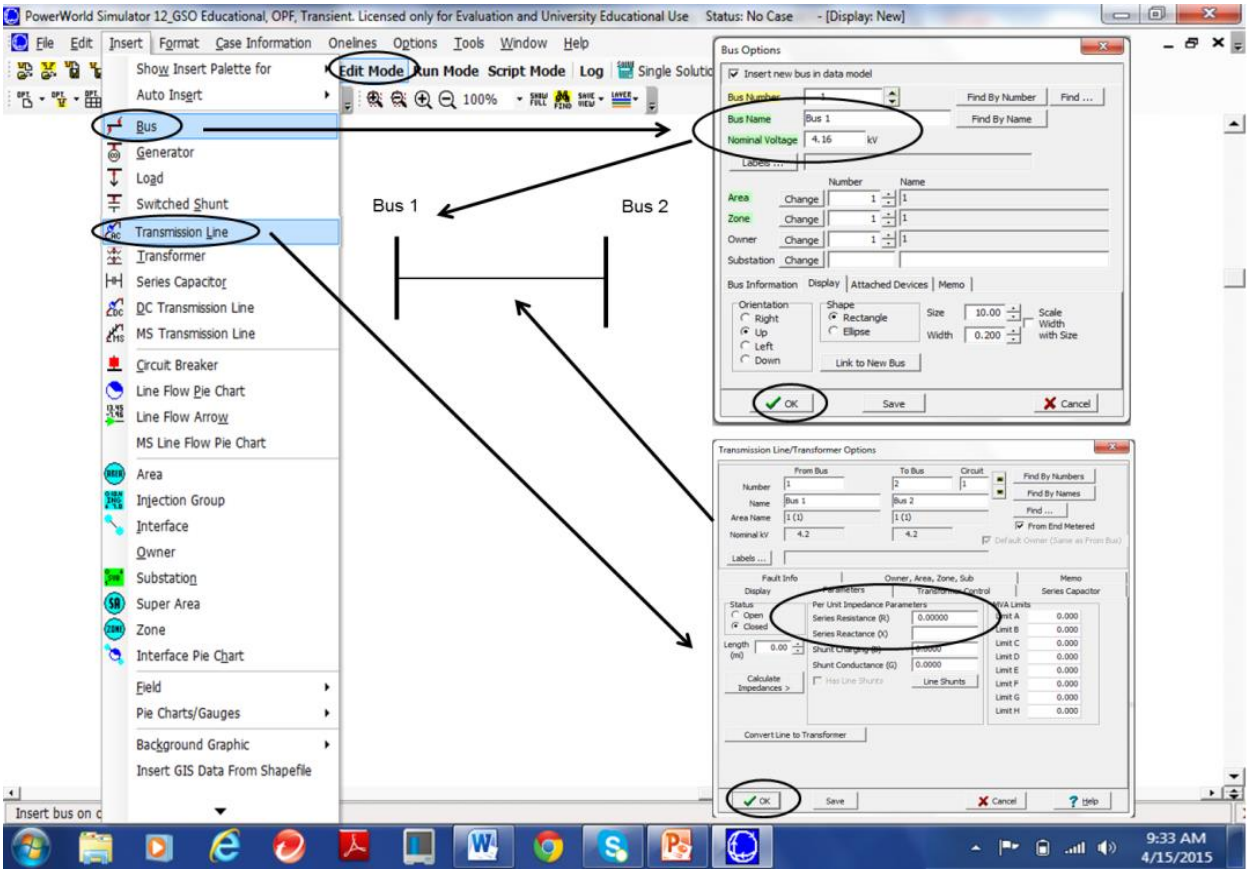

Figure 3.4: Steps to insert power lines using Power World® software [10]

Positive and zero sequence impedances of power lines per-unit, as shown in Table 3.5, were then set using Power World® software [10]. In the "Line Information Dialog" box, the positive sequence resistance and reactance per-unit of power lines were set in the "Parameters" option, and the zero sequence resistance and reactance per-unit of power lines were set in the "Fault Info" option. Figure 3.5 shows positive (A) and zero (B) sequence resistance and reactance per-unit set using Power World® software [10] for 1-2, 2-3, 6-7, and 7-8 power lines of the microgrid. Figure 3.6 shows positive (A) and zero (B) sequence resistance and reactance per-unit set using Power World® software [10] for 3-4 and 5-6 power lines of the microgrid.

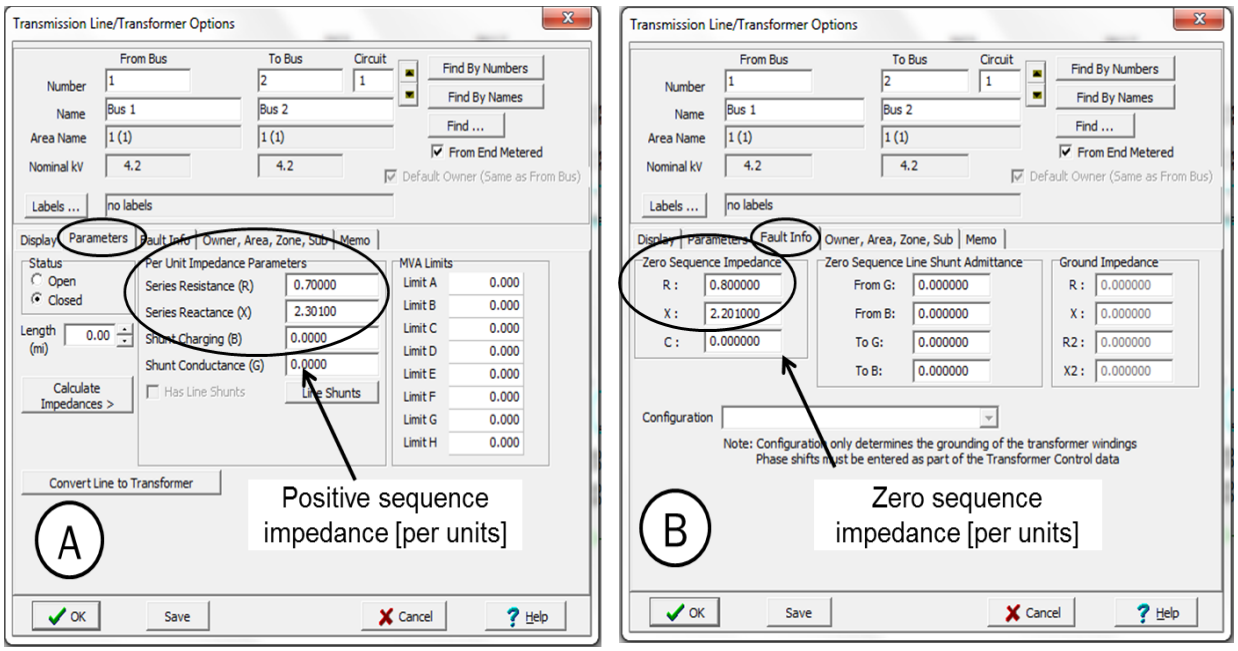

Figure 3.5: Positive (A) and zero (B) sequence impedances of 1-2, 2-3, 6-7, 7-8 power lines

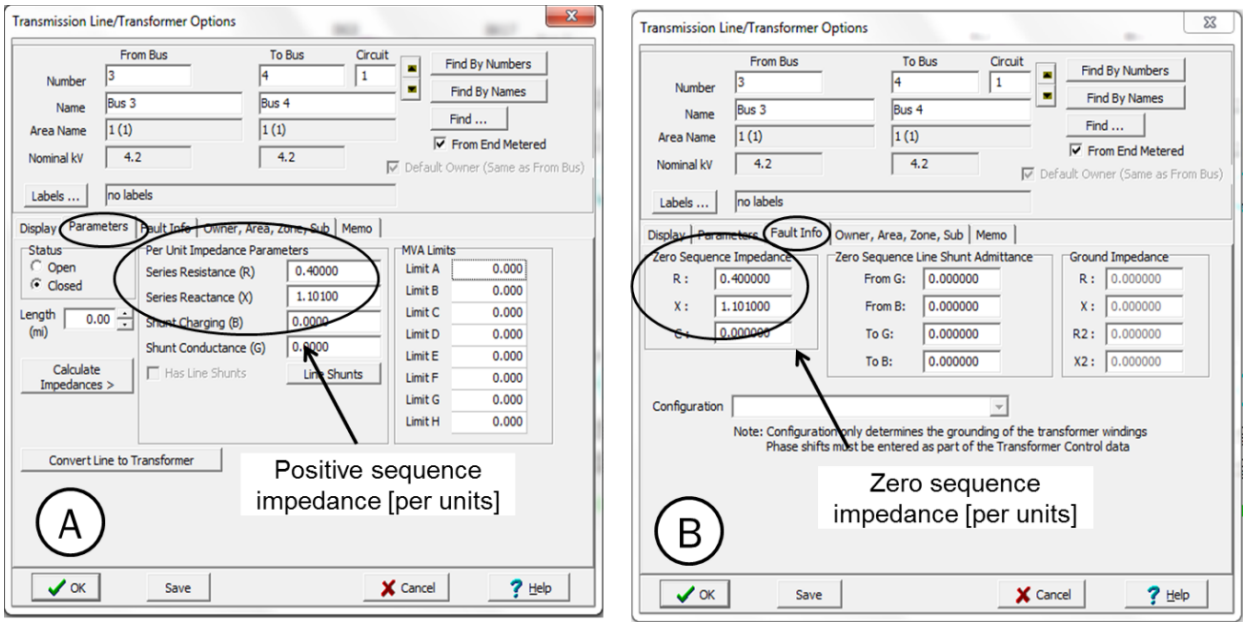

Figure 3.6: Positive (A) and zero (B) sequence impedances of 3-4 and 5-6 power lines

3.2.2 Utility and distribution transformers

The microgrid with distributed generators had one utility and three distribution transformers. Figure 3.7 presents a transformer bay with two-bus (A) and one-bus (B) substation

configurations. The transformer bay with two-bus configuration was applied for utility and DG1 distribution transformers. However, the transformer bay with one-bus configuration was applied for the DG2 and DG3 distribution transformers.

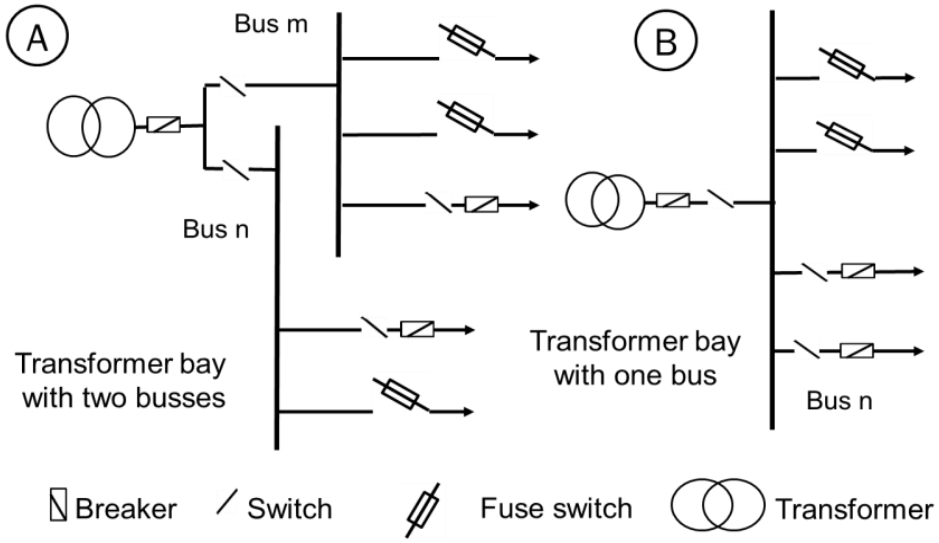

Figure 3.7: Transformer bay with two-bus (A) and one-bus (B) substation configurations

In substation configurations of Figure 3.7, switches ensured that breakers were not energized during maintenance operations [77]. In substations of the microgrid, breakers and MV fuse-switches operated power lines and load feeders, respectively. The utility and three distribution transformers in the microgrid had a Delta-high / Wye-low side configuration, creating a line-to-line / line-to-ground voltage distribution system of 7.2/4.16 kV, as shown in Figure 3.8.

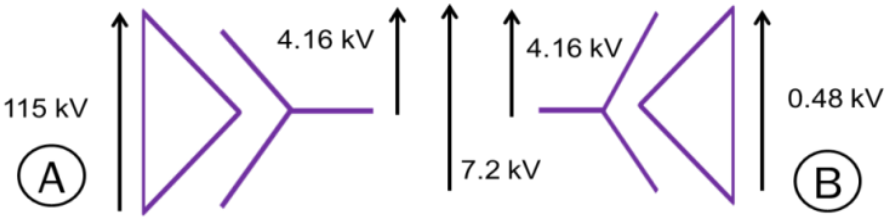

High side	Low side
115 kV–D	4.16 kV–y (ground)

High side	Low side
4.16 kV–Y (ground)	0.48 kV–d

Figure 3.8: Utility (A) and distribution transformer (B) configurations

Utility and distribution transformer data were collected from IEEE 13 node test feeder [9] and manufacturer publication [78], respectively. Total power, voltage levels, configurations, and resistance and reactance of utility and distribution transformers are indicated in Table 3.6.

Table 3.6: Utility and distribution transformers

Transformers	**Total power S_T [MVA]**	**Voltage levels and configurations**		**Resistance in percent $R_{T\%}$ [%]**	**Reactance in percent $j\,X_{T\%}$ [%]**
		kV-high	**kV-low**		
Utility	5	115 - D	4.16 – y (ground)	1	8
Distribution	2.5	4.16 – Y (ground)	0.48 - d	0.66	5.71

In utility and distribution transformers, values of positive, negative, and zero sequence impedances were considered identical. Because resistance and reactance of utility and distribution transformers are in percent in Table 3.6, resistances and reactances in percent were multiplied by area (old system) impedances in ohms. Transformer resistance and reactance in ohms were then converted per-unit by dividing resistances and reactances in ohms of the old system by base (new system) impedances in ohms. Reactance of a breaker was *j* 0.0005 per-unit based on the Power World® presentation [76]. Because utility and distribution transformers contained two breakers, reactance of *j* 0.001 per-unit was added to reactances of transformers per-unit. Resistance and reactance per-unit of utility and distribution transformers were estimated using Equation (3.3).

$$Z_{T\,pu} = \left[\frac{\frac{R_{T\%}}{100} \times Z_{T\,old}}{Z_{T\,new}}\right] + j\left[\frac{\frac{X_{T\%}}{100} \times Z_{T\,old}}{Z_{T\,new}} + 0.001\right] = \left[\frac{R_{T\%} \times S_{base}}{100 \times S_{T\,area}}\right] + j\left[\frac{X_{T\%} \times S_{base}}{100 \times S_{T\,area}} + 0.001\right] \quad (3.3)$$

where $Z_{T\,pu}$ is impedance of the transformer per-unit, $Z_{T\,old}$ is area impedance of the transformer for the old system in ohms, $Z_{T\,new}$ is base impedance of the transformer for the new system in ohms, $R_{T\%}$ is resistance of the transformer in percent, $X_{T\%}$ is reactance of the transformer in

percent, S_{base} is base total power of the new system in MVA, and $S_{T\,area}$ is area total power of the transformer for the old system in MVA.

As shown in Table 3.1, line-to-line voltage of utility and distribution transformers for Area 1 was 5 and 2.5 MVA, respectively, and base total power of the new system was 100 MVA. Resistance and reactance in percent of utility and distribution transformers were collected from Table 3.6. Positive, negative, and zero sequence impedances of the distribution and utility transformers were estimated using Equation 3.3. Resistance and reactance of utility and distribution transformers at the new base per-unit are shown in Table 3.7.

Table 3.7: Resistance and reactance of utility and distribution transformers in p.u.

Transformers	**Resistance in per-unit, $R_{T\,pu}$ [pu]**	**Reactance in per-unit, $j\,X_{T\,pu}$ [pu]**
Utility	0.200	1.601
Distribution	0.264	2.285

$R_{T\,pu} = R_{T\,1\,pu} = R_{T\,2\,pu} = R_{T\,0\,pu}$, $X_{T\,pu} = X_{T\,1\,pu} = X_{T\,2\,pu} = X_{T\,0\,pu}$

Resistances and reactances of transformers were rounded to 3 digits before summing breaker reactances of j 0.001

Figure 3.9 shows steps required to create a transformer with Power World® software [10], including a description of necessary tasks to create the distribution transformer on Bus 6 in the microgrid. The microgrid was placed in "Edit Mode," the "Insert" menu and "Transformer" option were selected, and the transformer object was connected between two busses. The "Parameter" tab was selected in the "Transmission Line / Transformer" window, and series resistance and reactance per-unit were completed based on Table 3.7. The "Fault Info" tab was then selected, zero sequence resistance and reactance per-unit were completed based on Table 3.7, and "Delta-Grounded Wye" configuration was selected.

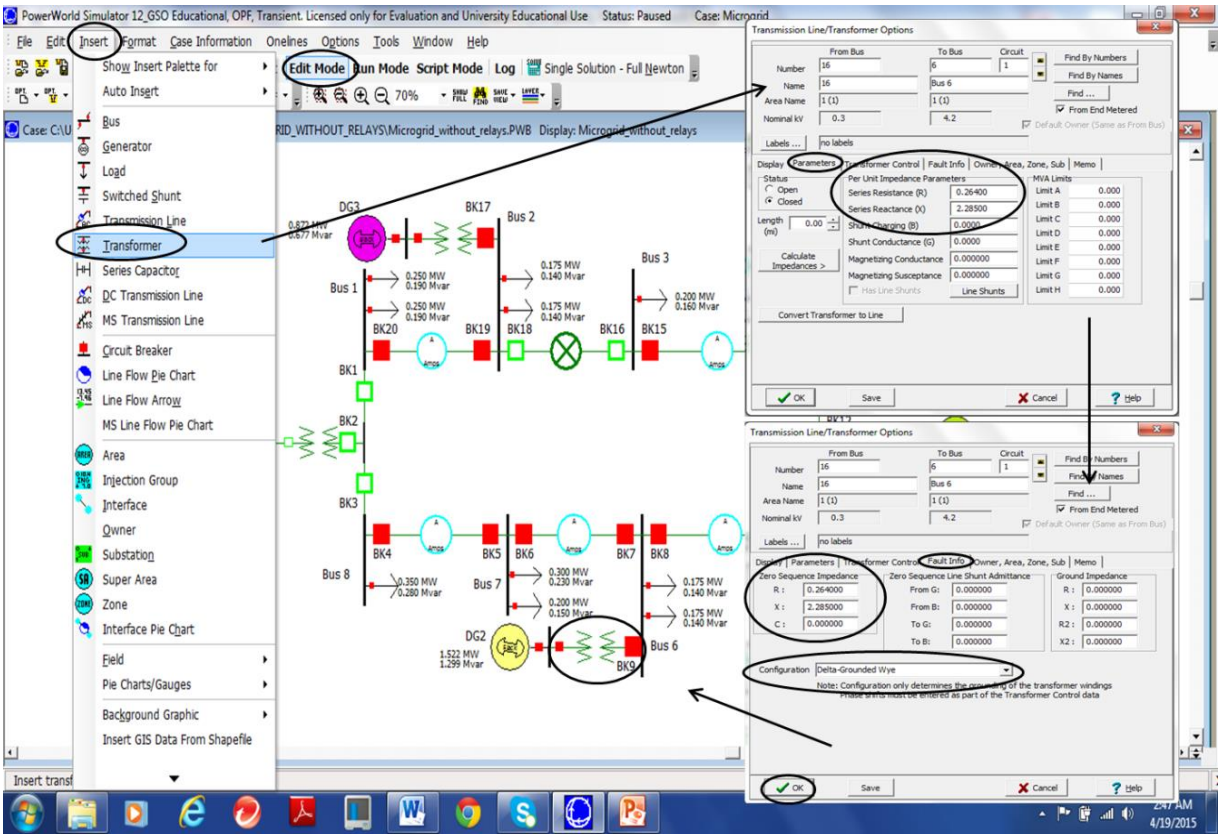

Figure 3.9: Steps to create a transformer with Power World® software [10]

3.3 Area 2 (115 kV)

Per-unit impedances of the utility source were estimated in Area 2 (115 kV). Total power of the utility source was 1500 MVA. Positive, negative, and zero sequence impedances per-unit in the new system based on 100 MVA were estimated in order to create the utility source with Power World ® software [10].

3.3.1 Utility source

The microgrid was formed by one utility source connected to the microgrid in normal operation, but the utility source was not connected in parallel with the distributed generators. Utility source data were collected from a short-circuit current calculation manual [79]. Table 3.8 shows the reactance/resistance ratio and ratio-1 of the utility source.

Table 3.8: Utility source

Source	*ratio = X/R*	*ratio^{-1} = R/X*
Utility	15	0.0666

In the utility source, positive, negative, and zero sequence impedances had the identical values; utility impedance was calculated using the reactance/resistance ratio indicated in Table 3.8. Breaker reactance was *j* 0.0005 per-unit based on Power World® presentation [76]. Because the utility source had one breaker, reactance of *j* 0.0005 per-unit was added to reactance of the utility source per-unit. The impedance, resistance, and reactance of the utility source are represented by the triangle in Figure 3.10.

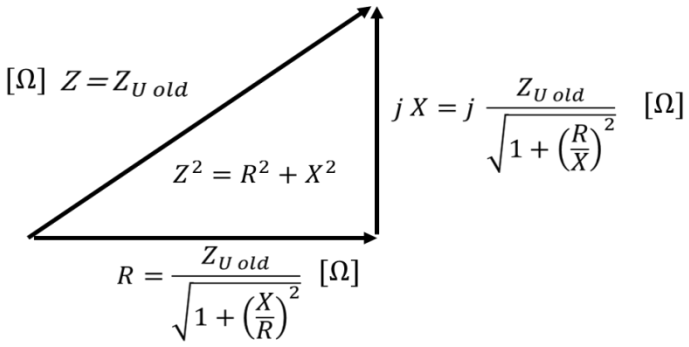

Figure 3.10: Impedance resistance and reactance of utility source

In Figure 3.10, horizontal (real part) and vertical (imaginary part) vectors represent resistance and reactance of the utility source, respectively. After dividing resistance and reactance of the utility source in ohms by the base (new system) impedance in ohms, resistance and reactance of the utility source per-unit were estimated using Equation (3.4).

$$Z_{U\,pu} = \left[\frac{Z_{U\,old}/Z_{U\,new}}{\sqrt{1+\left(\frac{X}{R}\right)^2}}\right] + j\left[\frac{Z_{U\,old}/Z_{U\,new}}{\sqrt{1+\left(\frac{R}{X}\right)^2}} + 0.0005\right] = \left[\frac{S_{base}/S_{U\,area}}{\sqrt{1+\left(\frac{X}{R}\right)^2}}\right] + j\left[\frac{S_{base}/S_{U\,area}}{\sqrt{1+\left(\frac{R}{X}\right)^2}} + 0.0005\right] \quad (3.4)$$

where $Z_{U\,pu}$ is impedance of the utility source per-unit, $Z_{U\,old}$ is area impedance of the utility source for the old system in ohms, $Z_{U\,new}$ is base impedance of the utility source for the new

system in ohms, X is reactance of the utility source in ohms, R is resistance of the utility source in ohms, S_{base} is base total power of the new system in MVA, and $S_{U\,area}$ is area total power of the utility source for the old system in MVA.

As shown in Table 3.1, line-to-line voltage and total power of the utility source for Area 2 were 115 kV and 1500 MVA, respectively, and base total power of the new system was 100 MVA. The reactance/resistance ratio and ratio^{-1} of the utility source were collected from Table 3.7. Using Equation (3.4), positive, negative, and zero sequence impedances of the utility source per-unit were estimated and presented, as shown in Table 3.9.

Table 3.9: Resistance and reactance of the utility source in p.u.

Source	**Resistance in per-unit, $R_{U\,pu}$ [pu]**	**Reactance in per-unit, $j\,X_{U\,pu}$ [pu]**
Utility	0.00443	0.06702

$R_{U\,pu} = R_{U\,1\,pu} = R_{U\,2\,pu} = R_{U\,0\,pu}$, $X_{U\,pu} = X_{U\,1\,pu} = X_{U\,2\,pu} = X_{U\,0\,pu}$

Resistances and reactances of the utility source were rounded to 5 digits before summing breaker reactance of j 0.0005

Figure 3.11 shows steps to create the utility source using Power World® software [10]. The microgrid was placed in "Edit Mode," and the "Insert" menu and "Bus" option were selected in order to place the utility bus. After selecting the "Bus Information" tab, the utility bus was placed as slack bus and a line-to-ground voltage of 66.5 kV was set at slack bus. The "Insert" menu and "Generator" option were selected, and the generator object was connected to the slack bus. In the "Generator Options" window, the "Fault Parameters" tab was selected, and positive, negative, and zero sequence resistances and reactances per-unit were completed based on Table 3.9. Generator base total power was set at 100 MVA, and the "Neutral Grounded" option was clicked. In the "Generator Options" window, the "Power and Voltage Control" tab was selected, and the maximum output was set at 5 MW for the utility source.

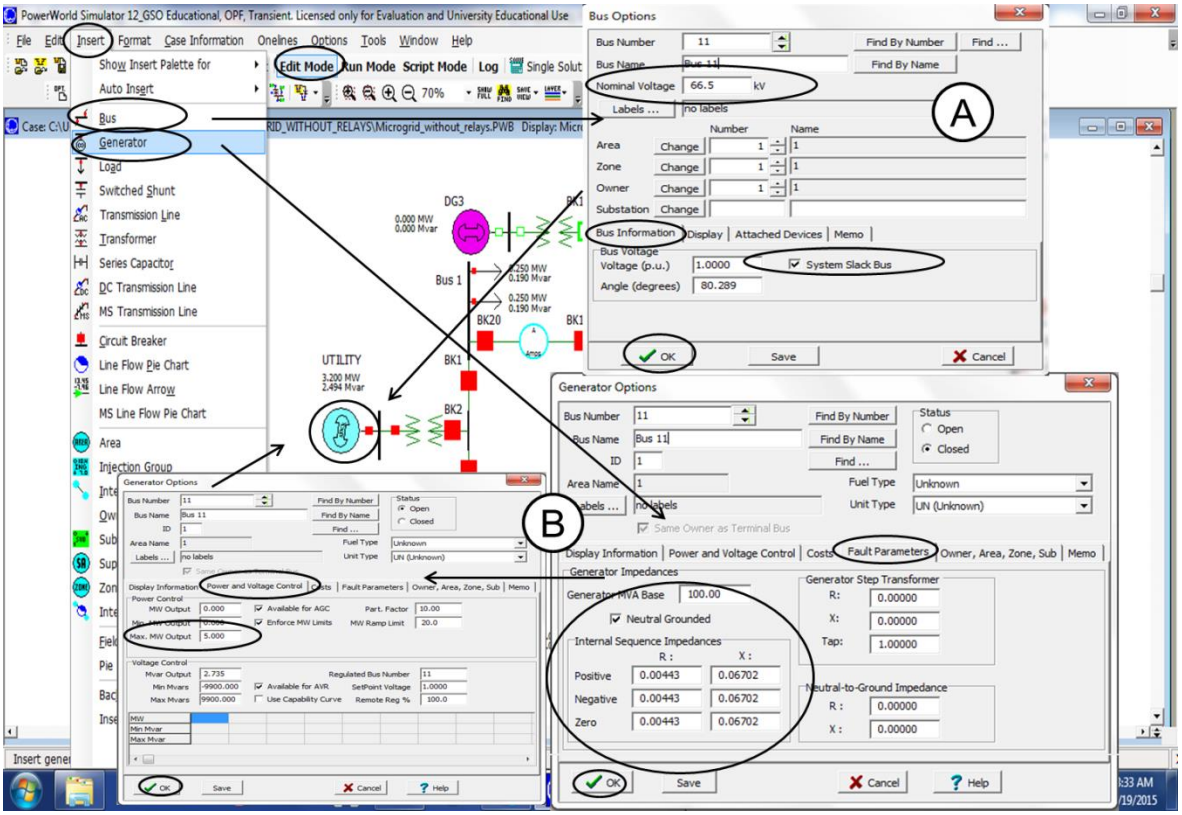

Figure 3.11: Steps to create utility bus (A) and source (B) by Power World® software [10]

3.4 Area 3 (0.48 kV)

Per-unit impedances of distributed generators were estimated in Area 3 (0.48 kV). Total power of distributed generators was 2281 MVA based on the diesel generator manufacturer data sheet [80]. Positive, negative, and zero sequence impedances per-unit in the new system based on 100 MVA were set using Power World ® software [10].

3.4.1 Distributed generators

The microgrid was formed by three distributed generators (DG1, DG2, and DG3) connected to the microgrid whenever a power line or utility source failure occurred (non-normal operation). The distributed generators were not connected in parallel with other generators. Diesel generators were presented as the most common application for utilities in distributed generation. Distribution projects that utilized generators of 1 to 10 MW power output range were

presented in the Electric Power Research Institute (EPRI) publication [1] in which utilities supplied distribution project data. Results showed that diesel-fueled distributed generation dominates the diesel segment of utility applications compared to natural gas and small combustion turbine units [1].

Each diesel generator contains standby, prime, and continuous power. Standby power diesel generators are used in emergency applications, such as power outages (i.e., backup generators for hospitals and commercial buildings). However, prime power diesel generators are used for unlimited run-time applications, such as when they are used as reliable continuous power sources (i.e., distributed generators for the utility microgrid). Continuous power is similar to prime power, but continuous power has a base load rating, meaning that the diesel generator can supply power continuously at a constant load, but it cannot handle overload conditions.

In the microgrid, data from the DG1, DG2, and DG3 distributed generators were collected from the diesel generator manufacturer data sheet [80]. Prime power and line-to-line voltage of the diesel generator was 2281 kVA and 0.48 kV, respectively. Table 3.10 shows the subtransient-direct axis (positive sequence), negative sequence, and zero sequence reactances of DG1, DG2, and DG3 diesel generators.

Table 3.10: Positive, negative, and zero sequence impedances of distributed generators [80]

Sources	$X''_{G\,d} = X_{G\,1}$ **[Ω]**	$X_{G\,2}$ **[Ω]**	$X_{G\,0}$ **[Ω]**
Distribution	0.0143	0.0130	0.0008

Positive, negative, and zero sequence impedances in ohms of distributed generators were collected from Table 3.10 in order to calculate positive, negative, and zero sequence reactances per-unit of distributed generators. Breaker reactance was *j* 0.0005 per-unit based on Power World® presentation [80]. Because the distributed generators had one breaker, reactance of

*j*0.0005 per-unit was added to positive, negative, and zero sequence reactances of distributed generators. Positive sequence reactance of distributed generators per-unit was estimated using Equation (3.5).

$$X_{G\,1\,pu} = \frac{X_{G\,1}}{Z_{G\,new}} = j\left[\frac{X_{G\,1}}{V_{G\,area}^2/S_{base}} + 0.0005\right] \tag{3.5}$$

where $X_{G\,1\,pu}$ is positive sequence impedance of the distributed generator per-unit, X_{G1} is positive sequence impedance of the distributed generator in ohms, $Z_{G\,new}$ is base impedance of the new system of distributed generator in ohms, $V_{G\,area}$ is area line-to-line voltage of the distributed generator in kV, and S_{base} is base total power of the new system in MVA.

Negative sequence reactance of distributed generators per-unit was estimated with Equation (3.6).

$$X_{G\,2\,pu} = \frac{X_{G\,2}}{Z_{G\,new}} = j\left[\frac{X_{G\,2}}{V_{G\,area}^2/S_{base}} + 0.0005\right] \tag{3.6}$$

where $X_{G\,2\,pu}$ is positive sequence impedance of the distributed generator per-unit, X_{G2} is positive sequence impedance of the distributed generator in ohms, $Z_{G\,new}$ is base impedance of the new system of the distributed generator in ohms, $V_{G\,area}$ is area line-to-line voltage of the distributed generator in kV, and S_{base} is base total power of the new system in MVA .

Zero sequence reactance of distributed generators per-unit was estimated with Equation (3.7).

$$X_{G\,0\,pu} = \frac{X_{G\,0}}{Z_{G\,new}} = j\left[\frac{X_{G\,0}}{V_{G\,area}^2/S_{base}} + 0.0005\right] \tag{3.7}$$

where $X_{G\,0\,pu}$ is zero sequence impedance of distributed generators per-unit, $X_{G\,0}$ is zero sequence impedance of the distributed generator in ohms, $Z_{G\,new}$ is base impedance of the new system of the distributed generator in ohms, $V_{G\,area}$ is area line-to-line voltage of the distributed generator in Kv, and $S_{\,base}$ is base total power of the new system in MVA.

Reactances for positive, negative, and zero sequence impedances of distributed generators per-unit were estimated using Equations (3.5), (3.6), and (3.7), respectively. As shown in Table 3.1, line-to-line voltage of distributed generators for Area 3 was 0.48 kV, and base total power of the new system was 100 MVA. Positive, negative, and zero reactances of the distributed generator in ohms were collected from Table 3.10. Positive, negative, and zero sequence reactances of distributed generators per-unit for the microgrid are indicated in Table 3.11.

Table 3.11: Positive, negative and zero sequence reactances of distributed generators in p.u.

Distributed generators	**Positive sequence reactance [pu]** $j\,X_{G\,1\,pu}$	**Negative sequence reactance [pu]** $j\,X_{G\,2\,pu}$	**Zero sequence reactance [pu]** $j\,X_{G\,0\,pu}$
DG1, DG2, DG3	6.2075	5.6425	0.3475

Reactances of distributed generators were rounded to 3 digits before summing breaker reactance of j 0.000

Figure 3.12 shows the steps to create distributed generators using Power World® software [10]. The microgrid was placed on "Edit Mode," and the "Insert" menu and "Bus" option were selected to place the distributed generator bus. After selecting the "Bus Information" tab, the distributed generator bus was placed as slack bus and set to a line-to-ground voltage of 0.27 kV. The "Generator" option was then selected from the "Insert" menu, and the generator object was connected to the slack bus. In the "Generator Options" window, the "Fault Parameters" tab was selected, and positive, negative, and zero sequence reactances per-unit were completed based on Table 3.11. Generator base total power was set to 100 MVA, and the

"Neutral Grounded" option was clicked. In the "Generator Options" window, the "Power and Voltage Control" tab was selected, and the maximum output was set to 1.825 MW based on diesel generator prime power [80].

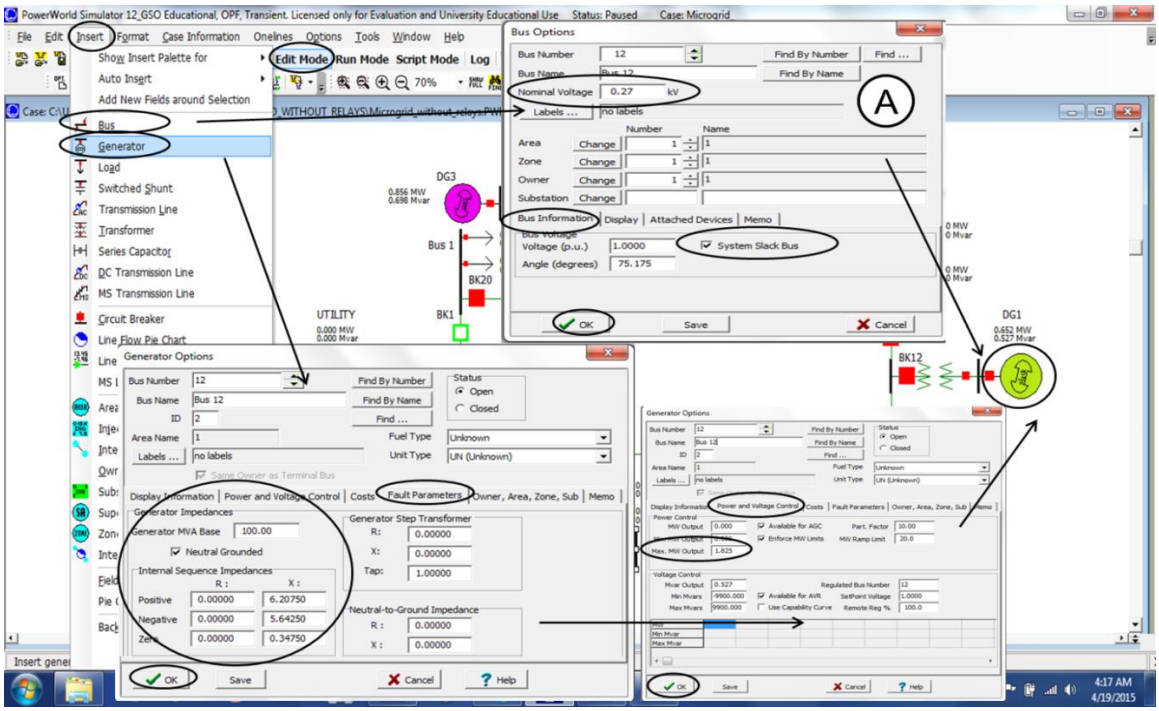

Figure 3.12: Steps to create distributed generator bus (A) and generator (B) by Power World® software [10]

3.5 Loads

In the microgrid, three-phase-balanced loads were set on feeder busses. The loads had a Wye configuration and were P-Q constant. Table 3.12 shows the maximum three-phase-balanced loads on bus feeders of the microgrid. In order to create loads on busses using Power World® software [10], the microgrid was placed in "Edit Mode," and the "Insert" menu and "Load" option were selected. In the "Load Options" window, the "Load Information" tab was selected, and the MW and MVAR values from Table 3.12 were placed in the "Constant Power" column for each load. Figure 3.13 shows the steps to create a P-Q constant load using Power World®

software [10]. For example, the maximum three-phase-balanced loads were referenced by the bus and load numbers: Load 61 corresponded to Load 1 placed on Bus 6, 175 kW / 140 kVar.

Table 3.12: Maximum three-phase-balanced loads on bus feeders of the microgrid

Branch No 1				Branch No 2			
Nodes	**Feeder loads**	**Real power [kW]**	**Reactive power [kVar]**	**Nodes**	**Feeder loads**	**Real power [kW]**	**Reactive power [kVar]**
Bus 1	11	250	190	Bus 5	51	300	230
	12	250	190				
Bus 2	21	175	140	Bus 6	61	175	140
	22	175	140		62	175	140
Bus 3	31	200	160	Bus 7	71	300	230
					72	200	150
Bus 4	41	250	200	Bus 8	81	350	280
	42	200	150				

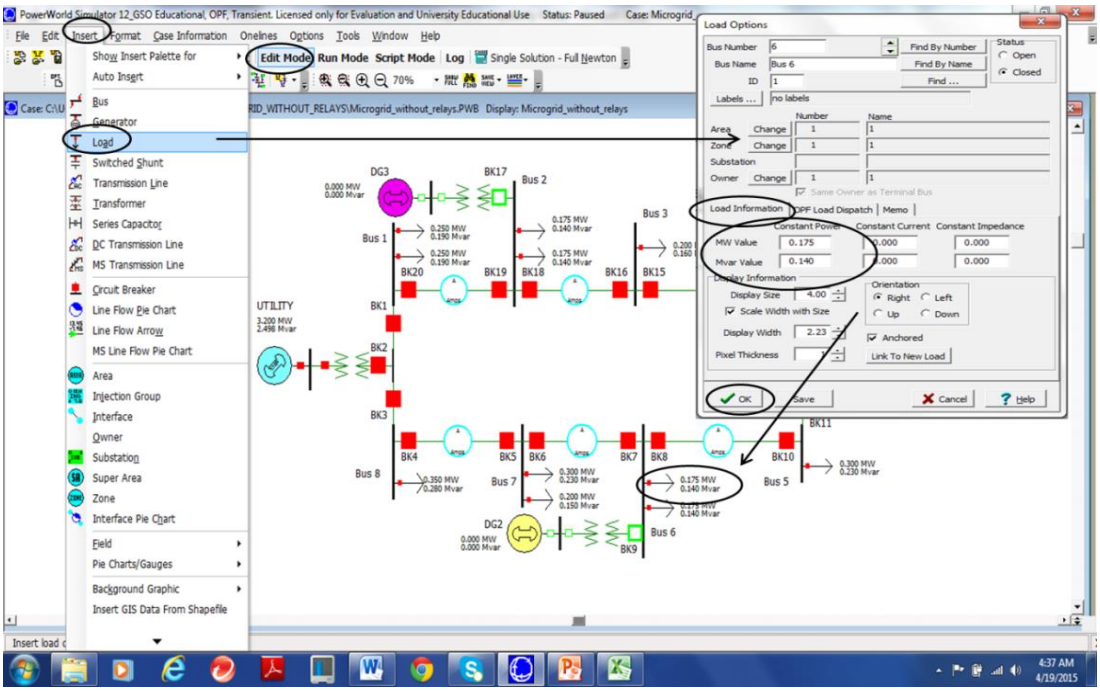

Figure 3.13: Steps to create a load using Power World® software [10]

3.6 Medium voltage fuses

Methods to select MV fuses for bus load feeders were based on the maximum full load and feeder conductor size methods. Use of the maximum full load method to select MV fuses of

load feeders ensures that MV fuses do not open overloads. In general, the minimum MV fuse rating should be at least 1.4 times the circuit's maximum load current [81]. Equation (3.8) indicates the condition to select MV fuses of load feeders in the microgrid based on the maximum full load method.

$$I_{fuse\ rating} \geq 1.4\ I_{max.full\ load} \tag{3.8}$$

where $I_{fuse\ rating}$ is the MV fuse rating current in amps, and $I_{max.\ full\ load}$ is maximum full load current in amps.

Use of the feeder conductor size method to select MV fuses of load feeders guarantees conductor overcurrent protection at load feeders. According to the National Electrical Code article, NEC 240.101-A [82], in the conductor size method, MV fuse rating cannot be more than 3 times the conductor ampacity. Equation (3.9) indicates the condition to select MV fuses of load feeders in the microgrid based on the feeder conductor size method.

$$I_{fuse\ rating} \leq 3\ I_{\ conductor\ rated\ ampacity} \tag{3.9}$$

where $I_{fuse\ rating}$ is MV fuse rating current in amps, and $I_{conductor\ rated\ ampacity}$ is rated ampacity of load feeder conductors in amps.

MV fuses of load feeders in the microgrid were selected based on the maximum full load and feeder conductor size methods, thereby ensuring that MV fuses were not open for overloads and that MV fuses provided overcurrent protection for conductors, respectively. In Table 3.13, selection of MV fuses based on maximum full load (rule of thumb) and feeder conductor size (NEC 240.101-A) methods were verified for the microgrid. In the load feeders, Raven and Penguin aluminum conductor steel-reinforced (ACSR) conductors had 1/0 and 4/0 American wire gauge (AWG) size, respectively. The name, size, and ampere ratings of ACSR conductors were collected from a cable manufacturer publication [83].

Table 3.13: MV fuse selection based on maximum full load (rule of thumb) and feeder conductor size (NEC 240.101-A.) methods

Branch		Feeder			ACSR Conductor				MV Fuse Selection			
Line	Node	Feeder	Max. Load [A]	kV	Type	Name	Size [AWG]	Rating [A]	$I_{fuse\ rating} \geq$ Eq. (3.8) [A]	$I_{fuse\ rating} <$ Eq. (3.9) [A]	Selected MV fuse rating	kV
1	Bus 1	11	43.4	4.16	ACSR	Raven	1/0	242	60.7	726	65E	4.16
		12	43.4			Raven	1/0	242	60.7	726	65E	
	Bus 2	21	31.0			Raven	1/0	242	43.3	726	50E	
		22	31.0			Raven	1/0	242	43.3	726	50E	
	Bus 3	31	35.4			Raven	1/0	242	49.5	726	50E	
	Bus 4	41	44.2			Raven	1/0	242	61.9	726	65E	
		42	34.5			Raven	1/0	242	48.3	726	50E	
2	Bus 5	51	52.2	4.16	ACSR	Penguin	4/0	357	73.1	1071	80E	4.16
	Bus 6	61	31.0			Raven	1/0	242	43.3	726	50E	
		62	31.0			Raven	1/0	242	43.3	726	50E	
	Bus 7	71	52.2			Penguin	4/0	357	73.1	1071	80E	
		72	34.5			Raven	1/0	242	48.3	726	50E	
	Bus 8	81	61.9			Penguin	4/0	357	86.7	1071	100E	

ACSR = Aluminum Conductor Steel Reinforced

As shown in Table 3.13, the 100E, 80E, 65E, and 50E fuses corresponded to SMU-40® standard speed fuses at 4.8 kV nominal rating [6]. As shown in Figure 3.14, maximum load currents and selected MV fuse ratings were based on the rule of thumb and NEC 240.101-A article.

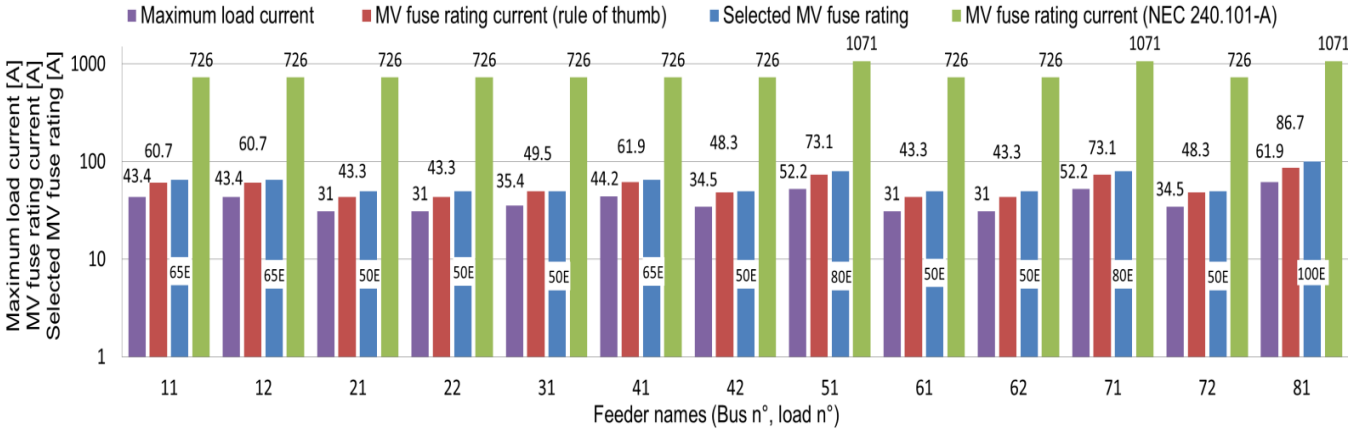

Figure 3.14: Maximum load current and selected MV fuse rating based on rule of thumb [81] and NEC 240.101-A article [82]

Figure 3.14 illustrates how the MV fuse ratings were placed between current ratings of rule of thumb and the NEC 240.101-A article. Therefore, MV fuses for load feeders selected by conditions of Equations (3.8) and (3.9) provided MV fuses that did not open for overloads and overcurrent protection for conductors.

In the 100E, 80E, 65E, and 50E MV fuses, the current-time area was limited by melting and clearing curves. When an MV fuse reached the area between melting and clearing curves, the fuse began the melting process, thereby limiting MV fuse current capacity and protecting feeder conductors. In Figure 3.15, dashed and full lines represent MV fuse melting and clearing curves, respectively. The brown, green, pink, and blue lines represent 100E, 80E, 65E, and 50E MV fuse curves, respectively. Based on load feeder names, MV fuses in Table 3.13 were placed in the microgrid, as shown in Figure 3.16.

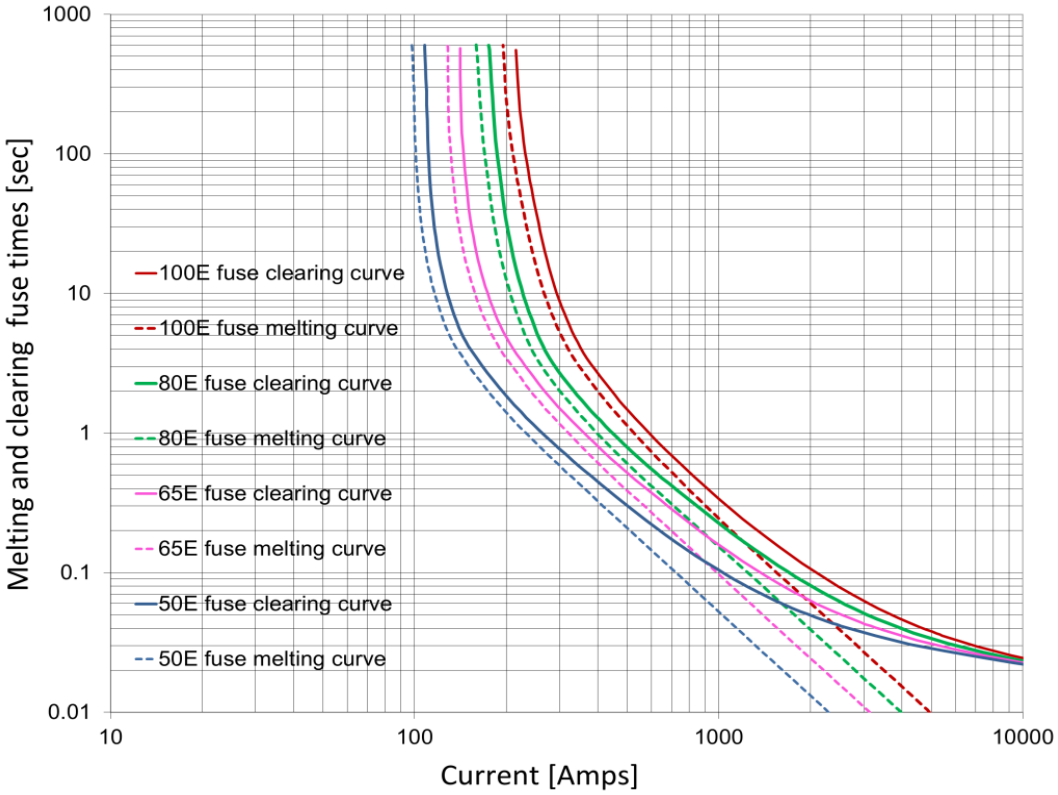

Figure 3.15: Current-time curves of 100E, 80E, 65E, and 50E standard speed 4.8 kV SMU-40® fuses [6]

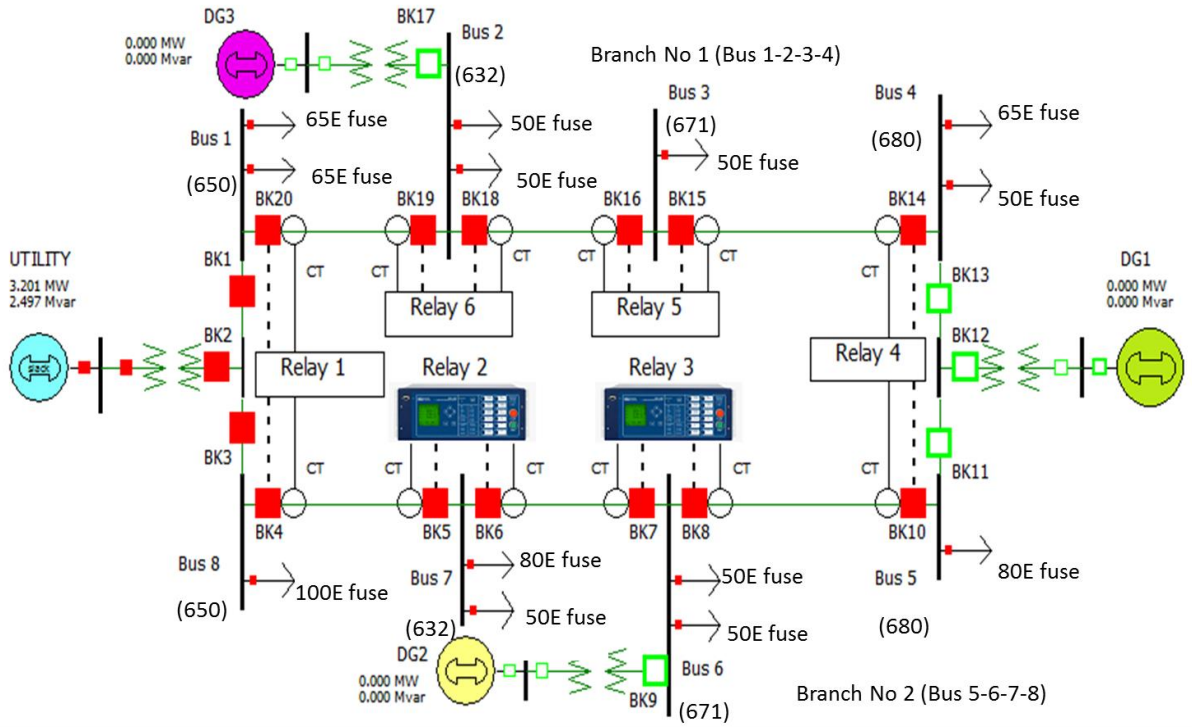

Figure 3.16: Microgrid with MV fuses for bus load feeders

Because the microgrid contained distributed generators, currents of power lines along branches 1 and 2 could flow in both directions; therefore, adaptive overcurrent protection with SEL 451relays [5] instead of MV fuses were applied to control breakers along the power lines. Consequently, adaptive overcurrent protection could select the relay setting group in order to maintain selectivity coordination with MV fuses and relays placed on load feeders and busses, respectively, based on circuit paths of the microgrid. Adaptive overcurrent protection for power lines of branches 1 and 2 allowed selective coordination of MV fuses for circuit paths of utility and distributed generators of the microgrid. Adaptive overcurrent protection was based on use of SEL-451 relays [5] on each bus to control power line breakers that measured fault overcurrents using current transformers (CTs). Adaptive overcurrent protection of the microgrid with distributed generators is described in Chapter 4.

3.7 Chapter summary

This chapter included a single-line diagram and description of equipment of a microgrid with distributed generators. The per-unit method was applied using Power World® software [10], and per-unit impedances of power lines, distribution and utility transformers, and generators were estimated based on equal voltage areas of the microgrid. Table B.1 of Appendix B details data and per-unit results of power lines, utility and distribution transformers, utility sources, and distributed generators. The steps to create power lines, transformers, generators, and loads of the microgrid using Power World® software [10] were described in order to simulate power flow and fault analysis described in the following chapter.

MV fuses of load feeders were selected based on a rule of thumb that states that the minimum MV fuse rating should be at least 1.4 times the circuit's maximum load current [81], and the NEC 240.101-A [82] article that states that the rating of MV fuse cannot be more than 3 times the conductor ampacity. Because the microgrid had distributed generators, currents of power lines along Branches 1 and 2 could flow in both directions, and adaptive overcurrent protection instead of MV fuses were applied to control breakers along the power lines. Adaptive overcurrent protection is further described in Chapter 4.

Chapter 4 - Adaptive overcurrent protection

This chapter describes adaptive overcurrent protection based on relay setting groups and protection logics. Microgrid circuits (test modes) were selected based on microgrid constraints (operation, maximum load demand, equipment, and utility service limitations). Adaptive overcurrent protection was verified by real-time and non-real-time simulators with Relays 2 and 3 in the loop. Circuit paths for Relay 2 and 3 busses were selected from microgrid circuits (test modes). Power flow and fault analysis were performed for circuit paths, collecting current magnitudes on relay breakers. Fault analysis was performed at line-to-line (LL), three-phase balanced (3PB), single-line-to ground (SLG), and double-line-to-ground (DLG) faults. Power lines of the microgrid were defined as protection areas in circuit paths. Based on circuit paths and fault locations, the expected tripped and non-tripped relay's breakers were selected, and maximum ampere rating fuses on busses for circuit paths were picked up to calculate inverse time overcurrent settings of relays.

Inverse time-current curve models of relays and fuses were created. In the inverse time overcurrent elements of relays, based on U3 (very inverse) time-current curve, the time dial settings (*TDS*) and secondary overcurrent pickups (*Ip*) were calculated. For all circuit paths of Relays 2 and 3, inverse time-current curves of the relay's overcurrent elements and maximum ampere rating fuses were plotted for each branch of circuit paths. Selectivity coordination between upstream (backup) and downstream (primary) protective devices was verified in time-current logarithmic plots. Maximum load and fault currents were plotted, verifying that the calculated inverse time overcurrent element settings did and did not trip the relay's breakers, respectively. CTIs between backup and primary protection devices at maximum fault currents were calculated, verifying that the calculated CTIs were not less than the minimum CTI.

Protection logics of relay's control outputs based on "AND" and "ZERO" gates were created to trip or not trip the relay's breakers at fault overcurrents, respectively. Breakers inside the protection areas needed to clear the fault overcurrents. In adaptive overcurrent protection, the setting groups of Relays 2 and 3 were selected by grouping the same inverse time overcurrent settings and protection logic gates of the relay's breakers for circuit paths in the microgrid.

4.1 Constraints of the microgrid

The microgrid with distributed generators was formed by one utility source and three diesel generator units. Utility and distributed generators were not allowed to be connected in parallel. Depending on what distributed generators were connected to the microgrid, power lines inside the dashed red circles allowed currents to flow in both directions, while branches inside the dashed blue circles allowed currents to flow in one direction. In addition, depending on current direction along the power lines, the relays needed to be coordinated with different feeder fuses and relays. Therefore, non-adaptive and adaptive overcurrent protection had to be developed for load feeders and power lines, respectively, as shown in Figure 4.1.

In the microgrid shown in Figure 4.1, inverse time overcurrent relays and MV fuses were applied in power lines and load feeders, respectively. Adaptive overcurrent protection was formed by six overcurrent relays. However, only adaptive overcurrent protection for Relays 2 and 3 was calculated and verified with relays in the loop test techniques.

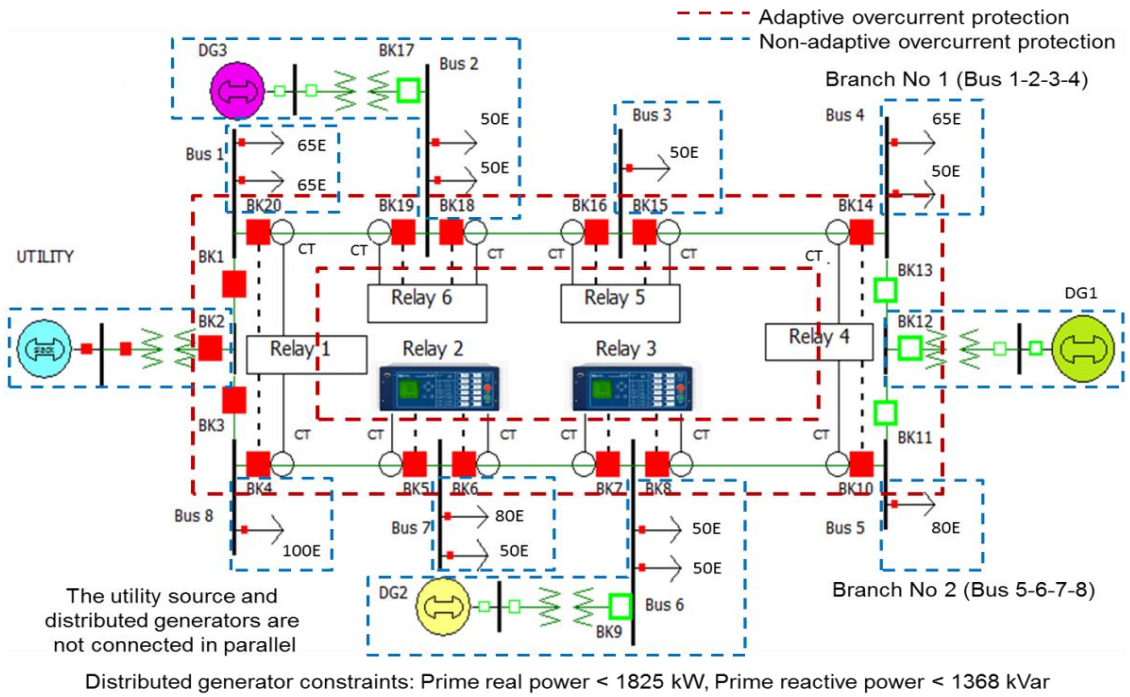

Figure 4.1: Non-adaptive and adaptive overcurrent protection in the microgrid

In adaptive overcurrent protection, circuit paths were allowed based on microgrid constraints. Constraints are limitations of the microgrid to operate breakers conforming to various paths. These constraints corresponded to operation, microgrid loads, equipment, and utility service limitations. Table 4.1 shows microgrid constraints.

Table 4.1: Constraints of the microgrid

Group	N°	Constraints
Operation	1	Normal operation: Utility source was connected to microgrid[(1)]
	2	Non-normal operation: Distributed generators were connected to microgrid[(2)]
Loads	3	Load scenarios of microgrid were based on maximum load demand.
Equipment	4	Distributed generators and utility source were not connected in parallel.
	5	Loads connected to distributed generators were limited by the prime real (1825 kW) and reactive (1368 kVar) power [80].
	6	Tap changers of distribution and utility transformers were sized from 0.9-1.1 per-unit.
Service	7	Bus voltage limit range was from 95-105 % (0.95-1.05 per-unit) based on Service Voltage Limits [84, 85]

[(1)] Utility source was connected to microgrid, [(2)] Distributed generators were connected to microgrid in case of equipment (utility source, power lines, and/or breakers) failure, and/or maintenance operation.

4.2 Microgrid test modes

Circuit paths of the microgrid were grouped into microgrid test modes. These test modes could be segregated into non-normal and normal operations. In normal operation, the utility source was connected to the microgrid. In non-normal operation, distributed generators were connected to the microgrid in case of equipment (utility source, power lines, and/or breakers) failure, and/or maintenance operation. For maximum load demand and normal operation, the utility source was connected to the microgrid, feeding all loads by two branches (UTILITY-8765/1234). However, the utility source could not feed all loads of the microgrid with one branch (UTILITY-87654321 or UTILITY-12345678) because voltages on busses dropped below 95% minimum service voltage limits [84, 85]. However, for maximum load demand and non-normal operation, distributed generators could not be connected in parallel. Also, the maximum prime real (1825 kW) and reactive (1368 kVar) power of DG1, DG2, and DG3 distributed generators limited the number of load feeders (busses) that could be connected to circuit paths. As an example, Figure 4.2 shows the test mode No 14 formed by the DG1-45, DG2-678, and DG3-21/23 circuit paths with maximum load demand.

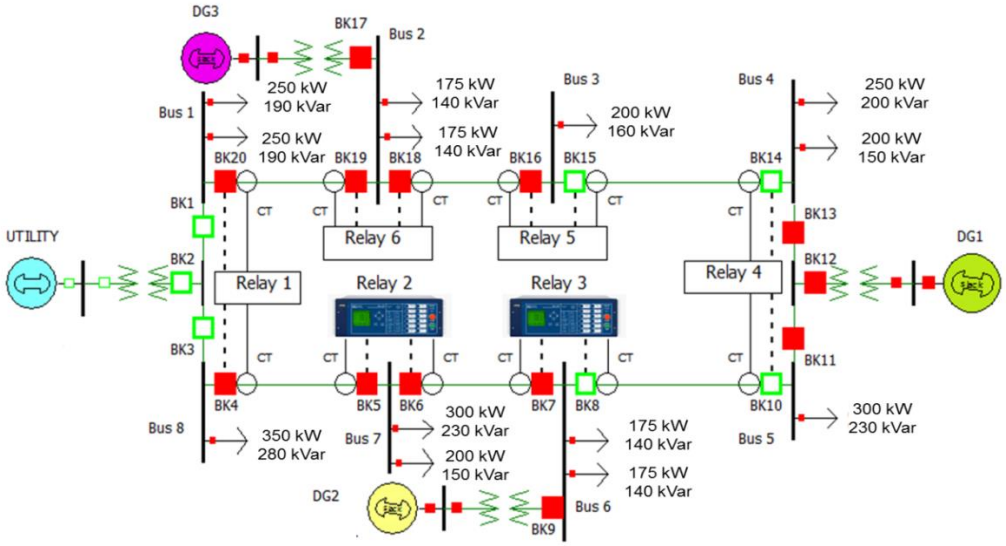

Figure 4.2: Microgrid with maximum load demand

Because circuit paths in the microgrid were limited by the prime real (1825 kW) and reactive (1368 kVar) power of DG1, DG2, and DG3 distributed generators, the real and reactive power of circuit paths were calculated without considering transformer tap ratios and power losses in the microgrid, adding real and reactive power of loads for circuit paths in the microgrid. As a result, DG1-43218 (1850 kW, 1450 kVar), DG1-4321/5 (1800 kW, 1400 kVar), DG1-56781(2000 kW, 1550 kVar), DG1-5678/4 (1950 kW, 1520 kVar), DG2-67812 (2050 kW, 1600 kVar), DG2-6781/65 (2000 kW, 1550 kVar), DG2-654321 (2150 kW, 1680 kVar), DG2-65432/67 (2150 kW, 1680 kVar), DG2-6543/67 (1800 kW, 1400 kVar), DG3-234567 (2150 kW, 1680 kVar), DG3-23456/21(2150 kW, 1680 kVar), DG3-2345/21(1800 kW, 1400 kVar), DG3-21876 (2050 kW, 1600 kVar), and DG3-2187/23 (1900 kW, 1480 kVar) circuit paths in the microgrid were not allowed. Also, DG2-65432 and DG3-23456 circuit paths were not permitted because Bus 1 and 8 were not allowed to connect to DG3 and DG2 distributed generators, respectively (distributed generators must not be connected in parallel).

Circuit paths allowed in the microgrid are shown in Table 4.2. In non-normal operation microgrid test modes, equipment (utility source, power lines, and/or breakers) failure, and maintenance operations were presented as possible scenarios. Although the Test Mode 1 represented the microgrid in normal operation, the 2-22 test modes represented the microgrid in non-normal operation. As shown in Table 4.2, opened breakers were indicated for circuit paths of the microgrid test modes. These breakers could be repaired (maintenance operations), allowing all busses in the microgrid to be fed. Microgrid test modes with distributed generators improved the reliability in case of equipment (utility source, power lines, and/or breakers) failure, and maintenance operation. Adaptive overcurrent protection was based on the 22 microgrid test modes indicated in Table 4.2.

Table 4.2: Circuit paths of microgrid test modes and non-operational equipment (utility source, power lines, and/or breakers) in case of failure and maintenance operation

Microgrid test modes		■ Non-operational equipment in case of failure and/or maintenance operation									
Test Modes	Circuit paths	Opened breakers	Utility and distributed generators				Power lines				
			UTILITY	DG1	DG2	DG3	L12	L23	L34	L56	L67	L78
1	UTILITY-8765/1234	9, 11, 12, 13, 17		■	■	■						
2	DG1-4321, DG2-678/65	1,2,3,11,17	■			■						
3	DG1-432/5, DG2-6781	2, 8,10,17,19,20	■			■	■			■		
4	DG1-5678, DG3-21/234	1, 2, 3, 9, 13	■		■							
5	DG1-34/56, DG3-2187	2,6,7,9,16,18	■		■			■			■	
6	DG2-678/65, DG3-21/234	1,2,3,11,12,13	■	■								
7	DG2-6781, DG3-2345	2,8,10,12,19,20	■	■			■			■		
8	DG2-6543, DG3-2187	2,6,7,12,16,18	■	■				■			■	
9	DG1-4, DG2-678/65, DG3-21/23	1,2,3,11,14,15	■						■			
10	DG1-4, DG2-67/65, DG3-218/23	2,4,5,11,14,15	■						■			■
11	DG1-5, DG2-678, DG3-21/234	1,2,3,8,10,13	■							■		
12	DG1-5, DG2-6781, DG3-234	2,8,10,13,19,20	■				■			■		
13	DG1-4/5, DG2-67, DG3-218/23	2,4,5,8,10,14,15	■						■	■		■
14	DG1-4/5, DG2-678, DG3-21/23	1,2,3,8,10,14,15	■						■	■		
15	DG1-4/5, DG2-6781, DG3-23	2,8,10,14,15,19,20	■				■		■	■		
16	DG1-34, DG2-67/65, DG3-218	2,4,5,11,16,18	■					■				■
17	DG1-34, DG2-65, DG3-2187	2,6,7,11,16,18	■					■			■	
18	DG1-34, DG2-678/65, DG3-21	1,2,3,11,16,18	■					■				
19	DG1-34/5, DG2-678, DG3-21	1,2,3,8,10,16,18	■					■		■		
20	DG1-34/5, DG2-6781, DG3-2	2,8,10,16,18,19,20	■				■	■		■		
21	DG1-34/5, DG2-67, DG3-218	2,4,5,8,10,16,18	■					■		■		■
22	DG1-34/5, DG2-6, DG3-2187	2,6,7,8,10,16,18	■					■		■	■	

4.2.1 Microgrid test modes at 1.00 tap ratio

With Power World® software [10], a power flow analysis was run for circuit paths of microgrid test modes indicated in Table 4.2. Power flow analysis was run at a transformer tap ratio of 1.00 in order to verify that the calculated real and reactive power of DG1, DG2, and DG3 distributed generators were not greater than the prime real (1825 kW) and reactive (1368 kVar) power of distributed generators, respectively [80], and that the calculated bus voltages were within the service voltage limit range (95-105 %) of ANSI Std. C84.1 [85]. Figure 4.3 shows the calculated real (A) and reactive (B) power of utility source and DG1, DG2, and DG3 distributed generators at transformer tap ratio of 1.00. Based on the prime reactive (1368 kVar) power of DG1, DG2, and DG3 distributed generators, test modes 3, 5, 7, 8, 12, 15, 17, 20, and 22 were not permitted because the calculated reactive power of distributed generators was greater than 1368 kVar. Figure 4.4 shows calculated bus voltages of microgrid test modes at a transformer tap ratio of 1.00. Because all microgrid test modes had bus voltages outside the 95.0-105.0% service voltage range, all 22 test modes were not permitted at transformer tap ratio of 1.00. Calculated real and reactive power of distributed generators and bus voltages of the microgrid test modes at transformer tap ratio of 1.00 are shown in Table C.1 of Appendix C. At a transformer tap ratio of 1.00, circuit paths of the microgrid test modes were not acceptable based on the service voltage limit range (95-105 %) constraint, according to the ANSI Std. C84.1 [85]. However, because transformer tap ratios could be regulated from 0.9 to 1.1, a new transformer tap ratio of 0.95 was defined to run another power flow analysis case.

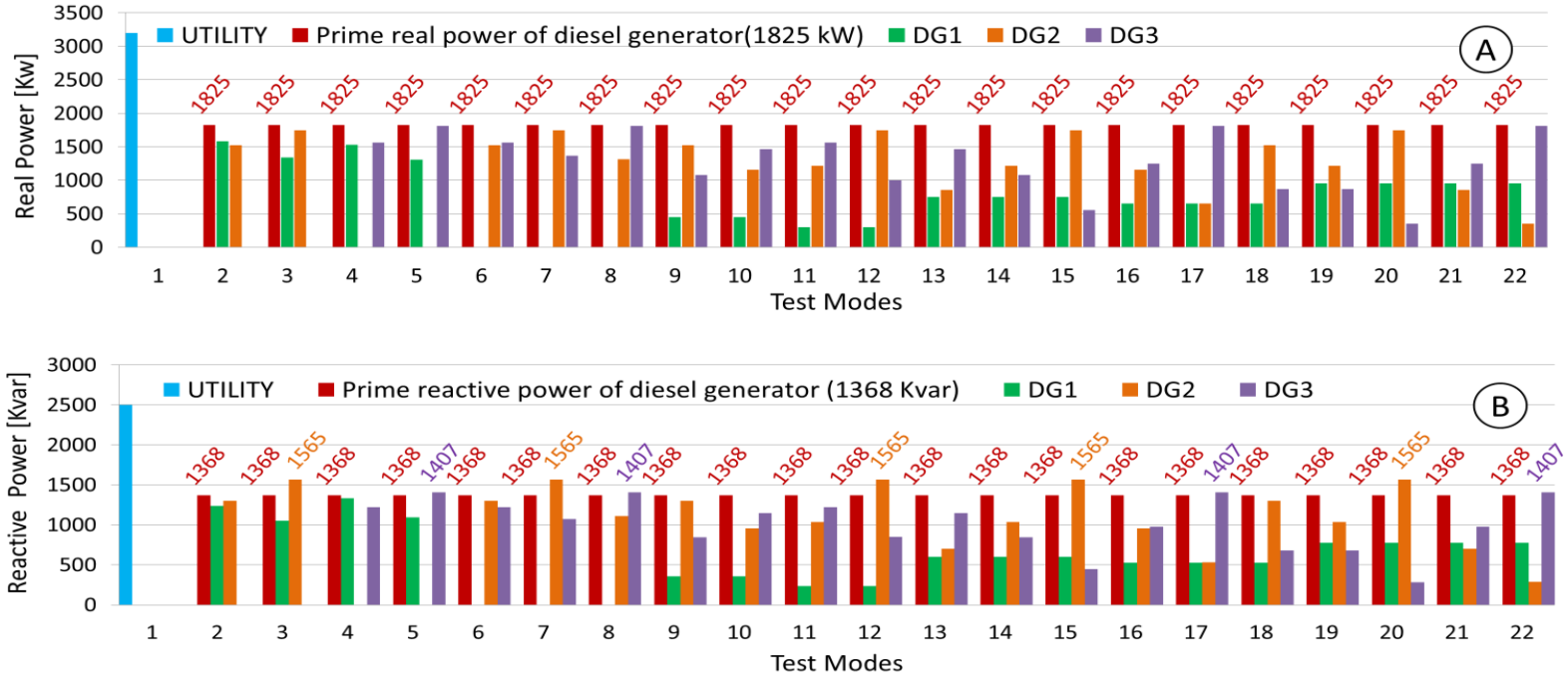

Figure 4.3: Utility and distributed generator real (A) and reactive (B) power of microgrid test modes versus prime real and reactive power of diesel generator for 1.00 tap ratio

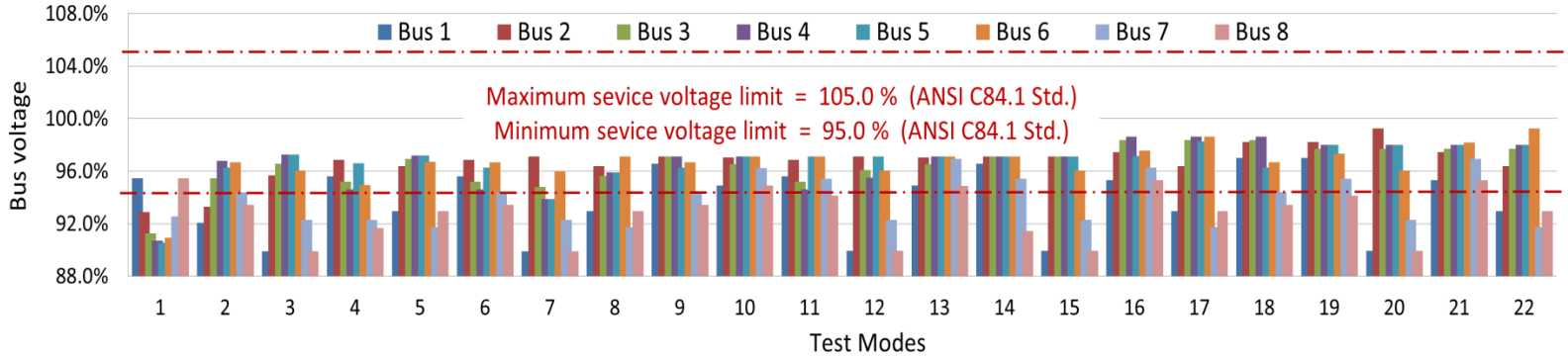

Figure 4.4: Bus voltages of microgrid test modes for 1.00 tap ratio

4.2.2 Microgrid test modes at 0.95 tap ratio

With Power World® software [10], power flow analysis was run at a transformer tap ratio of 0.95 in order to verify that the calculated real and reactive power real of DG1, DG2, and DG3 distributed generators were not greater than the prime real (1825 kW) and reactive (1368 kVar) power of distributed generators, respectively [80], and that the calculated bus voltages were within the service voltage limit range (95-105 %) of ANSI Std. C84.1 [85]. Figure 4.5 shows the calculated real (A) and reactive (B) power of the utility source and DG1, DG2, and DG3 distributed generators at transformer tap ratio of 0.95. At a transformer tap ratio of 0.95, the calculated real and reactive power of DG1, DG2, and DG3 distributed generators were less than 1825 kW and 1368 kVar. Figure 4.6 shows calculated bus voltages of microgrid test modes at a transformer tap ratio of 0.95. Because all microgrid test modes had bus voltages within the 95.0-105.0% service voltage range, all 22 test modes were permitted. Calculated real and reactive power of distributed generators and bus voltages of microgrid test modes at a transformer tap ratio of 0.95 are shown in Table C.2 of Appendix C. At a transformer tap ratio of 0.95, circuit paths of microgrid test modes were acceptable based on the service voltage limit range (95-105 %) constraint, according to the ANSI Std. C84.1 [85] and prime real (< 1825 kW) and reactive (<1368 kVar) power limit constraint of distributed generators [80].

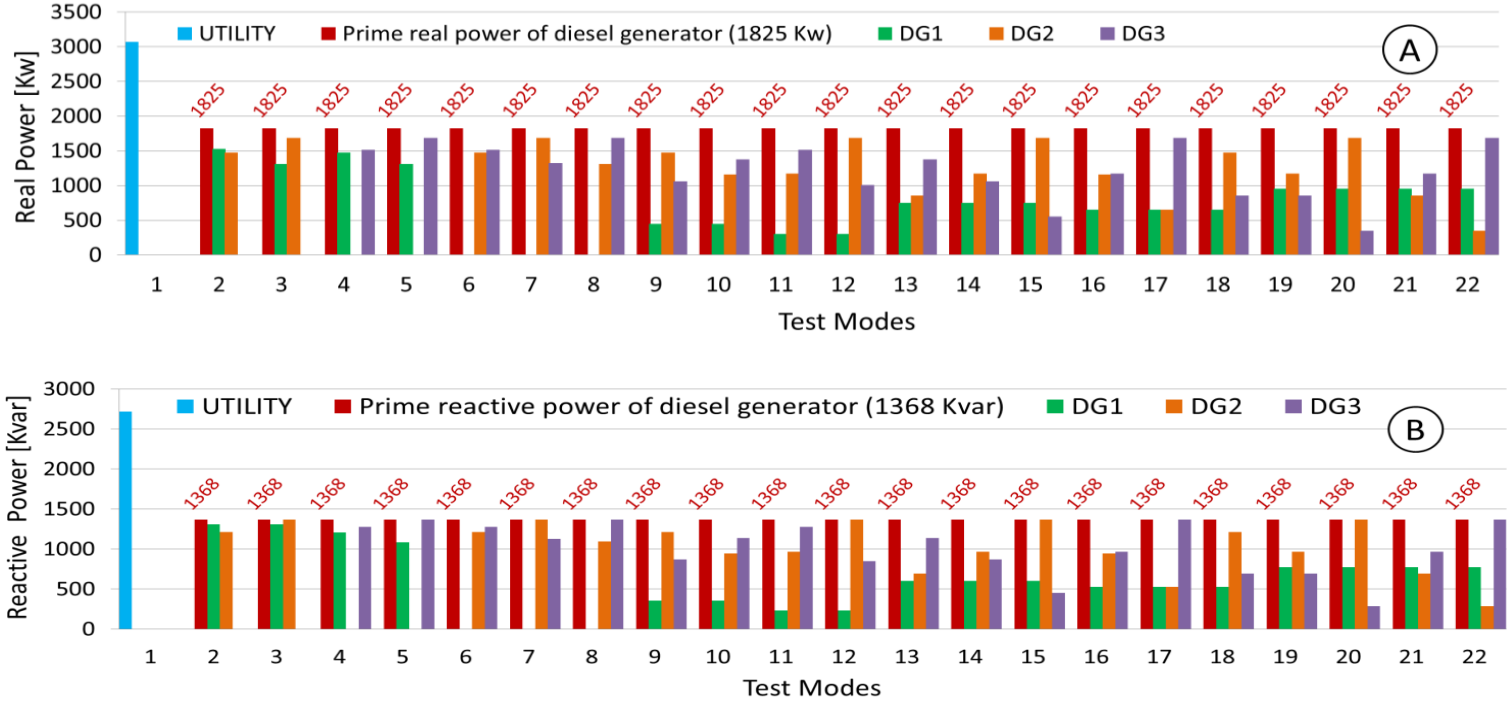

Figure 4.5: Utility and distributed generator real (A) and reactive (B) power of microgrid test modes versus prime real and reactive power of diesel generator for 0.95 tap ratio

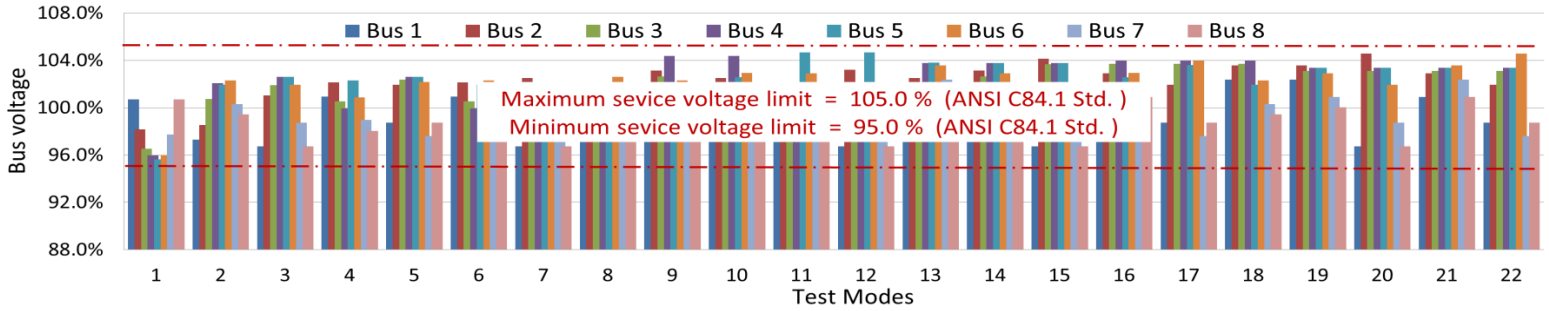

Figure 4.6: Bus voltages of microgrid test modes for 0.95 tap ratio

4.3 Circuit paths for Relays 2 and 3

In this research, adaptive overcurrent protection of the microgrid with distributed generators was verified for Relays 2 and 3 placed on Bus 7 and 6, respectively. Microgrid test modes that included circuit paths for Relays 2 and 3 represented the cases of study for adaptive overcurrent protection. These microgrid test modes are shown in Table 4.3.Circuit paths corresponding to Relays 2 and 3 are indicated in bold. Circuit paths of Relays 2 and 3 were collected. Circuit paths for Relays 2 and 3 corresponded to circuit paths with Bus 7 and 6, respectively. In Table 4.3, the microgrid had 12 circuit paths for Relays 2 and 3. Circuit paths for test modes are shown in Figures D.1-12 of Appendix D.

Table 4.3: Microgrid test modes and circuit paths

Microgrid test modes		
Test Modes	**Circuit paths**	**Circuit paths of Relays 2 and 3**
1	**UTILITY-8765/1234**	**UTILITY-1234/5678** (Test mode:1) **DG2-678/65** (Test modes: 2, 6, 9 and 18) **DG2-67/65** (Test modes: 10 and 16) **DG2-6543** (Test mode: 8) **DG2-65** (Test mode: 17) **DG2-6781** (Test modes: 3, 7, 12, 15 and 20) **DG2678** (Test modes: 11, 14 and 19) **DG2-67** (Test modes: 13 and 21) **DG1-5678** (Test mode: 4) **DG1-34/56** (Test mode: 5) **DG2-6** (Test mode 22) **DG3-2187** (Test modes: 5, 8, 17 and 22)
2	DG1-4321, **DG2-678/65**	
3	DG1-432/5, **DG2-6781**	
4	**DG1-5678**, DG3-21/234	
5	**DG1-34/56**, **DG3-2187**	
6	**DG2-678/65**, DG3-21/234	
7	**DG2-6781**, DG3-2345	
8	**DG2-6543**, **DG3-2187**	
9	DG1-4, **DG2-678/65**, DG3-21/23	
10	DG1-4, **DG2-67/65**, DG3-218/23	
11	DG1-5, **DG2-678**, DG3-21/234	
12	DG1-5, **DG2-6781**, DG3-234	
13	DG1-4/5, **DG2-67**, DG3-218/23	
14	DG1-4/5, **DG2-678**, DG3-21/23	
15	DG1-4/5, **DG2-6781**, DG3-23	
16	DG1-34, **DG2-67/65**, DG3-218	
17	DG1-34, **DG2-65**, **DG3-2187**	
18	DG1-34, **DG2-678/65**, DG3-21	
19	DG1-34/5, **DG2-678**, DG3-21	
20	DG1-34/5, **DG2-6781**, DG3-2	
21	DG1-34/5, **DG2-67**, DG3-218	
22	DG1-34/5, **DG2-6**, **DG3-2187**	

4.4 Protection areas for Relays 2 and 3

In this research, adaptive overcurrent protection for Relays 2 and 3 was implemented and verified with a real-time and non-real-time simulator with relays. Based on circuit paths in Figures D.1-12 of Appendix D, Relays 2 and 3 had to protect microgrid power lines by selective coordination inverse time overcurrent protection. Table 4.4 shows the backup and primary protection relays for circuit paths in the microgrid with distributed generators.

Table 4.4: Microgrid test modes, circuit paths, protection areas, and selectivity

Microgrid test modes		**Circuit paths**	**Protection areas and selectivity for Relays 2 and 3**		
Test modes	**Circuit paths**		**Relay 2**	**Relay 3**	**Power lines**
1	UTILITY-8765/1234	UTILITY-8765/1234	Backup	Primary	L56
			Primary		L67
2	DG1-4321, DG2-678/65	DG2-678/65		Primary	L56
6	DG2-678/65, DG3-21/234			Primary	L67
9	DG1-4, DG2-678/65, DG3-21/23				
18	DG1-34, DG2-678/65, DG3-21		Primary	Backup	L78
10	DG1-4, DG2-67/65, DG3-218/23	DG2-67/65		Primary	L56
16	DG1-34, DG2-67/65, DG3-218			Primary	L67
8	DG2-6543, DG3-2187	DG2-6543		Backup	L34
				Primary	L56
17	DG1-34, DG2-65, DG3-2187	DG2-65		Primary	L56
3	DG1-432/5, DG2-6781	DG2-6781		Primary	L67
7	DG2-6781, DG3-2345				
12	DG1-5, DG2-6781, DG3-234				
15	DG1-4/5, DG2-6781, DG3-23		Primary	Backup	L78
20	DG1-34/5, DG2-6781, DG3-2				
11	DG1-5, DG2-678, DG3-21/234	DG2-678		Primary	L67
14	DG1-4/5, DG2-678, DG3-21/23				
19	DG1-34/5, DG2-678, DG3-21		Primary	Backup	L78
13	DG1-4/5, DG2-67, DG3-218/23	DG2-67		Primary	L67
21	DG1-34/5, DG2-67, DG3-218				
4	DG1-5678, DG3-21/234	DG1-5678		Primary	L67
			Primary	Backup	L78

Protection areas (power lines) for Relays 2 and 3 were not available for test modes 5 (DG1-34/56, DG3-2187) and 22 (DG1-34/5, DG2-6, DG3-2187).

In DG1-34/56, DG3-2187, and DG2-6 circuit paths, breakers of Relays 2 (Bus 7) and 3 (Bus 6) did not have to trip. Table 4.5 shows observations of DG1-34/56, DG3-2187, and DG2-6 circuit paths. Based on observations in Table 4.5, inverse time overcurrent elements for "BK8 (Relay 3)" and "BK5 (Relay 2)" breakers must not be enabled for the DG1-34/56 and DG3-2187 circuit paths, respectively. However, the DG2-6 circuit path could allow the inverse time overcurrent settings of Relay 2 for any circuit path because the "BK7" and "BK8" breakers were opened. As an example, Figure 4.7 shows the DG1-34/56 circuit path.

Table 4.5: DG1-34/56, DG3-2187, and DG2-6 circuit paths

Microgrid test modes		**Observations**
Test modes	**Circuit paths**	
5	DG1-34/56	"BK7" and "BK8" breakers controlled by Relay 3 were open and closed, respectively.
5, 8, 17 and 22	DG3-2187	"BK5" and "BK6" breakers controlled by Relay 2 were closed and open, respectively.
22	DG2-6	"BK7" and "BK8" breakers controlled by Relay 3 were open.

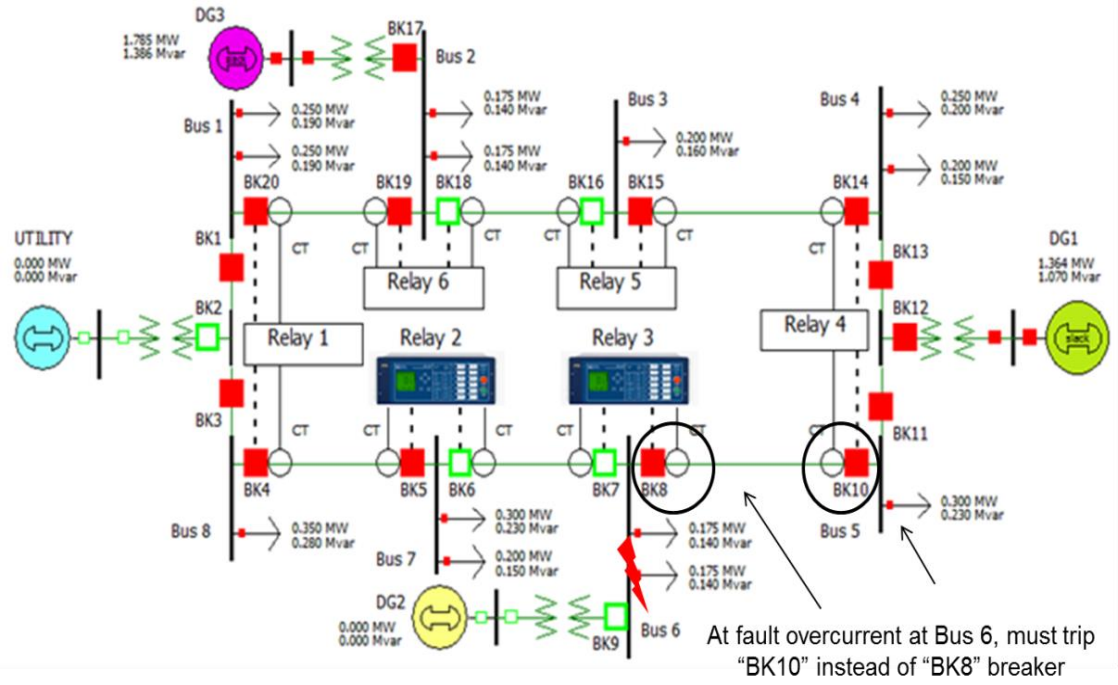

Figure 4.7: DG1-34/56 (Test Mode: 5)

At overcurrent fault on Bus 6, Relay 3 (Bus 6) must not trip “BK8” breaker and Relay 4 (Bus 5) must trip “BK10” breaker. Therefore, the L56 power line was completely de-energized after clearing overcurrent fault on Bus 6. In order to set adaptive inverse time overcurrent protection for Relays 2 and 3, protection areas of circuit paths in Table 4.4 were defined, calculating the magnitude of maximum and minimum fault overcurrents of the power lines defined as protection areas. Since the setting of Relays 2 and 3 as backup-primary or primary-backup protections depended on the circuit paths, minimum CTI between the backup and primary relays was defined to coordinate protective devices, expecting primary relays to trip faster than backup relays at fault overcurrent in the power lines (protection areas).

4.5 Inverse time-current curves

In the microgrid, MV fuses and overcurrent relays were considered to be protective devices. Although MV fuses were placed on load feeders, overcurrent relays were placed on power line busses. In order to define inverse time overcurrent settings of overcurrent relays based on selectivity coordination, models of inverse time-current curves for MV fuses and overcurrent relays were developed.

4.5.1 Inverse time-current curves of relays

Inverse time-current curves of Relays 2 and 3 were collected from SEL 451 relay’s manufacturer manual [5]. In SEL 451 relays, IEC (International Electrotechnical Commission) and U.S. (United States) families were presented as inverse time-current curves. The IEC family had the C1 (Standard Inverse), C2 (Very Inverse), C3 (Extremely Inverse), C4 (Long-Time Inverse), and C5 (Short-Time Inverse) curves, and the US family had the U1 (Moderately Inverse), U2 (Inverse), U3 (Very Inverse), U4 (Extremely Inverse), and U5 (Short-Time Inverse) curves. In adaptive overcurrent protection in the microgrid, the U3 (Very Inverse) curve was set

to Relays 2 and 3. Based on the U3 (Very Inverse) curve from the SEL 451 relay's instruction manual [5], the relay time of U3 (Very Inverse) curve was represented by Equation (4.1):

$$T_R = TDS \times \left(0.0963 + \frac{3.88}{M^2 - 1}\right) \tag{4.1}$$

where T_R is the relay time in seconds, *TDS* is the inverse time overcurrent time dial setting, and *M* is the multiple of pickup.

In order to coordinate relays with fuses, Equation (4.1) was represented as a function of the primary current instead of a multiple of pickup, considering that the multiple of pickup of relay was defined by Equation (4.2):

$$M = \frac{I}{CTR \times I_P} \tag{4.2}$$

where *M* is the multiple of pickup, *I* is the primary pickup fault current in amps, *CTR* is the current transformer ratio, and I_P is the secondary overcurrent pickup in amps.

Placing Equation (4.2) into (4.1), the U3 (Very Inverse) relay time curve as a function of the primary current was represented by Equation (4.3):

$$T_R = TDS \times \left(0.0963 + \frac{3.88}{\left(I/CTR/I_p\right)^2 - 1}\right) \tag{4.3}$$

where T_R is the relay time in seconds, *TDS* is the inverse time overcurrent time dial setting , *I* is the primary pickup fault current in amps, *CTR* is the current transformer ratio, and I_P is the secondary overcurrent pickup in amps.

With Equation (4.3), the CTI was calculated at maximum fault overcurrent for relay-relay and relay-fuse protection devices in adaptive overcurrent protection. Inverse time-current curves of SEL 451 relays were represented by Equation (4.3). The relay time represented the interval the relay took to trip the signal in order to open the breaker at fault overcurrent. Each relay measured primary currents by current transformers to control the breakers at overcurrent faults. In the

NRTS experiment, the current transformer ratios were 200. In the SEL 451 relays, the U3 (Very Inverse) curve was selected, and the *TDS* and *Ip* in amps were selected in order to set the inverse time-current curves of Relays 2 and 3 for the setting groups.

4.5.2 Inverse time-current curves of 4.8 kV fuses

The 100E, 80E, 65E, and 50E 4.8 kV fuses were placed on load feeders of the microgrid. In the MV fuses, the time-current area was limited by the melting and clearing curves. Relay times were calculated by relay curves represented by Equation (4.3). However, clearing times of fuses were calculated based on clearing time curves. Clearing curves of 100E, 80E, 65E, and 50E MV fuses were represented by the red, green, pink, and blue lines, respectively, shown in Figure 4.8.

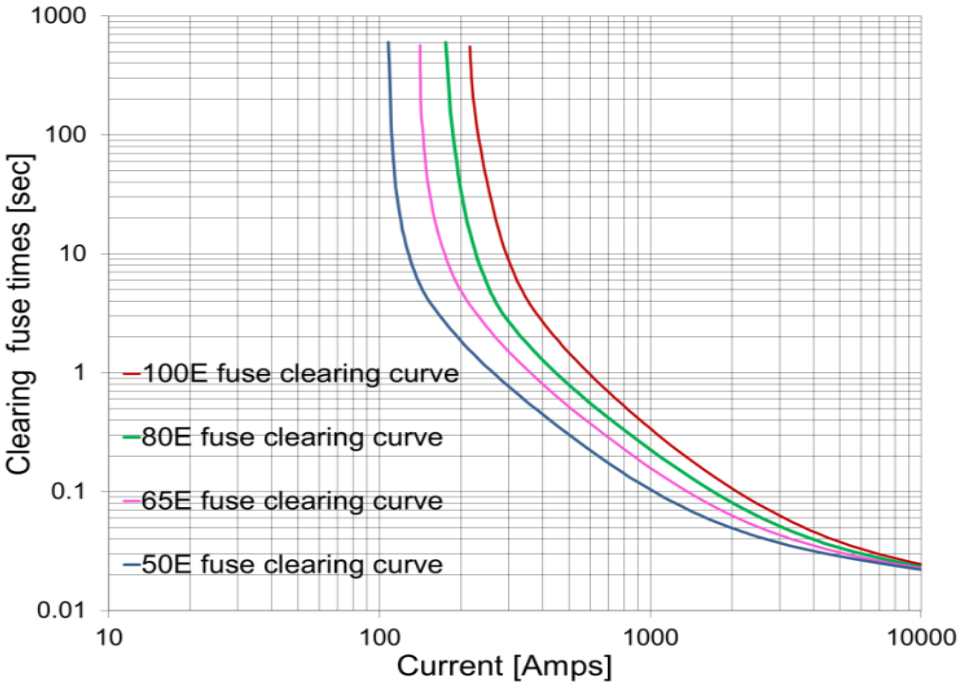

Figure 4.8: Clearing time curves of 100E, 80E, 65E, and 50E standard speed 4.8 kV SMU-40® fuses [6]

In Figure 4.8, clearing curves of 100E, 80E, 65E, and 50E 4.8 kV fuses were plotted by data points provided by the manufacturer's literature [6]. Clearing time curves of 100E, 80E, 65E, and

50E 4.8 kV fuses had to be represented by a mathematical model instead of a curve by points in order to coordinate fuses with relays. The clearing time curve for 65E standard speed 25 kV SMU-20® fuse based on logarithmic coefficients was presented by Yang and Gu [86]. The fuse model of this clearing time curve was represented by Equation (4.4):

$$T_f = 10^{\left(\sum_{n=0}^{6} \frac{d_n}{(\log I)^n}\right)} \tag{4.4}$$

where T_f is fuse total clearing time in seconds, I is current passing through the fuse in amps, and d_n are logarithmic coefficients from Table 4.5.

Table 4.5: Coefficients of 65E standard speed 25 kV SMU-20® fuse based on Yang and Gu [86]

d0	d1	d2	d3	d4	d5	d6
1943.968	-3743.1245	2986.37123	-1261.72	297.4204	-37.0748	1.909126

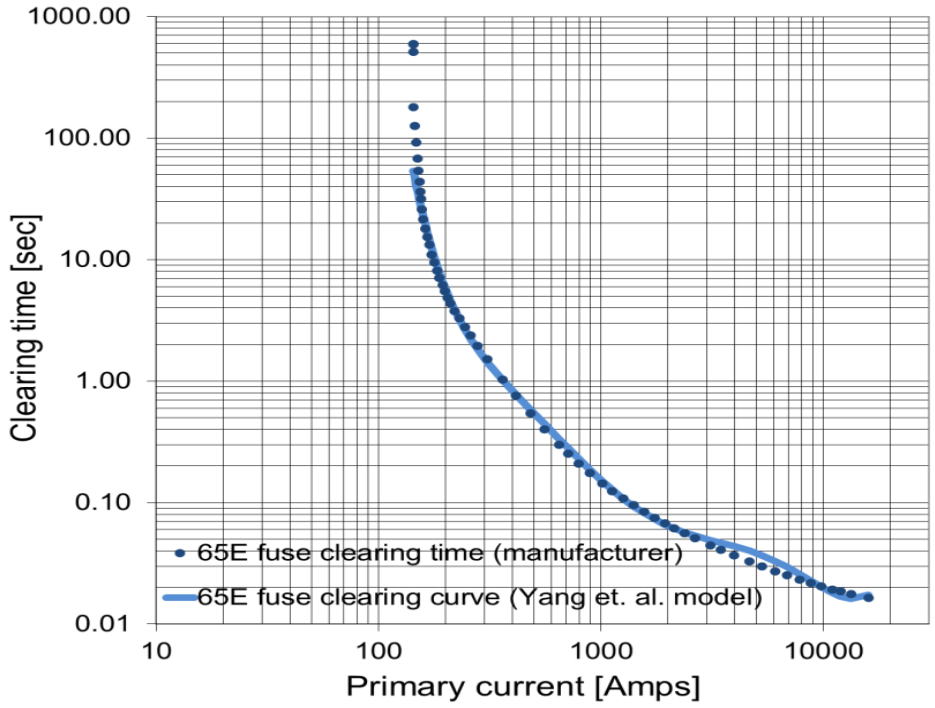

Figure 4.9: Yang and Gu [86] model and manufacturer clearing time curve of 65E standard speed 25 kV SMU-20® fuse

In Figure 4.9, Yang and Gu's [86] model based on Equation (4.4) and manufacturer clearing time curve of 65E fuse are plotted. The full and dotted blue curves represent the Yang and Gu [86] model and manufacturer clearing time curve of 65E standard speed 25 kV SMU-20® fuse [87].

In the microgrid, standard speed fuses of 4.8 kV instead of 25 kV were located on bus feeders. A new fuse model of clearing time curves based on fitting curves was presented for 50 E, 65E, 80E, and 100E standard speed 4.8 kV SMU-40® fuses placed in the microgrid. This new model was based on fitting clearing time curves with points of clearing time curves of 50E, 65E, 80E, and 100E standard speed 4.8 kV SMU-40® fuses provided by the manufacturer [6].

The fitted clearing time curves of 50E, 65E, 80E, and 100E standard speed 4.8 kV SMU-40® fuses were based on US curves as a function of primary current. The U4 (Extremely Inverse) and U5 (Short-Time Inverse) curves were considered in order to create 4.8 kV fuse clearing time curves from 0-3000 and 3001-12000 amps, respectively. From Equation (4.3), *TDS*, *Ip*, and *CTR* were named F_S, F_P, and 200, respectively. Equation (4.5) represents clearing time curves of 4.8 kV fuses up to a primary current of 12000 amps.

$$T_f = F_S \times \left(K_1 + \frac{K_2}{(I/200/F_P)^{K_3-1}}\right) \tag{4.5}$$

where T_f is clearing time of 4.8 kV fuse in seconds, F_S is the fuse factor setting, I is the primary pickup fault current in amps, and F_P is the secondary overcurrent pickup factor in amps. Table 4.6 shows US curve constants and selected F_S and F_P values to fit clearing time curves of 50E, 65E, 80E, and 100E 4.8 kV fuses.

Table 4.6: US curve constants, F_{S5}, and F_P values for clearing time curve models of MV fuses

Primary pickup fault currents [A]	US curves	US curve constants			50E		65E		80E		100E	
		K_1	K_2	K_3	F_S	F_P [A]	F_S	F_P [A]	F_S	F_P [A]	F_S	F_P [A]
0 to 3000	U4	0.02434	5.64	2	1.17	0.51	1.19	0.67	1.15	0.83	1.15	1.08
3001 to12000	U5	0.00262	0.00342	0.02	0.367	2.78	0.336	3.90	0.30	5.50	0.28	7.00

In Figure 4.10,the fuse model and manufacturer clearing time data from 0-3000 (A) and 3001-12000 (B) amps for 100E, 80E, 65E, and 50E standard speed 4.8 kV SMU-40® fuses are shown. Because the maximum fault current of the microgrid was not higher than 12000 amps, clearing time curve models for 100E, 80E, 65E, and 50E fuses were represented up to 12000 amps.

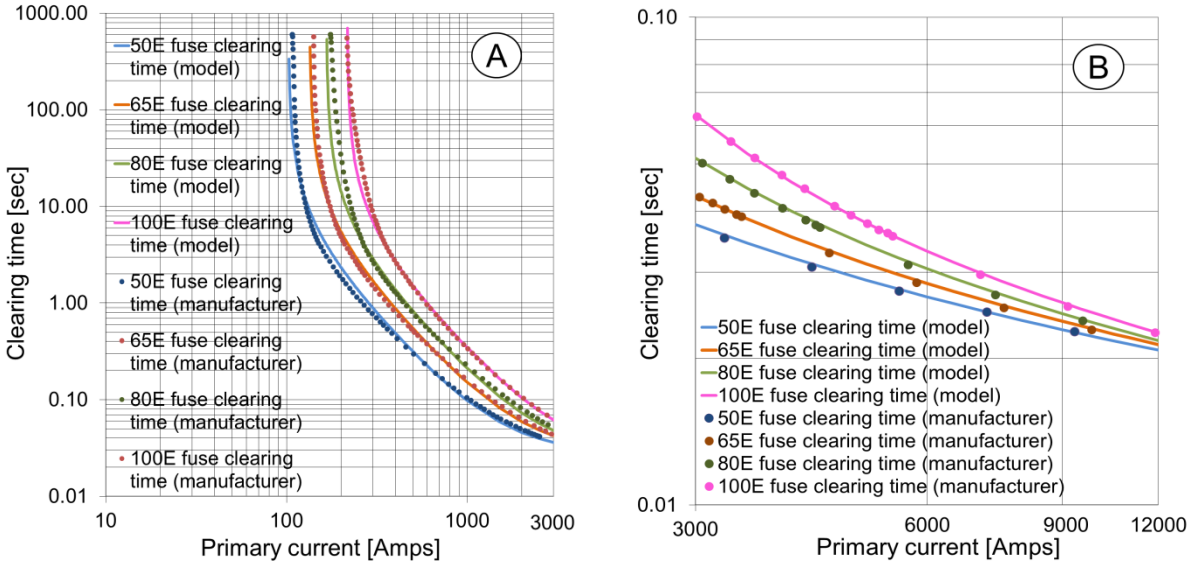

Figure 4.10: Model and manufacturer clearing time curves from 0-3000 (A) and 3001-12000 (B) amps for 100E, 80E, 65E, and 50E standard speed 4.8 kV SMU-40® fuses

In Figure 4.10, clearing time curve models for 100E, 80E, 65E, and 50E 4.8 kV fuses were plotted with Equation (4.5).Clearing time models of 4.8 kV fuses were needed to calculate selectivity coordination between relays and fuses in the adaptive overcurrent protection.

4.6 Minimum coordination time interval

In the microgrid with distributed generators, upstream (backup) and downstream (primary) protective devices were coordinated. Backup-primary protective devices in the microgrid were relay-fuse or relay-relay devices. For a backup and primary protective device, the maximum interrupting current was the value at which the protection devices reached the minimum CTI. Table 4.7 shows CTIs between upstream (backup) and downstream (primary) protective devices based on IEEE Std. 242-2001 [7]. CTIs for static relay were the sum of the circuit breaker operating time (0.08 sec. = 5 cycles) and the relay tolerance and setting error time (0.12 sec. = 7.2 cycles) based on IEEE Std. 242-2001 [7]. Table 4.8 shows components of CTIs with field calibration for static relays.

Table 4.7: Coordination time intervals, IEEE Std. 242-2001 [7]

Downstream	**Upstream**
	Static relay
Fuse	0.12 sec. (7.2 cycles)
Static relay (5 cycles)	0.20 sec.(12.2 cycles)

Table 4.8: Components of coordination time intervals with field testing for static relay [7]

Components	**Coordination time intervals with field testing for static relay**
Circuit breaker operating time	0.08 sec. (5 cycles)
Relay tolerance and setting error time	0.12 sec. (7.2 cycles)
Total coordination time interval	0.20 sec. (12.2 cycles)

In the RTS and NRTS experiments, Relays 2 and 3 tests for minimum and maximum fault currents were run, verifying selective coordination between backup and primary relays. Minimum CTI between the fuse and static relay was 0.12 sec. (7.2 cycles) based on Table 4.8. However, the minimum CTI between backup and primary relays was 0.12 sec. (7.2 cycles)

instead of 0.20 sec. (12.2 cycles) because the circuit breaker operating time was not added in the real-time simulation. Therefore, inverse time overcurrent settings of relays were calculated considering the minimum CTI of 0.12 sec. (7.2 cycles) for relay-fuse and relay-relay selectivity coordination. Figure 4.11 shows fuse-relay minimum CTI and relay-relay CTI components based on IEEE Std. 242-2001 versus relay-relay minimum CTI based on RTS experiment (without circuit breaker operating time).

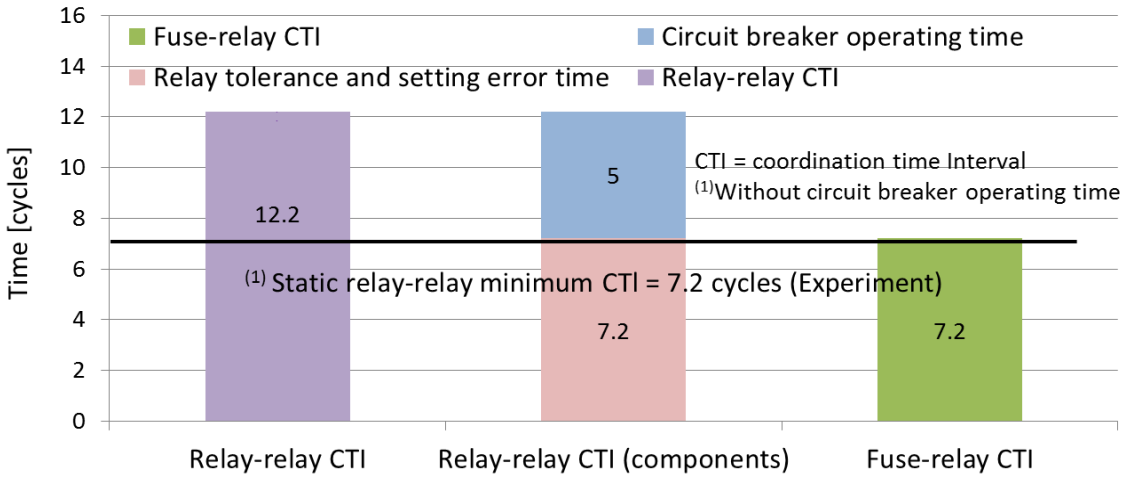

Figure 4.11: Relay-relay and relay-fuse CTIs

Measured CTIs were estimated by the difference between the backup and primary measured relay times at maximum fault overcurrents. In the NRTS experiment, Relays 2 and 3 were tested individually, and CTIs were calculated by collecting measured relay times. However, in the RTS experiment, Relays 2 and 3 were tested with a real-time simulator (power system real-time simulation) that allowed both relays to be tested simultaneously (synchronized). Then selectivity coordination between Relays 2 and 3 could be observed during real-time tests. The primary relay tripped faster than the backup relay, validating application of the minimum CTI of 0.12 sec. (7.2 cycles) instead of 0.20 sec. (12.2 cycles) between Relays 2 and 3 for the RTS experiment.

4.7 Power flow and fault analysis

Power flow and fault analysis of circuit paths for Relays 2 and 3, were run with Power World® software [10]. Power flow analysis allowed calculation of maximum load current magnitudes of relay breakers for circuit paths in the microgrid, and fault analysis allowed calculation of maximum and minimum fault current magnitudes of relay breakers for circuit paths. Table 4.9 shows calculation methods, results, and application of power flow and fault analysis.

Table 4.9: Calculation methods, results, and applications of power flow and fault analysis

Calculation methods	**Results**	**Application**
Power flow analysis	Select maximum load current magnitudes on relay breakers at power lines.	Plot maximum fault current magnitudes and verify that relays did not trip.
Fault analysis	Select maximum and minimum fault currents on relay breakers from the LL, 3PB, SLG, and double-line-to-ground (DLG) faults at power lines and feeder busses.	Plot maximum and minimum fault current magnitudes and verify relays tripped.
		Calculate CTIs at maximum fault currents between backup and primary protective devices and verify that calculated CTI were not less than 7.2 cycles [(1).]

[(1)]Relay-relay and relay-fuse minimum CTIs based on RTS experiment (without breaker operating time) and IEEE Std. 242-2001 [7], respectively.

Maximum load current magnitudes on relay breakers were calculated to verify that the relays did not trip at inverse time overcurrent settings. Maximum and minimum fault current magnitudes on relay breakers in power lines were calculated to verify that the relays tripped at inverse time overcurrent settings, protecting power lines (protection areas) in the microgrid. In addition, maximum fault current magnitudes at power lines and feeder busses allowed calculation of protection device times and CTIs between backup and primary protection devices, verifying that calculated CTIs for maximum fault currents were not less than 7.2 cycles.

Minimum CTI of 7.2 cycles refers to relay-relay and relay-fuse minimum CTIs based on RTS experiment (without breaker operating time) and IEEE Std. 242-2001 [7], respectively.

4.7.1 Power flow analysis

Power flow analysis with Power World® software [10] was run for all circuit paths of Relays 2 and 3 in the microgrid. Circuit paths are shown in Figures D.1-12 in Appendix D. Once power flow analysis was run, current magnitudes of power lines for relay breakers were collected. Table 4.10 shows calculated maximum load current magnitudes of relay breakers from circuit paths by power flow analysis.

Table 4.10: Maximum load current magnitudes of relay breakers for circuit paths

Microgrid test modes		**Maximum load current magnitudes of relay breakers [A]**											
		Bus 1/8		**Bus 7**		**Bus 6**		**Bus 4/5**		**Bus 3**		**Bus 2**	
Test modes	**Circuit Paths of Relays 2 and 3**	**Relay 1**		**Relay 2**		**Relay 3**		**Relay 4**		**Relay 5**		**Relay 6**	
		BK20	**BK4**	**BK5**	**BK6**	**BK7**	**BK8**	**BK10**	**BK14**	**BK15**	**BK16**	**BK18**	**BK19**
1	UTILITY-8765/1234	191	215	215	122	122	56	56	86	86	124	124	191
2, 6, 9, 18	DG2-678/65			65	156	156	55	55					
10, 16	DG2-67/65				90	90	54	54					
8	DG2-6543						173	173	37	37			
17	DG2-65						53	53					
3, 7, 12, 15, 20	DG2-6781		160	160	253	253							
11, 14, 19	DG2-678		65	65	156	156							
13, 21	DG2-67				89	89							
4	DG1-5678		66	66	158	158	224	224					
5	DG1-34/56						64	64	37	37			
22	DG2-6					0	0						
5, 22	DG3-2187	252	93	93	0								252

In Table 4.10, maximum load current magnitudes of relay breakers also represent pre-fault current magnitudes. Inverse time overcurrent settings of relays and maximum load current

magnitudes of relay breakers are represented by inverse time-current curves and current lines, respectively. For each circuit path, inverse time-current curves of relays and maximum load current lines of relay breakers were plotted at a logarithmic time-current (vertical - horizontal) plane, verifying that maximum load current lines of relay breakers did not intersect the inverse time-current curves of relays, confirming that relays must not trip at maximum load currents.

4.7.2 Fault analysis

Fault analysis by Power World® software [10] was run at circuit paths for Relays 2 and 3 in the microgrid. Circuit paths are shown in Figures D.1-12 in Appendix D (UTILITY-8765/1234, DG2-678/65, DG2-67/65, DG2-6543, DG2-65, DG2-6781, DG2-678, DG2-67, DG1-5678, DG1-34/56, DG2-6, and DG3-2187). For power lines as protection areas, maximum and minimum fault currents of the power lines were located near and far away of power lines, respectively. Fault analysis was run for all circuit paths except the DG2-6 circuit path because that circuit path was not connected to power lines. The LL at B-C, 3PB at A-B-C, SLG at A, and DLG at B-C phase faults were estimated at 10% and 90% of power line lengths, collecting A, B, and C phase current magnitudes on power lines. Fault current magnitudes on relay breakers at faults located in power lines are indicated in Tables E.1-12 of Appendix E.

In adaptive overcurrent protection, three-pole breakers instead of single-pole breakers were controlled by relays. Each breaker was tripped by one overcurrent element pickup that tripped A-B-C phases for the LL, 3PB, SLG, and DLG faults. In the minimum faults, relays tripped the three-pole breakers for the greatest A, B, C current magnitude. Therefore, the minimum fault current was the greatest A, B and C current magnitude at minimum fault. From calculated fault currents in Tables E.1-12 of Appendix E, maximum and minimum fault currents of relay breakers were collected; maximum fault currents of relay breakers for common power

lines and maximum fault currents of relay breakers and fuses for feeder busses were collected. Maximum and minimum fault currents of relay breakers were needed in order to verify that the relays tripped at inverse time overcurrent settings of relays. Maximum fault currents of relay breakers for common power lines were needed to verify minimum CTIs between backup and primary relays. Maximum fault currents of relay breakers and fuses for feeder busses were needed to verify the minimum CTI between relays and fuses as backup and primary protections, respectively. As an example, Figure 4.12 shows maximum (red) and minimum (green) fault currents of relay breakers, maximum fault currents of relay breakers for common power lines (pink), and maximum fault currents of relay breakers and fuses at feeder busses (brown) in the DG2-678/65 circuit path for Relays 2 and 3.

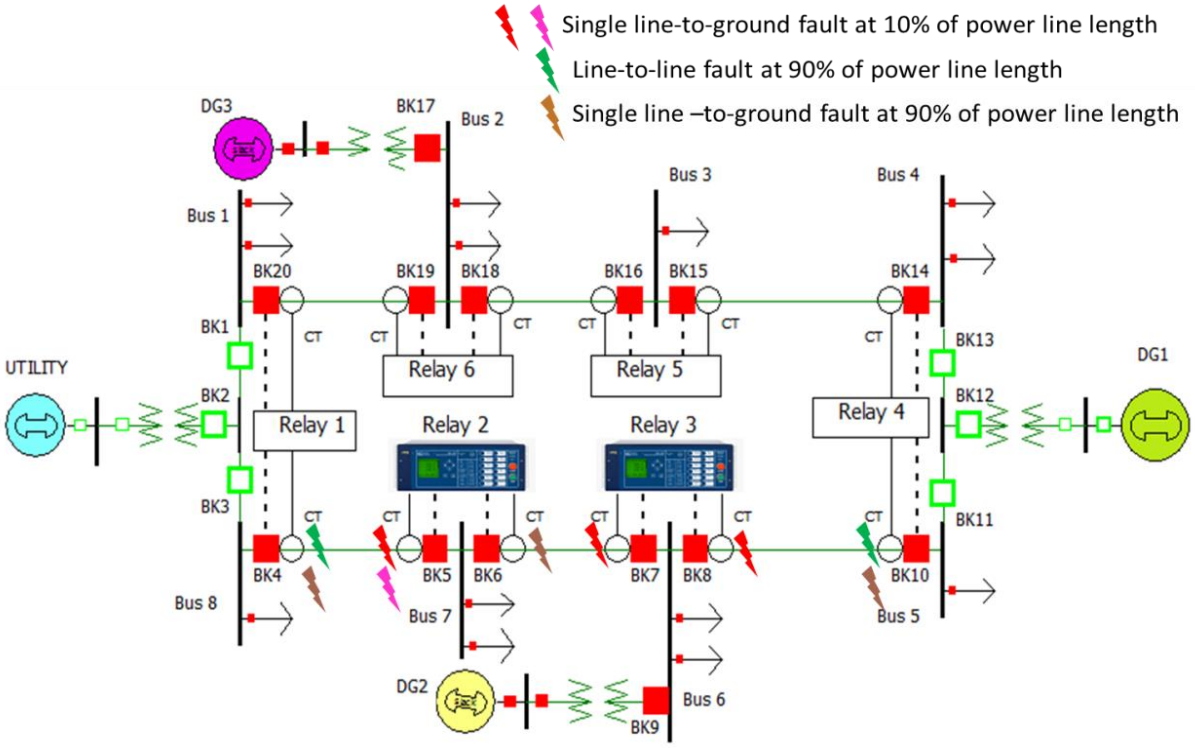

Figure 4.12: Location and type of fault currents for the DG2-678/65 circuit path

In order to verify that the relays tripped at inverse time overcurrent settings of relays, thereby protecting the power lines, maximum and minimum fault current magnitudes of relay

breakers had to be collected from Tables E.1-12 of Appendix E. For the utility source circuit path, maximum and minimum fault currents corresponded to the DLG (BC) and LL (BC) faults, respectively. However, for the DG1, DG2, and DG3 distributed generators circuit paths, maximum and minimum fault currents corresponded to the SLG (A) and LL (BC) faults, respectively. Maximum (DLG and SLG) and minimum (LL) fault currents were referenced to faults located at 10% and 90% of power line lengths, respectively. In addition, when the relay breakers were working as backup protective devices, minimum fault current magnitudes were referenced to common fault locations for all relay breakers in the same branch. Table 4.11 shows maximum and minimum fault current magnitudes in order to verify that the relays tripped the breakers at inverse time overcurrent settings.

Table 4.11: Maximum and minimum fault current magnitudes of relay breakers for circuit paths of Relays 2 and 3

[1]Circuit paths of Relays 2 and 3	Relays	Breakers	Protection areas	Maximum fault current magnitudes			Protection areas	Minimum fault current magnitudes		
				Fault location	Fault type	Currents [A]		Fault location	Fault type	[2]Currents [A]
UTILITY-8765/1234	3	BK8	L56	Bus 6 (10% L56)	DLG(BC)	2046	L56	Bus 5 (90% L56)	LL(BC)	1539
	2	BK6	L67	Bus 7 (10% L67)	DLG(BC)	3170			LL(BC)	1564
	1	BK4	L78	Bus 8 (10% L78)	DLG(BC)	7279			LL(BC)	1622
		BK20	L12	Bus 1 (10% L12)	DLG(BC)	7266	L34	Bus 4 (90% L34)	LL(BC)	1624
	4	BK18	L23	Bus 2 (10% L23)	DLG(BC)	3162			LL(BC)	1581
	5	BK15	L34	Bus 3 (10% L34)	DLG(BC)	2047			LL(BC)	1567
DG2-678/65	3	BK8	L56	Bus 6 (10% L56)	SLG(A)	2371	L56	Bus 5 (90% L56)	LL(BC)	1392
		BK7	L67	Bus 6 (10% L67)	SLG(A)	2369	L78	Bus 8 (90% L78)	LL(BC)	1036
	2	BK5	L78	Bus 7 (10% L78)	SLG(A)	1650			LL(BC)	996
DG2-67/65	3	BK8	L56	Bus 6 (10% L56)	SLG(A)	2330	L56	Bus 5 (90% L56)	LL(BC)	1369
		BK7	L67	Bus 6 (10% L67)	SLG(A)	2327	L67	Bus 7 (90% L67)	LL(BC)	1221
DG2-6543	4	BK14	L34	Bus 4 (10% L34)	SLG(A)	1942	L34	Bus 3 (90% L34)	LL(BC)	1235
	3	BK8	L56	Bus 6 (10% L56)	SLG(A)	2355			LL(BC)	1275
DG2-65	3	BK8	L56	Bus 6 (10% L56)	SLG(A)	2282	L56	Bus 5 (90% L56)	LL(BC)	1342
DG2-6781	3	BK7	L67	Bus 6 (10% L67)	SLG(A)	2400	L78	Bus 8 (90% L78)	LL(BC)	1088
	2	BK5	L78	Bus 7 (10% L78)	SLG(A)	1681			LL(BC)	1047
DG2-678	3	BK7	L67	Bus 6 (10% L67)	SLG(A)	2339	L78	Bus 8 (90% L78)	LL(BC)	1031
	2	BK5	L78	Bus 7 (10% L78)	SLG(A)	1639			LL(BC)	989
DG2-67	3	BK7	L67	Bus 6 (10% L67)	SLG(A)	2298	L67	Bus 7 (90% L67)	LL(BC)	1209
DG1-5678	4	BK10	L56	Bus 5 (10% L56)	SLG(A)	2350	L78	Bus 8 (90% L78)	LL(BC)	992
	3	BK7	L67	Bus 6 (10% L67)	SLG(A)	1940			LL(BC)	955
	2	BK5	L78	Bus 7 (10% L78)	SLG(A)	1453			LL(BC)	915
DG1-34/56	4	BK14	L34	Bus 4 (10% L34)	SLG(A)	2303	L34	Bus 3 (90% L34)	LL(BC)	1387
	4	BK10	L56	Bus 5 (10% L56)	SLG(A)	2306	L56	Bus 6 (90% L56)	LL(BC)	1399
DG3-2187	6	BK19	L12	Bus 2 (10% L12)	SLG(A)	2330	L78	Bus 7 (90% L78)	LL(BC)	1112
	1	BK4	L78	Bus 8 (10% L78)	SLG(A)	1671			LL(BC)	1038

[1]The DG2-6 circuit path was not included above because it did not have power lines, [2]Current fault magnitudes at relays tripped the three-pole breakers.

In order to verify minimum CTIs between backup and primary relays, current magnitudes of relay breakers at maximum faults for common protection areas (power lines) had to be collected from Tables E.1-12 of Appendix E. Maximum fault current magnitudes of relay breakers for common protection areas were located at 10% of power lines. Table 4.12 shows maximum fault current magnitudes to calculate relay times for relay-relay CTIs.

Table 4.12: Maximum fault current magnitudes of relay breakers for common power lines.

[(1)]Circuit paths (Branch) of Relays 2 and 3	Relays	Breakers	Protection areas	Maximum fault current magnitudes		
				Fault location	Fault type	Currents [A]
UTILITY-8765/1234 (UTILITY-8765)	3	BK8	L56	Bus 6 (10% L56)	DLG(BC)	2046
	2	BK6				2101
	1	BK4				2143
	2	BK6	L67	Bus 7 (10% L67)	DLG(BC)	3170
	1	BK4				3198
UTILITY-8765/1234 (UTILITY-1234)	5	BK15	L34	Bus 3 (10% L34)	DLG(BC)	2047
	6	BK18				2059
	1	BK20				2093
	6	BK18	L23	Bus 2 (10% L23)	DLG(BC)	2179
	1	BK20				2211
DG2-678/65 (DG2-678)	2	BK5	L78	Bus7 (10% L78)	SLG(A)	1650
	3	BK7				1709
DG2-6543	3	BK8	L34	Bus 4 (10% L34)	SLG(A)	1989
	4	BK14				1942
DG2-6781	2	BK5	L78	Bus7 (10% L78)	SLG(A)	1681
	3	BK7				1742
DG2-678	2	BK5	L78	Bus7 (10% L78)	SLG(A)	1639
	3	BK7				1698
DG1-5678	2	BK5	L78	Bus 8 (10% L78)	SLG(A)	1453
	3	BK7				1503
	4	BK10				1523
	3	BK7	L67	Bus 7 (10% L67)	SLG(A)	1940
	4	BK10				1950
DG3-2187	6	B19	L78	Bus 8 (10% L78)	SLG(A)	1702
	1	BK4				1671

[(1)]DG2-67/65, DG2-65, DG2-67, DG1-34/56, and DG2-6 circuit paths were not included above because they did not have common protection areas (power lines).

In order to verify minimum CTI between relays and fuses as backup and primary protections, respectively, maximum fault current magnitudes of relay breakers and fuses for

feeder busses were collected from Tables E.1-12 of Appendix E. Power World® software [10] allows calculation of faults in power line or bus locations but not load feeders. In order to calculate CTIs between relays and fuses, maximum faults were located near feeder busses (90% of power line length), and magnitudes of maximum fault currents for fuse feeders and relay breakers were considered to have the same value. Table 4.13 shows maximum fault currents magnitudes to calculate fuse and relay times and CTIs between the fuse and relay.

Table 4.13: Maximum fault current magnitudes of relay breakers and feeder fuses.

[(1)]Circuit paths of Relays 2 and 3	Relays	Breakers	Fuses	Protection areas	Maximum fault current magnitudes		
					Fault location	Fault type	[(2)]Currents [A]
UTILITY-8765/1234	3	BK8	80E	Bus 5	Bus 5 (90% L56)	DLG(BC)	1781
	2	BK6	50E	Bus 6	Bus 6 (90% L67)	DLG(BC)	2182
	1	BK4	80E	Bus 7	Bus 7 (90% L78)	DLG(BC)	3597
		BK20	50E	Bus 2	Bus 2 (90% L12)	DLG(BC)	3583
	4	BK18	50E	Bus 3	Bus 3 (90% L23)	DLG(BC)	2179
	5	BK15	65E	Bus 4	Bus 4 (90% L34)	DLG(BC)	1785
DG2-678/65	3	BK8	80E	Bus 5	Bus 5 (90% L56)	SLG(A)	2013
		BK7	80E	Bus 7	Bus 7 (90% L67)	SLG(A)	1762
	2	BK5	100E	Bus 8	Bus 8 (90% L78)	SLG(A)	1340
DG2-67/65	3	BK8	80E	Bus 5	Bus 5 (90% L56)	SLG(A)	1956
		BK7	80E	Bus 7	Bus 7 (90% L67)	SLG(A)	1680
DG2-6543	4	BK14	50E	Bus 3	Bus 3 (90% L34)	SLG(A)	1715
	3	BK8	80E	Bus 5	Bus 5 (90% L56)	SLG(A)	2022
DG2-65	3	BK8	80E	Bus 5	Bus 5 (90% L56)	SLG(A)	1928
DG2-6781	3	BK7	80E	Bus 7	Bus 7 (90% L67)	SLG(A)	1403
	2	BK5	100E	Bus 8	Bus 8 (90% L78)	SLG(A)	1373
DG2-678	3	BK7	80E	Bus 7	Bus 7 (90% L67)	SLG(A)	1364
	2	BK5	100E	Bus 8	Bus 8 (90% L78)	SLG(A)	1336
DG2-67	3	BK7	80E	Bus 7	Bus 7 (90% L67)	SLG(A)	1669
DG1-5678	4	BK10	50E	Bus 6	Bus 6 (90% L56)	SLG(A)	2051
	3	BK7	80E	Bus 7	Bus 7 (90% L67)	SLG(A)	1545
	2	BK5	100E	Bus 8	Bus 8 (90% L78)	SLG(A)	1204
DG1-34/56	4	BK14	50E	Bus 3	Bus 3 (90% L34)	SLG(A)	1995
		BK10	50E	Bus 6	Bus 6 (90% L56)	SLG(A)	2001
DG3-2187	6	BK19	65E	Bus 1	Bus 1 (90% L12)	SLG(A)	1799
	1	BK4	80E	Bus 7	Bus 7 (90% L78)	SLG(A)	1353

[(1)]The DG2-6 circuit path was not included above because it did not have available power lines, [(2)]Maximum fault currents for fuse feeder and relay breaker were considered to have the same value.

4.8 Relay settings in circuit paths

In this research, adaptive overcurrent protection of the microgrid with distributed generators was verified for Relays 2 and 3 placed on Busses 7 and 6, respectively. Therefore, adaptive overcurrent protection was developed for circuit paths corresponding to Relays 2 (Bus 7) and 3 (Bus 6), shown in Figures D.1-12 of Appendix D. In adaptive overcurrent protection, inverse time overcurrent settings of the relays were calculated for all circuit paths. The microgrid with distributed generators had six relays, and each relay controlled two breakers. Pickup overcurrent elements of the relays were enabled or disabled based on the current direction for the circuit paths. In the microgrid, MV fuses and relays were the protective devices. Although the MV fuses were placed on load feeders, the relays were placed on power line busses.

Adaptive overcurrent protection was created by the relays. In order to set inverse time overcurrent protection of the relays for each circuit path, clearing time curves of maximum ampere rating fuse on busses were plotted into Equation (4.5). Then inverse time-current curves of the relays were plotted into Equation (4.3) before selecting the *TDS* and *Ip* of relays. Therefore, verifications that relays did not trip at maximum load currents and relays tripped at maximum and minimum fault currents were observed in logarithmic time-current plots. Also, CTIs between backup and primary protective devices were calculated, verifying that CTIs of protective devices at maximum faults were less than minimum CTI (7.2 cycles). Inverse time overcurrent settings of relays for adaptive overcurrent protection in the UTILITY-8765/1234, DG2-678/65, DG2-67/65, DG2-6543, DG2-65, DG2-6781, DG2-678, DG2-67, DG1-5678, DG1-34/56, and DG2-6, DG3-2187 circuit paths are shown in Table 4.14. The pink and gray cells indicate inverse time overcurrent settings of Relays 2 and 3, respectively.

Table 4.14: Adaptive inverse time overcurrent settings of protective devices for circuit paths of Relays 2 and 3 (U3 curve and *CTR* = 200)

Busses		**1 / 8**				**7**				**6**				**5 / 4**				**3**				**2**			
MV fuses		**65E-65E / 100E**				**50E-80E**				**50E-50E**				**80E / 50E-65E**				**50E**				**50E-50E**			
Relays		**Relay 1**				**Relay 2**				**Relay 3**				**Relay 4**				**Relay 5**				**Relay 6**			
Breakers		**BK20**		**BK4**		**BK5**		**BK6**		**BK7**		**BK8**		**BK10**		**BK14**		**BK15**		**BK16**		**BK18**		**BK19**	
Overcurrent element pickup		**2**		**1**		**2**		**1**		**2**		**1**		**2**		**1**		**2**		**1**		**2**		**1**	
Time dial setting (*TDS*) Secondary overcurrent pickup (*Ip*)		***TDS***	***Ip***	***TDS***	***Ip***	***TDS***	***Ip***	***TDS***	***Ip***	***TDS***	***Ip***	***TDS***	***Ip***	***TDS***	***Ip***	***TDS***	***Ip***	***TDS***	***Ip***	***TDS***	***Ip***	***TDS***	***Ip***	***TDS***	***Ip***
Circuit paths (micro grid test modes)	**UTILITY-8765/1234** (1)	2.10	2.50	2.10	2.50			1.13	2.25			0.68	2.01					0.68	2.01			1.13	2.25		
	DG2-678/65 (2, 6, 9, 18)					0.78	1.86			1.18	1.95	0.77	1.97												
	DG2-67/65 (10, 16)									1.18	1.95	0.77	1.97												
	DG2-6543 (8)									**1.18**	**1.95**	0.77	1.97			1.50	2.00								
	DG2-65 (17)									**1.18**	**1.95**	0.77	1.97												
	DG2-6781 (3, 7, 12, 15, 20)					0.78	1.86			1.19	1.97														
	DG2-678 (11, 14, 19)					0.78	1.86			1.19	1.97														
	DG2-67 (13, 21)									0.67	1.97														
	DG1-5678 (4)					0.71	1.89			1.12	1.90			1.54	2.25										
	DG1-34/56 (5)													0.71	1.89	0.71	1.89								
	DG3-2187 (5, 8, 17, 22)			2.30	1.35																			1.22	1.46
	[(1)]DG2-6 (22)																								

MV = medium voltage, *CTR* = current transformer ratio, [(1)] DG1-34/56, DG2-6 and DG3-2187 circuit paths did not have available tripped breakers for Relays 2 and 3.
Bold *TDS* and *Ip* settings were added to minimize the number of setting groups for Relay 3, grouping DG2-6543 and DG2-6 with DG2-678/65 and DG2-67/65 circuit paths.

In order to validate settings of relays in Table 4.14, inverse time-current curves of relays and fuses (maximum ampere rating fuse on each bus) were plotted for the UTILITY-8765/1234, DG2-678/65, DG2-67/65, DG2-6543, DG2-65, DG2-6781, DG2-678, DG2-67, DG1-5678, DG1-34/56, and DG3-2187 circuit paths, verifying conditions in Table 4.15

Table 4.15: Conditions of inverse time overcurrent settings for relays.

N°	Conditions	Currents		Comments
		Analysis	Tables	
1	Relays did not trip at maximum load currents	Power flow	Table 4.10	Inverse time-current curves of relays were plotted with maximum load currents of relay breakers, verifying that relays did not trip for maximum load currents
2	Relays tripped at maximum and minimum fault currents	Fault analysis	Table 4.11	Inverse time-current curves of relays were plotted with maximum and minimum fault current of relay breakers, verifying that relays tripped for maximum and minimum fault currents.
3	Relay-relay CTIs at maximum fault currents must be less than minimum CTI		Table 4.12	CTIs between backup and primary relays at maximum fault currents were calculated, verifying that calculated CTIs were not less than the minimum CTI for RTS experiment (7.2 cycles)
4	Relay-fuse CTIs at maximum fault currents must be less than minimum CTI		Table 4.13	CTIs between relays and fuses as backup and primary protections, respectively, were calculated at maximum fault currents, verifying that calculated CTIs were not less than 7.2 cycles based on IEEE Std. 242-2001 [7].

CTI: coordination time interval, RTS: real-time simulation

Inverse time-current curves of relays for circuit paths were plotted into Equation (4.3), considering a *CTR* of 200. The *TDS* and *Ip* of relays were collected from Table 4.14. Inverse time-current curves of MV fuses in circuit paths were plotted based on fuse models represented by Equation (4.5) at maximum fuse ampere ratings (50E, 65E, 80E, and 100E) of each bus collected from Table 4.14.

In maximum load current verification of relay settings, a logarithmic time-current (vertical-horizontal) plane was plotted for each circuit path; inverse time-current curves of relays and maximum load current of breakers were compared, verifying that maximum load currents of the breakers did not intersect the inverse time-current curves of the relays, so relays did not trip at maximum load currents. Maximum load currents of breakers for circuit paths were collected from Table 4.10.

In maximum and minimum fault current verification of relay settings, inverse time-current curves of relays and fuses (maximum ampere rating fuse on each bus) were plotted for each circuit path. Also, maximum and minimum fault currents of the relay breakers were plotted, verifying that maximum and minimum fault currents of the relay breakers intersected the inverse time-current curves of the relays, so relays tripped at minimum and maximum fault currents. Maximum and minimum fault currents of relay breakers were collected from Table 4.11.

In CTI verification of primary and backup protective devices at maximum fault currents, the relay-relay and relay-fuse CTIs were calculated. CTIs between the backup and primary protective devices were estimated with Equation (4.6):

$$CTI = [T_B - T_P] \times 60 \tag{4.6}$$

where *CTI* is the calculated CTI between backup (upstream) and primary (downstream) protective devices in cycles, T_B is the calculated time of backup (upstream) protective device in seconds, and T_P is the calculated time of primary (downstream) protective device in seconds.

For the relay-relay CTI calculation, backup and primary relay times at maximum fault currents were calculated with Equation (4.3) and relay breaker currents (primary pickup fault currents) and relay settings (time dial settings and secondary overcurrent pickups) were collected

from Tables 4.12 and 4.14, respectively. Calculated relay-relay CTIs must not be less than 7.2 cycles, the minimum relay-relay CTI without breaker operating time for the RTS experiment.

For the relay-fuse CTI calculation, backup (upstream) relay times and primary (downstream) fuse clearing times at maximum fault currents were calculated with Equations (4.3) and (4.5), respectively. In order to calculate relay times, relay breaker currents (primary pickup fault currents) and relay settings (time dial settings and secondary overcurrent pickups) were collected from Tables 4.13 and 4.14, respectively. However, in order to calculate fuse clearing times, fuse currents were collected from Table 4.13. Power World® software [10] allows calculation of faults in power line or bus locations but not load feeders. In order to calculate CTIs between relays and fuses, maximum faults were located near feeder busses (90% of power line length), and magnitudes of maximum fault currents for the fuse feeder and relay breaker were considered to have the same value.

Inverse time overcurrent settings of relays in Table 4.14 were validated for the UTILITY-8765/1234, DG2-678/65, DG2-67/65, DG2-6543, DG2-65, DG2-6781, DG2-678, DG2-67, DG1-5678, DG1-34/56, and DG3-2187 circuit paths, verifying conditions in Table 4.15.

4.8.1 UTILITY-8765/1234 (Test mode 1)

The UTILITY-8765/1234 circuit path represented normal operation of the microgrid. A utility source was connected to all microgrid loads. The UTILITY-8765/1234 circuit path is shown in Figure D.1 of Appendix D. This circuit path was formed by the UTILITY-1234 and UTILITY-8765 branches. Although the UTILITY-1234 branch had the L12, L23, and L34 power lines, the UTILITY-8765 branch had the L56, L67, and L78 power lines.

In the UTILITY-1234 branch, fault overcurrents at L12, L23, and L34 power lines were cleared by Relays 1 (BK20), 6 (BK18), and 5 (BK15), respectively. Relays 1 (BK20) and 6

(BK18) were coordinated as backup and primary protection of L23 power line, respectively. Relays 6 (BK18) and 5 (BK15) were coordinated as backup and primary protection of L34 power line, respectively. Relays 1 (BK20), 6 (BK18), and 5 (BK15) were coordinated as backup protection of fuses on Busses 2, 3, and 4, respectively. In the UTILITY-8765 branch, fault overcurrents at L56, L67, and L78 power lines were cleared by Relays 3 (BK8), 2 (BK6), and 1 (BK4), respectively. Relays 1 (BK4) and 2 (BK6) were coordinated as backup and primary protection of L67 power line, respectively. Relays 2 (BK6) and 3 (BK8) were coordinated as backup and primary protection of L56 power line, respectively. Relays 1 (BK4), 2 (BK6), and 3 (BK8) were coordinated as backup protection of fuses on Buses 7, 6, and 5, respectively.

Figure 4.13 shows inverse time-current curves of relays and maximum ampere rating fuses for busses in the UTILITY-8765(A) and UTILITY-1234(B) branches versus maximum load currents of breakers. Maximum load currents of breakers were not intersected by inverse time-current curves of relays, verifying that relays did not trip to maximum load currents of breakers in the microgrid. Figure 4.14 shows inverse time-current curves of relays and maximum ampere rating fuses for busses in the UTILITY-8765(A) and UTILITY-1234(B) branches and maximum and minimum fault currents. Maximum and minimum fault currents flowing along breakers were intersected by inverse time-current curves of relays, verifying that relays tripped at fault overcurrents, thereby protecting power lines of UTILITY-8765(A) and UTILITY-1234(B) branches.

Figure 4.15 shows calculated CTIs between backup and primary protective devices at maximum fault currents for the UTILITY-8765(A) and UTILITY-1234(B) branches. The blue and pink bars represent calculated relay-relay and relay-fuse CTIs, respectively. Calculated CTIs between backup and primary protection devices at maximum fault currents were not less than 7.2

cycles. Minimum CTI of 7.2 cycles refers to the relay-relay and relay-fuse minimum CTIs based on RTS experiment (without breaker operating time) and IEEE Std. 242-2001 [7], respectively.

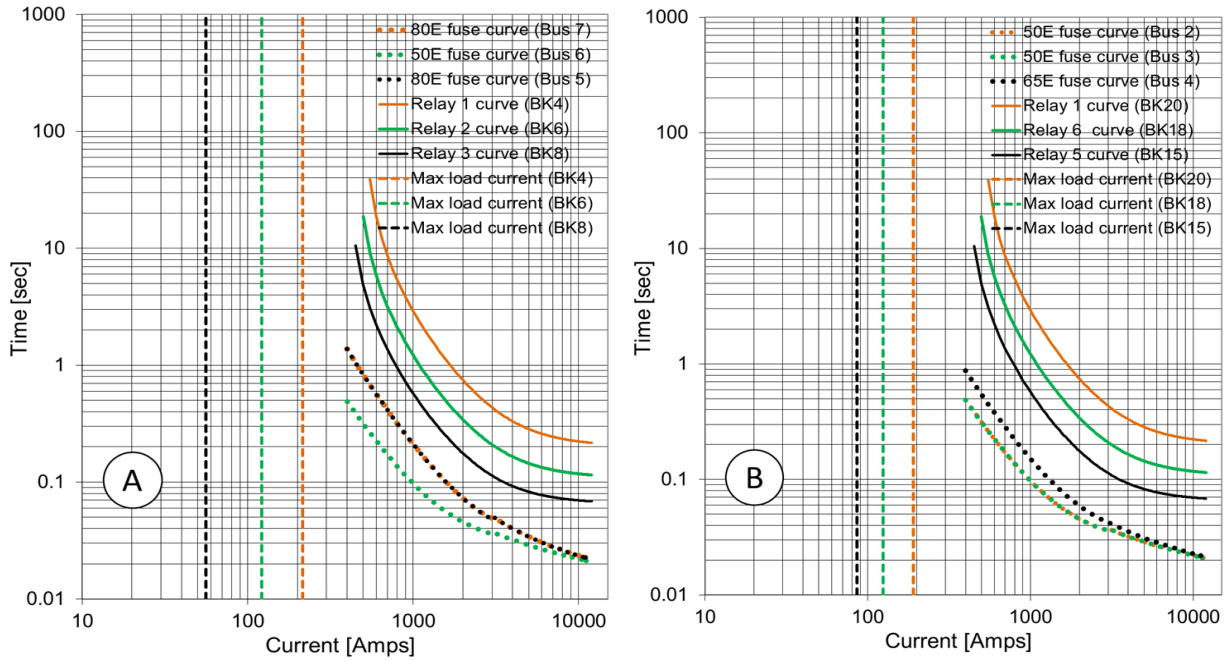

Figure 4.13: Maximum load currents versus fuse and relay curves of UTILITY-8765 (A) and UTILITY-1234 (B) branches for UTILITY-8765-1234 circuit path

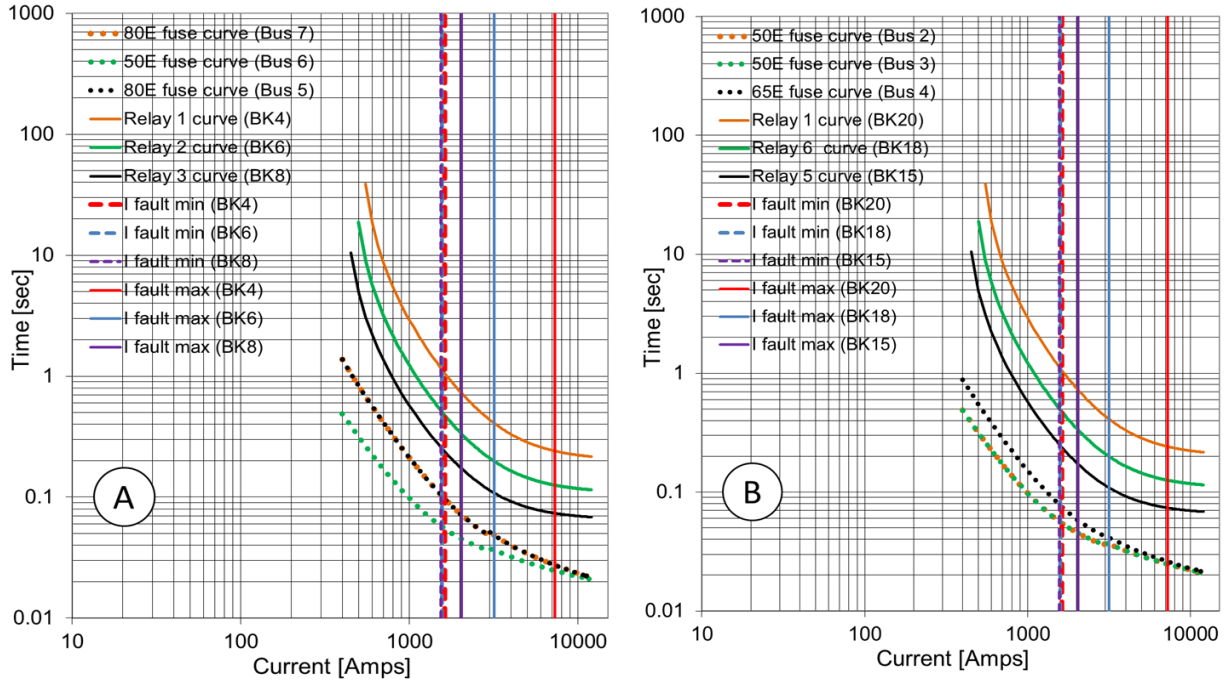

Figure 4.14: Maximum and minimum fault currents versus fuse and relay curves of UTILITY-8765 (A) and UTILITY-1234 (B) branches for UTILITY-8765/1234 circuit path

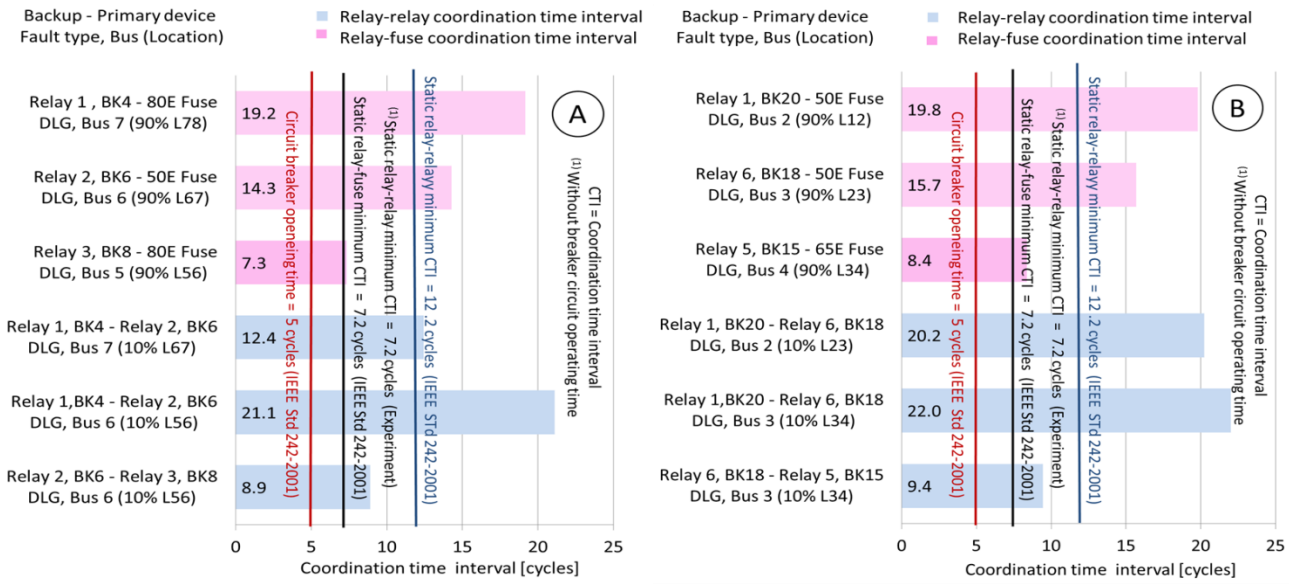

Figure 4.15: CTIs between backup and primary protections at maximum fault currents for UTILITY-8765 (A) and UTILITY-1234 (B) branches of UTILITY-8765/1234 circuit path

4.8.2 DG2-678/65 (Test modes 2, 6, 9, and 18)

The DG2-678/65 circuit path represented a non-normal operation of the microgrid; the DG2 source was connected to Busses 5, 6, 7, and 8. The DG2-678/65 circuit path is shown in Figure D.2 of Appendix D. This circuit path was formed by the DG2-678 and DG2-65 branches. Although the DG2-678 branch contained the L67 and L78 power lines, the DG2-65 branch had the L56 power line. In the DG2-678 branch, fault overcurrents at L67 and L78 power lines were cleared by Relays 3 (BK7) and 2 (BK5), respectively. Relays 3 (BK7) and 2 (BK5) were coordinated as backup and primary protection of the L78 power line, respectively. Relays 3 (BK7) and 2 (BK5) were coordinated as backup protection of fuses on Busses 7 and 8, respectively. In the DG2-65 branch, fault overcurrents at L56 power lines were cleared by Relay 3 (BK8). Relay 3 (BK8) was coordinated as backup protection of fuses on Bus 5.

Figure 4.16 shows inverse time-current curves of relays and maximum ampere rating fuses for busses in the DG2-678(A) and DG2-65(B) branches versus maximum load currents of breakers. Maximum load currents of breakers were not intersected by inverse time-current curves

of relays, verifying that the relays did not trip to maximum load currents of breakers in the microgrid.

Figure 4.17 shows inverse time-current curves of relays and maximum ampere rating fuses for busses in the DG2-678(A) and DG2-65(B) branches versus maximum and minimum fault currents. Maximum and minimum fault currents flowing along breakers were intersected by the inverse time-current curves of relays, verifying that the relays tripped at fault overcurrents, thereby protecting power lines of the DG2-678(A) and DG2-65(B) branches.

Figure 4.18 shows calculated CTIs between backup and primary protective devices at maximum fault currents for the DG2-678/65 circuit path. The blue and pink bars represent the calculated relay-relay and relay-fuse CTIs, respectively. Calculated CTIs between backup and primary protection devices at maximum fault currents were not less than 7.2 cycles. Minimum CTI of 7.2 cycles refers to the relay-relay and relay-fuse minimum CTIs based on RTS experiment (without breaker operating time) and IEEE Std. 242-2001 [7], respectively.

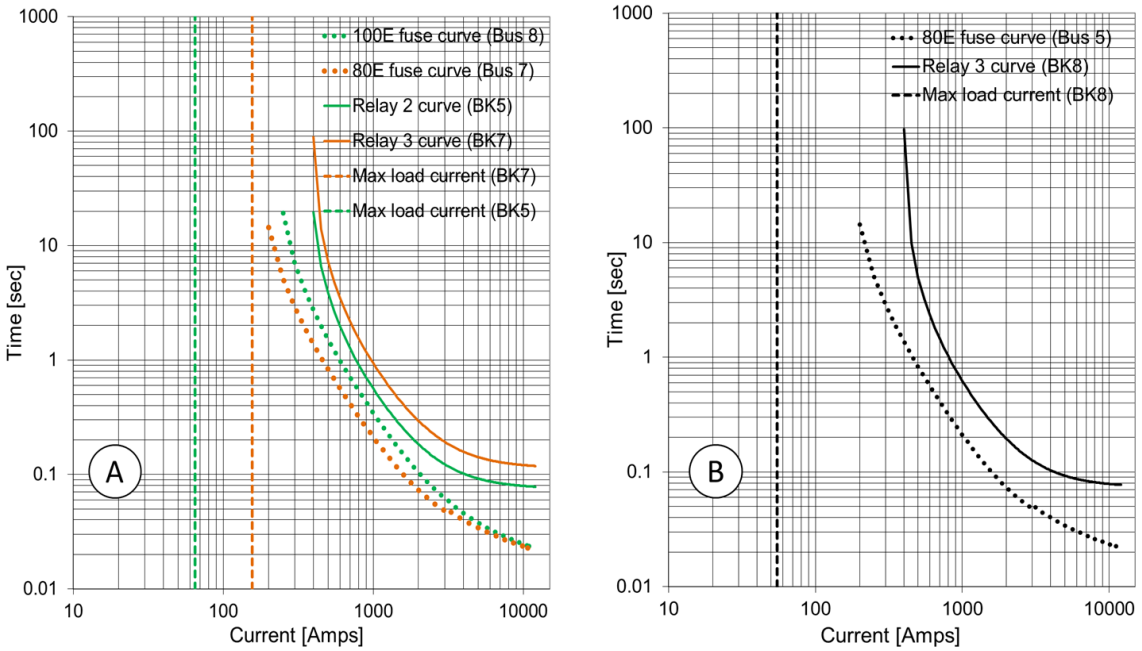

Figure 4.16: Maximum load currents versus fuse and relay curves of DG2-678 (A) and DG2-65 (B) branches for DG2-678/65 circuit path

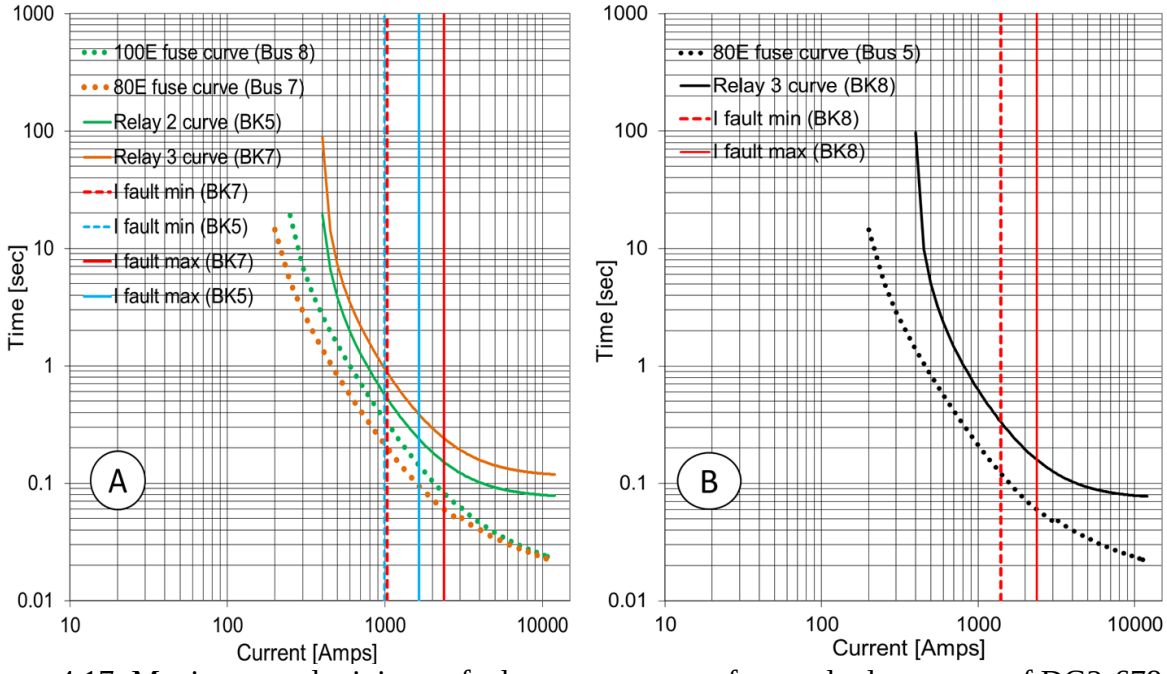

Figure 4.17: Maximum and minimum fault currents versus fuse and relay curves of DG2-678 (A) and DG2-65 (B) branches for DG2-678/65 circuit path

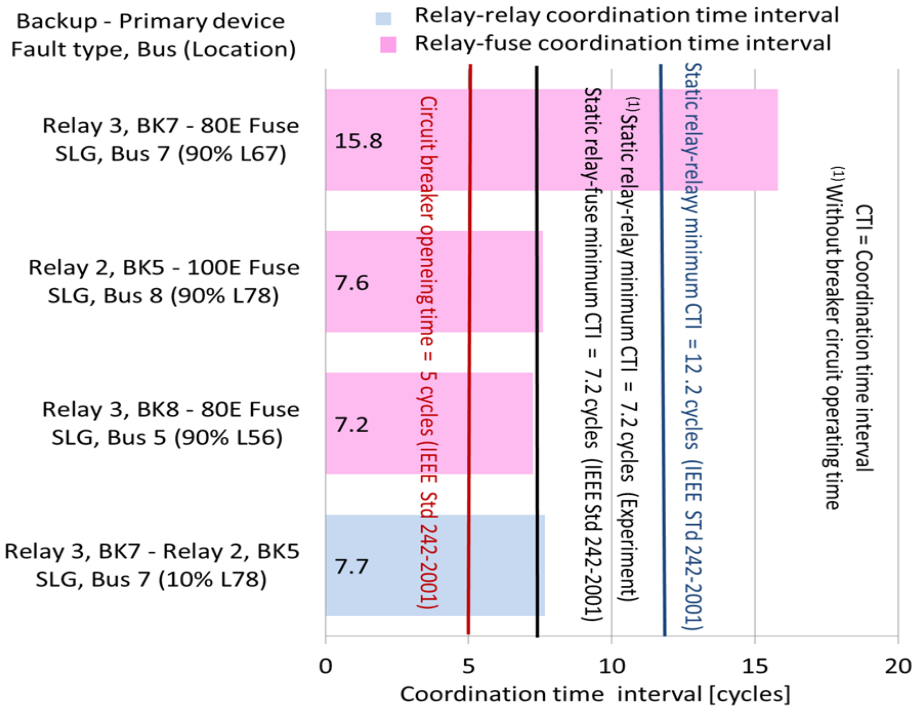

Figure 4.18: CTIs between backup and primary protections at maximum fault currents for DG2-678/65 circuit path

4.8.3 DG2-67/65 (Test modes 10 and 16)

The DG2-67/65 circuit path represented a non-normal operation of the microgrid. The DG2 source was connected to Busses 5, 6, and 7. The DG2-67/65 circuit path, formed by the DG2-67 and DG2-65 branches, is shown in Figure D.3 of Appendix D. The DG2-67 and DG2-65 branches had the L67 and L56 power lines, respectively. In the DG2-67 branch, fault overcurrents at L67 power lines were cleared by Relay 3 (BK7). Relay 3 (BK7) was coordinated as backup protection of fuses on Bus 7. In the DG2-65 branch, fault overcurrents at L56 power lines were cleared by Relay 3 (BK8). Relay 3 (BK8) was coordinated as backup protection of fuses on Bus 5.

Figure 4.19 shows inverse time-current curves of relay and maximum ampere rating fuses for busses in the DG2-67(A) and DG2-65(B) branches versus maximum load currents of breakers. Maximum load currents of breakers were not intersected by inverse time-current curves of the relay, verifying that the relay did not trip to maximum load currents of breakers in the microgrid.

Figure 4.20 shows inverse time-current curves of relay and maximum fuse for the DG2-67 (A) and DG2-65 (B) branches versus maximum and minimum fault currents. Maximum and minimum fault currents flowing along breakers were intersected by inverse time-current curves of the relay, verifying that the relay tripped at fault overcurrents, thereby protecting power lines of the DG2-67(A) and DG2-65(B) branches.

Figure 4.21 shows calculated CTIs between backup and primary protective devices at maximum fault currents for the DG2-67/65 circuit path. The pink bars represent calculated relay-fuse CTIs. Calculated CTIs between backup and primary protection devices at maximum fault

currents were not less than 7.2 cycles; the relay-fuse minimum CTIs were based on IEEE Std. 242-2001 [7].

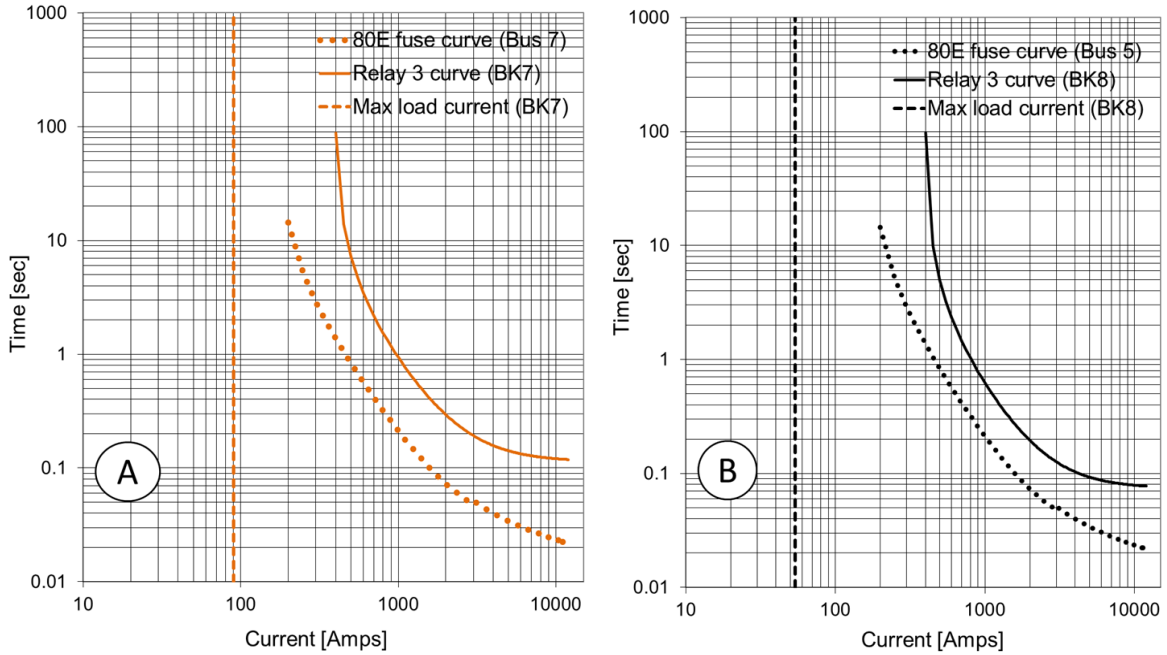

Figure 4.19: Maximum load currents versus fuse and relay curves of curves of DG2-67 (A) and DG2-65 (B) branches for DG2-67/65 circuit path

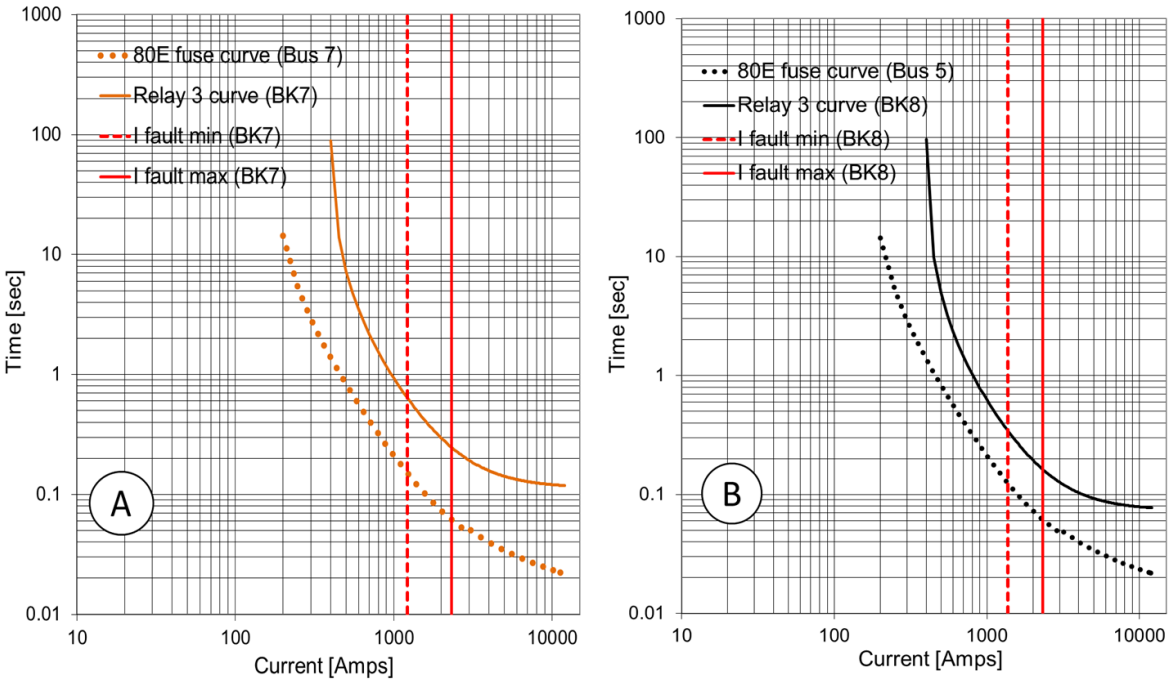

Figure 4.20: Maximum and minimum fault currents versus fuse and relay curves of curves of DG2-67 (A) and DG2-65 (B) branches for DG2-67/65 circuit path

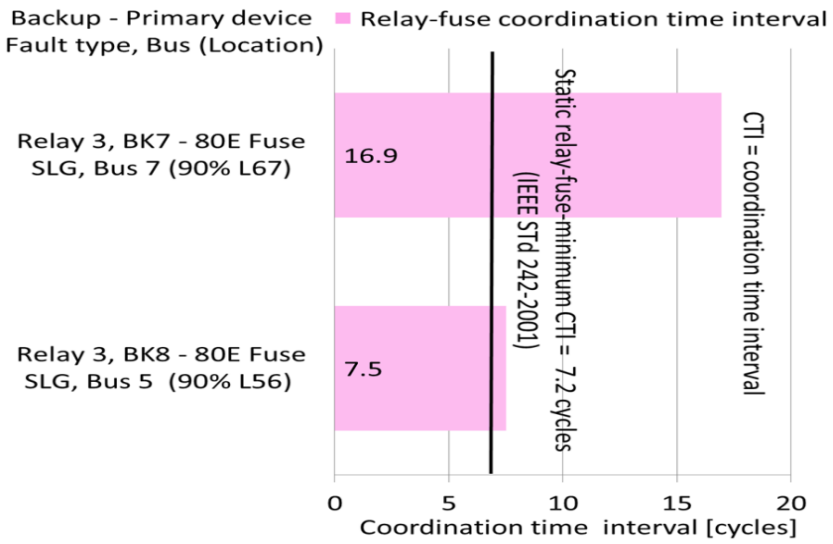

Figure 4.21: CTIs between backup and primary protections at maximum fault currents for DG2-67/65 circuit path

4.8.4 DG2-6543 (Test mode 8)

The DG2-6543 circuit path represented a non-normal operation of the microgrid. The DG2 source was connected to Busses 3, 4, 5, and 6. The DG2-6543 circuit path is shown in Figure D.4 of Appendix D. This circuit path had one branch (DG2-6543) formed by the L56 and L34 power lines. In the DG2-6543 branch, fault overcurrents at L56 and L34 power lines were cleared by Relays 3 (BK8) and 4 (BK14), respectively. Relays 3 (BK8) and 4 (BK14) were coordinated as backup and primary protection of the L34 power line and were coordinated as backup protection of fuses on Busses 5-4 and 3, respectively.

Figure 4.22 (A) shows inverse time-current curves of relays and maximum ampere rating fuses for busses in the DG2-6543 branch versus maximum load currents of breakers. Maximum load currents of breakers were not intersected by inverse time-current curves of relays, verifying that the relays did not trip to maximum load currents of breakers in the microgrid.

Figure 4.22 (B) shows inverse time-current curves of relays and maximum ampere rating fuses for busses in the DG2-6543 branch versus maximum and minimum fault currents. Maximum and minimum fault currents flowing along breakers were intersected by inverse time-

current curves of relays, verifying that the relays tripped at fault overcurrents, thereby protecting power lines of the DG2-6543 branch.

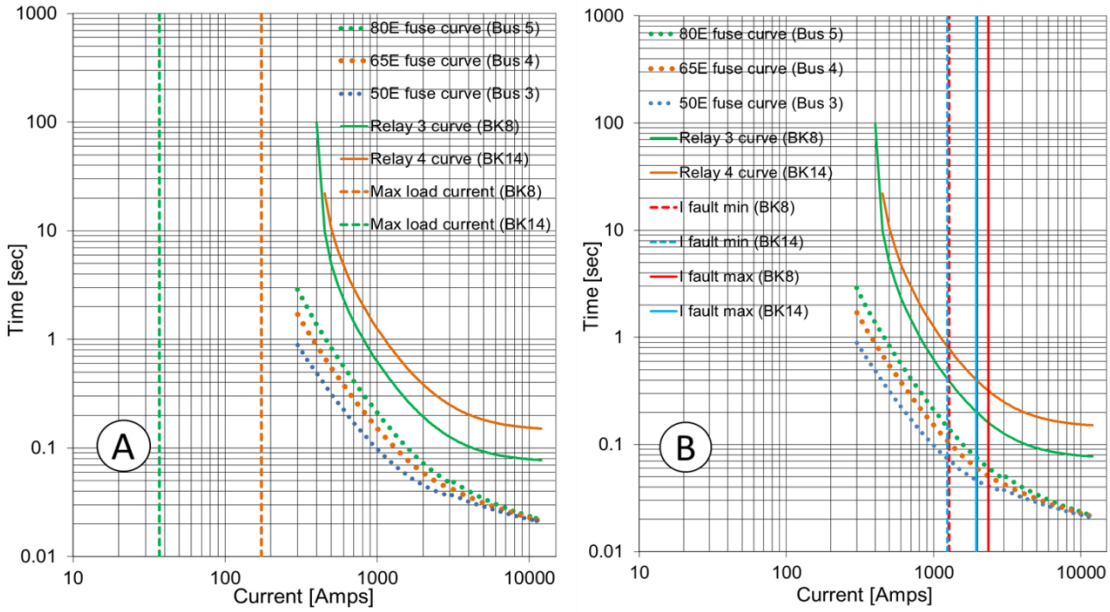

Figure 4.22: Maximum load (A), maximum and minimum fault currents (B) versus fuse and relay curves of DG2-6543 circuit path

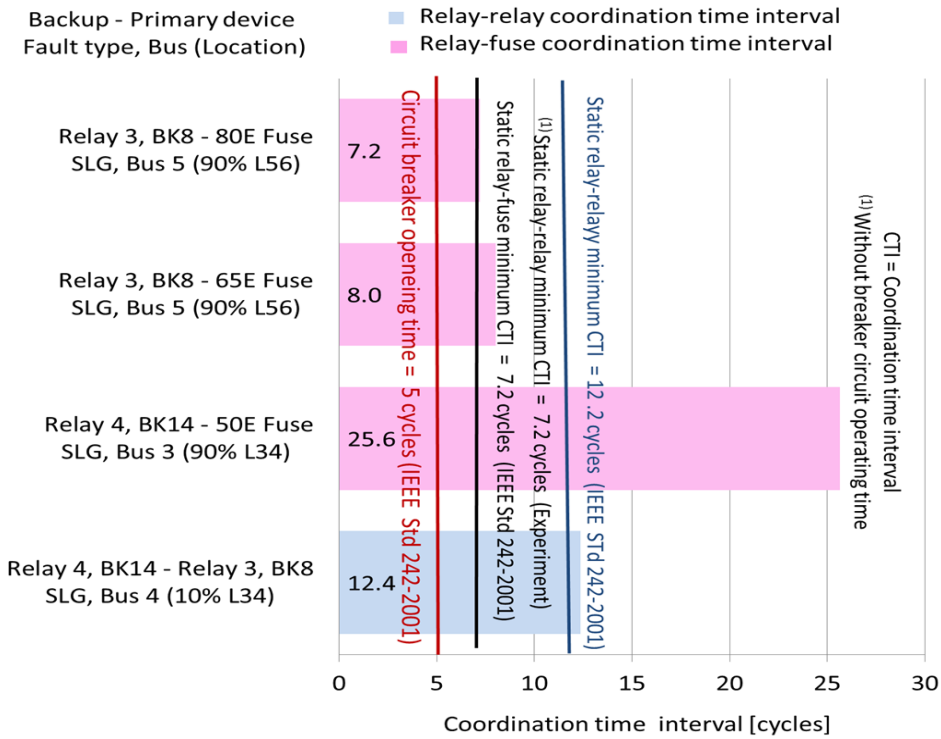

Figure 4.23: CTIs between backup and primary protections at maximum fault currents for DG2-6543 circuit path

Figure 4.23 shows calculated CTIs between backup and primary protective devices at maximum fault currents for the DG2-6543 circuit path. The blue and pink bars represent the calculated relay-relay and relay-fuse CTIs, respectively. Calculated CTIs between backup and primary protection devices at maximum fault currents were not less than 7.2 cycles. Minimum CTI of 7.2 cycles refers to the relay-relay and relay-fuse minimum CTIs based on RTS experiment (without breaker operating time) and IEEE Std. 242-2001 [7], respectively.

4.8.5 DG2-65 (Test mode 17)

The DG2-65 circuit path represented a non-normal operation of the microgrid. The DG2 source was connected to Busses 5 and 6. The DG2-65 circuit path is shown in Figure D.5 of Appendix D. This circuit path had one branch (DG2-65) formed by the L56 power line. In the DG2-65 branch, fault overcurrents at the L56 power line were cleared by Relay 3 (BK8). Relay 3 (BK8) was coordinated as a backup protection of fuses on Bus 5.

Figure 4.24 (A) shows the inverse time-current curve of the relay and maximum ampere rating fuse for busses in the DG2-65 branch versus maximum load currents of the breakers. Maximum load currents of the breakers were not intersected by the inverse time-current curves of the relay, verifying that the relay did not trip to maximum load currents of breakers in the microgrid. Figure 4.24 (B) shows inverse time-current curves of the relay and maximum ampere rating fuse for busses in the DG2-65 branch versus maximum and minimum fault currents. Maximum and minimum fault currents flowing along breakers were intersected by inverse time-current curves of the relay, verifying that the relay tripped at fault overcurrents, thereby protecting the power line of the DG2-65 branch.

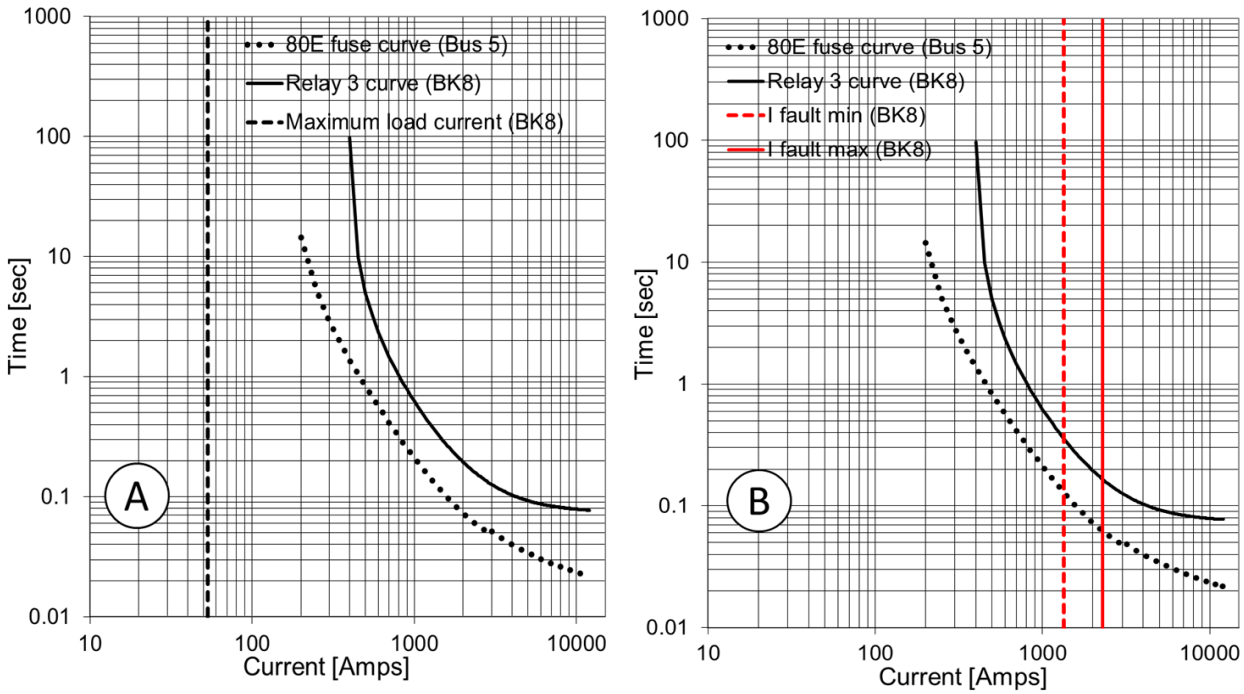

Figure 4.24: Maximum load (A), maximum and minimum fault currents (B) versus fuse and relay curves of DG2-65 circuit path

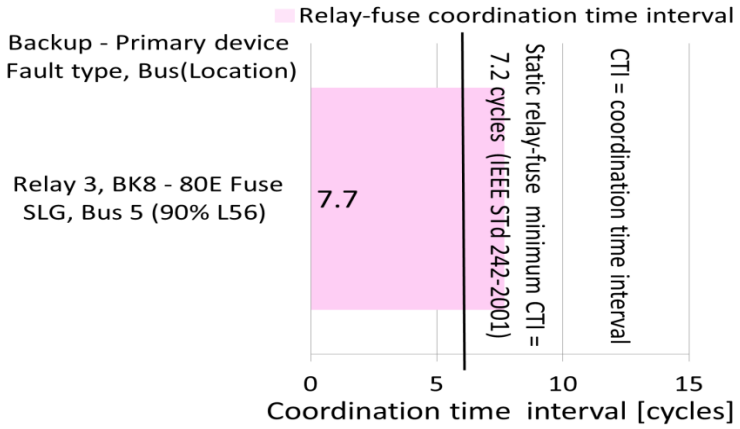

Figure 4.25: CTIs between backup and primary protections at maximum fault currents for DG2-65 circuit path

Figure 4.25 shows calculated CTIs between backup and primary protective devices at maximum fault currents for the DG2-65 circuit path. The pink bars represent the calculated relay-fuse CTIs. Calculated CTIs between backup and primary protection devices at maximum fault currents were not less than 7.2 cycles, the relay-fuse minimum CTIs based on IEEE Std. 242-2001 [7].

4.8.6 DG2-6781 (Test modes 3, 7, 12, 15, and 20)

The DG2-6781 circuit path represented a non-normal operation of the microgrid. The DG2 source was connected to Busses 6, 7, 8, and 1. The DG2-6781 circuit path is shown in Figure D.6 of Appendix D. This circuit path had one branch (DG2-6781) formed by the L67 and L78 power lines. In the DG2-6781 branch, fault overcurrents at L67 and L78 power lines were cleared by Relays 3 (BK7) and 2 (BK5), respectively. Relays 3 (BK7) and 2 (BK5) were coordinated as backup and primary protection of the L78 power line, respectively. Relays 3 (BK7) and 2 (BK5) were coordinated as backup protection of fuses on Busses 7 and 8-1, respectively.

Figure 4.26 (A) shows inverse time-current curves of relays and maximum ampere rating fuses for busses in the DG2-6781 branch versus maximum load currents of breakers. Maximum load currents of breakers were not intersected by inverse time-current curves of relays, verifying that the relays did not trip to maximum load currents of breakers in the microgrid. Figure 4.26 (B) shows inverse time-current curves of relays and maximum ampere rating fuses for busses in the DG2-6781 branch and maximum and minimum fault currents. Maximum and minimum fault currents flowing along breakers were intersected by inverse time-current curves of relays, verifying that the relays tripped at fault overcurrents, thereby protecting power lines of the DG2-6781 branch.

Figure 4.27 shows calculated CTIs between backup and primary protective devices at maximum fault currents for the DG2-6781 circuit path. The blue and pink bars represent the calculated relay-relay and relay-fuse CTIs, respectively. Calculated CTIs between backup and primary protection devices at maximum fault currents were not less than 7.2 cycles. Minimum

CTI of 7.2 cycles refers to the relay-relay and relay-fuse minimum CTIs based on RTS experiment (without breaker operating time) and IEEE Std. 242-2001 [7], respectively.

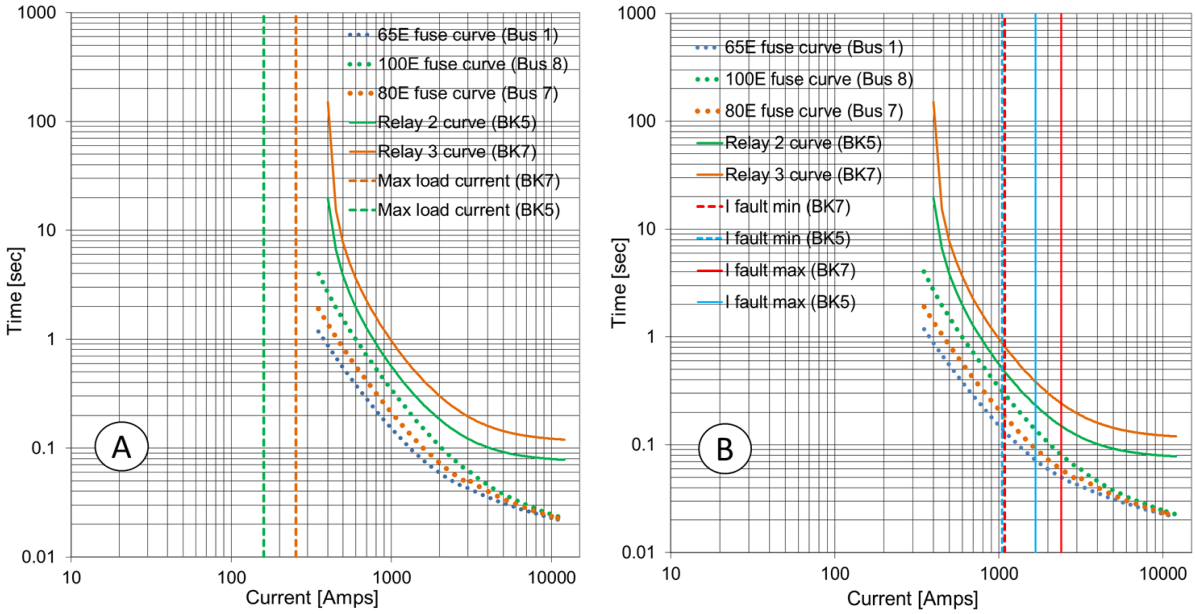

Figure 4.26: Maximum load (A), maximum and minimum fault currents (B) versus fuse and relay curves of DG2-6781 circuit path

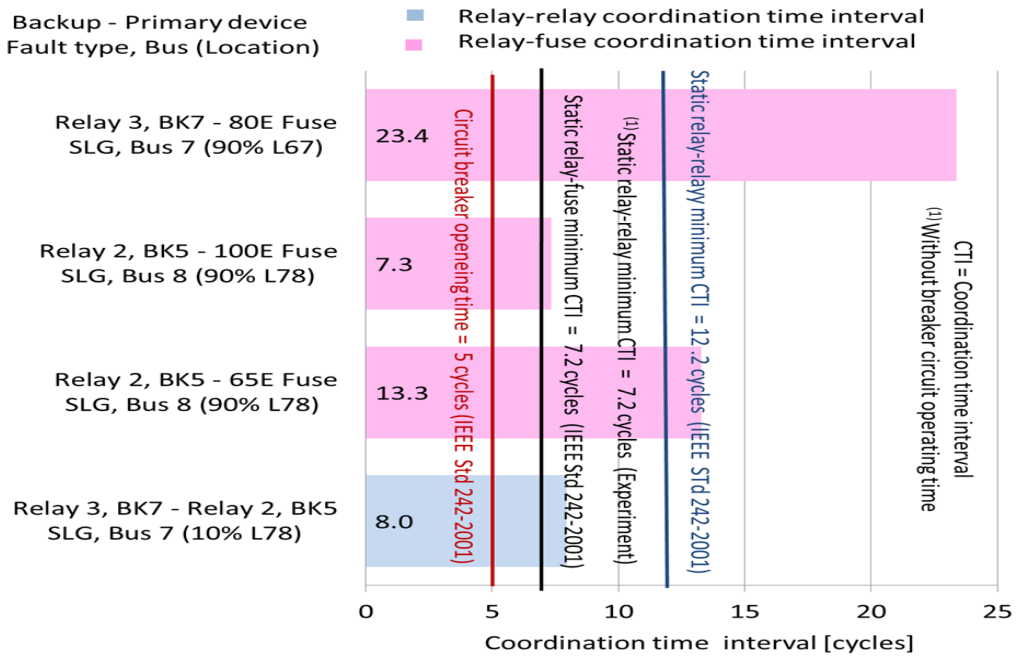

Figure 4.27: CTIs between backup and primary protections at maximum fault currents for DG2-6781 circuit path

4.8.7 DG2-678 (Test modes 11, 14, and 19)

The DG2-678 circuit path represented a non-normal operation of the microgrid. The DG2 source was connected to Busses 6, 7, and 8. The DG2-678 circuit path is shown in Figure D.7 of Appendix D. This circuit path had one branch (DG2-678) formed by the L67 and L78 power lines. In the DG2-678 branch, fault overcurrents at L67 and L78 power lines were cleared by Relays 3 (BK7) and 2 (BK5), respectively. Relays 3 (BK7) and 2 (BK5) were coordinated as backup and primary protection of the L78 power line, respectively. Relays 3 (BK7) and 2 (BK5) were coordinated as backup protection of fuses on Busses 7 and 8, respectively.

Figure 4.28 (A) shows inverse time-current curves of relays and maximum ampere rating fuses for busses in the DG2-678 branch versus maximum load currents of breakers. Maximum load currents of breakers were not intersected by inverse time-current curves of relays, verifying that the relays did not trip to maximum load currents of breakers in the microgrid. Figure 4.28 (B) shows inverse time-current curves of relays and maximum ampere rating fuses for busses in the DG2-678 branch versus maximum and minimum fault currents. Maximum and minimum fault currents flowing along breakers were intersected by inverse time-current curves of relays, verifying that the relays tripped at fault overcurrents, thereby protecting power lines of the DG2-678 branch.

Figure 4.29 shows calculated CTIs between backup and primary protective devices at maximum fault currents for the DG2-6781 circuit path. The blue and pink bars represent the calculated relay-relay and relay-fuse CTIs, respectively. Calculated CTIs between backup and primary protection devices at maximum fault currents were not less than 7.2 cycles. Minimum CTI of 7.2 cycles refers to the relay-relay and relay-fuse minimum CTIs based on RTS experiment (without breaker operating time) and IEEE Std. 242-2001 [7], respectively

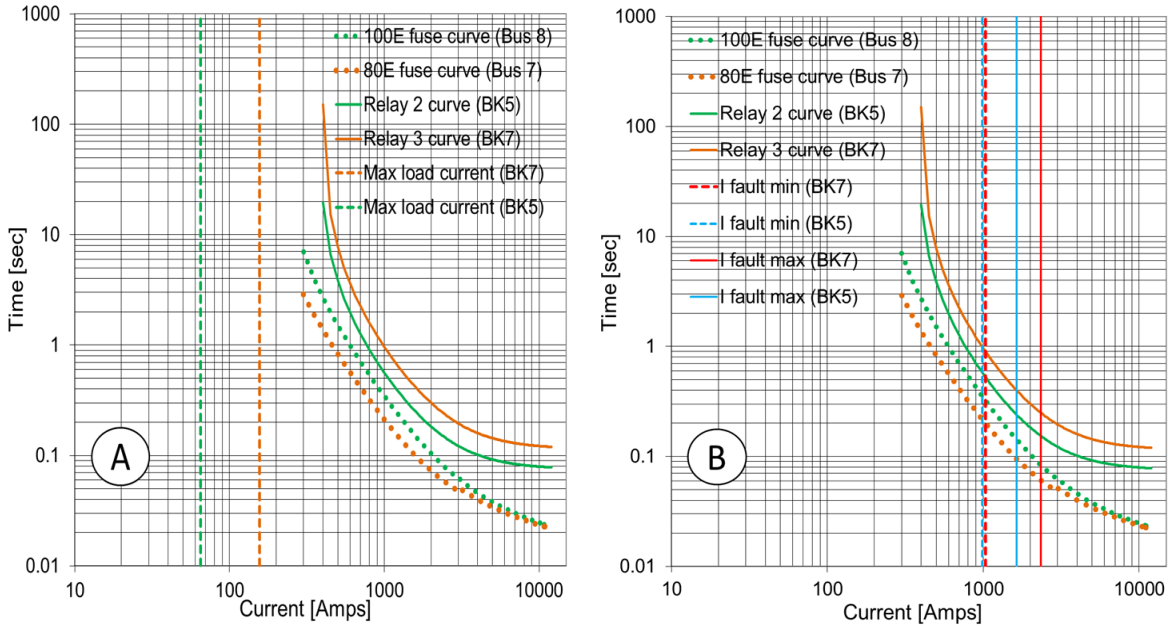

Figure 4.28: Maximum load (A), maximum and minimum fault currents (B) versus fuse and relay curves of DG2-678 circuit path

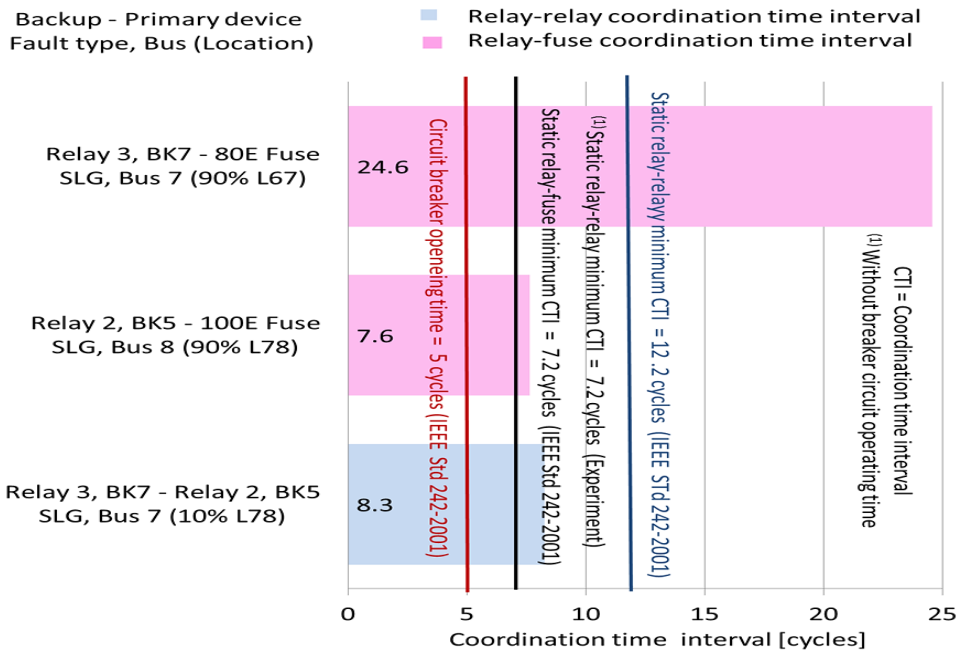

Figure 4.29: CTIs between backup and primary protections at maximum fault currents for DG2-678 circuit path

4.8.8 DG2-67 (Test modes 13 and 21)

The DG2-67 circuit path represented a non-normal operation of the microgrid. The DG2 source was connected to Busses 6 and 7. The DG2-67 circuit path is shown in Figure D.8 of

Appendix D. This circuit path had one branch (DG2-67) formed by the L67 power line. In the DG2-67 branch, fault overcurrents at the L67 power line were cleared by Relay 3 (BK7). Relay 3 (BK7) was coordinated as a backup protection of fuses on Bus 7.

Figure 4.30 (A) shows inverse time-current curves of the relay and maximum ampere rating fuse for busses in the DG2-67 branch versus maximum load current of breakers. Maximum load current of breakers was not intersected by the inverse time-current curve of relay, verifying that the relay did not trip to maximum load current of breakers in the microgrid. Figure 4.30 (B) shows inverse time-current curves of the relay and maximum ampere rating fuses for busses in the DG2-67 branch versus maximum and minimum fault currents. Maximum and minimum fault currents flowing along breakers were intersected by the inverse time-current curve of the relay, verifying that the relay tripped at fault overcurrents, thereby protecting power lines of the DG2-67 branch.

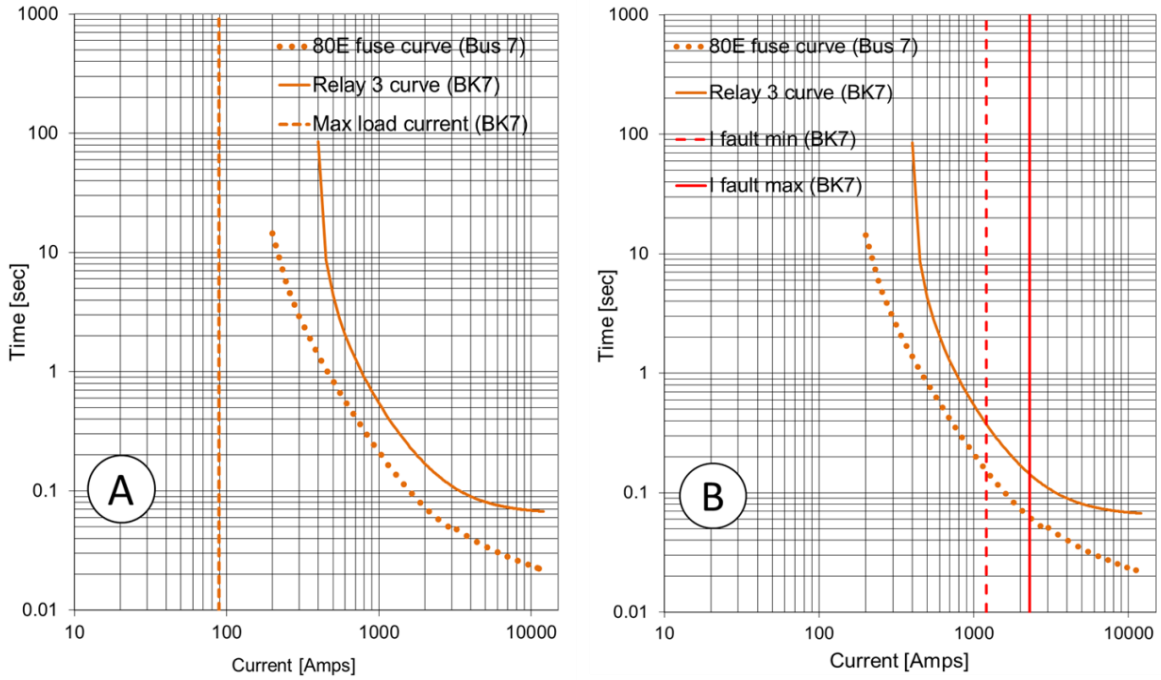

Figure 4.30: Maximum load (A), maximum and minimum fault currents (B) versus fuse and relay curves of DG2-67 circuit path

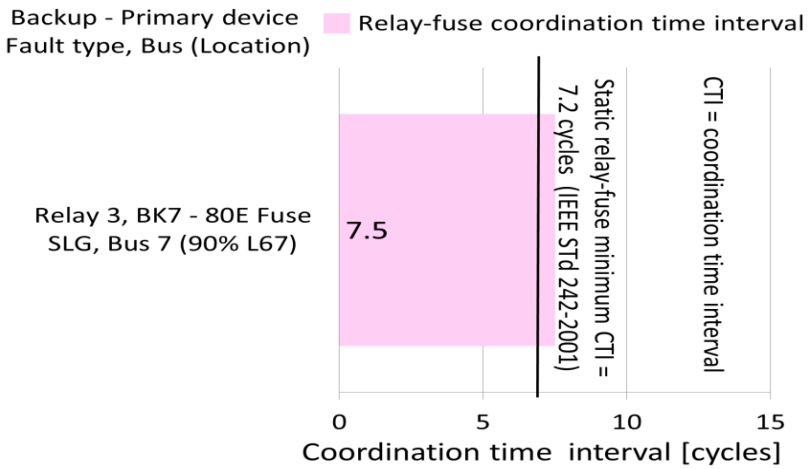

Figure 4.31: CTIs between backup and primary protections at maximum fault currents for DG2-67 circuit path

Figure 4.31 shows calculated CTIs between backup and primary protective devices at maximum fault currents for the DG2-67 circuit path. The pink bars represent the calculated relay-fuse CTIs. Calculated CTIs between backup and primary protection devices at maximum fault currents were not less than 7.2 cycles, the relay-fuse minimum CTIs based on IEEE Std. 242-2001 [7].

4.8.9 DG1-5678 (Test mode 4)

The DG1-5678 circuit path represented a non-normal operation of the microgrid. The DG1 source was connected to Busses 5, 6, 7, and 8. The DG1-5678 circuit path is shown in Figure D.9 of Appendix D. This circuit path had one branch (DG1-5678) formed by the L56, L67, and L78 power lines. In the DG1-5678 branch, fault overcurrents at L56, L67, and L78 power lines were cleared by Relays 4 (BK10), 3 (BK7), and 2 (BK5), respectively. Relays 4 (BK10) and 3 (BK7) were coordinated as backup and primary protection of the L67 power line, and Relays 3 (BK7) and 2 (BK5) were coordinated as backup and primary protection of the L78 power line. Relays 4 (BK10), 3 (BK7), and 2 (BK5) were coordinated as backup protection of fuses on Busses 6, 7, and 8, respectively.

Figure 4.32 (A) shows inverse time-current curves of relays and maximum ampere rating fuses for busses in the DG1-5678 branch versus maximum load currents of breakers. Maximum load currents of breakers were not intersected by inverse time-current curves of relays, verifying that the relays did not trip to maximum load currents of breakers in the microgrid. Figure 4.32 (B) shows inverse time-current curves of relays and maximum ampere rating fuses for busses in the DG1-5678 branch versus maximum and minimum fault currents. Maximum and minimum fault currents flowing along breakers were intersected by inverse time-current curves of relays, verifying that the relays tripped at fault overcurrents, thereby protecting power lines of the DG1-5678 branch.

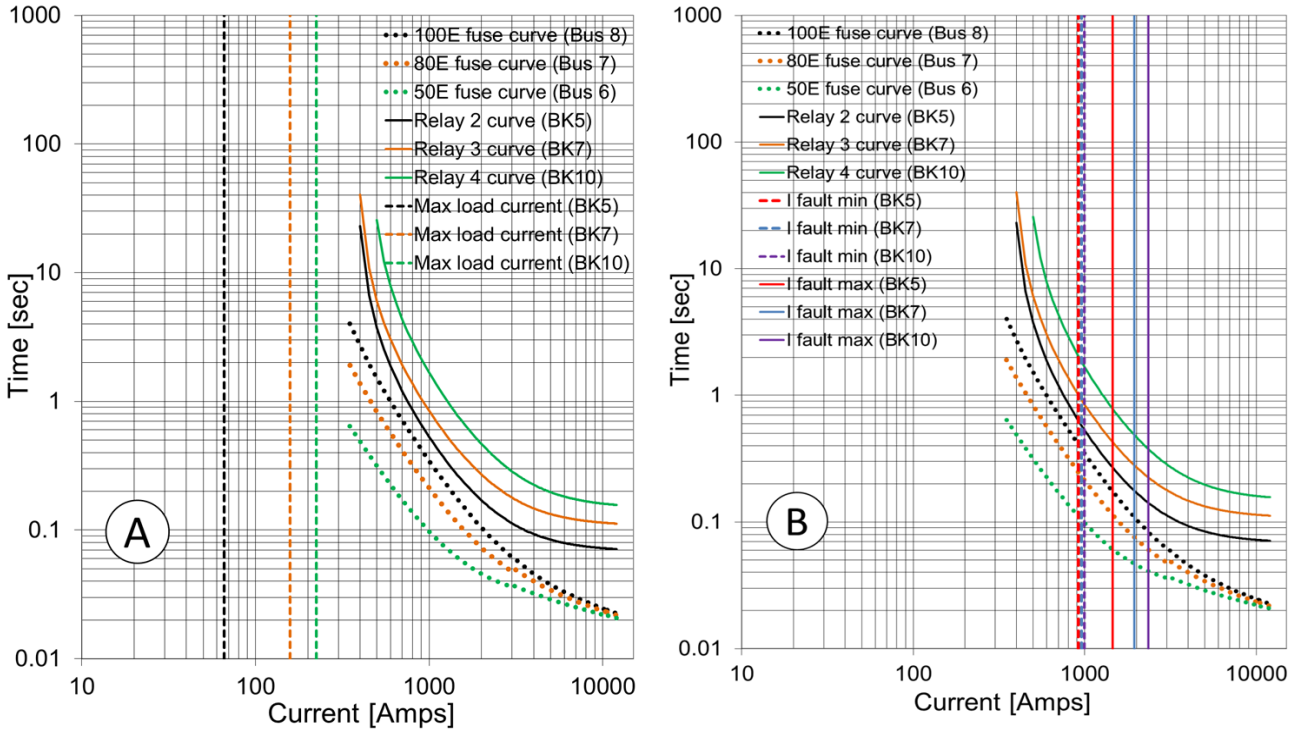

Figure 4.32: Maximum load (A), maximum and minimum fault currents (B) versus fuse and relay curves of DG1-5678 circuit path

Figure 4.33 shows calculated CTIs between backup and primary protective devices at maximum fault currents for the DG1-5678 circuit path. The blue and pink bars represent the

calculated relay-relay and relay-fuse CTIs, respectively. Calculated CTIs between backup and primary protection devices at maximum fault currents were not less than 7.2 cycles. Minimum CTI of 7.2 cycles refers to the relay-relay and relay-fuse minimum CTIs based on RTS experiment (without breaker operating time) and IEEE Std. 242-2001 [7], respectively.

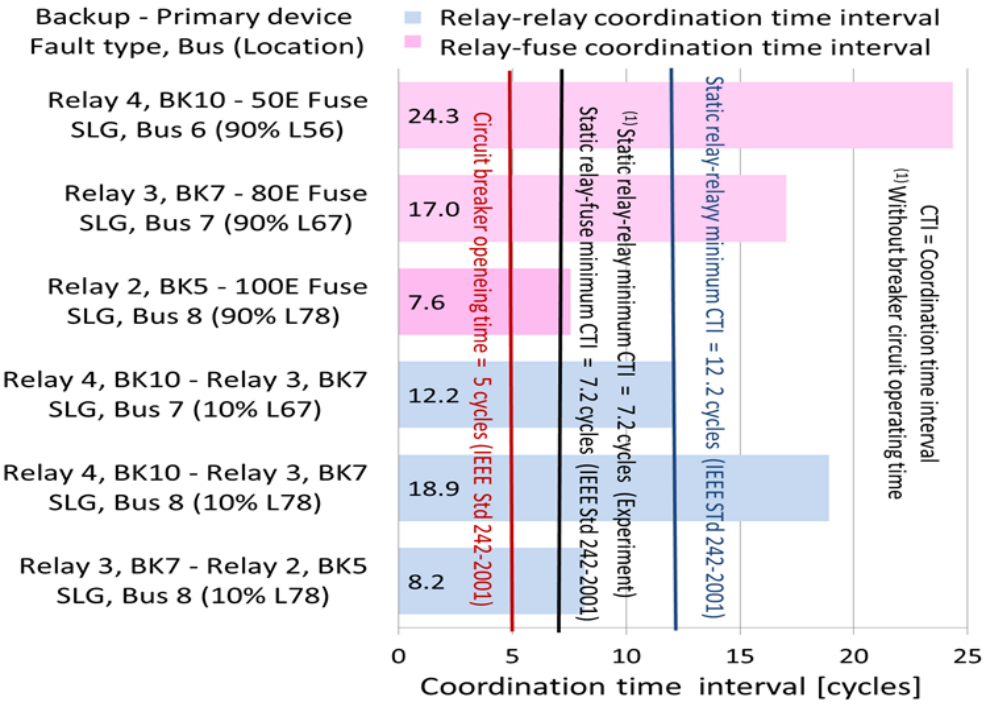

Figure 4.33: CTIs between backup and primary protections at maximum fault currents for DG1-5678 circuit path

4.8.10 DG1-34/56 (Test mode 5)

The DG1-34/56 circuit path represented a non-normal operation of the microgrid. The DG1 source was connected to Busses 3, 4, 5, and 6. The DG1-34/56 circuit path is shown in Figure D.10 of Appendix D. This circuit path was formed by the DG1-34 and DG1-56 branches that had the L34 and L56 power lines, respectively. In the DG1-34 branch, fault overcurrents at the L34 power line were cleared by Relay 4 (BK14). Relay 4 (BK14) was coordinated as backup protection of fuses on Bus 3. In the DG1-56 branch, fault overcurrents at L56 power lines were

cleared by Relay 4 (BK10). Relay 4 (BK10) was coordinated as backup protection of fuses on Bus 6.

Figure 4.34 shows inverse time-current curves of relay and maximum ampere rating fuses for busses in the DG1-34(A) and DG1-56(B) branches versus maximum load currents of breakers. Maximum load currents of breakers were not intersected by inverse time-current curves of relay, verifying that the relay did not trip to maximum load currents of breakers in the microgrid.

Figure 4.35 shows inverse time-current curves of relay and maximum ampere rating fuses for busses in the DG1-34 (A) and DG1-56 (B) branches versus maximum and minimum fault currents. Maximum and minimum fault currents flowing along breakers were intersected by inverse time-current curves of relay, verifying that the relay tripped at fault overcurrents, thereby protecting power lines of the DG1-34(A) and DG1-56 (B) branches.

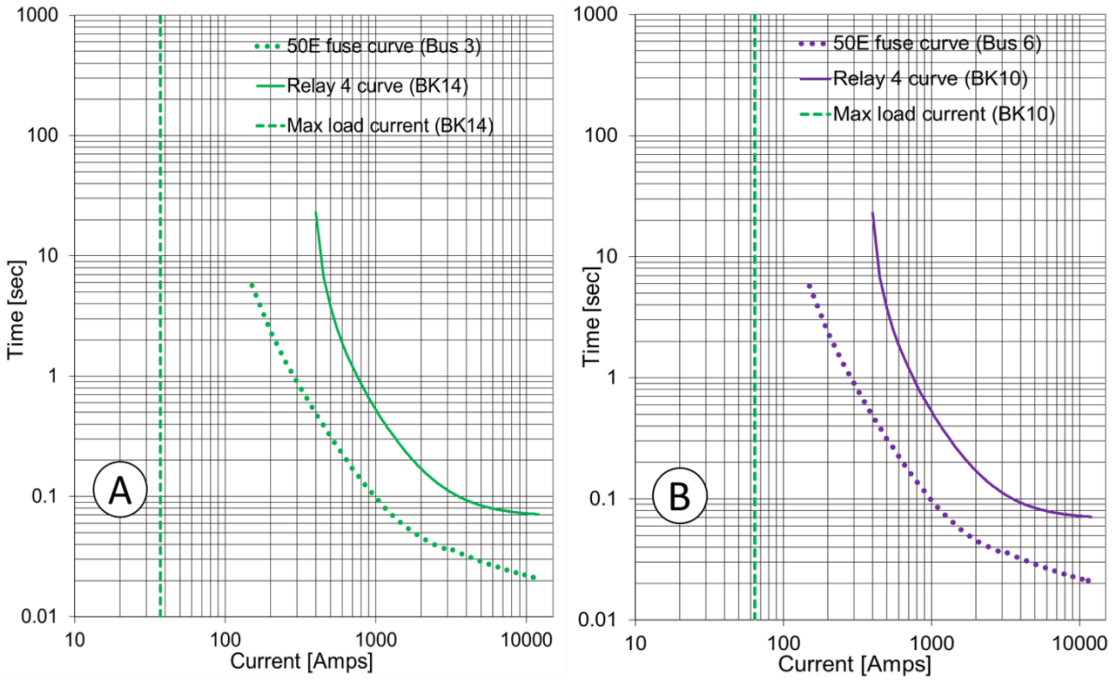

Figure 4.34: Maximum load versus fuse and relay curves of DG1-34 (A) and DG1-56 (B) branches for DG1-34/56 circuit path

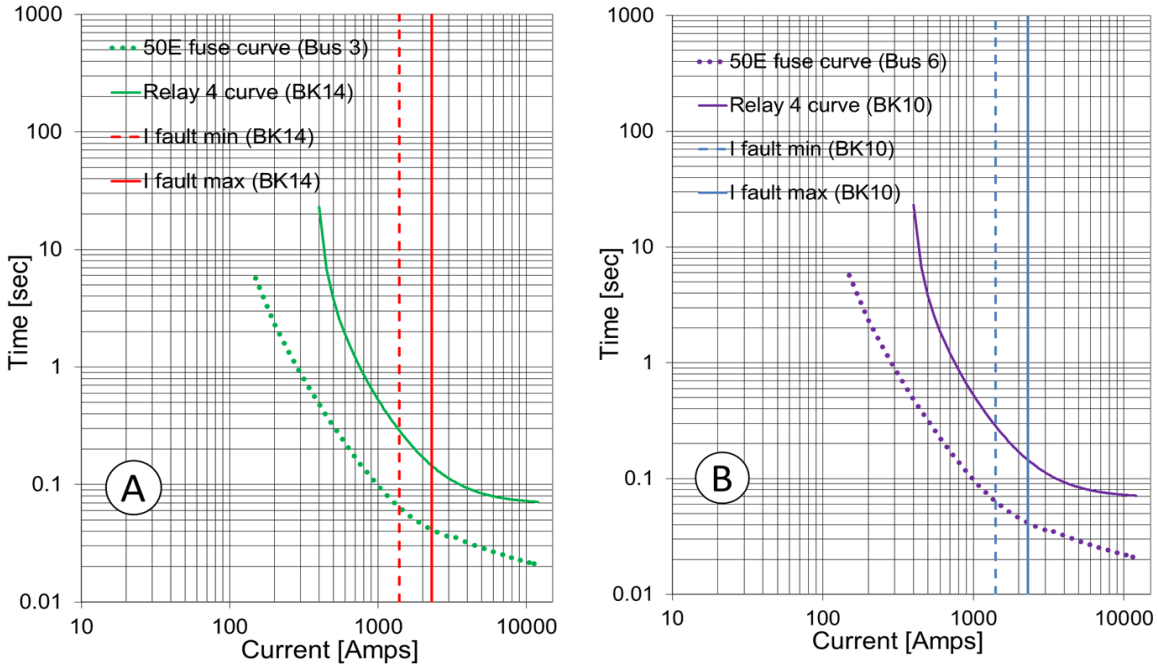

Figure 4.35: Maximum and minimum fault currents versus fuse and relay curves of DG1-34 (A) and DG1-56 (B) branches for DG1-34/56 circuit path

Figure 4.36 shows calculated CTIs between backup and primary protective devices at maximum fault currents for the DG1-34/56 circuit path. The pink bars represent the calculated relay-fuse CTIs. Calculated CTIs between backup and primary protection devices at maximum fault currents were not less than 7.2 cycles, the relay-fuse minimum CTIs based on IEEE Std. 242-2001 [7].

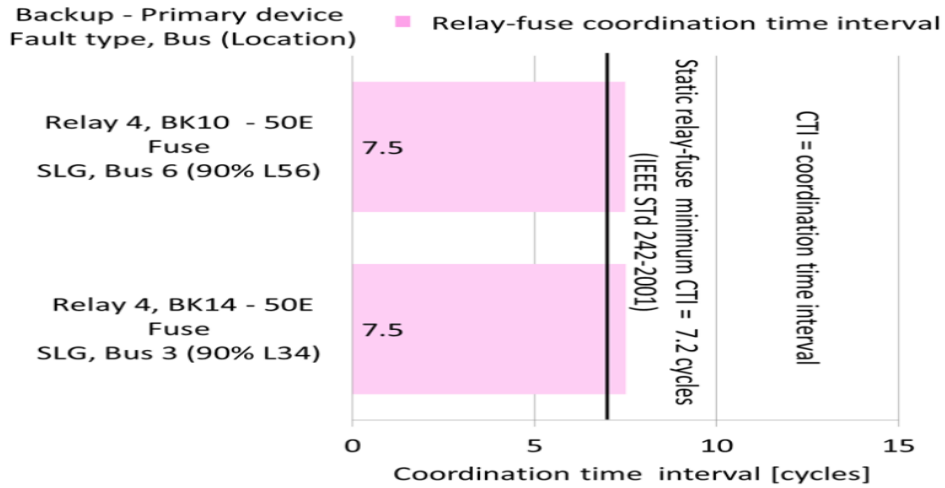

Figure 4.36: CTIs between backup and primary protections at maximum fault currents for DG1-34/56 circuit path

4.8.11 DG3-2187 (Test modes 5, 8, 17, and 22)

The DG3-2187 circuit path represented a non-normal operation of the microgrid. The DG3 source was connected to Busses 2, 1, 8, and 7. The DG3-2187 circuit path is shown in Figure D.12 of Appendix D. This circuit path had one branch (DG3-2187) formed by the L12 and L78 power lines. In the DG3-2187 branch, fault overcurrents at L12 and L78 power lines were cleared by Relays 6 (BK19) and 1 (BK4), respectively. Relays 6 (BK19) and 1 (BK4) were coordinated as backup and primary protection of the L78 power line, respectively. Relays 6 (BK19) and 1 (BK4) were coordinated as backup protection of fuses on Busses 8-1 and 7, respectively.

Figure 4.37 (A) shows inverse time-current curves of relays and maximum ampere rating fuses for busses in the DG3-2187 branch versus maximum load currents of breakers. Maximum load currents of breakers were not intersected by inverse time-current curves of relays, verifying that the relays did not trip to maximum load currents of breakers in the microgrid. Figure 4.37 (B) shows inverse time-current curves of relays and maximum ampere rating fuses for busses in the DG3-2187 branch versus maximum and minimum fault currents. Maximum and minimum fault currents flowing along breakers were intersected by inverse time-current curves of relays, verifying that the relays tripped at fault overcurrents, thereby protecting power lines of the DG3-2187 branch.

Figure 4.38 shows calculated CTIs between backup and primary protective devices at maximum fault currents for the DG3-2187 circuit path. The blue and pink bars represent the calculated relay-relay and relay-fuse CTIs, respectively. Calculated CTIs between backup and primary protection devices at maximum fault currents were not less than 7.2 cycles. Minimum

CTI of 7.2 cycles refers to the relay-relay and relay-fuse minimum CTIs based on RTS experiment (without breaker operating time) and IEEE Std. 242-2001 [7], respectively.

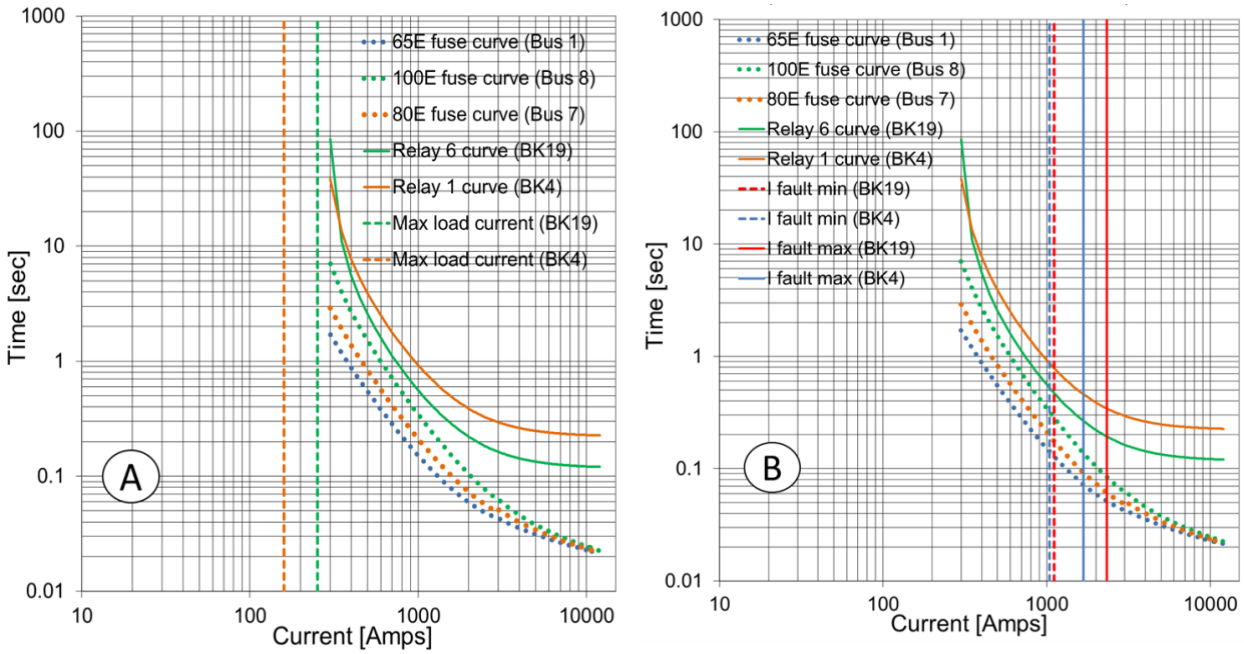

Figure 4.37: Maximum load (A), maximum and minimum fault currents (B) versus fuse and relay curves of DG3-2187 circuit path

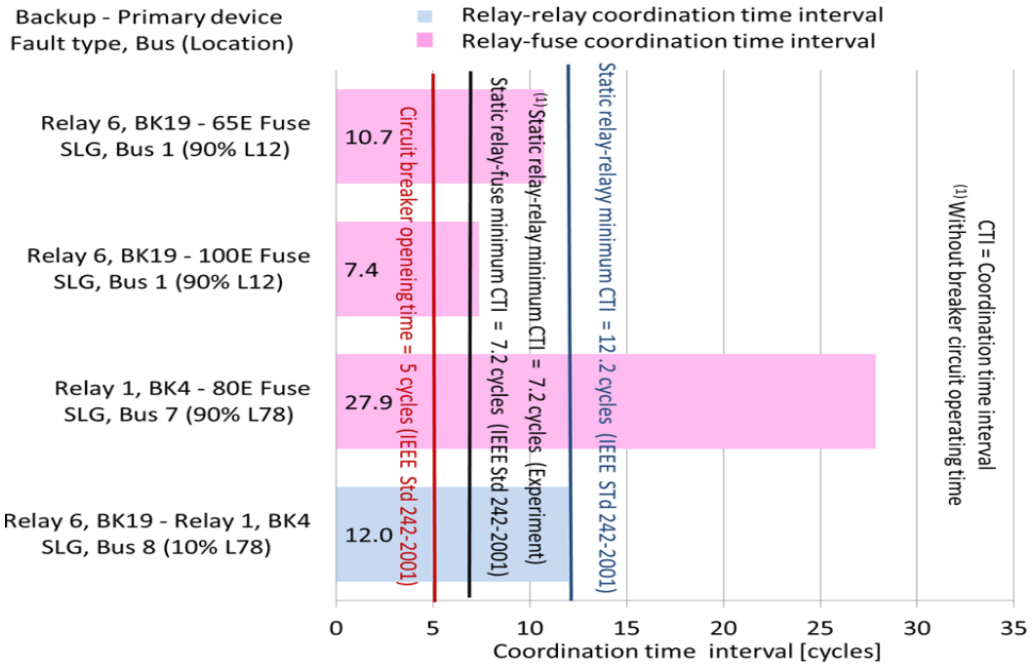

Figure 4.38: CTIs between backup and primary protections at maximum fault currents for DG3-2187 circuit path

4.9 Protection logic for Relays 2 and 3

In the circuit paths for Relays 2 and 3, protection logics to control the relay's breakers were created based on initial breaker states and expected breaker operations (no trip or trip) at overcurrent faults. Because each relay controlled two breakers, relays always tripped one breaker at fault overcurrent based on the circuit path and fault location. As an example, Figure 4.39 shows the DG2-678 circuit path and breaker operations at overcurrent faults located on power lines L67 and L78.

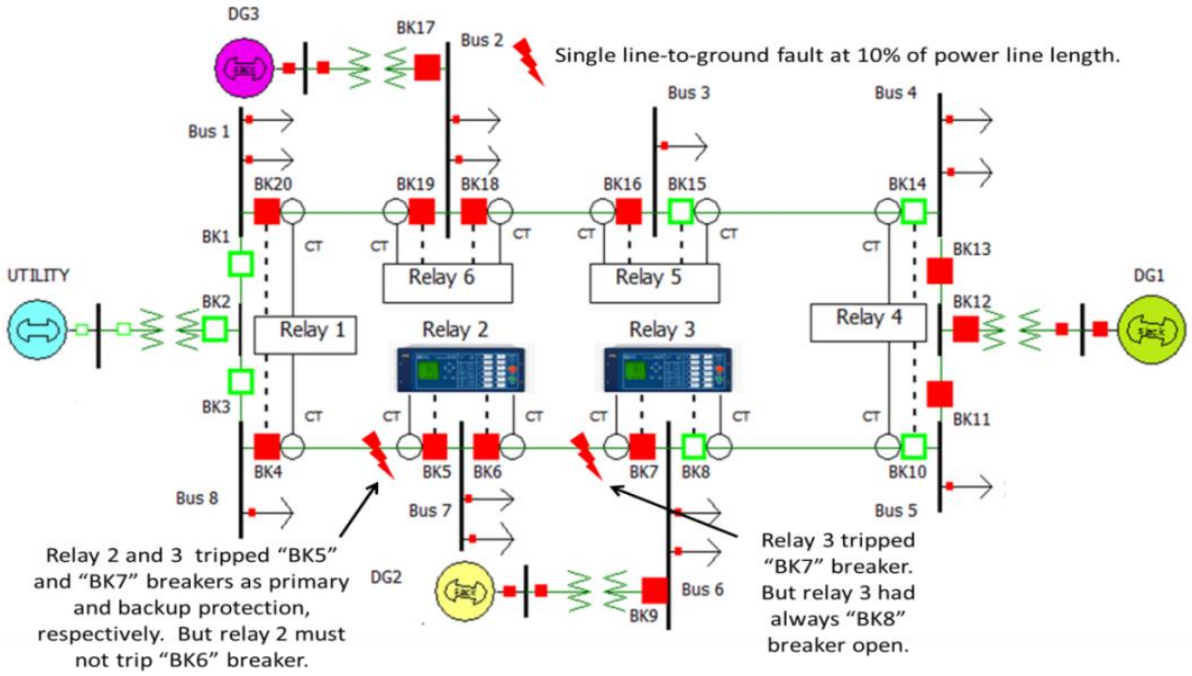

Figure 4.39: Breaker operations of Relays 2 and 3 in the DG2-678 circuit path

For Relay 2, "BK5" breaker was tripped at overcurrent fault in power line L78, while "BK6" breaker was always closed. For Relay 3, "BK7" breaker was tripped at overcurrent fault in power lines L78 and L67 as backup and primary protection, respectively, while "BK8" was always open. Therefore, at the DG2-678 circuit path, "BK7" or "BK5" breakers were tripped at overcurrent faults, and "BK6" and "BK8" breakers were always closed and open, respectively. Tables 4.16 and 4.17 show breaker operations at overcurrent faults, initial breaker states, current

directions, and protection logic gates for Relays 2 and 3, respectively. Based on initial state (open or closed) and current direction of breakers for relays in circuit paths, breakers of Relays 2 and 3 allowed the Trip (1), No Trip (2), and Any (3) breaker operations. "Trip" and "No Trip" breaker operations were represented by "AND" and "ZERO" protection logic gates. However, the "Any" breaker operation could be represented by the "AND" or "ZERO" protection logic gates.

Table 4.16: Initial breaker states and current directions of breakers for Relay 2

Microgrid test modes		**Relay 2 (Bus 7)**				
Test modes	**Circuit paths of Relays 2 and 3**	**Initial breaker states and current directions[1]**	**Breaker operations[2]**		**Protection logic gates**	
			BK5	**BK6**	**BK5**	**BK6**
1	UTILITY-8765/1234	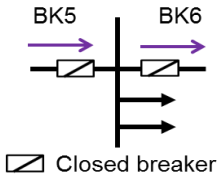	No Trip	Trip	ZERO	AND
2, 6, 9, 18	DG2-678/65	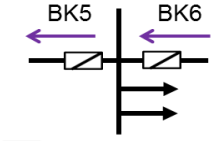	Trip	No Trip	AND	ZERO
3, 7, 12, 15, 20	DG2-6781					
11, 14, 19	DG2-678					
4	DG1-5678					
10, 16	DG2-67/65	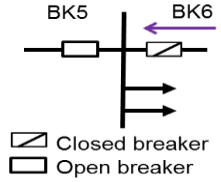	Any[3]	No Trip	ZERO	ZERO
13, 21	DG2-67					
8	DG2-6543	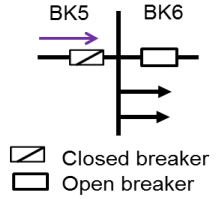	No Trip	Any[3]		
17	DG2-65					
5	DG1-34/56					
22	DG2-6					
5, 8, 17, 22	DG3-2187					

[1]At pre-fault sate, [2]At fault sate, [3]Permit "AND" or "ZERO" gates because breaker was always open.

Table 4.17: Initial breaker states and current directions of breakers for Relay 3

Microgrid test modes		Relay 3 (Bus 6)				
Test modes	Circuit paths of Relays 2 and 3	Initial breaker states and current directions[1]	Breaker operations[2]		Protection logic gates	
			BK7	BK8	BK7	BK8
1	UTILITY-8765/1234	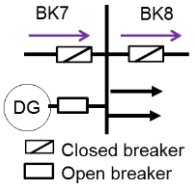	No Trip	Trip	ZERO	AND
2, 6, 9, 18	DG2-678/65	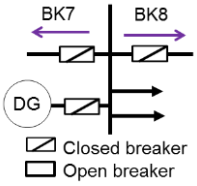	Trip	Trip	AND	AND
10, 16	DG2-67/65					
8	DG2-6543	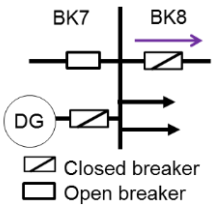	Any[3]	Trip		
17	DG2-65					
3, 7, 12, 15, 20	DG2-6781	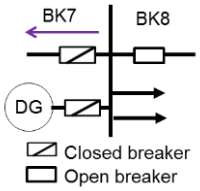	Trip	Any[3]	AND	ZERO
11, 14, 19	DG2-678					
13, 21	DG2-67					
4	DG1-5678	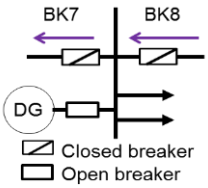	Trip	No Trip		
5	DG1-34/56	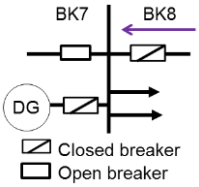	Any[3]	No Trip	ZERO	ZERO
5, 8, 17, 22	DG3-2187					
22	DG2-6	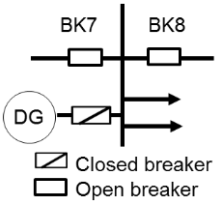	Any[3]	Any[3]		

[1]At pre-fault sate, [2]At fault sate, [3]Permit "AND" or "ZERO" gates because breaker was always open.

The “Trip” operation allowed the relay’s breakers to trip at fault overcurrent. However, the “No Trip” operation prevented the relay’s breaker from tripping at fault overcurrent. While the “Trip” operation was for relay breakers protecting a protection area (power lines and/or bus feeders), the “No trip” operation was for relay breakers that were not tripping and that had energized load feeder busses. The “Any” operation for relay breakers allowed a “Trip” or “No trip” operation because relay breakers were always open in circuit paths and no fault currents could flow along an open breaker. In addition, the “Any” operation allowed any inverse time overcurrent setting because relay breakers did not trip at an open breaker. Protection logic gates of Relays 2 and 3 were created based on the relay’s breaker operations (trip, no trip, and any), as shown in Table 4.16 and 4.17.

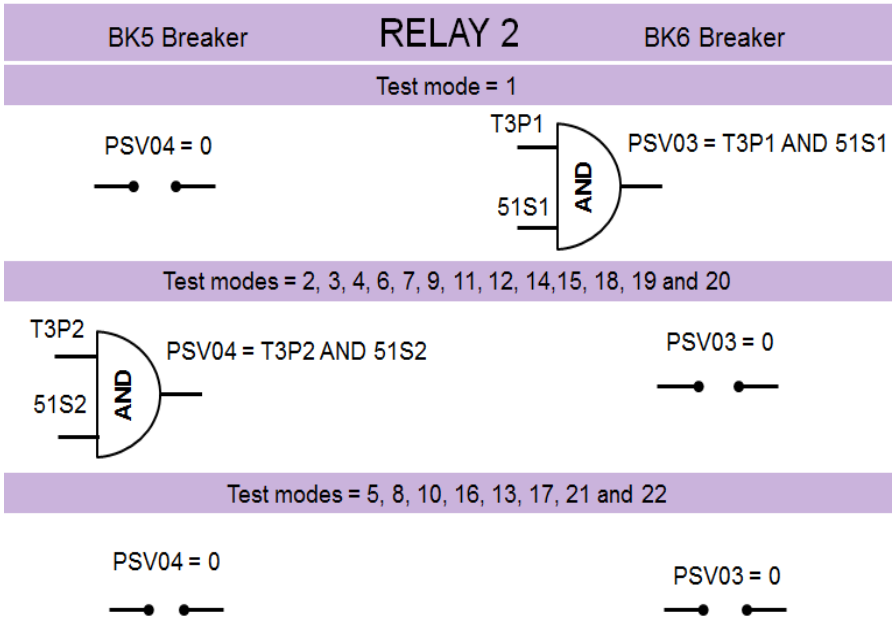

Figure 4.40: “AND” and “ZERO” gates for Relay 2 trip logics

Because Relay 2 had to trip “BK5” or “BK6” breakers, the inverse time overcurrent element pickup 51S2 and 51S1 digital signals were selected for “BK5” and “BK6” breakers, respectively. Based on breaker operations of Relay 2 in Table 4.16, Figure 4.40 shows the trip

logic gates of Relay 2. For test mode 1, “ZERO” and “AND” gates were selected for “BK5” and “BK6” breakers, respectively. For test modes 2, 3, 4, 6, 7, 9, 11, 12, 14, 15, 18, 19, and 20, “AND” and “ZERO” gates were selected for “BK5” and “BK6” breakers, respectively. However, for test modes 5, 8, 10, 13, 16, 17, 21, and 22, “ZERO” gates were selected for “BK5” and “BK6” breakers. “AND” gate inputs were formed by the inverse time overcurrent element pickup (51S1 or 51S2) and trip circuit breaker (T3P1 or T3P2) digital signals. The “AND” gate output was a SELogic variable (PSV0 3 or PSV04). The “ZERO” gate was represented by SELogic variable (PSV03 or PSV04) set to zero. Relay control outputs to trip the breakers were activated by the SELogic variables (PSV03 or PSV04).

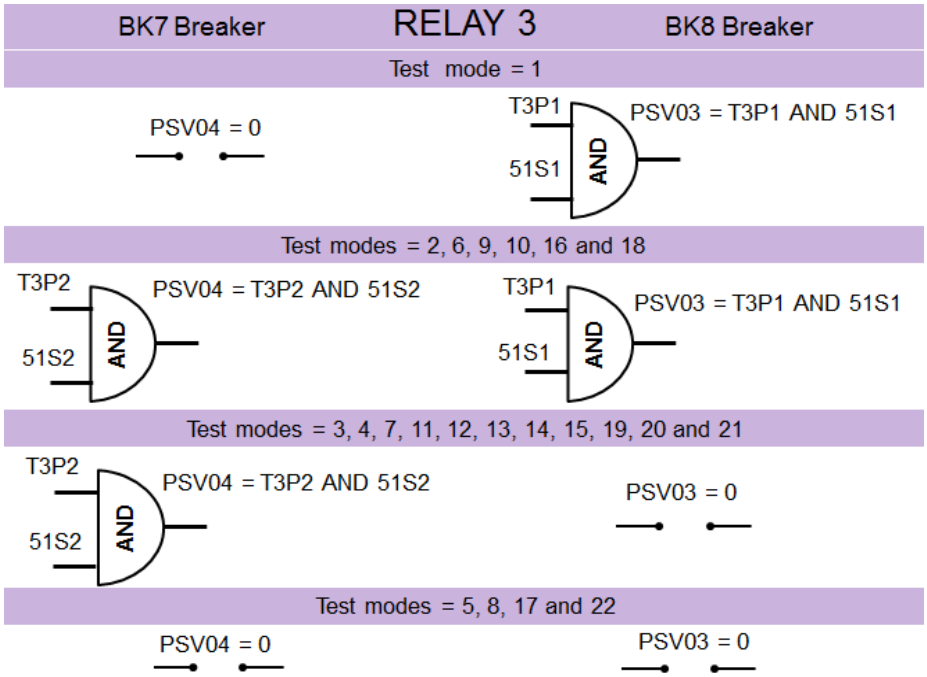

Figure 4.41: “AND” and “ZERO” gates for Relay 3 trip logics

Because Relay 3 had to trip “BK7” or “BK8” breakers, the inverse time overcurrent element pickup 51S2 and 51S1 digital signals were selected for “BK7” and “BK8” breakers, respectively. Based on breaker operations of Relay 3 in Table 4.17, Figure 4.41 shows trip logic gates of Relay 3. For test mode 1, “ZERO” and “AND” gates were selected for “BK7” and

"BK8" breakers, respectively. For test modes 2, 6, 9, 10, 16, and 18, "AND" gates were selected for "BK7" and "BK8" breakers. For test modes 3, 4, 7, 11, 12, 13, 14, 15, 19, 20, and 21, "AND" and "ZERO" gates were selected for "BK7" and "BK8" breakers, respectively. However, for test modes 5, 8, 17, and 22, "ZERO" gates were selected for "BK7" and "BK8" breakers.

As an example, Figure 4.42 shows A-B-C line currents and digital signals of HR_13115 event that corresponded to DG2-678/65-SLG(A)-Bus6-BK7 test from RTS experiment. The "BK7" breaker was tripped by Relay 3 at SLG fault near Bus 6 (10% of L67 power line length). When the inverse time overcurrent element pickup (51S2) and trip circuit breaker (T3P2) digital signals were activated, the SELogic variable (PSV04) was turned on, generating a trip signal at the relay's normally closed (NC) control output (OUT107) in order to trip "BK7" breaker at fault overcurrent. The "BK7" breaker state changed from closed to open according to the relay's control input (IN104).

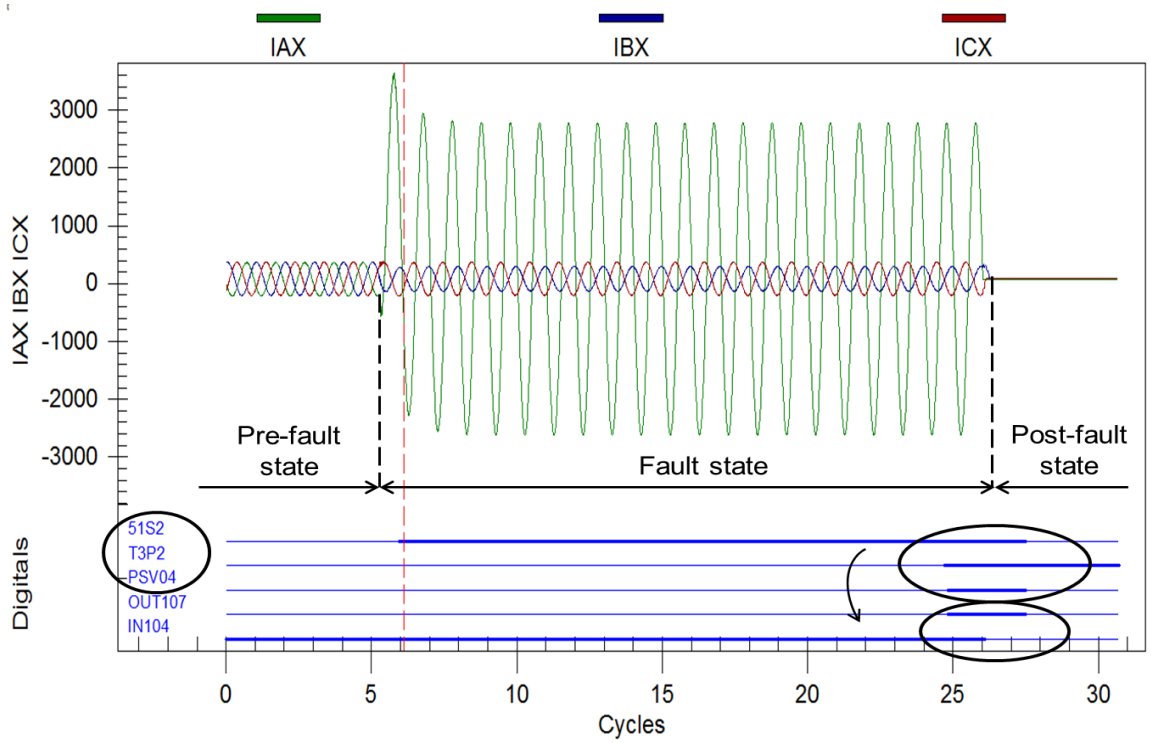

Figure 4.42: Trip logic digital signals of "AND" gate corresponded to "BK7" breaker of Relay 3 from collected HR_13115 event in RTS experiment

4.10 Setting groups for Relays 2 and 3

The adaptive overcurrent protection system was based on the setting group method and protection logics to control breakers of Relays 2 and 3. Setting groups for Relays 2 and 3 were created by collecting the identical inverse time overcurrent settings of Relays 2 and 3 from Table 4.14 and identical protection logic gates of Relays 2 and 3 from Tables 4.16 and 4.17, respectively. In this research, adaptive overcurrent protection was tested by a real and non-real-time simulator with Relays 2 and 3 in a loop. The setting group method was based on the application of up to six setting groups for each relay. Based on "AND" (trip) and "ZERO" (non-trip) protection logic gates, *TDS*, and *Ip* of Relays 2 and 3 for circuit paths, Relay 2 and 3 setting groups were grouped into SS1, SS2, SS3, SS4 and SS1, SS2, SS3, SS4, SS5, SS6, respectively. Table 4.18 shows the setting groups of Relays 2 and 3 in adaptive overcurrent protection of the microgrid. The "Any" breaker operation that allowed "AND" or "ZERO" gates permitted minimization of the number of setting groups for relays by grouping relay breakers with the identical protection logic gates.

Table 4.18: Settings groups of Relays 2 and 3 based on grouping same protection logic gates and inverse time overcurrent settings

Circuit paths of Relays 2 and 3 (Microgrid test modes)	**Protection logic gates**				**Inverse time overcurrent settings**								**Setting groups**	
	Relay 2		**Relay 3**		**Relay 2**				**Relay 3**				**Relay 2**	**Relay 3**
	BK5	**BK6**	**BK7**	**BK8**	**BK5**		**BK6**		**BK7**		**BK8**			
					TDS	***Ip***	***TDS***	***Ip***	***TDS***	***Ip***	***TDS***	***Ip***		
UTILITY-8765/1234 (1)	ZERO	AND	ZERO	AND			1.13	2.25			0.68	2.01	SS1	SS1
DG2-678/65 (2, 6, 9, 18)	AND	ZERO	AND	AND	0.78	1.86			1.18	1.95	0.77	1.97	SS2	SS2
DG2-67/65 (10, 16)	ZERO	ZERO											SS3	
DG2-6543 (8)														
DG2-65 (17)														
DG2-6781 (3, 7, 12, 15, 20)	AND	ZERO	AND	ZERO	0.78	1.86			1.19	1.97			SS2	SS3
DG2-678 (11, 14, 19)														
DG2-67 (13, 21)	ZERO	ZERO							0.67	1.97			SS3	SS4
DG1-5678 (4)	AND	ZERO			0.71	1.89			1.12	1.90			SS4	SS5
DG1-34/56 (5)	ZERO	ZERO	ZERO	ZERO									SS3	SS6
DG3-2187 (5, 8, 17, 22)														
DG2-6 (22)														

TDS : Time dial setting, *Ip*: Secondary overcurrent pickup [A].

Based on Table 4.18, circuit paths were segregated into Relay 2, 3 and 2-3 groups. The DG3-2187 circuit path was in the group of Relay 2. However, the DG2-65, DG2-6543, DG1-34/56, and DG2-6 circuit paths were in the group of Relay 3. In the group of Relays 2-3, Relays 2 and 3 share circuit paths (DG1-5678, DG2-678/65, UTILITY-8765/1234, DG2-6781, DG2-678, DG2-67/65, and DG2-67). Figure 4.43 shows circuit paths (A) and setting groups (B) for Relays 2 and 3.

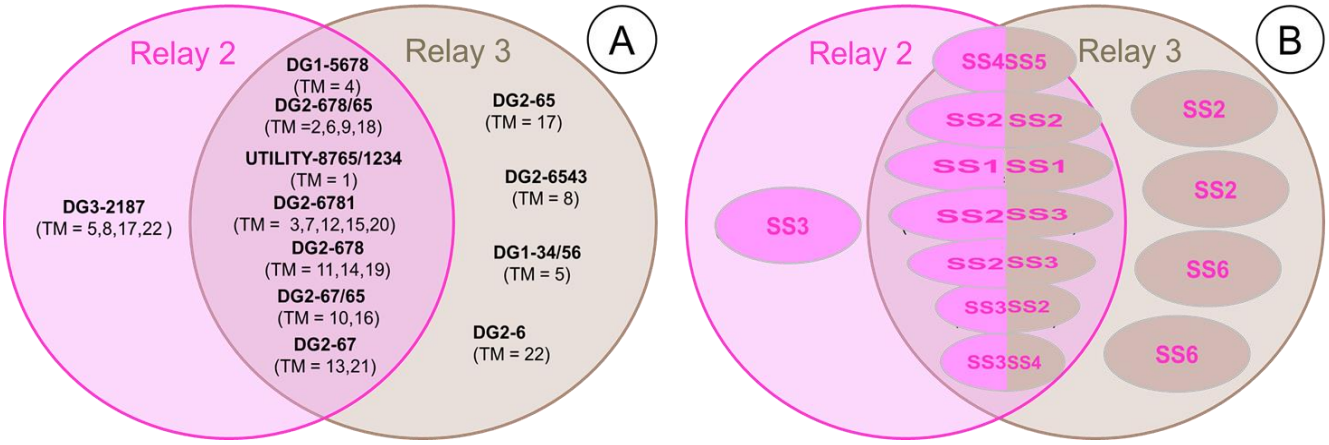

Figure 4.43: Circuit paths (A) and setting groups (B) for Relays 2 and 3

Setting groups of Relays 2 and 3 were selected based on the grouping of similar circuit paths with the identical protection logic gates and inverse time overcurrent settings. In adaptive overcurrent protection, each relay controlled two breakers and each breaker was controlled by "AND" or "ZERO" protection logic gates to trip or not trip the relay's breakers, respectively. "AND" protection logic gates depended on the inverse time overcurrent element pickup digital signals (51S1 or 51S2) of the relay's breakers. Inverse time overcurrent element settings of Relays 2 and 3 were selected based on upstream (backup) and downstream (primary) protective devices in the microgrid and circuit paths that had the identical current directions along the breakers of the same relay. Relays 2 and 3 were located at power line bus (Bus 7) and distributed generator bus (Bus 6), respectively. Because Relays 2 and 3 were located at power line and

distributed generator busses, respectively, Relay 2 required less setting groups than Relay 3. Relays 2 and 3 had four (SS1-2-3-4) and six (SS1-2-3-4-5-6) setting groups, respectively.

4.11 Algorithm of adaptive inverse time overcurrent protection

The algorithm to calculate and select adaptive inverse time overcurrent protection for Relays 2 and 3 in the microgrid with distributed generators is represented by a flow chart in Figure 4.44. The adaptive inverse time overcurrent protection algorithm was based on selection of inverse time overcurrent settings (*US* curve, *TDS*, *Ip*), creation of protection logic gates (AND, ZERO), and grouping of identical inverse time overcurrent settings and protection logic gates for circuit paths of Relays 2 and 3 in the microgrid.

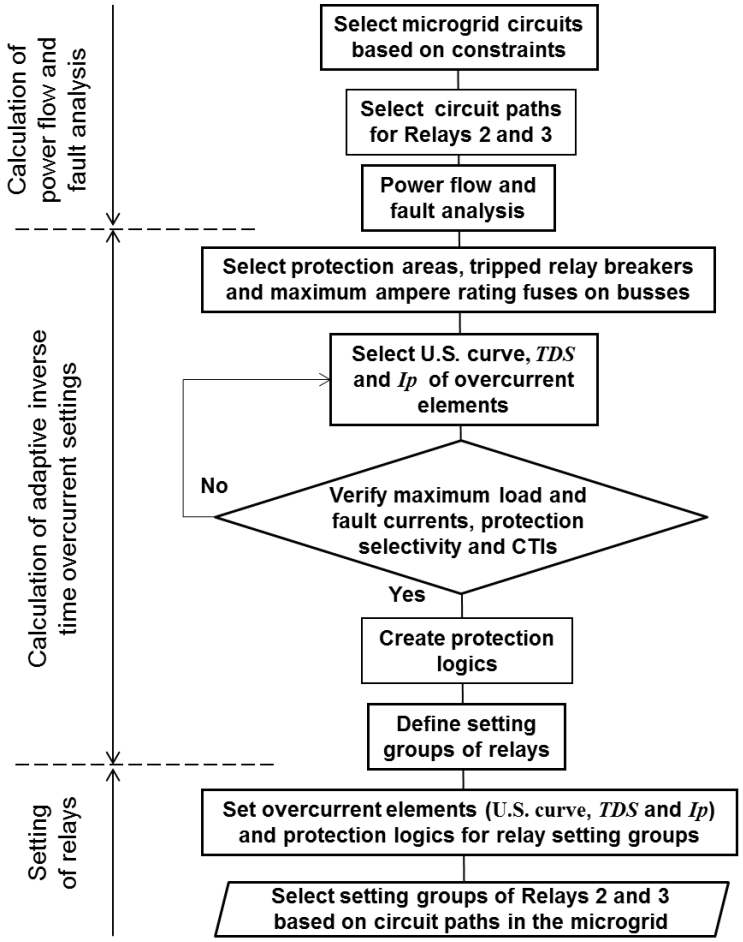

Figure 4.44: Adaptive inverse time overcurrent protection based on protection logic and setting group method

(1) Microgrid circuits (test modes) were selected based on microgrid constraints on operation, maximum load demand, equipment, and utility service limitations.

(2) Circuit paths for Relays 2 and 3 were selected because non-real and real-time experiments were performed with Relays 2 and 3 in the loop.

(3) Power flow and fault analysis were run for circuit paths, collecting current magnitudes on relay breakers. Fault analysis was performed at LL, 3PB, SLG and DLG faults located at 90% and 10% of power line lengths.

(4) Power lines of the microgrid were defined as protection areas based on circuit paths and fault locations. Expected tripped relay breakers were selected and maximum ampere rating fuses on busses of circuit paths were picked in order to calculate inverse time overcurrent settings for relay's breakers.

(5) Based on very-inverse U3 time-current curve for relays and current transformer ratio of 200, the *TDS* and *Ip* of inverse time overcurrent elements for expected tripped breakers on relays at overcurrent faults were selected.

(6) Inverse time-current curves of relay's overcurrent elements and maximum ampere rating fuses on busses were plotted for each branch of circuit paths, and selectivity coordination between upstream (backup) and downstream (primary) protective devices were verified in time-current logarithmic plots. Maximum load current magnitudes were plotted, verifying that the relays did not trip, and maximum and minimum fault current magnitudes were plotted verifying that the relays tripped. CTIs between backup and primary protection devices at maximum fault currents were calculated, verifying that calculated CTIs were not less than 7.2 cycles. If selectivity coordination, maximum load, maximum and minimum fault currents, and minimum CTI conditions were not satisfactory, the *TDS* and/or *Ip* had to select again.

(7) Protection logic gates of relay's control outputs were formed by "AND" and "ZERO" gates; the "AND" and "ZERO" gates represented the trip and non-trip breakers at overcurrent faults, respectively.

(8) Setting groups of Relays 2 and 3 were selected by grouping the relay's breakers with the identical inverse time overcurrent settings (*US* curve, *TDS*, *Ip*) and protection logic gates (AND, ZERO) for circuit paths of Relays 2 and 3.

(9) Inverse time overcurrent settings (U.S. curve, *TDS*, and *Ip*) and protection logic gates (AND, ZERO) for inverse time overcurrent elements of relay setting groups were set on Relays 2 and 3 (Chapter 5).

(10) In the non-real and real-time simulator experiments with Relays 2 and 3 in the loop, setting groups of Relays 2 and 3 were selected before running relay tests based on the circuit paths corresponding to the microgrid configurations (test modes).

4.12 Chapter summary

Adaptive overcurrent protection was based on the grouping of the identical inverse time overcurrent settings (U.S. curve, *TDS*, and *Ip*) and protection logic gates (AND, ZERO) into relay setting groups. Microgrid configurations (test modes) were selected based on microgrid constraints (operation, maximum load demand, equipment, and utility service limitations). In this research, adaptive overcurrent protection was verified by real and non-real-time simulators with Relays 2 and 3 in the loop. Circuit paths for Relay 2 and 3 busses were selected from microgrid configurations (test modes).

Power flow and fault analysis were run for circuit paths by collecting current magnitudes on relay breakers. Fault analysis was performed for LL, 3PB, SLG, and DLG faults at 90% and 10% of power line lengths. Power lines of the microgrid were defined as protection areas in

circuit paths. Based on circuit paths and fault locations, the expected tripped relay's breakers were selected, and maximum ampere rating fuses on busses for circuit paths were picked up in order to calculate inverse time overcurrent settings of the relay's breakers. Inverse time overcurrent settings (U.S. curve, *TDS*, and *Ip*) were assigned to each inverse time overcurrent element on the relays.

Inverse time-current curve models of relays and fuses were created. Based on very-inverse U3 time-current curve, the *TDS* and *Ip* of inverse time overcurrent elements were calculated in relays. In the UTILITY-8765/1234, DG2-678/65, DG2-67/65, DG2-6543, DG2-65, DG2-6781, DG2-678, DG2-67, DG1-5678, DG1-34/56, and DG3-2187 circuit paths, inverse time-current curves of relay's overcurrent elements and maximum ampere rating fuses were plotted for each branch of circuit paths. Selectivity coordination between upstream (backup) and downstream (primary) protective devices were verified in time-current logarithmic plots. Maximum load currents and fault currents were plotted, verifying that the relay's inverse time overcurrent settings did not trip and trip, respectively. CTIs between backup and primary protection devices at maximum fault currents were calculated, verifying that calculated CTIs were not less than 7.2 cycles. Minimum CTI of 7.2 cycles refers to the relay-relay and relay-fuse minimum CTIs based on RTS experiment (without breaker operating time) and IEEE Std. 242-2001 [7], respectively.

In adaptive overcurrent protection, setting groups of Relays 2 and 3 were selected by grouping the relay's breakers with the identical inverse time overcurrent settings (U.S. curve, *TDS*, and *Ip*) and protection logic gates (AND, ZERO) for circuit paths. Relays 2 and 3 were grouped into four and six setting groups, respectively.

Chapter 5 - Relay settings

This chapter describes how settings of Relays 2 and 3 were defined for adaptive overcurrent protection of a microgrid with distributed generators, based on the setting group method. Relays 2 and 3 had four and six setting groups, respectively, and each relay had two breakers. Overcurrent elements of the setting groups trip a signal during an overcurrent fault situation. The setting groups needed protection logic variables to trip breakers by the relay's control outputs. Figure 5.1 shows parameters set for Relays 2 and 3.

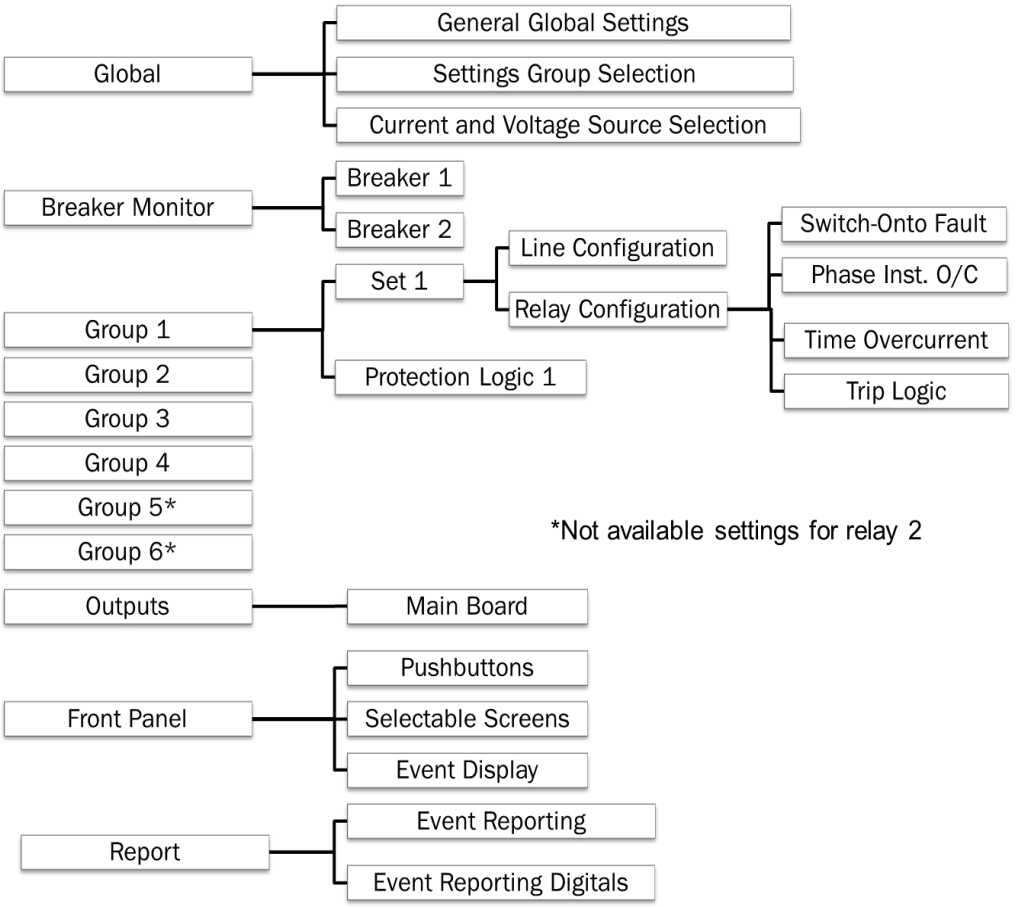

Figure 5.1: Parameters set for Relays 2 and 3

Global, Breaker Monitor, Groups, Outputs, Front Panel, and Report options were set for Relays 2 and 3. In the Global setting, power system characteristics were identified as station

names, system phase rotation, and nominal system frequency. In the Breaker Monitor setting, relay control inputs were defined in order to sense breaker pole states. In the Group setting, inverse time overcurrent settings and protection logic variables were set for overcurrent elements of the setting groups. In the Outputs relay control outputs were set to trip relay breakers. In the Front Panel setting, push-button light-emitting diodes (LEDs) and selectable screens were defined on the relay's front panel. In the Report setting, characteristics of the record event files were defined, including event reporting digital variables. The setting of Relays 2 and 3 were established for adaptive overcurrent protection of the microgrid with distributed generators. Default settings were used for other parameters.

5.1 Relay communication

In order to set SEL 451 relays and collect event files, the Human Machine Interface (HMI) computer had to communicate with the SEL 451 relays using AcSELerator Quickset® software [11]. Communication and setting parameters of the relays were needed to initiate the communication and relay setting process.

The relay communication process began by connecting the SEL C662 cable from the USB connection of the computer to the Port F (front panel) of the SEL 451 relay and opening the AcSELerator Quickset® program. The "Communication" option was selected using a SERIAL communication port device "SEL CP210x USB to UART Bridge." Data speed, data bits, stop bits, parity, Level 1 and 2 passwords were filled during the relay communication process based on SEL 451 relay's instruction manual [5]. The process to communicate with SEL 451 relays was:

- The SEL 451 relay was powered on.

- The SEL C662 cable was connected from the HMI computer's USB connector to the SEL 451 relay Port F located on the front panel.
- The AcSELerator Quickset® software [11] was opened and the "Communication" option was selected from the "Setup" list, Figure 5.2 (A).
- The "Serial" communication option was selected, and communication parameters were completed based on the SEL 451 relay instruction manual [5]. Then, Level 1 (OTTER) and 2 (TAIL) passwords were placed on the cells, Figure 5.2 (B).
- The communication status at the bottom of the computer screen was verified.

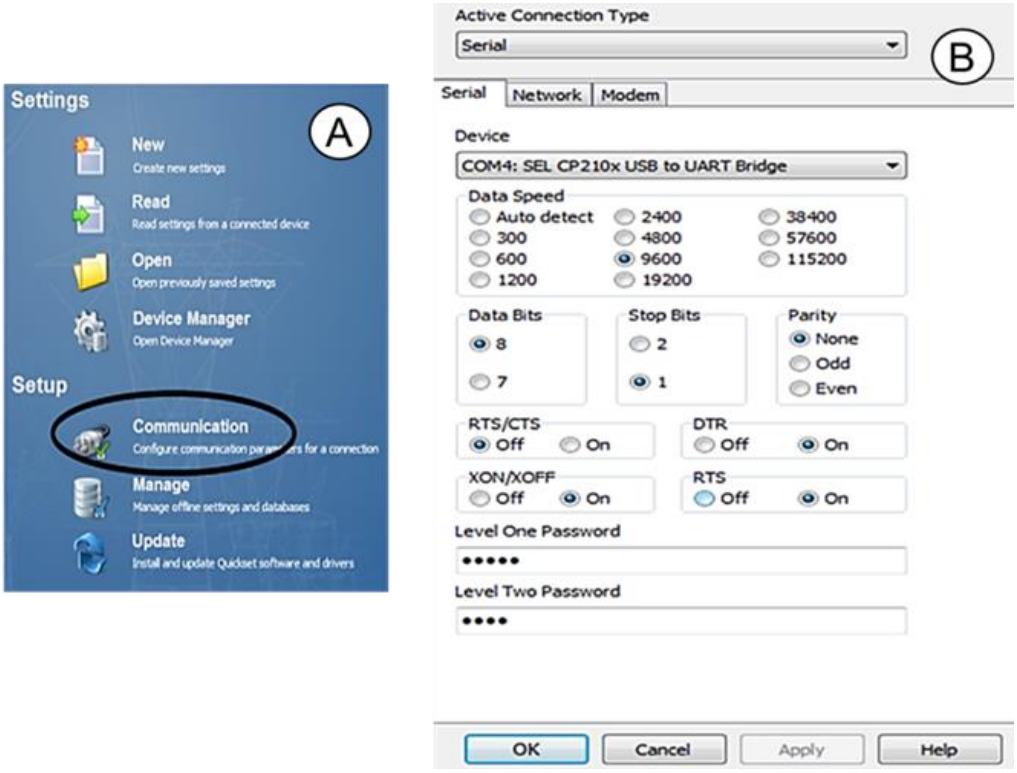

Figure 5.2: Setup (A) and communication parameters (B) of Relays 2 and 3

The relay setting process began after a successful relay communication was obtained and the "Create new setting" option was selected. Relays 2 and 3 had a rack-mount and panel-mount chassis, respectively. Firmware Identification (FID) and part numbers of SEL 451 relays were

needed to complete the “Setting Editor Selection” and “Device Part Number,” respectively. Table 5.1 shows FID and part numbers of Relays 2 and 3.

Table 5.1: FID and part numbers of SEL 451 relays

Relay name	Relay 2	Relay 3
Chassis	Rack-mount chassis	Panel-mount chassis
Part #	045126152B0B4H224XXXX	045124152XXAX3243XXXX
FID #	SEL-451-2-R125-V0-Z014011-D2011906	SEL-451-2-R126-V0-Z100011-D20121207

The process to begin setting SEL 451 relays required the following steps:

- After communicating with the SEL 451 relay, the “Create new setting” option was selected, as shown in Figure 5.3 (A).
- The “FID” number was completed based on Table 5.1, and “Device Family,” “Device Model,” and “Version” were selected from the “Settings Editor Selection.” Then “OK” was selected, as shown in Figure 5.3 (B).
- The “PART” number of the relay was selected from Table 5.1, and the “Device Part Number” was completed. Then “OK” was selected, as shown in Figure 5.4.

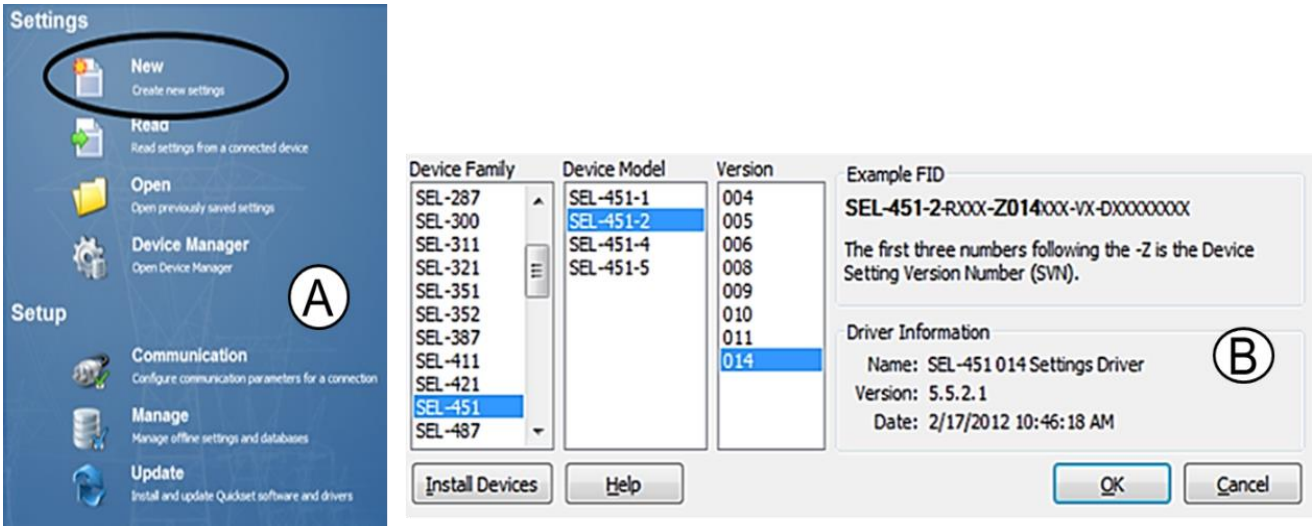

Figure 5.3: Settings (A) and settings editor selection (B) for Relay 2

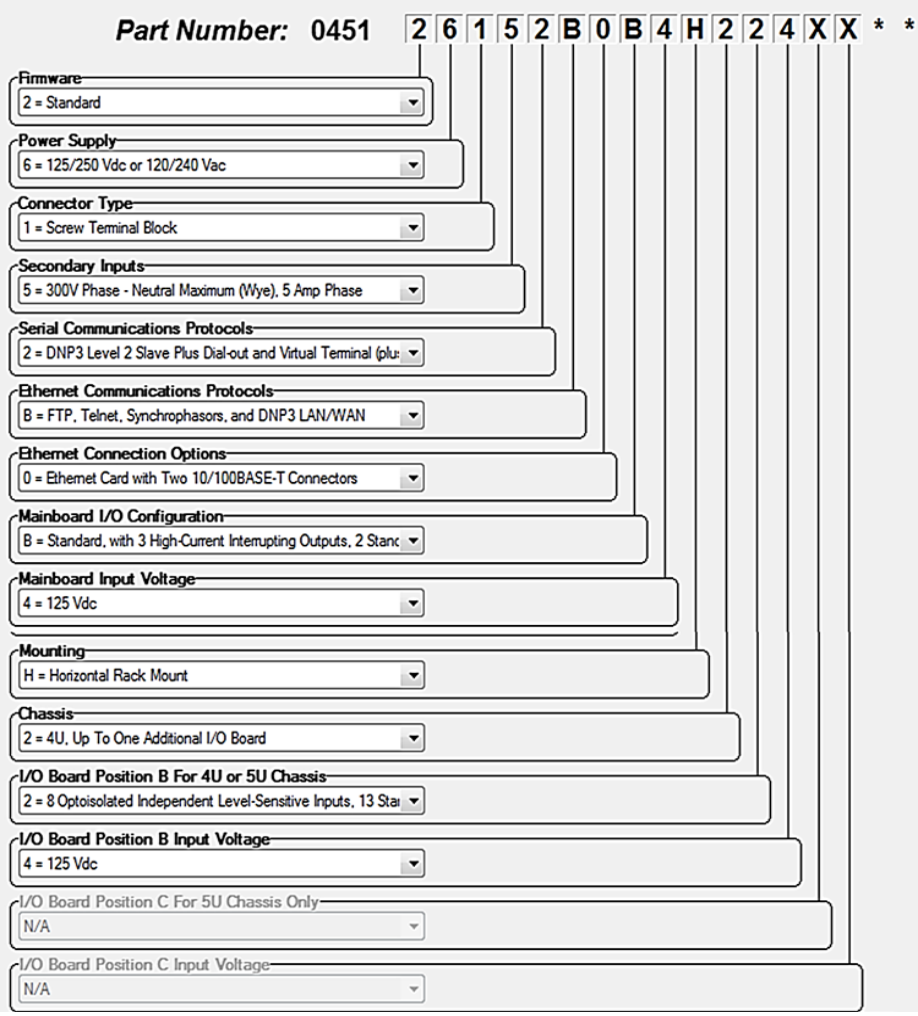

Figure 5.4: Device part number for Relay 2

5.2 Relay settings

Settings of Relays 2 and 3 were based on setting paths of SEL 451 relays indicated in Figure 5.5. In SEL 451 relays, main menu setting options were divided into “Aliases, Global, Breaker Monitor, Groups, Automation Logic, Outputs, Front Panel, Report, Ports, DNP MAP Settings, and Bay Control”. Relay manufacturer default settings were used for the “Aliases, Automation Logic, DNP MAP Settings, Bay Control and Port F, 1, 2, 3, 4, and 5”. However, “Global, Breaker Monitor, Outputs, Front Panel, Report, and Group 1, 2, 3, 4, 5, and 6” options were set to create adaptive overcurrent protection and run NRTS and RTS experiments with

relays in the loop. “Group 1, 2, 3, and 4” were set for Relay 2, and the “Group 1, 2, 3, 4, 5, and 6” were set for Relay 3.

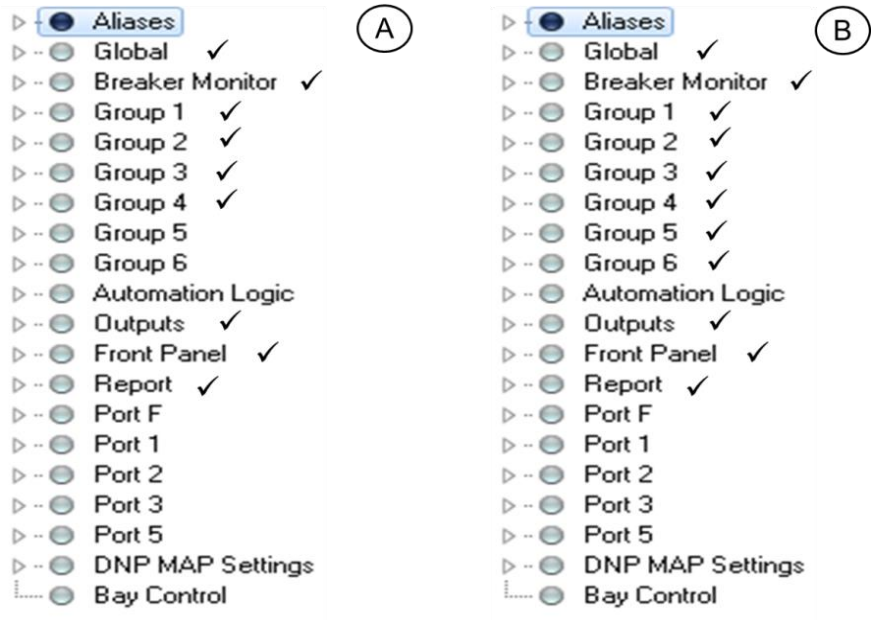

Figure 5.5: Settings of Relays 2 (A) and 3 (B)

5.2.1 Global

The main menu setting, “Global”, was divided into sub-menu options shown in Figure 5.6. From the “Global” menu, “General Global Settings, Settings Group Selection, and Current and Voltage Source Selection” were set. However, relay manufacturer default settings were used for other sub-menu options.

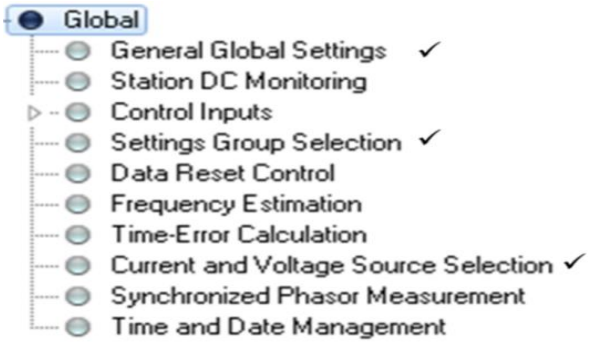

Figure 5.6: Global setting path of Relays 2 and 3

“General Global Settings” and identifiers of Relays 2 and 3 are shown in Figure 5.7. For the SEL 451 relay setting located on bus 7, “Bus 7” and “Relay 2” were chosen as the station

(SID) and relay (RID) identifiers, respectively. Breaker 1 (BID1) and 2 (BID2) identifiers of Relay 2 were named “BK6” and “BK5,” respectively. For the SEL 451 relay setting located on bus 6, “Bus 6” and “Relay 3” were chosen as the SID and RID, respectively. BID1 and BID2 identifiers of Relay 3 were named “BK8” and “BK7,” respectively.

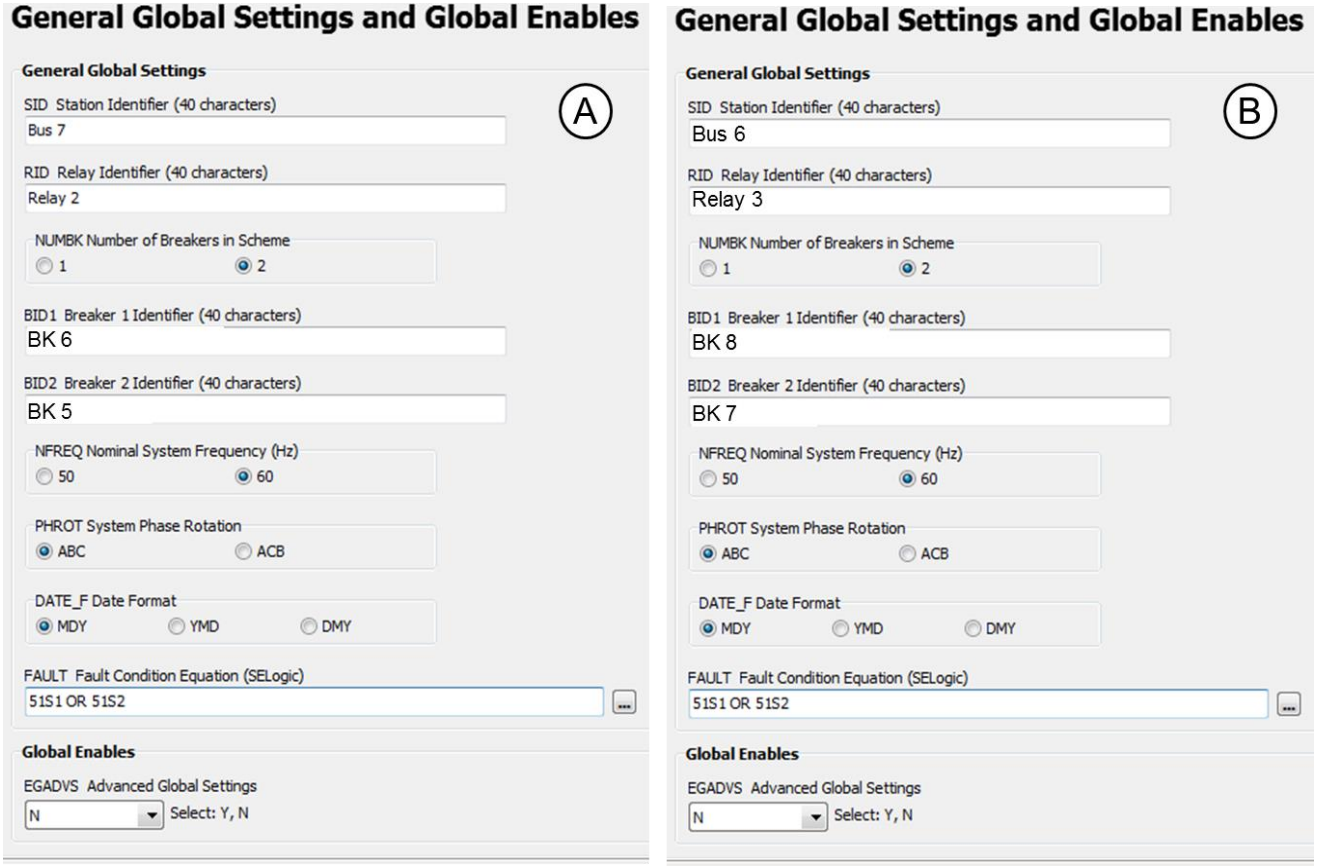

Figure 5.7: General global settings of Relays 2 (A) and 3 (B)

For Relays 2 and 3, the number of breakers in scheme (NUMBK) was “2” to activate two breakers for each relay. Nominal system frequency (NFREQ), system phase rotation (PHROT), and date format (DATE_F) were set at 60 Hz, ABC, and MDY, respectively. The fault condition equation “51S1 OR 51S2” was used to activate the inverse time overcurrent setting for overcurrent elements of BID1 and BID2. Advanced global settings (EGADVS) were not activated, selecting “N.”

In the RTS experiment with relays in the loop, Relays 2 and 3 were disabled for less than 1 sec. during the process of switching active setting groups, according to the relay instruction manual [5]. Hypothetically, if an overcurrent fault situation occurred in which Relays 2 and 3 were disabled, both relays may not detect the fault current at the time of disabling. Figure 5.8 shows the switch of setting groups of Relays 2 (B) and 3 (A) when the group change delay for both relays was 60 cycles. In this case, both relays were disabled at the same time, leaving no protection for less than 1 sec. and possibly leading to failure to detect an overcurrent fault.

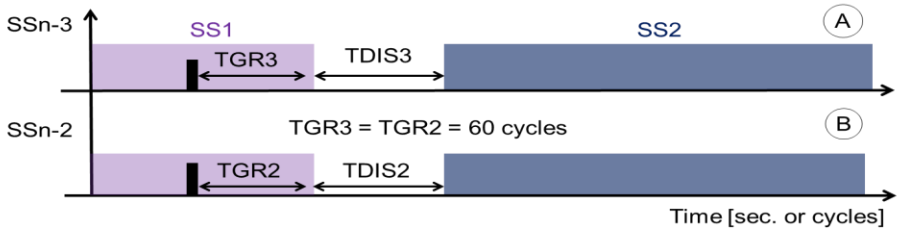

SSn-3 = setting group of relay 3, SSn-2 = setting group of relay 2
TGRn = group change delay of relay n, TDISn = disabled time of relay n < 1 sec.

Figure 5.8: Switch of Relays 3 (A) and 2 (B) setting groups with identical group change delay

However, setting Relays 2 and 3 with different group change delays improved the situation illustrated in Figure 5.8. Figure 5.9 shows the switch of the setting groups of Relays 2 (B) and 3 (A) when the group change delay was 0 and 120 cycles, respectively. In this case, Relay 3 was disabled later than Relay 2, allowing consistent protection of one relay when the other relay was disabled.

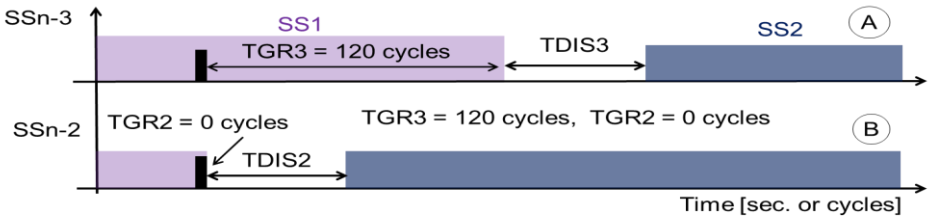

SSn-3 = setting group of relay 3, SSn-2 = setting group of relay 2
TGRn = group change delay of relay n, TDISn = disabled time of relay n < 1 sec.

Figure 5.9: Switch of Relays 3 (A) and 2 (B) setting groups with no identical group change delay

Therefore, in order to provide constant protection, group change delay of Relays 2 (TGR2) and 3 (TGR3) was set at 0 cycles and 120 cycles, respectively. In NRTS and RTS experiments with relays in the loops, prefault states were ≥ 3 seconds in order to allow enough time to switch the setting group of the relays before establishing fault states. In the NRTS experiment, the setting groups of relays were switched manually from the push buttons of the relay's front panel. However, in the RTS experiment, control inputs of the relay's rear side switched the relay setting groups. The "Settings Group Selection" of Relays 2 and 3 is shown in Figure 5.10. For Relay 2, control inputs 201, 202, 203, and 204 were applied to select the setting group 1 (SS1), 2 (SS2), 3 (SS3), and 4 (SS4), respectively. However, for Relay 3, control inputs 201, 202, 203, 213, 214, and 215 were applied to select the setting group 1 (SS1), 2 (SS2), 3 (SS3), 4 (SS4), 5 (SS5), and 6 (SS6), respectively. In order To avoid simultaneously switching the setting groups of Relays 2 and 3, group change delays (TGR) for Relay 2 and 3 were set at 0 and 120 cycles, respectively.

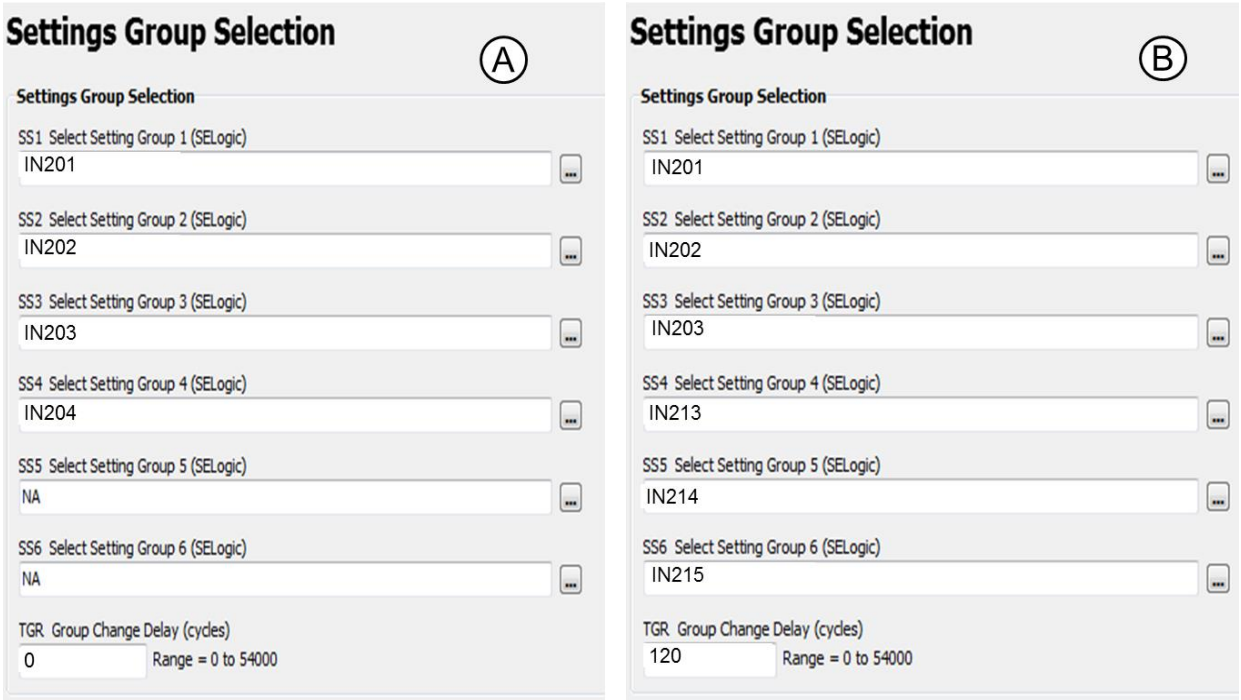

Figure 5.10: "Settings Group Selection" of Relays 2 (A) and 3 (B)

Figure 5.11 shows current source assignments from the relay instruction manual for SEL 451 relays [5]. The "Current and Voltage Source Selection" of SEL 451 relays allows the main and alternate line (A), combined currents for line (B), and breaker (C) current source assignments. Relays 2 and 3 of adaptive overcurrent protection in the microgrid required two breakers for each relay, so the main and alternate line current source assignment (A) was selected for Relays 2 and 3. The main and alternative breakers were Breakers 1 and 2, respectively. Breaker 1 represents "BK6" and "BK8" breakers from Relays 2 and 3, respectively, and Breaker 2 represents "BK5" and "BK7" breakers from Relays 2 and 3, respectively.

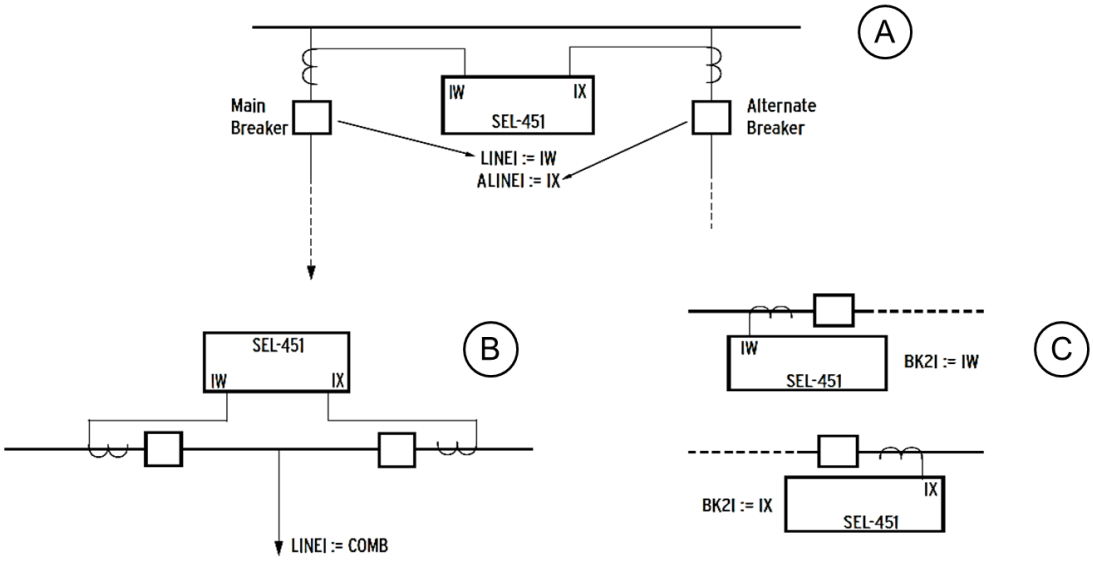

Figure 5.11: Main and alternate line (A), combined currents for line (B), and breaker (C) current source assignments

"Current and Voltage Source Selection" of Relays 2 and 3 is shown in Figure 5.12. The "Current and Voltage Selection" (ESS) was activated by selecting "Y" and then "Line" (LINEI) and "Alternate Current Source" (ALINEI) were selected as "IW" and "IX," respectively. "Alternate Current Source" (ALTI) was activated by the relay's IN105 control input, meaning that relays recorded "IW" and "IX" currents when IN105 control input was turned off and on, respectively. "IW" and "IX" represented line currents of Breakers 1 and 2, respectively.

Breaker 1 (BK1I) and 2 (BK2I) “Current Source” were set as “IW” and “IX” currents, respectively. “Polarizing Current” (IPOL) and “Alternate Line Voltage Source” (ALINEV) registered as “not available” (NA). For the NRTS experiment, no record event files were collected from Relays 2 and 3; however, record event files were collected from Relays 2 and 3 for the RTS experiment. In RTS experiment tests, IN105 control inputs from Relay 2 or 3 were activated according to the selected circuit path and fault location, saving the record event file from the breaker that was tripped during the relay tests.

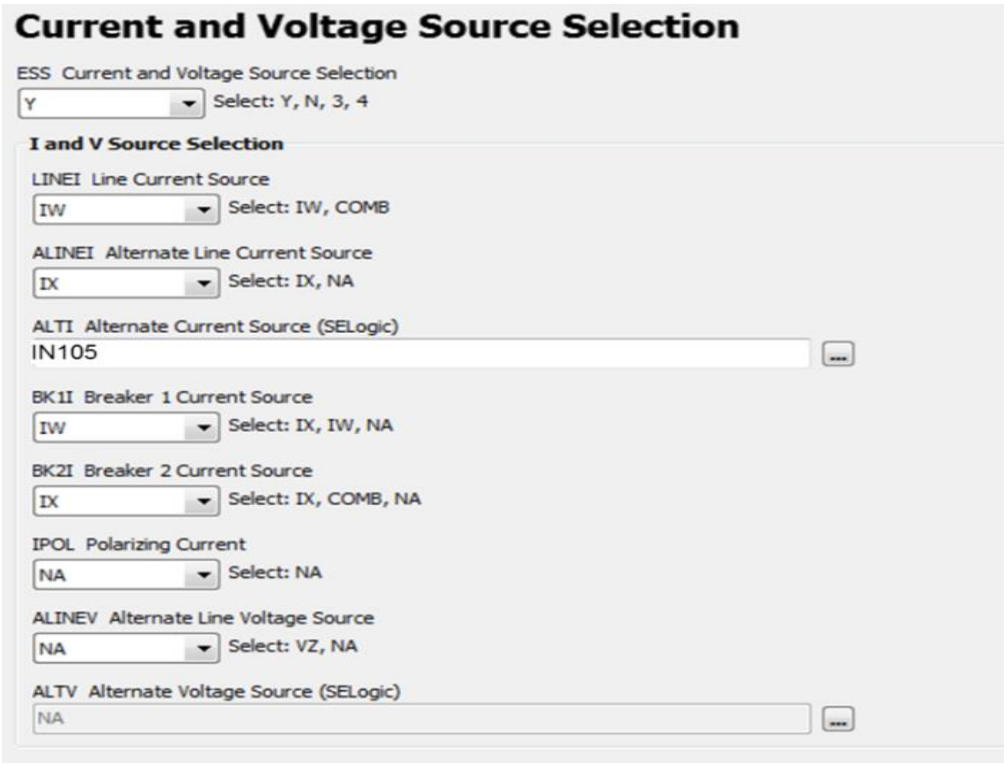

Figure 5.12: “Current and Voltage Source Selection” for Relays 2 and 3

5.2.2 Breaker monitor

The “Breaker Monitor” setting was divided into sub-menu options of Breaker 1 and 2. As shown in Figure 5.13, the “Breaker Monitor” for Relays 2 and 3 were set to monitor breaker status from relay control inputs.

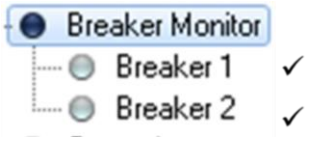

Figure 5.13: Breaker monitor setting path of Relays 2 and 3

Breaker 1 (EB1MON) and 2 (EB2MON) monitoring were not activated for Relays 2 and 3, and 52AA1 and 52AA2 represented open or closed states for Breakers 1 and 2, respectively. Relays 2 and 3 sensed their breaker states by using the relay control inputs. Breaker 1 inputs (52AA1) were activated by IN101 and IN103 control inputs for NRTS and RTS experimental circuits, respectively. However, Breaker 2 inputs (52AA2) were activated by IN102 and IN104 control inputs for NRTS and RTS experimental circuits, respectively. Figure 5.14 shows monitor settings of Breakers 1 and 2 for Relays 2 and 3.

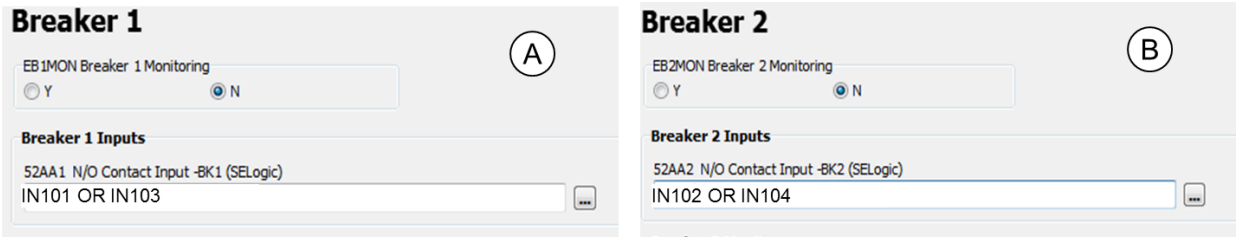

Figure 5.14: Monitor settings of Breakers 1(A) and 2 (B)

5.2.3 Groups

The setting group method was based on application of up to six setting groups for each relay. The U.S. time-current curve (U3) time dial settings (*TDS*) and secondary overcurrent pickups (I_P) were set at inverse time overcurrent elements of Relays 2 and 3. Overcurrent setting groups of Relays 2 and 3 were selected based on grouping same inverse time overcurrent settings (*TDS*, I_P) and protection logic gates (AND, ZERO) for relay's breakers of circuit paths for Relays 2 and 3. Figure 5.15 and 5.16 show the initial breaker states and current directions for setting groups of relays 2 and 3, respectively.

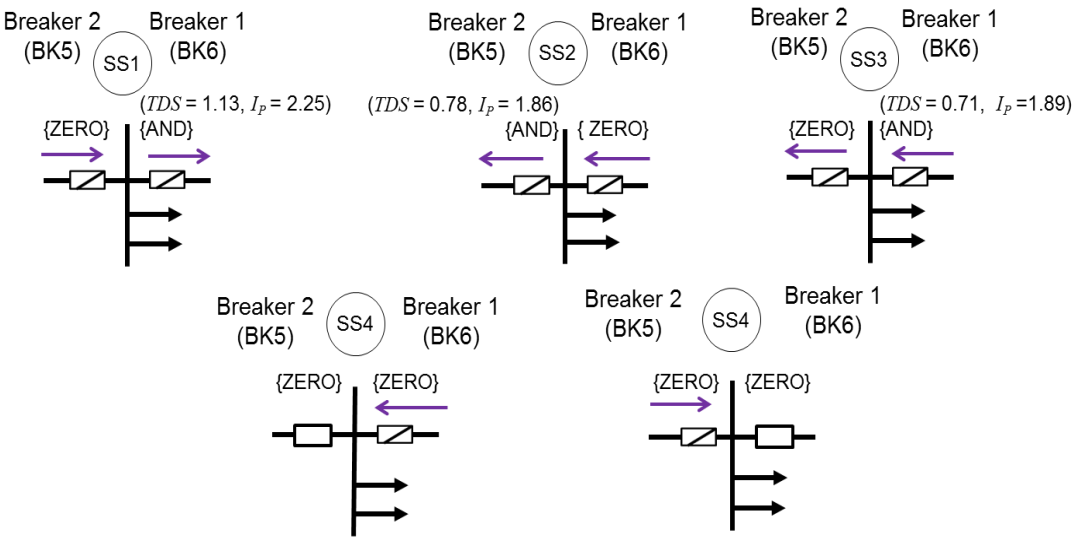

Figure 5.15: Initial breaker states and current directions for setting groups of Relay 2

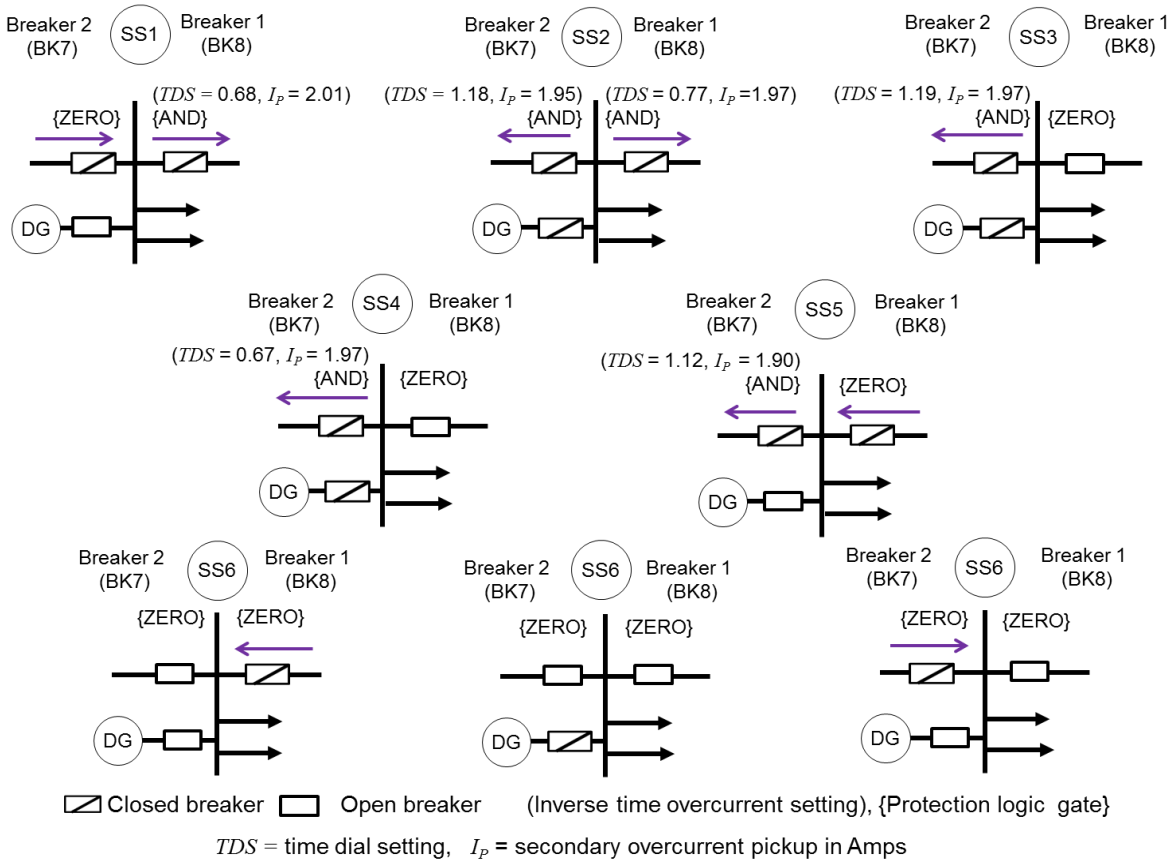

Figure 5.16: Initial breaker states and current directions for setting groups of Relay 3

In adaptive overcurrent protection, each relay controlled two breakers, and each breaker corresponded to an overcurrent element of the setting groups. The inverse time overcurrent element settings of relays 2 and 3 were selected based on upstream (backup) and downstream (primary) protective devices in the microgrid, and circuit paths that had the similar current directions along breakers of the same relay. Relays 2 and 3 had four and six setting groups, respectively. Although Relay 2 was located at line bus (Bus 7), Relay 3 was located at distributed generator bus (Bus 6). Line and distributed generator busses had two and three feeders, respectively. Relay 3 required more setting groups than Relay 2 because Relay 2 breaker currents were able to flow in the same direction and Relay 3 breaker currents flowed in the same and opposite direction, as shown in Figures 5.15 and 5.16, respectively. While the relays 2 had the SS1, SS2, SS3 and SS4 setting groups, Relay 3 had the SS1, SS2, SS3, SS4, SS5 and SS6 setting groups.

In relay 2, SS1 was selected for UTILITY-8765/1234 circuit, SS2 was selected for DG2-678/65, DG2-6781 and DG2-678 circuits, SS3 was selected for DG2-67/65, DG2-6543, DG2-65, DG2-67, DG1-34/56, DG3-2187 and DG2-6 circuits, and SS4 was selected for DG1-5678 circuit.

In Relay 3, SS1 was selected for UTILITY-8765/1234 circuit, SS2 was selected for DG2-678/65, DG2-67/65, DG2-6543 and DG2-65 circuits, SS3 was selected for DG2-6781 and DG2-678 circuits, SS4 was selected for DG2-67 circuit, SS5 was selected for DG1-5678 circuit, and SS6 was selected for DG1-34/56, DG3-2187 and DG2-6 circuits.

In the adaptive overcurrent protection system for a microgrid with distributed generators, the number of available circuit paths was limited by the constraint of maximum power of the distributed generators and bus loads along the microgrid. Based on this constraint, breaker states

along the microgrid were defined for up to 22 test modes grouped by circuit paths identified by four and six setting groups for Relays 2 and 3, respectively. In Relays 2 and 3, Breakers 1 and 2 were tripped by overcurrent elements 1 and 2, respectively. Overcurrent fault trip situations for circuit paths depended on breaker state configurations shown in Figures 5.15 and 5.16. In Relays 2 and 3, overcurrent elements 1 and 2 were set with the inverse time overcurrent setting for Breakers 1 and 2, respectively. Inverse time overcurrent settings of Relays 2 and 3 were estimated for a current transformer ratio (*CTR*) of 200, and overcurrent elements were set for maximum line current. Inverse time overcurrent settings for groups of Relays 2 and 3 were defined by the selected U3 curve presented in the relay instruction manual [5]. The overcurrent pickup and time dial were selected based on feeder fuses and selectivity of primary and backup protections. Based on the setting group method, Relays 2 and 3 had four and six setting groups for circuit paths of the microgrid with distributed generators. Figure 5.17 shows the group setting path for Relays 2 (A) and 3 (B). "Set" and "Protection Logic" settings were used in the active groups of Relays 2 and 3. "Protection Logic" instead of "Graphical Logic" was used to set protection logic variables for the relay setting groups.

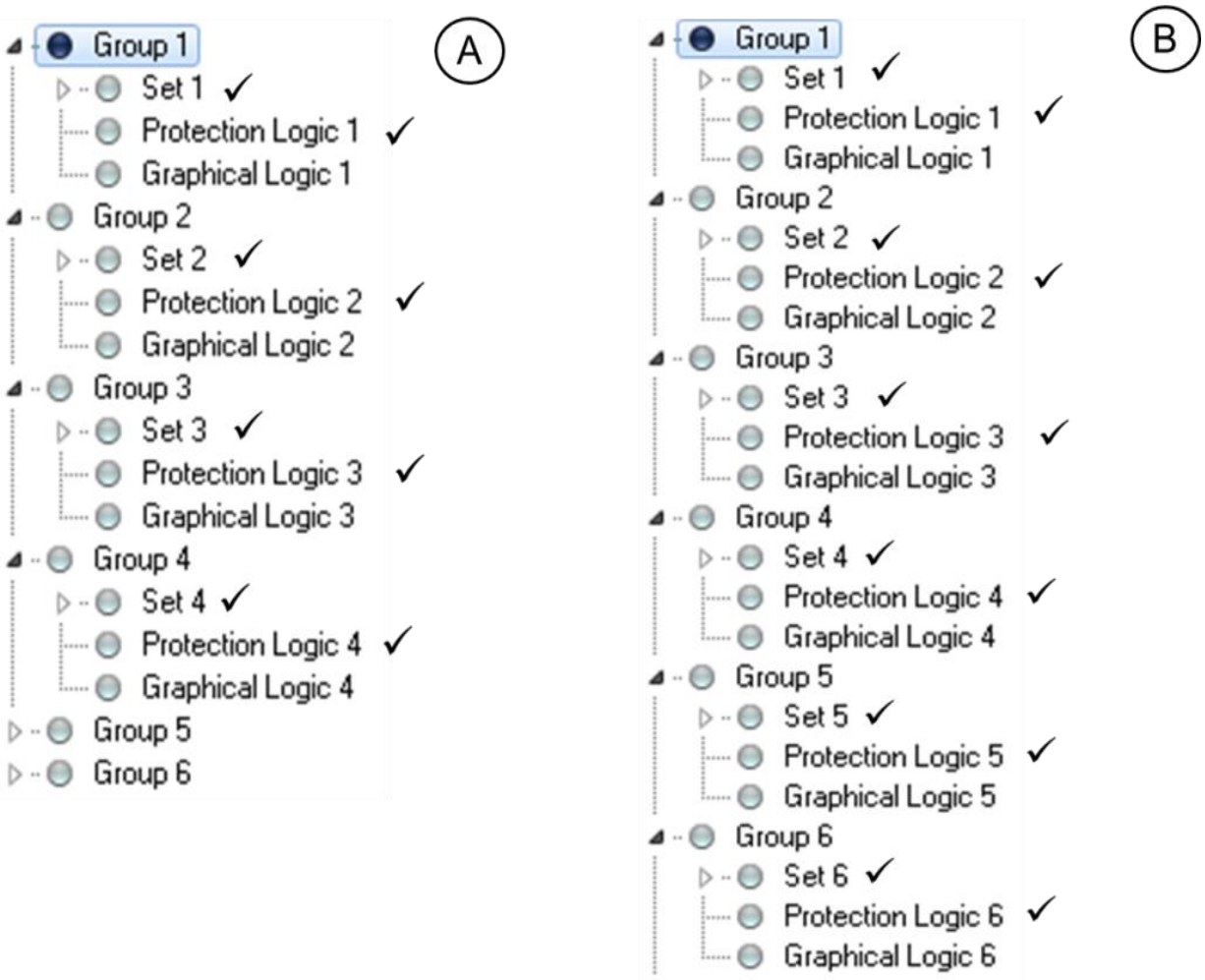

Figure 5.17: Group setting of Relays 2 (A) and 3 (B)

Figure 5.18 shows the setting path of the "Set 1" option, divided into "Line and Relay Configurations". For all active groups, "Line Configuration, Switch-Onto-Fault, Phase Inst O/C, Time Overcurrent, Trip Logic, and Protection Logic" were set. However, default settings provided by the relay manufacturer were used for "Load Encroachment, Residual Ground Inst O/C, Negative-Seq Inst O/C, Directional, Pole Open Detection, Trip Schemes, Breaker 1 and 2 Failure Logic, Synchronism Check, Reclosing and Manual Closing, Demand Metering and Graphical Logic" options.

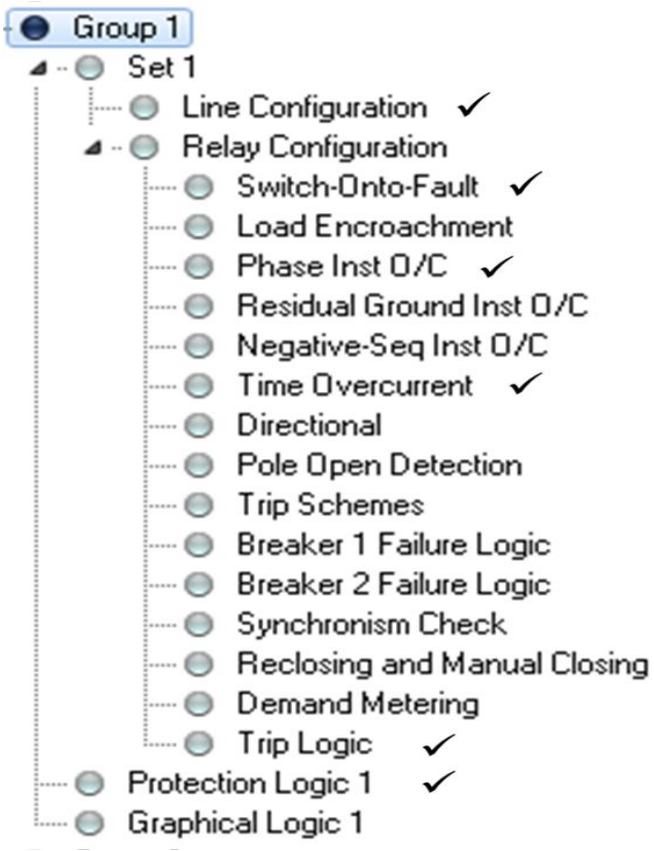

Figure 5.18: Set and protection logic of Relays 2 and 3

The "Line Configuration" setting of Relays 2 and 3 for NRTS (A) and RTS (B) experiments is shown in Figure 5.19. CTRW and CTRX values represented current transformer ratios of secondary currents of Breakers 1 (IAW, IBW and ICW) and 2 (IAX, IBC and ICX) for Relays 2 and 3. In NRTS and RTS experiments, current transformer ratios (CTRW and CTRX) were set to 200 and 50, respectively. Potential transformer ratios (PTRY and PTRZ) were set at 60. Nominal line-line secondary voltages for potential transformers (VNOMY and VNOMZ) were estimated by Equation (5.1).

$$VNOM_n = \frac{V_{LL}}{PTR_n} \tag{5.1}$$

where $VNOM_n$ is nominal line-line secondary voltage of the potential transformer in volts, V_{LL} is nominal line-line primary voltage of the potential transformer in volts, and PTR_n is the ratio of

the potential transformer. Nominal line-line primary voltage of the potential transformer was 7200 volts, and the potential transformer ratio was 60. From Equation (5.1), "VNOMY" and "VNOMZ" values were set at 120. Positive and negative line impedance secondary magnitudes and angles were the default values provided by the relay manufacturer because the fault location (EFLOC) was set as "N," meaning that the fault location was not activated.

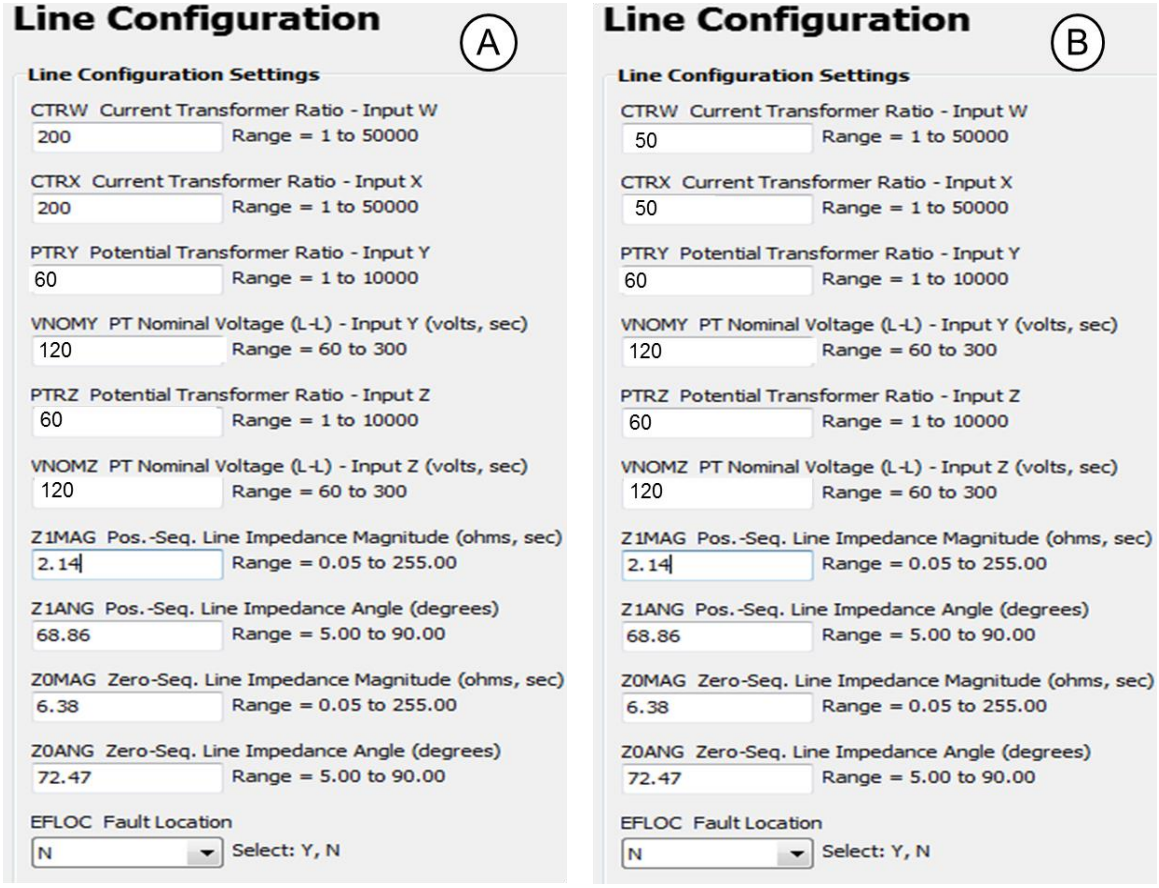

Figure 5.19: Line configuration setting of Relays 2 and 3 for NRTS (A) and RTS (B) experiments

Figure 5.20 shows "Switch-Onto-Fault (A) and Phase Instantaneous Overcurrent (B)" settings. The "Switch-Onto-Fault" (ESOTF) setting was set as "N" to disable the "Switch-Onto-Fault Trip" (TRSOFT) in the "Trip Logic" setting of Relays 2 and 3. The "Phase Instantaneous Overcurrent" setting was set as "N" for "Phase Inst./Definite-Time O/C Elements" (E50P)

because Relays 2 and 3 had to be set as an inverse time overcurrent instead of instantaneous overcurrent protection.

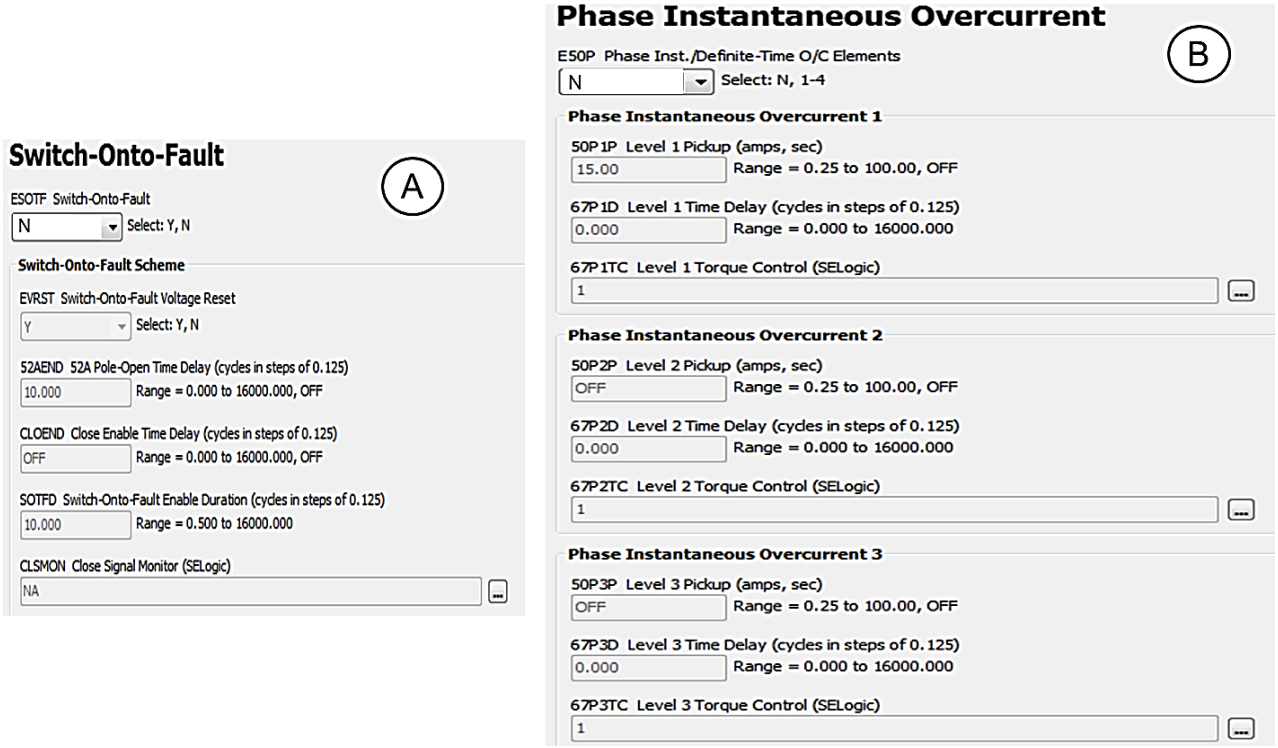

Figure 5.20: "Switch-Onto-Fault" (A) and "Phase Instantaneous Overcurrent" (B) settings of Relays 2 and 3

Figure 5.21 shows the "Time Overcurrent" element 1 (A) and 2 (B) of Group 2 for Relay 3. "Selectable Inverse-Time O/C Elements" (E51S) was set at "2" to activate time overcurrent elements 1 and 2 for Breakers 1 and 2 of Relay 2. "Operating Quantity" for the time overcurrent element 1 (51S1O) and 2 (51S2O) was defined by the maximum current of Phase A, B, or C, placing the "Imax1" and "Imax2" in the 51S1O and 51S2O cells, respectively. "Inv-Time O/C EM Reset" for the time overcurrent element 1 (51S1RS) and 2 (51S2RS) were not activated by setting "N," and the Torque Control (SELogic) for the time overcurrent element 1 (51S1TC) and 2 (51S2TC) were set to "1." Inverse time overcurrent settings of time overcurrent elements 1 and 2 for each group were secondary overcurrent pickups (51S1P and 51S2P), inverse time

overcurrent curves (51S1C and 51S2C), and time dials (51S1TD and 51S2TD). The "U3" curve based on the relay instruction manual [5] was selected to set time overcurrent elements 1 and 2. In Group 2 of Relay 3, secondary overcurrent pickups for time overcurrent elements 1(51S1P) and 2 (51S2P) were set at 1.97 and 1.95 amps, respectively. Inverse overcurrent time dials for time overcurrent elements 1 (51S1TD) and 2 (51S2TD) were set at 0.77 and 1.18, respectively.

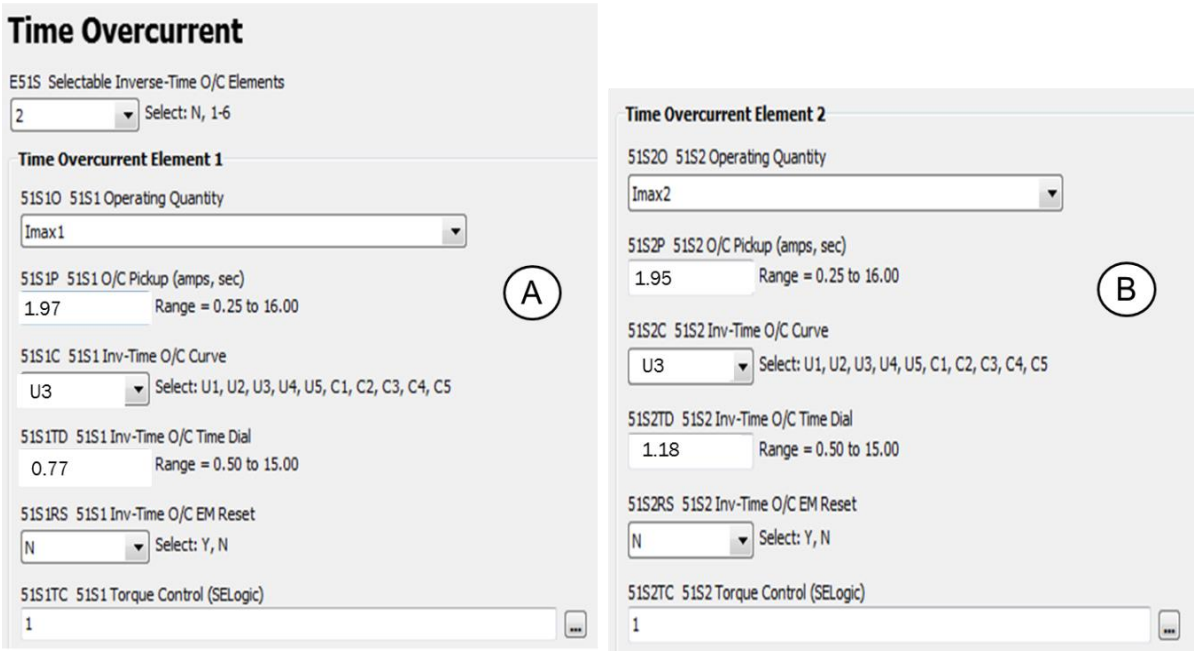

Figure 5.21: Time overcurrent element 1 (A) and 2 (B) of Group 2 for Relay 3

Current transformer ratios of 200 and 50 were used for relays in NRTS and RTS experiments, respectively. Secondary overcurrent pickups for time overcurrent elements 1 (51S1P) and 2 (51S2P) were not similar enough to maintain identical relay times for identical relay setting groups. Based on the inverse time overcurrent U3 curve from the relay instruction manual [5], relay time was represented by Equation (5.2).

$$T_R = TDS \times \left(0.0963 + \frac{3.88}{M^2 - 1}\right) \times 60 \tag{5.2}$$

where T_R is relay time in cycles, *TDS* is the inverse time overcurrent time dial setting, and *M* is the multiple of pickup. The multiple of relay pickup was defined by Equation (5.3).

$$M = \frac{I}{CTR\ I_P} \tag{5.3}$$

where M is the multiple of pickup , I is the primary pickup fault current in amps, CTR is the current transformer ratio, and I_P is the secondary overcurrent pickup in amps. Equations (5.2) and (5.3) revealed that the relay time was similar, using no identical current transformer ratios if the multiple of relay pickup was identical for NRTS and RTS experiments as is shown in Equation (5.4).

$$M_{NRTS} = M_{RTS} \tag{5.4}$$

where M_{NRTS} and M_{RTS} are the multiples of relay pickups for NRTS and RTS experiments, respectively. By representing the multiple of pickups of the relay for NRTS and RTS experiments as a function of Equation (5.3), Equation (5.4) is represented by Equation (5.5).

$$\frac{I}{CTR_{NRTS} \times I_{P\ NRTS}} = \frac{I}{CTR_{RTS} \times I_{P\ RTS}} \tag{5.5}$$

where I is the primary pickup fault current in amps, CTR_{NRTS} and CTR_{RTS} are current transformer ratios for NRTS and RTS experiments, respectively, and $I_{P\ NRTS}$ and $I_{P\ RTS}$ are secondary overcurrent pickups of relays in amps for NRTS and RTS experiments, respectively. Because primary pickup fault currents for NRTS and RTS experiments were identical, the secondary overcurrent pickup for relay settings during the RTS experiment was estimated by Equation (5.6).

$$I_{P\ RTS} = I_{P\ NRTS} \times \frac{CTR_{NRTS}}{CTR_{RTS}} \tag{5.6}$$

Using Equation (5.6), secondary overcurrent pickup for relay settings during the RTS experiment were estimated based on secondary overcurrent pickup for the relay setting during NRTS experiments in Table 5.2 and current transformer ratios of 200 and 50 for NRTS and RTS experiments, respectively.

In Table 5.2, "*TDS*" represents time dial settings to set groups of relays for NRTS and RTS experiments. The "$I_{P\ NRTS}$" and "$I_{P\ RTS}$" represent secondary overcurrent pickups for inverse time overcurrent elements 1 and 2 in order to set groups of Relays 2 and 3 during NRTS and RTS experiments. Inverse time overcurrent elements that must not trip were default settings provided by the relay manufacturer, but their overcurrent elements were disabled by not setting "51S1T" and "51S2T" trip logic equations for time overcurrent elements 1 and 2, respectively.

Table 5.2: Time overcurrent settings of groups for Relays 2 and 3

Relays	**Groups**	**Breaker**		**Time Overcurrent Settings**				
		No	**Name**	**Element**	**US Curve**	$I_{P\ NRTS}$	$I_{P\ RTS}$	***TDS***
2	1	1	BK6	1	U3	2.25	9.00	1.13
		2	BK5	2	No trip	No trip	No trip	No trip
	2	1	BK6	1	No trip	No trip	No trip	No trip
		2	BK5	2	U3	1.86	7.44	0.78
	3	1	BK6	1	No trip	No trip	No trip	No trip
		2	BK5	2	No trip	No trip	No trip	No trip
	4	1	BK6	1	No trip	No trip	No trip	No trip
		2	BK5	2	U3	1.89	7.56	0.71
3	1	1	BK8	1	U3	2.01	8.04	0.68
		2	BK7	2	No trip	No trip	No trip	No trip
	2	1	BK8	1	U3	1.97	7.88	0.77
		2	BK7	2	U3	1.95	7.80	1.18
	3	1	BK8	1	No trip	No trip	No trip	No trip
		2	BK7	2	U3	1.97	7.88	1.19
	4	1	BK8	1	No trip	No trip	No trip	No trip
		2	BK7	2	U3	1.97	7.88	0.67
	5	1	BK8	1	No trip	No trip	No trip	No trip
		2	BK7	2	U3	1.90	7.60	1.12
	6	1	BK8	1	No trip	No trip	No trip	No trip
		2	BK7	2	No trip	No trip	No trip	No trip

Figure 5.22 shows the "Trip Logic" setting of Group 2 for Relay 3. The "TR Trip" of Group 2 for Relay 3 tripped for time overcurrent elements 1 and 2 by selecting "51S1T OR 51S2T". "Switch-Onto-Fault Trip" (TRSOFT) was disabled because the "Switch-Onto-Fault"

(ESOTF) setting was set as “N.” Breakers 1 (BK1MTR) and 2 (BK2MTR) “Manual Trip” settings were set as “OC1 OR PB8_PUL” and “OC2 OR PB9_PUL”, respectively, meaning that Breakers 1 and 2 were opened by open circuit breakers (OC1 and OC2) or pulse push buttons (8 and 9). The “Unlatch Manual Trip” of Breakers 1 (ULMTR1) and 2 (ULMTR2) were set as “NOT 52AA1” and “NOT 52AA2,” respectively. The “52AA1” and “52AA2” represented auxiliary contacts that sensed phase “A” pole status for Breakers 1 and 2, respectively. ”Event Report Trigger Equations” (ER) was set as “R_TRIG 51S1 OR R_TRIG 51S2” in order to record event files when time overcurrent element 1 or 2 tripped during an overcurrent fault situation.

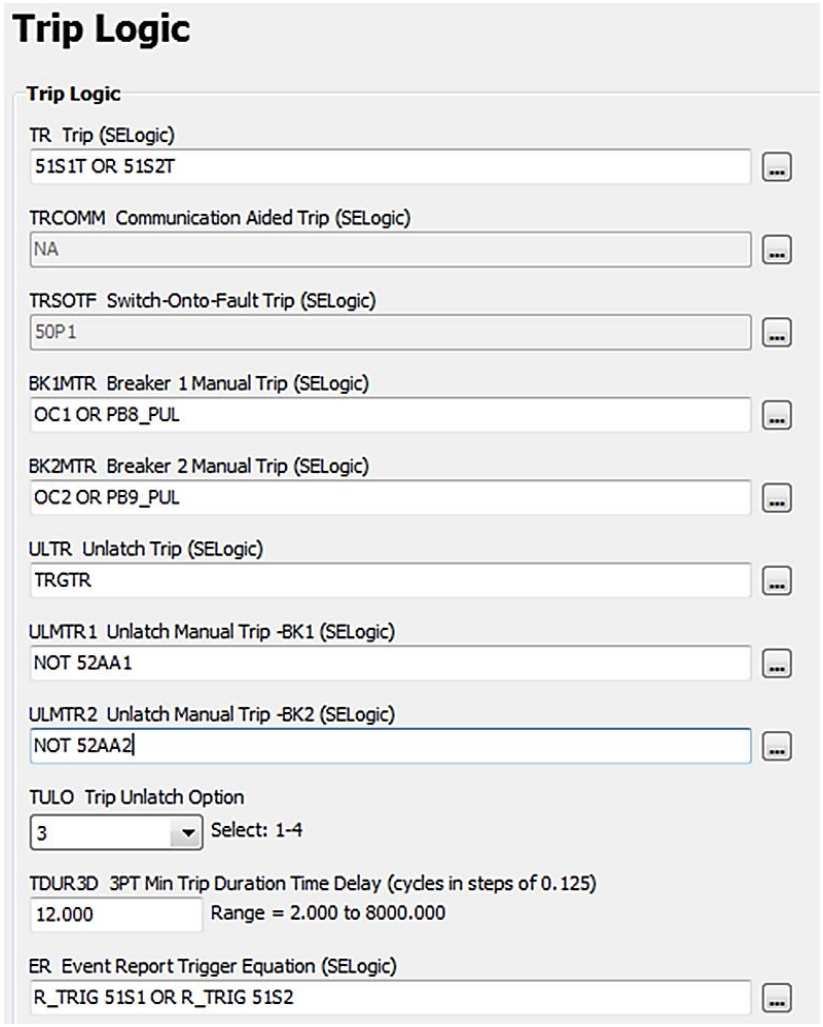

Figure 5.22: “Trip Logic” setting of Group 2 for Relay 3

In adaptive overcurrent protection for a microgrid with distributed generators, “Trip Logic” functions of overcurrent elements were activated to trip Breakers 1 and 2 operated by overcurrent elements from Relays 2 and 3. Therefore, if time overcurrent elements 1 and 2 needed to trip relay’s breakers at fault overcurrents, “51S1T OR 51S2T” was used in “TR Trip” settings. If time overcurrent element 1 needed to trip relay’s breaker at fault overcurrent, “51S1T” was used in “TR Trip” settings. However, if time overcurrent element 2 needed to trip relay’s breaker at fault overcurrent, “51S2T” was used in “TR Trip” settings. If time overcurrent elements 1 and 2 did not need to trip relay’s breakers at fault overcurrents, “NA” was used in “TR Trip” settings. Using Table 5.2, “TR Trip” SELogic settings for all groups of Relays 2 and 3 were created based on trip and non-trip situations of Breakers 1 and 2. Table 5.3 indicates “TR Trip” settings for groups of Relays 2 and 3.

Table 5.3: Trip settings of groups for Relays 2 and 3

Relays	Groups	Breaker		Element	Breaker Operation	TR Trip (SELogic)
		N°	Name			
2	1	1	BK6	1	Trip	51S1T
		2	BK5	2	No trip	
	2, 4	1	BK6	1	No trip	51S2T
		2	BK5	2	Trip	
	3	1	BK6	1	No trip	NA
		2	BK5	2	No trip	
3	1	1	BK8	1	Trip	51S1T
		2	BK7	2	No trip	
	2	1	BK8	1	Trip	51S1T OR 51S2T
		2	BK7	2	Trip	
	3, 4, 5	1	BK8	1	No trip	51S2T
		2	BK7	2	Trip	
	6	1	BK8	1	No trip	NA
		2	BK7	2	No trip	

Adaptive overcurrent protection system for a microgrid with distributed generators was based on the setting group method and protection logic to control Breakers 1 and 2 of the relays.

Protection logic variables controlled the trip of overcurrent elements 1 and 2 for setting groups of Relays 2 and 3. Control outputs OUT101and OUT106 tripped Breaker 1 of Relays 2 and 3 for NRTS and RTS experimental circuits, respectively. However, control outputs OUT102 and OUT107 tripped Breaker 2 of Relays 2 and 3 for NRTS and RTS experimental circuits, respectively. OUT101-2 and OUT106-7 were normally open (NO) and close (NC) control outputs, respectively.

Control outputs OUT101 and OUT106 tripped Breaker 1, and control outputs OUT102 and OUT107 tripped Breaker 2. Control outputs that tripped Breakers 1 and 2 needed SELogic variables PSV03 and PSV04, respectively. Therefore, Breakers 1 and 2 of Relays 2 and 3 needed to set protection logic variables for each setting group. Figure 5.23 shows protection logic variables of setting groups for Relay 2. In the adaptive overcurrent protection system, Relay 2 used four setting groups: SS1, SS2, SS3, and SS4. The "AND" gate was applied to Breaker 1/setting group1 and Breaker 2/setting groups 2 and 4.

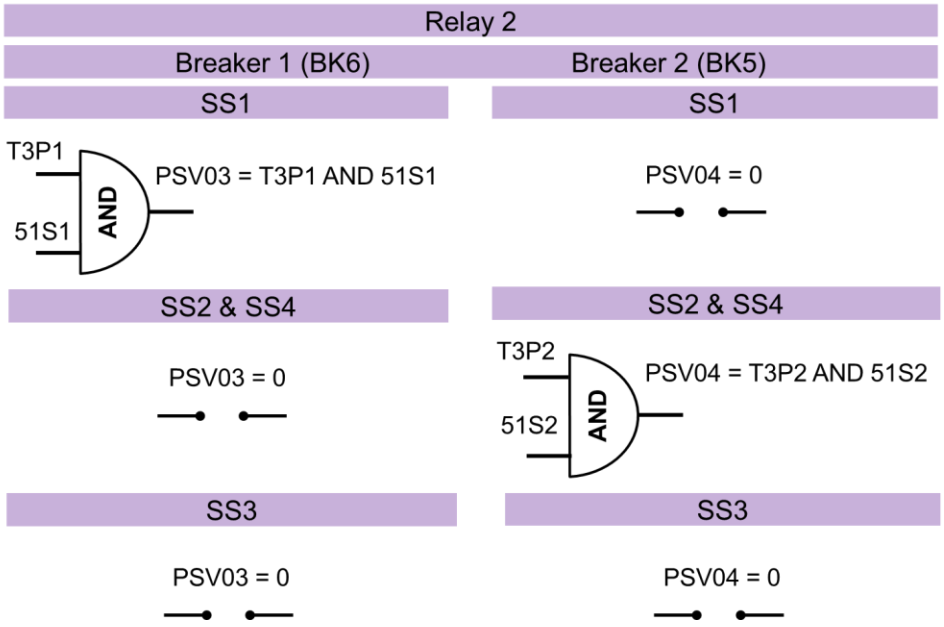

Figure 5.23: Protection logic variables of setting groups of Relay 2

Figure 5.24 shows protection logic variables of setting groups for Relay 3. In the adaptive overcurrent protection system, Relay 3 used six setting groups: SS1, SS2, SS3, SS3, SS4, SS5, and SS6. The “AND” gate was applied for Breaker 1/setting groups 1 and 2 and Breaker 2/setting groups 2, 3, 4, and 5.

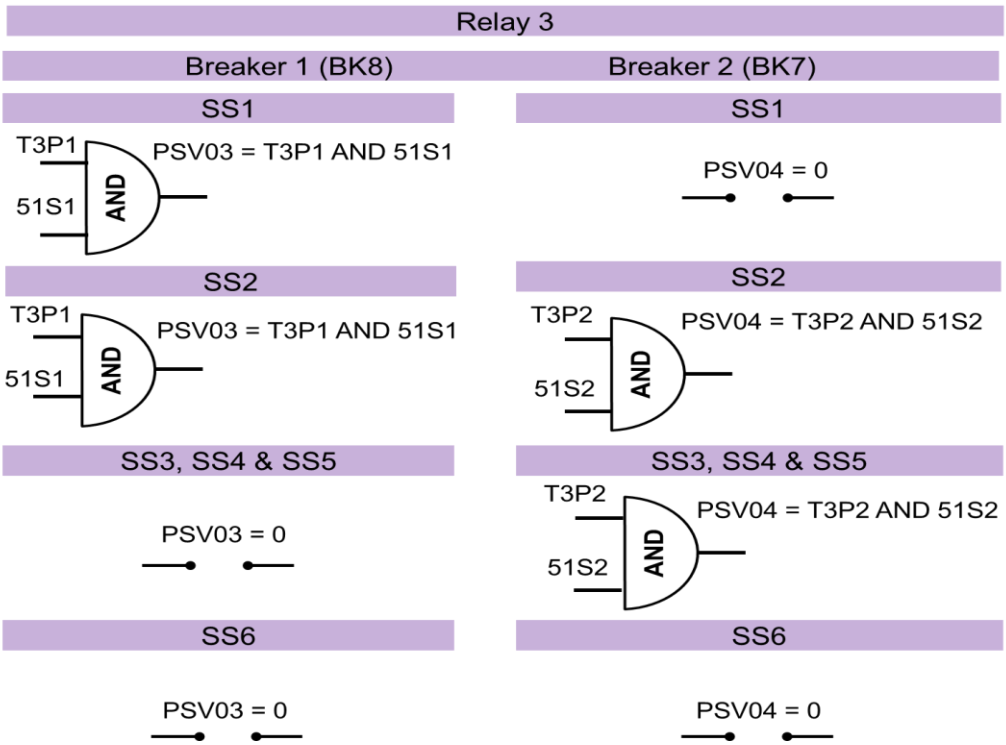

Figure 5.24: Protection logic variables of setting groups of Relay 3

The “AND” gate was applied to protection logic variables that must trip the breakers. The “AND” gate generated the relay’s trip to open the breakers during an overcurrent fault situation. The “AND” gate had to add the inverse time overcurrent element pickup (51S1 or 51S2) and trip circuit breaker (T3P1 or T3P2) digital signals in order to generate the trip signal. However, the “ZERO” gate (open circuit) gate was applied to protection logic variables that must not trip the breakers. Protection logic variables of Figures 5.23 and 5.24 were set on groups of Relays 2 and 3. Figure 5.25 shows protection logic variables for the setting group 2 of Relay 3. In this case, lines 15-16 were added to default protection logic settings provided by the relay manufacturer.

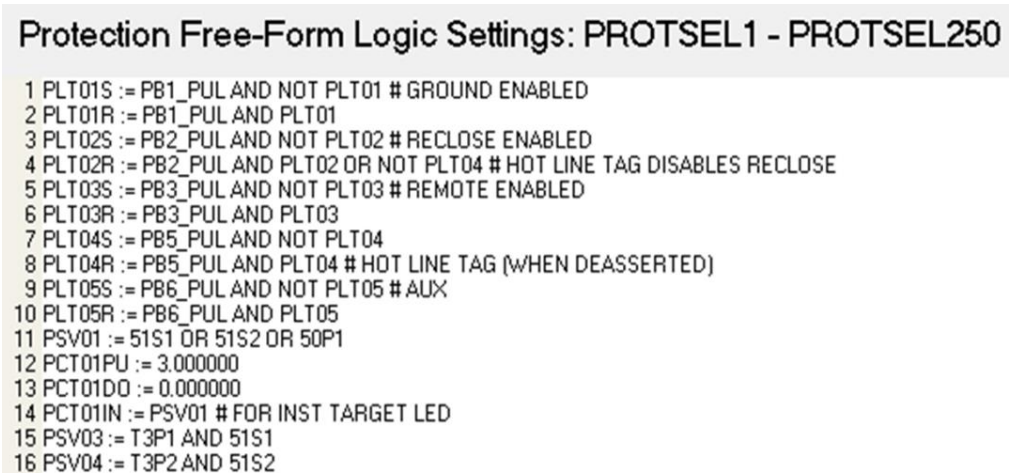

Figure 5.25: Protection logic for the setting group 2 of Relay 3

In protection logic settings, protection SELogic variables "PSV03:= T3P1 AND 51S1" and "PSV04:= T3P2 AND 51S2" were applied to trip Breakers 1 and 2 of Relay 3. Protection logic of each setting group for Relays 2 and 3 were defined by PSV03 and PSV04 variables in order to trip Breakers 1 and 2, respectively. Based on setting groups for Relays 2 and 3, protection logic settings were defined by "PSV03" and "PSV04" variables, as shown in Table 5.4.

Table 5.4: Protection logic settings

Setting groups of		**Protection Logic Variables**
Relay 2	**Relay 3**	
SS1	SS1	PSV03 := T3P1 AND 51S1, PSV04 := 0
-	SS2	PSV03 := T3P1 AND 51S1, PSV04 := T3P2 AND 51S2
SS2, SS4	SS3, SS4, SS5	PSV03 := 0, PSV04 := T3P2 AND 51S2
SS3	SS6	PSV03 := 0, PSV04 := 0

5.2.4 Outputs

The "Outputs" settings of Relays 2 and 3 for adaptive overcurrent protection were identical. The "Outputs" setting defined relay control outputs of Relays 2 and 3 for NRTS and RTS experimental circuits. Figure 5.26 shows the setting path of "Outputs" for Relays 2 and 3, was segregated into the "Main Board, Interface Board Outputs, Communication Card Outputs,

and Mirrored Bits Transmit Equations". The "Main Board" option was set for Relays 2 and 3. However, default settings provided by the relay manufacturer were used for "Interface Board Outputs, Communication Card Outputs, and Mirrored Bits Transmit Equations" options. "Outputs" settings for Relays 2 and 3 were based on tripping relays' breakers in NRTS and RTS experimental circuits. Control outputs of Relays 2 and 3 for NRTS and RTS experiments represented trip signals that opened breakers during the tests. These trip signals were represented by "PSV03" and "PSV04" variables in order to trip Breakers 1 and 2, respectively.

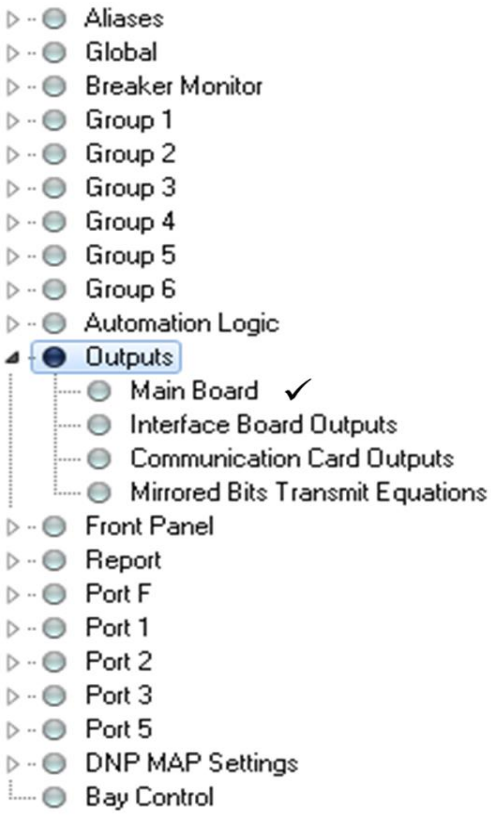

Figure 5.26: Setting path of outputs

In the NRTS experiment, Relays 2 and 3 had OUT101 and OUT102 control outputs to trip Breakers 1 and 2, respectively. However, in the RTS experiment, Relays 2 and 3 had OUT106 and OUT107 control outputs to trip Breakers 1 and 2, respectively. OUT101 and OUT102 were typically open (NO) control outputs, and OUT106 and OUT107 were typically

closed (NC) control outputs. Figure 5.27 shows settings of “Main Board Outputs” for Relays 2 and 3.After placing PSV03 and PSV04 variables on the cells, the “#” symbol allowed to indicate a reference, as e.g. the operational breaker and available experiment for each control output.

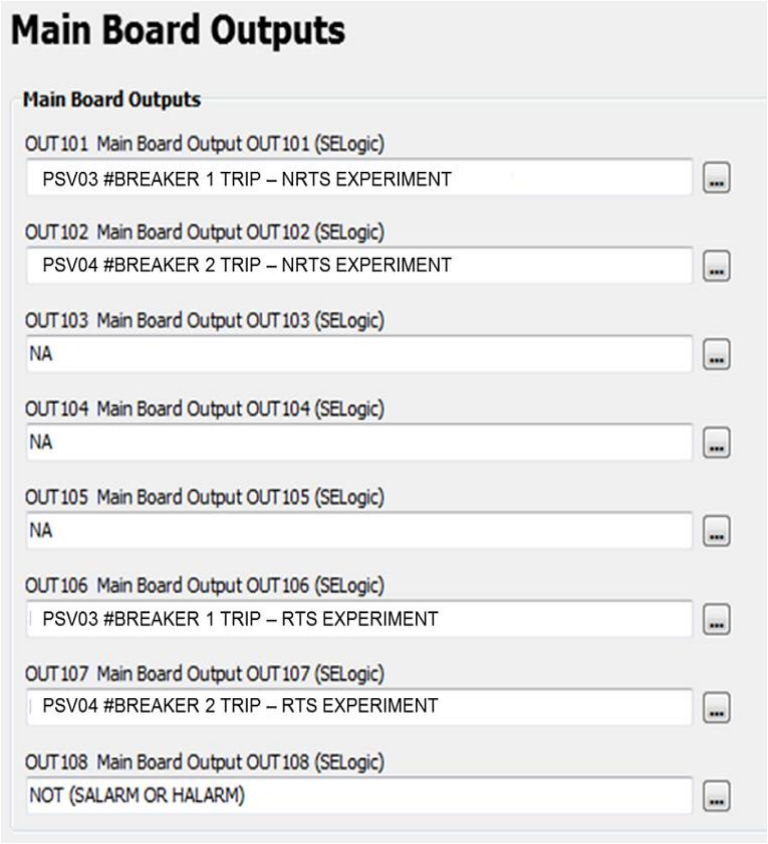

Figure 5.27: Main board outputs for Relays 2 and 3

5.2.5 Front panel

“Front Panel” settings of Relays 2 and 3 for adaptive overcurrent protection were similar. The “Front Panel” setting defined push-button LEDS on the front panel of the relays and selectable screens of the relay’s display. These selectable screens were defined based on information desired to be seen during tests for NRTS and RTS experiments with relays in the loop. These selectable screens could also be synchronized, showing selectable screens during a period of time that could be set on “Selectable Screen” settings, by sizing the “Front Panel Display Update Rate” in order to keep a selectable screen frozen for up to 15 sec..

Figure 5.28 shows the setting path of the “Front Panel” for Relays 2 and 3. Default settings provided by the relay manufacturer were used for “Front Panel, Target LEDs, Selectable Operator Pushbuttons, Display Points and Aliases, Local Control, and Local Bit SELogic” options. However, “Pushbuttons, Selectable Screens, and Event Display” options were set on Relays 2 and 3.

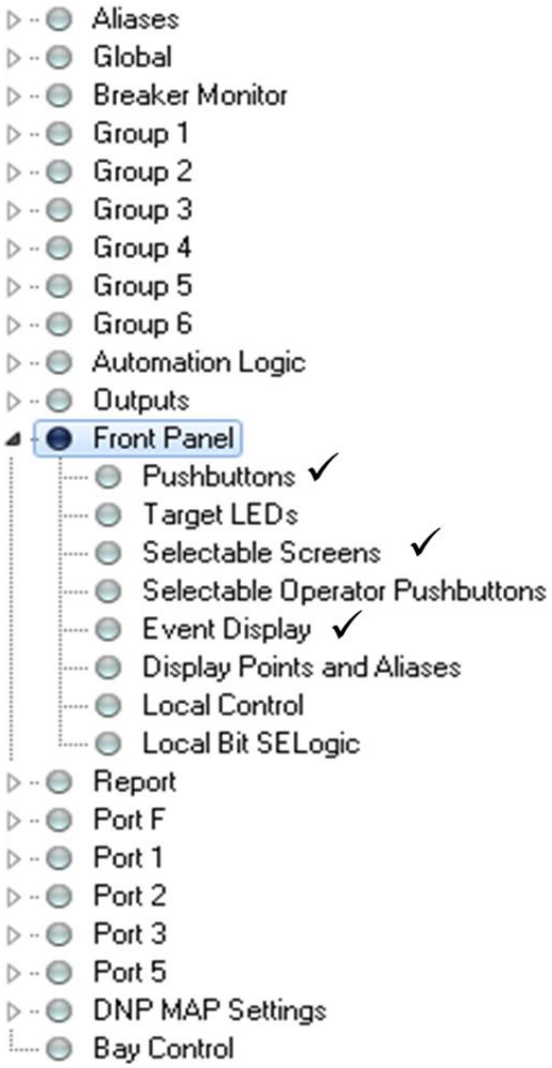

Figure 5.28: Setting path of the front panel

The “Pushbuttons” option was used to set functions of push-button LEDs on the front panel of Relays 2 and 3. Figure 5.29 (A) and (B) show the settings and location of push-button

LEDs, respectively. Push-button LEDs “PB1_LED,” “PB2_LED,” and “PB3_LED” indicated enabled ground, reclose, and remote functions, respectively. Push-button LEDs “PB4_LED” indicated alternative setting groups (2, 3, 4, 5, and 6). Push-button LEDs “PB5_LED” and “PB6_LED” indicated the close and trip of Breaker 1, and push-button LEDs “PB7_LED” and “PB8_LED” indicated the close and trip of Breaker 2.

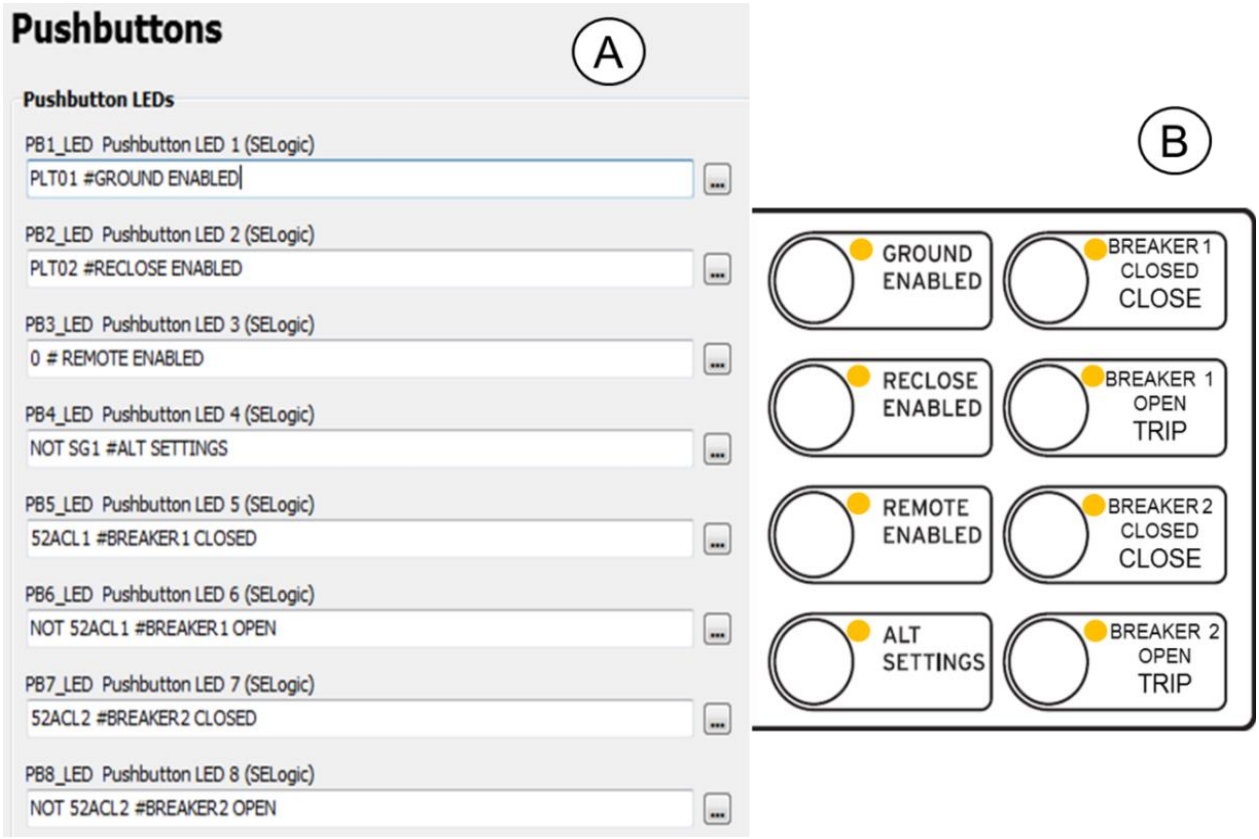

Figure 5.29: Settings (A) and location (B) of push-button LEDs

The “Event Display” setting is shown in Figure 5.30. “Enable HMI Auto Display of Event Summaries” (DISP_ER) was set as “N” in order to avoid seeing record events on the relay’s display every time the relay tripped. Only currents of Breakers 1 and 2 were shown on relay displays during tests for NRTS and RTS experiments.

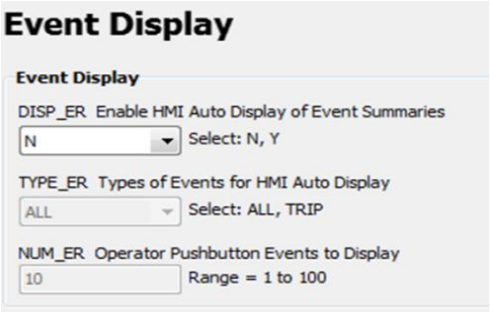

Figure 5.30: Event display settings

Figure 5.31 shows "Selectable Screens" settings of Relays 2 and 3. "Selectable Screens" had shown information on the relay's front panel displays by periodically updating the screens. However, screens of Relays 2 and 3 for NRTS and RTS experiments were kept fixed indicating currents of Breakers 1 and 2 in the relay settings. The "Front Panel Display Update Rate" (SCROLD) in sec. was set to "OFF," and only the "Fundamental Breaker Currents Screen" (FUND_BK) was activated by selecting the "Y" option. Therefore, selectable screens allowed simultaneous views of currents of Breakers 1 and 2 on the relay's front display during tests of NRTS and RTS experiments.

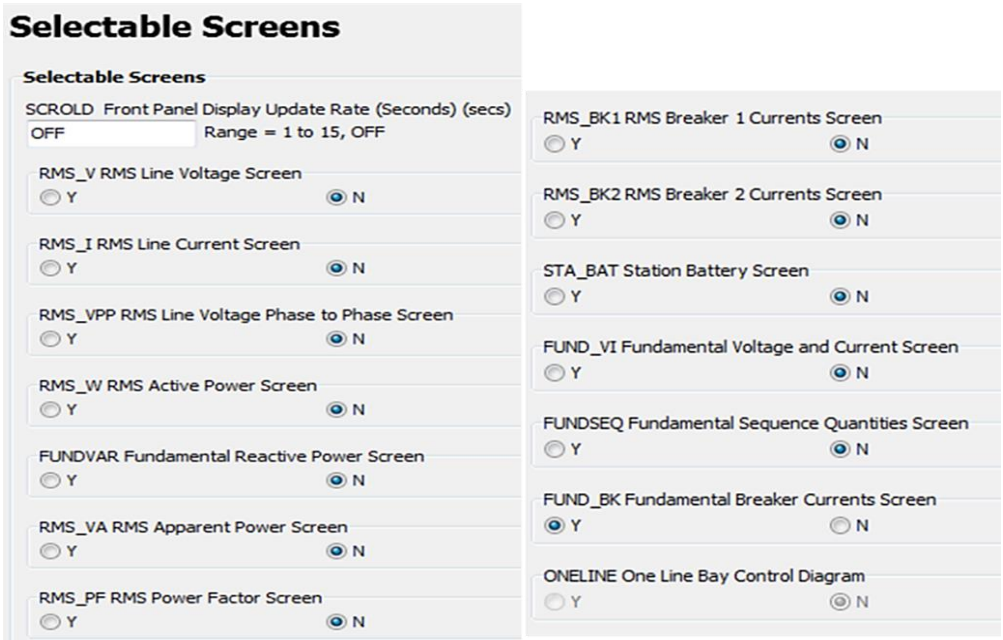

Figure 5.31: "Selectable Screens" setting

5.2.6 Report

The “Report” setting of Relays 2 and 3 for adaptive overcurrent protection were similar. The “Report” setting defined characteristics of record event files, including event reporting digital variables and cycle length of pre-fault, fault, and post-fault states for record event files of Relays 2 and 3. Figure 5.32 shows the setting path of “Report” for the record event of Relays 2 and 3. Default settings provided by the relay manufacturer were used for “SER Chatter Criteria” and “SER Points and Aliases” options. However, “Event Reporting” and “Event Reporting Digitals” were set on Relays 2 and 3 to record event files for tests of the RTS experiment.

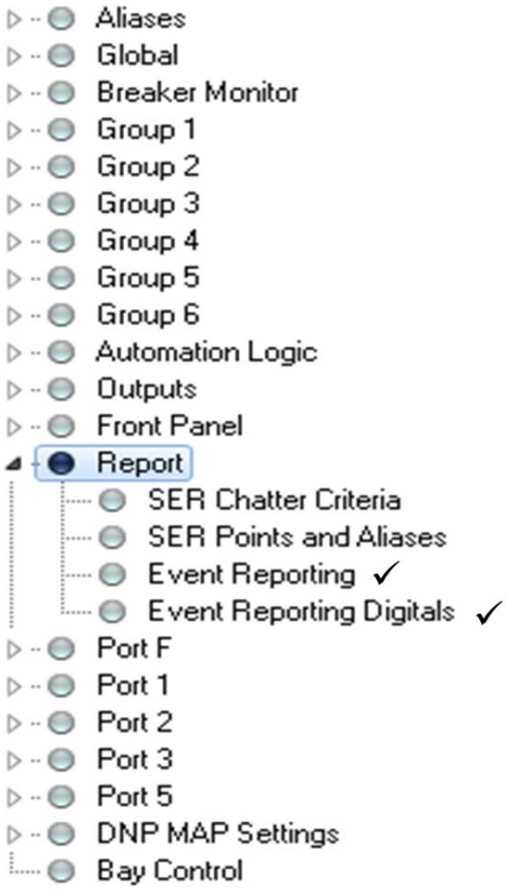

Figure 5.32: Setting path of the “Report” setting

"Event Reporting" settings for Relays 2 and 3 are shown in Figure 5.33. The "Sample Rate of Event Report" (SRATE) was 8 kHz in order to record an event file up to 3.0 sec. based on the relay instruction manual [5]. "Length of Event Report" (LER) was 2.00 sec. (120 cycles), and "Length of the Pre-Fault" (PRE) was set at 0.1 sec. (6 cycles). "Length of Event Report" was based on sizing a period of time that allowed view of breaker currents at fault state for the maximum clearing time, 120 cycles, during RTS experiments.

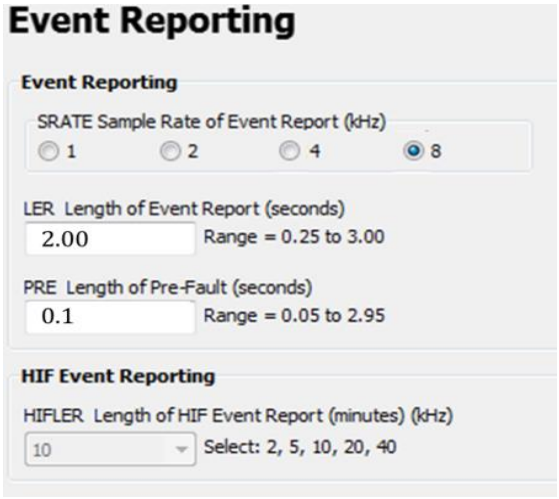

Figure 5.33: Event reporting setting

"Event Reporting Digitals" of Relays 2 (A) and 3 (B) are shown in Figure 5.34. "Event Reporting Digitals" settings allowed collection of relay word bits that corresponded to relay variables as trip signals (TRIP), SELogic variables (PSV03-4), trip circuit breaker 1 and 2 digital signals (T3P1-2), inverse time overcurrent element pickup 1 and 2 digital signals (51S1-2), 52A auxiliary contact of Breaker 1 and 2 (52AA1-2), relay control inputs of NRTS (IN101-2) and RTS (IN103-4) experiments, relay control outputs of NRTS (OUT101-2) and RTS (OUT106-7) experiments, setting groups of relays (SG1-6), relay control inputs of setting groups for the RTS experiment (IN201-4 and IN213-5), and relay control input for breaker record events (IN105) of the RTS experiment. These relay variables were collected from record event files in order to

analyze breaker status, setting groups, logic variables, control inputs and outputs, and trip signals during pre-fault, fault, and post-fault states.

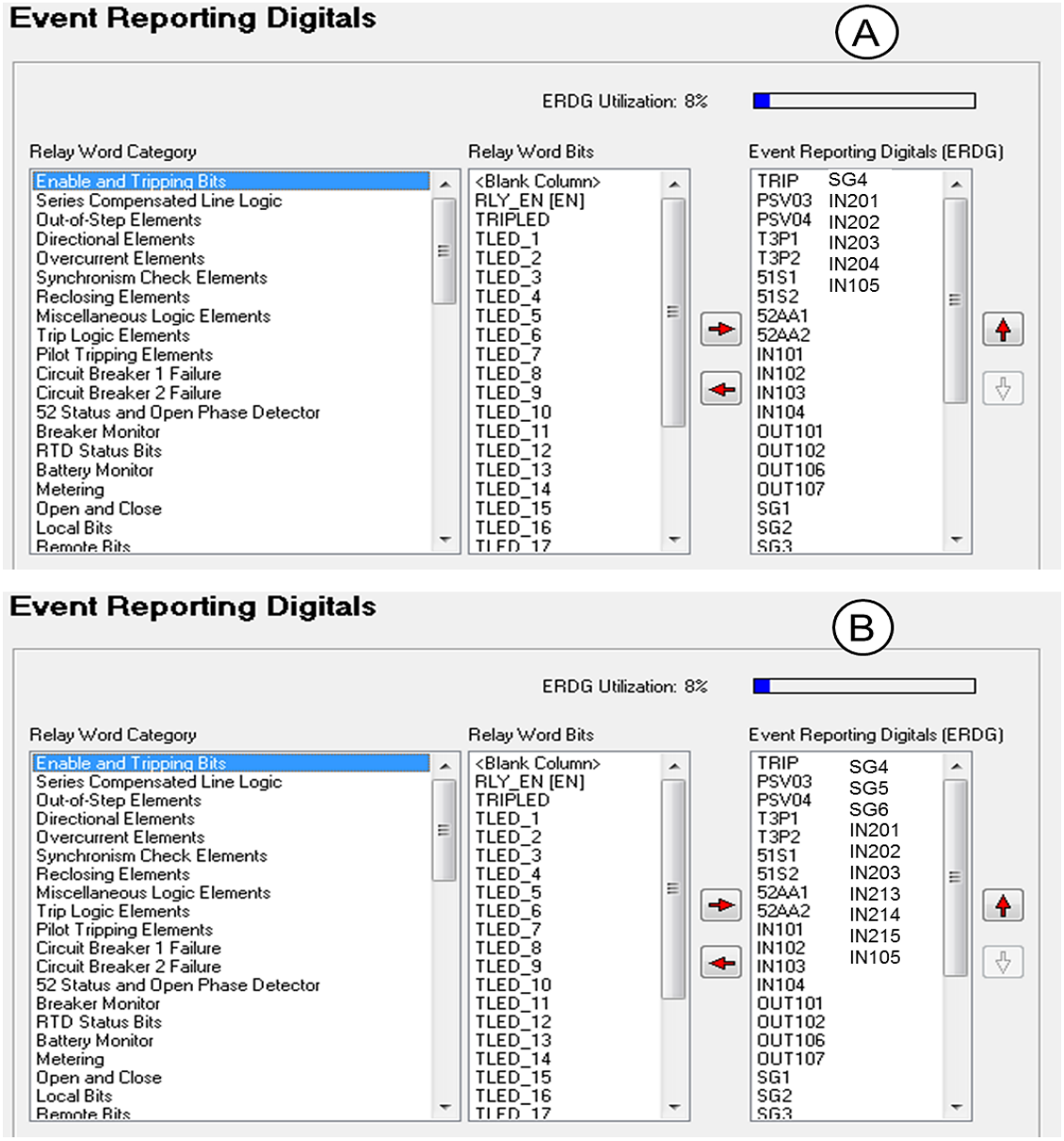

Figure 5.34: “Event Reporting Digitals” setting of Relays 2 (A) and 3 (B)

5.3 Chapter summary

This chapter described settings of Relays 2 and 3 for adaptive overcurrent protection of a microgrid with distributed generators. Using AcSELerator Quickset® software [11] and the SEL 451 relay instruction manual [5], Relays 2 and 3 were set. Adaptive overcurrent protection of

Relays 2 and 3 were based on the setting group method. The number of setting groups depended on available circuit paths and current directions along breakers of the relays. Relays 2 and 3 were located on a line and generator bus, respectively. In Relay 2, breaker currents could flow in the identical direction. However, in Relay 3, breaker currents could flow in the identical and opposite directions. Relays 2 and 3 had four and six setting groups, respectively.

In adaptive overcurrent protection, overcurrent elements of setting groups tripped a signal during an overcurrent fault situation. Each relay had two breakers, and setting groups had protection logic variables to trip breakers by relay control outputs. Protection logic variables "PSV03" and "PSV04" corresponded to Breakers 1 and 2 of Relays 2 and 3. Current transformer ratios for NRTS and RTS experiments were 200 and 50, respectively. Therefore, inverse time overcurrent settings of overcurrent elements 1 and 2 of Relays 2 and 3 were set with no identical overcurrent pickups for the setting groups based on Equation (5.6) but with the identical multiple of pickup for setting groups of relays in NRTS and RTS experiments.

"Global, Breaker Monitor, Groups, Outputs, Front Panel, and Report" options were set for Relays 2 and 3. In the "Global" setting, power system characteristics were identified as station names, system phase rotation, and nominal system frequency. In "Breaker Monitor" setting, relay control inputs were defined in order to sense breaker pole states. In the "Group" setting, inverse time overcurrent settings and protection logic variables were set for overcurrent elements of setting groups. In "Outputs", relay control outputs were set to trip relay breakers. In "Front Panel" setting, push-button LEDs and selectable screens were defined on the relay's front panel. Finally, in the "Report" setting, characteristics of record event files were defined, including event reporting digital variables and length in cycles of pre-fault, fault, and post-fault states for record event files of the relays.

Chapter 6 - Experimental circuits

The adaptive overcurrent protection for a microgrid with distributed generation was verified with a NRTS and RTS with two SEL 451 relays in loop experiments. This chapter defines the hardware and software for both experiments and experimental circuits using an SEL-AMS and OP5600 as a NRTS and RTS, respectively. The relay's LLTI, mainboard input voltages, and control inputs and outputs were described for the relays using the SEL 451 relay instruction manual [5] and SEL website.

The NO and NC relay trip circuits for NRTS and RTS experiments were described during pre-fault, fault, and post-fault sequence. Analog and digital signals applied on experimental circuits were described based on the SEL-AMS instruction manual [3] and OP5600 user guide [4]. The interface between relay control inputs and RTS digital outputs was presented as a high voltage interface panel (HVIP). NRTS and RTS experiments were segregated into sub-circuits that were named current and voltage measurement, breaker trip, breaker state pole, setting group, and breaker record event circuit. Diagrams of the sub-circuits were compared for NRTS and RTS experiments.

6.1 Equipment and software

NRTS and RTS experiments with two relays in the loop were developed in the Burns & McDonnell – K-State Smart Grid Laboratory [8], Kansas State University, Manhattan, Kansas, using computers located on the power desk (A) and RTS, NRTS, HVIP, and relays installed on the rack panels (B), as shown in Figure 6.1.

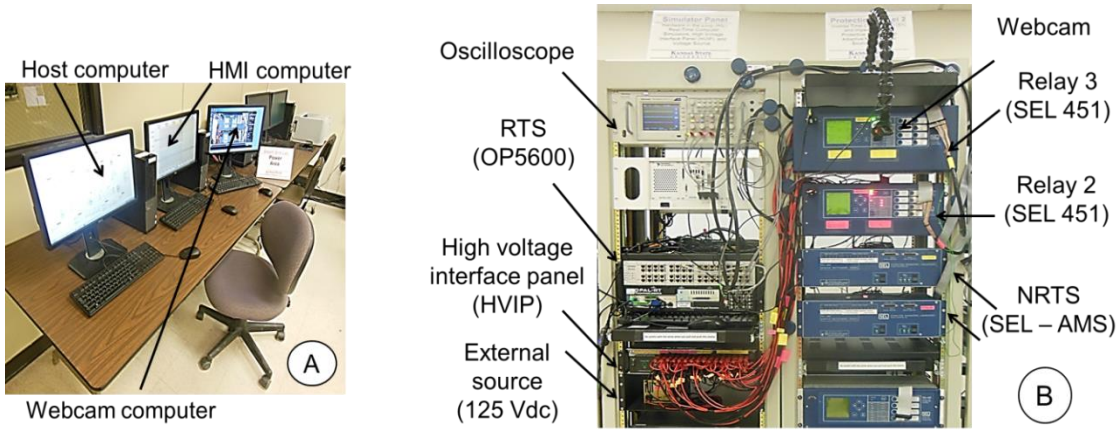

Figure 6.1: Power desk (A) and rack panels (B)

The power desk, a human machine interface (HMI) area applied to set SEL451 relays and NRTS and RTS, runs the tests and collects results from the experiments. The power desk contained an HMI computer, host computer, and webcam computer. The HMI computer was used to set SEL451 relays and NRTS tests, collect the relay and clearing time from the NRTS experiment, and relay record events from the RTS experiment. The host computer created the RT-LAB® project, set RTS tests, run the RTS experiment, and collected breaker currents, states, and trips after running RTS tests. The webcam computer was used to record relay display and supervise relay front panel LEDs during the tests. Tasks developed for each computer during NRTS and RTS experiments are shown in Table 6.1.

Table 6.1: Computers and experiments

Computer	NRTS Experiment	RTS Experiment
HMI	Set SEL451 relays and NRTS tests, run the NRTS experiment, collect the relay and clearing time from tests	Set SEL451 relays and collect relay record events after running tests
Host	Not available	Create the RT-LAB® project, set RTS tests, run the RTS experiment, and collect breaker currents, states, and trips after running RTS tests
Webcam	Make relay videos and supervise relay front panel LEDs during tests	Supervise relay front panel LEDs during tests

In the NRTS and RTS experiments, an SEL-AMS and OP5600 were installed as relay test systems, respectively. The NRTS experiment required calculation of pre-fault, fault, and post-fault currents and line-ground voltages in order to set the NRTS tests. However, the RTS experiment was based on building the microgrid with distributed generators and running tests in real-time. In the NRTS experiment, Power World Simulator software [10] was used to calculate bus line-ground voltages and line currents and AcSELerator Quickset software [11] was used to communicate and set SEL 451 relays. SEL-5401 software [12] was used to set NRTS tests, run the NRTS experiment, and collect the relay and clearing time. In the RTS experiment, AcSELerator Quickset software was used to communicate, set, and collect record events of SEL 451 relays; the Redhat software [88] was used to connect the OP5600 target and host computer; the RT-LAB® 10.5 software [13] was used to create the RT-LAB® project, run the RTS experiment, and collect breaker states (closed or open) and currents after running the tests. Matlab® Simulink® software [14] was also integrated into the RT-LAB® 10.5 software to create the RT-LAB® project using Simulink®, Simscape, Artemis, RT-LAB®, and RT-LAB® I/O libraries. Figure 6.2 shows the software for NRTS (A) and RTS (B) experiments with SEL 451 relays in the loop.

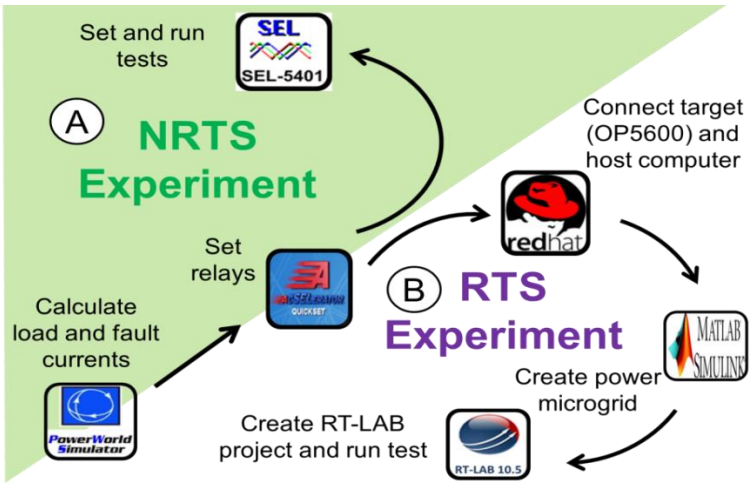

Figure 6.2: NRTS and RTS experiments and software

Before running the tests of RTS experiment, the LabView Signal Express software [89] was applied to measure analog output and input signals of OP5600 that represented breaker currents and bus line-ground voltages and relay trip signals, respectively. Table 6.2 lists equipment applied in the NRTS and RTS experiments, including equipment name, description, and manufacturer.

Table 6.2: List of equipment

Exp.		**Equipment**				
NRTS	**RTS**	**Item**	**Qty.**	**Name**	**Description**	**Manufacturer**
		1	1	SEL 451	SEL 451-2 relay, 300 V phase - neutral maximum (wye), 5 A phase, 125 Vdc mainboard input	Schweitzer Engineering Laboratories
		2	1	SEL 451	SEL 451-2 relay, 300 V phase - neutral maximum (wye), 5 A phase, 110 Vdc mainboard input	
		3	2	SEL-AMS	SEL relay test system, 110 Vac	
		4	1	Oscilloscope	Oscilloscope with digital storage, 200MHz, 2GS/s, 4-CH, TFT color display, USB ports	Tektronix
		5	1	OP5600 HIL	OP5600 HIL box real-time computer 3.46 GHz, 12 cores (OP5142 platform)	OPAL-RT Technologies Inc.
		6	1	High voltage interface panel	High voltage solid state relay box, 16 channels (250 Vdc, 250 mA)	OPAL-RT Technologies Inc.
		7	1	Source	Linear regulated power supply, 125 Vdc, ± 1 V, model L125MC50	Acopian
		8	1	Webcam	Microsoft LifeCam, 720p HD widescreen, autofocus for desktop with windows OS	Microsoft

(1) Desktop computers and cables are not indicated in this equipment list

6.2 NRTS and RTS with relays in the loop circuit

Methods to verify adaptive overcurrent protection for a microgrid with distributed generators were based on use of two relay test systems with relays in the loop. Relay test systems used in this research were SEL-AMS and OP5600 as NRTS and RTS, respectively. Application of SEL-AMS [3] and OP5600 [4] as relay test systems validated the adaptive overcurrent protection system presented in this research. Relay engineers must validate a new protection system before placing protective relays in substation panels. Figure 6.3 shows the NRTS with relays in the loop circuits. The experimental circuit for the NRTS with two relays in the loop used one SEL-AMS for each relay. Tasks developed from the HMI and webcam computers are indicated in solid arrows. Setting groups of the relays were set from the HMI computer, NRTS tests were downloaded and run, and the relay and clearing time were collected. The webcam computer recorded relay display and supervised tests. Dot arrows represent analog and digital signals in Figure 6.3, and analog outputs and digital outputs and inputs are referenced to the SEL-AMS. Therefore, an output for SEL-AMS represents an input for the relay and vice versa. NRTS analog outputs and digital inputs and outputs are represented by dash green, blue and grey arrows, respectively. Analog outputs represent Phase A, B, and C currents for Breaker 1 (IAW, IBW, ICW) and 2 (IAX, IBX, ICX) and line-ground bus voltages (VAY, VBY, VCY). Digital inputs represent the trip signal sent by relay control outputs to open Breaker 1 or 2 during an overcurrent fault situation. Digital outputs represent Breaker 1 and 2 states (closed or open) simulated by SEL-AMS during pre-fault, fault, and post-fault states. In the NRTS experiment, setting groups for the relays were selected manually before running the tests.

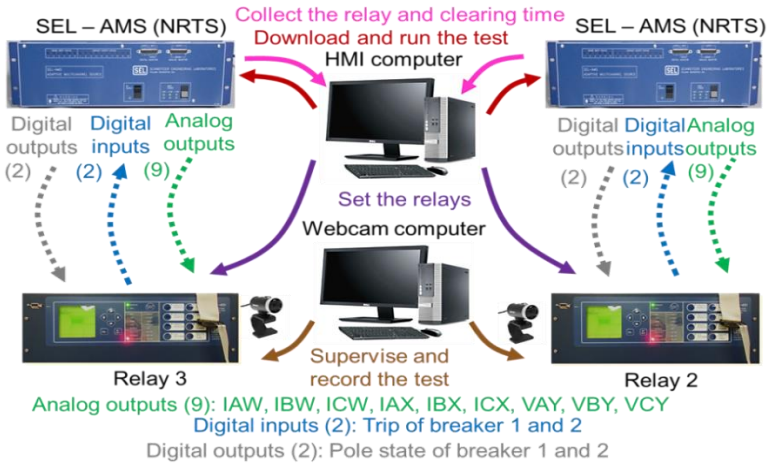

Figure 6.3: NRTS with relays in the loop

The experimental circuit for RTS with two relays in the loop used an OPAL- RT OP5600 real-time simulator with two relays in the loop. Tasks developed from the HMI, host, and webcam computers are indicated in solid arrows in Figure 6.4. The HMI computer set relay setting groups and collected relay record events. The host computer downloaded and ran the tests, and the webcam computer supervised relay front panel LEDs during the tests.

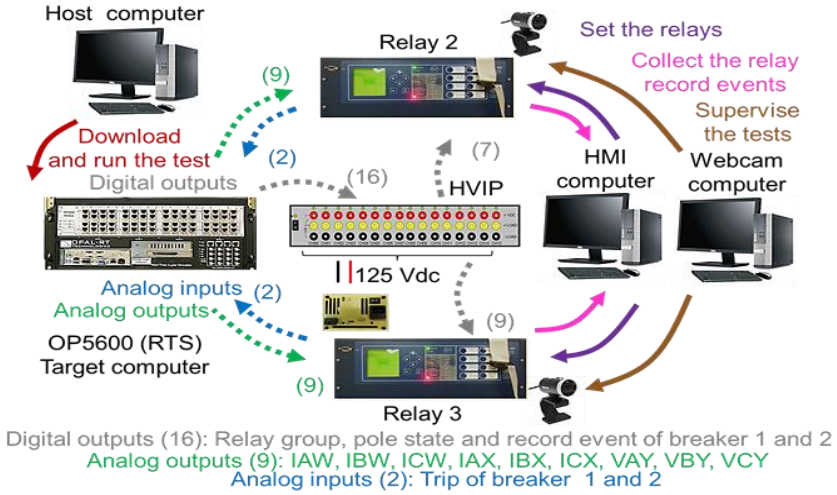

Figure 6.4: RTS with relays in the loop

In Figure 6.4, the dotted lines represent analog and digital signals. Analog outputs and digital outputs and inputs were referenced to OP5600 (RTS). Therefore, an output for OP5600 represented an input for the relay and vice versa. The HVIP was a voltage interface [90] between

RTS digital outputs and relay control inputs that connected 125 Vdc external source to the HVIP. In the RTS experiment, setting groups and breaker record event for Relays 2 and 3 were selected from the host computer based on the circuit path and fault location, respectively. Relays 2 and 3 had to be connected to seven and nine digital outputs, respectively. Two digital outputs sensed pole states of Breaker 1 and 2, and one digital output selected the breaker record event. Four and six digital outputs switched setting groups of Relays 2 and 3, respectively.

6.3 Protective relays

Two SEL 451 relays were used in the NRTS and RTS experiments. In both experiments, one relay was located on a line bus and the other relay was located on the distributed generator bus. The line bus relay was named Relay 2 and the distributed generator bus relay was named Relay 3. Both relays sensed currents from two feeders in order to trip Breaker 1 or 2. SEL 451 relays had two breakers named Breaker 1 and 2. Breaker 1 of Relays 3 and 2 were named "BK8" and "BK6", respectively, and Breaker 2 of Relays 3 and 2 were named "BK7" and "BK5", respectively. Figure 6.5 shows breakers of Relays 2 and 3 for the DG2-678/65 circuit path.

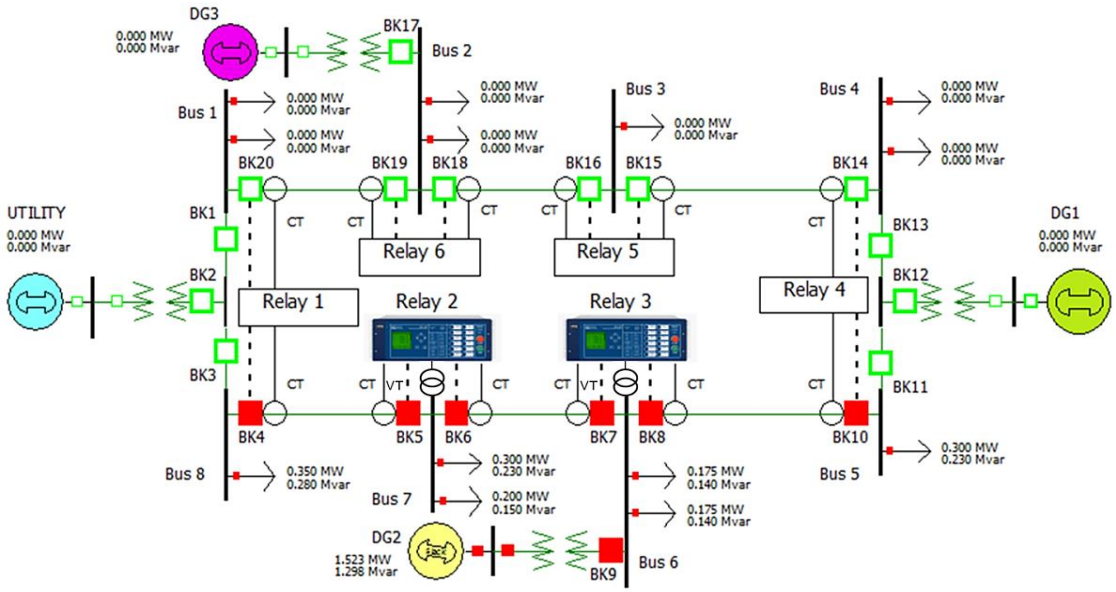

Figure 6.5: Breakers of Relays 2 and 3, DG2-678/65

Serial port F, relay display, LEDs, and LLTI connector were located at the front side of the relays. Serial port F was used to communicate to relay with HMI computer and set setting groups of the relays. The relays were set to close and trip Breakers 1 and 2. The relay display and LEDs were used to supervise tests of the NRTS and RTS experiments with a webcam. Currents of Breakers 1 and 2 were read on the relay display for pre-fault, fault, and post-fault states. The test was also supervised by reading relay front panel LEDs of the breaker states, trip, type of fault, and time overcurrent. Figure 6.6 shows relay front panel LEDs.

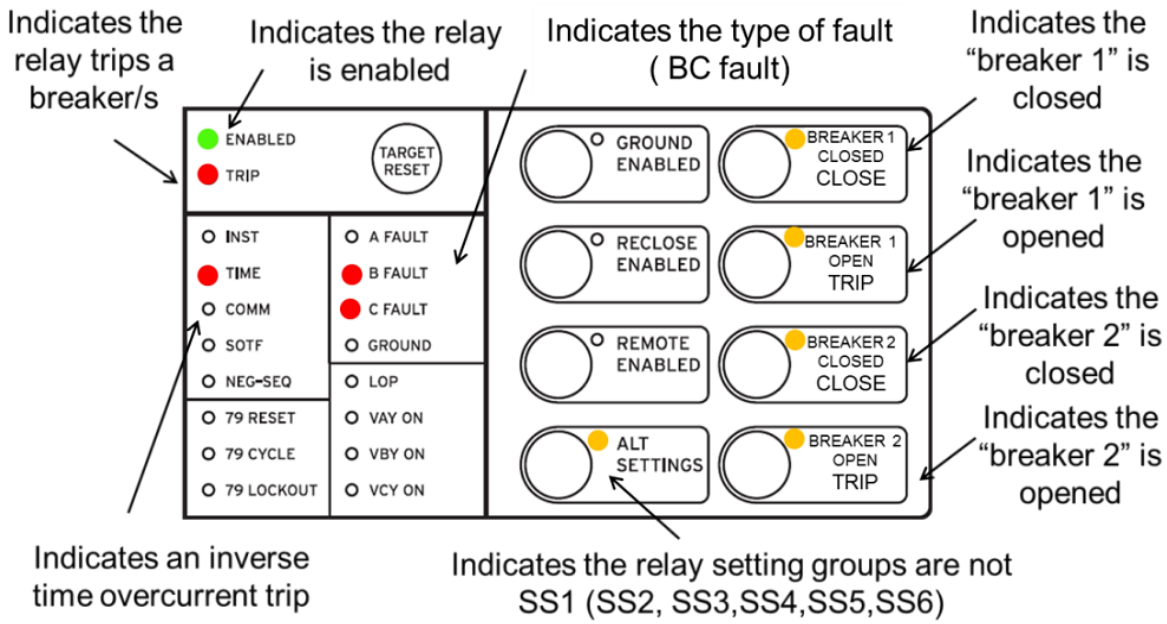

Figure 6.6: Relay front panel LEDs

In SEL 451 relays, current and voltage transformers were connected on the rear side of the relay. However, in RTS and NRTS experiments with relays in the loop, LLTI located on the relay's front side was used to sense secondary currents and voltages from the breaker feeder/s and bus, respectively. LLTI analog signals of the relays were limited to a maximum peak voltage of 3.3 volts based on the SEL 451 relay instruction manual [5]. Maximum peak voltage must be

avoided in order to prevent damage to the LLTI of SEL 451 relays. Figure 6.7 shows LLTI of the SEL 451 relay formed by a 34 PIN male-connector.

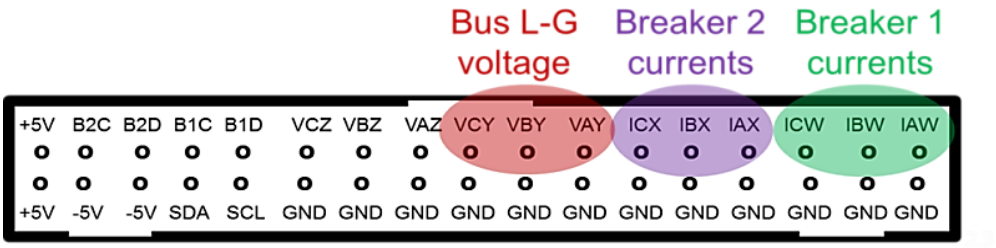

Figure 6.7: Low level test interface of SEL 451 relay

Relay control inputs and outputs were located on the rear side of the relays. In Relays 2 and 3, control outputs tripped (opened) the breakers. Control inputs sensed breaker states, switched relay setting groups, and selected breaker record events. Control output used a signal generated by a 14.3 Vdc source placed on the SEL-AMS to trip relay breakers.

The control input voltage level of Relays 2 and 3 depended on the relay part number usually located on a sticker in the rear side of the relay. Collecting the relay part number and searching the SEL website determined the control input voltage level for SEL 451 relays. After logging onto the relay manufacturer website (https://www.selinc.com), from the main page, "Products" and "Product Configuration (MOT)" were selected from the main page. Relay part numbers were placed on SEL website cells, and the "Display Configuration" tab was selected. Consequently, the "Product Configuration" indicated mainboard input voltage for the relays: 125 Vdc and 110 Vdc for Relays 2 and 3, respectively. Figure 6.8 shows the sequence to find product configuration on the SEL website.

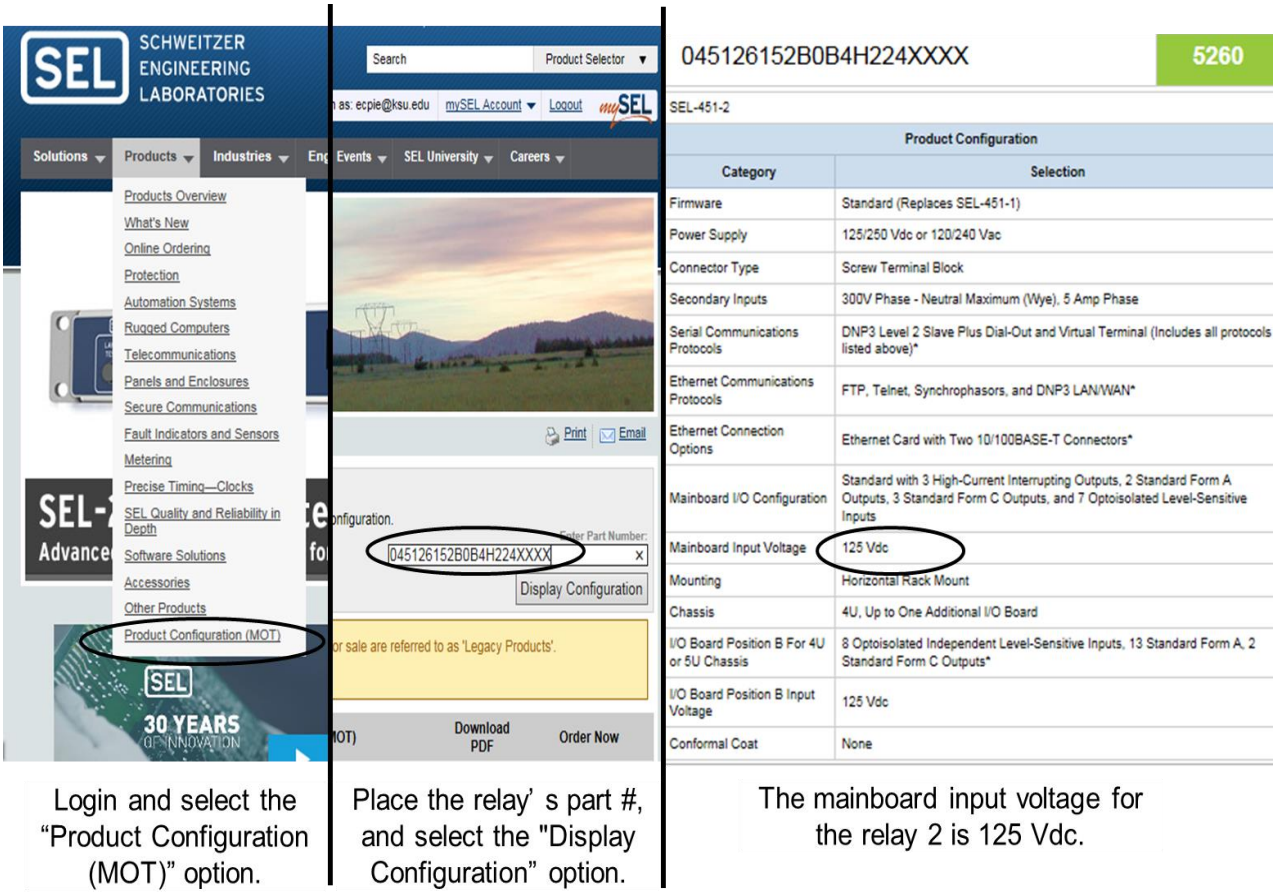

Figure 6.8: SEL website and product configuration

According to the SEL 451 relay instruction manual [5], pickup voltage for 125 and 110 Vdc control inputs were 105-150 Vdc and 88 -132 Vdc, respectively. These voltage ranges defined control inputs for both relays connected at 125 Vdc source. Table 6.3 lists characteristics of Relays 2 and 3.

Table 6.3: Characteristics of SEL 451 relays

Relay name	**Relay 2**	**Relay 3**
Part #	045126152B0B4H224XXXX	045124152XXAX3243XXXX
Control input voltage	125 Vdc : Pickup 105 - 150 Vdc 125 Vdc : Dropout < 75 Vdc	110 Vdc: Pickup 88 - 132 Vdc 110 Vdc: Dropout < 66 Vdc
LLTI	3.3 V (peak value)	

Figure 6.9 shows the rear side of Relays 2 (A) and 3 (B). Relay 2 for NRTS and RTS experiments had four setting groups, SS1, SS2, SS3, and SS4, enabled with relay control inputs IN201, IN202, IN203, and IN204, respectively. However, Relay 3 for NRTS and RTS experiments had six setting groups, SS1, SS2, SS3, SS4, SS5, and SS6, enabled with relay control inputs IN201, IN202, IN203, IN213, IN214, and IN215 respectively. In the NRTS experiment, relay control inputs IN101 and IN102 sensed pole states of Breakers 1 and 2, respectively. In the RTS experiment, however, relay control inputs IN103 and IN104 sensed pole states of Breakers 1 and 2, respectively. In the RTS experiment, the relay control input designated IN105 for both relays in order to select the Breaker 1 or 2 record events.

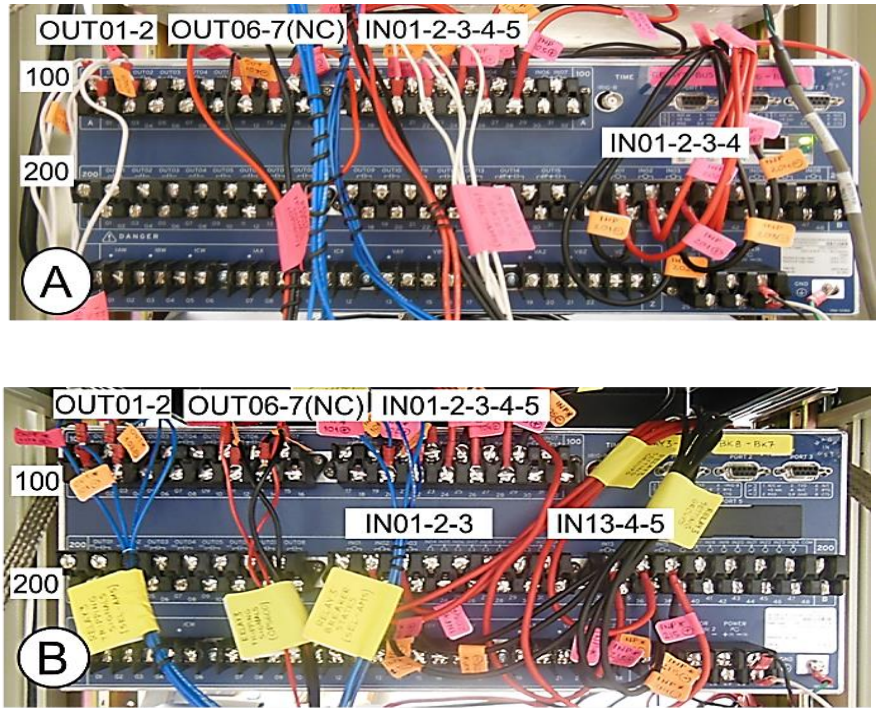

Figure 6.9: Rear side of Relay 2 (A) and 3 (B)

In the NRTS experiment, relay control outputs OUT101 and OUT102 applied trip signals of Breakers 1 and 2, respectively. In the RTS experiment, however, relay control outputs OUT106 and OUT107 applied trip signals of Breakers 1 and 2, respectively. OUT106 and

OUT107 relay control outputs were NC contacts, but OUT101 and OUT102 relay control outputs were NO contacts. Tables 6.4 and 6.5 show relay control inputs and outputs for NRTS and RTS experiments based on Figure 6.9.

Table 6.4: Control digital inputs and outputs of Relay 2

Exp.	Breaker Name	Control Digital Outputs		Control Digital Inputs	
		Name	Function	Name	Function
NRTS	BK6	OUT101	Trips Breaker 1	IN101	Sense pole states of Breaker 1
	BK5	OUT102	Trips Breaker 2	IN102	Sense pole states of Breaker 2
RTS	BK6	OUT106-NC	Trips Breaker 1	IN103	Sense pole states of Breaker 1
	BK5	OUT107-NC	Trips Breaker 2	IN104	Sense pole states of Breaker 2
				IN105	Save record event of Breaker 2
				IN201	Activate the group setting SS1, SS2, SS3 and SS4
				IN202	
				IN203	
				IN204	

Table 6.5: Control digital inputs and outputs of Relay 3

Exp.	Breaker Name	Control Digital Outputs		Control Digital Inputs	
		Name	Function	Name	Function
NRTS	BK8	OUT101	Trips Breaker 1	IN101	Sense pole states of Breaker 1
	BK7	OUT102	Trips Breaker 2	IN102	Sense pole states of Breaker 2
RTS	BK8	OUT106-NC	Trips Breaker 1	IN103	Sense pole states of Breaker 1
	BK7	OUT107-NC	Trips Breaker 2	IN104	Sense pole states of Breaker 2
				IN105	Save record event of Breaker 2
				IN201	Activate the group setting SS1, SS2, SS3, SS4, SS5 and SS6
				IN202	
				IN203	
				IN213	
				IN214	
				IN215	

6.4 Trip circuits

In the NRTS experiment with relays in the loop, relay NO control outputs sent trip signals according to the SEL 451 instruction manual [5]. The AC circuit breaker and auxiliary contacts were based on the Device 52, ANSI/IEEE device number system [40]. An electrical contact (auxiliary contact) associated with a circuit breaker that opens or closes to indicate the breaker position. The 52A auxiliary contacts close when the breaker is closed and open when the breaker is open. However, the 52B auxiliary contacts open when the breaker is closed and close when the breaker is open. The breaker trip circuit (52) was defined by a NO control output of the relay and the trip coil (TC) and NO auxiliary contact (52A) of the breaker. Figure 6.10 indicates the NO trip circuit for the NRTS experiment. The breaker (52) was tripped when the TC coil was energized.

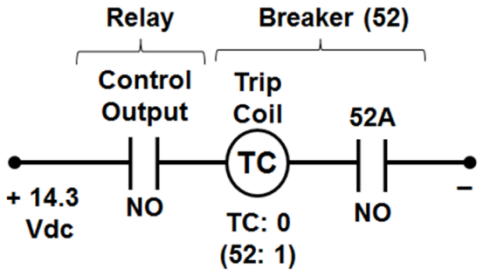

Relay	Breaker (52)		
OUT (NO)	Trip Coil (TC)	Main Poles (52)	52A (NO)
Close	Energized	Trip (0)	Open
Open	No-energized	Close (1)	Close

NO: Normally open, 52: Breaker
52A: NO auxiliary contact of 52 breaker

Figure 6.10: Normally open trip circuit for the NRTS experiment

In Figure 6.11, the following sequence represents the trip circuit sequence of the NRTS experiment: (A) *Pre-fault state*: As the 52 breaker is closed, the 52A breaker NO auxiliary contact is closed, the load current flows along the 52 breaker, and the TC coil is not energized, (B) *Fault state*: The relay detects a fault overcurrent, thereby closing the NO control output (Trip), and then the TC coil is energized, and (C) *Post-fault state*: The 52 breaker is opened clearing the fault overcurrent, thereby the 52A breaker NO auxiliary opened, and the TC coil is not energized.

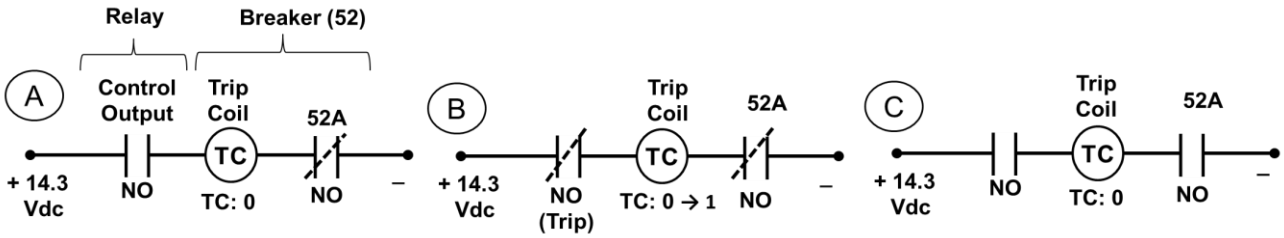

Figure 6.11: Pre-fault (A), fault (B), and post-fault (C) trip circuit sequence for NRTS

Based on the sequence shown in Figure 6.11, pre-fault, fault, and post-fault RMS currents, NO trip signal, and breaker NO auxiliary contact (52A) states are represented in Figure 6.12.

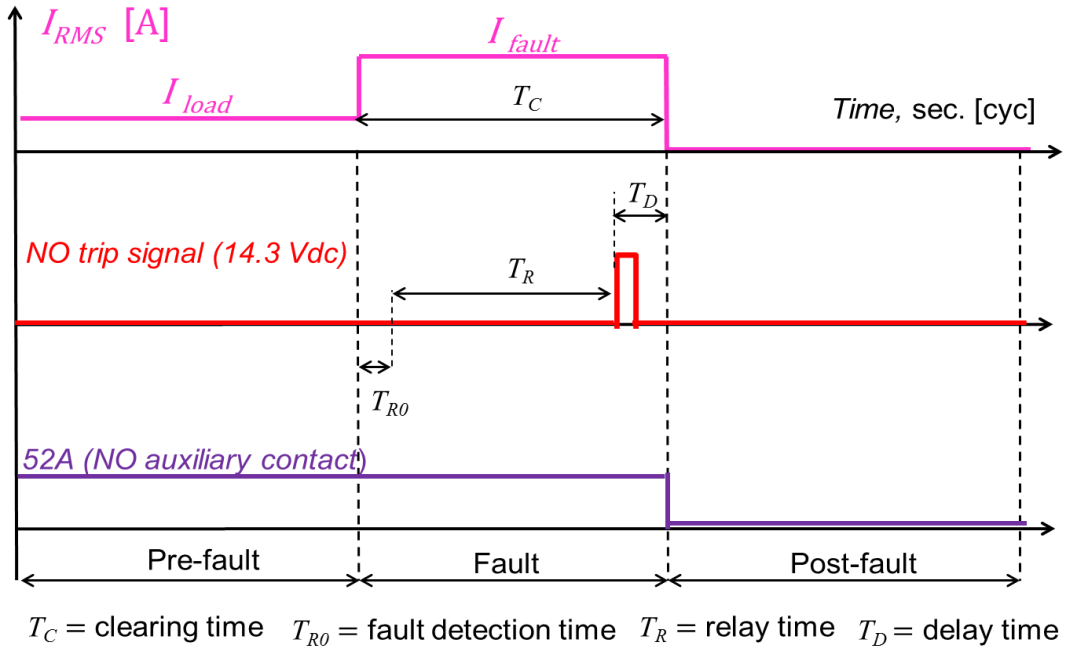

Figure 6.12: Signals of normally open trip circuit

Relays detect a fault overcurrent in less than ¼ cycle (4.16 msec), or the time relays need to calculate operation relay time based on secondary RMS fault current and inverse time overcurrent relay settings. Once the relay generates the trip signal, the fault is cleared after a delay time that represents the breaker (52) and NO auxiliary contact (52A) operation, breaker arc-flash, and relay-breaker communication time.

An NC relay control output was used in the RTS experiment with relays in the loop. Selection of the NC control output of the relay was based on a real-time hardware-in-the-loop (HIL) simulation experiment that validated a relay test for instantaneous overcurrent protection using OPAL-RT OP5600 as a real-time simulator with an SEL421 relay in the loop [68]. With use a NC relay control output, the breaker (52) was tripped when the TC coil was de-energized. The trip circuit for RTS with relays in the loop is presented in Figure 6.13.

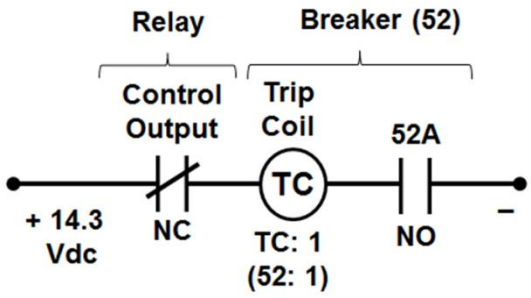

Relay	Breaker (52)		
OUT (NC)	Trip Coil (TC)	Main Poles (52)	52A (NO)
Close	Energized	Close (1)	Close
Open	No-energized	Trip (0)	Open

NC: Normally closed, 52: Breaker
52A: NO auxiliary contact of 52 breaker

Figure 6.13: Normally closed trip circuit for the RTS experiment

In Figure 6.14, the following sequence represents the trip circuit sequence of the RTS experiment: (A) *Pre-fault state*: As the 52 breaker is closed, the 52A breaker NO auxiliary contact is also closed, the load current flows along the 52 breaker, and the TC coil is energized, (B) *Fault state*: The relay that opens the NC control output (Trip) detects a fault overcurrent and then the TC coil begins to be de-energized, and (C) *Post-fault state*: The TC coil is de-energized, the 52 breaker and the 52A breaker NO auxiliary contact are opened, then fault overcurrent is cleared.

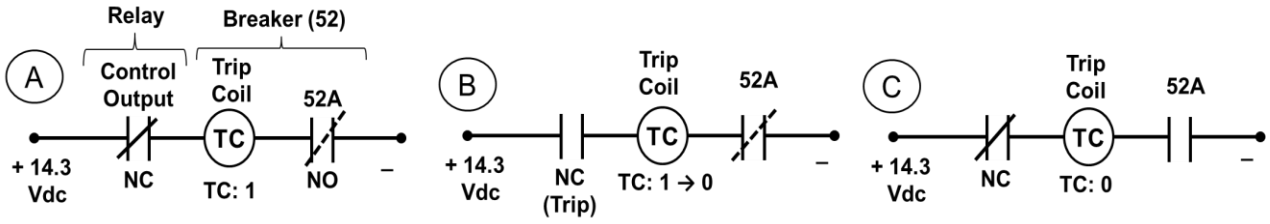

Figure 6.14: Pre-fault (A), fault (B), and post-fault (C) trip circuit sequence for RTS

Based on the sequence shown in Figure 6.14, pre-fault, fault, and post-fault RMS currents, trip signal, and breaker NO auxiliary contact (52A) states are represented in Figure 6.15.

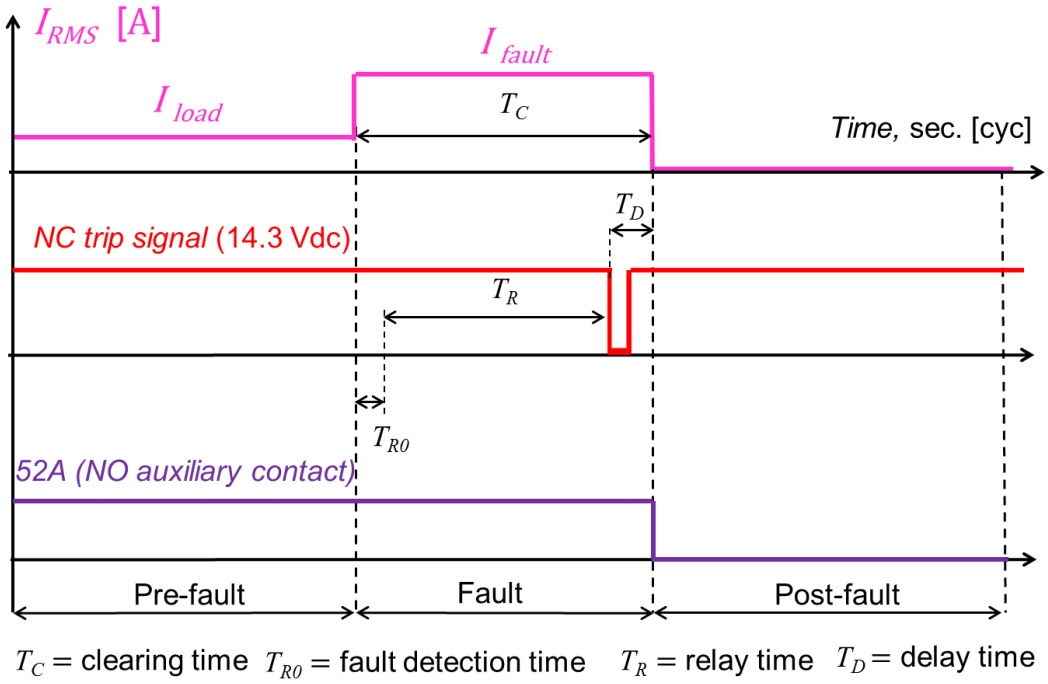

Figure 6.15: Normally closed trip circuit signals

6.5 NRTS and RTS

NRTS and RTS were used as relay test systems to verify the relay setting of adaptive overcurrent protection for a microgrid with distributed generators. Both relay test systems had to simulate current and voltages for pre-fault, fault, and post-fault states and breakers states controlled by relays in the loop.

6.5.1 SEL-AMS

The non-real-time simulator, or SEL-AMS, was a Schweitzer Engineering Laboratory relay test system [3] that simulated secondary currents and voltages, breaker NO auxiliary contacts (52A), and breaker states during pre-fault, fault, and post-fault states. In order to run a

test with SEL-AMS, SEL 5401 software [12] created a relay test with a pre-fault, fault, and post-fault state. These states had to be completed with the breaker NO auxiliary contact (52A) and trip coil states and the magnitude and angle of secondary line currents and line-ground voltages.

The breaker NO auxiliary contact (52A), or contact output, was connected to the relay control input that sensed if the breaker was closed or open. The trip signal turned on the sense input that represents the trip coil of the trip circuit. The sense input was connected to the relay control output that generated a trip signal when the relay detected an overcurrent fault situation. Figure 6.16 shows sense input and contact output LEDs on the front side of SEL-AMS.

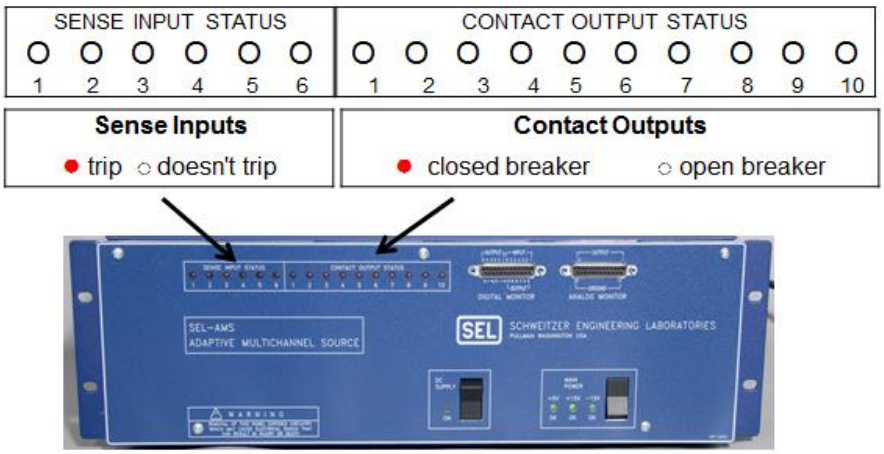

Figure 6.16: SEL- AMS front side

Power flow and fault analysis had to estimate secondary currents and voltages, or analog outputs, before the tests were run. Power flow analysis was used to calculate primary line currents and line-ground bus voltages during pre-fault and post-fault states, and fault analysis was used to calculate primary line currents and line-ground bus voltages during the fault state. In the NRTS experiment, Power World software performed the power flow and fault analysis. Secondary line currents and line-ground voltages were estimated by dividing calculated primary line currents and line-ground voltages by current and voltage transformer ratios, respectively.

Figure 6.17 shows contact outputs, sense inputs, analog outputs and DC supply output connections from the rear side of the SEL-AMS. Contact outputs represented the NO auxiliary contact (52 a) of the breakers and were connected in series with a DC supply output voltage (125 Vdc) and relay control inputs that sensed breaker states (closed or open).

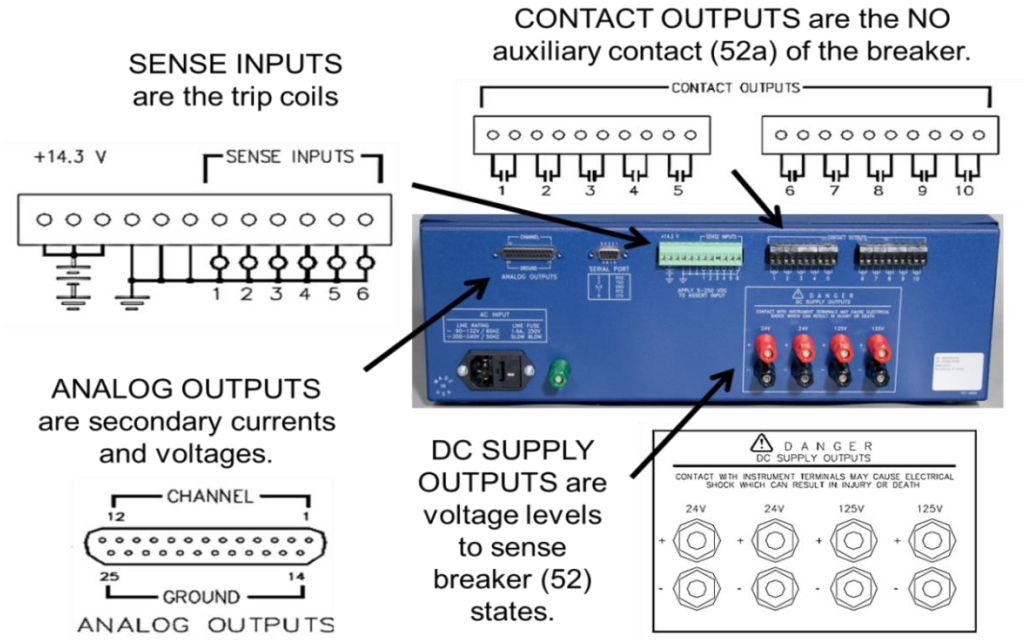

Figure 6.17: SEL- AMS rear side

Sense inputs, the trip coil of the trip circuit, were connected in series with the 14.3 Vdc source and relay control output that generated the trip signal in order to open the breaker during an overcurrent fault situation. Analog outputs, the secondary line currents and line-ground voltages, were connected from the rear side of the SEL-AMS to the relay's LLTI connector.

Figure 6.18 shows the wired connection for one SEL 451 relay and SEL-AMS for the NRTS experiment. This circuit was valid for Relays 2 and 3. For each SEL 451 relay, the 101 control input and output were used to sense and trip poles of Breaker 1, respectively, and the 102 control input and output were used to sense and trip poles of Breaker 2, respectively.

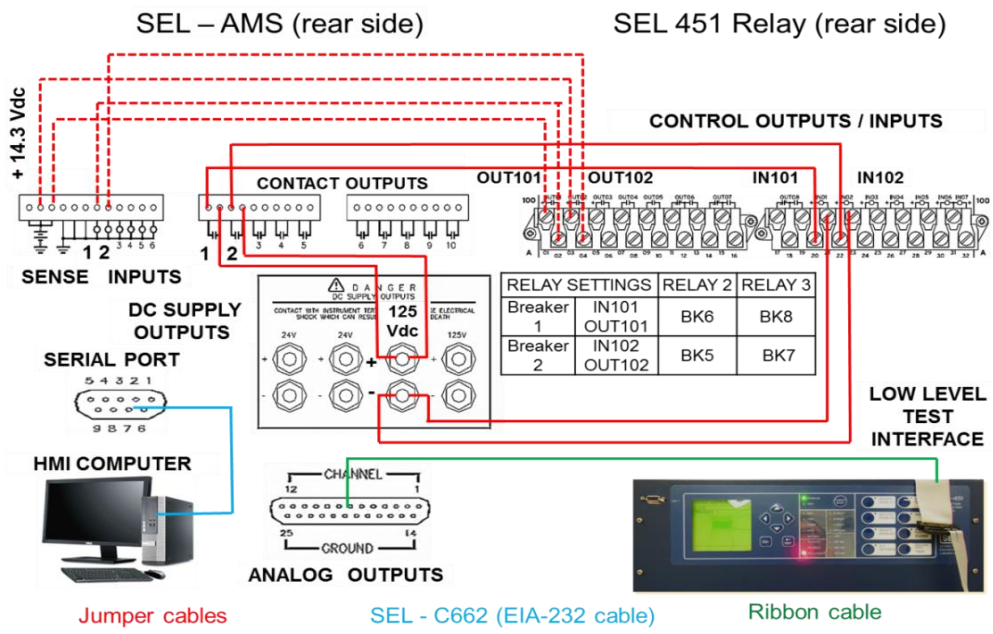

Figure 6.18: NRTS with relay in the loop circuit

Jumper cables connected relay control inputs and outputs and SEL-AMS sense inputs and contact outputs. A ribbon cable connected the relay LLTI and SEL-AMS analog outputs, and a SEL-C662 cable connected the USB port of the HMI computer and serial port of the SEL-AMS. The rear side of SEL-AMS for Relays 2 and 3 are shown in Figure 6.19.

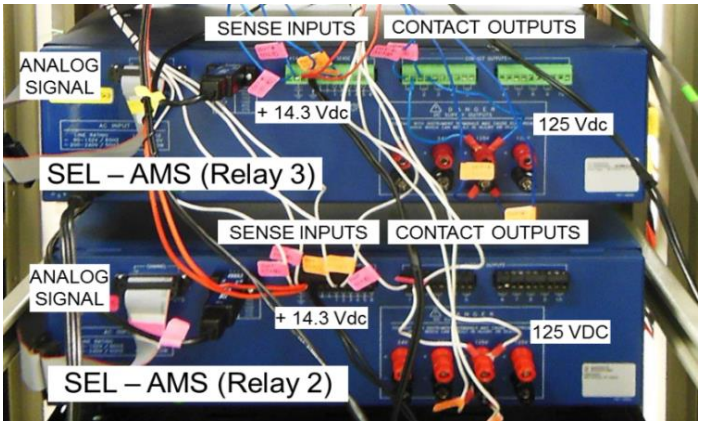

Figure 6.19: SEL-AMS rear side

Table 6.6 shows sense inputs, contact outputs, and analog outputs used in the NRTS experiment with two relays in the loop. Voltage levels of sense inputs and contact outputs were 14.3 Vdc and 125 Vdc, respectively.

Table 6.6: NRTS experiment with two relays in the loop

Sense Inputs			Contact Outputs			Analog Outputs	
Name	Description	Vdc	Name	Description	Vdc	Name	Description
1	Trip coil of Breaker 1	14.3 V	1	NO auxiliary contact (52A1) of Breaker 1	125 V	Low level test interface (LLTI)	Secondary line currents and line-ground voltages for Breakers 1 and 2
2	Trip coil of Breaker 2	14.3 V	2	NO auxiliary contact (52A2) of Breaker 2	125 V		

6.5.2 OP5600

The RTS, or OP5600 [4], was an OPAL-RT real-time simulator that could be used as a relay test system [70]. The OP5600 is the target computer that was connected to a host computer via ethernet cable. The host computer controlled the OP5600 and ran the real-time simulation test with relays in the loop. With the host computer and use of RT-LAB® and Matlab® software and their libraries, a microgrid with breakers, power lines, transformers, and distributed generators was created and sent to the OP5600. The front and rear side of the OP5600 are shown in Figure 6.20. The OP5600 has four inputs/outputs (I/O) groups. OP5600 analog inputs and digital outputs are limited to ± 16 V. However, OP5600 analog outputs are limited to ±5 V.

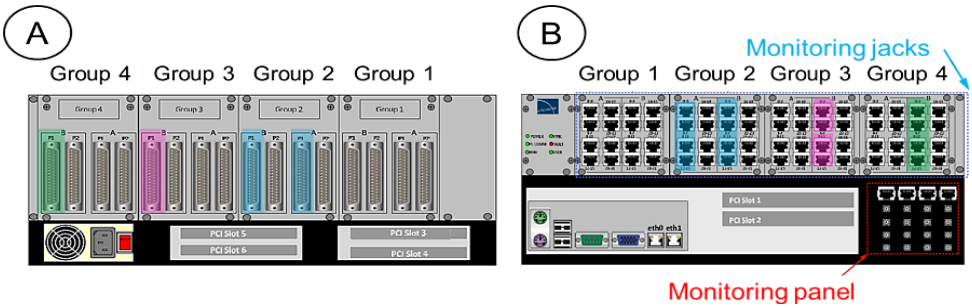

Figure 6.20: OP5600 rear (A) and front (B) side

I/O groups on the OP5600's front side contained monitoring jacks, and an ethernet cable connected the jacks to the monitoring panel. Probe scope cables connected the monitoring panel to a Tektronix oscilloscope [91]. Therefore, OP5600 analog and digital signals were verified

before running the tests to avoid damaging OP5600 and/or hardware in the loop. Three I/O groups were used in the RTS experiment: Analog inputs, digital outputs, and analog outputs are shown in green, pink, and blue, respectively (Table 6.7). Each I/O group was segregated into an A and B section, and each section was divided into a P1 and P2 DB37 connector. DB37 connector pins were connected or wired to the relays and HVIP. Table 6.7 shows group/section/connector/signals of the OP5600. The G4/B/P1/AI, G3/B/P1/DO, G2/B/P1/AO, and G2/A/P1/AO groups/sections/connectors/signals of the OP5600 were used in the RTS experiment.

Table 6.7: Groups, sections, connectors, and signals of the OP5600

Group	G4				G3				G2				G1			
Section	B		A		B		A		B		A		B		A	
DB37 Connector	P1	P2	P1	P2	P1	P2	P1	P2	P1	P2	P1	P2	P1	P2	P1	P2
Signal	AI	NA	DI	DI	DO	DO	DI	DI	AO	NA	AO	NA	AO	NA	AO	NA

AI: analog inputs, DI: digital inputs, DO: digital outputs, AO: analog outputs, NA: not available

G4/B/P2, G2/B/P2 and G2/A/P2, G1/B/P2, and G1/A/P2 connectors were not connected to I/O cards inside the OP5600, so those connectors were not connected in the RTS experiment. In the RTS experiment, analog outputs in Group 2 were connected to LLTI of the relays. Digital outputs in Group 3 were connected to relay control inputs using a high voltage interface panel. Analog inputs in Group 4 were connected to relay control outputs.

Figure 6.21 shows I/O cards located on the rear side of the OP5600. OP5600 analog outputs, digital inputs, and analog inputs were provided by the OP5330 [92], OP5354 [93], and OP5340 [94] cards, respectively. A DB37M - IDC34F cable connected OP5330 analog outputs to the relay's LLTI. This cable was specially designed for use with the SEL 451 relay's LLTI connector and OP5330 card's connector. A DB37M – DB37F cable connected OP5354's digital inputs to the rear side of the HVIP. An external source [95] connected to the HVIP [90]

amplified OP5354's digital inputs from 16 to 125 Vdc by so the relay control inputs could receive their pick-up voltage. Jumper cables and a DB37 slim breakout board connected OP5340's analog inputs to relay control outputs.

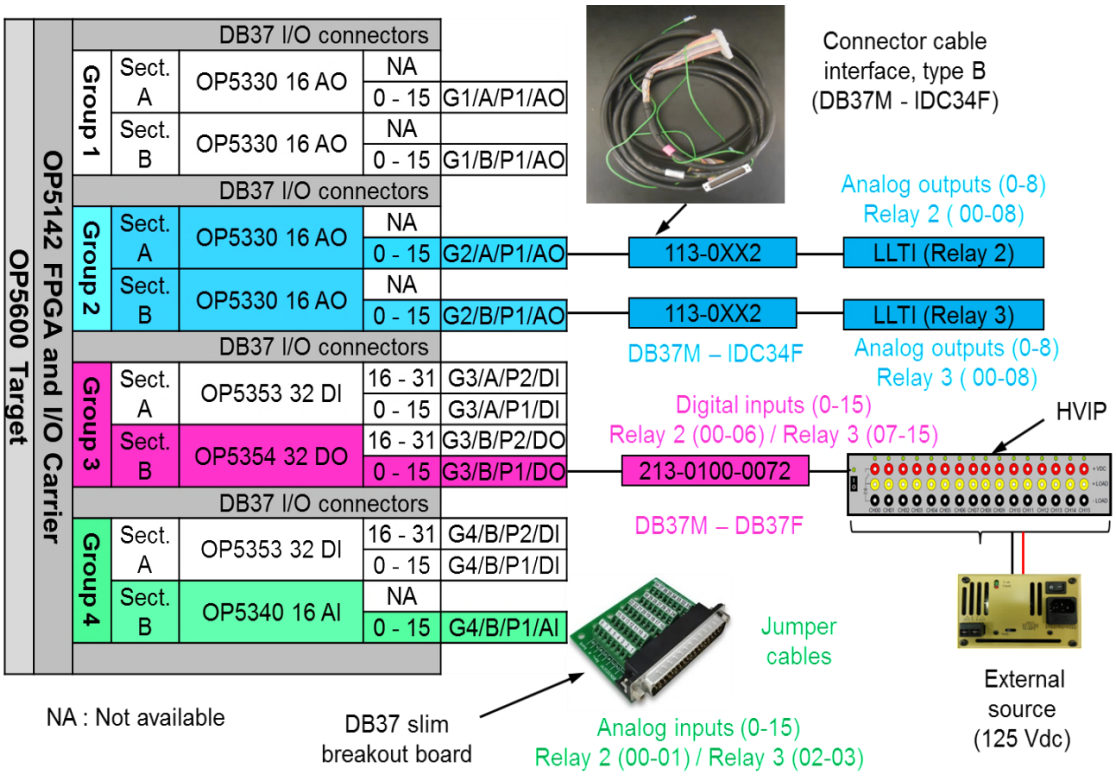

Figure 6.21: OP5600 and I/O cards

Figure 6.22 shows the group, section, connector, and signals connected to relays in the RTS experiment. Figure 6.23 shows DB37 connector pins used from the OP5330, OP5340, and OP5354 cards.

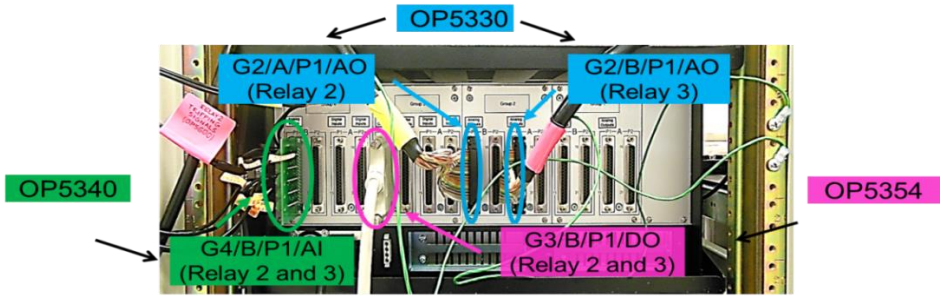

Figure 6.22: Rear side of OP5600

In the OP5330 card, G2/A/P1/AO and G2/B/P1/AO DB37 connectors had nine pairs of pins for Relays 2 and 3, respectively. These pairs of pins sent secondary currents for Breakers 1 (IAW, IBW, ICW) and 2 (IAX, IBX, ICX) and secondary line-ground bus voltages (VAY, VBY, VCY). In the OP5340 card, the G4/B/P1/AI DB37 connector had two pairs of pins for each relay, and each pair of pins received breaker trip signals from relay control outputs. In the OP5354 card, the G3/B/P1/DO DB37 connector had seven and nine pairs of pins for Relays 2 and 3, respectively. These pairs of pins sent breaker pole states, setting groups, and breaker record events to control inputs of Relays 2 and 3.

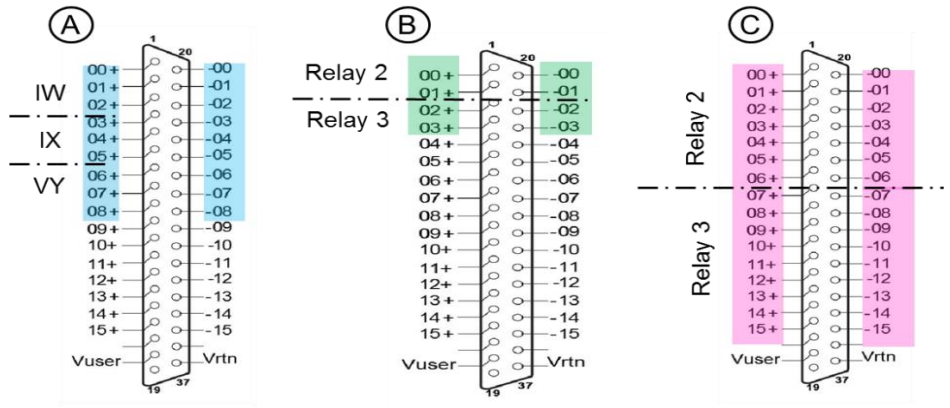

Figure 6.23: OP5330-AO (A), OP5340-AI (B), and OP5354-DO (C) DB37 connectors

Tables 6.8 and 6.9 show DB37 connector pins of OP5330 cards that were connected from G2/B/P1/AO and G2/A/P1/AO to the LLTI of Relays 2 and 3, respectively. Table 6.10 shows relay control outputs, voltage source level, and DB37 connector pins of the OP5340 card that were connected from G4/B/P1/AI to the relay control inputs. Table 6.11 indicates relay control inputs and DB37 connector pins of the OP5354 card that were connected from G3/B/P1/DO to HVIP channels and relay control inputs. Tables 6.8 to 6.11 also indicate the ‘OP5142EX1 Ctrl’

controller, DatIn Port #, and # of Channels selected to integrate the RT-LAB® project with I/O cards.

Table 6.8: OP5330 analog outputs for the LLTI of Relay 3

Group 2 - Section B - P1 - Analog Outputs (G2/B/P1/AO)																			
Relay 3	**Breakers/ Bus**	Breaker 1 (BK8)						Breaker 2 (BK7)						Bus 6					
	LLTI	IAW		IBW		ICW		IAX		IBX		ICX		VAY		VBY		VCY	
OP5330	**DB37 Pin #**	1	20	2	21	3	22	4	23	5	24	6	25	7	26	8	27	9	28
	Analog Outputs	+00	-00	+01	-01	+02	-02	+03	-03	+04	-04	+05	-05	+06	-06	+07	-07	+08	-08
	Controller	‘OP5142EX1 Ctrl’																	
	DatIn Port #	7																8	
	# of Channel	8																8	

Table 6.9: OP5330 analog outputs for the LLTI of Relay 2

Group 2 - Section A - P1 - Analog Outputs (G2/A/P1/AO)																			
Relay 2	**Breakers/ Bus**	Breaker 1 (BK6)						Breaker 2 (BK5)						Bus 7					
	LLTI	IAW		IBW		ICW		IAX		IBX		ICX		VAY		VBY		VCY	
OP5330	**DB37 Pin #**	1	20	2	21	3	22	4	23	5	24	6	25	7	26	8	27	9	28
	Analog Outputs	+00	-00	+01	-01	+02	-02	+03	-03	+04	-04	+05	-05	+06	-06	+07	-07	+08	-08
	Controller	‘OP5142EX1 Ctrl’																	
	DatIn Port #	5																6	
	# of Channel	8																8	

Table 6.10: OP5340 analog inputs for control inputs of Relays 2 and 3

Group 4 - Section B - P1 - Analog Inputs (G4/B/P1/AI)									
Relays	**Relays**	Relay 2				Relay 3			
	Trip	Breaker 1 (BK6)		Breaker 2 (BK5)		Breaker 1 (BK8)		Breaker 2 (BK7)	
	Control Outputs	106 - NC		107 - NC		106 - NC		107 - NC	
		–	+	–	+	–	+	–	+
SEL-AMS	**Source**	+14.3 V	Gnd	+14.3 V	Gnd	+14.3 V	Gnd	+14.3 V	Gnd
OP5340	**Channel**	0		1		2		3	
	DB37 Pin #	1	20	2	21	3	22	4	23
	Analog Input	+00	-00	+01	-01	+02	-02	+03	-03
	Controller	‘OP5142EX1 Ctrl’							
	DatIn Port #	1							
	# of Channel	4							

The front side of HVIP for the RTS experiment is shown in Figure 6.24. When HVIP channel LEDs located on the front side of HVIP were green, HVIP switches were closed or relay control inputs had 125 Vdc.

Table 6.11: OP5354 digital outputs for control inputs of Relay 2 and 3

Group 3 - Section B - P1 - Digital Outputs (G3/B/P1/DO)																																			
Relays	**Relays**	Relay 2														Relay 3																			
	Functions	Sense the pole state of				Select the relay setting group								Select the breaker record event of		Sense the pole state of				Select the relay setting group																	
		Breaker 1		Breaker 2		SS1		SS2		SS3		SS4		Relay 2		Relay 3		Breaker 1		Breaker 2		SS1		SS2		SS3		SS4		SS5		SS6			
	Control Inputs	103		104		201		202		203		204		105		105		103		104		201		202		203		213		214		215			
HVIP	**Channel**	00		01		02		03		04		05		06		07		08		09		10		11		12		13		14		15			
OP5354	**DB37 Pin #**	1	20	2	21	3	22	4	23	5	24	6	25	7	26	8	27	9	28	10	29	11	30	12	31	13	32	14	33	15	34	16	35		
	Digital Out	+00	-00	+01	-01	+02	-02	+03	-03	+04	-04	+05	-05	+06	-06	+07	-07	+08	-08	+09	-09	+10	-10	+11	-11	+12	-12	+13	-13	+14	-14	+15	-15		
	Controller	'OP5142EX1 Ctrl'																																	
	DatIn Port #	9																10																	
	# of Channel	8																8																	

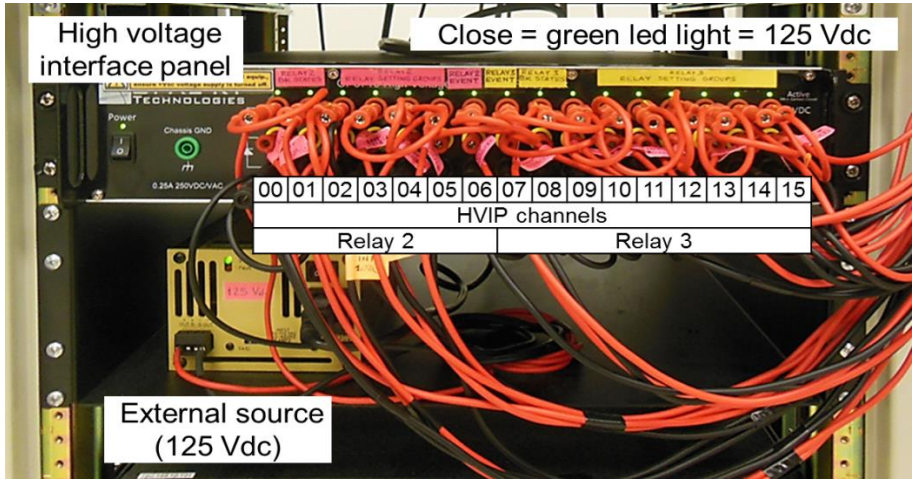

Figure 6.24: High voltage interface panel

Figure 6.25 illustrates an HVIP circuit [90] based on a solid-state relay carrier that received digital outputs from the OP5600. In the RTS experiment, the HVIP was connected to digital outputs from the OP5354 [93] card located on Group 3, Section B, and DB37 connector P1. In this circuit, the HVIP grounded the Vuser_RTN pin. When OP5600's digital output was activated, the solid state relay (SSR) switch was closed by collecting 125 Vdc from the external source that activated the relay control input.

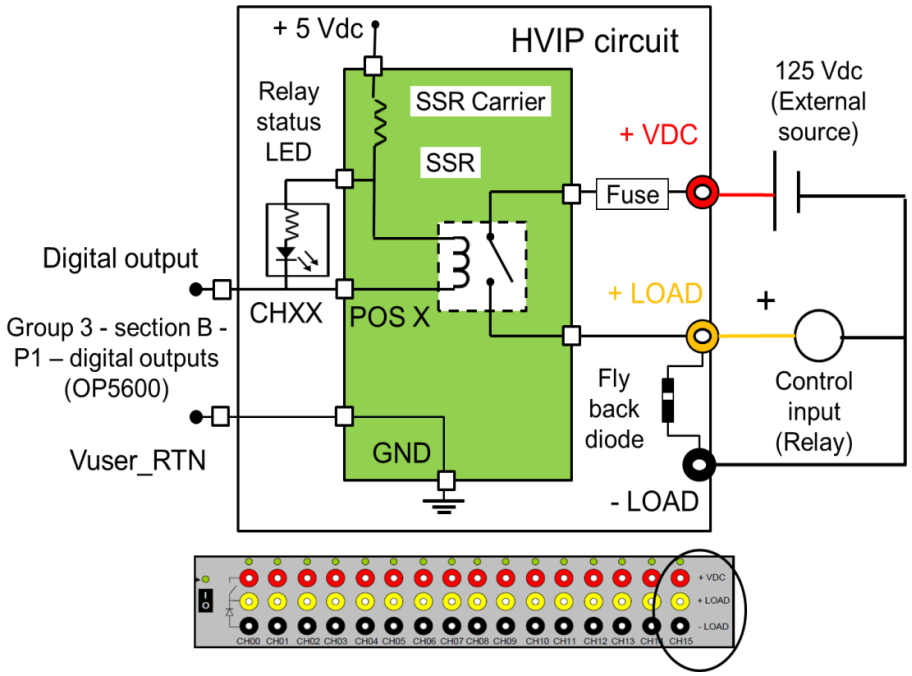

Figure 6.25: HVIP circuit

6.6 Sub-circuits

The circuits of the NRTS and RTS experiments with relays in the loop could be segregated into sub-circuits: (1) current and voltage measurement, (2) breaker trip, (3) breaker pole state, (4) setting group, and (5) breaker record event circuit. Table 6.12 lists sub-circuits for NRTS and RTS experiments with relays in the loop.

The current and voltage measurement, breaker trip, and breaker pole state circuits were included in the NRTS and RTS experiments with relays in the loop. However, the setting group

and breaker record event circuits were included only in the RTS experiment with relays in the loop. The relay signal of the current and voltage measurement circuit was the LLTI. The breaker trip circuit was connected to relay control outputs, and the breaker state pole, setting group, and record event circuits were connected to relay control inputs.

Table 6.12: Sub-circuits of NRTS and RTS experiments

Experiments		**N°**	**Sub-circuits**	**Relay's Signal**
NRTS	RTS	1	Current and voltage measurement circuit	LLTI[(1)]
		2	Breaker trip circuit	Control Outputs
		3	Breaker state pole circuit	Control Inputs
		4	Setting group circuit	
		5	Breaker record event circuit	

[(1)] Low level test interface

6.6.1 Current and voltage measurement circuit

The current and voltage measurement circuit connected NRTS and RTS analog outputs to the relay's LLTI, which collected secondary line breaker currents and line-ground bus voltages. The SEL 451 relay's LLTI had a current and voltage scaling factor for adapting secondary line current and line-ground voltages into analog signals. Based on the SEL 451 instruction manual [5], an analog signal of 0.0666 V corresponded to a nominal secondary current of 5 A, and an analog signal of 0.446 V corresponded to a nominal secondary line-ground voltage of 67 V. Dividing the nominal value by the analog signal, the current and voltage scaling factors of SEL 451 relay's LLTI were 75 A/V and 150 V/V, respectively. In order to prevent damage to the relay's LLTI, maximum secondary line current and line-ground voltage could be estimated with Equations (6.1) and (6.2), respectively.

$$I_{RMS\,max} = 0.707 \times SF_A \times V_{p\,max} \tag{6.1}$$

$$V_{RMS\,max} = 0.707 \times SF_V \times V_{p\,max} \quad (6.2)$$

where $I_{RMS\,max}$ and $V_{RMS\,max}$ are RMS secondary line current and line-ground voltage in amps and volts, respectively. SF_A and SF_V are the current and voltage scaling factors in amps/volts and volts/volts, respectively, and V_{pmax} is the maximum peak voltage of the SEL 451 relay's LLTI, 3.3 volts.

Maximum secondary line current and line-ground voltages were estimated completing the scaling factors and maximum peak voltage into Eq. (6.1) and (6.2) by. The SEL 451 relay's LLTI was prevented from reaching a secondary line current and line-ground voltage of 190 amps and 350 volts, respectively. Therefore, the scaling factors and maximum peak voltage of the LLTI limited secondary line currents and line-ground voltages during NRTS and RTS experiments. In those experiments, the relay's LLTI was connected by a black round and grey ribbon control cable, respectively. Figure 6.26 shows analog cables for the SEL 451 relay's LLTI.

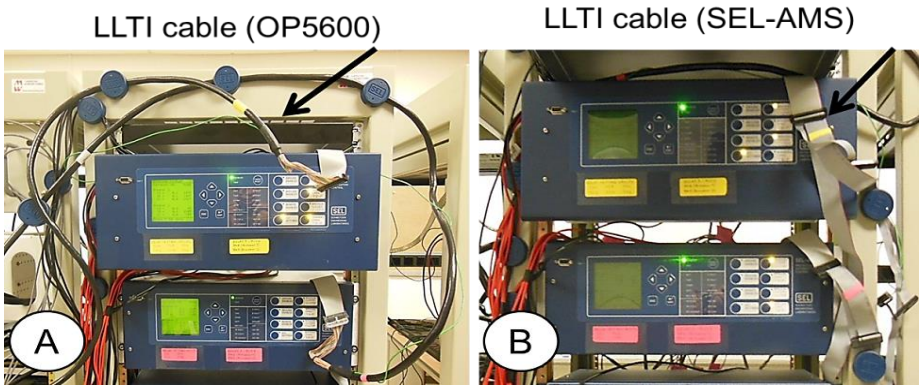

Figure 6.26: LLTI cables for RTS (A) and NRTS (B) experiment

6.6.2 Breaker trip circuit

The breaker trip circuit opens the breaker during an overcurrent fault situation. Breaker trip circuits for NRTS (A) and RTS (B) experiments are shown in Figure 6.27. The breaker trip circuit connected the sense and analog input of the SEL-AMS and OP5600, respectively. In

NRTS and RTS experiments, the breaker trip circuit had a 14.3 Vdc source in order to trip the breaker, so the same 14.3 Vdc source located on the SEL-AMS was used for the NRTS and RTS experiments.

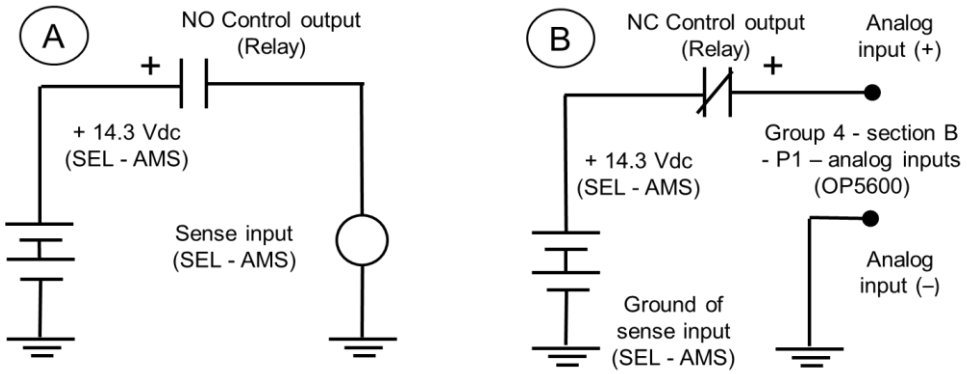

Figure 6.27: Breaker trip circuit for NRTS (A) and RTS (B) experiments

In the NRTS experiment, the breaker trip circuit had a relay NO control output. In the RTS experiment, however, the breaker trip circuit had a relay NC control output. Polarity of relay control outputs, SEL-AMS sources and sense inputs, and OP5600 analog inputs had to be considered in order to correctly connect breaker trip circuits correctly and avoid damaging relays, SEL-AMS or OP5600. Control outputs and sense inputs for each relay and breaker in breaker trip circuits of the NRTS experiment are indicated in Table 6.13.

Table 6.13: Breaker trip circuits for the NRTS experiment

Relays	**Relays**	Relay 2		Relay 3	
	Breakers	Breaker 1	Breaker 2	Breaker 1	Breaker 2
	Control Outputs	101	102	101	102
SEL-AMS	**Sense Inputs**	1	2	1	2

Control outputs and analog inputs for each relay and breaker in breaker trip circuits of the RTS experiment are indicated in Table 6.14. In the trip circuits for the RTS experiment, pin

polarity of the DB37 connector had to match the polarity of the 14.3 Vdc source and relay control outputs.

Table 6.14: Breaker trip circuits for the RTS experiment

Relays	**Relays**	Relay 2				Relay 3			
	Breakers	Breaker 1		Breaker 2		Breaker 1		Breaker 2	
	Control Outputs	106-NC		107-NC		106-NC		107-NC	
OP5600 (1)	**DB37 Pin #**	1	20	2	21	3	22	4	23
	Analog Inputs	+00	-00	+01	-01	+02	-02	+03	-03

(1) Group 4 - Section B - P1 - Analog Inputs (OP5340)

6.6.3 Breaker state pole circuit

The breaker state pole circuit sensed if the breaker was open or closed during pre-fault, fault, and post-fault states. Breaker pole state circuits for NRTS (A) and RTS (B) experiments are shown in Figure 6.28. In the NRTS experiment, the breaker pole state circuit connected the contact output of SEL-AMS to the relay control input. In the RTS experiment, the breaker pole state circuit was connected to the OP5600 digital output and the relay control input through an HVIP that converted OP5600's digital output of 16 into 125 Vdc. The SEL 451 relay control inputs needed a 125 Vdc supply to detect breaker pole states, so when the relay control input was 125 Vdc, the SEL 451 relay control input sensed that the breaker poles were closed.

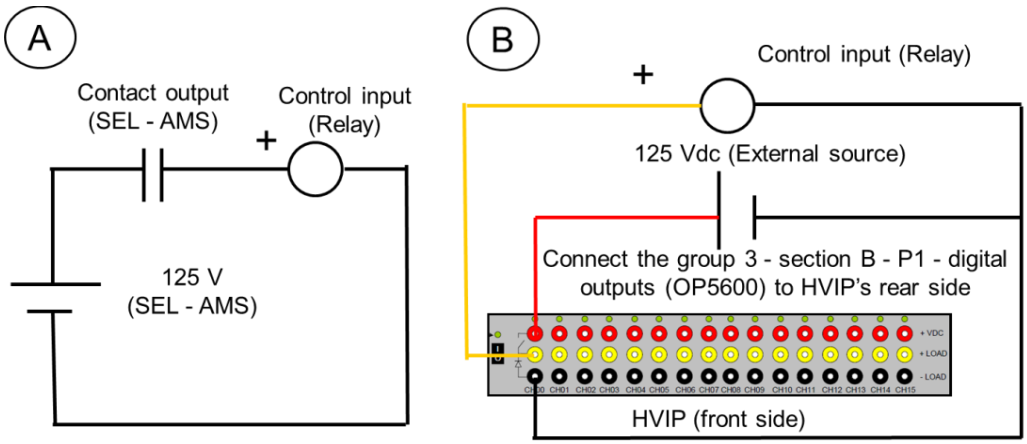

Figure 6.28: Breaker state pole circuit for the NRTS (A) and RTS (B) experiments

Table 6.15 indicates relay control inputs and SEL-AMS contact outputs for breakers and relays in breaker state pole circuits of the NRTS experiment with relays in the loop.

Table 6.15: Breaker state pole circuits for the NRTS experiment

Relays	**Relays**	Relay 2		Relay 3	
	Breakers	Breaker 1	Breaker 2	Breaker 1	Breaker 2
	Control Inputs	101	102	101	102
SEL-AMS	**Contact Outputs**	1	2	1	2

Table 6.16 indicates relay control inputs, HVIP channels, and OP5600 digital outputs for each breaker and relay in the breaker state pole circuits of the RTS experiment with relays in the loop.

Table 6.16: Breaker state pole circuits for the RTS experiment

Relays	**Relays**	Relay 2				Relay 3			
	Breakers	Breaker 1		Breaker 2		Breaker 1		Breaker 2	
	Control Inputs	103		104		103		104	
HVIP[(1)]	**Channels**	00		01		08		09	
OP5600[(2)]	**DB37 Pin #**	1	20	2	21	9	28	10	29
	Digital Output	+00	-00	+01	-01	+08	-08	+09	-09

[(1)]High voltage interface panel [(2)] Group 3 - Section B - P1- Digital Outputs (OP5354)

6.6.4 Setting group circuit

The setting group circuit selects inverse time overcurrent settings of the relay based on circuit path. The setting group circuit was used only for the RTS experiment because pushbuttons on the relay's front panel manually selected setting groups in the NRTS experiment before running the tests. The setting group circuit for RTS experiments is shown in Figure 6.29. In the RTS experiment, the setting group circuit connected OP5600 digital output and relay control input through a HVIP that converted OP5600 digital output of 16 into 125 Vdc. SEL 451 relay control inputs required a 125 Vdc supply to activate a new setting group, so the SEL 451 relay picked up the activated setting group when the relay control input was 125 Vdc.

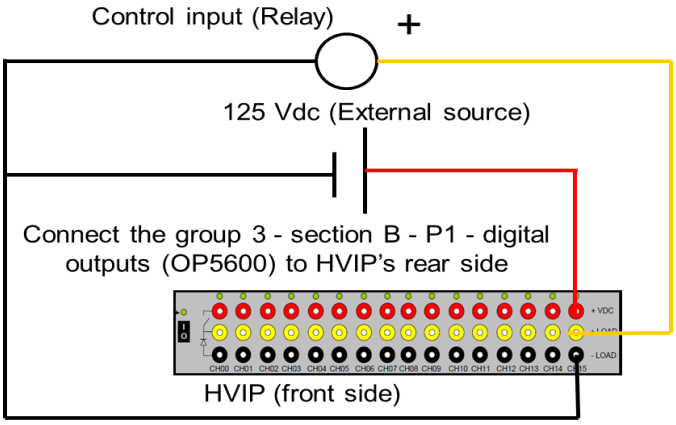

Figure 6.29: Setting group circuit for the RTS experiment

In the setting group circuit of the RTS experiment, Relay 2 required four setting groups. Control inputs, HVIP channels, and OP5600 digital outputs of Relay 2 are indicated in Table 6.17.

Table 6.17: Setting group circuits for Relay 2 in the RTS experiment

Relay 2		**HVIP**[1]	**OP5600**[2]			
Setting Group	Control Input	Channel	DB37 Pin #		Digital Output	
SS1	IN201	02	3	22	+02	-02
SS2	IN202	03	4	23	+03	-03
SS3	IN203	04	5	24	+04	-04
SS4	IN204	05	6	25	+05	-05

[1] High voltage interface panel [2] Group 3 - Section B - P1 - Digital Outputs (OP5354)

In the setting group circuit of the RTS experiment, Relay 3 required six setting groups. Control inputs, HVIP channels, and OP5600 digital outputs of Relay 3 are indicated in Table 6.18.

Table 6.18: Setting group circuits for Relay 3 in the RTS experiment

Relay 3		**HVIP**[1]	**OP5600**[2]			
Setting Group	Control Input	Channel	DB37 Pin #		Digital Output	
SS1	IN201	10	11	30	+10	-10
SS2	IN202	11	12	31	+11	-11
SS3	IN203	12	13	32	+12	-12
SS4	IN213	13	14	33	+13	-13
SS5	IN214	14	15	34	+14	-14
SS6	IN215	15	16	35	+15	-15

[1] High voltage interface panel [2] Group 3 - Section B - P1 - Digital Outputs (OP5354)

6.6.5 Breaker record event circuit

The record event of Breaker 1 or 2 was saved by the relay after running the tests for the RTS experiment. This circuit was only applied to the RTS experiment because record event files were not collected in the NRTS experiment. The breaker record event circuit for RTS experiments is shown in Figure 6.30. In the RTS experiment, the breaker record event circuit connected OP5600 digital output and relay control input through HVIP that converted OP5600 digital output of 16 into 125 Vdc.

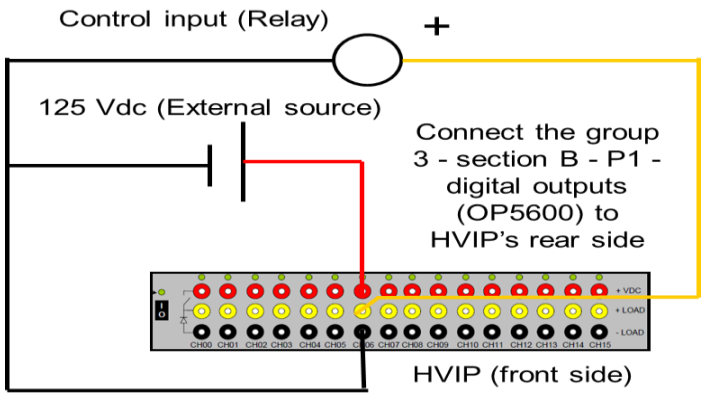

Figure 6.30: Breaker record event circuit for the RTS experiment

The SEL 451 relay recorded the event file of Breakers 1 and 2 when relay control input was connected or disconnected to the 125 Vdc supply. Relay control inputs, HVIP channels, and OP5600 digital outputs for each relay in the breaker record event circuits of the RTS experiment with relays in the loop are indicated in Table 6.19.

Table 6.19: Breaker record event circuits for the RTS experiment

Relays	**Relays**	Relay 2		Relay 3	
	Breakers	Breaker 1	Breaker 2	Breaker 1	Breaker 2
	Control Inputs	105		105	
HVIP[(1)]	**Channels**	06		07	
OP5600[(2)]	**DB37 Pin #**	7	26	8	27
	Digital Output	+06	-06	+07	-07

[(1)]High voltage interface panel [(2)] Group 3 - Section B - P1 - Digital Outputs (OP5354)

6.7 Chapter summary

This chapter described the equipment, software, and circuits of NRTS and RTS experiments with SEL 451 relays in the loop. NRTS and RTS were based on application of SEL-AMS and OP5600 as relay test systems, respectively. Diagrams for NRTS and RTS experiments were presented that described analog and digital signals of SEL 451 relay, OP5600, and SEL-AMS. OP5600 I/O cards, external voltage sources, and high voltage interface panel were described for the NRTS experiment.

For the NRTS and RTS experiments, the external source for relay control input circuits had to be sized based on relay control input pickup voltage; the method to obtain this voltage was described in this chapter. This method was based on determining the mainboard input voltage according to the part number on the SEL website and then finding the pickup voltage range according to the main board input voltage in the relay instruction manual. SEL's website indicated that mainboard input voltages for Relays 2 and 3 were 125 Vdc and 110 Vdc, respectively. According to the relay instruction manual, the pickup voltage range for Relays 2 and 3 were 105-150 Vdc and 88-132 Vdc; therefore, a 125 Vdc voltage supply was applied for relay control input circuits. The SEL 451 relay's LLTI was determined to avoid relay damage. Therefore, based on the current (75 A/V) and voltage (150 V/V) scaling factors and maximum LLTI peak voltage (3.3 V), maximum secondary RMS current (190 A) and line-ground voltage (350 V) that limited the LLTI of the SEL 451 relay were estimated for RTS and NRTS experiments.

In the NRTS experiment, relay control inputs and outputs sensed breaker poles and sent breaker trip signals, respectively. However, the relay's LLTI sensed line breaker currents and line-ground bus voltages. In the RTS experiment, relay control inputs also selected setting

groups and breaker record event. Relay trip circuits were based on two circuits that applied relay NO or NC control outputs: NO and NC trip circuits. The NRTS experiment contained NO trip circuits based on the SEL 451 relay instruction manual [5], but the RTS experiment had NC trip circuits based on relay test validation that applied an OPAL-RT OP5600 with a relay in the loop [68].

NRTS and RTS experimental circuits were segregated into sub-circuits. These sub-circuits were segregated based on their functions as (1) current and voltage measurement, (2) breaker trip, (3) breaker state pole, (4) setting group, and (5) breaker record event sub-circuits. Diagrams of these sub-circuits were compared for NRTS and RTS experiments. Although the RTS experiment contained all sub-circuits, the NRTS experiment contained only current and voltage measurement, breaker trip, and breaker state pole sub-circuits.

Chapter 7 - Test steps of NRTS experiment

This chapter describes test steps to run non-real-time simulation with relays in the loop. Before initiating test steps of the NRTS experiment, Relays 2 and 3 were set with adaptive inverse time overcurrent protection and the NRTS experiment circuit was built as indicated in Chapters 5 and 6, respectively. In the NRTS experiment, tripping and non-tripping tests were run for adaptive overcurrent protection of the microgrid with distributed generators. The non-real-time simulator simulated the trip coil and auxiliary contacts of the breakers and the pre-fault, fault, and post-fault states of the non-real-time tests. As shown in Figure 7.1, test steps for tripping and non-tripping tests were Calculation (1), Preparation (2), Execution (3), and Collection (4). Relays 2 and 3 were verified by tripping and non-tripping tests. In the process on a loop of Figure 7.1, when the Collection phase of the tripping test was finished, a new tripping test began. In the Collection phase of tripping tests, measured relay times were collected to estimate the fault state time of non-tripping tests. Then the tripping test loop (A) was run before the non-tripping test loop (B) for Relays 2 and 3.

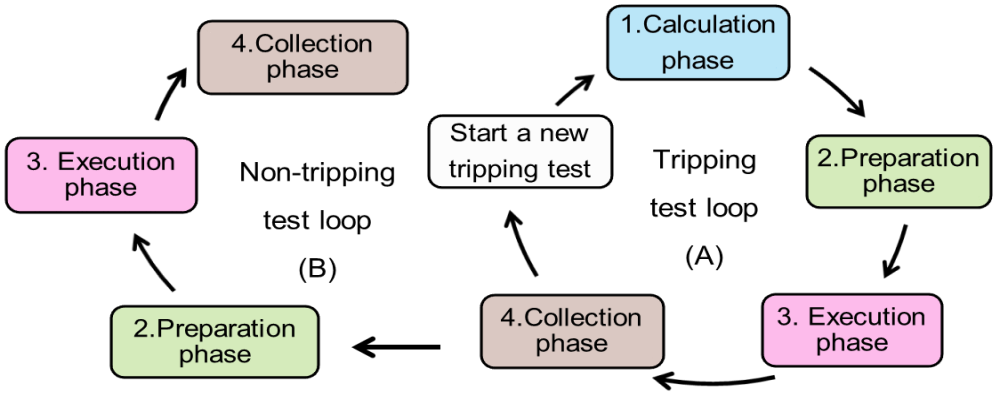

Figure 7.1: Phases of test steps for the NRTS experiment

In the NRTS experiment, tripping and non-tripping tests were run individually for each relay; therefore, selective coordination between primary and backup relays could not be verified

with both relays connected to the experimental circuit. Each relay was wired to an individual non-real-time simulator called SEL-AMS [3]. Figure 7.2 presents tasks of the phases for tripping tests in the NRTS experiment.

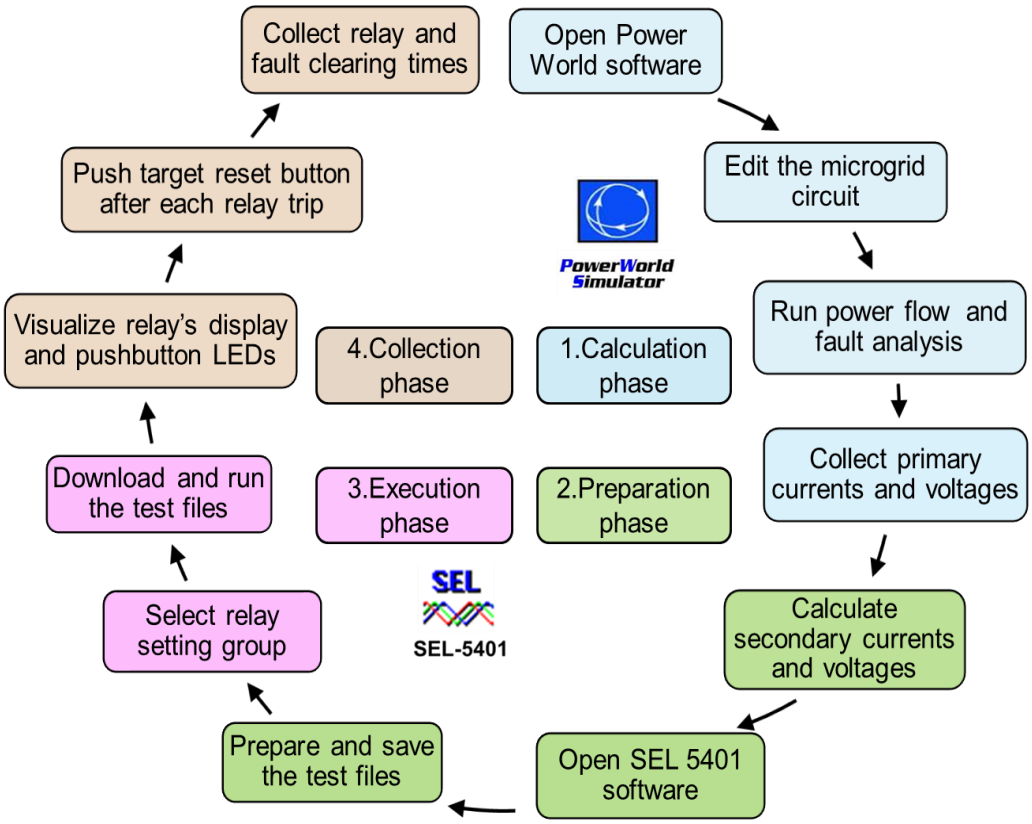

Figure 7.2: Tasks of phases for tripping tests

Power World® software [10] was used to calculate currents and voltages of pre-fault, fault, and post-fault states, SEL-5401® software [12] was used to run the tripping and non-tripping tests. In the tripping tests, Relays 2 and 3 tripped for a fault overcurrent and measured relay and fault clearing times of the fault states were collected from the HMI computer. However, in the non-tripping tests, relay and fault clearing times were not collected because relays did not trip. Table 7.1 describes the tasks and summary of each phase for tripping and non-tripping tests of Relays 2 and 3.

Table 7.1: Phases and tasks of tripping and non-tripping tests

Phases	Task Codes and Names		Phase Descriptions
	Code	Name	
1. Calculation	1.1	Open Power World® software [10]	Power World® software [10] was opened and the microgrid circuit was edited based on the circuit path of each non-real-time test. As Relays 2 and 3 controlled breakers placed on buses, breaker primary currents and bus primary voltages for pre-fault and post-fault states were calculated by running a power flow analysis. However, breaker primary currents and bus primary voltages for the fault state were calculated by running a fault analysis.
	1.2	Edit the microgrid circuit	
	1.3	Run power flow and fault analysis	
	1.4	Collect primary currents and voltages	
2. Preparation	2.1	Calculate secondary currents and voltages	Secondary currents and voltages for the breakers and buses of Relays 2 and 3 were estimated by dividing calculated primary currents and voltages by the current and potential transformer ratios, respectively. Then SEL-5401® software [12] was opened to create test files for tripping and non-tripping tests.
	2.2	Open SEL-5401® software [12]	
	2.3	Prepare and save test files	
3. Execution	3.1	Select relay setting group	For each test, the relay setting group was selected from the relay's display front. Then tripping and non-tripping tests were executed by downloading and running test files with SEL-5401® software [12].
	3.2	Download and run test files	
4. Collection	4.1	Visualize relay's display and push-button LEDs	While non-real-time tests were run, the relay's display and push-button LEDs were evaluated at first sight from a webcam. At the end of the tripping tests, measured relay and fault clearing times were collected from fault state results. After each relay tripped, the target reset button on the relay's front panel was pushed to allow measurement of the relay and fault clearing times of the next tripping test. After collecting measured relay times of the tripping tests, the fault state time for the non-tripping tests was estimated to run the non-tripping tests. Therefore, in the NRTS experiment, tripping tests were run before non-tripping tests.
	4.2	Push target reset button after each relay trip	
	4.3	Collect measured relay and fault clearing times	

7.1 Tripping and non-tripping tests

The NRTS experiment was divided into tripping and non-tripping tests. Figure 7.3 shows pre-fault, fault, and post-fault states of tripping test (A) and pre-fault and fault states of non-tripping test (B). In the tripping tests, pre-fault, fault, and post-fault state times were set at 600 cycles (10 sec). In the non-tripping tests, the post-fault state was not available because the relays did not trip; therefore, the pre-fault state time was set at 600 cycles (10 sec) and the fault states were set at a time less than the measured relay time of the tripping test.

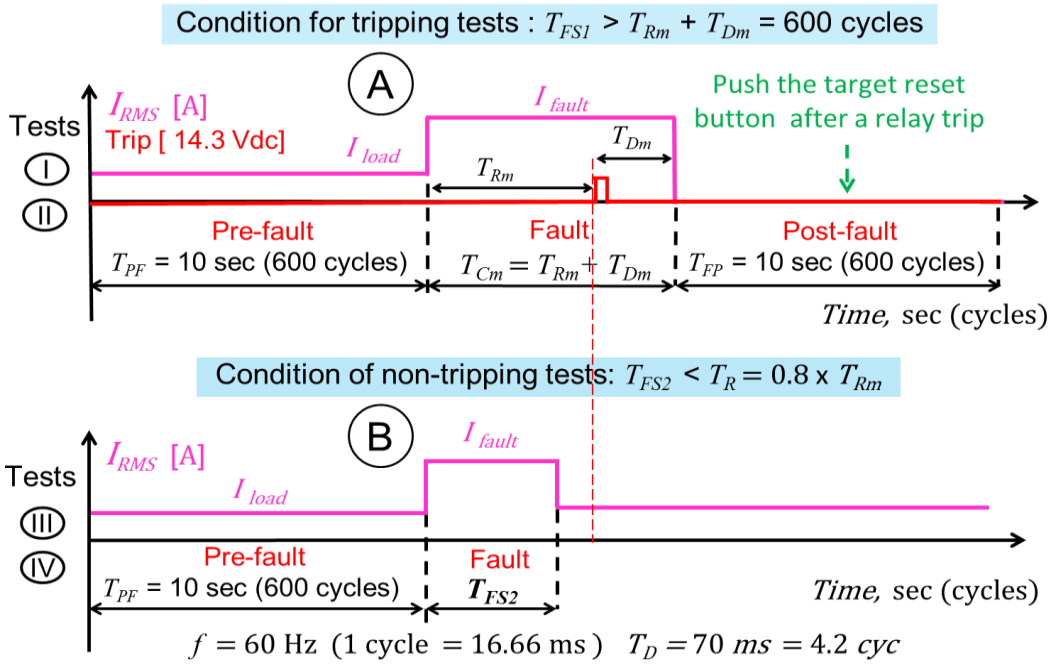

T_{PF} = pre-fault state time T_{PF} = post-fault state time T_{Rm} = measured relay time of tripping test
T_{Cm} = measured fault clearing time of tripping test T_{Dm} = measured delay time of tripping test
T_{FS1} = fault state time of tripping test T_{FS2} = fault state time of non-tripping test

Figure 7.3: Pre-fault, fault, and post-fault states of tripping test (A) and pre-fault and fault states of non-tripping test (B)

As shown in Figure 7.3-A, the load current flowed along the breaker during the pre-fault state for the tripping test. The fault overcurrent then flowed along the breaker, and the relay tripped during the fault state. Once the relay tripped, the fault overcurrent was cleared after a

delay time at post-fault state. However, as shown in Figure 7.3-B, the load current flowed along the breaker during the pre-fault state for the non-tripping test. The fault overcurrent then flowed along the breaker, but the relay did not trip during the fault state because the fault state time was less than the relay time.

Tripping tests verified adaptive overcurrent protection of the microgrid for a protection area represented by a power line. Considering maximum and minimum faults along a power line, tripping tests were verified for maximum and minimum fault overcurrents. Tripping tests were formed by a pre-fault, fault, and post-fault state. In the tripping tests, fault state time was greater than measured fault clearing time to relay trip. However, in the non-tripping tests, fault state time was less than the measured relay time of the tripping test, so the relay did not trip. Figure 7.4 shows fault state time conditions of tripping and non-tripping tests for maximum and minimum fault currents of a power line.

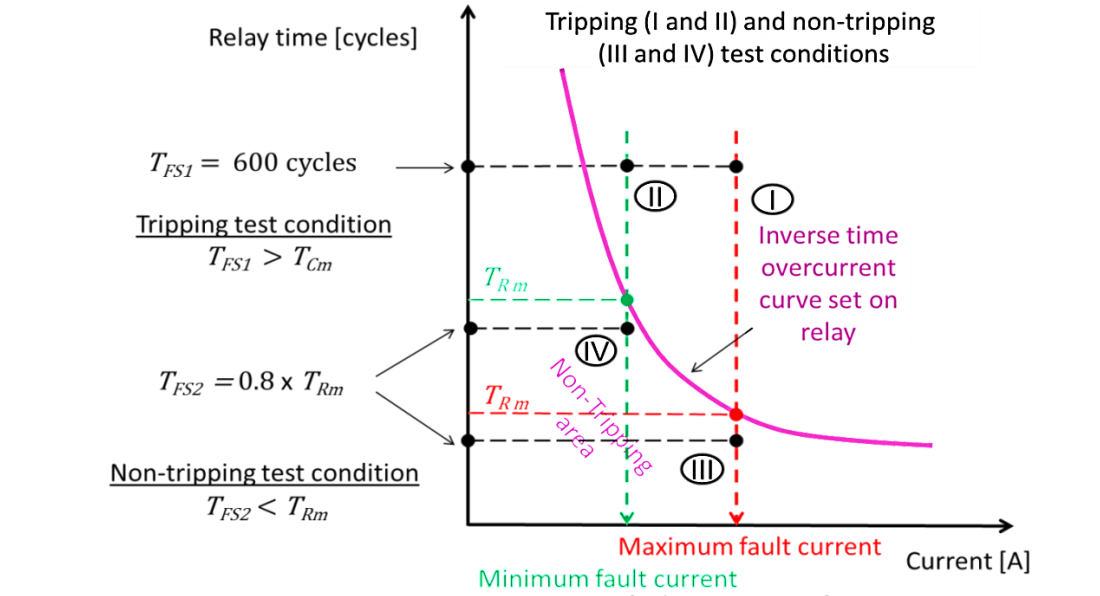

Figure 7.4: Conditions of tripping and non-tripping tests

In Figure 7.4, the horizontal and vertical axes represent the primary currents in amps and the relay time in cycles, respectively. The pink curve represents the inverse time overcurrent curve set for the setting group of the relay. For tripping tests, if the fault state time for the test file was set at 600 cycles for the maximum and minimum fault overcurrent tests, the relay tripped based on the inverse time overcurrent curve. However, for non-tripping tests, the fault state time for test files was set at the measured relay time of the tripping test multiplied by 0.8, so the relay did not trip. Table 7.2 shows test characteristics and fault state conditions for tripping and non-tripping tests.

Table 7.2: Tripping and non-tripping tests

Test Characteristics			**Fault State Conditions**			
N°	**Type**	**Overcurrent**	**Secondary Currents**	**Condition**	**Time [cycles]**	**Results**
I	Tripping	Maximum	DLG(BC) SLG(A)	$T_{FS1} > T_{Cm}$	600	Non-Trip
II		Minimum	LL(BC)			
III	Non-Tripping	Maximum	DLG(BC) SLG(A)	$T_{FS2} < T_{Rm}$	$T_{FS2} = 0.8 \times T_{Rm}$	Trip
IV		Minimum	LL(BC)			

DLG(BC): double line-to-ground fault at B-C phases, SLG(A): single line-to-ground fault at A phase, LL(BC): line-to-line fault at B-C phases, T_{FS1}: fault state time of test file for tripping test, T_{FS2}: fault state time of test file for non-tripping test, T_{Cm}: measured fault clearing time of tripping test, T_{Rm}: measured relay time of tripping test

Figure 7.5 shows test groupings for Relays 2 and 3 for the NRTS experiment. Non-tripping tests were formed by pre-fault and fault states because the relays did not trip. Because tripping tests were run before non-tripping tests, the NRTS experiment was segregated into tripping and non-tripping tests. Because tripping and non-tripping tests were run individually for each relay, tripping and non-tripping tests were segregated into Relays 2 and 3. Because Relays 2 and 3 were set with no identical setting groups for circuit paths of the microgrid, tests of Relays 2 and 3 were segregated into SS1 to SS4 and SS1 to SS6 setting groups, respectively. Also,

setting groups were grouped into circuit paths and protection areas (power lines) for maximum and minimum fault overcurrents. For tests that corresponded to utility circuit paths, maximum and minimum fault overcurrents were DLG and LL faults, respectively. However, for tests that corresponded to distributed generator circuit paths, maximum and minimum fault overcurrents were SLG and LL faults, respectively.

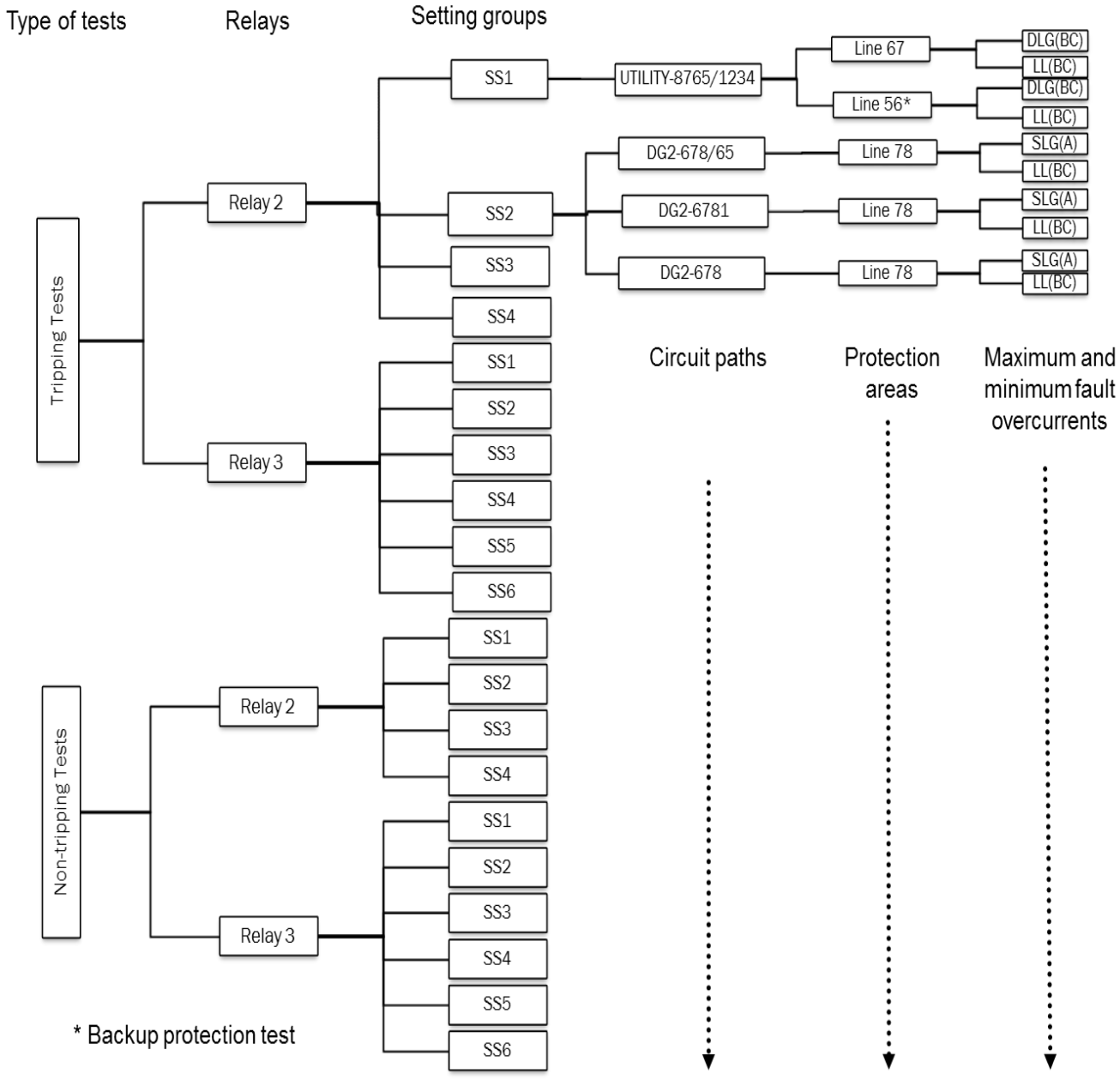

Figure 7.5: Grouping of tripping and non-tripping test files

Tests were referenced by source, circuit, type of fault, fault site, and desired tripped breaker. For example, the "DG2-678/65-LL(BC)-Bus8-BK5" test means that the test was performed for the LL (BC) fault located on "Bus8" in the circuit conformed by "distributed generator 2" and two power line branches formed by 6-5 and 6-7-8 power lines that expected "BK5" breaker to trip.

In adaptive overcurrent protection for the microgrid with distributed generators, Relays 2 and 3 tripped as primary and backup protections and vice versa, depending on the circuit path selected to run the non-real-time simulation. Circuit paths of the tests are shown in Figures D.1-12 of Appendix D. Tripping and non-tripping tests for Relays 2 and 3 are shown in Tables 7.3 and 7.4, respectively, in which the bold lines represent backup protection tests for Relays 2 and 3.

Table 7.3: Tripping and non-tripping tests for Relay 2

Relay	**Fault Overcurrent**	**Setting Groups**	**Protection Areas**	**Test Name**	**Number of Tests**	
				Source – Circuit - Fault Type – Fault Site - Tripped Breaker	**Tripping Tests**	**Non-Tripping Tests**
2	Maximum	SS1	**L56**	**UTILITY-8765/1234-DLG(BC)-Bus6-BK6**	12	12
			L67	UTILITY-8765/1234-DLG(BC)-Bus7-BK6		
		SS2	L78	DG2-678/65-SLG(A)-Bus7-BK5		
			L78	DG2-6781-SLG(A)-Bus7-BK5		
			L78	DG2-678-SLG(A)-Bus7-BK5		
		SS4	L78	DG1-5678-SLG(A)-Bus7-BK5		
	Minimum	SS1	**L56**	**UTILITY-8765/1234-LL(BC)-Bus5-BK6**		
			L67	UTILITY-8765/1234-LL(BC)-Bus6-BK6		
		SS2	L78	DG2-678/65-LL(BC)-Bus8-BK5		
			L78	DG2-6781-LL(BC)-Bus8-BK5		
			L78	DG2-678-LL(BC)-Bus8-BK5		
		SS4	L78	DG1-5678-LL(BC)-Bus8-BK5		
				Total Tests of Relay 2	24	

Bold represents backup protection tests

Table 7.4: Tripping and non-tripping tests for Relay 3

Relay	Fault Overcurrent	Setting Groups	Protection Areas	Test Name Source – Circuit - Fault Type – Fault Site - Tripped Breaker	Number of Tests Tripping Tests	 Non-Tripping Tests
3	Maximum	SS1	L56	UTILITY-8765/1234-DLG(BC)-Bus6-BK8	32	32
		SS2	**L78**	**DG2-678/65-SLG(A)-Bus7-BK7**		
			L56	DG2-678/65-SLG(A)-Bus6-BK8		
			L67	DG2-678/65-SLG(A)-Bus6-BK7		
			L56	DG2-67/65-SLG(A)-Bus6-BK8		
			L67	DG2-67/65-SLG(A)-Bus6-BK7		
			L34	DG2-6543-SLG(A)-Bus4-BK8		
			L56	DG2-6543-SLG(A)-Bus6-BK8		
			L56	DG2-65-SLG(A)-Bus6-BK8		
		SS3	**L78**	**DG2-6781-SLG(A)-Bus7-BK7**		
			L67	DG2-6781-SLG(A)-Bus6-BK7		
			L78	**DG2-678-SLG(A)-Bus7-BK7**		
			L67	DG2-678-SLG(A)-Bus6-BK7		
		SS4	L67	DG2-67-SLG(A)-Bus6-BK7		
		SS5	**L78**	**DG1-5678-SLG(A)-Bus7-BK7**		
			L67	DG1-5678-SLG(A)-Bus6-BK7		
	Minimum	SS1	L56	UTILITY-8765/1234-LL(BC)-Bus5-BK8		
		SS2	**L78**	**DG2-678/65-LL(BC)-Bus8-BK7**		
			L56	DG2-678/65-LL(BC)-Bus5-BK8		
			L67	DG2-678/65-LL(BC)-Bus7-BK7		
			L56	DG2-67/65-LL(BC)-Bus5-BK8		
			L67	DG2-67/65-LL(BC)-Bus7-BK7		
			L34	DG2-6543-LL(BC)-Bus3-BK8		
			L56	DG2-6543-LL(BC)-Bus5-BK8		
			L56	DG2-65-LL(BC)-Bus5-BK8		
		SS3	**L78**	**DG2-6781-LL(BC)-Bus8-BK7**		
			L67	DG2-6781-LL(BC)-Bus7-BK7		
			L78	**DG2-678-LL(BC)-Bus8-BK7**		
			L67	DG2-678-LL(BC)-Bus7-BK7		
		SS4	L67	DG2-67-LL(BC)-Bus7-BK7		
		SS5	**L78**	**DG1-5678-LL(BC)-Bus8-BK7**		
			L67	DG1-5678-LL(BC)-Bus7-BK7		
				Total Tests of Relay 3	64	

Bold represents backup protection tests

7.2 Calculation phase

In the Calculation phase, line breaker primary currents and line-to-ground bus primary voltages for Relays 2 and 3 in the microgrid with distributed generators were calculated for test circuit paths in Figures D.1-12 of Appendix D.

Power World® software [10] was used to estimate line breaker primary currents and line-to-ground bus primary voltages for pre-fault, fault, and post-fault states. Although line breaker primary currents and line-to-ground bus primary voltages for pre-fault and post-fault states were estimated by power flow analysis, line breaker primary currents and line-to-ground bus primary voltages for the fault state were estimated by fault analysis.

7.2.1 Power flow analysis

In power flow analysis, line breaker primary currents and line-to-ground bus primary voltages were estimated for pre-fault, fault, and post-fault states for power flow analysis, considering test circuit paths in Figures D.1-12 of Appendix D. Test circuit paths for pre-fault and post-fault states were also considered. In the pre-fault state, breakers were closed and load line currents flowed along the power lines. However, in the post-fault state, the tripped breaker opened after an overcurrent fault. For example, circuit paths for pre-fault (A) and post-fault (B) states of the "UTILITY-8765/1234-DLG(BC)-Bus7-BK6" test are presented in Figure 7.6. As shown in the figure, power flow analysis was run for circuit paths of pre-fault (A) and post-fault (B) states in order to collect line primary currents for "BK6" and "BK5" breakers and line-to-ground primary voltage for Bus 7.

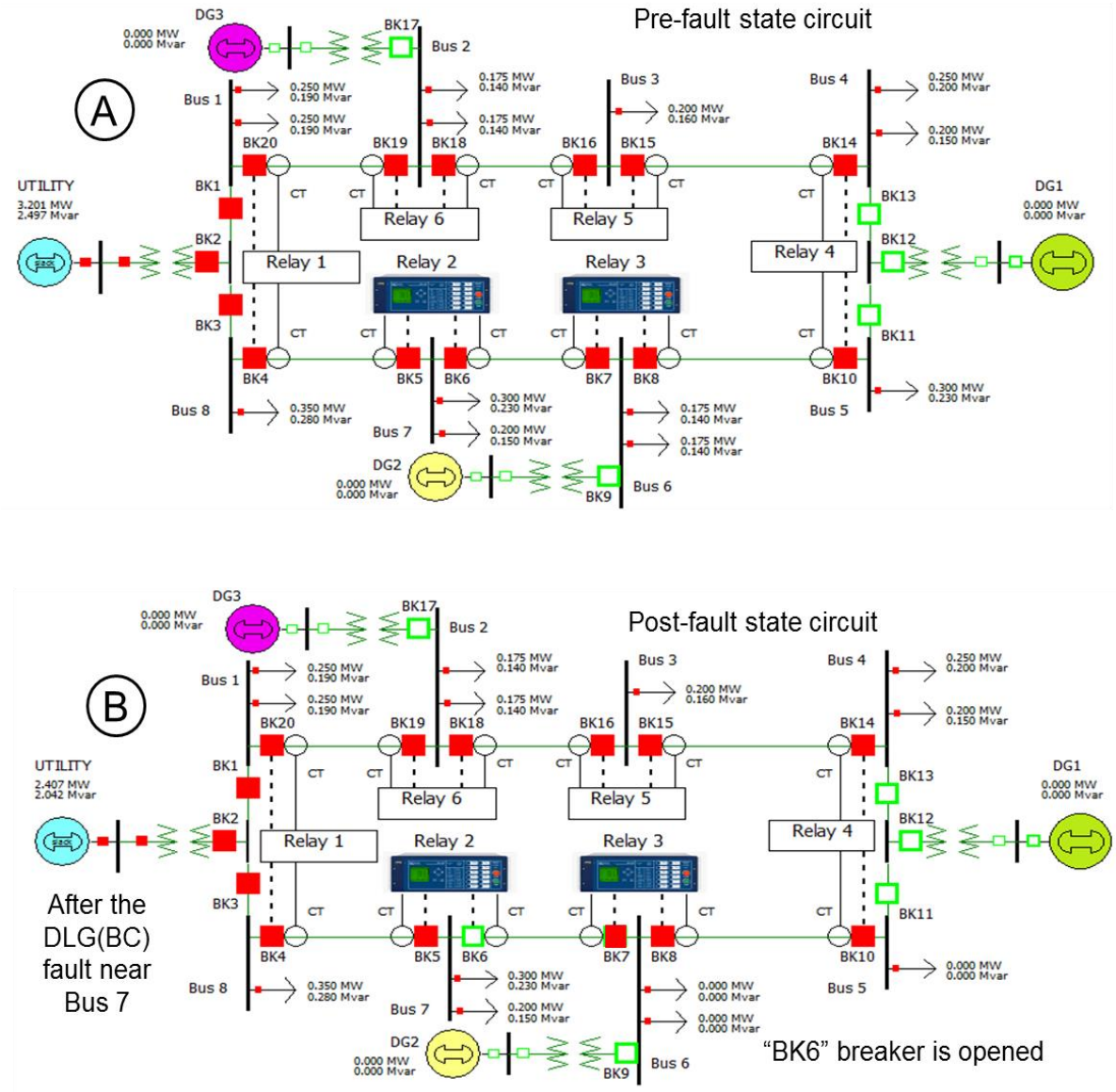

Figure 7.6: Pre-fault (A) and post-fault (B) state circuit path for "UTILITY-8765/1234-DLG(BC)-Bus7-BK6" test

Steps to collect magnitudes and angles of voltages on Bus 7 are shown in Figure 7.7. After running power flow analysis, a click was made on Bus 7, the "Bus Information Dialog" menu was selected, and the line-to-ground voltage magnitude and angle of Phase A were collected.

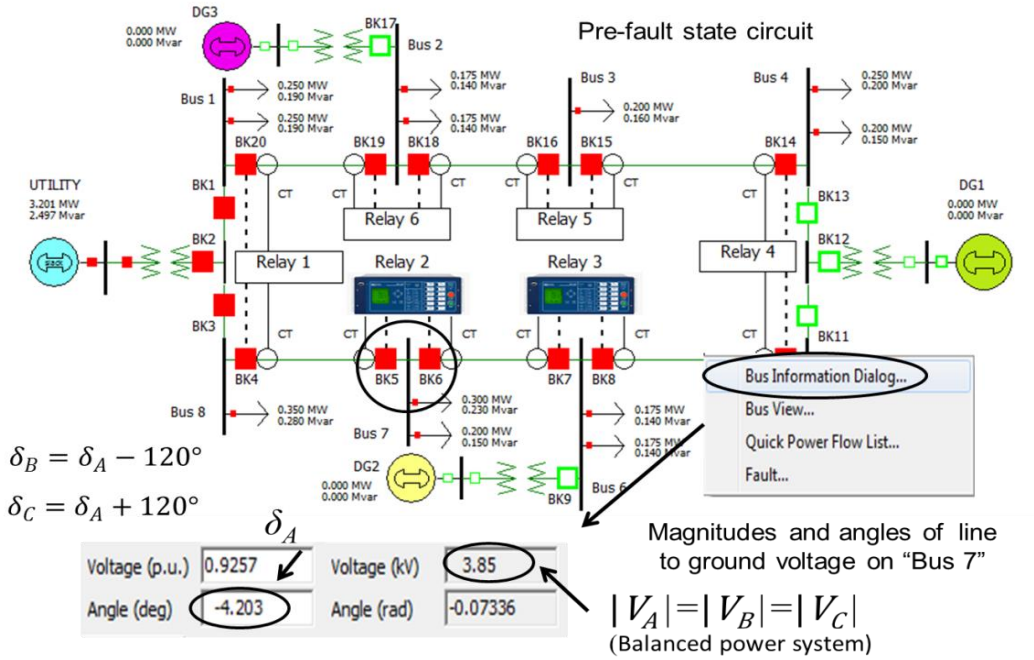

Figure 7.7: Steps to collect line-to-ground voltages on Bus 7 during power flow analysis

Because the circuit shown in Figure 7.7 represented a balanced power system, the magnitude of A, B, and C line-to-ground voltages on Bus 7 were 3.85 kV. The angle of A line-to-ground voltage on Bus 7 was -4.20 degrees, and the angles of B and C line-to-ground voltages on Bus 7 were estimated by Equations (7.1) and (7.2), respectively.

$$\delta_B = \delta_A - 120° \tag{7.1}$$

$$\delta_C = \delta_A + 120° \tag{7.2}$$

where δ_A is the line-to-ground voltage angle of Phase A in degrees, δ_B is the line-to-ground voltage angle of Phase B in degrees, and δ_C is the line-to-ground voltage angle of Phase C in degrees.

As shown in Figure 7.7, the magnitude and angle of A line-to-ground voltage on Bus 7 were collected. Because the microgrid was represented by a balanced power system, the magnitude of A, B, and C line-to-ground voltages on Bus 7 was 3850 volts. The estimated angle

of A line-to-ground voltage on Bus 7 was -4.20 degrees, and according to Equations (7.1) and (7.2), B and C line-to-ground voltage angles on Bus 7 were -124.20 and 115.80 degrees, respectively.

The steps to collect magnitudes and angles of line currents flowing along the "BK6" breaker are shown in Figure 7.8. After running the power flow analysis, a click was made along the power line between Bus 6 and 7, the "Line Information Dialog" was selected, and the line current magnitude of Phase A, real and reactive power were collected.

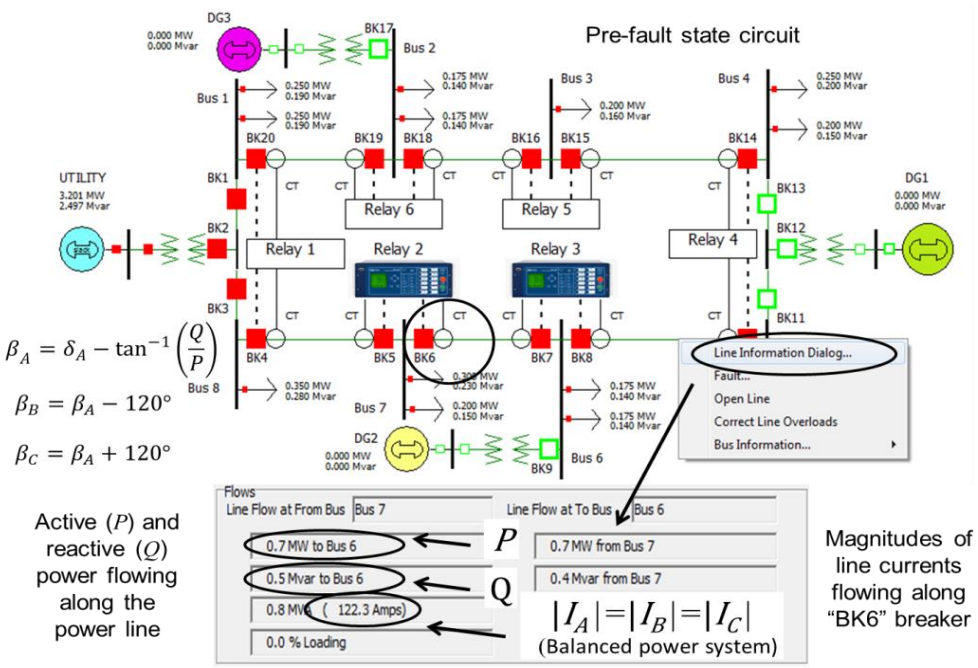

Figure 7.8: Steps to collect line currents of "BK6" breaker during power flow analysis

Apparent power of Phase A, flowing along the power line between Bus 6 and 7 as shown in Figure 7.8, is represented by Equation (7.3):

$$S_A = V_A \times I_A^* \tag{7.3}$$

where S_A is apparent power of Phase A in MVA, V_A is line-to-ground voltage of Phase A in kV, and I_A is conjugate line current of Phase A in kA.

Equation (7.4) represents Equation (7.3) in a polar form:

$$S_A = |V_A| \ \delta_A \times \ |I_A| - \beta_A = \ |V_A| \times |I_A| \ \theta_A \tag{7.4}$$

where $|V_A|$ is line-to-ground voltage magnitude of Phase A in kV, δ_A is line-to-ground voltage angle of Phase A in degrees, $|I_A|$ is line current magnitude of Phase A in kA, β_A is line current angle of Phase A in degrees, and θ_A is the angle between the line-to-ground voltage and line current of Phase A in degrees.

Considering a balanced power system derived from Equation (7.4), the angle between the line-to-ground voltage and line current of Phase A was represented by the power factor angle of Phase A, as shown in Equation (7.5):

$$\theta_A = \delta_A - \beta_A = \tan^{-1}\left(\frac{Q_A}{P_A}\right) = \tan^{-1}\left(\frac{Q/_3}{P/_3}\right) = \tan^{-1}\left(\frac{Q}{P}\right) \tag{7.5}$$

where Q_A is reactive power of Phase A in MVAR, P_A is real power of Phase A in MW, Q is total reactive power in MVAR, and P is total real power in MW.

Using results from Equation (7.5), the angle of line current for Phase A is represented by Equation (7.6) and, considering a balanced power system, angles of line currents for Phases B and C are represented by Equations (7.7) and (7.8), respectively:

$$\beta_A = \delta_A - \tan^{-1}\left(\frac{Q}{P}\right) \tag{7.6}$$

$$\beta_B = \beta_A - 120° \tag{7.7}$$

$$\beta_C = \beta_A + 120° \tag{7.8}$$

where β_A is line current angle of Phase A in degrees, δ_A is line-to-ground voltage angle of Phase A in degrees, Q is total reactive power in MVAR, P is total real power in MW, β_B is line current angle of Phase B in degrees, and β_C is line current angle of Phase C in degrees.

As shown in Figure 7.7, the A line-to-ground voltage angle on Bus 6 was collected, and Figure 7.8 shows that A, B, and C line current magnitude and real and reactive power were

collected from power flow analysis before running the relay tests for NRTS experiment . Because the microgrid was represented by a balanced power system, the magnitude of A, B, and C line currents had identical values, and the magnitudes of A, B, and C line currents of "BK6" breaker were 122 amps. According to Equations (7.6), (7.7), and (7.8), A, B, and C line current angles of "BK6" breaker were -39.74, -159.74, and 80.26 degrees, respectively. Table 7.6 shows A, B, and C line primary currents on "BK6" breaker for the pre-fault state of the "UTILITY-8765/1234-DLG(BC)-Bus7-BK6" test.

The A, B, C line currents and line-to-ground voltages for pre-fault and post-fault states were estimated for all circuit path tests. Line primary currents and line-to-ground primary voltages for the pre-fault state of Relays 2 and 3 are presented in Tables F.1 and F.2 in Appendix F. However, line primary currents and line-to-ground primary voltages for the post-fault state of tests for Relays 2 and 3 are presented in Tables G.1 and G.2 in Appendix G.

7.2.2 Fault analysis

Based on protection areas of the adaptive overcurrent protection system, tests for Relays 2 and 3 in the fault analysis were defined by protection areas of the microgrid for maximum and minimum fault overcurrents of the power lines. Maximum and minimum fault overcurrents were located at the beginning and end of each power line, respectively. The maximum fault overcurrent for the utility and distributed generator circuit paths was the DLG fault at B-C phases and SLG fault at Phase A. The minimum fault overcurrent for utility and distributed generator circuit paths was the LL fault at C-D phases. The A, B, and C line currents of the breakers controlled by the relays and the A, B, and C SLG voltages of relay busses were calculated by running a fault analysis with Power World® software [10].

In the fault analysis, line breaker primary currents and line-to-ground bus primary voltages were estimated for fault states, considering test circuit paths in Figures D.1-12 of Appendix D. For example, Figure 7.9 presents the "UTILITY-8765/1234-DLG(BC)-Bus7-BK6" test circuit for the maximum fault overcurrent. Fault analysis was run for the DLG fault at B-C phases located at 10% length of the power line 6-7 (L67) and line primary currents of "BK6" and "BK5" breakers and line-to-ground primary voltage of Bus 7 were collected.

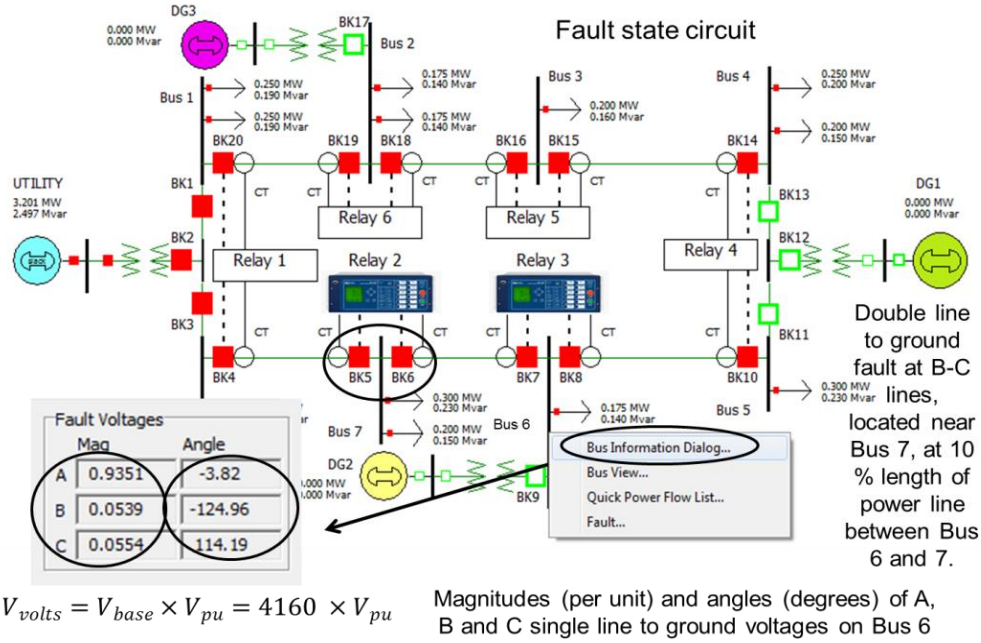

Figure 7.9: Steps to collect line-to-ground voltages on Bus 7 during fault analysis

Steps to collect magnitudes and angles of voltages on Bus 7 are shown in Figure 7.9. After running the fault analysis, a click was made on Bus 7, then the "Bus Information Dialog" menu and "Fault Voltages" tab were selected, and magnitudes and angles of the line-to-ground voltages for Phases A, B, and C were collected. Because magnitudes of the line-to-ground voltages were categorized per-unit and assuming a bus line-to-ground voltage level of 4160 volts as base voltage, magnitudes of the line-to-ground primary voltages in volts were estimated by Equation (7.9):

$$V_{volts} = V_{base} \times V_{pu} = 4160 \times V_{pu} \quad (7.9)$$

where V_{volts} is the line-to-ground voltage in volts, V_{base} is the base line-to-ground voltage of 4160 volts, and V_{pu} is the line-to-ground voltage in per-units.

As shown in Figure 7.9, angles of A, B, C line-to-ground voltages were -3.82, -124.96, and 114.19 degrees, respectively. Using Equation (7.9) and magnitudes of A, B, C line-to-ground voltages per-unit from Figure 7.9, the magnitudes of A, B, C line-to-ground voltages were 3890, 224, and 230 volts, respectively.

Steps to collect magnitudes and angles of line currents on "BK6" and "BK5" breakers are shown in Figure 7.10. After running the fault analysis, a click was made between the fault location and Bus 7 to collect magnitudes and angles of A, B, and C line currents on "BK6" breaker. Another click was made between Bus 7 and 8 to collect magnitudes and angles of A, B, and C line currents on "BK5" breaker. Then the "Line Information Dialog" menu and "Fault Info" tab were selected.

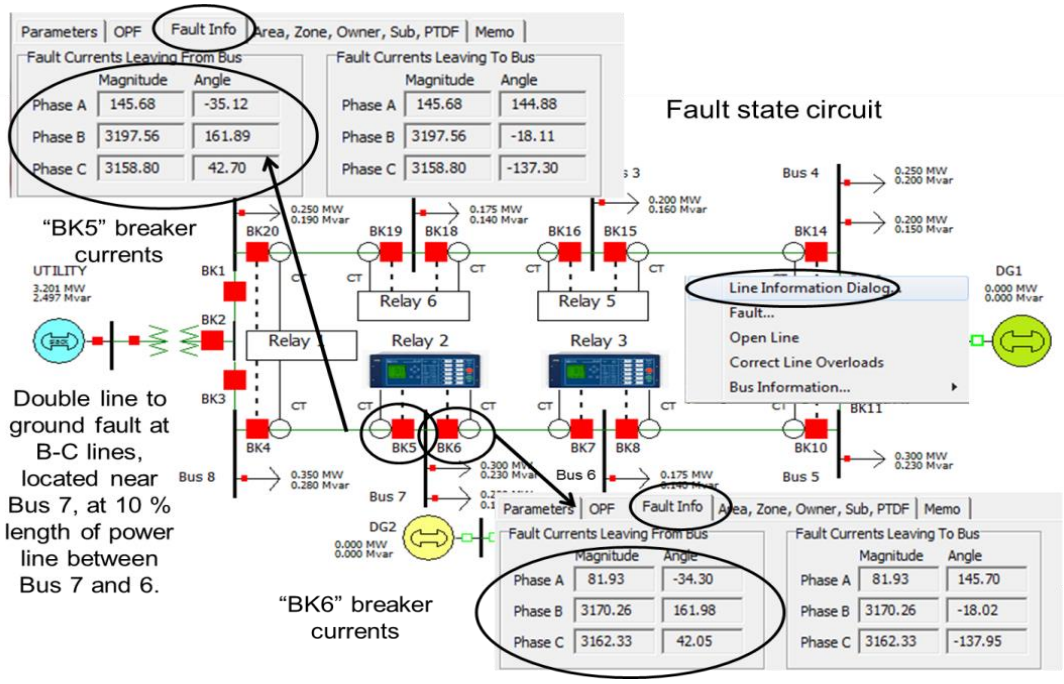

Figure 7.10: Steps to collect line currents of breakers during fault analysis

Magnitudes and angles of A, B, and C line currents for “BK6 and “BK5” breakers were read from the microgrid circuit in Figure 7.10 and are presented in Table 7.5.

Table 7.5: Line primary currents of “BK5” and “BK6” breakers for the fault state, “UTILITY-8765/1234-DLG(BC)-Bus7-BK6” tripping test

A, B, and C line currents of “BK5” breaker						A, B, and C line currents of “BK6” breaker					
I_A		I_B		I_C		I_A		I_B		I_C	
Mag [A]	Angle [°]	Mag [A]	Angle [°]	Mag [A]	Angle [°]	Mag [A]	Angle [°]	Mag [A]	Angle [°]	Mag [A]	Angle [°]
146	-35.12	3197	161.89	3158	42.70	82	-34.30	3170	161.98	3162	42.05

The A, B, C line currents and line-to-ground voltages for fault states were estimated for all circuit path tests. Line primary currents and line-to-ground primary voltages for fault states of maximum and minimum fault overcurrents of Relay 2 tests are presented in Tables H.1 and H.2, respectively, and line primary currents and line-to-ground primary voltages for fault states of maximum and minimum fault overcurrents of Relay 3 tests are presented in Tables H.3 and H.4, respectively, in Appendix H.

Similar to fault states of the tripping tests, LEDs on the relay’s front panels required magnitudes and angles of A, B, and C line currents and line-to-ground voltages in order to detect fault type. Magnitudes and angles of A, B, C line currents and line-to- ground voltages for fault states estimated with Power World® software [10] were also verified when the relays tripped during the tripping tests.

7.3 Preparation phase

In the Preparation phase, test files prepared with the SEL-5401® software [12] were created to run the tripping and non-tripping tests. The non-real-time simulator, SEL-AMS [3], simulated the line secondary currents and line-to-ground secondary voltages, as well as breaker

coils (sense inputs) and auxiliary contacts (contact outputs) for pre-fault, fault, and post-fault states of the test files.

The SEL-5401® software [12] was opened in order to create a new test file. The “File” menu and “New” option were selected to create a new test file, and then the “Relay Configuration” window was opened and the SEL-451 was selected as “Relay Type”. The 75 A/V current and 150 V/V voltage scale factors for the new test file on the “Relay Configuration” window were shown, and the “OK” tab was clicked. Figure 7.11 shows the steps to create a new test file and select current and voltage scaling factors of the SEL-451 relay.

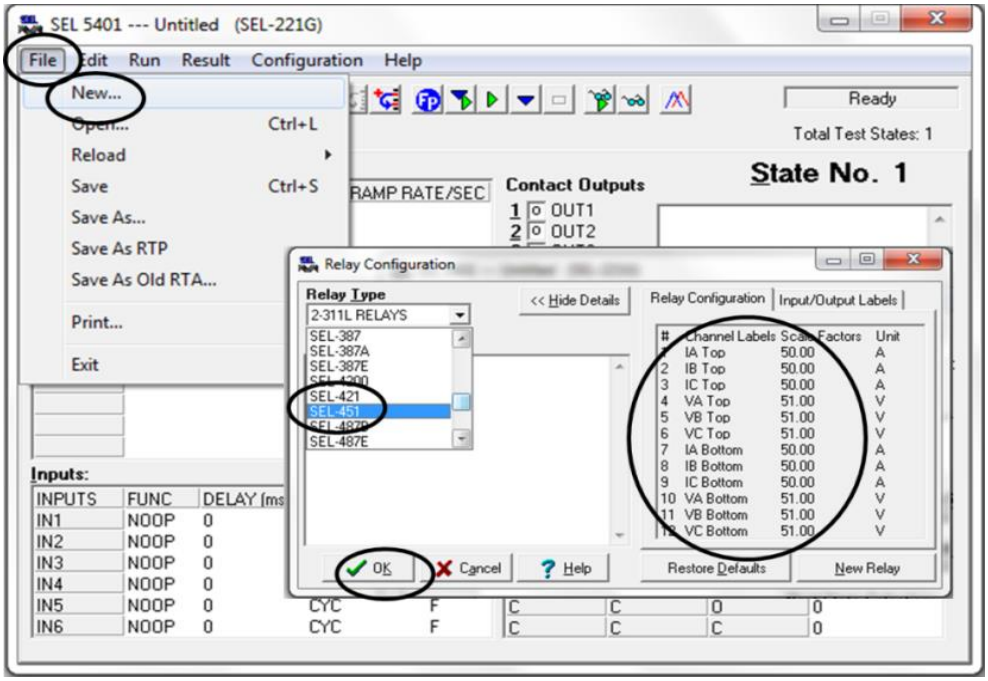

Figure 7.11: Creating a new test file and selecting scaling factors for the SEL-451 relay

In order to create states of the new test file, the “Insert State Before Current” tab was clicked three times to insert pre-fault, fault, and post-fault sates; then the “Frequency” of 60 Hz was set for all states. Figure 7.12 shows the steps to insert the states into a new test file.

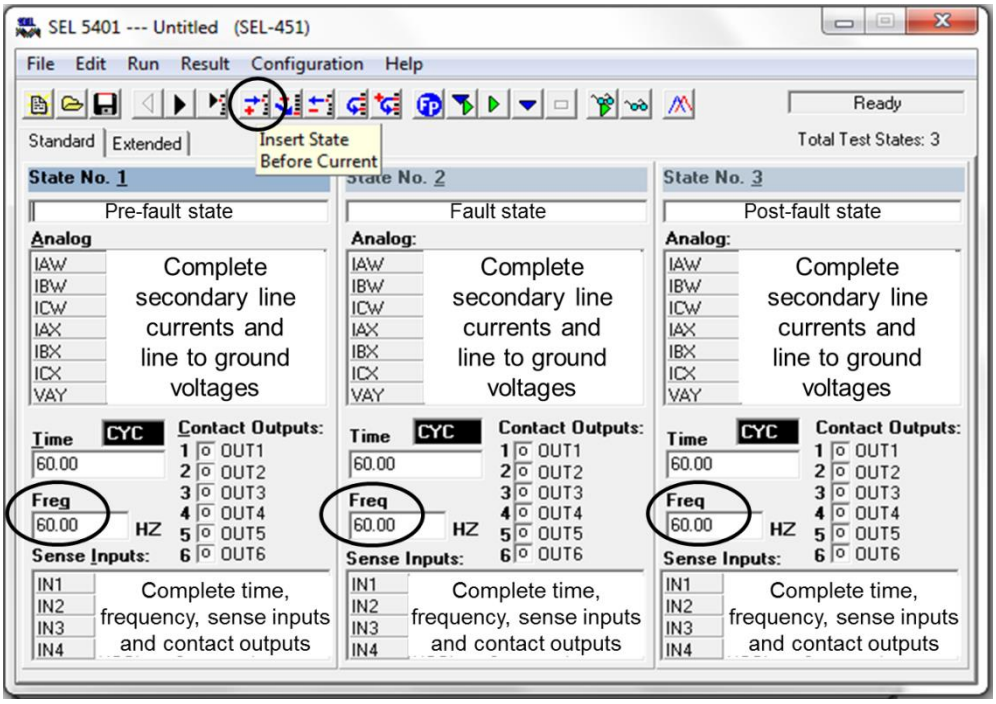

Figure 7.12: Steps to insert states into a new test file

The A, B, and C line secondary currents and line-to-ground secondary voltages, state times, sense inputs, and contact outputs for pre-fault, fault, and post-fault states of the new test file were completed.

7.3.1 Secondary currents and voltages

The non-real-time simulator, SEL-AMS [3], simulated pre-fault, fault and post-fault states for the tripping tests and pre-fault and fault states for the non-tripping tests. Line secondary currents and line-to-ground secondary voltages corresponded to values measured by the current transformers and power transformers, respectively. Line secondary currents and line-to-ground secondary voltages were simulated as analog signals, and the LLTI of the relays was connected to the SEL-AMS [3]. The SEL-5401® software [12] was applied in order to set the line secondary currents and line-to-ground secondary voltages for the tripping and non-tripping tests.

Magnitudes of line secondary currents for the A, B, and C phases were estimated using Equation (7.10):

$$I_{secondary} = \frac{I_{primary}}{CTR} = \frac{I_{primary}}{200} \tag{7.10}$$

where $I_{secondary}$ is magnitude of line secondary currents in amps, $I_{primary}$ is magnitude of line primary currents in amps, and *CTR* is the current transformer ratio of 200.

Magnitude of line-to-ground secondary voltages for the A, B, and C phases was estimated using Equation (7.11):

$$V_{secondary} = \frac{V_{primary}}{PTR} = \frac{V_{primary}}{60} \tag{7.11}$$

where $V_{secondary}$ is magnitude of line-to-ground secondary voltages in volts, $V_{primary}$ is magnitude of line-to-ground primary voltages in volts, and *PTR* is the potential transformer ratio of 60. In order to calculate magnitudes of line secondary currents and line-to-ground secondary voltages using Equations (7.10) and (7.11), respectively, magnitude of the line primary currents and line-to-ground primary voltages were estimated with Power World® software [10] before setting the test files.

Although line primary currents and line-to-ground primary voltages for pre-fault and post-fault states were estimated by power flow analysis using the Power World® software [10], line primary currents and line-to-ground primary voltages for fault states were estimated by fault analysis using the Power World® software [10]. Line secondary currents and line-to-ground secondary voltages for pre-fault, post-fault, and fault states for test files of maximum and minimum fault overcurrents are presented in Tables I.1-.2, J.1-.2, and K.1-.2-.3-.4 of Appendixes I, J, and K, respectively.

As an example of setting line secondary currents and line-to-ground secondary voltages for the non-real-time simulator, the line secondary currents and line-to-ground secondary

voltages for the “UTILITY-8765/1234-LL(BC)-Bus5-BK6” tripping and non-tripping tests are shown in Figures 7.13 and 7.14, respectively.

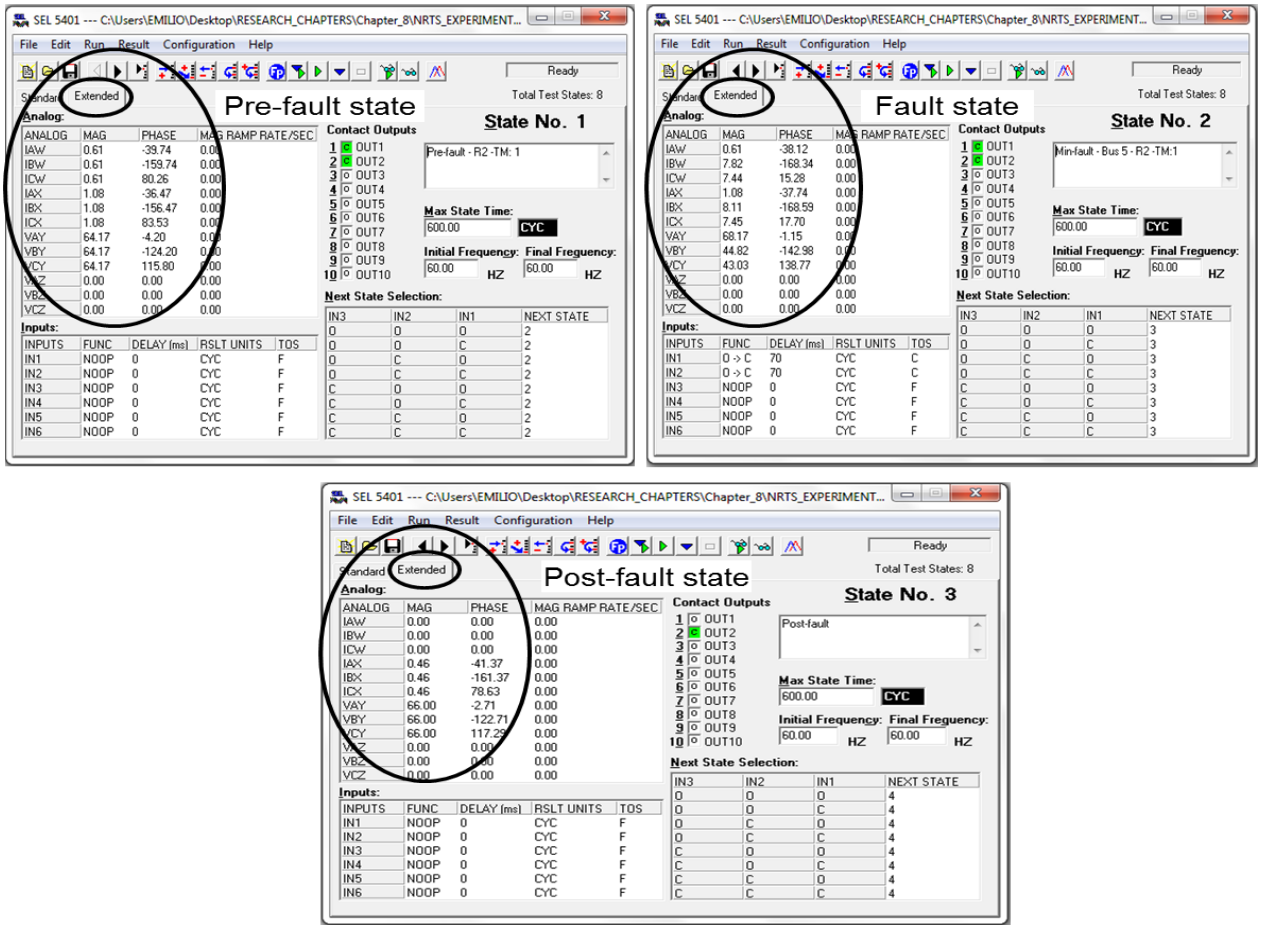

Figure 7.13: Line secondary currents and line-to-ground secondary voltages of the “UTILITY-8765/1234-LL(BC)-Bus5-BK6” tripping test file

Using SEL-5401® software [12], line secondary currents and line-to-ground secondary voltages for pre-fault, fault, and post-fault states were set, and the Extended mode was selected instead of the Standard mode in order to set the IAW- IBW- ICW, IAX- IBX-ICX, and VAY-VBY-VCY analog signals. Pre-fault states of the “UTILITY-8765/1234-LL(BC)-Bus5-BK6” tripping and non-tripping tests were identical in Figures 7.13 and 7.14.For the “UTILITY-8765/1234-LL(BC)-Bus5-BK6” tripping (Figure 7.13) and non-tripping (7.14) test files, magnitudes and angles of line secondary currents and line-to-ground secondary voltages for the

analog signals were set. The A, B, and C line secondary currents of Breakers 1 and 2 were represented by the IAW-IBW-ICW and IAX-IBX-ICX analog signals, respectively. The A, B, and C line-to-ground secondary voltages of Bus 7 were represented by VAY-VBY-VCY analog signals. On Bus 7, Breakers 1 and 2, named “BK6” and “BK5”, respectively, were controlled by Relay 2 for the “UTILITY-8765/1234-LL(BC)-Bus5-BK6” tripping and non-tripping tests.

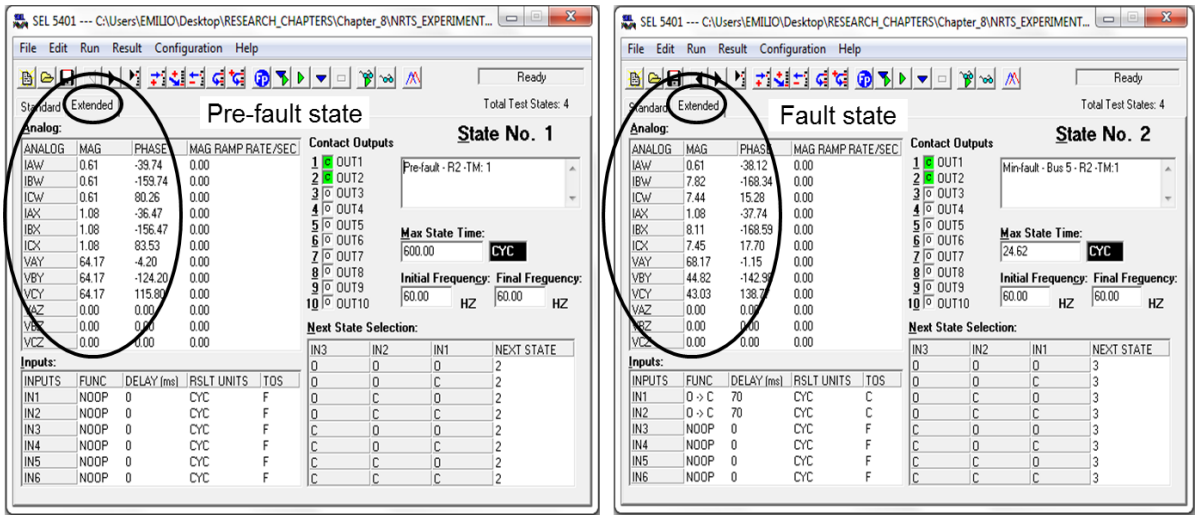

Figure 7.14: Line secondary currents and line-to-ground secondary voltages of the “UTILITY-8765/1234-LL(BC)-Bus5-BK6” non-tripping test file

In Figure 7.13, the “UTILITY-8765/1234-LL(BC)-Bus5-BK6” tripping test was formed by the pre-fault, fault, and post-fault states. In Figure 7.14, the “UTILITY-8765/1234-LL(BC)-Bus5-BK6” non-tripping test was formed by the pre-fault and fault states; the post-fault state was not required because the relay did not trip.

7.3.2 Sense inputs, contact outputs, and state times

SEL-AMS [3] simulated sense inputs and contact outputs of the breakers. The sense inputs (O symbol) and contact outputs (| | symbol) represented the breaker coils and auxiliary contacts, respectively. Sense inputs of the SEL-AMS [3] represented the trip (TC1, TC2) and close (CC1, CC2) coils of breakers that received 14.3 Vdc signals from the relay’s control

outputs to open or close the breakers. However, contact outputs of the SEL-AMS [3] represented the NO auxiliary contacts (52A1, 52A2) of breakers that sent the breaker pole status (closed or open) to the relay. In the relay, the open state of the NO auxiliary contact (52A1, 52A2) was 0 Vdc if the circuit breaker was open, and the closed state of the NO auxiliary contact (52A1, 52A2) was 125 Vdc if the circuit breaker was closed, based on the relay's instruction manual [5]. Figure 7.15 shows the tripping, closing, and breaker state circuits of a SEL-451 relay operating two breakers (52AA1, 52AA2) during pre-fault (A), fault (B), and post-fault (C) states. Tripping and closing circuits were represented by a 14.3 Vdc source, breaker coil, and relay's control output connected in series. However, breaker state circuits were represented by a 125 Vdc source, breaker NO auxiliary contacts (52A1, 52A2), and the relay's control inputs connected in series.

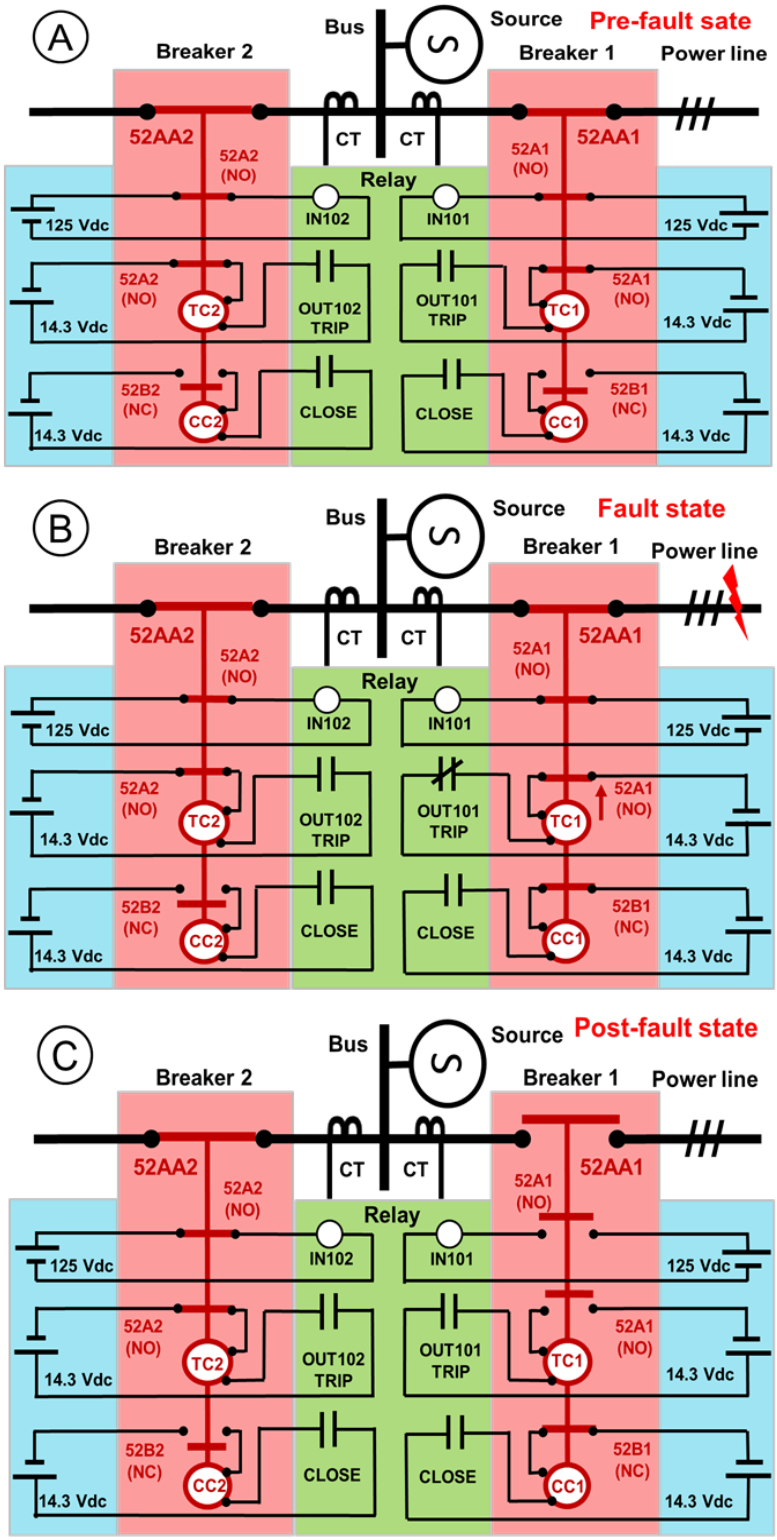

Breaker status: NO contact output (52A1, 52A2), Trip coil: sense inputs (TC1, TC2), Close coil: sense inputs (CC1, CC2)

Figure 7.15: Pre-fault (A), fault (B), and post-fault (C) states

In Figures 7.16, the RMS line breaker primary currents, breaker pole status (contact outputs), and trip coil states (sense inputs) for pre-fault, fault, and post-fault states were plotted for Breakers 1 (A) and 2 (B). In the NRTS experiment, the tripping and closing circuits with trip coils (TC1, TC2) and close coils (CC1, CC2) were wired and not wired, respectively, for experimental circuits of Relays 2 and 3. Therefore, only sense inputs represented by breaker trip coils (TC1, TC2) and contact outputs represented by breaker NO auxiliary contacts (52A1, 52A2) were considered to create test files for the tripping and non-tripping tests.

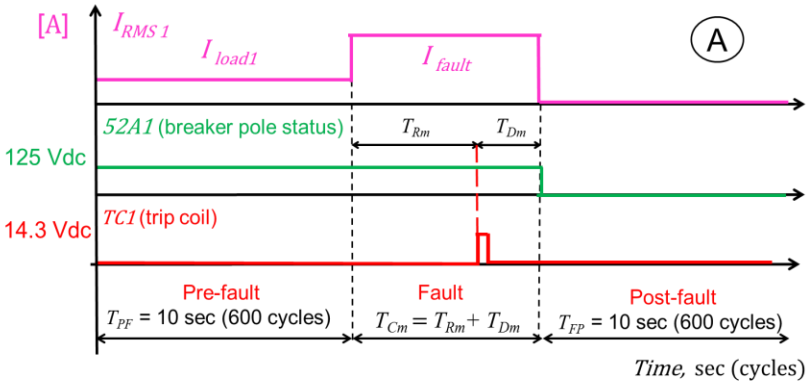

f = 60 Hz (1 cycle = 16.66 ms) T_D = 70 ms = 4.2 cyc

T_{PF} = pre-fault state time T_{PF} = post-fault state time T_{Rm} = measured relay time of tripping test

T_{Cm} = measured fault clearing time of tripping test T_{Dm} = measured delay time of tripping test

52A1 = NO auxiliary contact of breaker 1 pole status (SEL-AMS's contact output)

TC1 = trip coil status of breaker 1 (SEL-AMS's sense input)

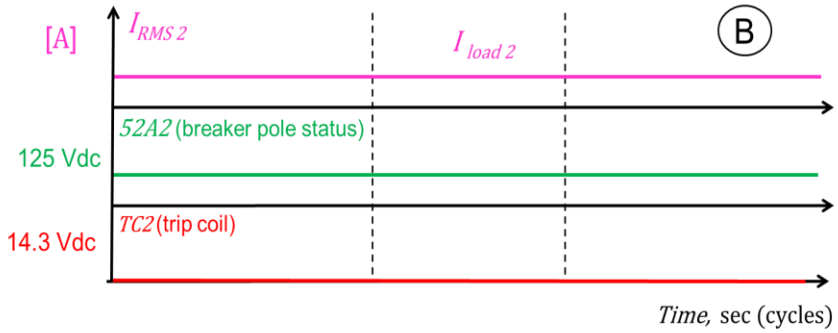

52A2 = NO auxiliary contact of breaker 2 pole status (SEL-AMS's contact output)

TC2 = trip coil status of breaker 2 (SEL-AMS's sense input)

Figure 7.16: Contact outputs and sense inputs of Breaker 1 (A) and 2 (B)

Table 7.6 shows sense inputs, contact outputs, and state times for tripping and non-tripping test files. In the tripping tests, fault state times were set at a time greater than the measured fault clearing time and relays tripped for fault overcurrents. Tripping test files were formed by pre-fault, fault, and post-fault states. However, in the non-tripping tests, the fault state was set at a time less than the measured relay time of the tripping test; therefore, the relays did not trip. Non-tripping test files were formed by pre-fault and fault states.

Table 7.6: Sense inputs, contact outputs, and state times

Type of test	**States**	**Time [cycles]**	**Sense inputs (trip coils)**		**Contact outputs (NO auxiliary contacts)**	
			IN1 (TC1)	**IN2 (TC2)**	**OUT1 (52A1)**	**OUT2 (52A2)**
Tripping	Pre-fault	600	NOOP	NOOP	c	c
	Fault	600	O=>C	O=>C	c	c
	Post-fault	600	NOOP	NOOP	o (or) c	o (or) c
Non-tripping	Pre-fault	600	NOOP	NOOP	c	c
	Fault	0.8 x T_{Rm}	O=>C	O=>C	c	c

NOOP: non-operation, O = >C: trip coil off = >trip coil on, c: closed contact, o: open contact
T_{Rm} : measured relay time of tripping tests

In the adaptive overcurrent protection system, fault overcurrent was cleared by the breaker nearest to the fault. In the fault state, fault overcurrent was detected by the relay, the relay's control output (OUT101) was closed, and the trip coil (TC1) was energized by the 14.3 Vdc source, thereby moving the mechanical support of Breaker 1 (52AA1) to open the poles of Breaker 1 (52AA1) at the post-fault state. Although only one trip coil (TC1) was energized in the fault state, all sense inputs (IN1 and IN2) were set at "O = >C" for all tripping and non-tripping test files. Based on setting groups of the relays, the breaker nearest to the fault was always tripped for adaptive overcurrent protection. In the post-fault state, OUT1 (52A1) and OUT2 (52A2) contact outputs were set as "o" or "c" contacts, depending on which breaker of the relay

was expected to trip or remain closed, respectively, for each tripping test. The OUT1 (52A1) and OUT2 (52A2) NO auxiliary contacts corresponded to Breakers 1 and 2, respectively.

Fault state times for non-tripping tests were set at a time less than the measured relay time of the tripping test. Fault state times for non-tripping tests were calculated using Equation (7.12):

$$T_{FS2} = 0.8 \times T_{Rm} \tag{7.12}$$

where T_{FS2} is the fault state time of non-tripping tests in cycles and T_{Rm} is the measured relay time of tripping tests in cycles. As an example of setting the sense inputs, contact outputs, and state times for the non-real-time simulator, the sense inputs, contact outputs, and state times for the "UTILITY-8765/1234-LL(BC)-Bus5-BK6" tripping (A) and non-tripping (B) tests are indicated in Figure 7.17.

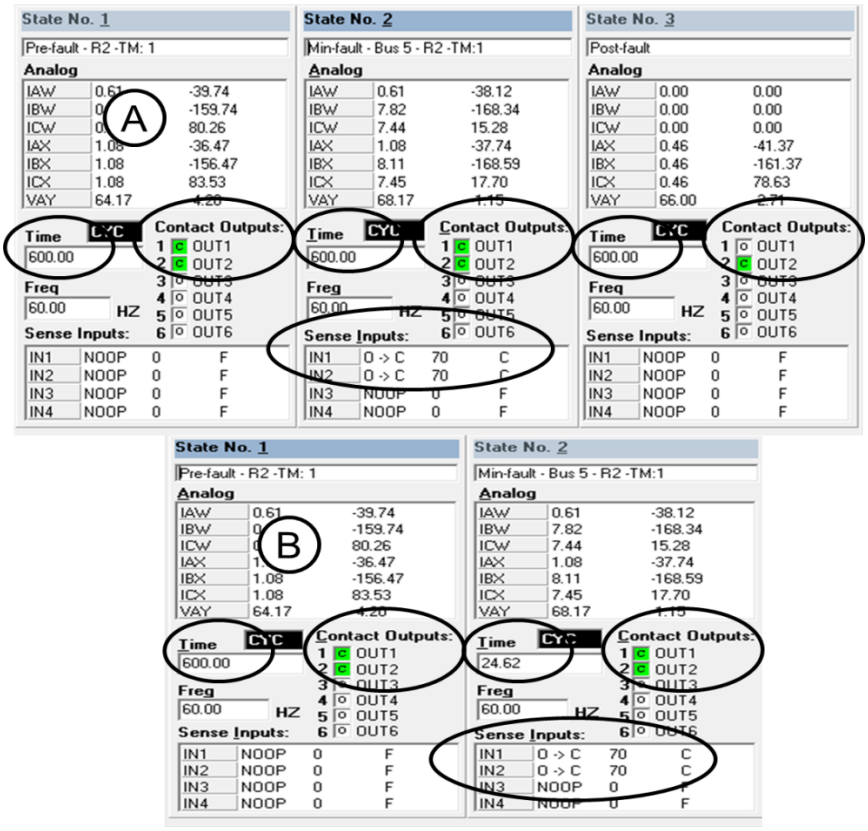

Figure 7.17: Sense inputs, contact outputs, and state times for the "UTILITY-8765/1234-LL(BC)-Bus5-BK6" tripping (A) and non-tripping (B) tests

Sense inputs, contact outputs, and state times were set with the SEL-5401® software [12]. For the fault state, sense inputs (O = >C) were set at "C" as final state, and delay time of the breaker was set at 70 milliseconds (4.22 cycles) based on the manufacturer's literature [96]. In Figure 7.17-B, the fault state time for the non-tripping test was estimated using Equation (7.12). The "UTILITY-8765/1234-LL(BC)-Bus5-BK6" tripping test was run before the non-tripping test, and the measured relay time of the tripping tests was 30.774 cycles. A fault state time of 24.62 cycles was calculated with Equation (7.12) and set for the "UTILITY-8765/1234-LL(BC)-Bus5-BK6" non-tripping test file in Figure 7.17-B.

7.4 Execution phase

In the Execution phase, tripping and non-tripping tests were run. Before executing tripping and non-tripping tests for Relays 2 and 3, the following steps were conducted in order to manually select the setting group from the relay's front panel:

- Push the "ENT" button on the relay's front panel.
- Select the "SET / SHOW" option and push the "ENT" button.
- Select the "ACTIVE GROUP" and push the "ENT" button.
- Enter the password "TAIL" and select "ACCEPT".
- Place the new relay setting group in "NEW GROUP" option and push the "ENT" button.

Based on the circuit path of the tripping and non-tripping tests, setting groups of Relays 2 and 3 are indicated in Figure 7.18.

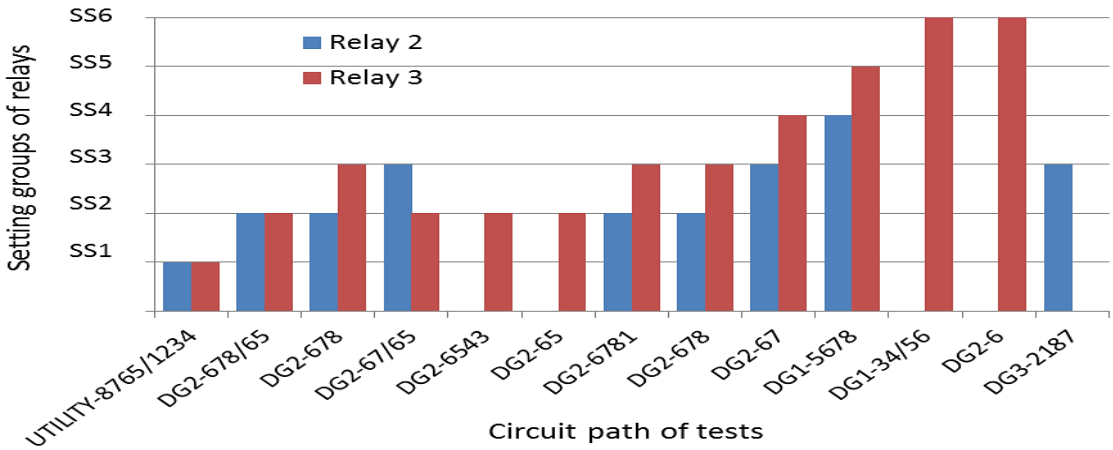

Figure 7.18: Setting groups of Relays 2 and 3 for circuit paths of tripping and non-tripping tests

The SEL-5401® software [12] opened the tripping and non-tripping test files (.RTA) created in the Preparation phase. Steps for executing tripping and non-tripping test files are indicated in Figure 7.19. The SEL-5401® software [12] opened the test file. As shown in Figure 7.19-A, the "Configuration" menu was clicked, the "Communications" option was selected, and then the number of the "Comm Port" was matched to the USB port of the HMI computer connected by the SEL-C662 cable to the SEL-AMS [3]. As shown in Figure 7.19-B, the baud date (data speed) was set at 9600, the "OK" tab was clicked, and the "Download and run this test" menu was selected to run the test file.

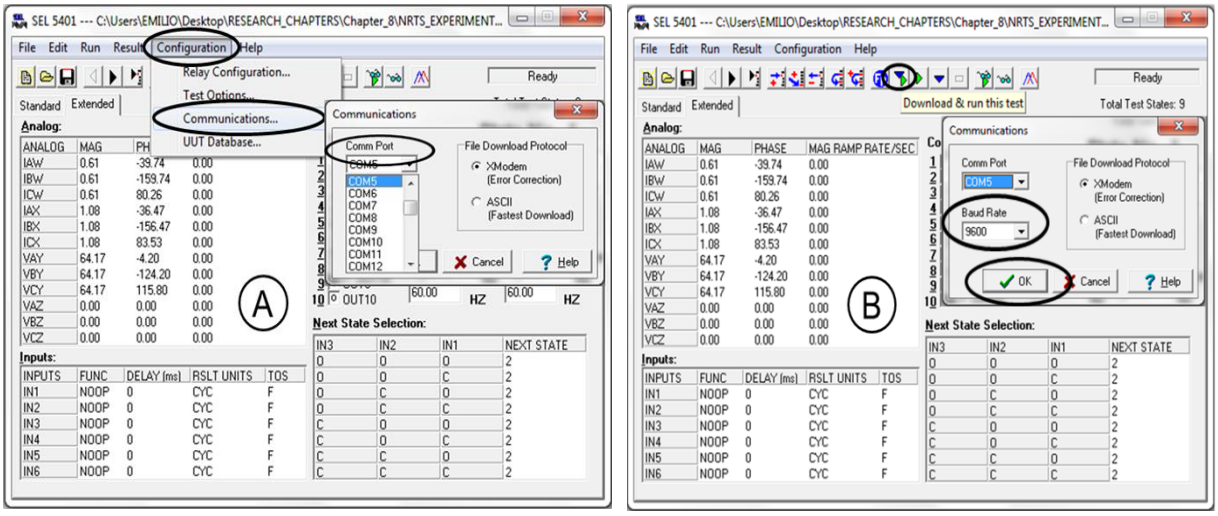

Figure 7.19: Configuration (A) and download and run this test (B)

While test files of Relays 2 or 3 were run with SEL-5401® software [12], the relay's display and push-button LEDs from the HMI computer were observed, indicating magnitudes of A, B, and C line currents and status of Breakers 1 and 2. At end of the Execution phase, measured relay and fault clearing times were collected.

7.5 Collection phase

In the Collection phase, the relay's display and push-button LEDs and measured relay and fault clearing times were collected from the webcam and HMI computer. The relay's display and push-button LEDS were collected to verify adaptive overcurrent protection at first sight during execution of the non-real-time tests. Table 7.7 shows collected data, sites, sources, and measurements of the non-real-time tests.

Table 7.7: Collected data for the non-real-time tests

Collected Data	Sites	Sources	Measurements
Display and push-button LEDs	Webcam computer	Relays 2 and 3	Breaker line currents, breaker trips, and fault type were measured from the relay's front panel.
Relay and fault clearing times	HMI computer	SEL-AMS	Relay and fault clearing times from the fault states were measured from test results.

HMI: Human machine interface

Figure 7.20 shows the power desk and rack area in the NRTS Experiment. Non-real-time tests were executed and supervised from the power desk (A). In Figure 7.20-A, the webcam and HMI computers were connected to collect the display and push-button LEDs, as well as test results (measured relay and fault clearing times), respectively.

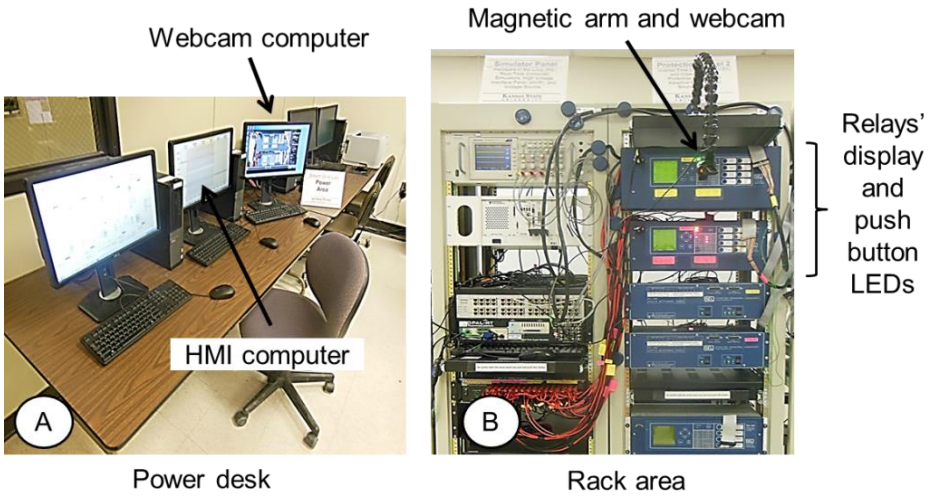

Figure 7.20: Power desk (A) and rack area (B) in the NRTS Experiment

7.5.1 Display and push-button LEDs

The relay's display and push-button LEDs were measured during the execution of the non-real-time tests. The relays' display and push-button LEDs were evaluated at first sight from the webcam computer (Figure 7.20-A), and a webcam placed in a magnetic arm attached to the relay rack observed the relay's displays and push-button LEDs were for Relays 2 and 3 (Figure 7.20-B). The A, B, and C line currents of Breakers 1 and 2 were observed on the relay's display during execution of the non-real-time tests, verifying load and fault currents for pre-fault and fault states, respectively, and zero current at post-fault state. Breaker 1 and 2 states (closed and open) were observed on the push-button LEDs on the relay's front panel, verifying breaker status during tripping and non-tripping tests. In addition, the status of LEDs that indicated enabled relay, trip, inverse time overcurrent protection, fault types, line-to-ground voltage level, breaker status, and alternative setting groups were measured from the relay's front panel. Figure 7.21 shows LEDs on the relay's front panel according to the relay's instruction manual [5]. As soon as the relay tripped, the "TARGET RESET" button was pushed to reset LEDs of the relay's front panel.

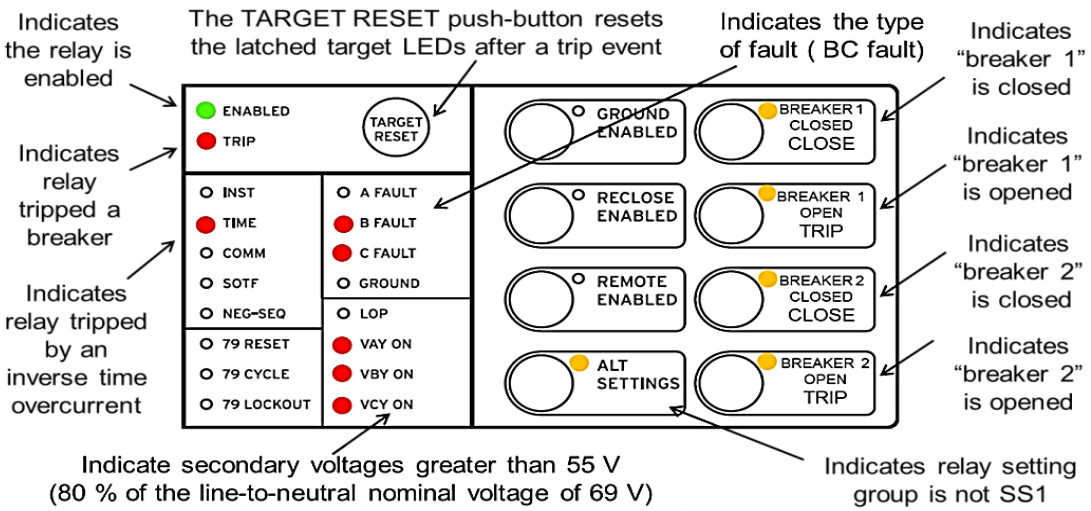

Figure 7.21: LEDs on SEL-451 relay's front panel [5]

In the tripping tests, "TRIP" and" TIME" LEDs were turned on when the relay tripped. Maximum fault overcurrents corresponded to the DLG(BC) and SLG(A) faults of the utility and distributed generator circuit path tests, respectively. Minimum fault overcurrents corresponded to the SLG(A) fault of the utility and distributed generator circuit path tests. Because the type of fault detected by LEDs on the relay's front panel depended on the magnitude and angle of the currents and line-to-ground voltages, currents and line-to-ground voltages estimated by fault analysis with Power World® software [10] were also verified by LEDs on the relay's front panel. DLG (A), SLG (B), and LL (C) faults on the relay's front panel are shown in Figure 7.22.

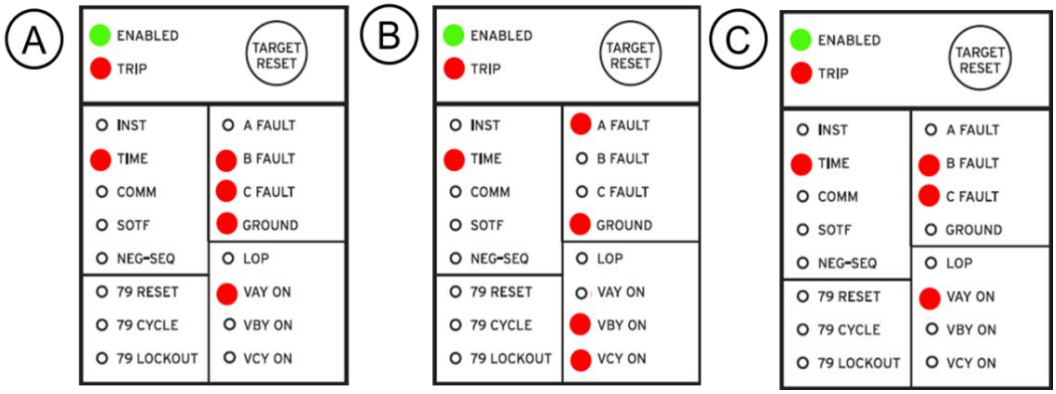

Figure 7.22: DLG (A), SLG (B), and LL (C) faults on SEL 451 relay's front panel [5]

7.5.2 Measured relay and fault clearing times

The measured relay and fault clearing times were collected from fault states of tripping tests after the relay was tripped. The measured relay and fault clearing times represented the sense input and total state times of the fault states, respectively. The measured relay and fault clearing times were generated by the non-real-time simulator, SEL-AMS [3], that simulated breaker trip coils (sense inputs) and NO auxiliary contacts (contact outputs) during pre-fault, fault, and post-fault states. The trip coil (TC1, TC2) was energized by the relay trip signal to open the breaker and the NO auxiliary contacts (52A1, 52A2) sensed the breaker poles. Once the tripping tests were run, the measured relay and fault clearing times were collected by clicking on the "Test Results" tab and selecting the fault states from the "Go To" cell, as shown in Figure 7.23.

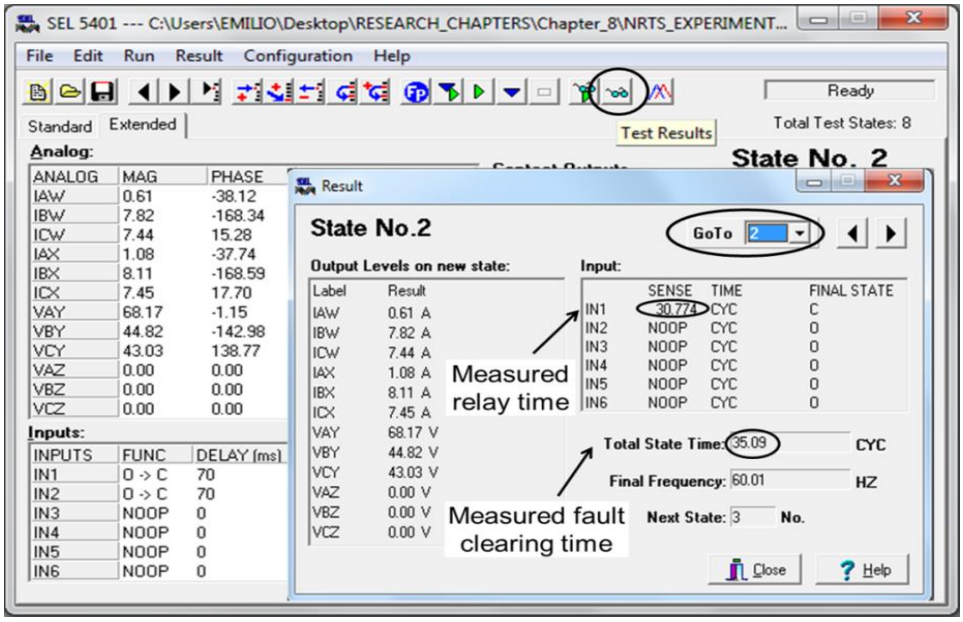

Figure 7.23: Test results of "UTILITY-8765/1234-LL(BC)-Bus5-BK6" test

As demonstrated in Figure 7.23, time from the "Input" represented the measured relay time in cycles and the "Total State Time" represented the measured fault clearing time in cycles. The measured delay time was estimated using Equation (7.13):

$$T_{Dm} = T_{Cm} - T_{Rm} \tag{7.13}$$

where T_{Dm} is the measured delay time in cycles, T_{Rm} is the measured relay time in cycles, and T_{Cm} is the measured fault clearing time in cycles for the tripping tests. For example, State No. 2 in Figure 7.23 indicated results of the "UTILITY-8765/1234-LL(BC)-Bus5-BK6" test. The LL fault at B-C phases was located on Bus 5, and Breaker 1 (BK6) was tripped; the measured relay and fault clearing times were 30.774 and 35.09 cycles, respectively. According to Equation (7.13), the measured delay time was 4.316 cycles. Although the delay time was set at 4.22 cycles for the "UTILITY-8765/1234-LL(BC)-Bus5-BK6" test, the measured delay time was greater than 4.22 cycles because the wired experimental circuit added delay time.

7.5.3 Percent error of relay time

Theoretical and measured relay time values for tripping tests were evaluated. Although theoretical relay times were based on the inverse time overcurrent U3 curve from the relay's instruction manual [5], measured relay times were collected from test results. The percent error of relay times was calculated with Equation (7.14):

$$E_{TR\%} = \frac{T_{Rm} - T_R}{T_R} \times 100 \tag{7.14}$$

where $E_{TR\%}$ is percent error of relay time, T_{Rm} is measured relay time in cycles, and T_R is theoretical relay time in cycles. Theoretical relay time values were estimated with Equation (7.15), based on the inverse time overcurrent U3 curve from relay's instruction manual [5]:

$$T_R = TDS \times \left(0.0963 + \frac{3.88}{(I/CTR/\,I_P)^2 - 1}\right) \times 60 \tag{7.15}$$

where T_R is the theoretical relay time in cycles, *TDS* is the inverse time overcurrent time dial setting, *I* is the primary pickup fault current in amps, *CTR* is the current transformer ratio, and I_P is the secondary overcurrent pickup in amps.

In the NRTS experiment, percent error values for tripping tests of maximum and minimum fault overcurrents in Relays 2 and 3 were estimated.

7.6 Chapter summary

In this chapter, test steps to run tripping and non-tripping tests for adaptive overcurrent protection of the microgrid with distributed generators were described. The test steps, based on tripping and non-tripping tests, included Calculation (1), Preparation (2), Execution (3), and Collection (4) phases. In the NRTS experiment, tripping tests were run before non-tripping tests.

In the Calculation (1) phase, the microgrid circuit was edited based on the circuit path test. Line breaker primary currents and SLG bus primary voltages of Relays 2 and 3 were estimated for pre-fault and post-fault states by running a power flow analysis. However, line breaker primary currents and SLG bus primary voltages of Relays 2 and 3 were estimated for the fault state by running a fault analysis. Power flow and fault analysis were run with Power World® software [10].

In the Preparation (2) phase, secondary currents and voltages for the breakers and buses of Relays 2 and 3 were estimated by dividing the calculated line breaker primary currents and SLG bus primary voltages by the current and potential transformer ratios, respectively. Test files for tripping and non-tripping tests were created with the SEL-5401® software [12].

In the Execution (3) phase, relay setting groups to run the tests were selected from the relay's display front. Tripping and non-tripping tests were then executed by downloading and running test files with the SEL-5401® software [12].

In the Collection (4) phase, non-real-time tests were run and the relay's display and push-button LEDs were evaluated at first sight from a webcam. Upon completion of the tripping tests, the measured relay and fault clearing times were collected from the fault state results. Tripping

tests were run before non-tripping tests because fault state times of the non-tripping tests were set with measured relay times of the tripping tests multiplied by 0.8.

Chapter 8 - Results of NRTS experiment

NRTS experiment results are analyzed in this chapter. The NRTS experiment was segregated into tripping tests, including backup protection tests, and non-tripping tests. Inputs (tripped breakers), relays, and fault clearing times were collected from tripping test results. Table 8.1 shows characteristics of tests and methods used to collect test results.

Table 8.1: Characteristics and results of tests for NRTS experiment

Characteristics of tests					**Methods for collecting results**	
Type of Test	**Stop Time**	**Overcurrent**	**Type of Fault**	**Number of Tests**	**Relay Test System**	**Relays**
Tripping Tests	> pre-fault state time + fault clearing time	Maximum	DLG(BC), SLG(A)	17	Test results from fault state	Pushbutton LEDs and relay's display
		Minimum	LL(BC)	17		
Backup Tests		Maximum	DLG(BC), SLG(A)	5		
		Minimum	LL(BC)	5		
Non-Tripping Tests	< pre-fault time + relay time	Maximum	DLG(BC), SLG(A)	17	NA	
		Minimum	LL(BC)	17		

DLG(BC): double line-to-ground BC fault, SLG(A): single line-to-ground A fault, LL(BC): line-to-line BC fault, NA: not available

The fault state time in tripping tests was greater than the fault clearing time required to observe if relays tripped. However, in non-tripping tests, the fault state time was less than the relay time required to observe if relays did not trip. Percent error values and mean ± SEM of Relays 2 and 3 were calculated for measured and theoretical relay time values for tripping tests. In order to observe protection coordination scenarios, measured coordination time intervals between primary and backup relays were estimated.

8.1 Tripping tests

Tripping tests of the NRTS experiment for adaptive overcurrent protection of the microgrid with distributed generators were performed for nine circuit paths, as shown in Appendix D. SEL-5401 test system software [12] was applied to run tripping tests. In the tripping tests, fault state time had to be greater than the fault clearing time, thereby allowing the relay to trip for the inverse time overcurrent protection curve setting on the relays. Tripping tests were performed for each relay in the loop, using SEL-AMS [3] as a relay test system. Tripping tests verified that Relays 2 and 3 tripped for various overcurrent fault situations along the microgrid. Overcurrent faults were located on power line busses assuming the maximum and minimum fault overcurrents, and power lines were defined as protection areas of Relays 2 and 3. Table 8.2 describes tripping tests developed for the NRTS experiment.

Table 8.2: Tripping tests for the NRTS experiment

Type of tests	Objectives
Maximum fault overcurrent tests	Verified that the primary relay tripped for the maximum fault overcurrent along the power line.
Minimum fault overcurrent tests	Verified that the primary relay tripped for the minimum fault overcurrent along the power line.
Backup protection tests	Verified that the primary relay tripped faster than the backup relay for minimum and maximum fault overcurrents along the power line.

The maximum fault overcurrent corresponded to the double line-to-ground (DLG) faults and single line-to-ground (SLG) faults. However, the minimum fault overcurrent corresponded to the line-to-line (LL) fault. When considering a power line between two busses, the maximum overcurrent fault was located on the bus closest to the source, and the minimum overcurrent fault was located on the bus farthest away from the source.

To define test characteristics, the tests were referenced by the source, circuit, type of fault, fault site, and desired tripped breaker. The “DG2-678/65-LL(BC)-Bus8-BK5” test was performed for the LL (BC) fault located on “Bus8” in the circuit conformed by “distributed generator 2” and two power line branches formed by 6-5 and 6-7-8 power lines, with the expectation that “BK5” breaker would trip.

Maximum and minimum fault overcurrent and backup protection tests were performed in the NRTS experiment to complete A-B-C line breaker secondary currents and line-to-ground bus secondary voltages for pre-fault, fault, and post-fault states. Figure 8.1 shows the “DG2-678/65” circuit path applied to estimate A-B-C line breaker primary currents and line-to-ground bus primary voltages before running maximum and minimum fault overcurrent and backup protection tests for the 7-8 power line. Power World® software [10] estimated A-B-C line breaker primary currents and line-to-ground primary bus voltages for pre-fault, fault, and post-fault states by applying the circuit within the red dashed lines, as shown in Figure 8.1.

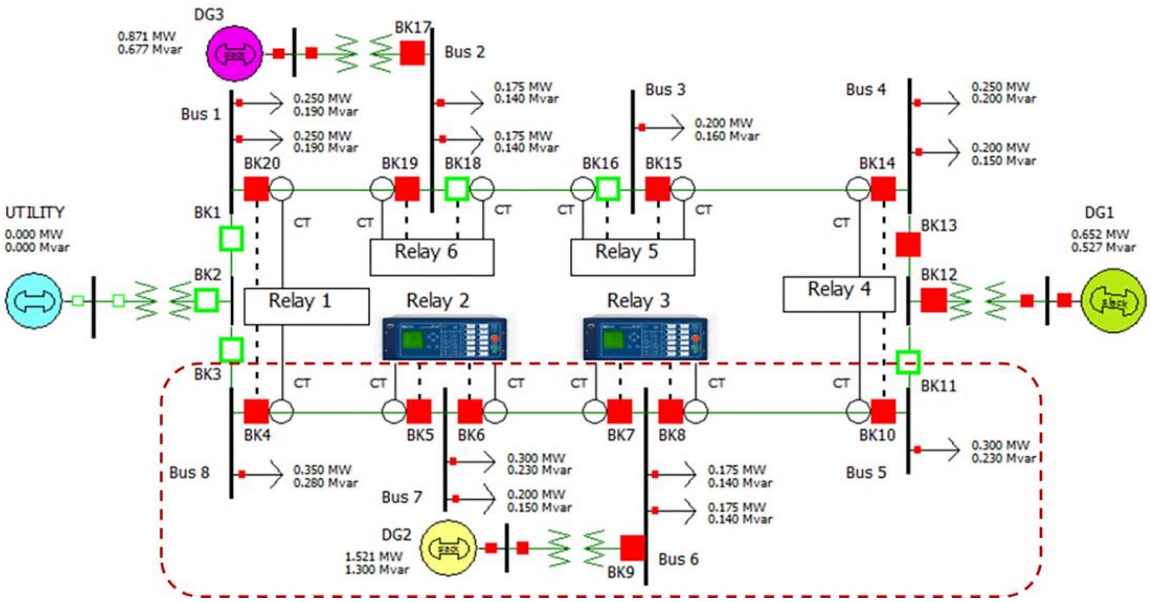

Figure 8.1: Circuit for “DG2-678/65-SLG(A)-Bus7-BK5, -LL(BC)-Bus8-BK5, -SLG(A)-Bus7-BK7, and -LL(BC)-Bus8-BK7” tests for protection of the 7-8 power line

The A-B-C line breaker primary currents and line-to-ground bus primary voltages for pre-fault and post-fault states were calculated using power flow analysis, and A-B-C line breaker currents and line-to-ground bus voltages for the fault state were estimated using fault analysis. Secondary currents and voltages were calculated by dividing primary currents and voltages by current and potential transformer ratios, which were 200 and 60, respectively. Using the circuit in Figure 8.1, the A-B-C line breaker secondary currents and line-to-ground bus secondary voltages for pre-fault, fault, and post-fault states were calculated for the maximum and minimum fault overcurrent tests. Pre-fault, fault, and post-fault state files were completed with SEL-5401 test system software [12] for maximum and minimum tripping tests for Relay 2. In the maximum and minimum fault overcurrent tests for the 7-8 power line of the "DG2-678/65" circuit path, Relay 2 tripped the BK5 breaker. Maximum fault overcurrent DG2-678/65-SLG(A)-Bus7-BK5 test verifying that the BK5 breaker tripped for an SLG fault of Line A at Bus 7. Minimum fault overcurrent DG2-678/65-LL(BC)-Bus8-BK5 test verifying that the BK5 breaker tripped for an LL fault of Lines B and C at Bus 8.

Using the circuit in Figure 8.1, A-B-C line breaker secondary currents and line-to-ground bus secondary voltages for pre-fault, fault, and post-fault states were calculated for the backup protection tests. SEL-5401 test system software [12] was then used to complete pre-fault, fault, and post-fault states for backup protection tests of Relay 3 for maximum and minimum fault overcurrent. In the backup protection tests for the 7-8 power line of the "DG2-678/65" circuit path, Relay 3 tripped the BK7 breaker. Backup protection DG2-678/65-SLG (A)-Bus7-BK7 test verifying that the BK7 breaker tripped for an SLG fault of Line A at Bus 7. Backup protection DG2-678/65-LL (BC)-Bus8-BK7 test verifying that the BK7 breaker tripped for a LL fault of Lines B and C at Bus 8.

In the backup protection DG2-678/65-SLG(A)-Bus7-BK7 and DG2-678/65-LL(BC)-Bus8-BK7 tests, LLTI of the primary protection (Relay 2) was not disconnected to simulate a current transformer (CT) failure on Relay 2 because the tests were performed individually for each relay in the NRTS experiment. Therefore, in order to confirm that the backup protection (Relay 3) tripped after the primary protection (Relay 2), CTIs between the upstream (backup relay) and downstream (primary relay) protections were measured from the test results, verifying that the primary relay cleared the fault faster than the backup relay.

In adaptive overcurrent protection for the microgrid with distributed generators, Relays 2 and 3 tripped as "primary and backup" or "backup and primary" protections, depending on the circuit path selected to run the non-real-time simulation. Backup protection tests were performed for the maximum and minimum fault overcurrent, and CTIs between the upstream (backup relay) and downstream (primary relay) protections were measured from test results, verifying that the primary relay cleared the fault faster than the backup relay. Tripping tests of maximum and minimum fault overcurrent for Relays 2 and 3 are shown in Tables 8.3 and 8.4, respectively. Backup protection tests for maximum and minimum fault overcurrent for Relays 2 and 3 are shown in Table 8.5. Circuit paths of the tests are shown in Figures D.1-12 in Appendix D. The DLG and SLG faults set the maximum fault overcurrents for the circuits fed by the utility source and distributed generators, respectively. DLG and SLG faults were placed at BC and A lines-to-ground, respectively. Minimum fault overcurrent was the LL fault at BC lines for circuit paths. Relays 2 and 3 were verified for tripping and backup protection tests of the maximum and minimum fault overcurrent.

Table 8.3: Tripping tests of maximum fault overcurrent for Relays 2 and 3

Relays	Setting Groups	Protection Areas	Tests	
			N°	Source – Circuit - Fault Type – Fault Site - Tripped Breaker
2	SS1	L67	1	UTILITY-8765/1234-DLG(BC)-Bus7-BK6
	SS2	L78	2	DG2-678/65-SLG(A)-Bus7-BK5
		L78	3	DG2-6781-SLG(A)-Bus7-BK5
		L78	4	DG2-678-SLG(A)-Bus7-BK5
	SS4	L78	5	DG1-5678-SLG(A)-Bus7-BK5
3	SS1	L56	6	UTILITY-8765/1234-DLG(BC)-Bus6-BK8
	SS2	L56	7	DG2-678/65-SLG(A)-Bus6-BK8
		L67	8	DG2-678/65-SLG(A)-Bus6-BK7
		L56	9	DG2-67/65-SLG(A)-Bus6-BK8
		L67	10	DG2-67/65-SLG(A)-Bus6-BK7
		L34	11	DG2-6543-SLG(A)-Bus4-BK8
		L56	12	DG2-6543-SLG(A)-Bus6-BK8
		L56	13	DG2-65-SLG(A)-Bus6-BK8
	SS3	L67	14	DG2-6781-SLG(A)-Bus6-BK7
		L67	15	DG2-678-SLG(A)-Bus6-BK7
	SS4	L67	16	DG2-67-SLG(A)-Bus6-BK7
	SS5	L67	17	DG1-5678-SLG(A)-Bus6-BK7

Table 8.4: Tripping tests of minimum fault overcurrent for Relays 2 and 3

Relays	Setting Groups	Protection Areas	Tests	
			N°	Source – Circuit - Fault Type – Fault Site - Tripped Breaker
2	SS1	L67	1	UTILITY-8765/1234-LL(BC)-Bus6-BK6
	SS2	L78	2	DG2-678/65-LL(BC)-Bus8-BK5
		L78	3	DG2-6781-LL(BC)-Bus8-BK5
		L78	4	DG2-678-LL(BC)-Bus8-BK5
	SS4	L78	5	DG1-5678-LL(BC)-Bus8-BK5
3	SS1	L56	6	UTILITY-8765/1234-LL(BC)-Bus5-BK8
	SS2	L56	7	DG2-678/65-LL(BC)-Bus5-BK8
		L67	8	DG2-678/65-LL(BC)-Bus7-BK7
		L56	9	DG2-67/65-LL(BC)-Bus5-BK8
		L67	10	DG2-67/65-LL(BC)-Bus7-BK7
		L34	11	DG2-6543-LL(BC)-Bus3-BK8
		L56	12	DG2-6543-LL(BC)-Bus5-BK8
		L56	13	DG2-65-LL(BC)-Bus5-BK8
	SS3	L67	14	DG2-6781-LL(BC)-Bus7-BK7
		L67	15	DG2-678-LL(BC)-Bus7-BK7
	SS4	L67	16	DG2-67-LL(BC)-Bus7-BK7
	SS5	L67	17	DG1-5678-LL(BC)-Bus7-BK7

Table 8.5: Backup protection tests for Relays 2 and 3

Fault Overcurrent	Relays	Setting Groups	Protection Areas	Tests	
				N°	Source – Circuit - Fault Type – Fault Site -Tripped Breaker
Maximum	2	SS1	L56	1	UTILITY-8765/1234-DLG(BC)-Bus6-BK6
	3	SS2	L78	2	DG2-678/65-SLG(A)-Bus7-BK7
		SS3	L78	3	DG2-6781-SLG(A)-Bus7-BK7
			L78	4	DG2-678-SLG(A)-Bus7-BK7
		SS5	L78	5	DG1-5678-SLG(A)-Bus7-BK7
Minimum	2	SS1	L56	1	UTILITY-8765/1234-LL(BC)-Bus5-BK6
	3	SS2	L78	2	DG2-678/65-LL(BC)-Bus8-BK7
		SS3	L78	3	DG2-6781-LL(BC)-Bus8-BK7
			L78	4	DG2-678-LL(BC)-Bus8-BK7
		SS5	L78	5	DG1-5678-LL(BC)-Bus8-BK7

Test results from the fault states were collected after execution of each tripping test. Figure 8.2 shows fault states and results for the DG2-678/65-SLG(A)-Bus7-BK5 and DG2-678/65-SLG(A)-LL(BC)-Bus8-BK5 tripping tests of Relay 2. In Figures 8.2-A and 8.2-B, “IN1” and “IN2” inputs represent the states (trip or closed) of “BK6” and” BK5” breakers, respectively. For both cases, the “IN1” input was not operated (NOOP) and “IN2” input was operated, indicating that the “BK5” breaker was tripped.

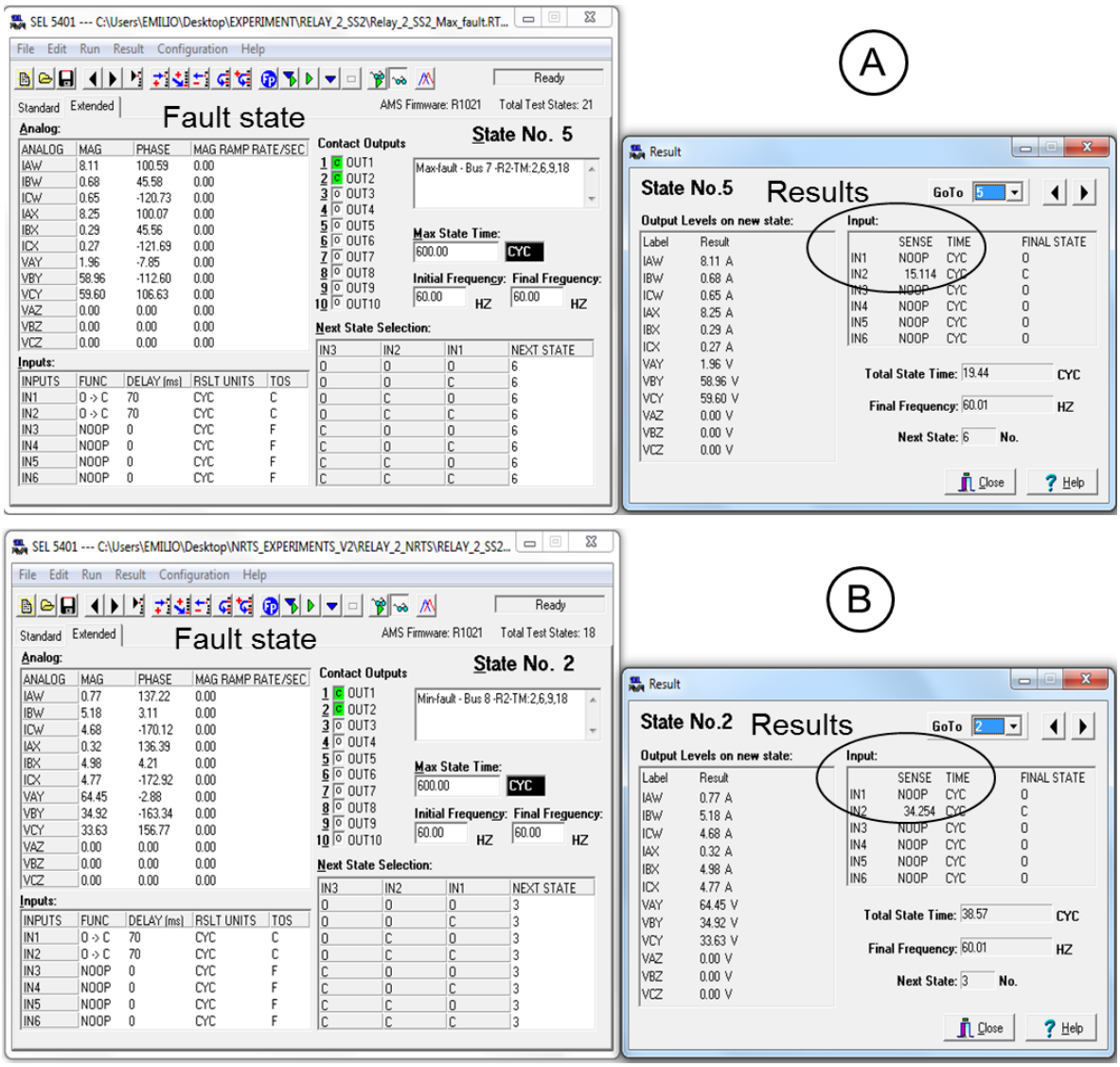

Figure 8.2: DG2-678/65-SLG(A)-Bus7-BK5 (A) and -LL(BC)-Bus8-BK5 (B) tripping tests for Relay 2

Figure 8.3 shows fault states and results for the DG2-678/65-SLG(A)-Bus7-BK7 and DG2-678/65 -LL(BC)-Bus8-BK7 backup tests of Relay 3. In Figures 8.3-A and 8.3-B, the "IN1" and "IN2" inputs represent the states (trip or closed) of "BK8" and" BK7" breakers, respectively. For both cases, the "IN1" input was not operated (NOOP) and "IN2" input was operated, indicating that the "BK7" breaker was tripped.

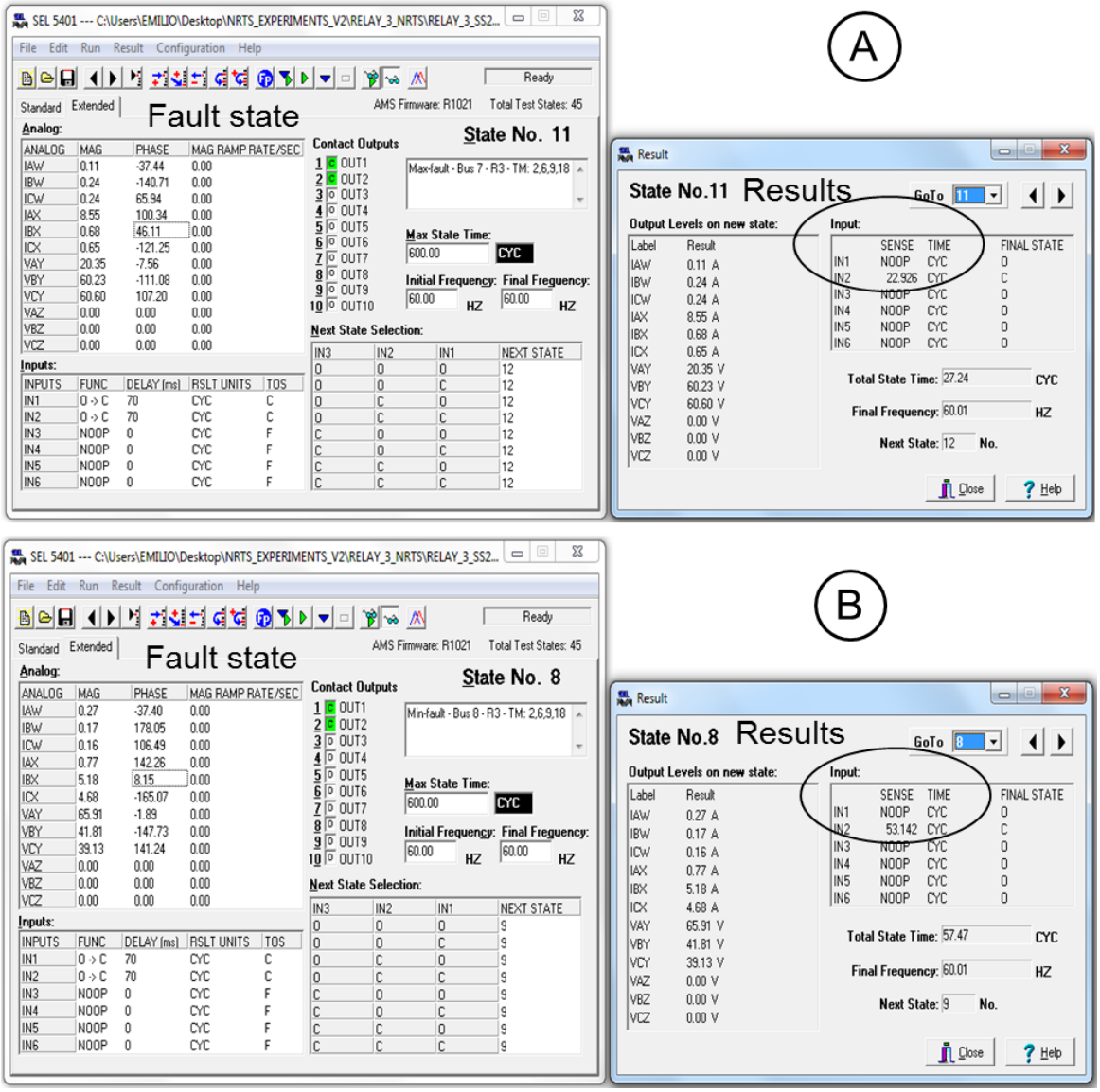

Figure 8.3: DG2-678/65-SLG(A)-Bus7-BK7 (A) and -LL(BC)-Bus8-BK7 (B) backup tests for Relay 3

Using relay test results, breaker states of the tripping and backup tests were measured for maximum and minimum fault overcurrents. Figures 8.4 and 8.5 show the state (open or closed) of Breakers 1 and 2 for Relays 2 and 3, respectively, verifying that the desired breaker tripped for the maximum fault overcurrent during the tripping tests.

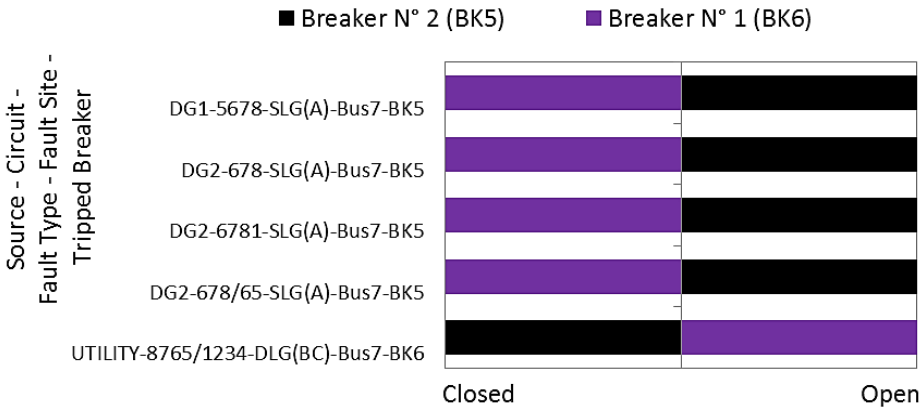

Figure 8.4: Maximum fault overcurrent, tripping tests for Relay 2

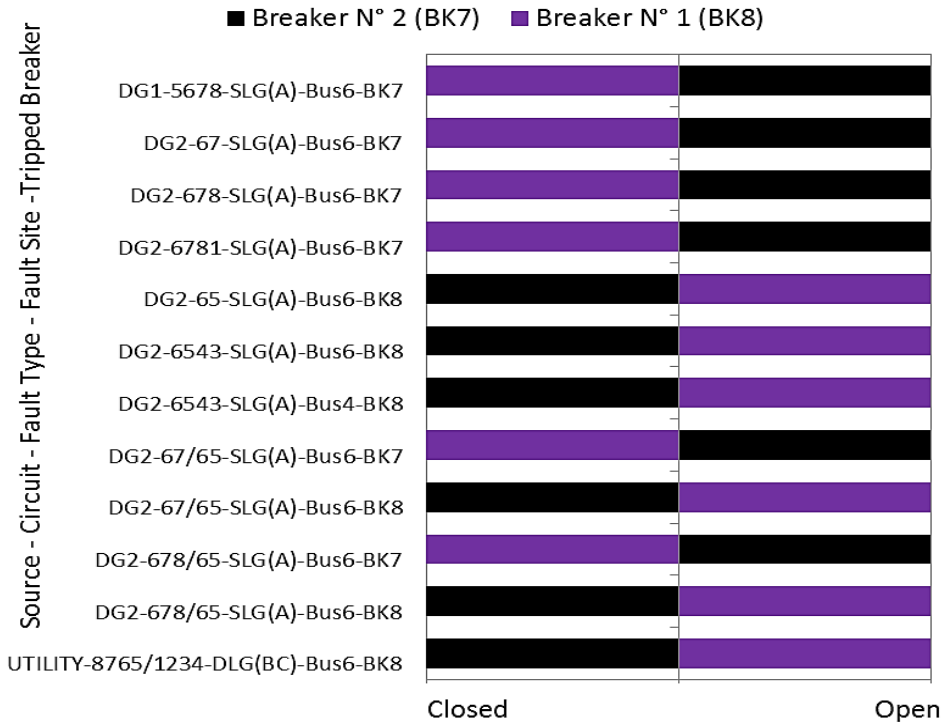

Figure 8.5: Maximum fault overcurrent, tripping tests for Relay 3

Figures 8.6 and 8.7 show the states (open or closed) of Breakers 1 and 2 for Relays 2 and 3, respectively, verifying that the desired breaker tripped for the minimum fault overcurrent during the tripping tests.

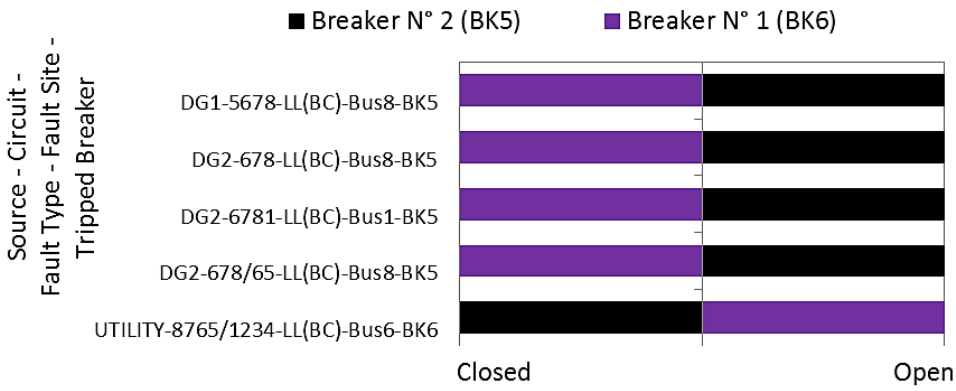

Figure 8.6: Minimum fault overcurrent, tripping tests for Relay 2

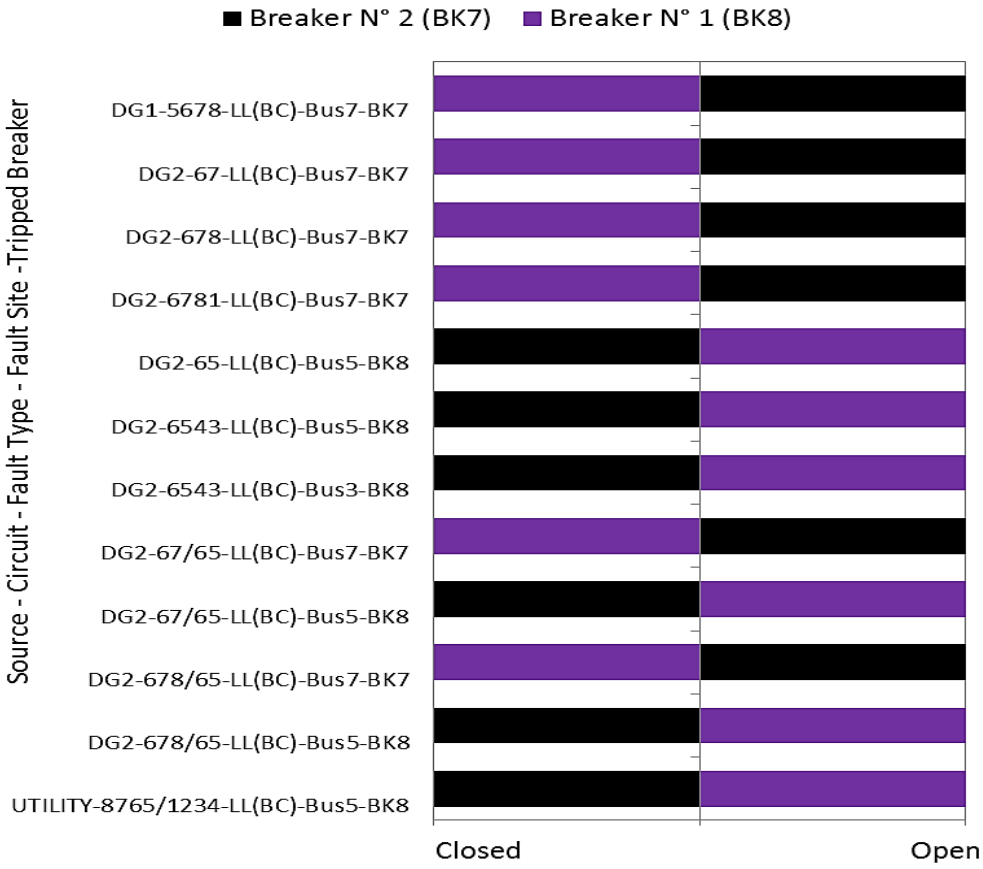

Figure 8.7: Minimum fault overcurrent, tripping tests for Relay 3

Figures 8.8 and 8.9 show the state (open or closed) of Breakers 1 and 2 for Relays 2 and 3, respectively, verifying that the desired breaker tripped during backup protection tests.

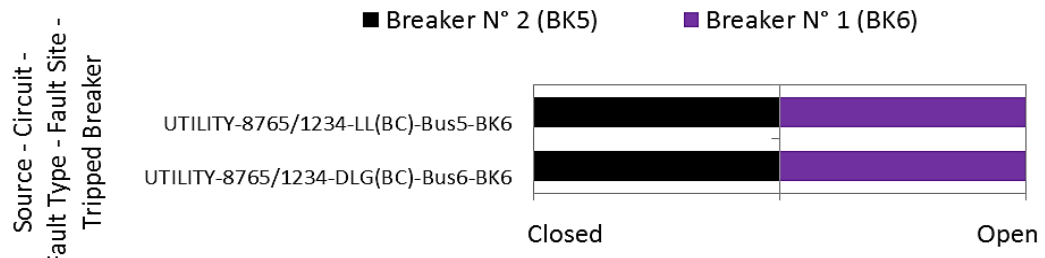

Figure 8.8: Backup protection tests for Relay 2

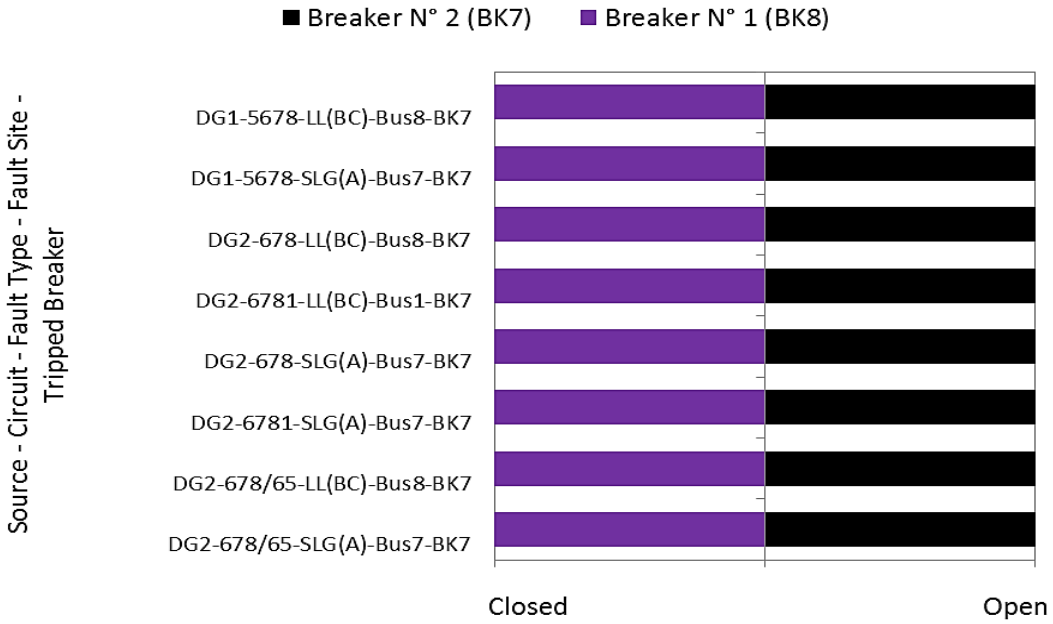

Figure 8.9: Backup protection tests for Relay 3

8.2 Non-tripping tests

SEL-5401 test system software [12] was applied to run non-tripping tests of the NRTS experiment for adaptive overcurrent protection of microgrid with distributed generators. The non-tripping tests were run for maximum and minimum fault overcurrents. Although the fault state time was greater than the fault clearing time for tripping tests, the fault state time was less than relay times for non-tripping tests to prohibit relays from tripping during the fault state for non-real-time simulation, thereby preventing relays from tripping for inverse time overcurrent protection curve setting. Figure 8.10 shows the RMS breaker current of tripping and non-tripping

tests for maximum and minimum fault overcurrents. For tripping tests (A), relays tripped, clearing the overcurrent fault. However, for non-tripping tests (B), relays did not trip because fault states were stopped before relays could trip. The fault state times of non-tripping tests for maximum and minimum (T_{FS2}) fault overcurrents were estimated before collecting the measured relay times from tripping tests.

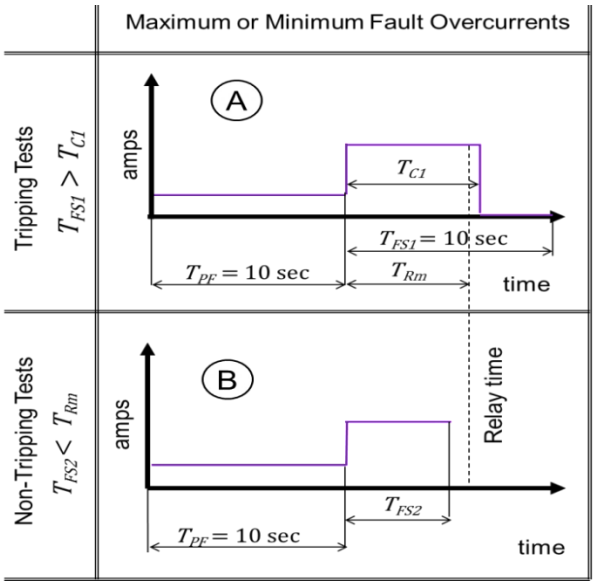

Figure 8.10: Tripping and non-tripping tests for minimum and maximum fault overcurrents

Based on plots (A) and (B) in Figure 8.10, the fault state time of non-tripping tests was given by Equation (8.1):

$$T_{FS2} = 0.8 \times T_{Rm} \tag{8.1}$$

where T_{FS2} is the fault state time of non-tripping tests in cycles and T_{Rm} is measured relay time in cycles from tripping tests.

Based on Equation (8.1), tripping tests had to be performed before non-tripping tests in order to obtain measured relay times from test results of fault states. Equation (8.1) was used to calculate fault state time of non-tripping tests for maximum and minimum fault overcurrent. Table 8.6 shows primary pickup fault currents of Relay 3 during the tests and fault state time

values collected from test results of fault states for tripping tests when Relay 3 tripped. Fault state time values of non-tripping tests for maximum and minimum fault overcurrents were calculated with Equation (8.1).

Table 8.6: Fault state time for non-tripping tests - Relay 3 - NRTS experiment

Fault Overcurrent	Test Name	Primary pickup fault current, [I] A	Tripping Test		Non-Tripping Tests
	Source - Circuit - Type of Fault - Fault Location - Opened Breaker		Fault State Time, [T_{FS1}] cycles	Measured Relay Time, [T_{Rm}] cycles	Fault State Time, [T_{FS2}] cycles T_{FS2} = 0.8 x T_R
Maximum	UTILITY-8765/1234-DLG(BC)-Bus6-BK8	2046	600	11.154	8.92
	DG2-678/65-SLG(A)-Bus6-BK8	2371	600	10.146	8.12
	DG2-678/65-SLG(A)-Bus6-BK7	2369	600	15.114	12.09
	DG2-678/65-SLG(A)-Bus7-BK7	**1709**	**600**	**22.926**	**18.34**
	DG2-67/65-SLG(A)-Bus6-BK8	2330	600	10.374	8.30
	DG2-67/65-SLG(A)-Bus6-BK7	2327	600	15.426	12.34
	DG2-6543-SLG(A)-Bus4-BK8	1989	600	12.426	9.94
	DG2-6543-SLG(A)-Bus6-BK8	2355	600	10.134	8.11
	DG2-65-SLG(A)-Bus6-BK8	2282	600	10.374	8.30
	DG2-6781-SLG(A)-Bus6-BK7	2400	600	15.150	12.12
	DG2-6781-SLG(A)-Bus7-BK7	**1742**	**600**	**22.674**	**18.14**
	DG2-678-SLG(A)-Bus6-BK7	2339	600	15.654	12.52
	DG2-678-SLG(A)-Bus7-BK7	**1698**	**600**	**23.370**	**18.70**
	DG2-67-SLG(A)-Bus6-BK7	2298	600	9.594	7.68
	DG1-5678-SLG(A)-Bus6-BK7	1940	600	17.898	14.32
	DG1-5678-SLG(A)-Bus7-BK7	**1503**	**600**	**25.398**	**20.32**
Minimum	UTILITY-8765/1234-LL(BC)-Bus5-BK8	1539	600	16.350	13.08
	DG2-678/65-LL(BC)-Bus5-BK8	1392	600	20.706	16.56
	DG2-678/65-LL(BC)-Bus7-BK7	1265	600	36.378	29.10
	DG2-678/65-LL(BC)-Bus8-BK7	**1036**	**600**	**53.142**	**42.51**
	DG2-67/65-LL(BC)-Bus5-BK8	1369	600	21.666	17.33
	DG2-67/65-LL(BC)-Bus7-BK7	1221	600	38.670	30.94
	DG2-6543-LL(BC)-Bus3-BK8	1275	600	24.138	19.31
	DG2-6543-LL(BC)-Bus5-BK8	1427	600	19.914	15.93
	DG2-65-LL(BC)-Bus5-BK8	1342	600	22.410	17.93
	DG2-6781-LL(BC)-Bus7-BK7	1318	600	34.890	27.91
	DG2-6781-LL(BC)-Bus8-BK7	**1088**	**600**	**49.350**	**39.48**
	DG2-678-LL(BC)-Bus7-BK7	1253	600	37.878	30.30
	DG2-678-LL(BC)-Bus8-BK7	**1031**	**600**	**54.894**	**43.92**
	DG2-67-LL(BC)-Bus7-BK7	1210	600	23.010	18.41
	DG1-5678-LL(BC)-Bus7-BK7	1145	600	39.618	31.69
	DG1-5678-LL(BC)-Bus8-BK7	**955**	**600**	**56.178**	**44.94**

Bold represents the backup protection tests

Table 8.7 shows primary pickup fault currents of Relay 2 during the tests and fault state time values collected from test results of fault states for tripping tests when Relay 2 tripped.

Table 8.7: Fault state time for non-tripping tests - Relay 2 - NRTS experiment

Fault Overcurrent	Test Description	Primary pickup fault current, [I] A	Tripping Test		Non-Tripping Tests
	Source - Circuit - Type of Fault - Fault Location - Opened Breaker		Fault State Time, [T_{FS1}] cycles	Measured Relay Time, [T_{Rm}] cycles	Fault State Time, [T_{FS2}] cycles T_{FS2} = 0.8 x T_R
Maximum	**UTILITY-8765/1234-DLG(BC)-Bus6-BK6**	**2101**	**600**	**19.626**	**15.70**
	UTILITY-8765/1234-DLG(BC)-Bus7-BK6	3170	600	12.426	9.94
	DG2-678/65-SLG(A)-Bus7-BK5	1650	600	15.114	12.09
	DG2-6781-SLG(A)-Bus7-BK5	1681	600	14.418	11.53
	DG2-678-SLG(A)-Bus7-BK5	1639	600	15.102	12.08
	DG1-5678-SLG(A)-Bus7-BK5	1453	600	16.854	13.48
Minimum	**UTILITY-8765/1234-LL(BC)-Bus5-BK6**	**1564**	**600**	**30.774**	**24.62**
	UTILITY-8765/1234-LL(BC)-Bus6-BK6	1845	600	23.658	18.93
	DG2-678/65-LL(BC)-Bus8-BK5	996	600	34.254	27.40
	DG2-6781-LL(BC)-Bus8-BK5	1047	600	31.842	25.47
	DG2-678-LL(BC)-Bus8-BK5	989	600	34.878	27.90
	DG1-5678-LL(BC)-Bus8-BK5	915	600	38.358	30.69

Bold represents backup protection tests

8.3 Tripping and non-tripping tests

In the NRTS experiment, tripping and non-tripping tests were developed to observe if breakers tripped or did not trip, respectively. Tripping tests were set to a fault state time greater than the fault clearing time in order to observe if relays tripped. However, non-tripping tests were set at a fault state time less than the relay time to observe if relays did not trip.

Measured fault clearing and relay times from tripping test results were collected to compare ending fault times for tripping and non-tripping tests and then measured ending fault times for tripping and non-tripping tests were estimated with Equations (8.2) and (8.3), respectively.

$$T_{EF1} = T_{PF} + T_{C1} = 600 + T_{C1} \tag{8.2}$$

where T_{EF1} is measured ending fault time in cycles for tripping tests, T_{PF} is pre-fault state time set at 600 cycles (10 sec.), and T_{C1} is measured fault clearing time in cycles for tripping tests.

$$T_{EF2} = T_{PF} + 0.8 \times T_{Rm} = 600 + 0.8 \times T_{Rm} \quad (8.3)$$

where T_{EF2} is measured ending fault time in cycles for non-tripping tests, T_{PF} is pre-fault state time set at 600 cycles (10 sec.), and T_{Rm} is measured relay time in cycles for tripping tests.

In order to calculate measured ending fault times for tripping and non-tripping tests from Equations (8.2) and (8.3), respectively, measured fault clearing and relay times of test results were collected from fault states after running non-real-time simulation. Figure 8.11 shows the test result of the fault state for the "DG2-67-SLG(A)-Bus6-BK7" tripping test for maximum fault overcurrent. The measured fault clearing (13.91 cycles) and relay (9.594 cycles) times were collected after running non-real-time simulation.

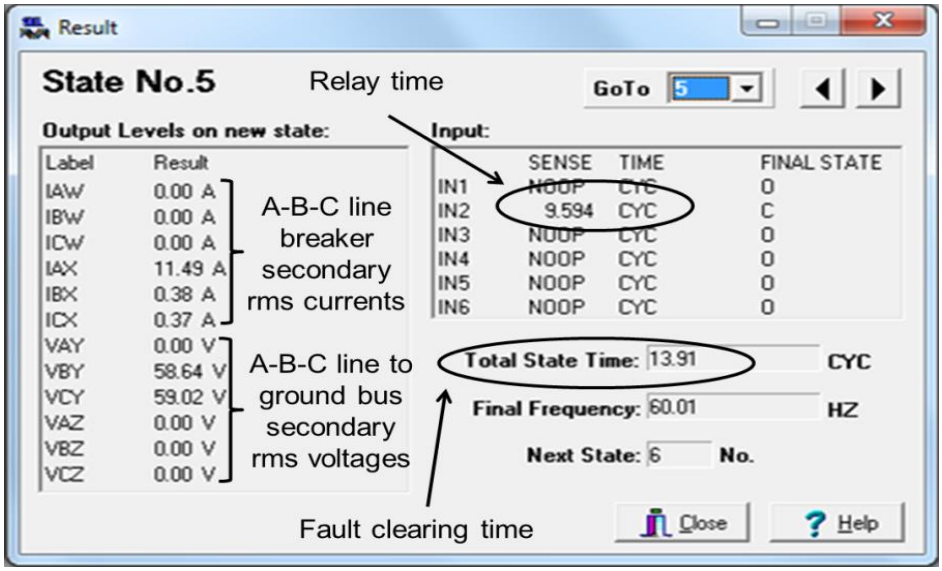

Figure 8.11: "DG2-67-SLG(A)-Bus6-BK7" test result

Application of Equations (8.2) and (8.3) revealed that the measured ending fault time in cycles for tripping and non-tripping "DG2-67-SLG(A)-Bus6-BK7" tests were 613.91 cycles and 608.634 cycles, respectively.

From Tables L.1 and L.2 of Appendix L and Equations (8.2) and (8.3), the measured ending fault time in cycles of all tripping and non-tripping tests were estimated for Relays 2 and 3. Figure 8.12 shows tripping and non-tripping tests for Relays 2 (A) and 3 (B), respectively. The horizontal and vertical axes represent primary pickup fault currents and time in cycles, respectively. The red line represents the pre-fault state for tripping and non-tripping tests, and violet dots and green squares represent the ending fault time for tripping and non-tripping states, respectively. For the same "source-circuit-fault type-fault site-tripped breaker" tripping and non-tripping tests, the ending fault time of the tripping test was greater than the ending fault time of the non-tripping test. For non-tripping tests, fault overcurrents flowed along relay breakers but the relay did not trip, verifying the non-trip condition. However, for tripping tests, fault currents flowed along relay breakers and the relay tripped, verifying the tripping condition.

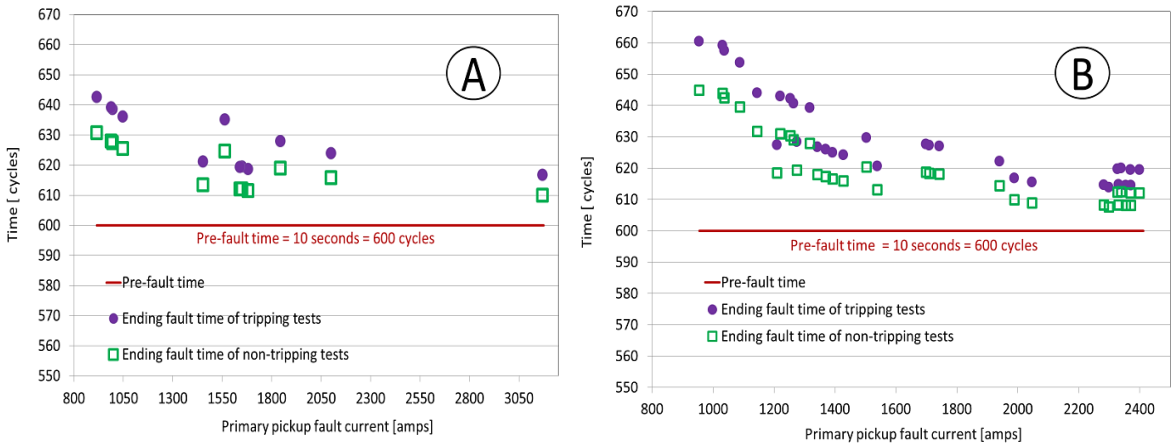

Figure 8.12: Ending fault time for tripping and non-tripping tests of Relays 2 (A) and 3 (B)

8.4 Measured delay time

In non-real-time simulation with relays in the loop, the measured delay time of tripping tests for Relays 2 and 3 was defined by the sum of the setting delay time (4.22 cycles) and NRTS experimental circuit delay time. The setting delay time of 4.22 cycles was collected from the

vacuum circuit breaker publication [96]. In Table 8.8, the setting delay time is presented as the sum of auxiliary relay operation, breaker operation, and arc times.

Table 8.8: Times of 5 kV vacuum circuit breaker [96]

Times of 5 kV vacuum circuit breaker	
Auxiliary relay operation time [cycles]	0.5
Breaker operation time [cycles]	2.7
Arc time [cycles]	1.02
Total time (Setting delay time) [cycles]	**4.22**

In the tripping tests, the measured clearing fault and relay times were collected from test results of the fault state and then measured delay times of tripping tests for Relays 2 and 3 were estimated by Equation (8.4):

$$T_{Dm} = T_{C1} - T_{Rm} \tag{8.4}$$

where T_{Dm} is measured delay time in cycles, T_{C1} is measured fault clearing time in cycles for tripping tests, and T_{Rm} is measured relay time in cycles for tripping tests.

Figure 8.13 shows the test result of the fault state for the "DG2-678/65-SLG(A)-BUS7-BK5" tripping test for maximum fault overcurrent. The measured fault clearing and relay times were collected after running non-real-time simulation.

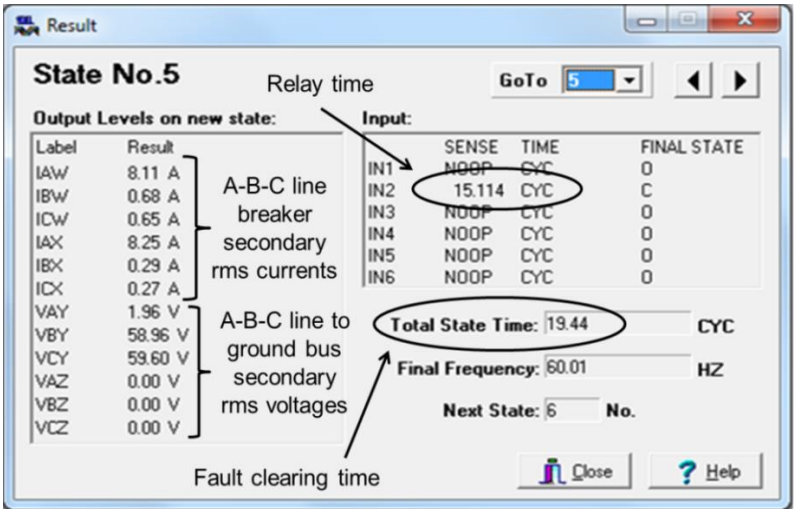

Figure 8.13: "DG2-678/65-SLG(A)-BUS7-BK5" test result

Based on application of Equation (8.4) and measured fault clearing (19.44 cycles) and relay (15.114 cycles) times collected from Figure 8.13, the measured delay time in cycles for tripping "DG2-678/65-SLG(A)-BUS7-BK5" test was 4.326 cycles.

Using measured fault clearing and relay times of Tables M.1 and M.2 from Appendix M and Equation (8.4), the measured delay time in cycles was estimated for Relays 2 and 3, respectively. Measured delay time values of Relays 2 and 3 for tripping tests are plotted in Figure 8.14.

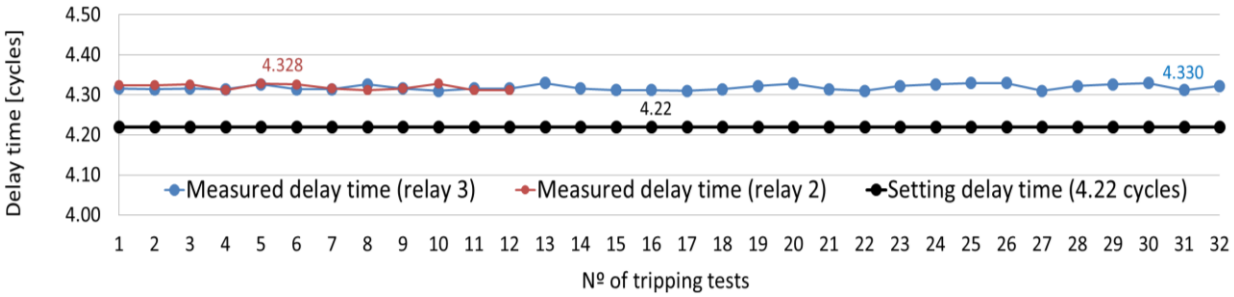

Figure 8.14: Measured delay time of tripping tests for Relays 2 and 3

In Figure 8.14, black dots represent the setting delay time of 4.22 cycles set for relay tests of the NRTS experiment, and red and blue dots represent measured delay times of tripping tests for Relays 2 and 3, respectively. The maximum measured delay time for Relays 2 and 3 were 4.328 and 4.330 cycles, respectively. Based on the setting delay time for tripping tests, the maximum delay time of the NRTS experimental circuit was 0.11 cycles (4.33 cycles - 4.22 cycles = 0.11 cycles).

8.5 Theoretical and measured relay time

Theoretical and measured relay time values were compared for the tripping tests. Although theoretical relay time values were based on the inverse time overcurrent U3 curve from the relay's instruction manual [5], measured relay time values were collected from test results. In order to verify inverse time overcurrent settings for the groups of Relays 2 and 3, theoretical and

measured relay time values for tripping tests were evaluated. Theoretical relay time values were estimated by Equation (8.5):

$$T_R = TDS \times \left(0.0963 + \frac{3.88}{(I/CTR/\, I_P)^2 - 1}\right) \times 60 \qquad (8.5)$$

where T_R is theoretical relay time in cycles, *TDS* is the inverse time overcurrent time dial setting, *I* is the primary pickup fault current in amps, *CTR* is the current transformer ratio, and I_P is the secondary overcurrent pickup in amps. Primary pickup fault currents from Tables N.1 and N.2 in Appendix N and inverse time overcurrent settings from Table 8.9 were collected in order to use Equation (8.5) to calculate theoretical relay time values of tripping tests for Relays 2 and 3.

Table 8.9: Inverse time overcurrent settings of active settings for Relays 2 and 3

Setting Groups	Element	Relay 2				Relay 3			
		Breakers	**Curve**	**Secondary Overcurrent Pickup, amps [I_P]**	**Time Dial Setting [*TDS*]**	**Breakers**	**Curve**	**Secondary Overcurrent Pickup, amps [I_P]**	**Time Dial Setting [*TDS*]**
SS1	1	BK6	U3	2.25	1.13	BK8	U3	2.01	0.68
	2	BK5				BK7			
SS2	1	BK6				BK8	U3	1.97	0.77
	2	BK5	U3	1.86	0.78	BK7	U3	1.95	1.18
SS3	1	BK6				BK8			
	2	BK5				BK7	U3	1.97	1.19
SS4	1	BK6				BK8			
	2	BK5	U3	1.89	0.71	BK7	U3	1.97	0.67
SS5	1					BK8			
	2					BK7	U3	1.90	1.12
SS6	1					BK8			
	2					BK7			

Current transformer ratio (*CTR*) = 200

Measured relay time values of Relay 2 collected from tripping test results are presented in Tables N.1 and N.2 of Appendix N. Figure 8.15 presents measured and theoretical relay time values for tripping tests for Relays 2 (A) and 3 (B). Horizontal and vertical axes represent primary pickup fault currents and relay time values, respectively. As shown in Figure 8.15, measured and theoretical relay time values represented by green square and orange dots,

respectively, had matched visually, verifying the inverse time overcurrent setting groups of Relays 2 and 3 that were indicated in Table 8.9.

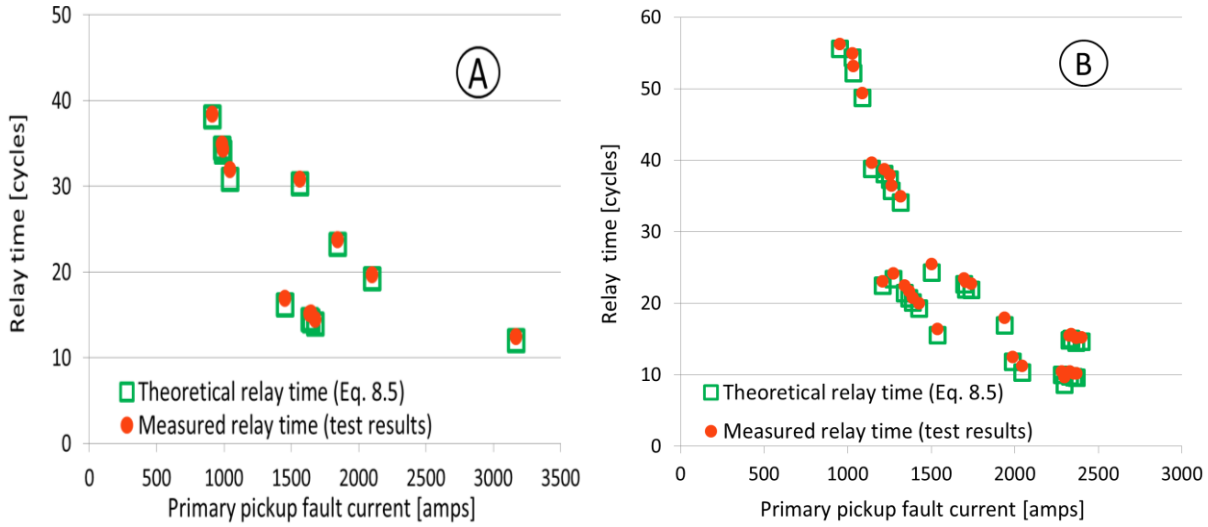

Figure 8.15: Theoretical and measured relay time values for Relays 2 (A) and 3 (B)

Theoretical and measured relay time values in Figure 8.15 were used to estimate percent error of relay time values for tripping tests. The percent error of relay time values was calculated using Equation (8.6):

$$E_{TR\%} = \frac{T_{Rm} - T_R}{T_R} \times 100 \tag{8.6}$$

where $E_{TR\%}$ is percent error of relay time, T_{Rm} is measured relay time in cycles, and T_R is theoretical relay time in cycles.

SAS® software [97] was used for correlation analysis. The correlation between primary pickup fault currents and relay time percent error values was evaluated for each relay using Pearson's analysis; significance was considered when $P < 0.05$. No correlation existed between the relay time percent error and pickup fault current values for Relay 2 ($P = 0.2134$). However, correlation coefficient (R) was high ($R = 0.7046$, $P < 0.0001$) for Relay 3. Figure 8.16 presents the percent error of relay time values for Relays 2 and 3 based on tripping tests. Horizontal and

vertical axes represent primary pickup fault currents and percent error of relay time values, respectively. The red diamonds and violet circles represent the relay time percent error values for Relays 2 and 3, respectively.

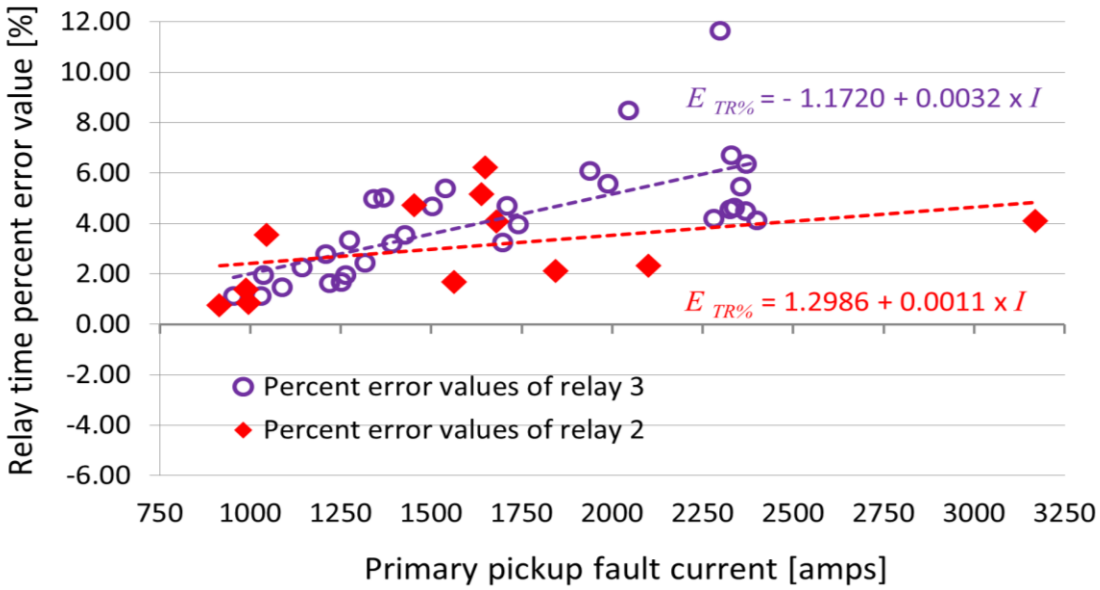

Figure 8.16: Percent error values of Relays 2 and 3

In Figure 8.16, the red and violet dashed lines represent trend lines of the relay time percent error values of tripping tests for Relays 2 and 3, respectively. Based on these trend lines, the higher the primary pickup fault current, the higher the relay time percent error. Measured and theoretical relay time values and percent error values of tripping tests for Relays 2 and 3 are shown in Tables N.1 and N.2 of Appendix N.

8.6 Coordination time intervals

CTIs between upstream (backup relay) and downstream (primary relay) protections were measured from test results of Relays 2 and 3 for protection coordination scenarios. Relays 2 and 3 were applied as backup and primary relays or vice versa, depending on the selected circuit of the microgrid and fault location. Table 8.10 shows protection coordination scenarios for Relays 2

and 3. Each protection coordination scenario consisted of a backup and tripping test that corresponded to the upstream (backup relay) and downstream (primary relay) protections, respectively.

Table 8.10: Protection coordination scenarios for Relays 2 and 3

Fault Overcurrent	Scenarios	Protection Area	Tests	Results		
			Source - Circuit - Type of Fault -Fault Location - Opened Breaker	**Measured Relay Time[(1)] of Backup Protection, cycles [T_{RBm}]**	**Measured Relay Time[(1)] of Primary Protection, cycles [T_{RPm}]**	**Measured Coordination Time Interval, cycles [CTI_m]**
Maximum	1	L56	**UTILITY-8765/1234-DLG(BC)-Bus6-BK6**	**19.626**		8.47
			UTILITY-8765/1234-DLG(BC)-Bus6-BK8		11.154	
	2	L78	**DG2-678/65-SLG(A)-Bus7-BK7**	**22.926**		7.81
			DG2-678/65-SLG(A)-Bus7-BK5		15.114	
	3	L78	**DG2-6781-SLG(A)-Bus7-BK7**	**22.674**		8.26
			DG2-6781-SLG(A)-Bus7-BK5		14.418	
	4	L78	**DG2-678-SLG(A)-Bus7-BK7**	**23.370**		8.27
			DG2-678-SLG(A)-Bus7-BK5		15.102	
	5	L78	**DG1-5678-SLG(A)-Bus7-BK7**	**25.398**		8.54
			DG1-5678-SLG(A)-Bus7-BK5		16.854	
Minimum	6	L56	**UTILITY-8765/1234-LL(BC)-Bus5-BK6**	**30.774**		14.42
			UTILITY-8765/1234-LL(BC)-Bus5-BK8		16.350	
	7	L78	**DG2-678/65-LL(BC)-Bus8-BK7**	**53.142**		18.89
			DG2-678/65-LL(BC)-Bus8-BK5		34.254	
	8	L78	**DG2-6781-LL(BC)-Bus8-BK7**	**49.350**		17.51
			DG2-6781-LL(BC)-Bus8-BK5		31.842	
	9	L78	**DG2-678-LL(BC)-Bus8-BK7**	**54.894**		20.02
			DG2-678-LL(BC)-Bus8-BK5		34.878	
	10	L78	**DG1-5678-LL(BC)-Bus8-BK7**	**56.178**		17.82
			DG1-5678-LL(BC)-Bus8-BK5		38.358	

Bold represents backup protection tests, [(1)] Values from Tables N.1 and N.2 in Appendix N.

Measured relay times for backup and primary relays were collected from Tables N.1 and N.2 in Appendix N. Measured CTIs between backup and primary relays were estimated using Equation (8.7):

$$CTI_m = T_{RBm} - T_{RPm} \tag{8.7}$$

where CTI_m is the measured CTI in cycles, T_{RBm} is the measured relay time of backup (upstream protection) relay in cycles, and T_{RPm} is the measured relay time of the primary (downstream protection) relay in cycles. As shown in Figure 8.17, measured CTIs for protection coordination scenarios for Relays 2 and 3 were plotted based on Table 8.10. The blue and green bars represent measured CTIs for minimum and maximum fault overcurrents, respectively. Measured CTIs for maximum fault overcurrent tests were expectedly smaller than the minimum fault overcurrent tests because the inverse time overcurrent curve settings of Relays 2 and 3 for maximum fault overcurrents tripped faster than for the minimum fault overcurrents.

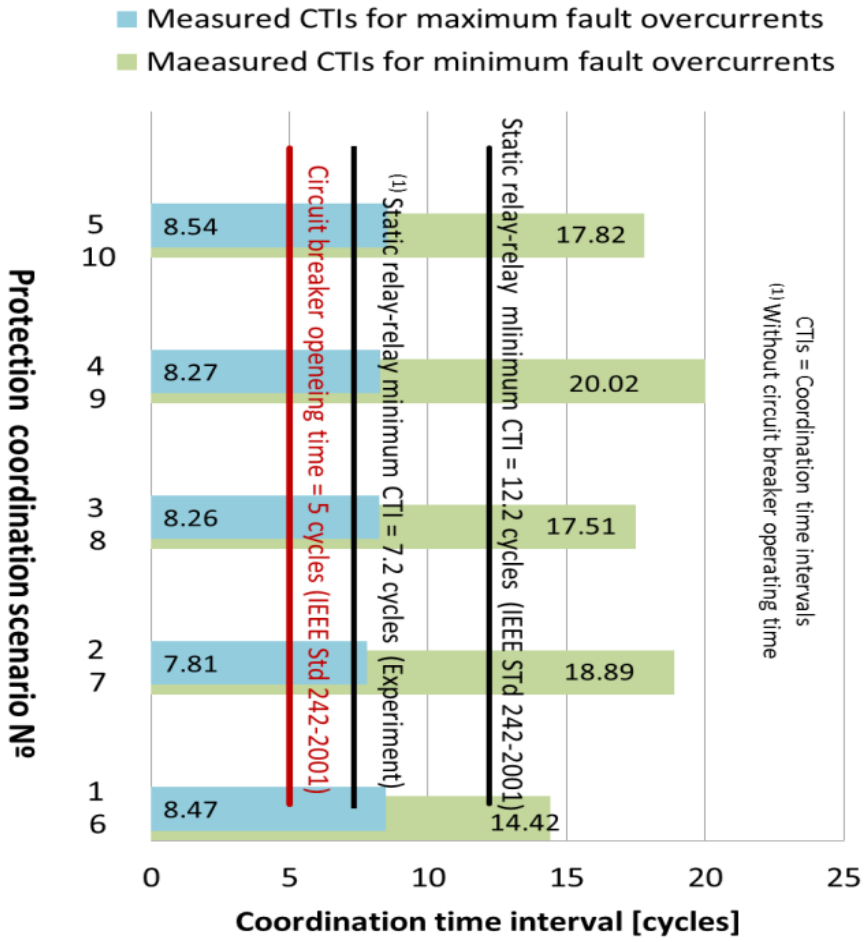

Figure 8.17: Measured CTIs for protection coordination scenarios

Based on the IEEE Std. 242-2001 [7], the minimum CTI for “static relay- static relay” coordination was 0.20 sec. (12 cycles) for the maximum fault current, based on the sum of the circuit breaker opening time (0.08 sec. = 5 cycles) and relay tolerance and setting error time (0.12 sec. = 7.2 cycles). However, since the circuit breaker operating time was not added in the RTS experiment, inverse time overcurrent curves of relays 2 and 3 were the same for the RTS and NRTS experiments. The minimum CTI between primary and backup relays was 0.12 sec. (7.2 cycles) instead of 0.20 sec. (12.2 cycles). In Figure 8.17, the measured CTIs for maximum fault current tests were not smaller than 7.2 cycles, verifying the inverse time overcurrent settings of relays 2 and 3.

In the NRTS experiment, relays 2 and 3 tested as primary and backup protection or vice versa, were not simulated at the same time. Relays 2 and 3 were connected to a different non-real-time simulator. Then, the selectivity coordination for relays 2 and 3 could not be observed in the NRTS experiment because primary and backup relays were tested individually, and what relay tripped and non-tripped during tests could not be compared.

8.7 Chapter summary

This chapter presented NRTS experiment results. The NRTS experiment was divided into tripping and non-tripping tests, including backup protection tests into tripping tests. Inputs (tripped breakers), relay, and fault clearing times were collected for relay tests.

In tripping tests, non-real-time simulation was stopped at a time greater than the sum of pre-fault and fault clearing times in order to observe if relays tripped. However, non-tripping tests were stopped at a time less than the sum of pre-fault and relay times in order to observe if

relays did not trip. Breaker state plotting verified that relays tripped breakers during tripping tests; however, during non-tripping tests, the relays did not trip breakers.

Measured and theoretical relay time values were identical, verifying inverse time overcurrent protection settings for groups of Relays 2 and 3. Measured relay time values allowed calculation of the percent error and measured CTIs between the backup and primary relays for protection coordination scenarios.

Conclusions of this chapter were based on collected results that demonstrated that the selectivity, speed, and reliability of the adaptive inverse time overcurrent protection were achieved satisfactorily.

Selectivity: In adaptive inverse time overcurrent protection, each relay had two breakers. The protection logic of the setting groups allowed breakers to be tripped based on circuit paths. For maximum and minimum fault overcurrents of tripping and non-tripping tests, breaker state sequences were verified satisfactorily, breakers were open or remained closed for tripping and non-tripping tests, respectively.

Speed: In adaptive inverse time overcurrent protection, setting groups were set with inverse time overcurrent settings based on upstream fuses and/or relays. Application of various inverse time overcurrent settings achieved the speed to clear a fault overcurrent because inverse time overcurrent settings were adequate for each circuit path. The inverse time overcurrent settings of Relays 2 and 3 were verified by evaluating measured and theoretical relay times.

Reliability: Protection coordination was applied to achieve the reliability of adaptive inverse time overcurrent protection. When the primary relay did not trip because of a CT failure, the backup relay tripped the breaker, thereby clearing the fault overcurrent. Measured CTIs between primary and backup relays were verified.

Chapter 9 - Project model of RTS experiment

This chapter describes how the project model was built for adaptive overcurrent protection of the microgrid. The project model was based on an IEEE publication [70] that presented an OP5600 real-time simulator with a relay in the loop. The relays were set with inverse time overcurrent protection that tripped breakers at fault overcurrent. In the project model created for this research, the OP5600 contained two relays in the loop that were set with adaptive overcurrent protection; each relay controlled two breakers that tripped for a fault overcurrent. Application of two relays displayed their integration into selective coordination as primary and backup protections during real-time simulation. In the RTS experiment, the project model was built before running real-time tests. Figure 9.1 shows phases of the RTS experiment.

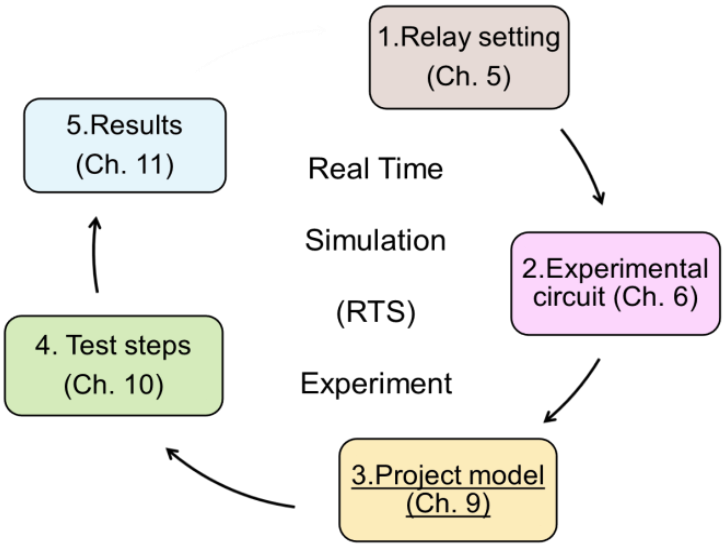

Figure 9.1: Phases of the RTS experiment

The SM_Network (master) and SC_console subsystems were configured in the project model. The SM_Network (master) subsystem simulated the microgrid and recorded test results after real-time simulation. However, the SC_console subsystem triggered the external control signal for the fault block and supervised the real-time test during execution of RTS experiment.

9.1 Project model phase

The RT-LAB® [13] and Matlab®/Simulink® software [14] were used to create the project model. In order to create a new project, step1 (create a new project) of the "six steps to real time" tutorial of the RT-LAB® software [13] was described. Steps to create a new project included the following:

- RT-LAB® software was opened by clicking the RT-LAB® icon (Figure 9.2-A).
- The new project wizard was opened: File → New → RT-LAB® Project.
- The project was named, and the model to be added to the project was selected.

The project and model were named "EMILIO" and "Relay_Test_Model," respectively (Figure 9.2-B).

- The new project was created into the Project Explorer (Figure 9.2-B).
- The model was built by placing and configuring the SM_Network (master) and SC_console subsystems (Figure 9.2-C).
- The ".bin" and ".conf" files were added to the directory of the RT-LAB® project (Figure 9.2-D).

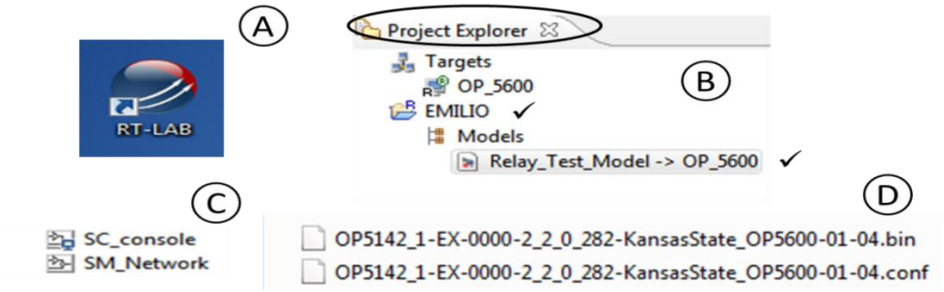

Figure 9.2: Steps to create a new project and model

Based on an OPAL-RT website article [98], inclusion of bitstream (.bin) and configuration (.conf) files was required in the project when the project had an OP5142 card. The ".bin" and ".conf" files of the OP5600 were added to the directory of the project model. The

".bin" file configured the target computer prior to execution of real-time simulation; however, the ".conf" file specified available inputs/outputs of the model. The purpose of the ".conf" file was to configure the OP5142 card according to the input/output card assembled on the target computer (OP5600), and the purpose of the ".bin" file was to link the OP5142 bitstream to the model. Figure 9.3 shows the "OP5142_1-EX-0000-2_2_0_282-KansasState_OP5600-01-04.conf" file that corresponded to the OP5600 target computer in the Burns & McDonnell - K-State Smart Grid Laboratory [8].

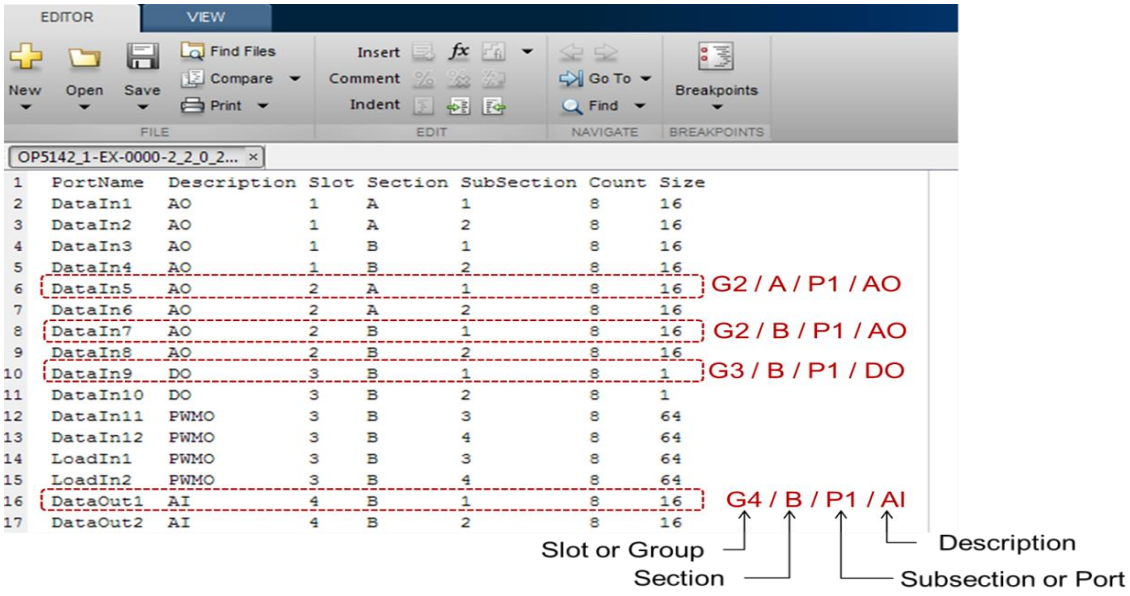

Figure 9.3: "Conf." file of the OP5600 in the Burns & McDonnell - K-State Smart Grid Laboratory [8]

The "conf." file was opened with a right click, and the "Edit with Notepad++" option was selected. In Figure 9.3, the "slot/section/subsection/description" inside the red dashed circles refers to connectors applied in the RTS experimental circuit of Chapter 5.

Two subsystems, the SM_Network and SC_console, formed the model. In the SM_Network (master) subsystem, the microgrid with distributed generators contained a fault block controlled by an external signal. In the fault block, the control fault timing circuit of the

SC_console subsystem triggered the external signal. Objectives of the SM_Network (master) and SC_console subsystems are indicated in Table 9.1.

Table 9.1: SM_Network (master) and SC_console subsystems

Subsystems	Objectives
SM_Network (master)	The SM_Network (master) subsystem simulated overcurrent fault at the microgrid with distributed generators and recorded test results after real-time simulation.
SC_console	The SC_console subsystem triggered the external control fault timing block and supervised the real-time test during the execution of real-time simulation.

Figure 9.4 shows the model formed by SM_Network (master) and SC_console subsystem blocks, including the ARTEMIS Guide and powergui blocks on the left-hand side of the figure.

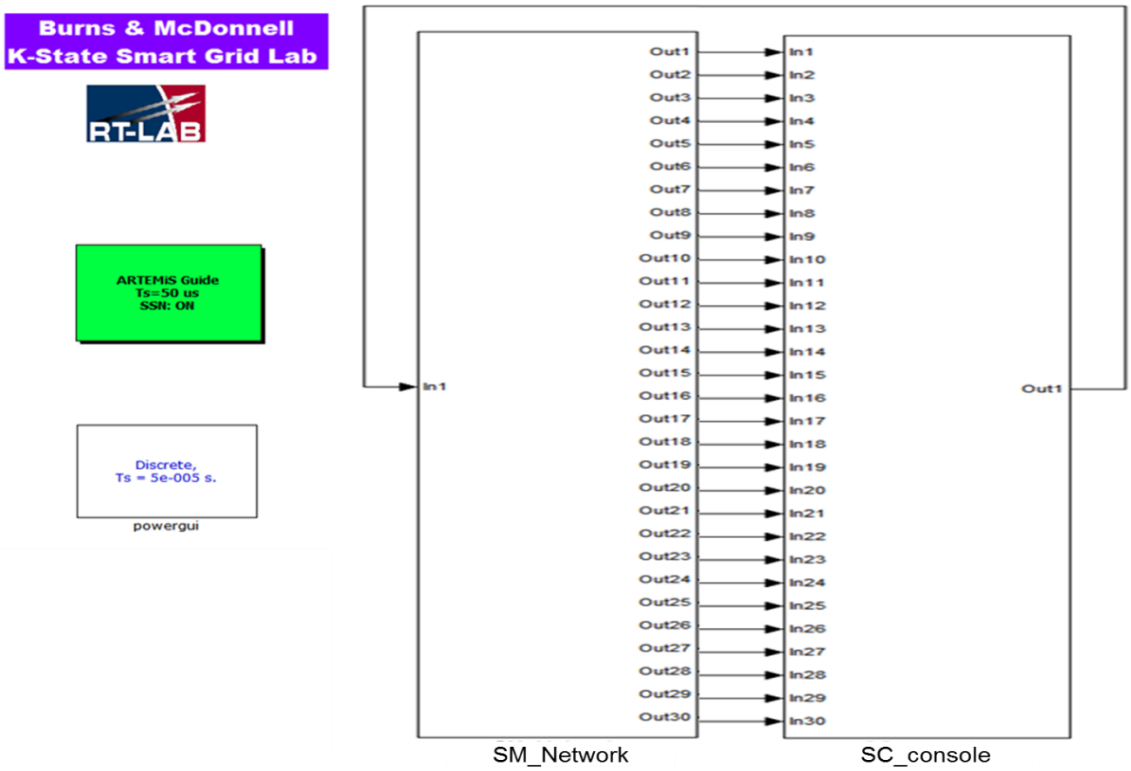

Figure 9.4: Model formed by the SM_Network (master) and SC_console subsystems

In Figure 9.4, the powergui and ARTEMIS Guide block were environment blocks from the Simscape/ SimPowerSystems and Artemis libraries, respectively. The powergui and

ARTEMIS Guide blocks allowed simulation of the microgrid with distributed generators. Settings of the powergui and ARTEMIS Guide blocks are shown in Figure 9.5.

In the powergui block, simulation parameters were set with a Discrete simulation and Tustin solver type (Figure 9.5-A). In the ARTEMIS Guide block, the state-space nodal (SSN) method was enabled, and the art5 state-space discretization method was applied (Figure 9.5-B). In the powergui and ARTEMIS Guide blocks, a fixed time step of 50 microseconds was set as sample time.

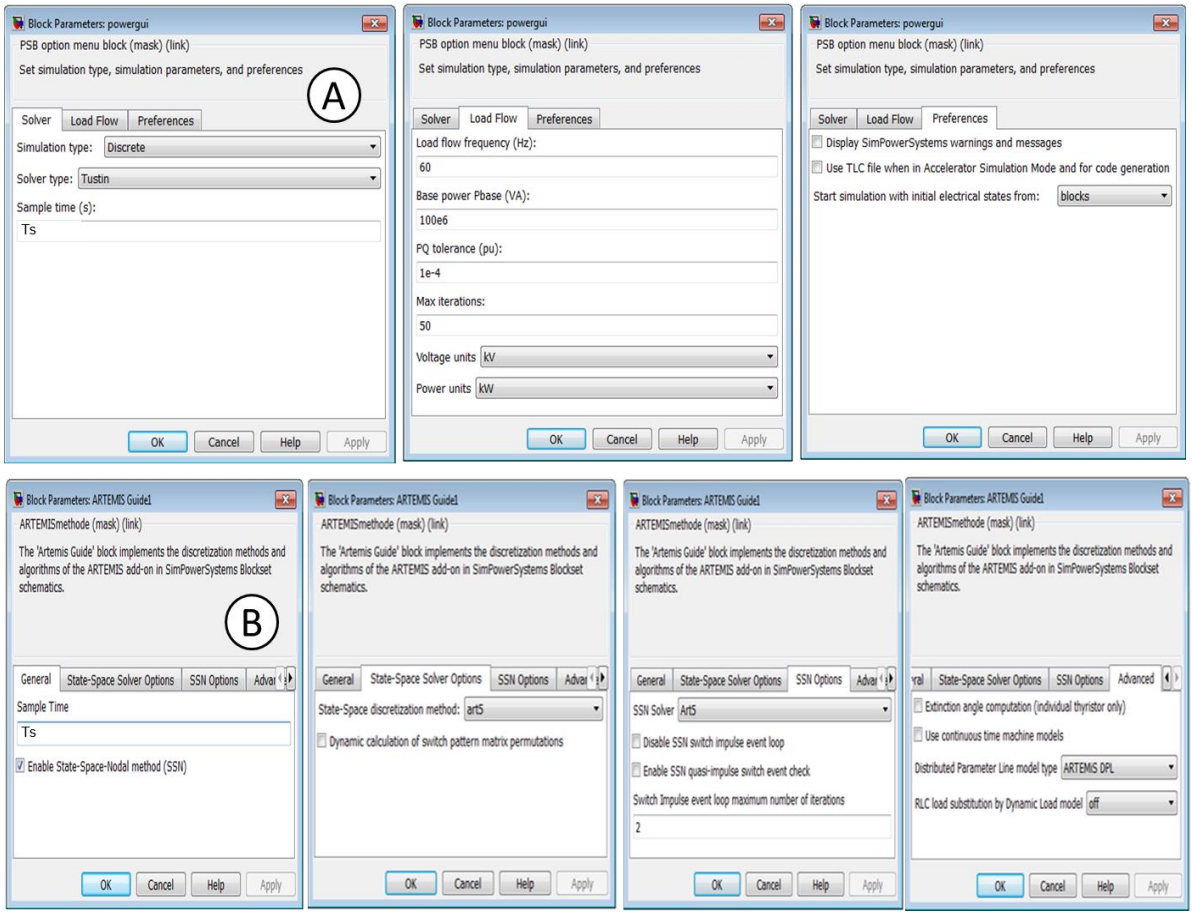

Figure 9.5: Setting of the powergui (A) and ARTEMIS Guide (B) blocks (Ts = 50e-6 seconds)

9.2 SM_Network subsystem

The SM_Network (master) subsystem was designed for application to the OP5600 and Relays 2 and 3 as a real-time relay test system. The SM_Network (master) subsystem

represented the microgrid with distributed generators, and the control circuits applied to Relays 2 and 3 in the loop. These control circuits were the link between the relays and microgrid with distributed generators during real-time tests. Table 9.2 indicates SM_Network (master) subsystem circuit and block functions.

Table 9.2: Functions of circuits and blocks of the SM_Network (master) subsystem

Circuits and blocks	**Figure 9.6**	**Functions**
Interface block	(A)	The interface block controlled the "OP5142EX1 Ctrl" controller by the "Bitstream Filename" of the OP5600 target computer.
Microgrid circuit	(B)	The microgrid circuit simulated pre-fault, fault, and post-fault states of the microgrid with distributed generators.
Fault block	(C)	The fault block simulated overcurrent faults (DLG, SLG, and LL) for real-time tests.
External control fault timing block	(D)	The external control fault timing block received the control fault timing signal from the SC_console subsystem in order to trigger the fault block.
Breaker record event selector-circuit	(E)	The breaker record event selector-circuit selected the recorded event file for breakers of Relays 2 and 3 during the real-time test.
Acquisition circuit	(F)	The acquisition circuit measured A-B-C line breaker currents, breaker pole states, trip signals, and setting groups of Relays 2 and 3.
Tripping circuit	(G)	The tripping circuit received trip signals from Relays 2 and 3 in the loop and sent breaker pole states (open or closed) to Relays 2 and 3 in the loop.
Setting group selector-circuit	(H)	The setting group selector-circuit defined the setting group of Relays 2 and 3 for each real-time test.
LLTI circuits	(I)	LLTI circuits measured A-B-C line breaker currents and the A-B-C line-to-ground bus voltages of Relays 2 and 3.

DLG: double line-to-ground, SLG: single line-to-ground, LL: line-to-line

In Figure 9.6, the interface block (A), microgrid circuit (B), fault block (C), external control fault timing block (D), breaker record event selector-circuit (E), acquisition circuit (F), tripping circuit (G), setting group selector-circuit (H), and LLTI circuits (I) are indicated inside red dashed circles.

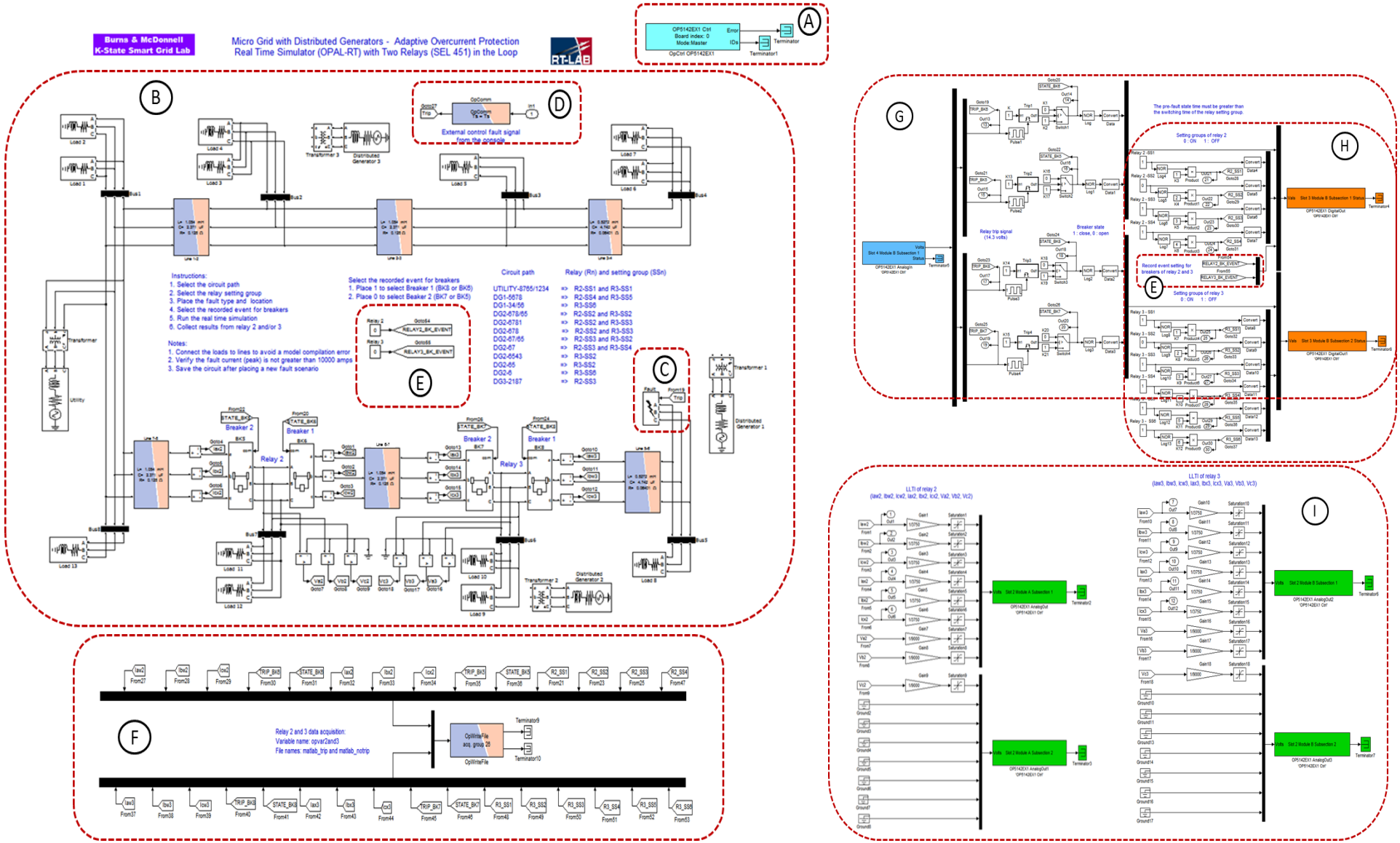

Figure 9.6: Circuits and blocks of the SM_Network (master) subsystem : interface block (A), microgrid circuit (B), fault block (C), external control fault timing block (D), breaker record event selector-circuit (E), acquisition circuit (F), tripping circuit (G), setting group selector-circuit (H), and LLTI circuits (I)

9.2.1 Interface block

The interface block contained an “OP5142EX1 Ctrl” mask. The interface block (Figure 9.6-A) controlled the “OP5142EX1 Ctrl” controller by the “OP5142_1-EX-0000-2_2_0_282-KansasState_OP5600-01-04.bin” file. The controller name, bitstream file name, synchronization mode, and sample time were set in the “OpCtrl OP5142EX1” block. Figure 9.7 shows settings of the “OpCtrl OP5142EX1” mask. Sample time (*Ts*) was set at 50 microseconds for the project model.

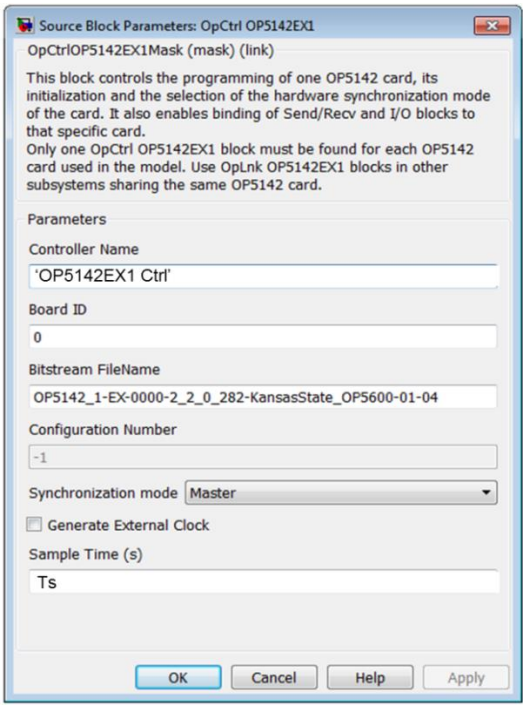

Figure 9.7: Settings of the “OpCtrl OP5142EX1” mask

9.2.2 Microgrid circuit

The microgrid circuit (Figure 9.6-B) was the electrical circuit of the microgrid with the utility and distributed generators, transformers, power lines, loads, busses, and breakers controlled by Relays 2 and 3 in the loop. Masks of the microgrid originated from Simulink, Simscape, and Artemis libraries. Table 9.3 shows the libraries and masks applied in the microgrid circuit (Figure 9.6-B).

Table 9.3: Libraries and masks applied in the microgrid circuit

Library	Sublibraries	Masks
Simulink	Signal Routing	Goto and from tags
Simscape	SimPowerSystems	Three-phase source
		Three-phase transformer (two windings), three-phase series RLC load, three-phase breaker, and ground
		Current, voltage, and three-phase V-I measurement
Artemis	ARTEMIS	Stubline

"Goto" tags were applied in order to send signals from the microgrid (Figure 9.6-A) to the control circuits (Figures 9.6-F and -I). However, "From" tags were applied to receive signals from the control circuits (Figures 9.6-D and -G) to the microgrid (Figure 9.6-A).

For example, "Goto" tags connected to current measurement blocks sent measured A-B-C line breaker currents from the microgrid circuit (Figure 9.6-A) to LLTI circuits (Figure 9.6-I). In addition, "From" tags connected to three-phase breaker blocks received trip signals from the tripping circuit (Figure 9.6-G) connected to Relays 2 and 3 in the loop.

In the microgrid circuit (Figure 9-6-A), current and voltage measurement masks were applied in order to measure A-B-C line breaker currents and A-B-C line-to-ground bus voltages. Busses of the microgrid were created with "three-phase V-I measurement" masks.

In the microgrid circuit (Figure 9.6-A), three-phase breaker blocks were applied in order to simulate breakers controlled by the tripping circuit (Figure 9.6-G) through Relays 2 and 3 in the loop. In the microgrid circuit (Figure 9.6-A), if relays in the loop detected a fault overcurrent, a breaker tripped. Although Relay 2 tripped "BK5" and "BK6" breakers, Relay 3 tripped "BK7" and "BK8" breakers.

Three-phase series resistance, inductance and capacitance (RLC) load blocks were applied in order to simulate bus loads along the microgrid (Figure 9.6-A). These loads were

identical to loads simulated by the Power World® software [10] in the NRTS experiment. Load dialog in the Power World® software [10] was set with the single-phase load, and load masks in the microgrid circuit (Figure 9.6-A) were set with the three-phase load (single-phase load multiplied by 3). Setting parameters of three-phase series RLC load masks are listed in Table O.1 of Appendix O. Power lines of the microgrid circuit (Figure 9.6-A) were shorter than 15 km. Initially, three-phase transmission line models with lumped (short lines) and distributed parameters (long lines) from the SimPowerSystems library were applied without success with real-time simulation because three-phase transmission line models with lumped and distributed parameters had length limitations. Based on an OPAL-RT website article [99], Equation (9.1) limited these three-phase transmission line models.

$$l_{min} = \frac{Ts}{1/c} \tag{9.1}$$

where l_{min} is minimum line length in km, *Ts* is the sample in seconds, and *c* is the speed of light in km per sec. Considering the sample time of 50 x10^{-6} seconds (50 microseconds), minimum line length according to Equation (9.1) was 15 km. Therefore, the stubline model from the ARTEMIS library was applied in order to model power lines with lengths less than 15 km in the microgrid circuit (Figure 9.6-A). Parameter settings of Artemis stubline masks for power lines 1-2, 2-3, 3-4, 5-6, 6-7, and 7-8 are indicated in Table O.1 of Appendix O.

Three-phase transformer (two windings) blocks configured the utility and distributed transformers along the microgrid (Figure 9.6-A). The configuration, parameters, and advanced settings of three-phase transformer (two windings) masks for the utility and distributed transformers are presented in Table O.1 of Appendix O.

Three-phase source blocks configured the utility and distributed generators in the microgrid circuit (Figure 9.6-A). Because microgrid constraint prevented the utility and

distributed generators from being connected in parallel, they were set as swing generators for load flow analysis. Setting parameters of three-phase source masks for the utility and distributed generators are indicated in Table O.1 of Appendix O.

9.2.3 Fault and external control fault timing block

The fault block (Figure 9.6-C), selected from the "Simscape/ SimPowerSystems" library, simulated overcurrent faults for real-time tests. Fault types simulated for real-time tests included double line-to-ground faults at B-C phases, single line-to-ground faults at A phase, and line-to-line faults at B-C phases. Fault block location and type of faults were selected for real-time tests based on circuit paths. When the fault block was located close to or far away from the tripped breaker, real-time tests corresponded to a maximum or minimum fault overcurrent, respectively. The fault block (Figure 9.6-C) was applied to simulate minimum and maximum fault overcurrents along power lines for circuit paths of real-time tests. Figure 9.8 shows masks of the three-phase fault (A) and "OpComm" (B) blocks.

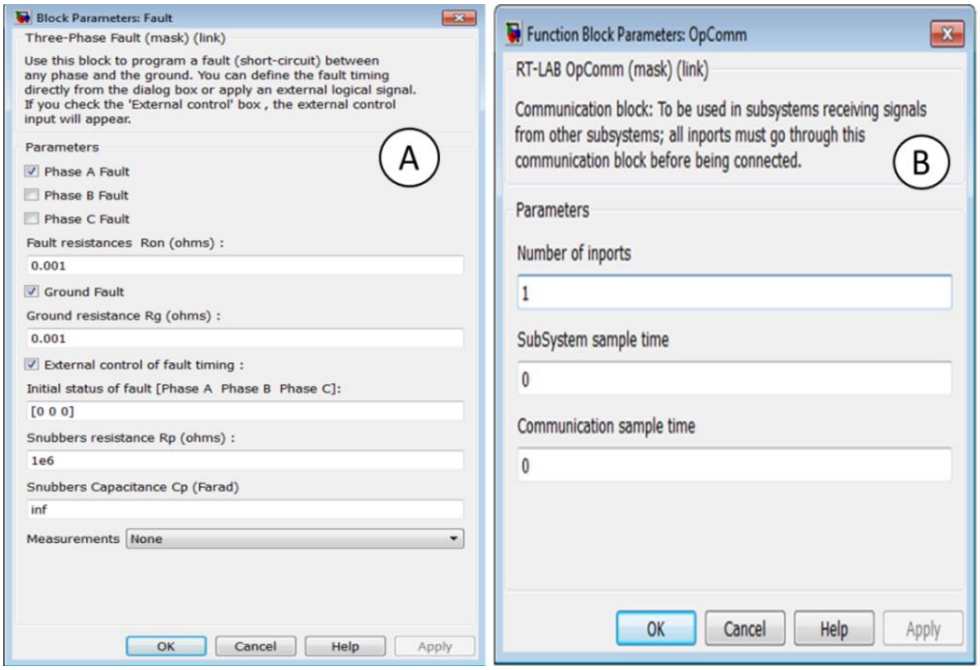

Figure 9.8: Three-phase fault (A) and OpComm (B) masks of the SM_Network subsystem

An external signal sent by the external control fault timing block (Figure 9.6-D), or "OpComm" block, triggered the fault block (Figure 9.6-C). The "OpComm" block was selected from the "RT-LAB®/ Communication" library, and the "OpComm" block in the SM_Network (master) subsystem received a signal from the SC_console subsystem. Although the fault (Figure 9.6-C) and external control fault timing (Figure 9.6-D) blocks were located in the SM_Network (master) subsystem, the control fault timing circuit that triggered the fault was located in the SC_console subsystem. Therefore, the external control fault timing block (Figure 9.6-D), represented by an "OpComm" block, received the external signal from the "Out1" of the SC_console subsystem during execution of real-time simulation.

9.2.4 Breaker record event selector-circuit

In the SM_Network (master) subsystem, the breaker record event selector-circuit (Figure 9.6-E) defined the recorded event from breakers of Relays 2 and 3. As shown in Figure 9.9, the breaker record event selector-circuit could be segregated into a selector (A) and circuit (B) section.

The selector (Figure 9.9-A) picked up the record event from the breaker expected to trip based on the circuit path and fault location of the real-time test. In the circuit (Figure 9.9-B), signals from the selector were received and then sent to the "OP5142EX1 DigitalOut" block.

The recorded event file for breakers of Relays 2 and 3 was selected by placing "0" or "1" in cells of the record event selector before running the real-time test, thereby recording the record event of "BK5" and "BK7" breaker or "BK6" and "BK8" breaker in the "RELAY2_BK_EVENT" and "RELAY3_BK_EVENT" cells (Figure 9.9-A), respectively.

Breaker event files of Relays 2 and 3 were recorded based on "current and voltage source selection" settings of Relays 2 and 3 in Chapter 5. In real-time tests, IN105 control inputs from

Relays 2 or 3 activated the breaker recorded event according to the breaker expected to trip during tests by setting the breaker record event selector (Figure 9.9-A) . The breaker record event selector-circuit was connected to the “OP5142EX1 DigitalOut” block that activated IN105 control input of relays through the high voltage interface panel (HVIP). The HVIP converted 16 volt-level from the “OP5142EX1 DigitalOut” card’s digital outputs to 120 volt- level relay’s control input. The “OP5142EX1 DigitalOut” block was selected from the “RT-LAB®/ I/O / Opal-RT => OP5142EX1” library.

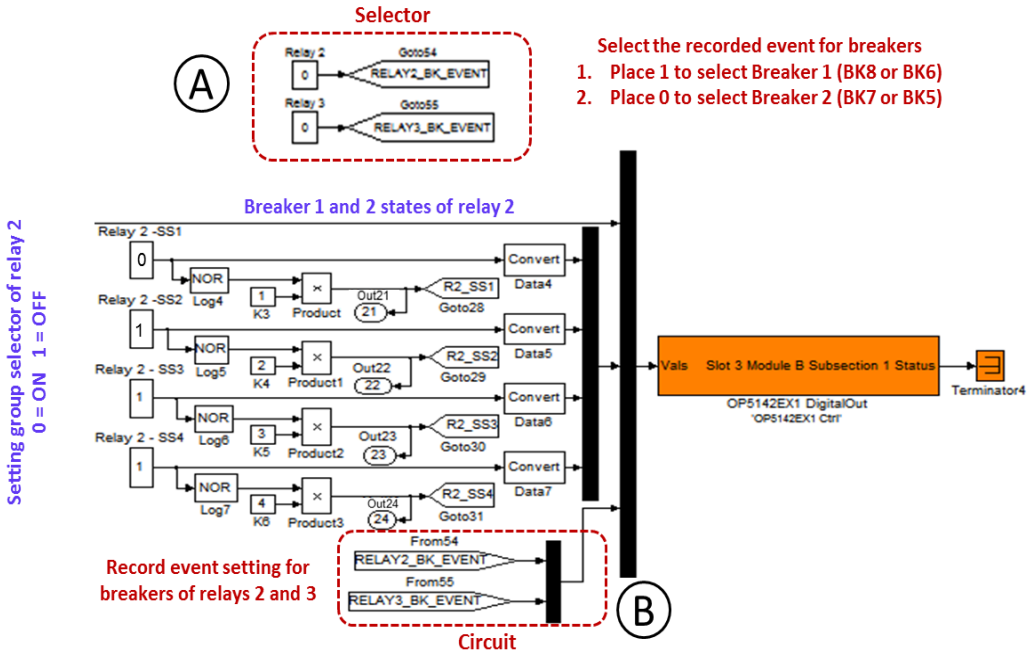

Figure 9.9: Breaker record event selector-circuit

9.2.5 Acquisition circuit

In the SM_Network (master) subsystem, the acquisition circuit (Figure 9.6-F) contained an “OpWriteFile” block that measured and recorded A-B-C line breaker currents, breaker pole states, trip signals, and setting groups of Relays 2 and 3. The “OpWriteFile” block collected these signals from the SM_Network (master) subsystem and generated a “mat.” file after executing real-time simulation that allowed results from the microgrid in the SM_Network

(master) subsystem to be plotted. The “OpWriteFile” block was selected from the “RT-LAB®/DataLogging” library. As shown in Figure 9.10, setting parameters of the “OpWriteFile” mask were defined to record A-B-C line breaker currents, breaker pole states, trip signals, and relay setting groups until real-time simulation stopped at 5 sec.. The default decimation factor, number of samples, buffer size in bytes, and file size limit in bytes were then set to record test results in “mat.” files collected from the “OpWriteFile” block.

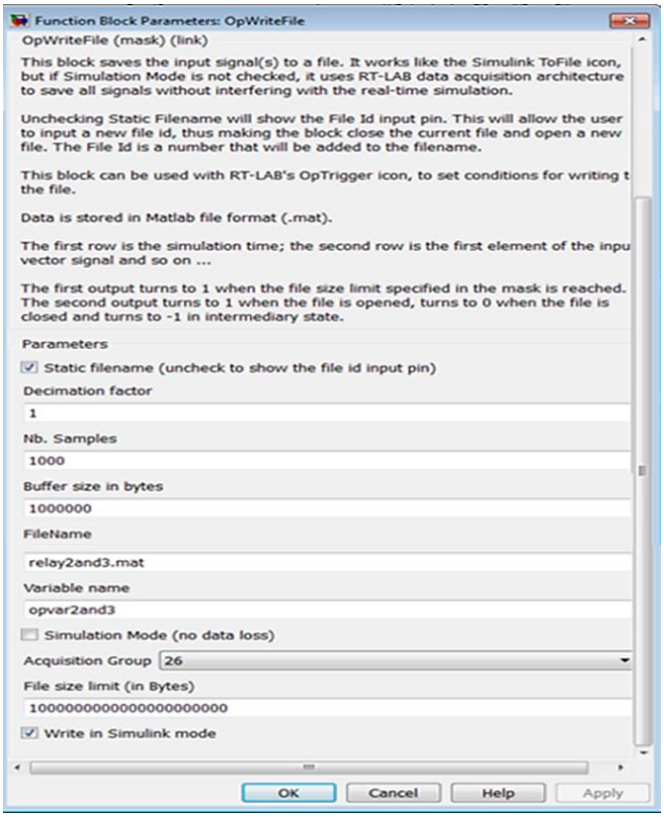

Figure 9.10: Settings of the “OpWriteFile” mask

Modification of the default file size limit in bytes from $10x10^6$ to $10x10^{20}$ bytes allowed A-B-C line breaker currents, breaker pole states, trip signals, and relay setting groups to be recorded for real-time tests with a stop time of 5 sec.. The “mat.” file and variable names were defined as “relay2and3.mat” and “opvar3and3.” As shown in Figure 9.10, the “Write in Simulink mode” cell was selected because real-time simulation was run in Simulink.

9.2.6 Tripping circuit

In the SM_Network (master) subsystem, the tripping circuit (Figure 9.6-G) tripped breakers of Relays 2 and 3 when an overcurrent fault occurred. In real-time tests, the tripping circuit received the trip signal from the relays when the relay's overcurrent elements detected a fault overcurrent, thereby tripping a breaker by clearing the overcurrent fault in the microgrid. In addition, the tripping circuit sent breaker pole states (open or closed) to Relays 2 and 3 in the loop. Tripping circuits received trip signals from relays through the "OP5142EX1 AnalogIn" block. Figure 9.11 shows settings of the "OP5142EX1 AnalogIn" mask (A) and system description (B). In the setting mask (Figure 9.11-A), the controller name was "OP5142EX1 Ctrl." Based on the system description (Figure 9.11-B), settings of the "DataOut port number," "Slot infos," and "Maximum number of AIn channels controlled by this block" were "1," "Slot 4 Module 8 Subsection 1," and "8," respectively. The "Number of AIn channels" was set at "4," applying one AIn channel for each breaker of Relays 2 and 3; "Sample Time" was set at zero seconds. The OP5142EX1 AnalogIn" block was collected from the "RT-LAB®/ I/O/ Opal-RT => OP5142EX1" library.

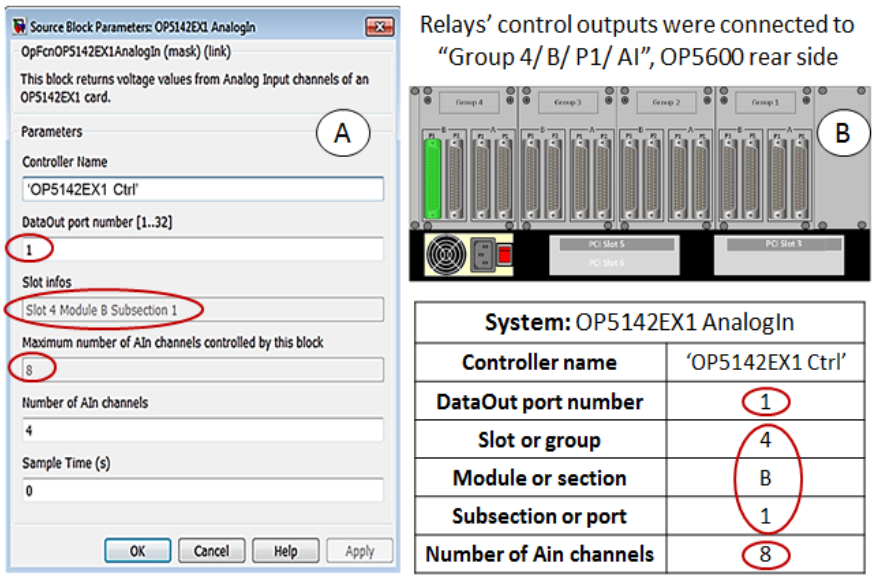

Figure 9.11: "OP5142EX1 AnalogIn" mask (A) and system description (B)

Figure 9.12 shows the tripping circuit of the "BK6" breaker. The tripping circuit was segregated into three phases: Phase I collected the measured trip signal from Relay 2 from the "OP5142EX1 AnalogIn" card connected to the relay's control output; Phase II generated the external signal to trip the "BK6" breaker of the microgrid; Phase III generated breaker pole states (open or closed); Phase IV sent the breaker pole state signal to the "OP5142EX1 DigitalOut" card connected to the relay's control input through the HVIP. The HVIP converted 16 volt-level from the "OP5142EX1 DigitalOut" card's digital outputs to 120 volt-level relay's control inputs. In the tripping circuit, the control output and input of Relay 2 had a NC and NO configuration, respectively.

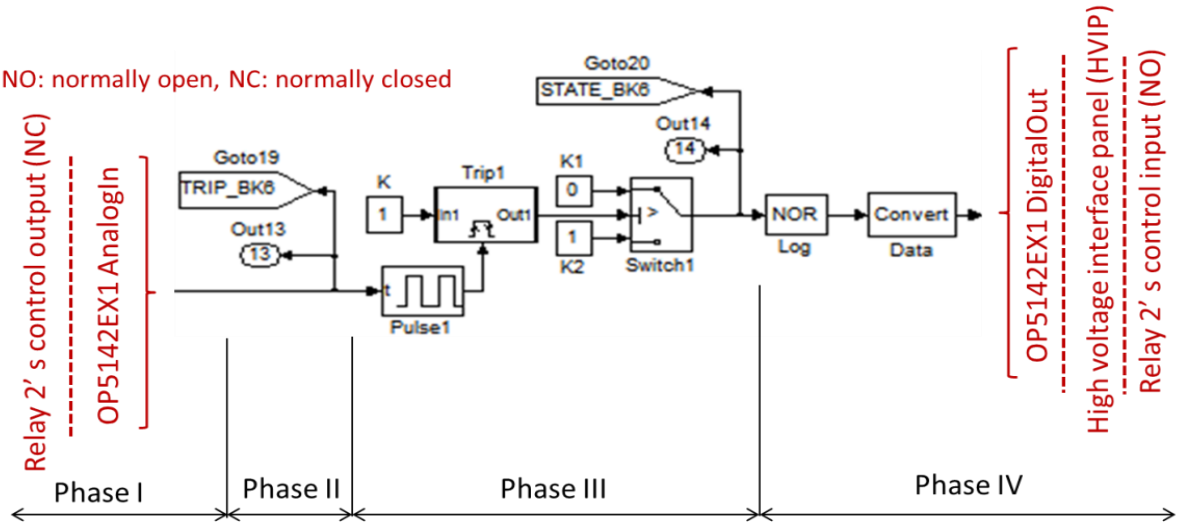

Figure 9.12: Tripping circuit of "BK6" breaker

As shown in Figure 9.12, the "Pulse 1" was activated by the trip signal from Relay 2 (TRIP_BK6)." The trip signal was represented by a falling-rising pulse that activated the pulse generator (Pulse 1) that controlled the trigger (Trip 1). "Trip 1" generated a constant value "1" when the pulse was falling or rising, and "Switch 1" generated an external signal (STATE_BK6) in order to open the "BK6" breaker, representing an open breaker state. The "Convert" block

converted the Boolean output signal from the “NOR” block into a real word value (RWV). Figure 9.13 shows settings of the pulse generator (A), trigger port (B), and switch (C) masks.

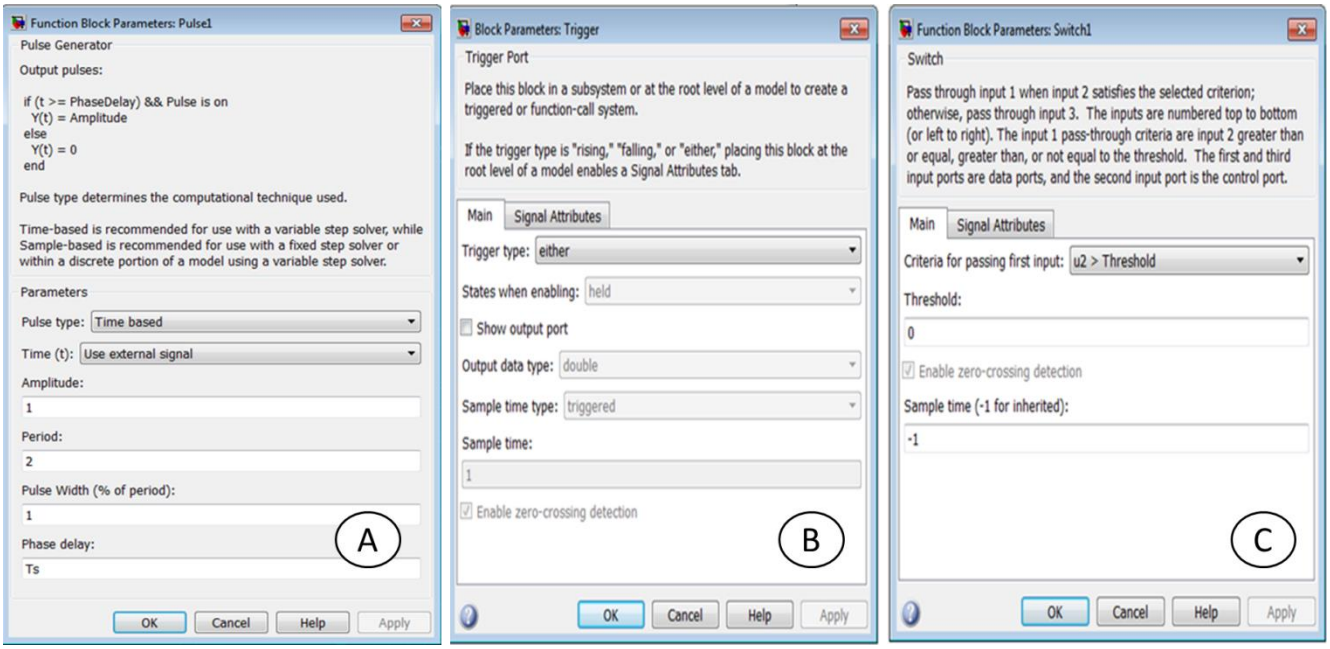

Figure 9.13: Settings of pulse generator (A), trigger port (B), and switch (C) masks

9.2.7 Setting group selector-circuit

In the SM_Network (master) subsystem, the setting group selector-circuit (Figure 9.6-H) defined setting groups of Relays 2 and 3 in the loop during execution of real-time tests. The setting group selector-circuit was divided into a setting group selector-circuit for Relays 2 and 3. Although Relay 2 had four available setting groups, Relay 3 had six available setting groups. Figure 9.14 shows the setting group selector-circuit of Relay 2 with “0” in the “Relay 2–SS2” cell and “1” in the other cells. The setting group 2 (SS2) for Relay 2 was selected. The “Relay 2 setting group” cells (Relay 2 –SS1 to –SS4) were set before executing real-time simulation. The “Convert” blocks converted the output signal into a RWV before sending relay setting group signals to the “OP5142EX1 DigitalOut” card connected to control inputs of Relay 2 through the HVIP. The HVIP converted the 16 volt-level from the “OP5142EX1 DigitalOut” card’s digital

outputs to the 120 volt-level relay's control inputs. The "Goto" tags sent the "R2_SS1- SS4" signals to the acquisition circuit (Figure 9.6-F) and the SC_console subsystem.

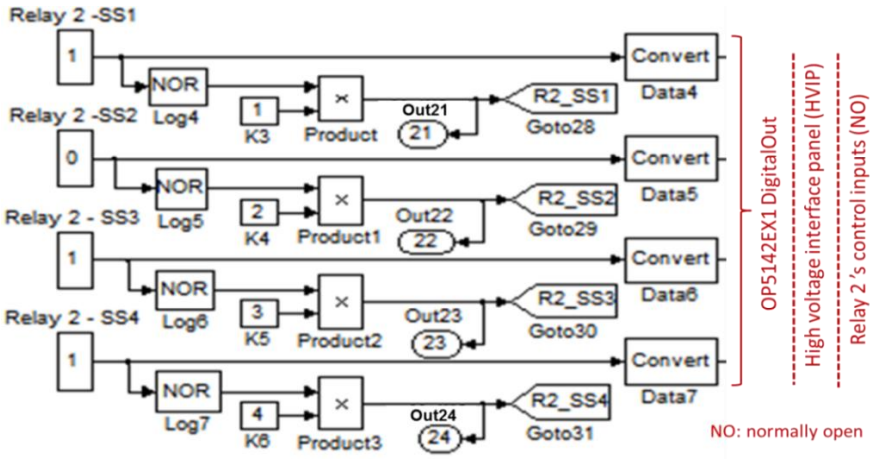

Figure 9.14: Setting group selector-circuit of Relay 2

In the adaptive inverse time overcurrent protection for the microgrid with distributed generators, setting groups of Relays 2 and 3 were selected based on circuit paths applied during real-time tests. The "relay setting group" cells had to be set at "0" to select the relay setting group, while the other setting group cells remained at "1." Table 9.4 shows relay setting groups of Relays 2 and 3 based on circuit paths for real-time tests.

Table 9.4: Relay setting groups for circuit paths

Circuit paths	**Relay setting groups**	
	Relay 2	**Relay 3**
UTILITY-8765/1234	SS1	SS1
DG2-678/65	SS2	SS2
DG2-67/65	SS3	SS2
DG2-6543, DG2-65	NA	SS2
DG2-6781, DG2-678	SS2	SS3
DG2-67	SS3	SS4
DG1-5678	SS4	SS5
DG1-34/56, DG2-6	NA	SS6
DG3-2187	SS3	NA

NA: not available

9.2.8 Low level test interface circuits

In the SM_Network (master) subsystem, the LLTI circuit (Figure 9.6-I) collected measured line breaker currents and line-to-ground bus voltages from the current and voltage measurement boxes of the mircrogrid circuit (Figure 9.6-B). LLTI circuits generated to analog input signals of Relays 2 and 3. LLTI circuits of Relays 2 and 3 were connected to "OP5142EX1 AnalogOut" cards connected to the relays' LLTI. These analog output signals represented A-B-C line breaker currents and A-B-C line-to-ground bus voltages. A-B-C line breaker currents corresponded to "BK6"/ "BK5" breakers for Relay 2 (Iaw2, Ibw2, Icw2/ Iax2, Ibx2, Icx2) and "BK8"/ "BK7" breakers for Relay 3 (Iaw3, Ibw3, Icw3/, Iax3, Ibx3, Icx3). A-B-C line-to-ground bus voltages corresponded to bus 7 for Relay 2 (Va2, Vb2, Vc2) and bus 6 for Relay 3 (Va3, Vb3, Vc3). Because each relay measured nine analog signals, two "OP5142EX1 AnalogOut" cards were applied in the LLTI circuit of each relay. Figures 9.15 and 9.16 show settings of "OP5142EX1 AnalogOut" masks (A-B) and system description (C) for the LLTI circuit of Relays 2 and 3, respectively.

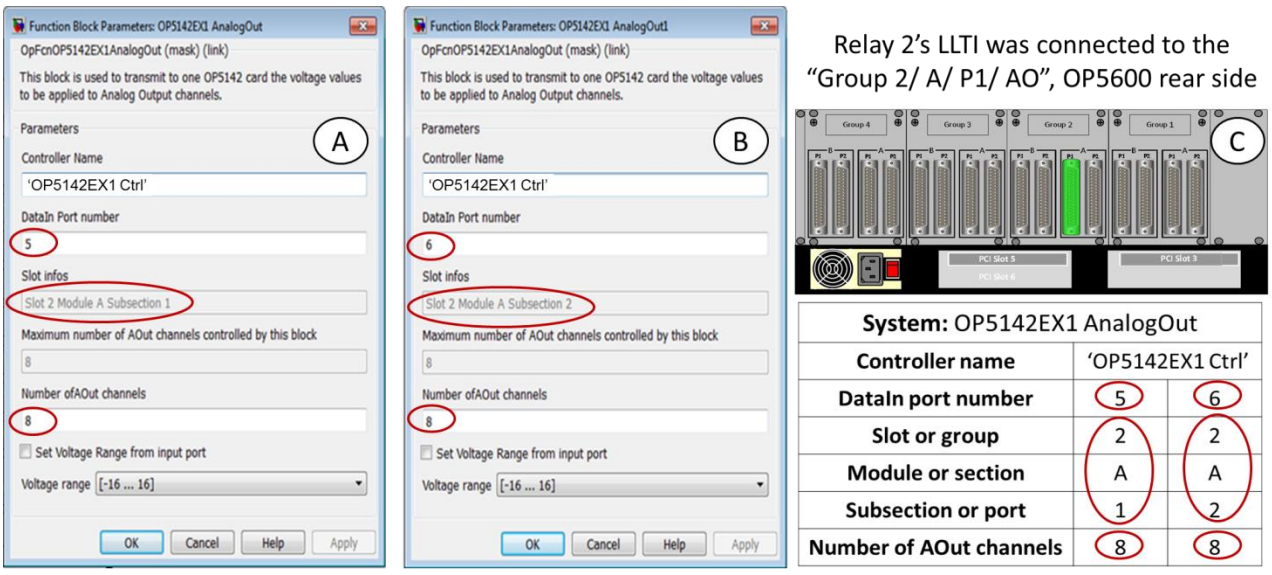

Figure 9.15: "OP5142EX1 AnalogOut" masks (A-B) and system description (C) for Relay 2's LLTI circuit

The setting of the “Controller Name” was ‘OP5142EX1 Ctrl’. However, the selected port of the system connected to the LLTI of the relay defined settings of the “DataIn port number,” “Slot infos,” and “Maximum number of AOut channels controlled by this block.”

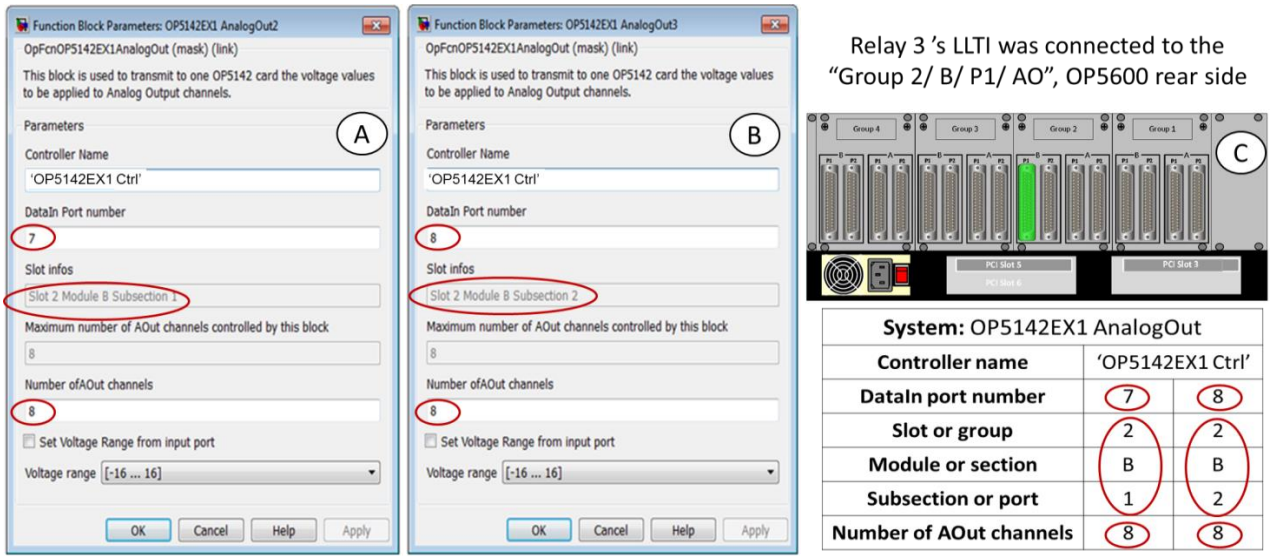

Figure 9.16: “OP5142EX1 AnalogOut” masks (A-B) and system description (C) for the LLTI circuit of Relay 3

The LLTI circuit was segregated into the current (Figure 9.17-A) and voltage (Figure 9.17-B) branches. The “From1” and “From7” tags received the measured A line current (Iaw2) and A line-to-ground voltage (Va2), respectively, from the microgrid circuit (Figure 9.6-B).

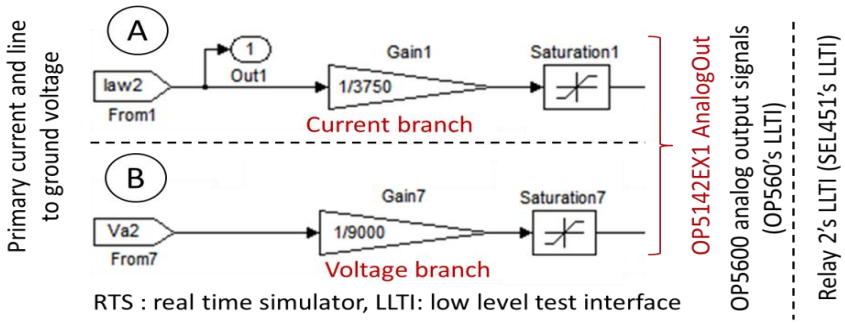

Figure 9.17: Current (A) and voltage (B) branches of the LLTI circuit for Relay 2

Because Relays 2 and 3 were SEL451 relays, the LLTI circuits were designed to achieve the protection and scaling requirements based on relay’s instruction manual [5]. The protection

requirement limited peak-to-peak voltage of the analog signal for the LLTI circuit in order to prevent damage to the SEL451 relay's LLTIs. The scaling requirement adapted the OP5600 analog output signal to the current and voltage scaling factors of the SEL 451 relays.

The protection requirement protected the SEL451 relay's LLTI by placing a saturation block in the current and voltage branches of the LLTI circuits for Relays 2 and 3. Maximum peak-to-peak voltage allowed by the relay's LLTI based on the instruction manual [5], specifically 6.6 volts for SEL451 relays, limited by the saturation blocks. Saturation blocks at end of the current and voltage branches were then set at upper/lower limit of + 3.3/ -3.3 volts, protecting the SEL451 relay's LLTIs from non-desired peak analog signals that could be generated by error during the real-time experiment. Figure 9.18 shows settings of the saturation mask.

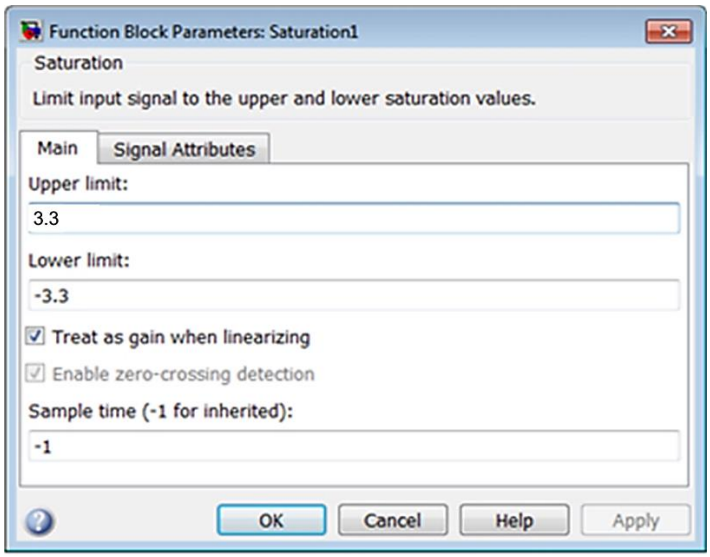

Figure 9.18: Setting of saturation mask

The scaling requirement adapted the measured primary currents and line-to-ground voltages of the microgrid circuit (Figure 9.6-B) to the SEL451 relay's LLTIs, applying a gain block. In other words, the scaling requirement allowed measurement the identical line breaker

rms currents and line-to-ground bus voltages in the microgrid circuit and relay displays. The scaling requirement was based on adaptation of the OP5600 analog output signals to the current and voltage scaling factors of the SEL451 relay's LLTI provided by the instruction manual [5].

A graphical method was applied to estimate gain of the current and voltage branches for the LLTI circuits. This method was based on determining gains of the current and voltage branches by plotting primary peak current and voltage as a function of the OP5600 and relay's LLTI peak analog signals. Gain of current branches for the LLTI circuit was estimated by matching lines represented by Equations (9.2) and (9.3).

$$I_{AI\ peak} = \frac{I_{P\ peak}}{CTR \times SF_A} \tag{9.2}$$

$$I_{AO\ peak} = I_{P\ peak} \times G_I \tag{9.3}$$

where $I_{AI\ peak}$ is the peak current analog input signal (relay's LLTI) in volts, $I_{P\ peak}$ is the primary peak current in amps, *CTR* is the current transformer ratio, SF_A is the current scaling factor in amps/volts, $I_{AO\ peak}$ is the peak current analog output signal (OP5600's LLTI) in volts, and G_I is the gain of the current branch for the LLTI circuit in volts/amps.

In the RTS experiment, current transformer ratios for Relays 2 and 3 were set at 50. The current scaling factor for LLTI of Relays 2 and 3 was 75 A/V based on the SEL 451 relay's instruction manual [5]. Figure 9.19 shows the OP5600 and relay's LLTI peak analog signals represented by dashed black and blue lines, respectively. The graphical method to determine gain of the current branch for the LLTI circuit is also shown in Figure 9.19, in which the relays had a current scaling factor of 75 A/V and they were set at *CTR* of 50. By plotting Equation (9.2) represented in a dashed blue line, gain of the current branch was estimated by plotting Equation (9.3) for various gain values (represented in dashed black lines) until matching the line of

Equation (9.2). As shown in Figure 9.19, the estimated gain of the current branch was 1/3750 V/A.

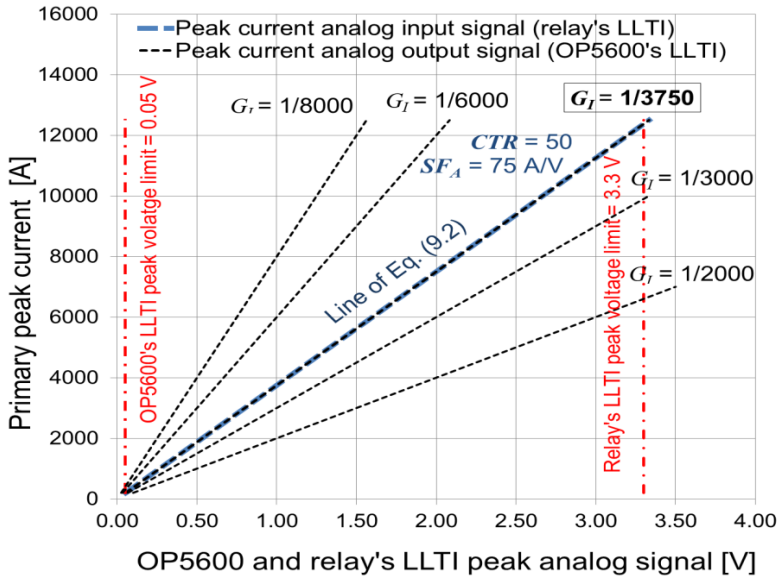

Figure 9.19: OP5600 and relay's LLTI peak analog signal lines for primary peak currents

Gain of voltage branches for the LLTI circuit of Relays 2 and 3 was estimated by matching lines represented by Equations (9.4) and (9.5).

$$V_{AI\ peak} = \frac{V_{P\ peak}}{PTR \times SF_V} \tag{9.4}$$

$$V_{AO\ peak} = V_{P\ peak} \times G_V \tag{9.5}$$

where $V_{AI\ peak}$ is the peak voltage analog input signal (relay's LLTI) in volts, V_{Ppeak} is the primary peak line-to-ground voltage in volts, *PTR* is the potential transformer ratio, SF_V is the voltage scaling factor in volts/volts, $V_{AO\ peak}$ is the peak voltage analog output signal (OP5600's LLTI) in volts, and G_V is gain of the voltage branch for the LLTI circuit in volts/volts.

In the RTS experiment, potential transformer ratios for Relays 2 and 3 were set at 60. The voltage scaling factor for LLTI of Relays 2 and 3 was 150 V/V based on the SEL 451 relay's instruction manual [5]. Figure 9.20 shows the OP5600 and relay's LLTI peak analog

signals represented by black and green dashed lines, respectively. The graphical method to determine gain of the voltage branch for the LLTI circuit is also shown in Figure 9.20, in which the relays had a voltage scaling factor of 150 V/V and they were set at *PTR* of 60. By plotting Equation (9.4) (represented by a dashed green line), gain of the voltage branch was estimated by plotting Equation (9.5) for various gain values (represented by dashed black lines) until matching the line of Equation (9.4). As shown in Figure 9.20, the estimated gain of the voltage branch was 1/9000 V/V. Figure 9.21 shows settings of gain masks for current (A) and voltage (B) branches of LLTI circuits for Relays 2 and 3.

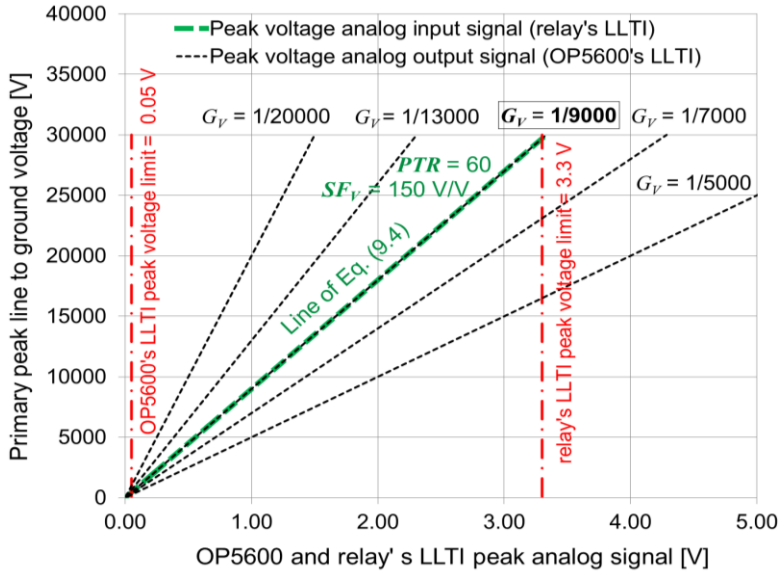

Figure 9.20: OP5600 and relay's LLTI peak analog signal lines for the primary peak line-to-ground voltages

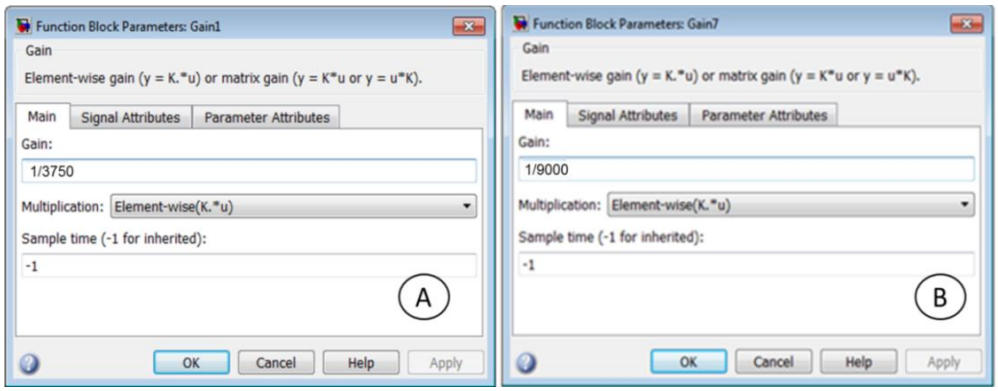

Figure 9.21: Gain masks of current (A) and voltage (B) branches for LLTI circuits

Based on estimated gains of current and voltage branches for LLTI circuits, maximum primary rms current and voltage values for the RTS experiment could be estimated. Primary rms current and voltage are represented by Equations (9.6) and (9.7).

$$I_{P\,rms} = \frac{\sqrt{2}}{2} \times I_{P\,peak} \tag{9.6}$$

$$V_{P\,rms} = \frac{\sqrt{2}}{2} \times V_{P\,peak} \tag{9.7}$$

where $I_{P\,rms}$ is the primary rms current in amps and $V_{P\,rms}$ is the primary rms voltage in volts.

Placing the Equations (9.6) and (9.7) into (9.3) and (9.5), respectively, and considering the maximum peak current and voltage analog output signals (OP5600's LLTI) were limited by 3.3 volts, in order to prevent damage to the relay's LLTI, gain of the current and voltage branches for the LLTI circuit were 1/3750 V/A and 1/9000 V/V, respectively. The maximum primary rms current and voltage were estimated with Equations (9.8) and (9.9), respectively.

$$I_{P\,rms\,max} = \frac{I_{AO\,peak\,max}}{\sqrt{2} \times G_I} = \frac{3.3\ |V|}{\sqrt{2} \times \left(\frac{1}{3750}\ \left|\frac{V}{A}\right|\right)} = 8750\ A \tag{9.8}$$

$$V_{P\,rms\,max} = \frac{V_{AO\,peak\,max}}{\sqrt{2} \times G_V} = \frac{3.3\ |V|}{\sqrt{2} \times \left(\frac{1}{9000}\ \left|\frac{V}{V}\right|\right)} = 21001\ V \tag{9.9}$$

where $I_{P\,rms\,max}$ is the maximum primary rms current in amps, $V_{P\,rms\,max}$ is the maximum primary rms line-to-ground voltage in volts, $I_{AO\,peak\,max}$ is the maximum peak current analog output signal (3.3 volts), and $V_{AO\,peak\,max}$ is the maximum peak voltage analog output signal (3.3 volts). According to results of Equations (9.8) and (9.9), if the measured primary rms current and line-to-ground voltage were greater than 8750 A and 21001 V, respectively, the saturation block that protected the relay's LLTI cut the sinusoidal shape of the current and line-to-ground voltage.

In order to avoid a noisy analog output signal with the OP5600's LLTI, the minimum peak voltage was limited to 0.05 volts. The minimum primary rms current and line-to-ground voltage values could be estimated with Equations (9.10) and (9.11).

$$I_{P\ rms\ min} = \frac{I_{AO\ peak\ min}}{\sqrt{2} \times G_I} = \frac{0.05\ |V|}{\sqrt{2} \times \left(\frac{1}{3750}\ \left|\frac{V}{A}\right|\right)} = 132\ A \tag{9.10}$$

$$V_{P\ rms\ min} = \frac{V_{AO\ peak\ min}}{\sqrt{2} \times G_V} = \frac{0.05\ |V|}{\sqrt{2} \times \left(\frac{1}{9000}\ \left|\frac{V}{V}\right|\right)} = 318\ V \tag{9.11}$$

where $I_{P\ rms\ min}$ is the minimum primary rms current in amps, $V_{P\ rms\ min}$ is the minimum primary rms line-to-ground voltage in volts, $I_{AO\ peak\ min}$ is the minimum peak current analog output signal (0.05 volts), and $V_{AO\ peak\ min}$ is the minimum peak voltage analog output signal (0.05 volts). According to results of Equations (9.10) and (9.11), if the measured primary rms current and line-to-ground voltage were less than 132 A and 318 V, respectively, a noise could be added to the sinusoidal current and line-to-ground voltage. Table 9.5 shows parameters of the current and voltage branches for LLTI circuits of Relays 2 and 3.

Table 9.5: Parameters of current and voltage branches of LLTI circuits

Parameters	**LLTI Circuits**			
	Current branch		**Voltage branch**	
Relay scaling factors	SF_A [A/V]	75	SF_V [V]	150
Transformer ratios	*CTR*	50	*PTR*	60
Gains of LLTI circuits	G_I [V/A]	1/3750	G_V [V/V]	1/9000
Peak analog output signal limits	$I_{AO\ peak\ max}$ [V]	3.3	$V_{AO\ peak\ max}$ [V]	3.3
	$I_{AO\ peak\ min}$ [V]	0.05	$V_{AO\ peak\ min}$ [V]	0.05
Primary current and line-to-ground voltage limits	$I_{P\ rms\ max}$ [A]	8750	$V_{P\ rms\ max}$ [V]	21001
	$I_{P\ rms\ min}$ [A]	132	$V_{P\ rms\ min}$ [V]	318

9.3 SC_Console subsystem

In the project model, the SC_console subsystem contained supervision and control functions. In the supervision, A-B-C line breaker currents, breaker pole states, trip signals, and setting groups of Relays 2 and 3 were plotted during execution of the real-time test. In the control, the initial fault time to trigger the fault block into the SM_Network (master) subsystem was set before executing the real-time test. Based on the supervision and control functions, the

"OpComm" blocks received signals from the SM_Network (master) and SC_console subsystems. The "OpComm" blocks were installed on the receiving subsystem to collect measurements or control signals from the transmitter subsystem. Table 9.6 shows measurements and control signals of the SC_console as a receiver and transmitter subsystem.

Table 9.6: Measurements and control signals

	SM_Network Subsystem (Transmitter)		**SC_console Subsystem (Receiver)**		
Measurements	Circuit	Outputs	Interface	Signal Names (Inputs)	Scopes
	LLTI circuit of Relay 2	1 to 3	OpComm (30 signals)	Iaw2, Ibw2, Icw2	Relay 2
		4 to 6		Iax2, Ibx2, Icx2	
	LLTI circuit of Relay 3	7 to 9		Iaw3, Ibw3, Icw3	Relay 3
		10, 12		Iax3, Ibx3, Icx3	
	Tripping Circuit	13, 14		BK6_TRIP, BK6_STATE	Relay 2
		15, 16		BK5_TRIP, BK5_STATE	
		17, 18		BK8_TRIP, BK8_STATE	Relay 3
		19, 20		BK7_TRIP, BK7_STATE	
	Setting group selector-circuit	21 to24		R2_SG	Relay 2
		25 to 30		R3_SG	Relay 3
Control Signal	**SC_console Subsystem (Transmitter)**		**SM_Network Subsystem (Receiver)**		
	Circuit	Outputs	Interface	Signal Name (Input)	Block
	Control fault timing circuit	1	OpComm (1 signal)	trip	Control fault timing circuit

Iaw2, Ibw2, Icw2: A, B, and C line currents of "BK6" breaker; Iax2, Ibx2, Icx2: A, B, and C line currents of "BK5" breaker; Iaw3, Ibw3, Icw3: A, B, and C line currents of "BK8" breaker; Iax3, Ibx3, Icx3: A, B, and C line currents of "BK7" breaker; BK6_TRIP , BK6_STATE: trip signal and state of "BK6" breaker; BK5_TRIP, BK5_STATE: trip signal and state of "BK5" breaker; BK8_TRIP, BK8_STATE: trip signal and state of "BK8" breaker; BK7_TRIP, BK7_STATE: trip signal and state of "BK7" breaker; R2_SG: setting groups of Relay 2; R3_SG: setting groups of Relay 3.

In the project model, the SC_console subsystem controlled and supervised the real-time test. The SC_console subsystem was segregated into the "OpComm" block (Figure 9.22-A), control fault timing circuit (Figure 9.22-B), and relay scopes (Figure 9.22-C).

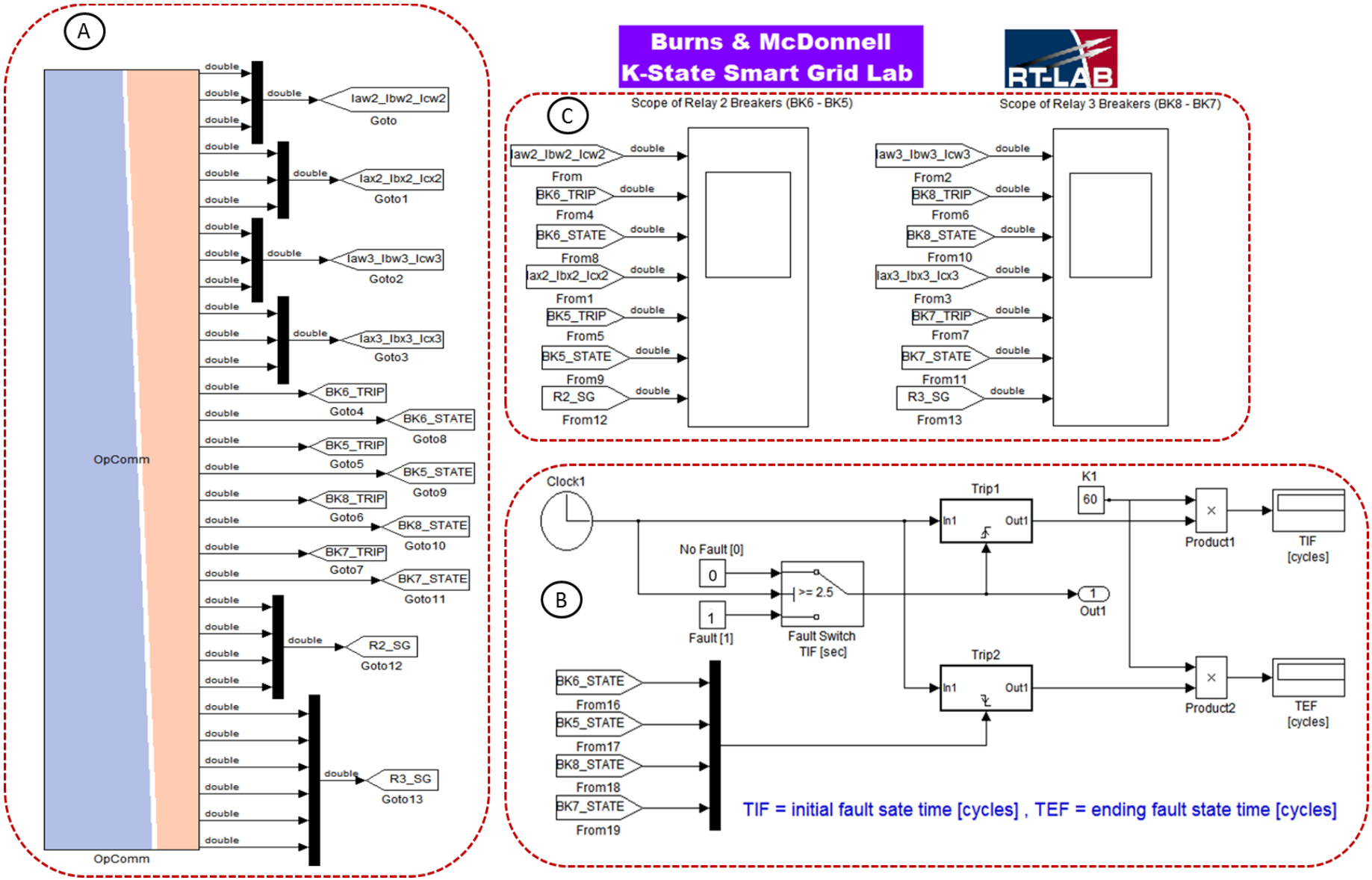

Figure 9.22: Circuits and blocks of the SC_console subsystem: OpComm (A), control fault timing circuit (B), and relay scopes (C)

9.3.1 “OpComm” block

In the SC_console subsystem, the “OpComm” block (Figure 9.22-A) received A-B-C line breaker currents, breaker pole states, trip signals, and setting groups of Relays 2 and 3 from the microgrid and control circuits in the SM_Network (master) subsystem. The “OpComm” was the communication interface between the SM_Network (master) and SC_console subsystems. The “OpComm” block (Figure 9.22-A), selected from the “RT-LAB®/ Communication” library, contained 30 signals (Table 9.6). The “OpComm” mask was set with “30” number of inports, and the “OpComm” block was set as the “1” acquisition group number for the SC_console subsystem. Synchronization and interpolation were enabled on the “OpComm” mask. Figure 9.23 shows settings of the “OpComm” mask for the SC_console subsystem.

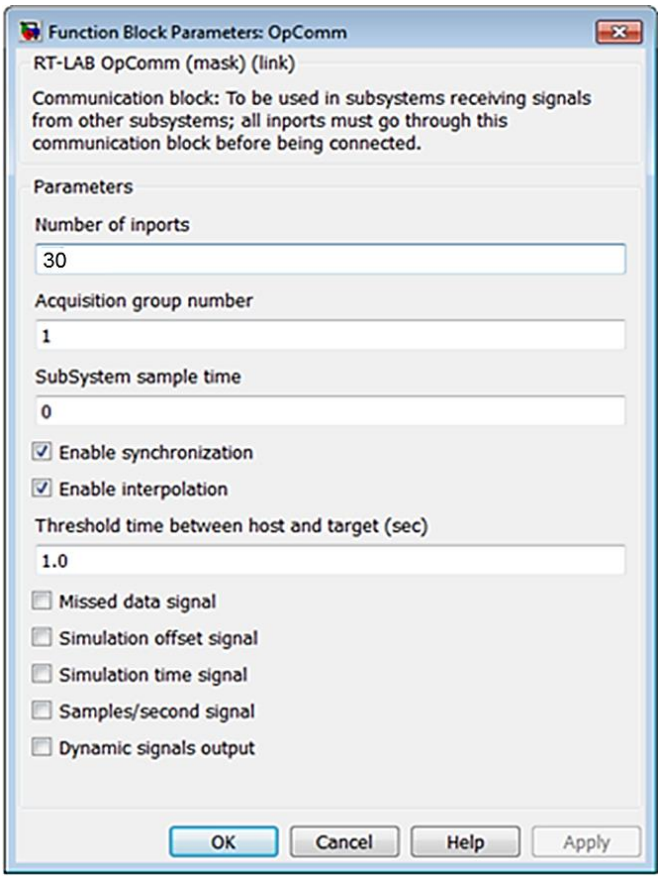

Figure 9.23: “Opcomm” mask of the SC_console subsystem

9.3.2 Control fault timing circuit

In the SC_console subsystem, the control fault timing circuit (Figure 9.22-B) contained control and measurement functions. The fault timing circuit controlled the initial fault time of the fault block in the SM_Network (master) subsystem and measured initial and ending fault state times after executing the real-time test. The control fault timing circuit of the SC_console subsystem is shown in Figure 9.24. This control fault timing circuit was segregated into initial fault state time level (1), control signal level (2), and ending fault state time level (3).

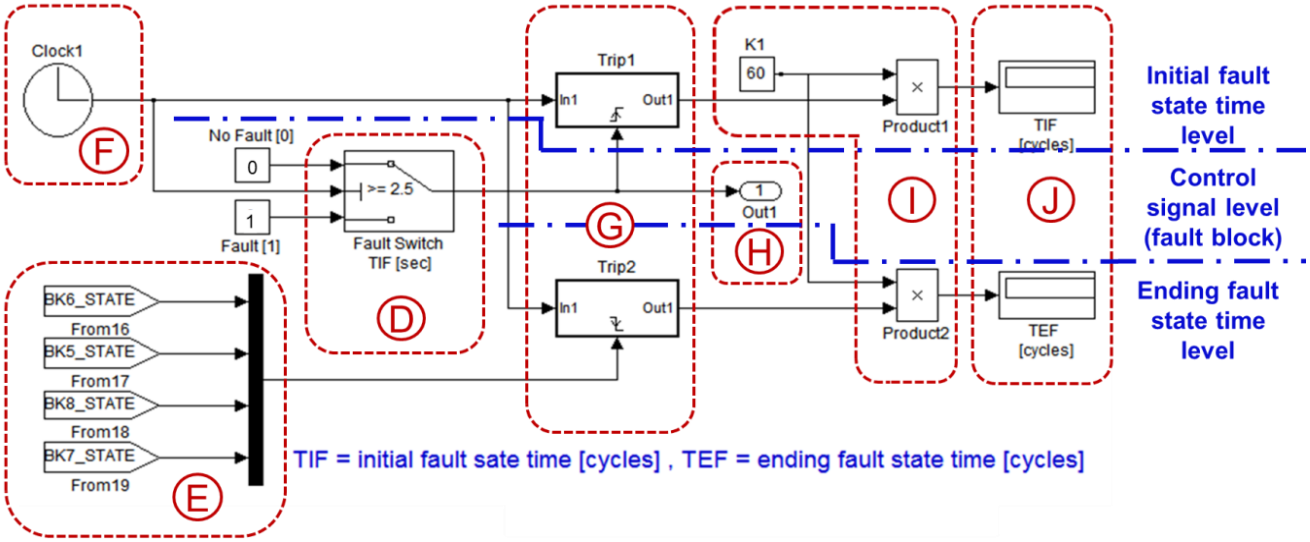

Figure 9.24: Control fault timing circuit of the SC_console subsystem

Initial fault state time, measured in the initial fault time level, was created by the "Trip1" block (Figure 9.24-G) and synchronized by Clock1 (Figure 9.24-F). The "Product1" block (Figure 9.24-I) converted the signal in seconds into cycles, and initial fault state time was measured from the display (Figure 9.24-J) at the end of the real-time test.

In the control signal level, the fault switch (Figure 9.24-D) was set at 2.5 sec., and the Clock1 (Figure 9.24-F) generated the trip for the fault switch connected to the Out1 (Figure 9.24-H). An "OpComm" in the SM_Network (master) subsystem received the Out1 signal, which

represented the output signal of the SC_console and trip signal of the fault block in the SM_Network (master) subsystem.

The ending fault state time, measured in the ending fault time level, was created by the "Trip2" block (Figure 9.24-G) controlled by breaker states from the bus (Figure 9.24-E). Breaker states (open or closed) were collected from the "OpComm" place in the SC-console. During the tripping tests, one breaker always tripped and then inputs (breaker states) of the ending fault time level were connected to an identical bus. The ending fault state time in cycles was measured from the display (Figure 9.24-J) at the end of the real-time test. Measured fault clearing time was then estimated by subtracting the ending and initial fault state times. In the "Trip1" block (Figure 9.24-G), the fault switch block (Figure 9.24-D) generated a signal from zero to one. However, in the "Trip2" block (Figure 9.24-G), breaker states from the bus (Figure 9.24-E) were initially closed; when a fault occurred and Relay 2 or 3 tripped, the breaker generated a signal from one to zero. Therefore, Trip masks for initial and ending fault time levels were set by a rising and falling trigger, respectively. Figure 9.25 shows settings of Trip1 (A) and Trip2 (B) block masks.

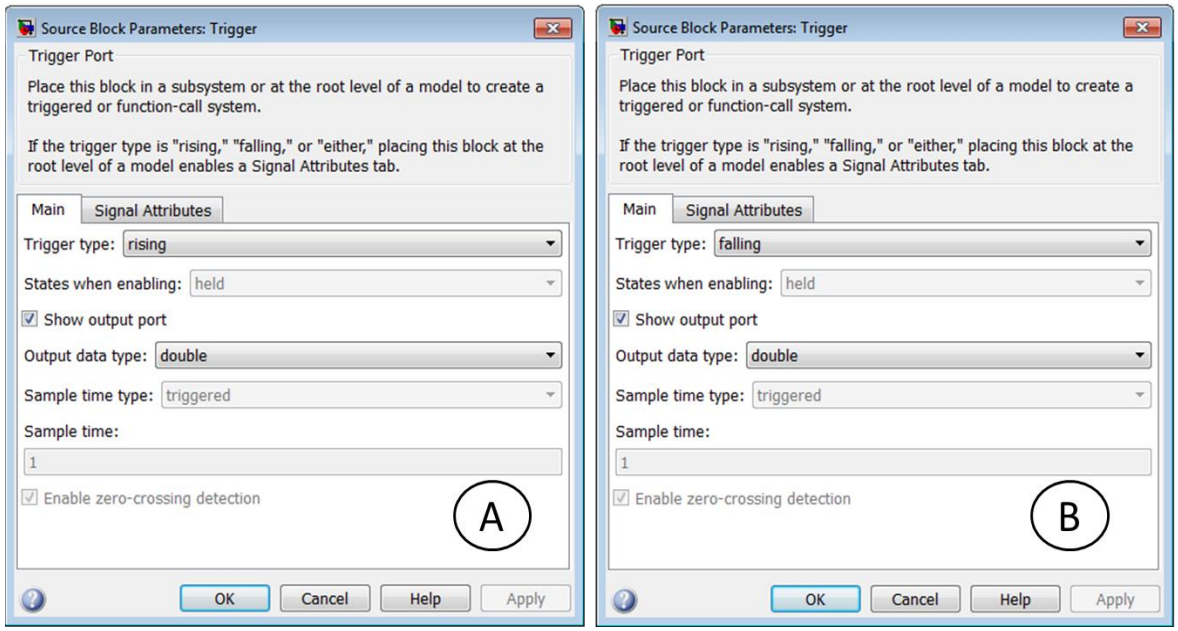

Figure 9.25: Settings of Trip1 (A) and Trip2 (B) block masks

9.3.3 Relay scopes

In the SC_console subsystem, relay scopes (Figure 9.22-C) plotted signals collected from the “OpComm” block (Figure 9.22-A) in the SC_console subsystem. Relay scopes supervised the real-time tests and plotted pre-fault, fault, and post-fault states for tripping and non-tripping tests, supervising both real-time simulations. In the relay scopes, A-B-C line currents, breaker states, trip signals, and relay setting groups were plotted for Relays 2 and 3.

Relay 2 plotted A-B-C line currents of “BK6” breaker (Iaw2, Ibw2, Icw2), A-B-C line currents of “BK5” breaker (Iax2, Ibx2, Icx2), trip signal and state of “BK6” breaker (BK6_TRIP, BK6_STATE), trip signal and state of “BK5” breaker (BK5_TRIP, BK5_STATE) and setting groups of Relay 2 (R2_SG). However, Relay 3 plotted A-B-C line currents of “BK8” breaker (Iaw3, Ibw3, Icw3), A-B-C line currents of “BK7” breaker (Iax2, Ibx2, Icx2), trip signal and state of “BK8” breaker (BK8_TRIP, BK8_STATE), trip signal and state of “BK7” breaker (BK7_TRIP, BK7_STATE), and setting groups of Relay 3 (R3_SG). Relays 2 and 3 contained four and six available setting groups, respectively.

9.4 Chapter summary

This chapter described the project model for adaptive overcurrent protection of the microgrid with distributed generators, in which the OP-5600 contained two relays in the loop and each relay controlled two breakers. The project was created with RT-LAB® software [13] and the model was created with Matlab®/Simulink® software [14].

In the project model, the SM_Network (master) and SC_console subsystems were configured. The SM_Network (master) subsystem simulated fault overcurrents at the microgrid with distributed generators and recorded test results after execution of real-time test. However, SC_console subsystems controlled the fault block and supervised real-time tests.

The SM_Network (master) subsystem contained the interface block, microgrid circuit, fault block, external control fault timing block, breaker record event selector-circuit, acquisition circuit, tripping circuit, setting group selector-circuit, and LLTI circuits. However, the SC_console subsystem contained the OpComm, control fault timing circuit, and relay scopes.

Chapter 10 - Test steps of RTS experiment

This chapter presents test steps to run real-time simulation with relays in the loop (Figure 10.1), including description of test steps to run tripping and non-tripping tests for adaptive overcurrent protection of the microgrid with distributed generators. Test steps consist of Edition (1), Preparation (2), Compilation (3), Execution (4), and Collection (5) phase. When the collection phase finished in the process on a loop, a new test was started again from the edition phase.

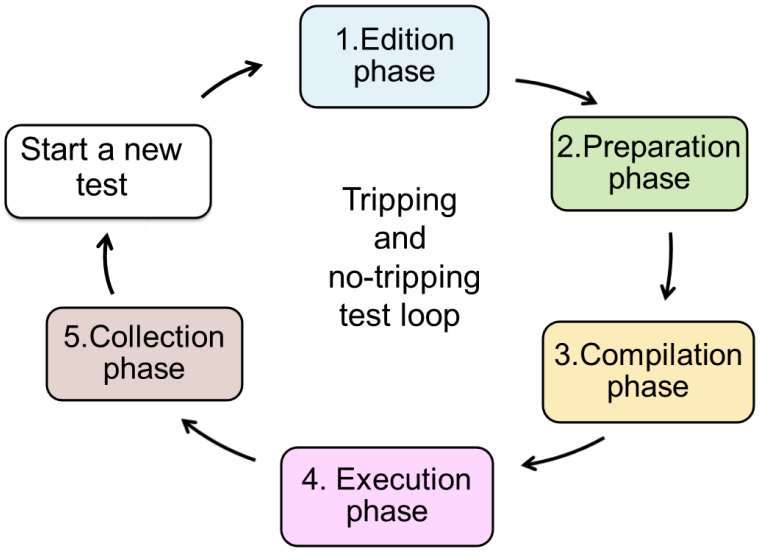

Figure 10.1: Test step phases

In the RTS experiment, test phase tasks were based on the project model (Chapter 9) built for adaptive overcurrent protection in the microgrid with distributed generators and the "Six Steps to Real-Time" tutorial in the RT-LAB® software [13]. As shown in Figure 10.2, tasks for Edition (1), Preparation (2), Compilation (3), Execution (4) and Collection (5) phases allowed the real-time tests to be run for adaptive overcurrent protection of the microgrid with distributed generators.

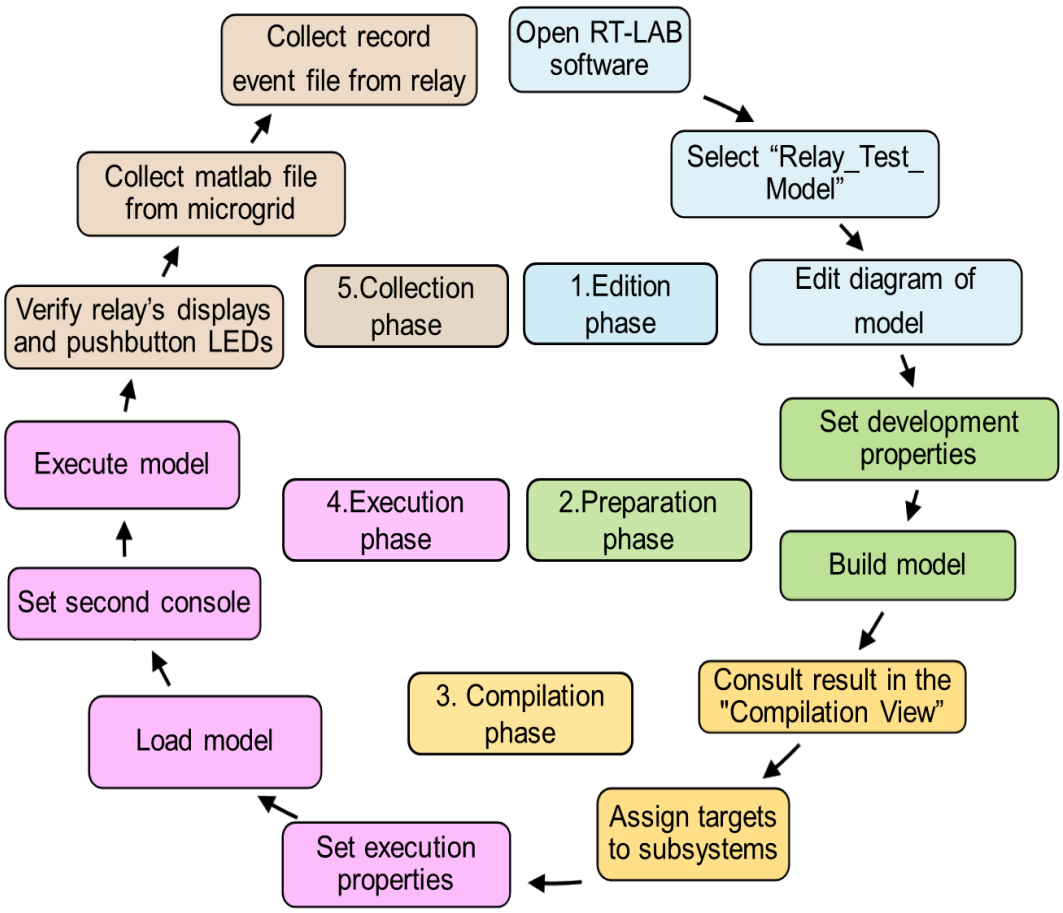

Figure 10.2: Test step tasks

Table 10.1 indicates the tasks and summary of each phase during real-time test steps. Tripping and non-tripping tests were run in the RTS experiment. In the tripping tests, relays tripped for an overcurrent fault situation, collecting the microgrid's Matlab® and relay record event files from the host and HMI computers, respectively. However, in the non-tripping tests, Matlab® files were collected because relays did not save record events if they did not trip.

Table 10.1: Phases and tasks during the test steps

Phases	Task Codes and Names		Phase Descriptions
	Code	Name	
1. Edition	1.1	Open RT-LAB® software [13]	RT-LAB® software [13] was opened and "Relay_Test Model" was selected. Then "Edit the diagram of the model" option was selected, and the SM_Network (master) subsystem was opened. In the SM_Netwotk (master) subsystem represented by the microgrid, the circuit path, fault type (SLG, DLG and LL) and location, relay setting groups (SS1 to SS6), and breaker to record event files were set for the microgrid.
	1.2	Select "Relay_Test_Model"	
	1.3	Edit the model diagram	
2. Preparation	2.1	Set development properties	The target platform was selected, and the model was built based on the diagram model edited in the previous phase.
	2.2	Build the model	
3. Compilation	3.1	Consult the "Compilation View"	Model compilation was consulted, and the OP-5600 target computer to run the real-time test was assigned.
	3.2	Assign targets to subsystems	
4. Execution	4.1	Set execution properties	Execution properties to run the real-time test were set, including the "stop time" to end the real-time test. Then the model was loaded in the target computer. When the second console was automatically generated and opened, the time to trigger the fault block by an external signal was set, and plots of the relay scopes were set to visualize A-B-C line breaker currents, breakers states, trip signals, and relay setting groups during the tests. Finally, the model was executed, running the real-time test.
	4.2	Load model	
	4.3	Set second console	
	4.4	Execute model	
5. Collection	5.1	Visualize relay's display and pushbutton LEDs	While the real-time test was running, the relay's display and pushbuttons were evaluated from a webcam. When the real-time test was finished, the Matlab® and record event (C8 and HR) files from the microgrid and relays were collected, respectively. In the Matlab® files, the A-B-C line breaker currents, breakers states, trip signals, and relay setting groups were measured. In the record events, the relay control inputs/outputs and SELogic variables were also added.
	5.2	Collect generated Matlab® file	
	5.3	Collect record event file	

SLG: single line-to-ground; DLG: double line-to-ground; LL: line-to-line; C8: compressed-8-samples-per-cycle; HR: high resolution

10.1 Edition phase

In the Edition phase, the SM_Netwotk (master) subsystem that represented the microgrid was edited based on the selected real-time test, and then the circuit path of the microgrid, fault type (SLG, DLG and DL) and location, relay setting groups of Relays 2 (SS1-4) and 3 (SS1-6), and breaker recorded event were set at the SM_Network (master) subsystem. Steps to edit the model diagram are presented in Figure 10.3. The RT-LAB® software [13] was opened by double left-clicking the RT-LAB® icon (A), and the "Relay_Test_Model → OP_5600" path was selected (B). Then the "Edit the diagram of the model" option was selected, and the SM_Network (master) subsystem was opened to edit the microgrid scenario based on the selected real-time test.

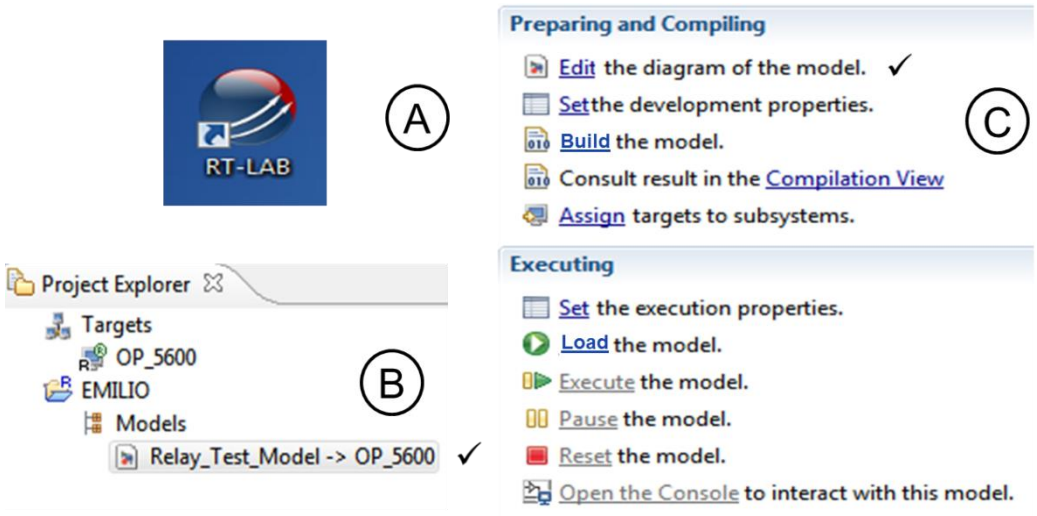

Figure 10.3: RT-LAB® icon (A), project explorer (B), and editor (C)

The SM_Network (master) subsystem contained the microgrid with distributed generators, breaker trip and LLTI circuits, and relay setting group and breaker record event selector-circuits. Initially, parameters of the real-time test were configured to define the circuit path, fault type and location, breaker record event, and setting group of Relays 2 and 3. Based on

a selected real-time test, the circuit path was connected to the microgrid, the fault type was selected for the fault block, and the fault block was connected to the fault site in the microgrid. Setting groups of Relays 2 and 3 were then selected from the relay setting group selector and the record event of the breaker expected to trip was selected from the breaker record event selector. Figure 10.4 shows the circuit of the "UTILITY-8765/1234-LL(BC)-Bus5-BK8" test. The circuit test was configured by connecting busses, power lines, source, and transformer in the microgrid. The utility source and transformer were connected to the "L12, L23, L34" and "L56, L67, L78" power lines. The fault block (Figure 10.4-A) was placed on Bus 5, with the expectation that the "BK8" breaker would trip. The record event for the "BK8" breaker of Relay 3 was selected by placing "1" on the "Relay3_BK_EVENT" cell in the breaker record event selector (Figure 10.4-B).

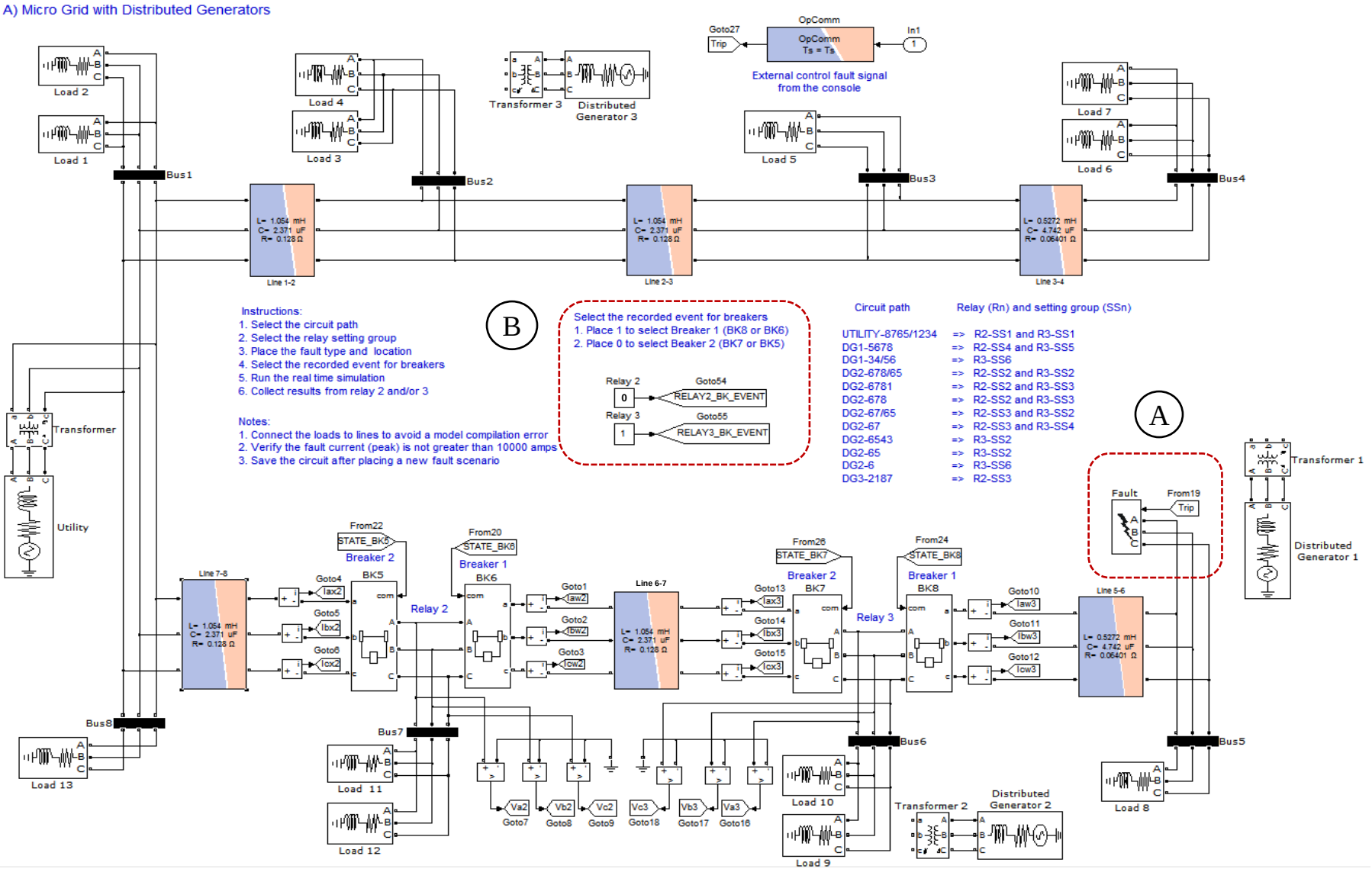

Figure 10.4: Microgrid with distributed generators in the SM_Network subsystem, “UTILITY-8765/1234-LL(BC)-Bus5-BK8” test

In the “UTILITY-8765/1234-LL(BC)-Bus5-BK8” test, the fault block was set for a line-to-line (LL) fault at B-C lines. In the fault block, the fault was triggered by the external control of fault timing controlled by the control fault timing circuit placed on the SC_console subsystem. Figure 10.5 shows the fault block’s mask.

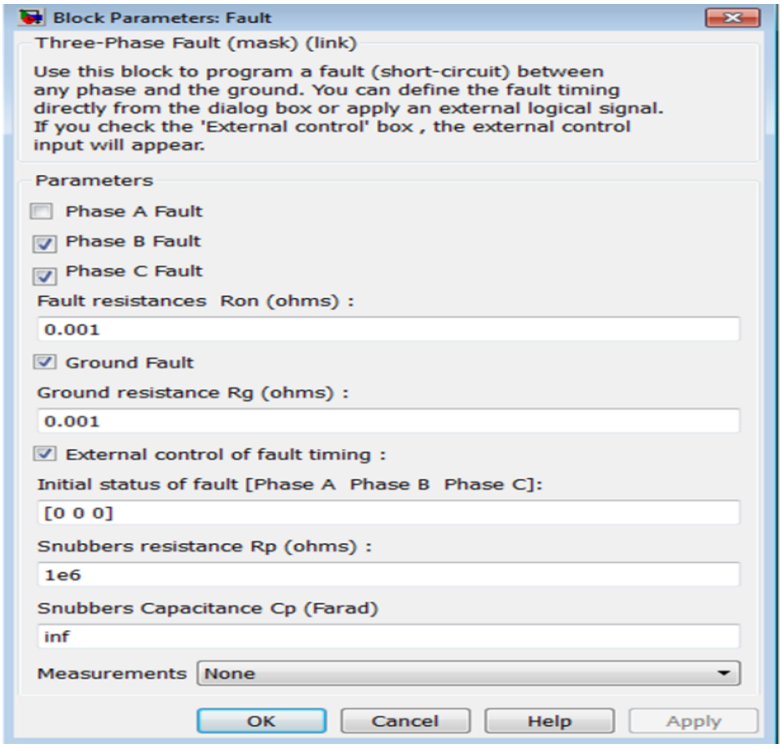

Figure 10.5: Fault block mask

In the “UTILITY-8765/1234-LL(BC)-Bus5-BK8” test, the “BK8” breaker was expected to trip. After the “BK8” breaker tripped as expected, the C8 record event of the “BK8” breaker for Relay 3 was recorded. Figure 10.4-B shows the breaker record event selector of the microgrid. Table 10.2 indicates settings of the breaker record event selector for recording event files of breakers for Relays 2 and 3.

Table 10.2: Settings of breaker record event selector

RELAY2_BK_EVENT[(1)]		RELAY3_BK_EVENT[(1)]	
BK5	BK6	BK7	BK8
0	1	0	1

[(1)]Based on the recording of C8 event files

As an example, to collect the C8 record event of the “BK8” breaker for the “UTILITY-8765/1234-LL(BC)-Bus5-BK8” test, in the “RELAY3_BK_EVENT” cell was set “1” instead of “0”, based on Table 10.2.

Setting groups of the relays were selected in the setting group circuit of the SM_Network subsystem. Figure 10.6 shows the setting group circuit for Relays 2 and 3. Dashed red circles indicate the four and six available setting groups for Relays 2 and 3, respectively.

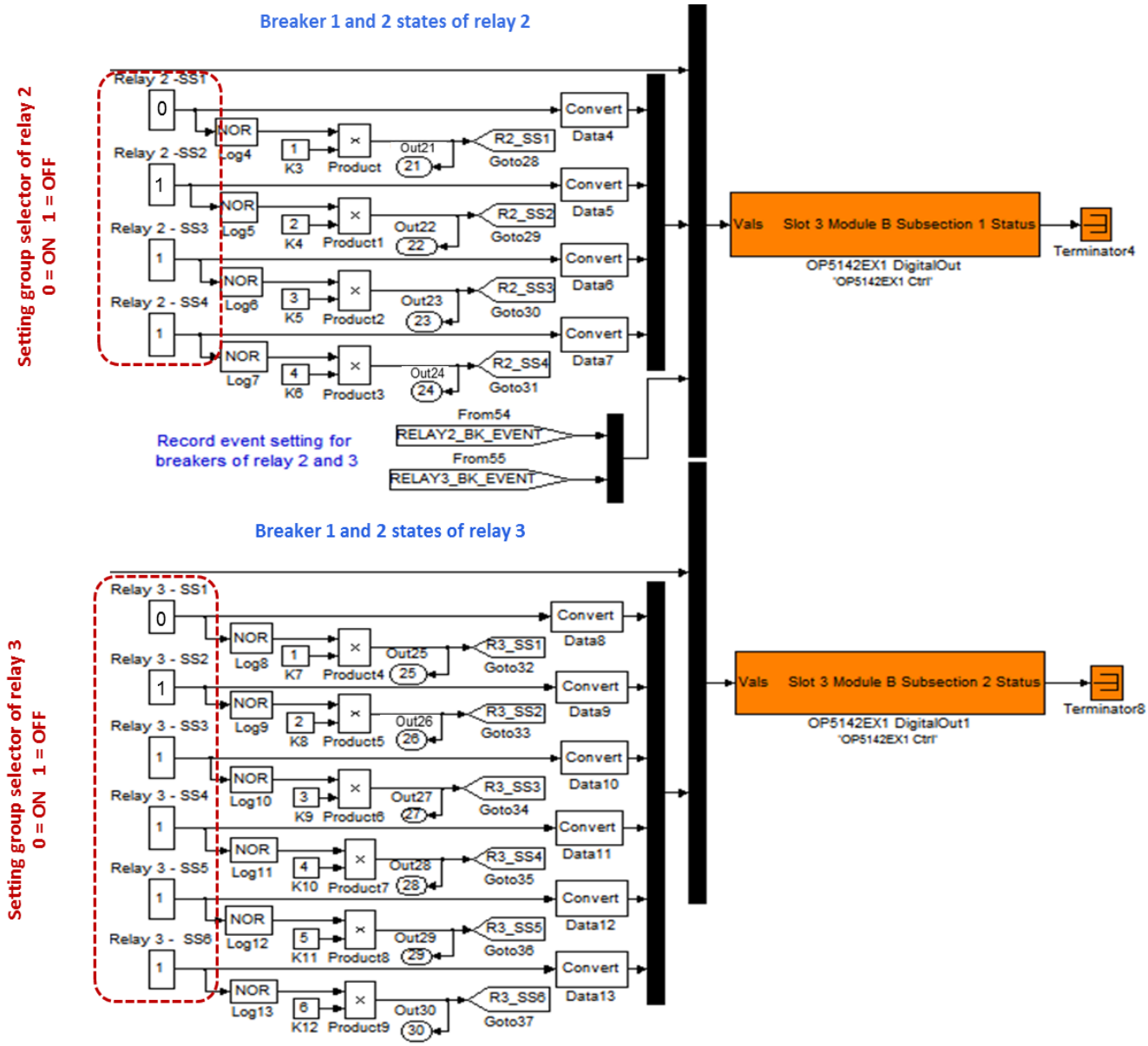

Figure 10.6: Setting group circuit in the SM_Network subsystem

Table 10.3 shows parameters for setting groups of Relays 2 and 3. In the microgrid for the "UTILITY-8765/1234-LL(BC)-Bus5-BK8" test, setting group 1 (SS1) for Relays 2 and 3 was set by placing "0" in the "Relay 2-SS1" and "Relay 3-SS1" cells and "1" in the other relay setting group cells.

Table 10.3: Parameters to set groups of Relays 2 and 3 in the setting group circuit

Circuit path	Setting groups of Relay 2				Setting groups of Relay 3					
	SS1	SS2	SS3	SS4	SS1	SS2	SS3	SS4	SS5	SS6
UTILITY-8765/1234	0	1	1	1	0	1	1	1	1	1
DG2-678/65	1	0	1	1	1	0	1	1	1	1
DG2-678	1	0	1	1	1	1	0	1	1	1
DG2-67/65	1	1	0	1	1	0	1	1	1	1
DG2-6543	1	1	1	1	1	0	1	1	1	1
DG2-65	1	1	1	1	1	0	1	1	1	1
DG2-6781	1	0	1	1	1	1	0	1	1	1
DG2-678	1	0	1	1	1	1	0	1	1	1
DG2-67	1	1	0	1	1	1	1	0	1	1
DG1-5678	1	1	1	0	1	1	1	1	0	1
DG1-34/56	1	1	1	1	1	1	1	1	1	0
DG2-6	1	1	1	1	1	1	1	1	1	0
DG3-2187	1	1	0	1	1	1	1	1	1	1

By defining the circuit path (1), placing the fault type and location (2), choosing the breaker record event (3), and setting the relay setting groups (4), real-time tests for the RTS experiment were edited before initiating the preparation phase.

10.2 Preparation phase

In the Preparation phase, the Redhat® [88] target platform was selected, and the model of the microgrid was built. Figure 10.7 shows "Set" and "Build" options selected in the editor during the Preparation phase. In the "Set the development properties" option was selected the Redhat® [88]

target as platform to communicate with host and target computers during the RTS experiment tests. Figure 10.8 shows the target platform selected on the development settings.

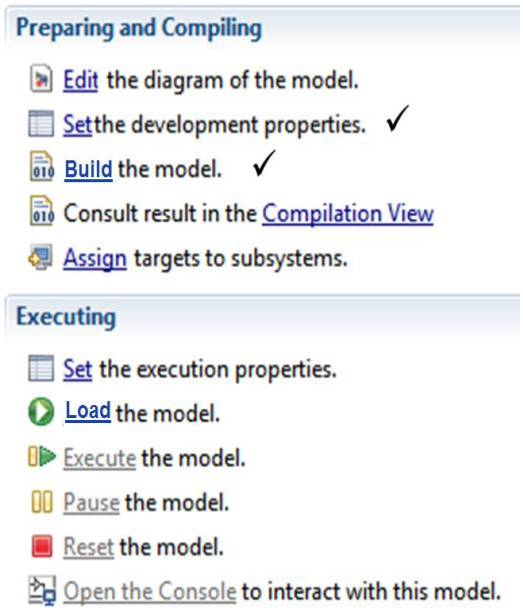

Figure 10.7: Set and build options in the editor

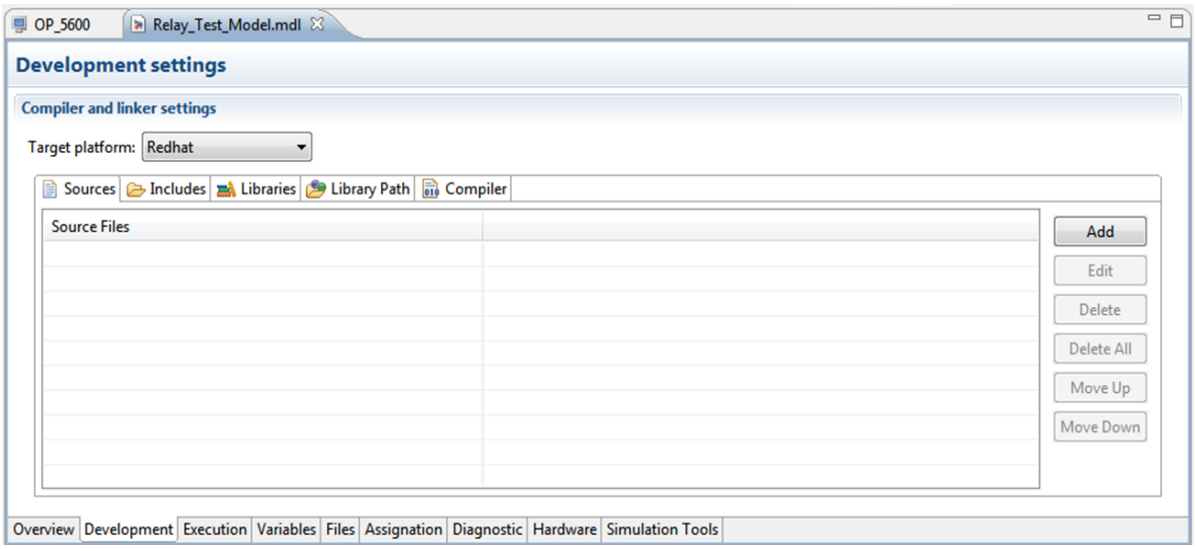

Figure 10.8: Development settings

The “Build the model” option was selected in the editor to build the model that was edited in the Edition phase. The test model was compiled after being built satisfactorily. Figure 10.9 shows the

"Progress" (left) and "Views" (right) windows when the model was built (A) and compiled (B). In the Preparation phase, the Redhat® [88] target platform was set and the model and compilation was built satisfactorily.

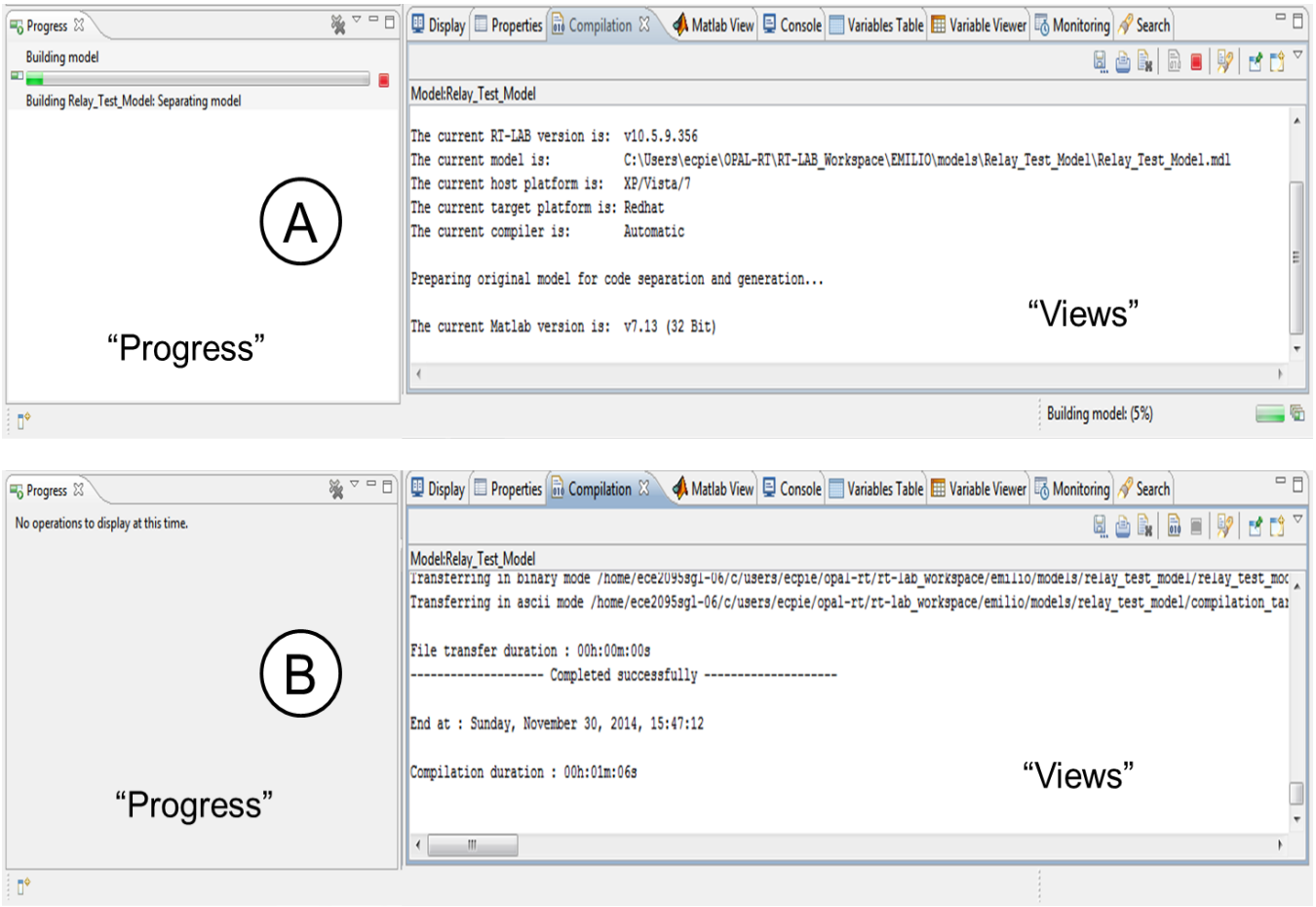

Figure 10.9: Views and progress windows when the model was built (A) and compiled (B)

10.3 Compilation phase

In the Compilation phase, the results from the compilation view were consulted and the target computer was assigned. However, if the model was built satisfactorily in the Preparation phase, the model was compiled successfully. Figure 10.10 shows the "Compilation View" and "Assign" options selected in the editor during the Compilation phase.

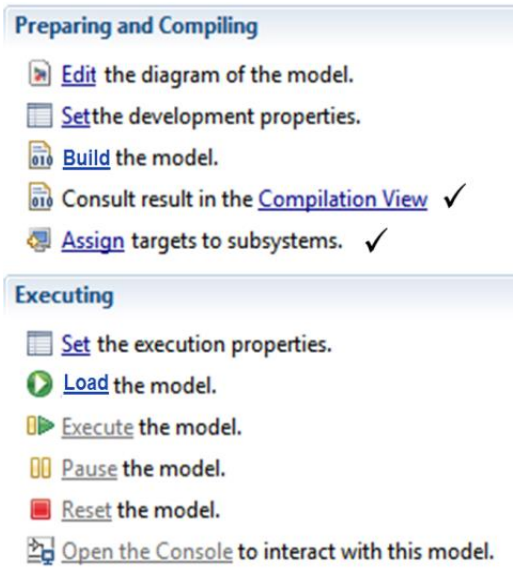

Figure 10.10: “Compilation View” and “Assign” options in the editor

In real-time simulation, the OP-5600 (target computer) was connected to the host computer in order to run the real-time test. Figure 10.11 shows subsystem settings. In the real-time tests, “OP_5600” was chosen as a physical node, and the subsystems were set to run in eXtreme High Performance (XHP) mode. The “Clean target” button could be clicked to eliminate the selected target computer or it could be clicked if a new target computer was selected. The selected target computer was “OP_5600” because it was connected to Relays 2 and 3. In the Compilation phase, compilation view results were consulted and the target computer was assigned to subsystems for real-time tests.

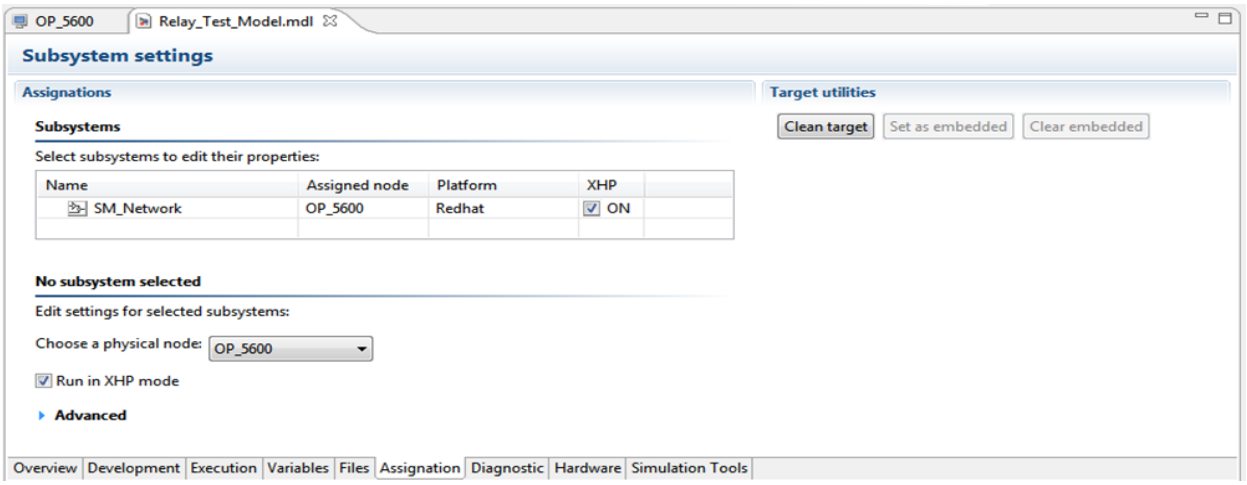

Figure 10.11: Subsystem settings

10.4 Execution phase

In the Execution phase, execution properties required to run the test were set and the model was loaded into the target computer and executed. However, the second console needed to be set after loading the model. The second console was set to supervise the real-time test during the execution of RTS experiment tests. Figure 10.12 shows the "Set," "Load," and "Execute" options selected in the editor during the Execution phase.

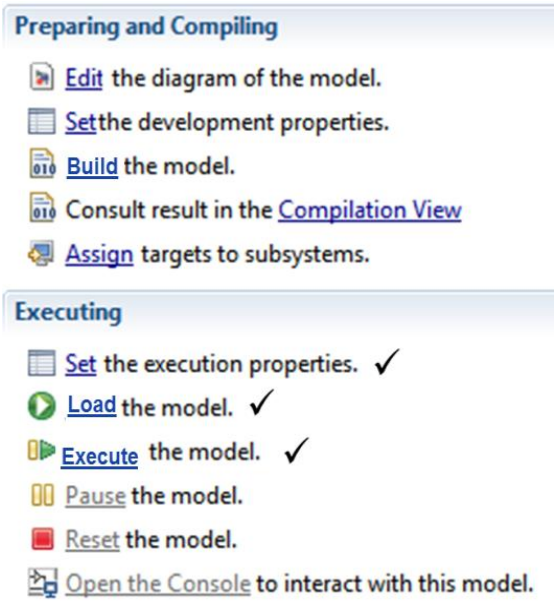

Figure 10.12: "Set," "Load," and "Execute" options in the editor

As shown in Figure 10.13, execution property settings were defined to perform real-time tests. Detection of overruns was enabled in the performance properties, and "Continue" was selected in the action to perform on overruns. The number of steps without overruns was set at 10. Execution of the test that detected overruns improved performance of the real-time simulation because it indicated any overrun situation during the simulation. Redhat® was selected as target platform for real-time properties. Hardware was synchronized as real-time simulation mode and UDP/IP as real-time communication link type. The "time factor" was set at 1.0 to perform the real-time test. If the "time

factor" was greater than 1.0, generated power system frequency was less than 60 Hz. Power system frequency was measured on the relay display, verifying that the "time factor" was set at 1.0.

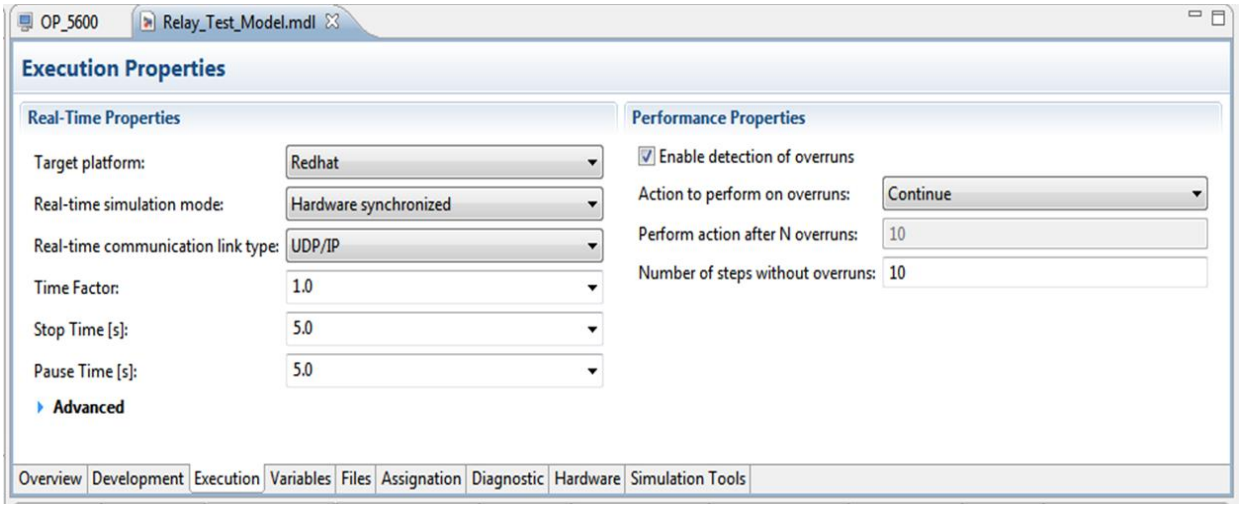

Figure 10.13: Execution properties of tripping tests for RTS experiment

In Figure 10.13, "stop time" defines the time when the real-time simulation test ended. "Stop time" had to be set at 5 sec. in order to complete pre-fault, fault, and post-fault states during tripping tests in real-time simulation. However, in non-tripping tests, "stop time" values were less than 5 sec., thereby preventing relays from tripping at fault state. Equations (10.1) and (10.2) indicate conditions of "stop time" for tripping and non-tripping tests, respectively.

$$T_{S1} > T_{PF} + T_{C1} \tag{10.1}$$

$$T_{PF} < T_{S2} < T_{PF} + T_{C1} \tag{10.2}$$

where T_{S1} is stop time of tripping tests set at 5 sec., T_{S2} is stop time of non-tripping tests in seconds, T_{PF} is pre-fault time set at 2.5 sec. in the second console, and T_{C1} is measured clearing time in seconds for tripping tests. "Pause time" was set at 5 sec. for tripping and non-tripping tests.

When execution properties were set, the "Load the model" option was selected from the editor in order to load the model. Figure 10.14 shows the progress (A) and view (B) windows when the

model was loaded. After the model was loaded and successfully transferred model files, the second console was opened.

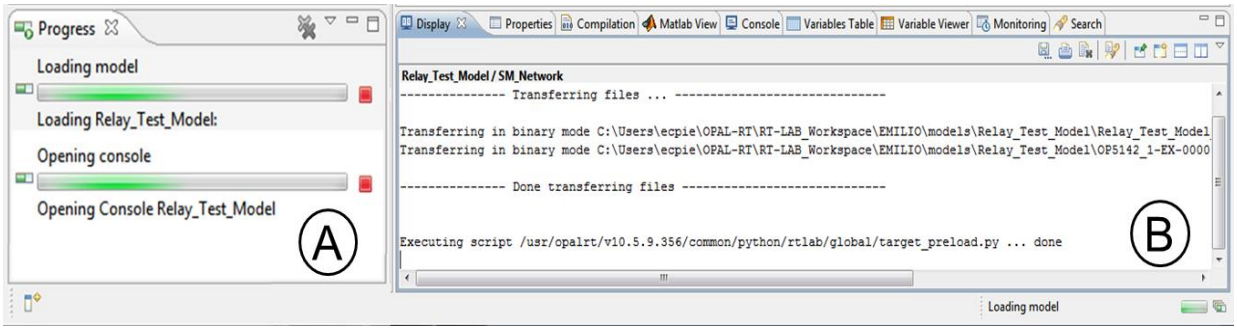

Figure 10.14: “View” (A) and “Progress" (B) windows when the model was loaded

Figure 10.15 shows the second console automatically generated by RT-LAB® during compilation when the model was loaded. The second console contained “OpComm” block (A), control fault timing circuit (B), and scopes of Relays 2 and 3 (C).

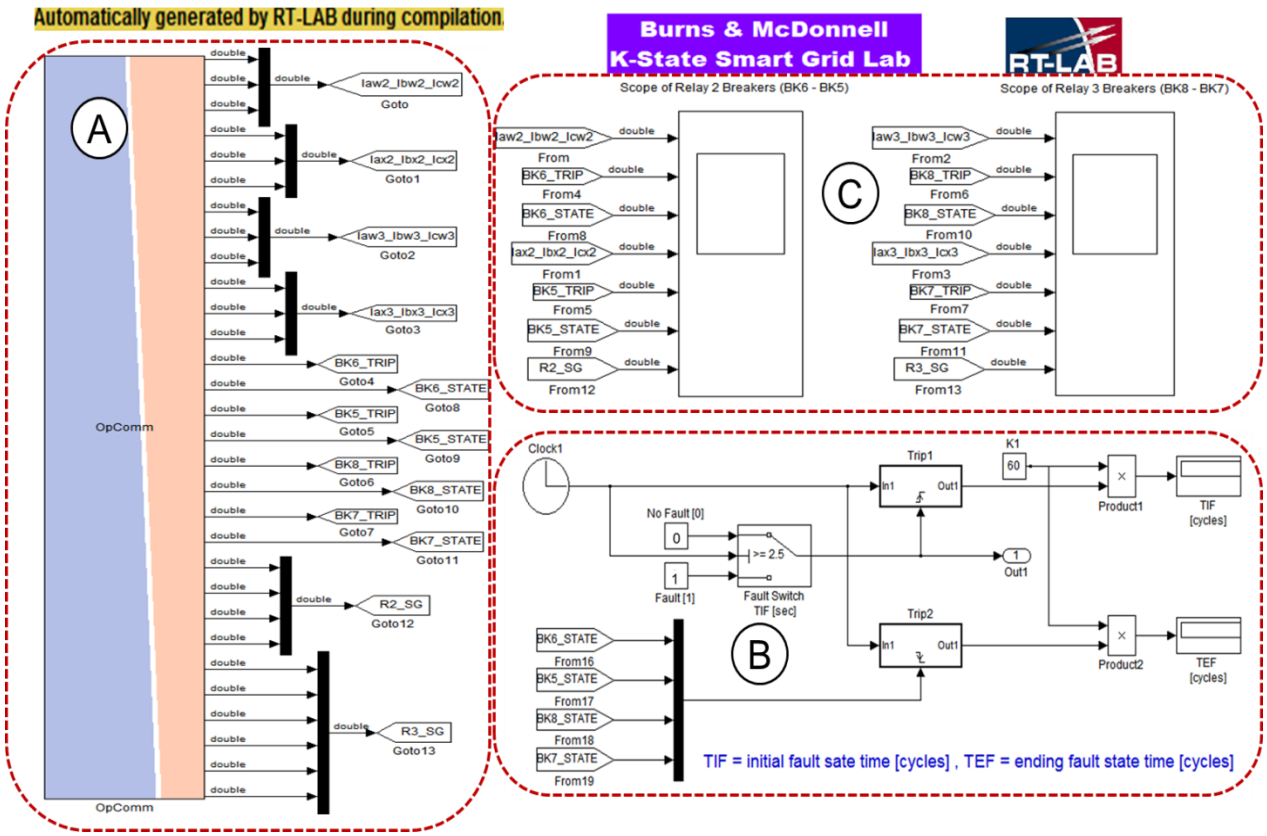

Figure 10.15: Second console automatically generated by RT-LAB® during compilation

The “OpComm” block, shown in Figure 10.5 (A), collected signals from the microgrid in the SM_Network (master) subsystem. These signals included A-B-C line currents, breaker states, trip signals, and relay setting groups. The control fault timing circuit, shown in Figure 10.5 (B), was used to control external fault timing of the fault block in the microgrid from the SM_Network (master) subsystem. Relay 2 and 3 scopes collected signals from the “OpComm” block during the test’s real-time simulation. Once model loading generated the second console, Relay 2 and 3 scopes were opened to set plots that measured A-B-C line currents, breaker states, trip signals, and relay setting groups. Scope plots of Relays 2 and 3 were applied with the identical settings. Figure 10.16 shows plot settings for the scope of Relay 2 in which the scope’s plot was picked up from the “Parameters” menu. The “General” submenu was defined at a time range of 5 sec. and sample time (*Ts*) of 50 microseconds, as shown in Figure 10.16 (A). The “Save data to workspace” option was selected in the “History” submenu, as well as the “Structure with time” option for the “Format,” as shown in Figure 10.16 (B). Finally, line size of 2.0 was selected in the “Graphics” submenu for all lines, as shown in Figure 10.16 (C).

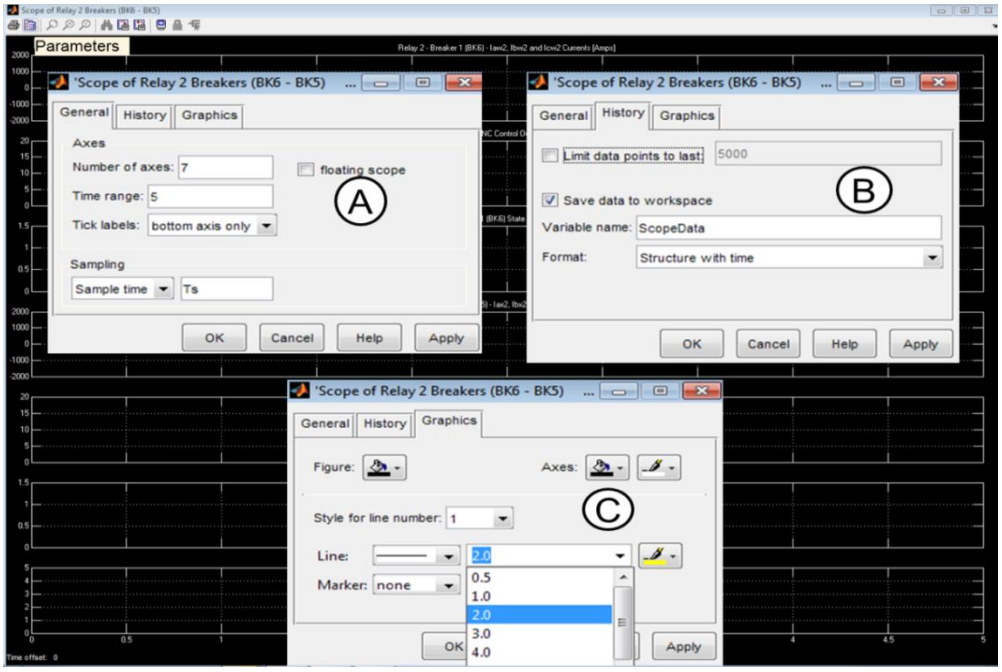

Figure 10.16: Plot settings of Relay 2 scope in second scope

Figure 10.17 shows plots of Relay 3's scope collected from the second scope during execution of the overcurrent fault test when Relay 3 tripped "BK8" breaker and kept the "BK7" breaker closed. Figure 10.17 (A) and (D) show A-B-C line currents of "BK8" and "BK7" breakers, respectively, and Figure 10.17 (B) and (E) show "BK8" and "BK7" trip signals, respectively. Figure 10.17 (C) and (F) show "BK8" and "BK7" breaker states, respectively, and Figure 10.17 (G) shows the active setting group (SS2) of Relay 3.

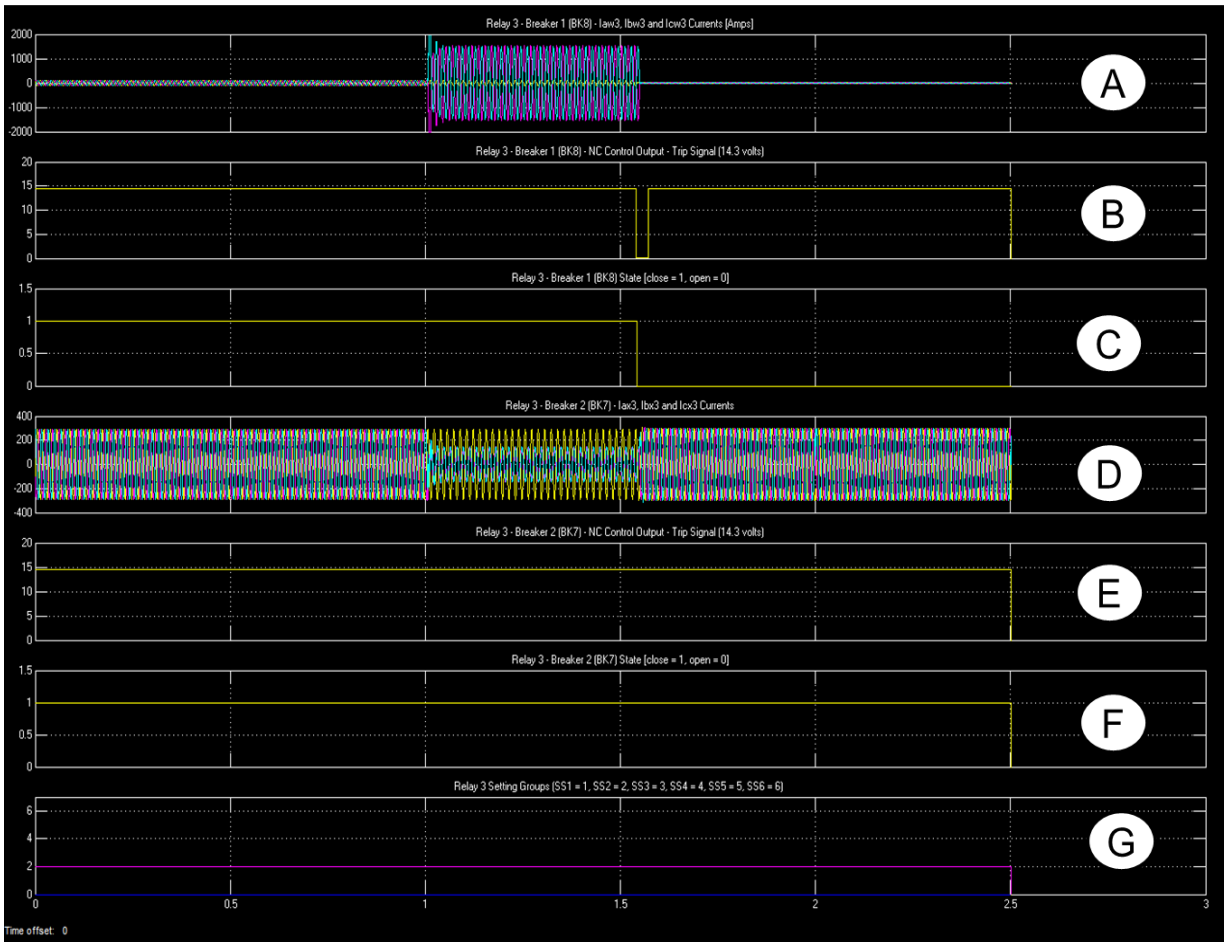

Figure 10.17: Plots of Relay 3 scope

Relay scopes were applied in order to supervise the tests during execution of real-time simulation; however, relay scopes were not applied to collect test results. In the second console, relay scope plots did not have a sinusoidal waveform of A-B-C line currents when "stop time" of real-time simulation was set at more than 3 sec.. Real-time tests were set at "stop time" of 5 sec. because setting

groups of relays were selected during the pre-fault state and Relay 3's setting group required more than 3 sec. (180 cycles) to perform pre-fault, fault, and post-fault states.

Plotted sinusoidal waveforms of A-B-C line currents were not sinusoidal in the second console because the console subsystem (SC_console) was not executed in real-time. The SM_Network (master) subsystem was executed in real-time, while the SC_console subsystem was executed on workstation in non-real-time. The SC_console subsystem communicated with the "OP-5600" real-time simulator to obtain a burst of data according to settings applied in the acquisition. For more than 3 sec., acquisition settings did not allow the plot of a sinusoidal waveform for A-B-C line currents, but test results were collected satisfactorily in real-time by placing an "OpWriteFile" block in the SM_Network (master) subsystem. The "OpWriteFile" block was configured to collect A-B-C line currents, breaker states, trip signals, and relay setting groups. When the test was executed in real-time, the "OpWriteFile" block created a Matlab® file that collected signals to be plotted as test results.

In the second console (SC_console), the control fault timing circuit was set to the time to initiate the fault by the external control of fault timing of the fault block (SM_Network). As shown in Figure 10.18, external control of the fault timing was controlled from the second console (SC_console), and the fault switch was set at 2.5 sec. after initiating the pre-fault state. Figure 10.18 shows the control fault timing circuit in the second console (SC_console).

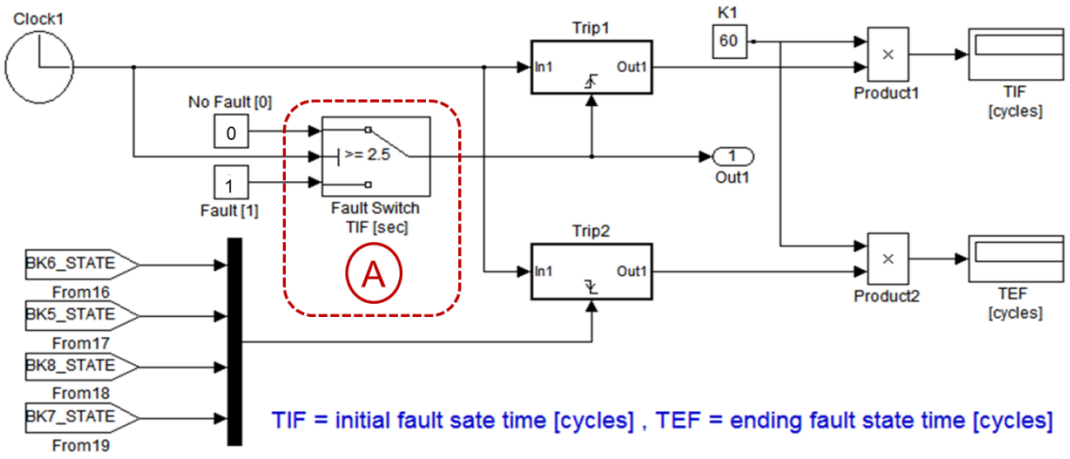

Figure 10.18: Control fault timing circuit in the second console (SC_console)

A clock with a fault switch (Figure 10.18 (A)) was set at 2.5 sec. controlled the control fault timing circuit. By the clock, "1" signal was generated at 2.5 sec. after executing the test, and "1" signal was sent by the "Out1" to the external control of the fault block in the microgrid (SM_Network). At the end of real-time simulation, initial and ending fault state times were collected in cycles from the control fault timing circuit in order to estimate the measured fault clearing time for tripping tests by Equation (10.3).

$$T_{C1} = T_{EF} - T_{IF} \tag{10.3}$$

where T_{C1} is measured fault clearing time for tripping tests in seconds, T_{EF} is measured ending fault time for tripping tests in seconds, and T_{IF} is measured initial fault clearing time for tripping tests in seconds. In the SM_Network (master) subsystem, the "OpWriteFile" block measured and recorded A-B-C line breaker currents, trip signals, breaker states, and relay setting groups of Relays 2 and 3 during real-time tests. The "OpWriteFile" block generated the "opvar2and3" variable at the end of each test that recorded real-time simulation results. The "OpWriteFile" block recorded results during real-time tests (Figure 10.19).

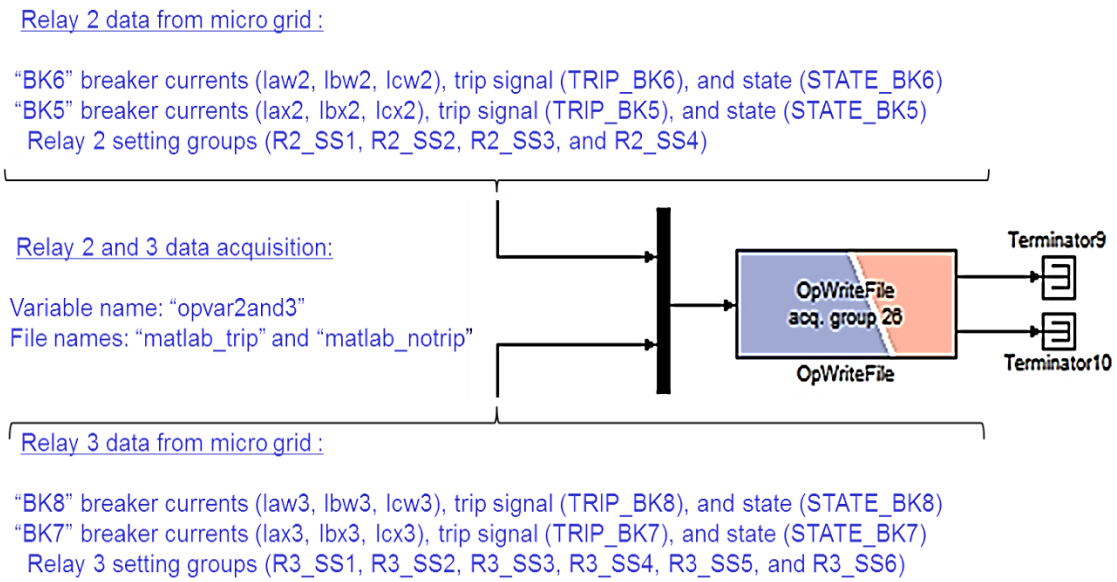

Figure 10.19: Data recorded from the "OpWriteFile" block

After setting plots of relay scopes and the control fault timing circuit in the second console (SC_console), the “Execute model” option was selected from the editor to execute real-time simulation. When the model was executed and the real-time test was finished, “Progress” indicated “No operations to display at this time” and a window was generated on the right corner of the “Views” screen that indicated “New file available.” The Matlab® file generated by the “OpWriteFile” block, containing signals plotted as test results, was saved into a folder when the “New file available” option was selected. Figure 10.20 shows “Progress” (A) and “Views” (B) windows after executing the model.

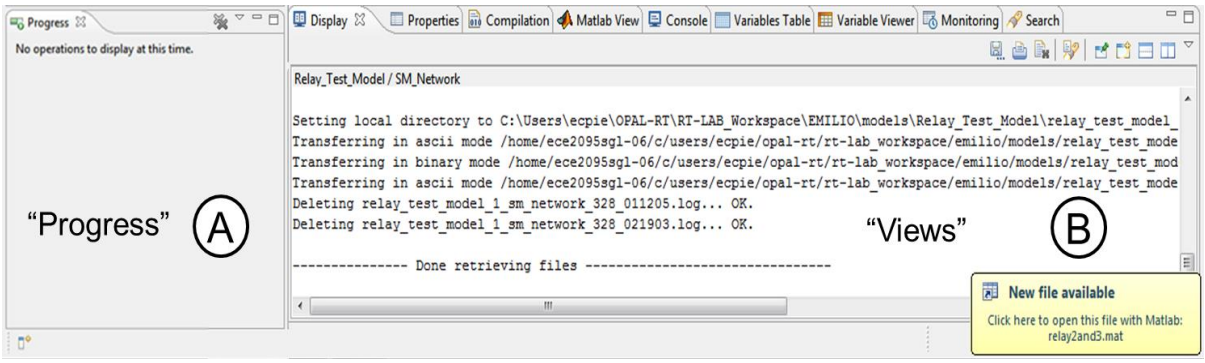

Figure 10.20: “Progress” (A) and “Views” (B) windows after executing the model

In the Execution phase, execution properties were set and the model was loaded. In the second console (SC_console), plots of the relay scopes and fault time were set before executing the real-time test. After the real-time test was executed, test results were collected from the generated Matlab® file.

10.5 Collection phase

In the Collection phase, the relay’s display and pushbutton LEDs (1), record event files (2), and generated Matlab® files (3) were collected. The Matlab® files and relay record events collected time, A-B-C line currents, trip signals, breaker states, and relay setting groups. Information related to Matlab® and record event files originated from the microgrid and relays, respectively. Test results were measured from the microgrid and relays in order to validate real-time simulation and application of the OP5600 as a real-time relay test system and evaluate the adaptive overcurrent protection system.

The relay's display and pushbutton LEDS were collected to verify adaptive overcurrent protection during the execution of real-time tests. Table 10.4 shows collected data, sites, sources, and measurements of real-time tests. Figure 10.21 shows the power desk (A) from which real-time tests were executed and supervised and the rack area. As shown in Figure 10.21 (A), the webcam, HMI and host computers were applied to measure the display and pushbutton LEDs, record events, and Matlab® files, respectively.

Table 10.4: Collected data for real-time tests

Collected Data	Sites	Sources	Measurements
Display and pushbutton LEDs	Webcam computer	Relays 2 and 3	Breaker line currents and breaker trips from the relay's front panel
Record events	HMI computer		A-B-C line currents and event reporting digitals (trip signals, control inputs and outputs, setting groups, SELogic variables, and breaker states)
Matlab® files (mat. files)	Host computer	Microgrid	Time, A-B-C line currents, trip signals, breaker states, and relay setting groups for the Relays 2 and 3

HMI: Human machine interface

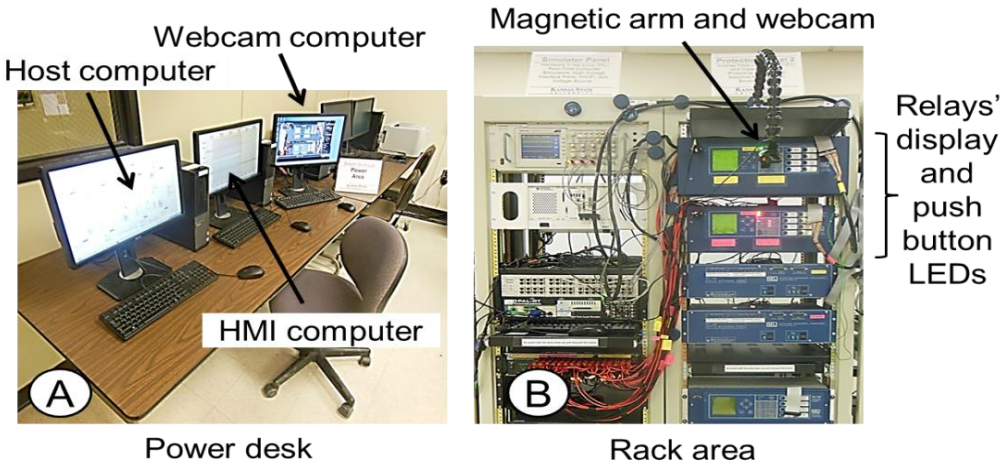

Figure 10.21: Power desk (A) and rack area (B)

10.5.1 Display and pushbutton LEDs

The relay's display and pushbutton LEDs were measured during execution of the real-time tests. Relays' display and pushbutton LEDs were evaluated from the webcam computer, as shown in Figure 10.21 (A). The relay's front panel (displays and pushbutton LEDs) was observed for Relays 2

and 3 with a webcam placed in a magnetic arm through the webcam computer on the power desk. Breaker 1 and 2 line currents for Relays 2 and 3 were observed on the relay's display during execution of the real-time tests, verifying load and fault currents for pre-fault and fault states, respectively, and zero current at post-fault state. Breaker 1 and 2 states (closed and open) were observed on pushbutton LEDs on the relay's front panel, verifying satisfactory performance of the breakers during tripping and non-tripping tests, respectively.

10.5.2 Record events

Record event files from the relays were collected only for tripping tests. Record events of relays were not recorded for non-tripping tests because the relays had to trip in order to generate event files. C8 and HR record events were collected from the relays and read after execution of each tripping test in real-time simulation. AcSELerator Quickset® [11] and AcSELerator Analytic Assistant® [100] software were applied to collect and read record events, respectively.

The HMI computer needed to communicate with the relay that tripped in the tripping test, so AcSELerator Quickset® software [11] was applied in order to communicate with the relay and collect record event files. The relay communication process was initiated by connecting the SEL C662 cable from the relay's Port F to HMI computer's USB connector. AcSELerator Quickset® software [11] was opened and the "Communication" option was selected, as shown in Figure 10.22 (A). The "SERIAL" communication and "SEL CP210x USB to UART Bridge" port device were selected (Figure 10.22 (B)), thereby completing the data speed, data bits, stop bits, parity, RTS/CTS, DTR, XON/XOFF, RTS, and Level 1 and 2 passwords based on the SEL 451 relay's instruction manual [5]. Level 1 and 2 passwords were "OTTER" and "TAIL," respectively. Figure 10.22 shows communication parameters of SEL 451 relays. As shown in Figure 10.23, when the relay communicated with the HMI computer, screen indicated "Open: Connected" at the lower bar of the computer screen. The "Tools" menu, "Events," and "Get Event Files" submenus were then selected.

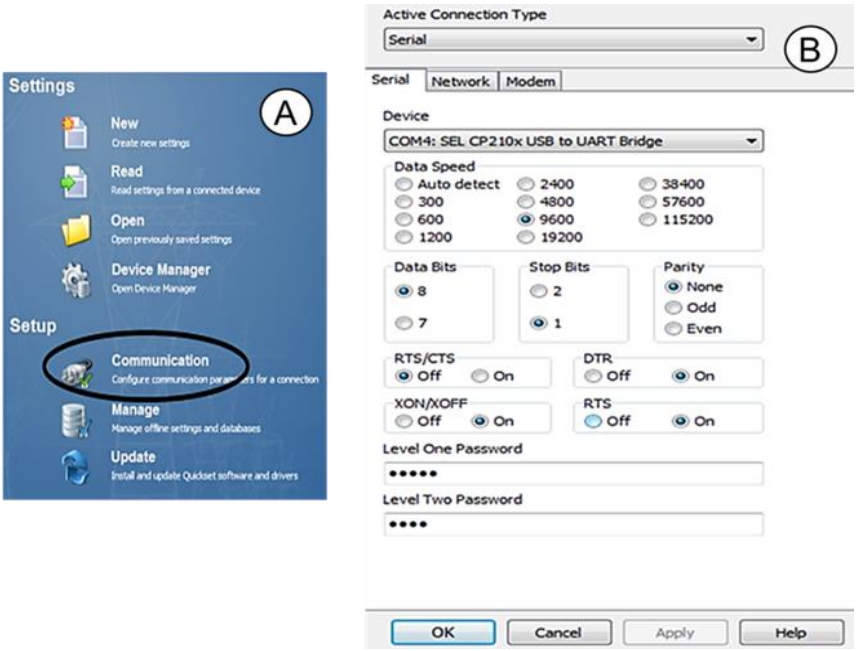

Figure 10.22: Communication parameters of SEL 451 relays

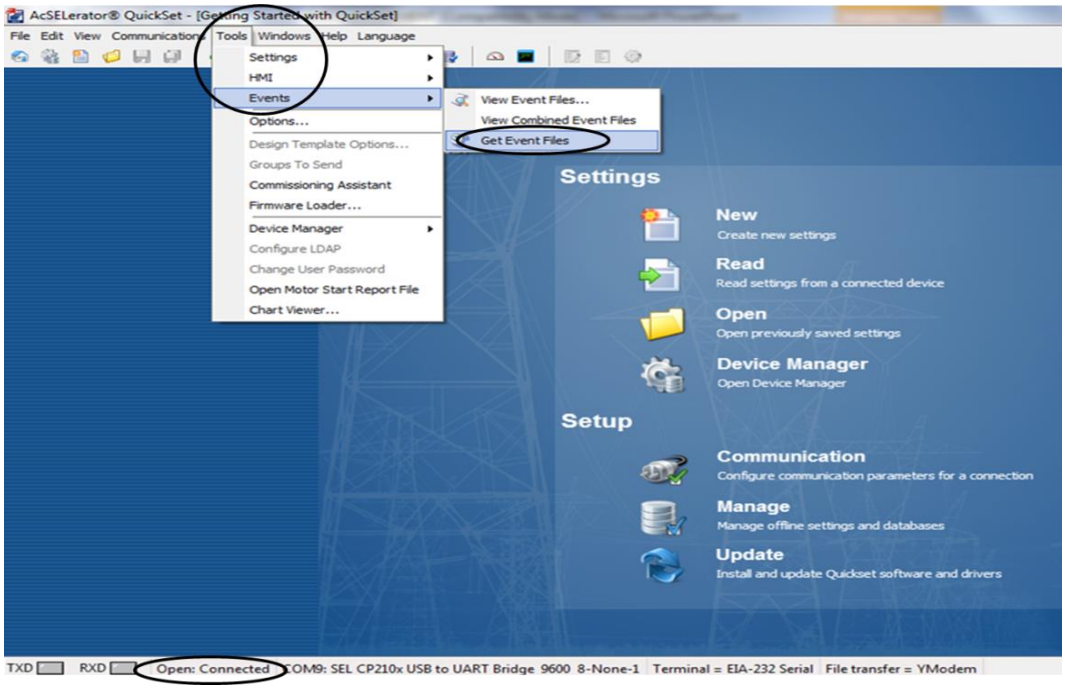

Figure 10.23: “Get event” files

When the list of event files was transferred from the relay, that list was read on the “Event History.” From the “Event Type” menu was selected the “Binary COMTRADE” and “CEV8” event types for HR and C8 event files, respectively, as shown in Figure 10.24 (A). When the selected record

event file was completely transferred, the record event file was saved into a folder that corresponded to tripping tests of this record event, demonstrated in Figure 10.24 (B).

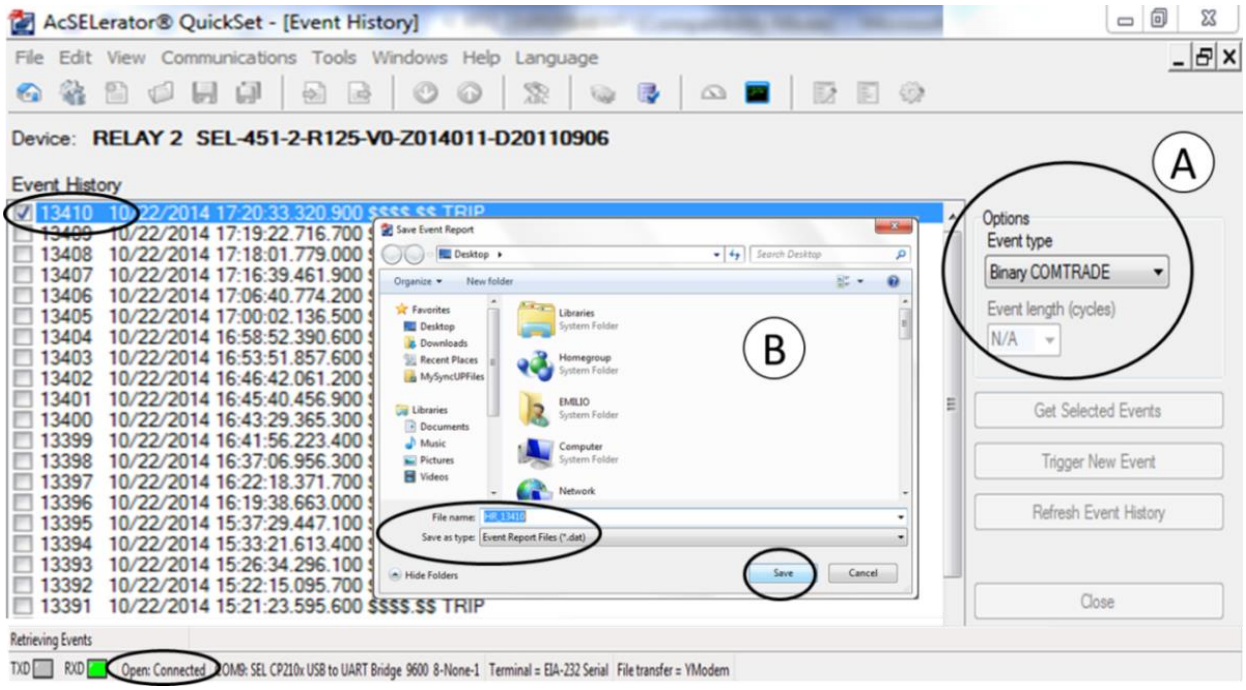

Figure 10.24: Transferring and saving record event file

SEL 451 relays provide two types of event data captures: event report oscillography with filtered sample per cycle data and unfiltered (raw) data [5]. In C8 record events, A-B-C line currents depended on how the “Current and Voltage Source Selection” (ESS) setting was defined on the relay, recording the IW, IX, or a combination (IW + IX) of line currents. Although C8 record events were filtered reports that included digital filtering, HR record events were raw reports that did not incorporate digital filtering. In addition, the size of HR event files was greater than size of C8 event files. The time required to collect HR event files was greater than the time required to collect C8 event files because C8 record events had fewer samples per cycle to plot A-B-C line currents than HR record events. Figure 10.25 shows data points for C8_13115 and HR_13115 event files that corresponded to the “DG2-678/65-SLG(A)-BUS6-BK7” test. A-B-C lines currents of C8_13115 and HR_13115 record events are shown in Figures 10.25 (A) and (B), respectively.

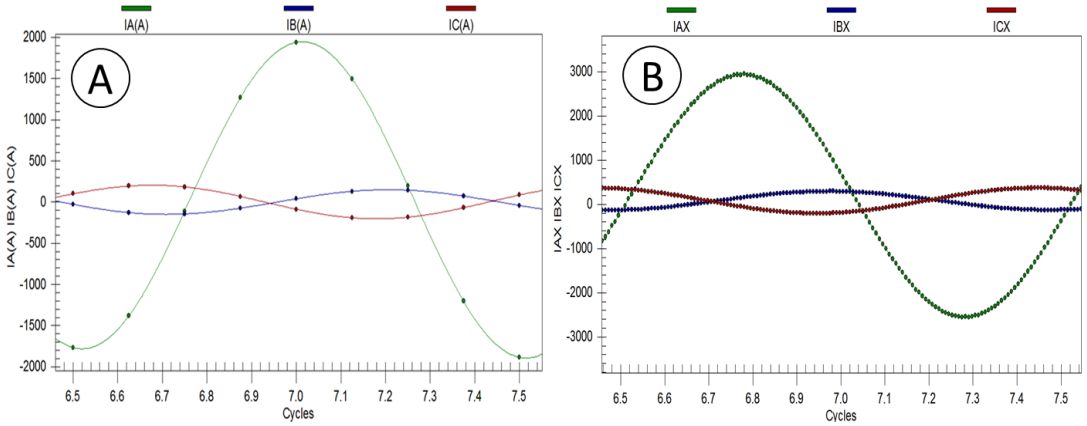

Figure 10.25: Line currents from C8_13115 (A) and HR_13115 (B) event files, respectively

AcSELerator Analytic Assistant® [100] software was used to read C8 and HR record event files. In tripping tests, plots with instantaneous and magnitude A-B-C line currents and trip digital signals were read from the event report summary of C8 event files. However, instantaneous A-B-C line currents and digital signals (setting groups, control inputs and outputs, SELogic variables, trip, overcurrent element, and breaker auxiliary contact) were plotted according to HR event files. Table 10.5 indicates the read information and plot signals from C8 and HR event files. For C8 event files, the breaker recorded event was set before executing the tripping test by selecting the recorded event of the breaker expected to trip.

Table 10.5: Information read from C8 and HR event files

C8 Event Files[(1)]	**HR Event Files**[(2)]
Event report summary	Plot of instantaneous A-B-C line currents and digital signals (setting groups, control inputs and outputs, SELogic variables, trip, overcurrent element, and breaker aux. contact)
Plot of instantaneous A-B-C line currents and trip digital signal	
Plot of magnitude A-B-C line currents and trip signal	

C8 (compressed-8-samples-per-cycle), HR (high resolution) [(1)] IW, IX or combination (IW+IX) line currents, [(2)] IW and IX line currents

Figures 10.26 to 10.28 show the steps required to read the event report summary of the C8_13115 event corresponding to the“DG2-678/65-SLG(A)-BUS6-BK7” tripping test. AcSELerator Analytic Assistant® [100] software was opened (Figure 10.26 (A)) and then the “File” menu and

"Open Event Report File" submenu were selected (Figure 10.26 (B)). When the C8_13115 event file was found in the Desktop, the "All files (*.*)" option was selected, and the C8_13115 file was opened, as shown in Figure 10.26 (C). A left click in the AcSELerator Analytic Assistant® [100] icon was made (Figure 10.27 (A)), the "View" menu and "Summary Data" submenu were selected (Figure 10.27 (B)), and the "Event Report Summary" of the file was opened (Figure 10.27 (C)). The C8_13115 event represented the "DG2-678/65-SLG(A)-BUS6-BK7" tripping test.

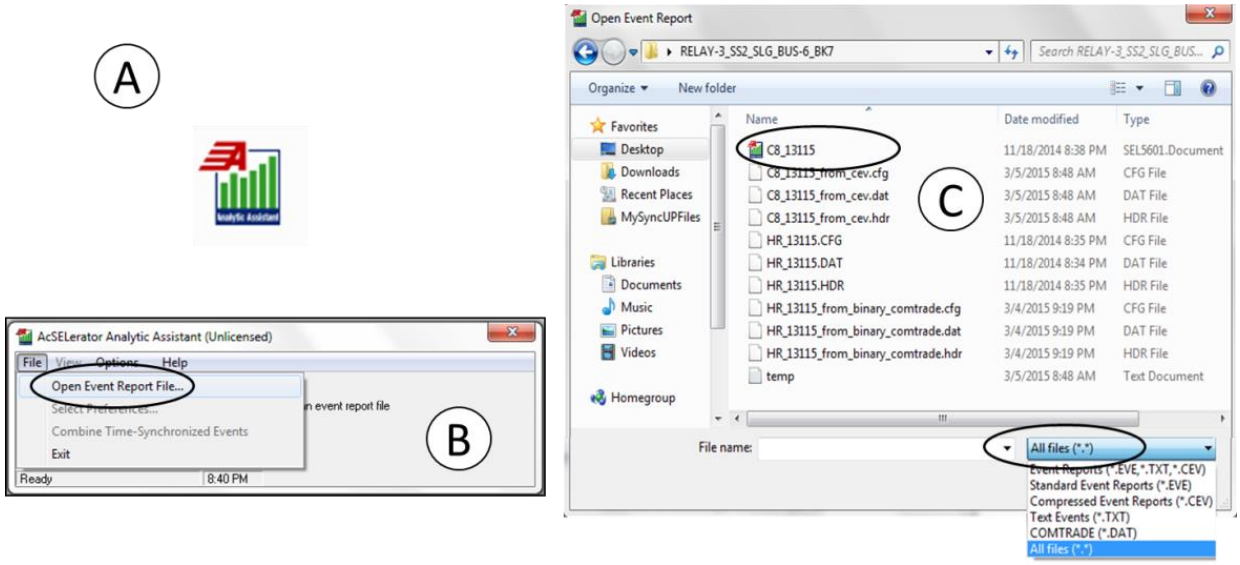

Figure 10.26: Opening a C8 event file

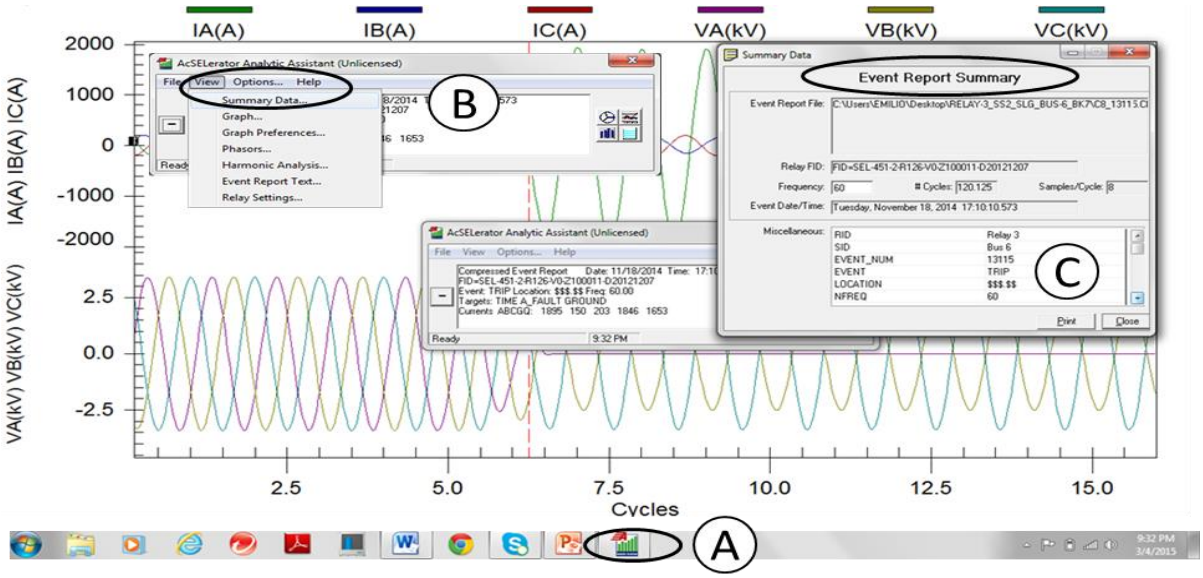

Figure 10.27: Event report summary

In Figures 10.28 (A) and (B), the event report summary of the C8_13115 event was read. From the C8_13115 event, the number and type of events were collected, and the magnitude of primary pickup fault currents were measured. According to the C8_13115 event report summary, states (open or closed) of Breakers 1 and 2 were also collected for Relay 3 from Figures 10.28 (C) and (D), respectively. Figure 10.28 shows the event report summary for the "DG2-678/65-SLG(A)-BUS6-BK7" tripping test.

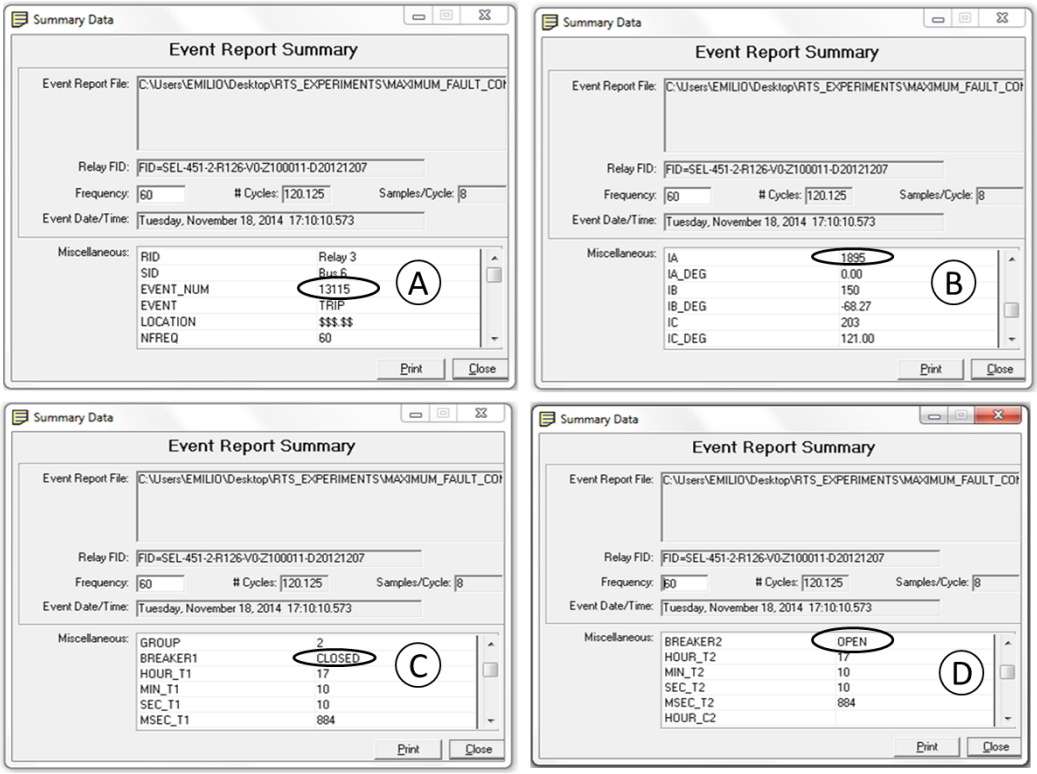

Figure 10.28: Event report summary, C8_13115 event, DG2-678/65-SLG(A)-Bus6-BK7 test

Figures 10.29 to 10.30 show the steps to plot instantaneous A-B-C line currents and trip digital signal of the C8_13115 event corresponding to the"DG2-678/65-SLG(A)-BUS6-BK7" tripping test. After opening the C8_13115 event file, a left click in the AcSELerator Analytic Assistant® [100] icon was made, as shown in Figure 10.29 (A). The "View" menu and "Graph Preferences" submenu were then selected (Figure 10.29 (B)), and the "Time Units, Starting/ Ending Row" option was set in cycles (Figure 10.30 (A)). IA(A) , IB(A), and IC(A) analog signals from the analog list were dragged into

Axis 1 , the TRIP digital signal from the digital list was dragged into the digital axis, and the “OK” cell was selected, as demonstrated in Figure 10.30 (B). As a result, A-B-C line currents and trip signals were plotted (Figures 10.30 (C)) for the C8_13115 event, “DG2-678/65-SLG(A)-BUS6-BK7” test.

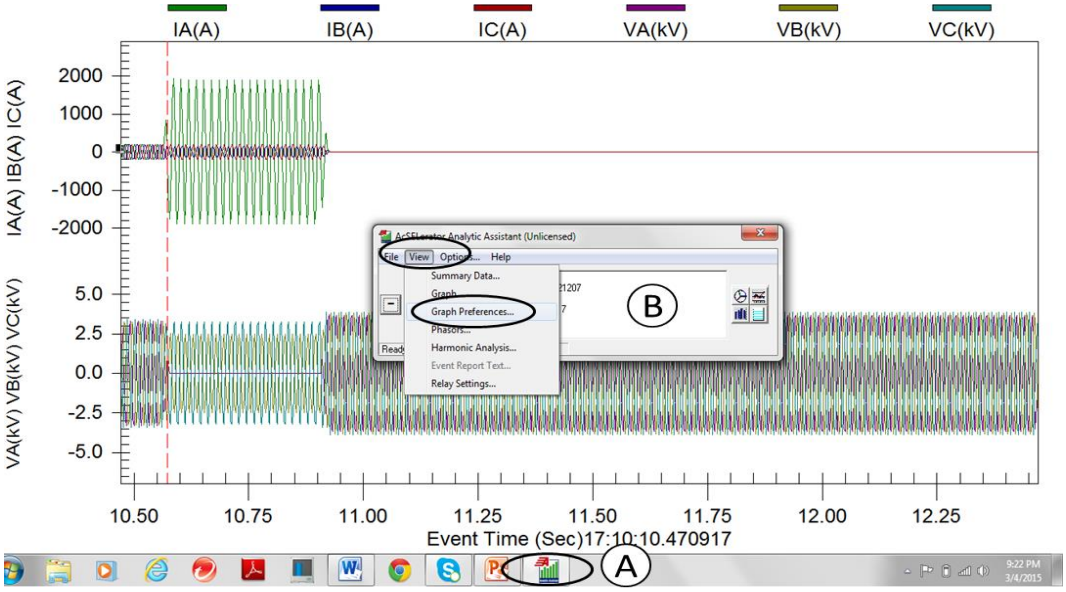

Figure 10.29: Graph preferences of C8 event file

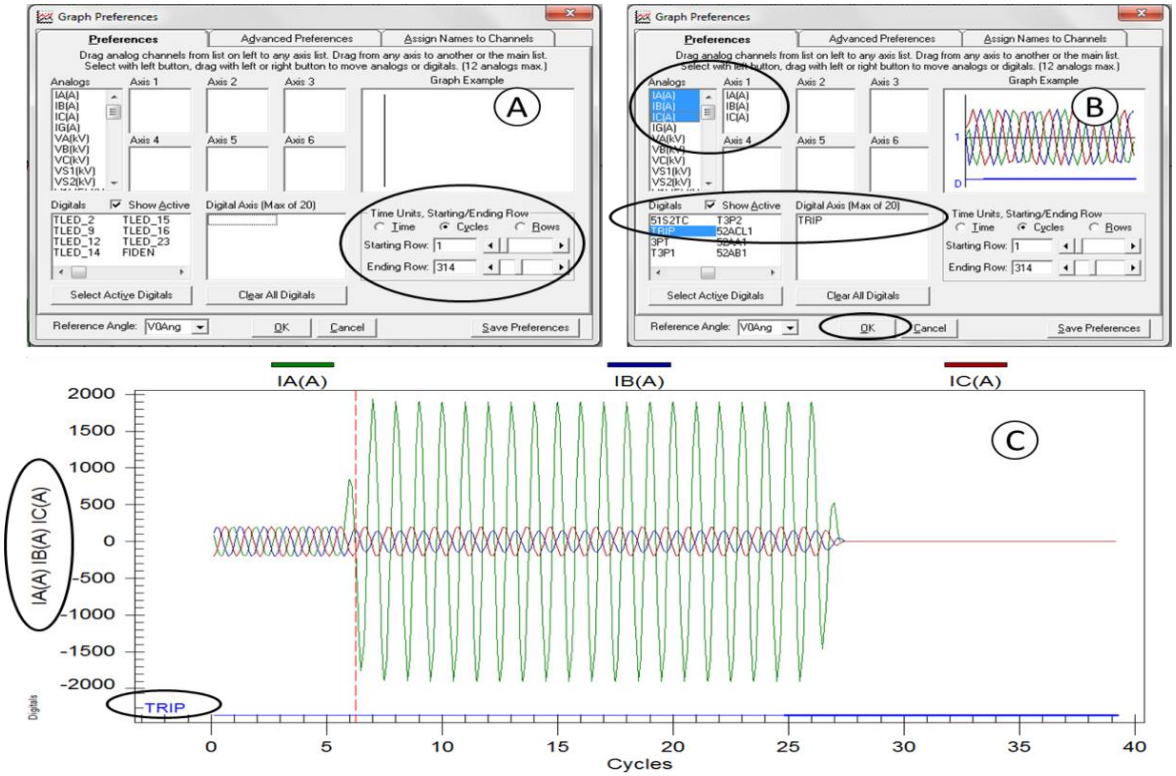

Figure 10.30: Plot of A-B-C line currents and trip signal, C8_13115 event

The magnitude of A-B-C line currents and trip signal of the C8_13115 event, “DG2-678/65-SLG(A)-BUS6-BK7” tripping test was plotted by selecting IA(A)Mag, IB(A)Mag, and IC(A)Mag analog signals. Figure 10.31 (A) shows selected graph preferences. The plot of magnitude A-B-C line currents and trip signal of the C8_13115 event, “DG2-678/65-SLG(A)-BUS6-BK7” test is shown in Figure 10.31 (B).

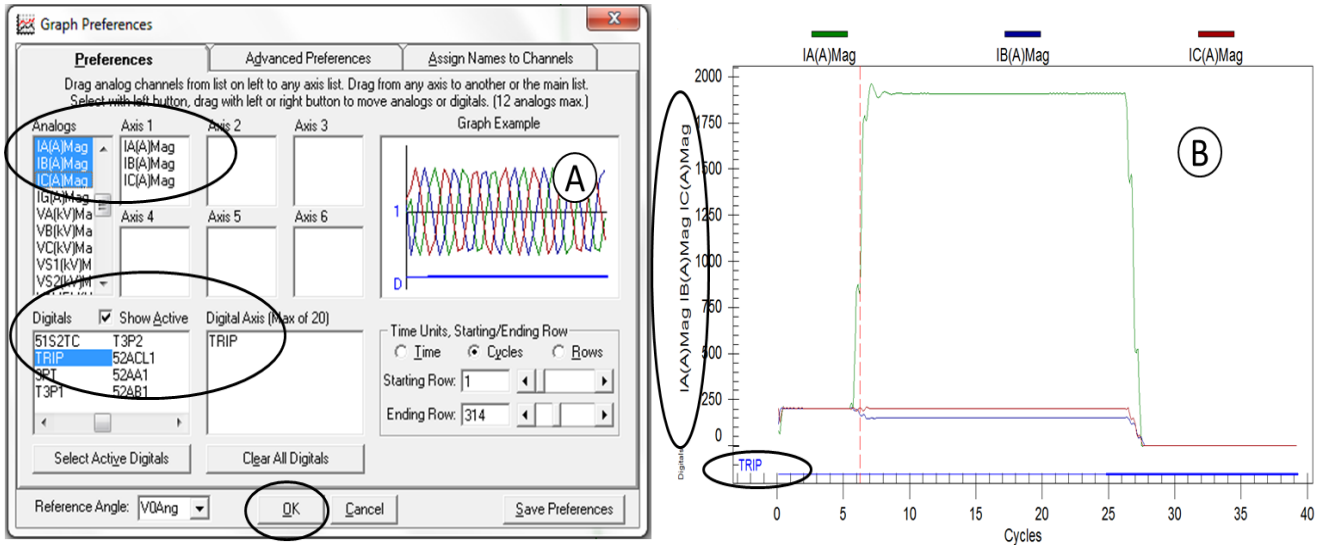

Figure 10.31: Plot of magnitude A-B-C line currents and trip signal, C8_13115 event, DG2-678/65-SLG(A)-Bus6-BK7 test

Figures 10.32 to 10.34 show the steps to plot instantaneous A-B-C line currents and digital signals (setting groups, control inputs and outputs, SELogic variables, trip, overcurrent element, and breaker auxiliary contact) for the HR_13115 event, DG2-678/65-SLG(A)-Bus6-BK7 test. AcSELerator Analytic Assistant® [100] software was opened, as shown in Figure 10.32 (A), and then the “File” menu and “Open Event Report File” submenu were selected, as shown in Figure 10.32 (B). When the HR_13115 event file was found in the Desktop, the “All files (*.*)” option was selected, and the HR_13115 file was opened, as shown in Figure 10.32 (C). After opening the HR_13115 event file, on the lower bar of the screen, a left click on the AcSELerator Analytic Assistant® [100] icon on the

screen's toolbar was made (Figure 10.33 (A)) and the "View" menu and "Graph Preferences" submenu were selected, as shown in Figure 10.33 (B).

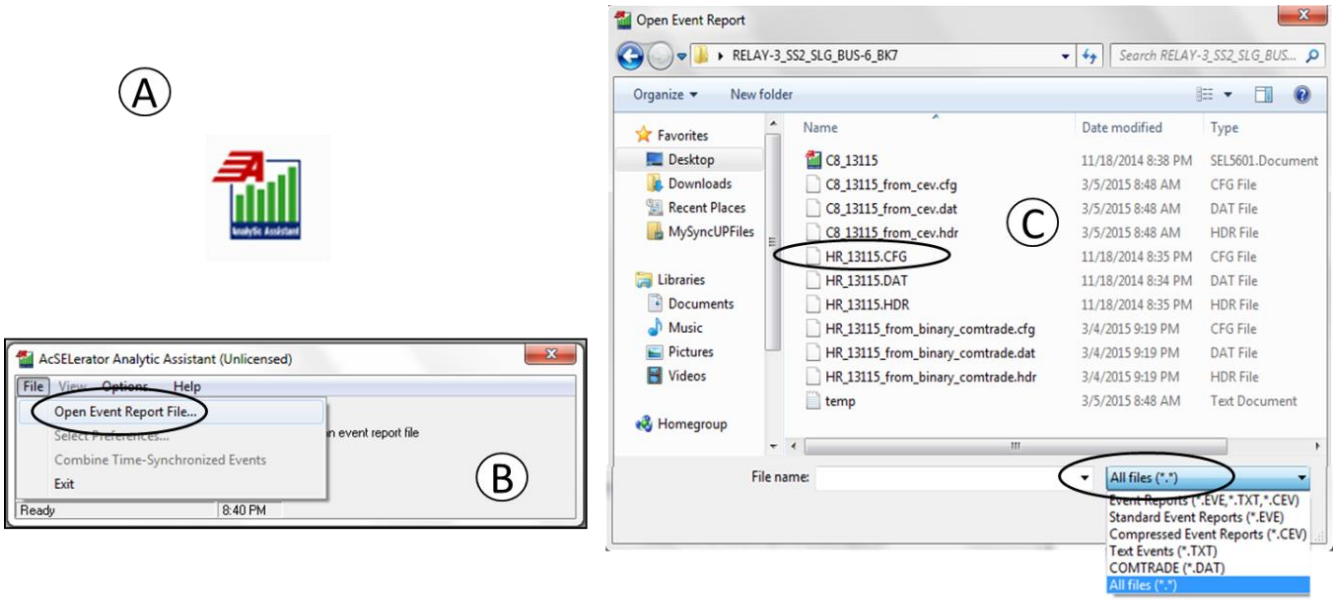

Figure 10.32: Opening an HR event file

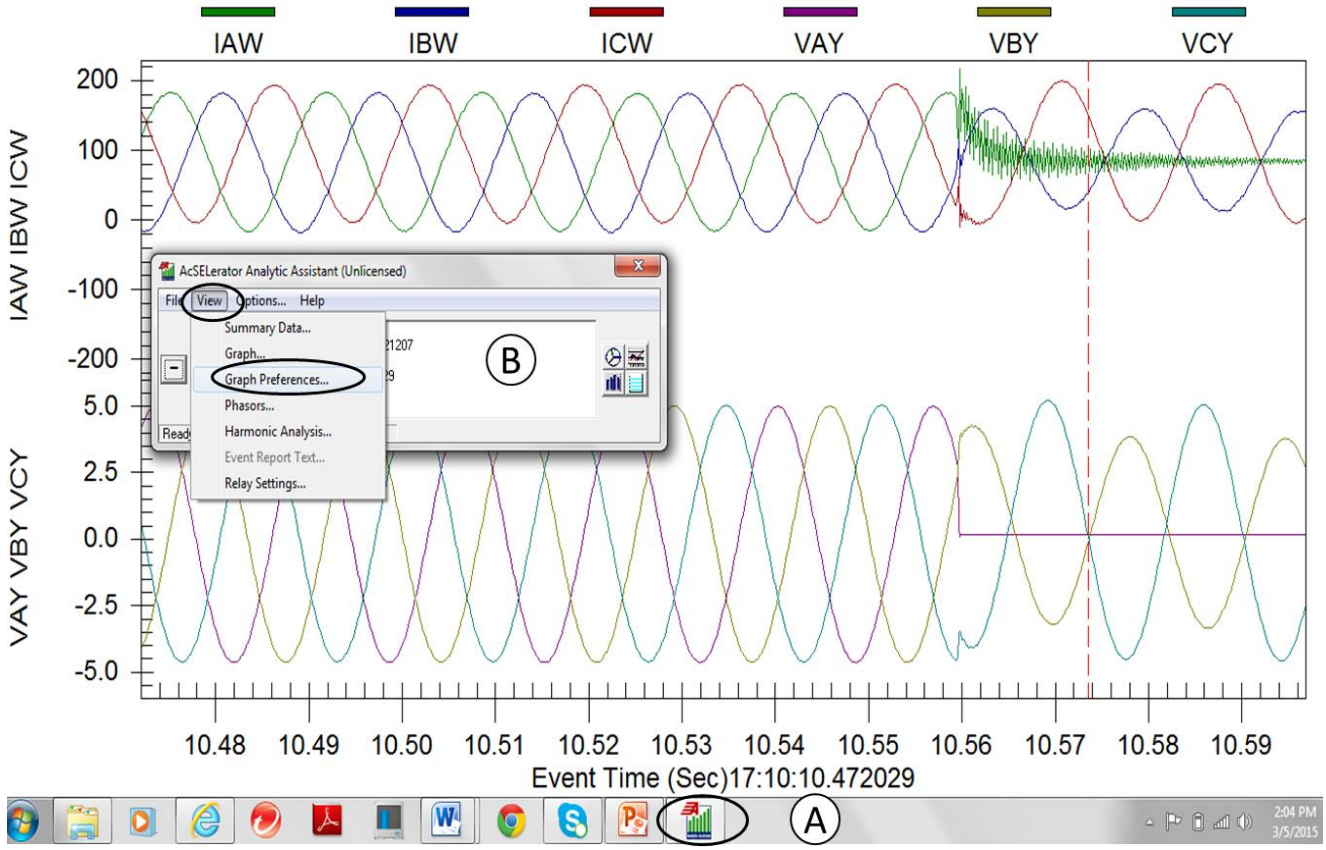

Figure 10.33: Graph preferences of HR event file

A-B-C line currents and digital signals were plotted after collecting the HR event files. The "Time Units, Starting/ Ending Row" option was set in cycles, shown in Figure 10.34 (A) and IAX, IBX, and ICX analog signals from the analog list were dragged to Axis 1 and SG2, IN202, PSV04, T3P2, 51S2, IN104, 52AA2, OUT107, and TRIP digital signals from the digital list were dragged to the digital axis. The "OK" cell was the selected, as shown in Figure 10.34 (B). The plot of A-B-C line currents and digital signals was created (Figures 10.34 (C)) for the HR_13115 event, "DG2-678/65-SLG(A)-BUS6-BK7" test. A-B-C line currents of "BK7" breaker and SG2, IN202, PSV04, T3P2, 51S2, IN104, 52AA2, OUT107, and TRIP digital signals were presented in the same plot, as shown in Figure 10.34 (C).

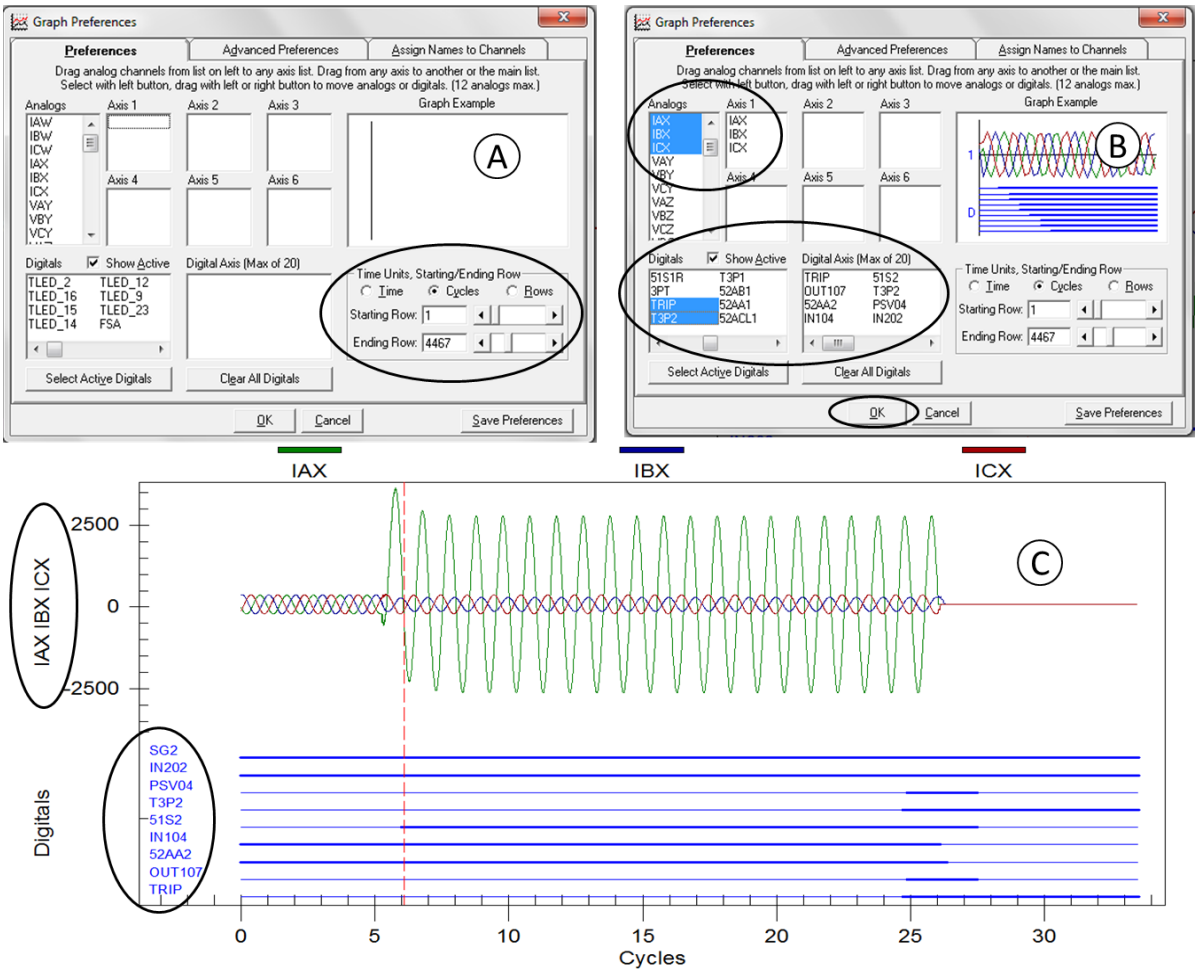

Figure 10.34: Plot of A-B-C line currents and digital signals, HR_13115 event, DG2-678/65-SLG(A)-Bus6-BK7 test

10.5.3 Matlab® files

In the power desk, Matlab® files were collected from the host computer. After the model was executed, the Matlab® file was generated. A left click selected the “New file available” window, shown in Figure 10.35 (A), the “Import Wizard” dialog was signed, and the “Finish” cell was selected, as shown in Figure 10.35 (B).

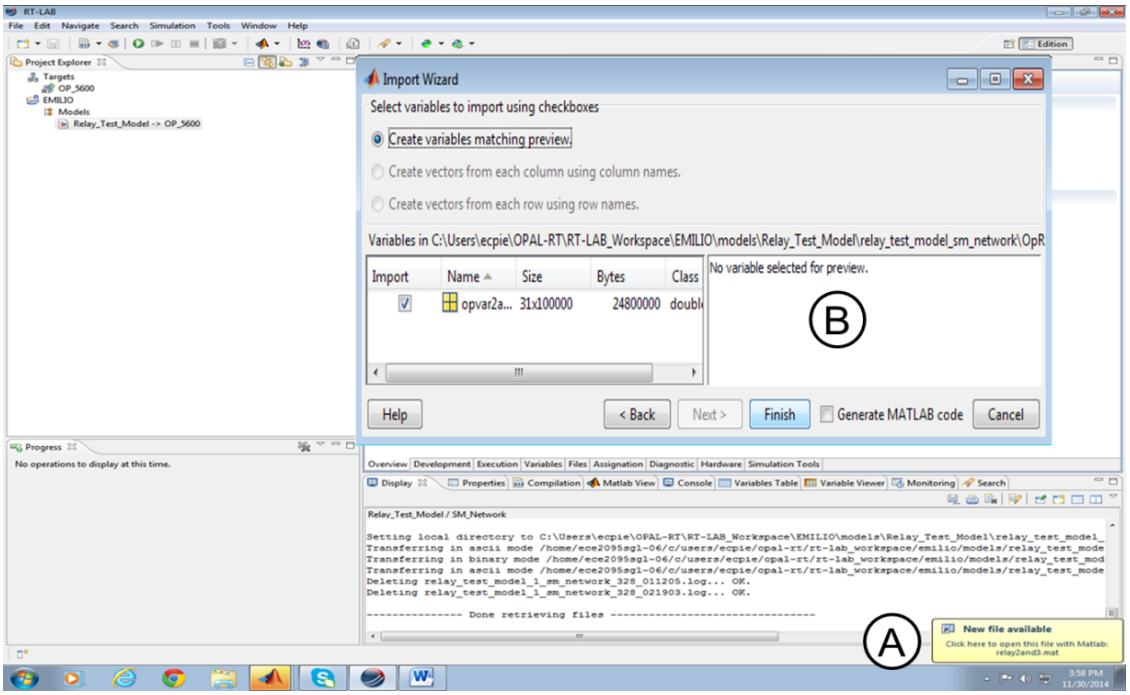

Figure 10.35: Importing wizard dialog

Figures 10.36 and 10.37 demonstrate the process to save a Matlab® file. In Figure 10.36, the Matlab® software [14] icon on the host computer screen was selected (A). Then, a double left click on the “opvar2and3” file was made to observe the collected data in the variable editor (B). The “opvar2and3” file was generated by the “OpWriteFile” block placed in SM_Network (master) subsystem. Signals in the variable editor represented time, A-B-C line currents, trip signals, breaker states, and relay setting groups from the microgrid. The “Save” icon was clicked, and the “relay2and3” file was selected (C). In Figure 10.37, the “Desktop” icon was clicked (D) and the “relay2and3” Matlab® file was renamed as “matlab_trip” or “matlab_notrip,” depending on whether the Matlab®

file was generated in a trip or non-tripping test, respectively (E). The “matlab_trip” and “matlab_notrip” files were saved into a folder referenced with the name of the test (F).

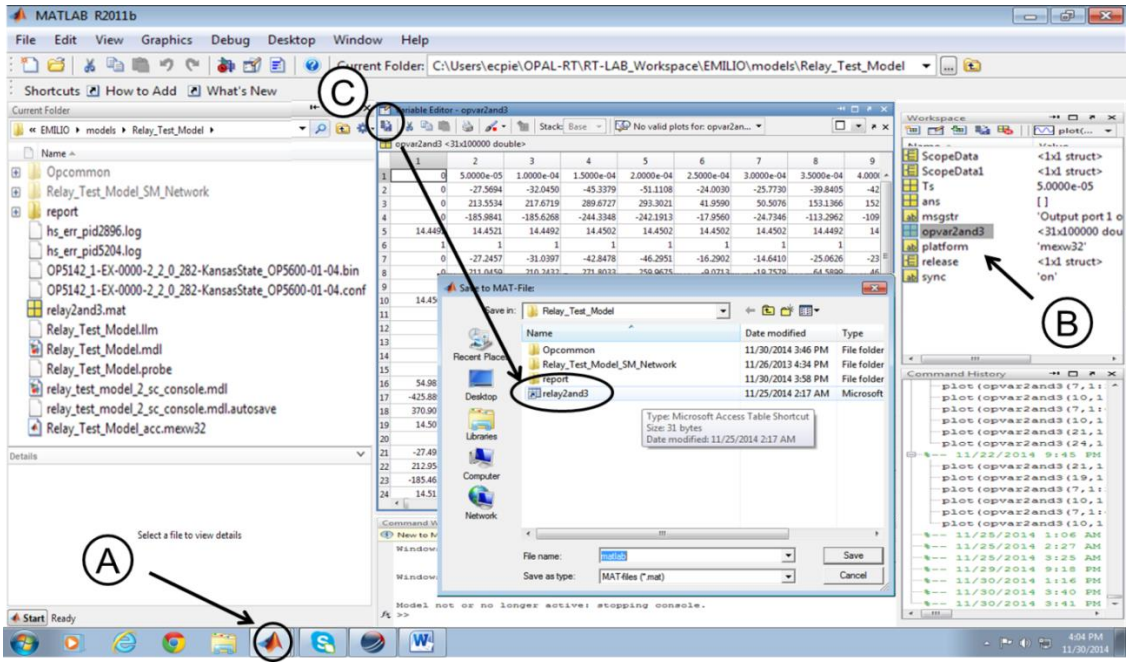

Figure 10.36: Process to save Matlab® files from microgrid

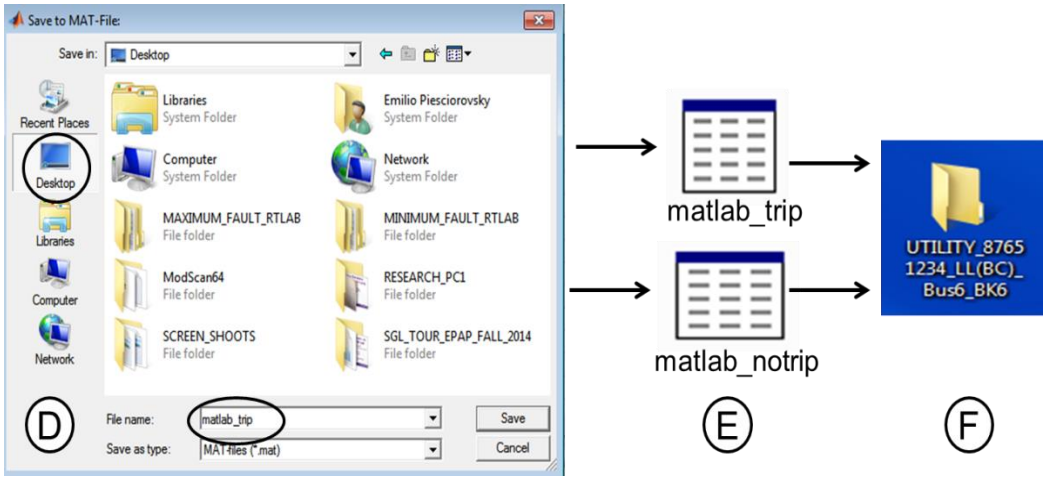

Figure 10.37: Process to save Matlab® files from microgrid (continued)

To a relay tripped and did not trip at fault overcurrent, the fault state time of relay test needed to be greater and smaller than the expected fault clearing time, respectively. In tripping tests, relays tripped because the clearing time was smaller than the fault state time. However, in non-tripping tests,

relays did not trip because the clearing time was greater than the fault state time. Variable lines, names, and descriptions of Matlab® files are shown in Table 10.6. In the Matlab® files, lines 2-15 and 16-31 represented Relay 2 and 3 variables, respectively.

Table 10.6: Variable lines, names, and descriptions of Matlab® file

Relays	Variable Lines	Variable Names	Variable Descriptions
2	1	time	Time of real-time simulation test
	2-3-4	Iaw2, Ibw2, Icw2	A-B-C line currents of Breaker 1 for relay 2
	5	tripw2	Trip of breaker 1 for relay 2
	6	bk1r2state	State of breaker 1 for relay 2
	7-8-9	Iax2, Ibx2, Icx2	A-B-C line currents of breaker 2 for relay 2
	10	tripx2	Trip of breaker 2 for relay 2
	11	bk2r2state	State of breaker 2 for relay 2
	12-13-14-15	ss1r2, ss2r2, ss3r2, ss4r2	Setting groups 1, 2, 3, and 4 for relay 2
3	16-17-18	Iaw3, Ibw3, Icw3	A-B-C line currents of breaker 1 for relay 3
	19	tripw3	Trip of breaker 1 for relay 3
	20	bk1r3state	State of breaker 1 for relay 3
	21-22-23	Iax3, Ibx3, Icx3	A-B-C line currents of breaker 2 for relay 3
	24	tripx3	Trip of breaker 2 for relay 3
	25	bk2r3state	State of breaker 2 for relay 3
	26-27-28-29-30-31	ss1r3, ss2r3, ss3r3, ss4r3, ss5r3, ss6r3	Setting groups 1, 2, 3, 4, 5 and 6 for relay 3

Figures 10.38 to 10.39 show the process to create the plot of A-B-C line currents of Breaker 1 for Relay 3. In Figure 10.38, the Matlab® software [14] icon in the lower bar on the screen was selected (A), and then the “File” menu and “Open” submenu were selected (B). The “matlab_trip” file for the “UTILITY-8765/1234-LL(BC)-Bus6-BK6” test was selected from the Desktop by clicking the “Open” tab (C). The “opvar2and3” file was then selected with a double left click (D).

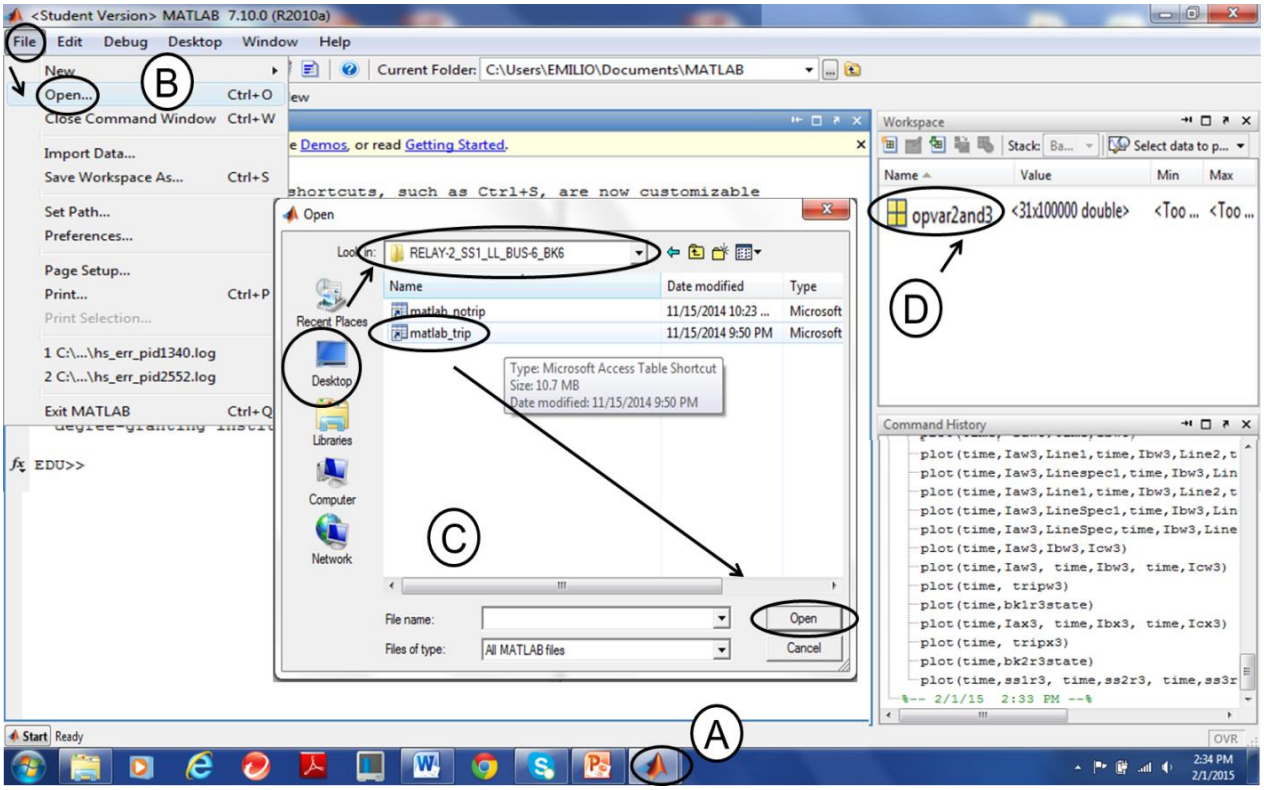

Figure 10.38: Reading the "matlab_trip" file

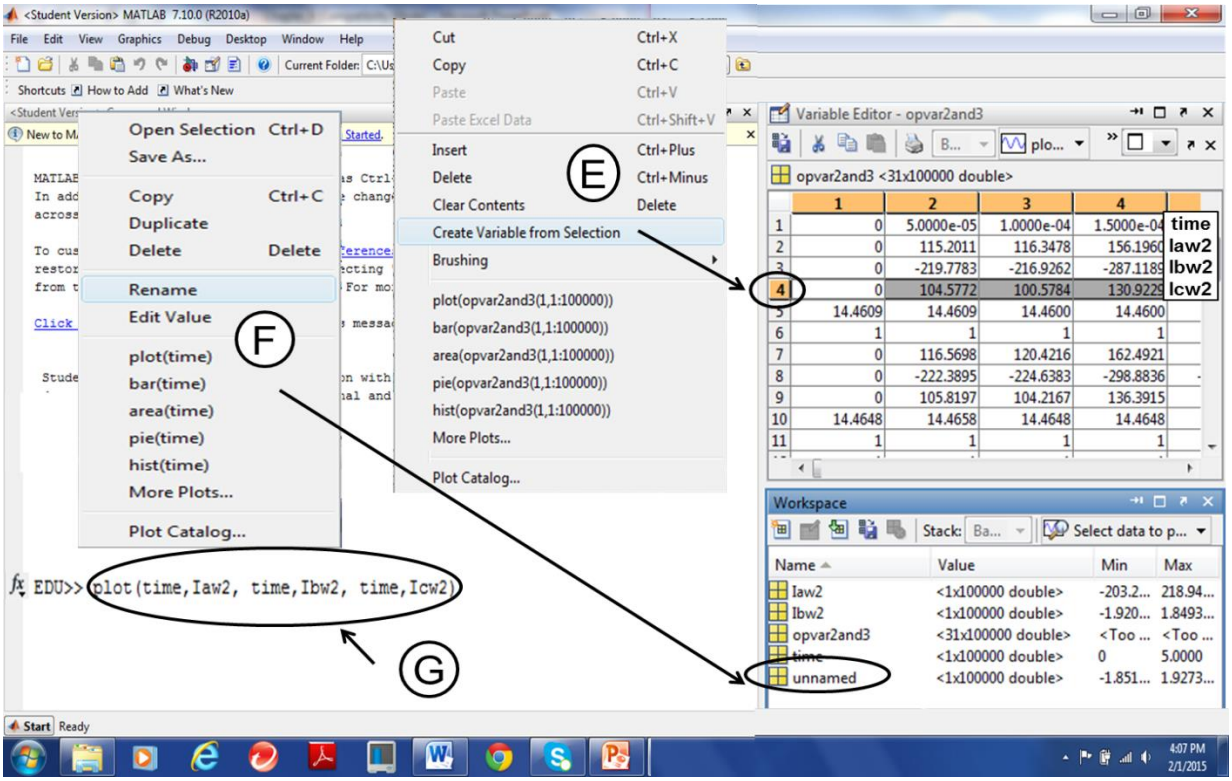

Figure 10.39: Plot A-B-C line currents of Breaker 1 for Relay 2 from "matlab_trip" file

As shown in Figure 10.39, the “opvar2and3” table was opened, and a right click on the first line of the“opvar2and3” table was made. Then the “Create Variable from Selection” menu was selected by creating an “unnamed” file in “Workspace” (E). A right click was made on the “unnamed” file in “Workspace,” and the “Rename” menu was selected to name the “unnamed” file as “time” file. This process was repeated for lines 2, 3, and 4 in order to name the “unnamed” files as “Iaw2,” “Ibw2,” and “Icw2” files, respectively (F). EDU>> plot(time,Iaw2, time, Ibw2, time, Icw2) was written without spaces between time and current variables, and the “Enter” tab was selected in order to plot the A-B-C line current-time plot.

Figure 10.40 shows the Matlab® plot of A-B-C line currents of “BK6” breaker for the “UTILITY-8765/1234-LL(BC)-Bus6-BK6” test. In this plot, the horizontal axis represents time in seconds and the vertical axis represents A-B-C line currents in amps. This plot presents pre-fault, fault, and post-fault states. In the pre-fault state, load currents flowed along the “BK6” breaker. In the fault state, fault overcurrent flowed along the “BK6” breaker until Relay 2 tripped and the fault was cleared. In the post-fault state, no currents flowed along the “BK6” breaker. The Matlab® plot was edited by selecting “Figure Properties,” “Axes Properties,” and “Copy Figure” options from the “Edit” menu and the “Legend” option from the “Insert” menu.

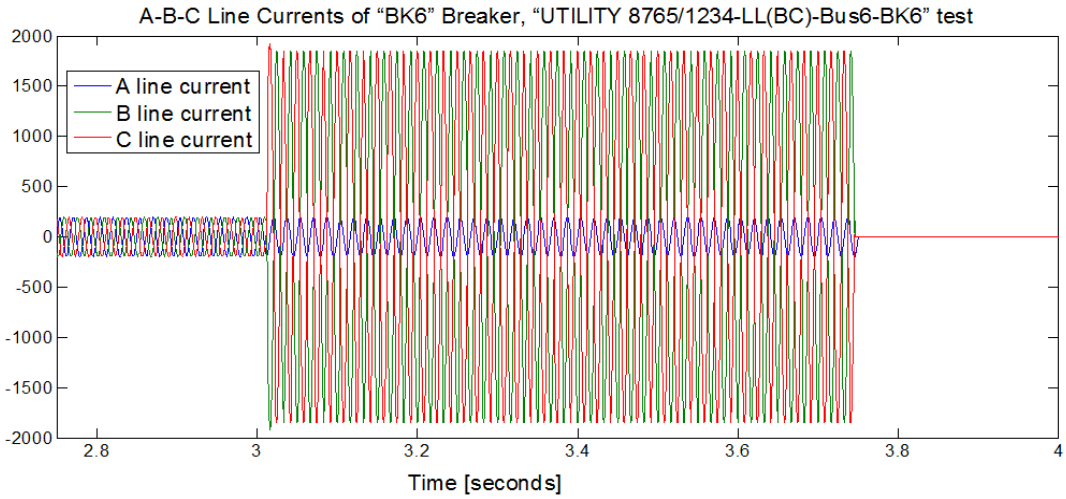

Figure 10.40: A-B-C line currents of “BK6” breaker, “UTILITY- 8765/1234-LL(BC)-Bus6-BK6” test

Variables indicated in Table 10.7, and collected from the “matlab_trip” and “matlab_notrip” files could be plotted from the real-time test. Table 10.7 shows Matlab® functions (*fx*) to plot line currents, trip signals, breaker states, and relay setting groups.

Table 10.7: Matlab® functions to plot variables

Variables	**Matlab® functions**
A-B-C line currents of breakers	EDU>> plot(time,Iaw2, time,Ibw2, time,Icw2)
	EDU>> plot(time,Iax2, time,Ibx2, time,Icx2)
	EDU>> plot(time,Iaw3, Ibw3,time, Icw3,time)
	EDU>> plot(time,Iax3, time,Ibx3, time,Icx3)
Trip signals	EDU>> plot(time,tripw2), EDU>> plot(time,tripx2)
	EDU>> plot(time,tripw3), EDU>> plot(time,tripx3)
Breaker states	EDU>> plot(time,bk1r2state), EDU>> plot(time,bk2r2state)
	EDU>> plot(time,bk1r3state), EDU>> plot(time,bk2r3state)
Setting groups	EDU>> plot(time,ss1r2, time,ss2r2, time,ss3r2, time,ss4r2)
	EDU>> plot(time,ss1r3, time,ss2r3, time,ss3r3, time,ss4r3, time,ss5r3, time,ss6r3)

10.6 Chapter summary

This chapter detailed test steps to run tripping and non-tripping tests for adaptive overcurrent protection of the microgrid with distributed generators. Test steps included Edition (1), Preparation (2), Compilation (3), Execution (4) and Collection (5) phase. The test step process was based on a loop: When the Collection phase ended, a new test was initiated starting from the Edition phase.

In the Edition (1) phase, the circuit path was defined, fault type and location were placed, the breaker record event was chosen, relay setting groups were defined, and real-time tests for the RTS experiment were edited before initiating the Preparation phase. In the Preparation (2) phase, the target platform was set and the model was built and compiled. In the Compilation (3) phase, compilation view results were consulted and the target computer was assigned to subsystems for real-time tests in which “OP_5600” was chosen as a physical node and the subsystems were set to run in XHP mode.

In the Execution (4) phase, execution properties to run the test were set, the model was loaded in the target computer, and the model was executed to run the test. However, an additional task was required when the second console was generated after loading the model. In the second console, plots

of the relay scopes and fault time were set before executing the real-time test. After execution, test results were collected from the generated Matlab® file. The second console was set to supervise the real-time test during execution. In the Collection (5) phase, the relay's display and pushbutton LEDs and record event files were collected and Matlab® files were generated. A-B-C line currents, trip signals, breaker states, and relay setting groups were plotted and read in Matlab® and relay record event files. Information related to Matlab® and record event files was provided from the microgrid and relays, respectively. Test results were measured from the microgrid and relays in order to validate real-time simulation and application of the OP5600 as a real-time relay test system and to evaluate the adaptive overcurrent protection system.

Chapter 11 - Results of RTS experiment

This chapter analyzes RTS experiment results. The RTS experiment was segregated into tripping and non-tripping tests. Backup protection tests were included in the tripping tests. Setting groups, A-B-C- line currents, trip signals, and breaker states were collected in the tripping and non-tripping tests. Table 11.1 shows characteristics of tests and methods used to collect test results.

Table 11.1: Characteristics and results of tests for RTS experiment

<table>
<tr><th colspan="5">Characteristics of tests</th><th colspan="3">Methods for collecting results</th></tr>
<tr><th>Type of Test</th><th>Stop Time</th><th>Overcurrent</th><th>Type of Fault</th><th>Number of Tests</th><th>RT-LAB® Second Console</th><th>Microgrid</th><th>Relays</th></tr>
<tr><td rowspan="2">Tripping Tests</td><td rowspan="4">> pre-fault state time + fault clearing time</td><td>Maximum</td><td>DLG(BC), SLG(A)</td><td>17</td><td rowspan="4">Scopes and displays(3)</td><td rowspan="8">Matlab® files</td><td rowspan="4">Event files</td></tr>
<tr><td>Minimum</td><td>LL(BC)</td><td>17</td></tr>
<tr><td rowspan="2">Backup Tests(1)</td><td>Maximum</td><td>DLG(BC), SLG(A)</td><td>5</td></tr>
<tr><td>Minimum</td><td>LL(BC)</td><td>5</td></tr>
<tr><td rowspan="2">Non-Tripping Tests</td><td rowspan="4">< pre-fault time + relay time</td><td>Maximum</td><td>DLG(BC), SLG(A)</td><td>17</td><td rowspan="4">Scopes</td><td rowspan="4">Pushbutton LEDs and relay display</td></tr>
<tr><td>Minimum</td><td>LL(BC)</td><td>17</td></tr>
<tr><td rowspan="2">Backup Tests(2)</td><td>Maximum</td><td>DLG(BC), SLG(A)</td><td>5</td></tr>
<tr><td>Minimum</td><td>LL(BC)</td><td>5</td></tr>
</table>

DLG(BC): double line-ground BC fault, SLG(A): single line to ground-A fault, LL(BC): line-to-line BC fault
(1)Included in tripping tests, (2) Included in non-tripping tests, (3)Displays located in the control fault timing circuit

In tripping tests, real-time simulation was stopped at a time greater than the sum of pre-fault and fault clearing times in order to observe if relays tripped. However, non-tripping tests were stopped at a time less than the sum of pre-fault and relay times in order to observe if relays did not trip. Mean ± SEM of each test result collecting method was calculated to verify if data collected from RT-LAB® second console, microgrid, and relays were acceptable for testing relays in the loop with OP5600 as a relay test system. Analysis of relay record events was also performed, plotting A-B-C line currents of

tripped breaker and digital variables to verify the protection logic of setting groups for relays. Percent error values and mean ± SEM of Relays 2 and 3 were calculated for measured and theoretical relay time values for tripping tests. Measured coordination time intervals between primary and backup relays were estimated for backup tests in order to observe protection coordination scenarios.

11.1 Tripping tests

Tripping tests of the RTS experiment for adaptive overcurrent protection of the microgrid with distributed generators were performed for nine circuit paths, shown in Appendix P. RT-LAB® software [13] was applied to run tripping tests. Tripping tests verified that Relays 2 and 3 tripped for inverse time overcurrent protection settings. In the tripping tests, fault state time had to be greater than the fault clearing time, allowing the relay to trip for the inverse time overcurrent protection curve setting on relays. “Real-Time Properties” to run tripping tests are shown in Figure 11.1. “Execution Properties”, “Stop Time,” and “Pause Time” were set at 5 sec., assuming the sum of pre-fault and fault clearing times to be less than 5 sec.

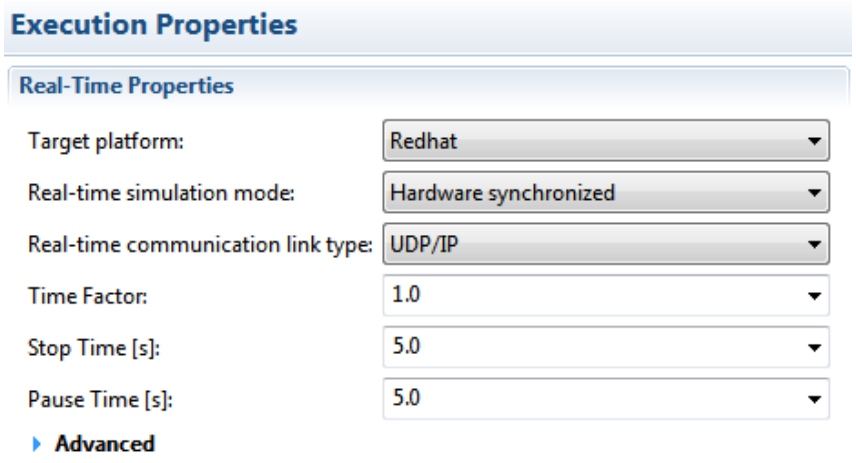

Figure 11.1: Real-time properties for tripping tests

Tripping tests, performed for Relays 2 and 3 in the loop with OP5600, verified that Relays 2 and 3 tripped at overcurrent fault situations along the microgrid. Overcurrent faults were located on

power line busses assuming maximum and minimum fault overcurrent. Power lines were defined as protection areas of Relays 2 and 3. Table 11.2 lists tripping tests developed for the RTS experiment.

Table 11.2: Tripping tests for the RTS experiment

Type of tests	Objectives
Maximum fault overcurrent tests	Verified that the primary relay tripped for the maximum fault overcurrent along the power line.
Minimum fault overcurrent tests	Verified that the primary relay tripped for the minimum fault overcurrent along the power line.
Backup protection tests	Verified that the backup relay tripped for the minimum and maximum fault overcurrent along the power line when a failure in the primary relay occurred.

The maximum fault overcurrent corresponded to the double (DLG) and single (SLG) line-to-ground faults. However, the minimum fault overcurrent corresponded to the line-to-line (LL) fault. When considering a power line between two busses, the maximum overcurrent fault was located on the power line bus nearest from the source, and the minimum overcurrent fault was located on the power line bus farthest from the source.

In order to define test characteristics, the tests were referenced by source, circuit, type of fault, fault site, and desired tripped breaker. Therefore, the "DG2-678/65-LL(BC)-Bus8-BK5" test means that the test was performed for the LL (BC) fault located on "Bus8" in the circuit conformed by the "distributed generator 2" and two power line branches formed by 6-5 and 6-7-8 power lines with the expectation that "BK5" breaker would trip.

Maximum and minimum fault overcurrent and backup protection tests were performed in the RTS experiment. Figure 11.2 shows the "DG2-678/65" circuit path to run minimum fault overcurrent and backup protection tests for the 7-8 power line. Tripping and backup protection tests for minimum fault overcurrent were performed by applying the circuit within the red dashed lines in Figure 11.2. The tests were described by the following:

- Minimum fault overcurrent DG2-678/65-LL(BC)-Bus8-BK5 test verifying that the BK5 breaker tripped for a LL fault of lines B and C at Bus 8.
- Backup protection DG2-678/65-LL (BC)-Bus8-BK7 test verifying that the BK7 breaker tripped for a LL fault of lines B and C at Bus 8. The LLTI of the primary protection (Relay 2) was disconnected, simulating a current transformer (CT) failure on Relay 2.

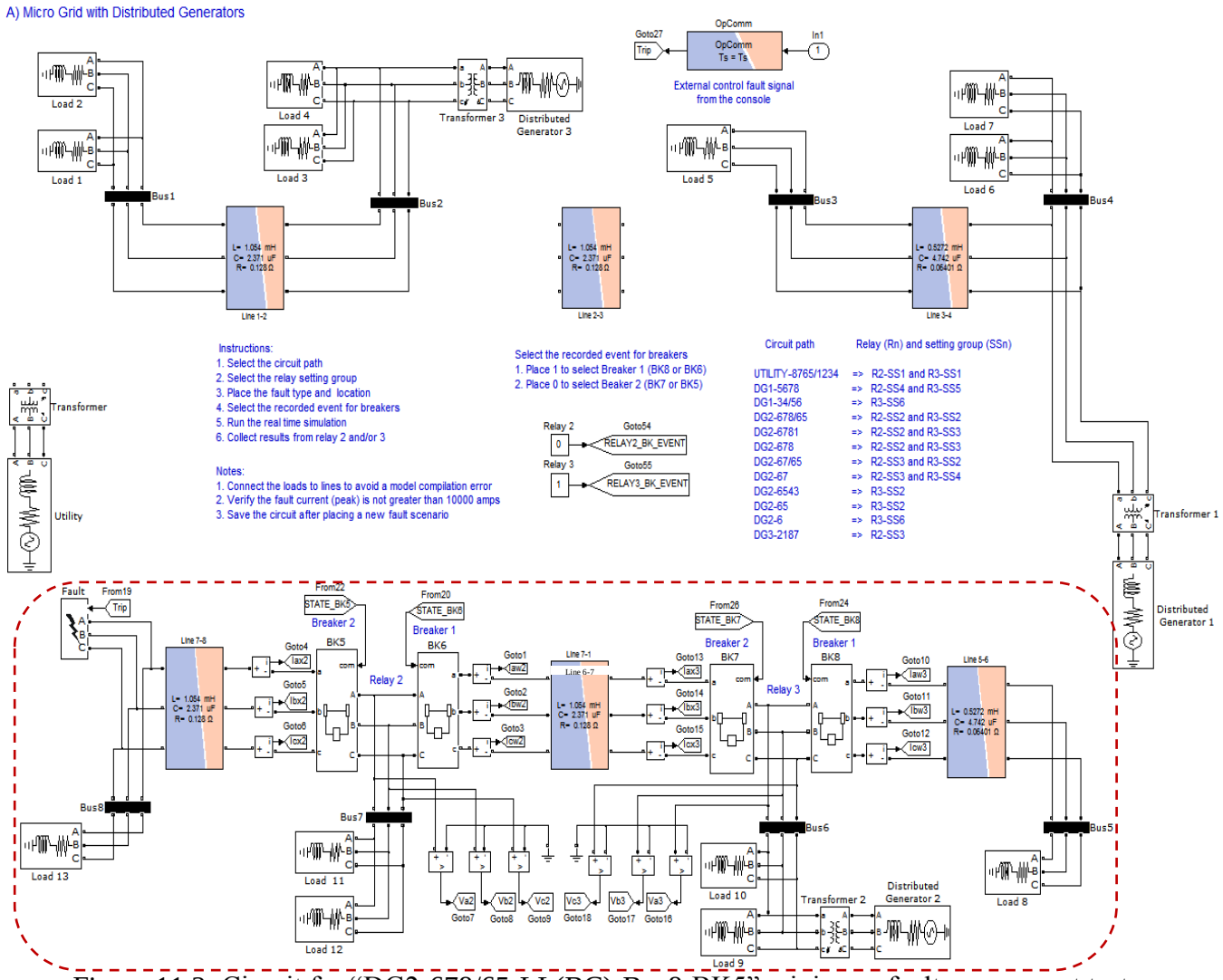

Figure 11.2: Circuit for "DG2-678/65-LL(BC)-Bus8-BK5" minimum fault overcurrent test

In addition, tripping and backup protection tests for maximum fault overcurrent were performed on the circuit in Figure 11.2 by moving the fault block to the other extreme of power line 7-8 and setting a SLG(A) fault. Tests were described by the following:

- Maximum fault overcurrent DG2-678/65-SLG(A)-Bus7-BK5 test verifying that the BK5 breaker tripped for a SLG fault of line A at Bus 7.
- Backup protection DG2-678/65-SLG (A)-Bus7-BK7 test verifying that the BK7 breaker tripped for a SLG fault of lines A at Bus 7. The LLTI of the primary protection (Relay 2) was disconnected, simulating a current transformer (CT) failure on Relay 2.

DLG fault set the maximum fault overcurrent for the circuit fed by the utility source and SLG fault for circuits fed by distributed generators. DLG and SLG faults were placed at BC and A lines to ground, respectively. The minimum fault overcurrent was the LL fault at BC lines for circuit paths. Relays 2 and 3 were verified for tripping and backup protection tests of maximum and minimum fault overcurrent.

In adaptive overcurrent protection for the microgrid with distributed generators, Relays 2 and 3 tripped as primary and backup protections depending on the circuit path selected to run the real-time simulation. Backup protection tests were performed for maximum and minimum fault overcurrent. The backup relay tripped as backup protection simulating a failure on primary relay. In order to verify Relays 2 and 3 as backup protections, CT failures were simulated by disconnecting the LLTI of the primary relay during the tests and observing if the backup relay tripped.

Tripping tests of maximum and minimum fault overcurrent for Relays 2 and 3 are shown in Tables 11.3 and 11.4, respectively. Backup protection tests for maximum and minimum fault overcurrent for Relays 2 and 3 are shown in Table 11.5. Setting groups, protection areas, tests, and record event files for Relays 2 and 3 are shown in Table 11.5. Bold lines in Tables 11.4 and 11.5 indicate tripping and backup tests that correspond to circuit paths shown in Figures P.1 to P.9 of Appendix P.

Table 11.3: Tripping tests of maximum fault overcurrent for Relays 2 and 3

Relays	Setting Groups	Protection Areas	Tests		Record Event File
			N°	Source – Circuit - Fault Type – Fault Site - Tripped Breaker	
2	SS1	L67	1	UTILITY-8765/1234-DLG(BC)-Bus7-BK6	C8_14167
	SS2	L78	2	DG2-678/65-SLG(A)-Bus7-BK5	C8_14169
		L78	3	DG2-6781-SLG(A)-Bus7-BK5	C8_14173
		L78	4	DG2-678-SLG(A)-Bus7-BK5	C8_14175
	SS4	L78	5	DG1-5678-SLG(A)-Bus7-BK5	C8_14177
3	SS1	L56	6	UTILITY-8765/1234-DLG(BC)-Bus6-BK8	C8_13193
	SS2	L56	7	DG2-678/65-SLG(A)-Bus6-BK8	C8_13106
		L67	8	DG2-678/65-SLG(A)-Bus6-BK7	C8_13115
		L56	9	DG2-67/65-SLG(A)-Bus6-BK8	C8_13127
		L67	10	DG2-67/65-SLG(A)-Bus6-BK7	C8_13131
		L34	11	DG2-6543-SLG(A)-Bus4-BK8	C8_13170
		L56	12	DG2-6543-SLG(A)-Bus6-BK8	C8_13175
		L56	13	DG2-65-SLG(A)-Bus6-BK8	C8_13120
	SS3	L67	14	DG2-6781-SLG(A)-Bus6-BK7	C8_13161
		L67	15	DG2-678-SLG(A)-Bus6-BK7	C8_13151
	SS4	L67	16	DG2-67-SLG(A)-Bus6-BK7	C8_13142
	SS5	L67	17	DG1-5678-SLG(A)-Bus6-BK7	C8_13207

Table 11.4: Tripping tests of minimum fault overcurrent for Relays 2 and 3

Relays	Setting Groups	Protection Areas	Tests		Record Event File
			N°	Source – Circuit - Fault Type – Fault Site - Tripped Breaker	
2	SS1	L67	1	UTILITY-8765/1234-LL(BC)-Bus6-BK6	C8_14042
	SS2	L78	2	**DG2-678/65-LL(BC)-Bus8-BK5**	C8_13953
		L78	3	**DG2-6781-LL(BC)-Bus8-BK5**	C8_14052
		L78	4	**DG2-678-LL(BC)-Bus8-BK5**	C8_14048
	SS4	L78	5	**DG1-5678-LL(BC)-Bus8-BK5**	C8_14044
3	SS1	L56	6	**UTILITY-8765/1234-LL(BC)-Bus5-BK8**	C8_13015
	SS2	L56	7	DG2-678/65-LL(BC)-Bus5-BK8	C8_12784
		L67	8	DG2-678/65-LL(BC)-Bus7-BK7	C8_12796
		L56	9	**DG2-67/65-LL(BC)-Bus5-BK8**	C8_12862
		L67	10	DG2-67/65-LL(BC)-Bus7-BK7	C8_12867
		L34	11	**DG2-6543-LL(BC)-Bus3-BK8**	C8_12854
		L56	12	DG2-6543-LL(BC)-Bus5-BK8	C8_12856
		L56	13	**DG2-65-LL(BC)-Bus5-BK8**	C8_12850
	SS3	L67	14	DG2-6781-LL(BC)-Bus7-BK7	C8_13002
		L67	15	DG2-678-LL(BC)-Bus7-BK7	C8_12990
	SS4	L67	16	**DG2-67-LL(BC)-Bus7-BK7**	C8_13012
	SS5	L67	17	DG1-5678-LL(BC)-Bus7-BK7	C8_12978

Table 11.5: Backup protection tests for Relays 2 and 3

Fault Overcurrent	Relays	Setting Groups	Protection Areas	Tests		Record Event File
				N°	Source – Circuit - Fault Type – Fault Site -Tripped Breaker	
Maximum	2(1)	SS1	L56	1	UTILITY-8765/1234-DLG(BC)-Bus6-BK6	C8_14156
	3(2)	SS2	L78	2	DG2-678/65-SLG(A)-Bus7-BK7	C8_13113
		SS3	L78	3	DG2-6781-SLG(A)-Bus7-BK7	C8_13157
			L78	4	DG2-678-SLG(A)-Bus7-BK7	C8_13149
		SS5	L78	5	DG1-5678-SLG(A)-Bus7-BK7	C8_13138
Minimum	2(1)	SS1	L56	1	**UTILITY-8765/1234-LL(BC)-Bus5-BK6**	C8_14026
	3(2)	SS2	L78	2	**DG2-678/65-LL(BC)-Bus8-BK7**	C8_12794
		SS3	L78	3	**DG2-6781-LL(BC)-Bus8-BK7**	C8_13000
			L78	4	**DG2-678-LL(BC)-Bus8-BK7**	C8_12987
		SS5	L78	5	**DG1-5678-LL(BC)-Bus8-BK7**	C8_12980

(1) Relay 3's LLTI was disconnected; (2) Relay 2's LLTI was disconnected.

After executing each tripping test, a C8 event file was collected from the relay that tripped and states (open or closed) of Breakers 1 and 2 were collected. The "Event Report Summary" of the C8_14169 event from Relay 2 that corresponds to DG2-678/65-SLG(A)-Bus7-BK5 test is shown in Figure 11.3. "EVENT_NUM," "BREAKER1," and "BREAKER2" states are indicated in (A), (B), and (C), respectively.

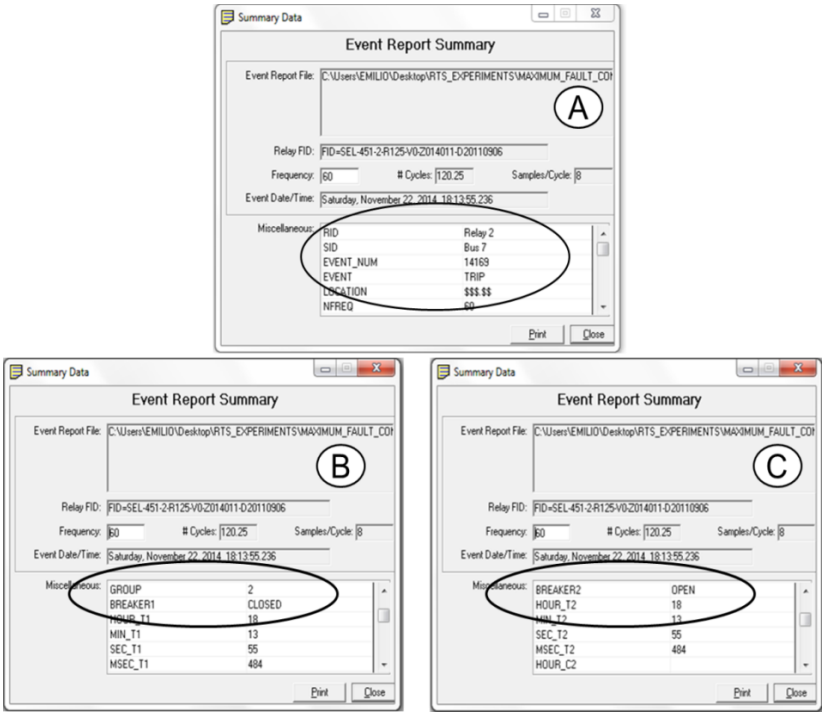

Figure 11.3: Event report summary of "DG2-678/65-SLG(A)-Bus7-BK5" tripping test

Figures 11.4 and 11.5 show the state (open or closed) of Breakers 1 and 2 for Relays 2 and 3, respectively, verifying that the desired breaker tripped for the maximum fault overcurrent during the tripping tests.

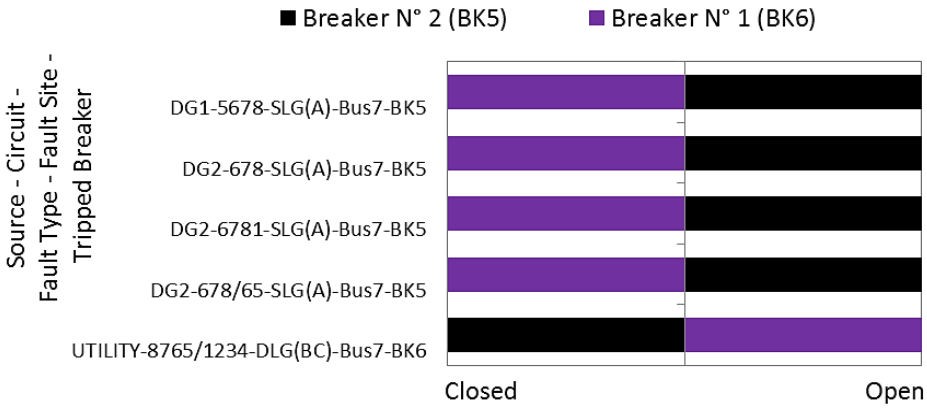

Figure 11.4: Maximum fault overcurrent, tripping tests for Relay 2

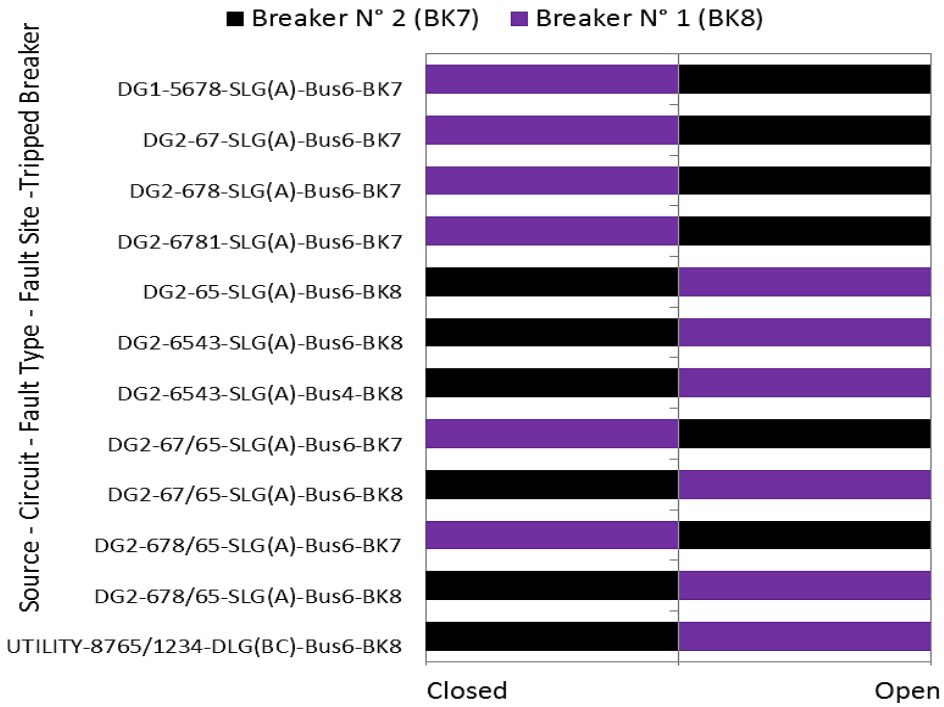

Figure 11.5: Maximum fault overcurrent, tripping tests for Relay 3

Figures 11.6 and 11.7 show the states (open or closed) of Breakers 1 and 2 for Relays 2 and 3, respectively, verifying that the desired breaker tripped for the minimum fault overcurrent during the tripping tests.

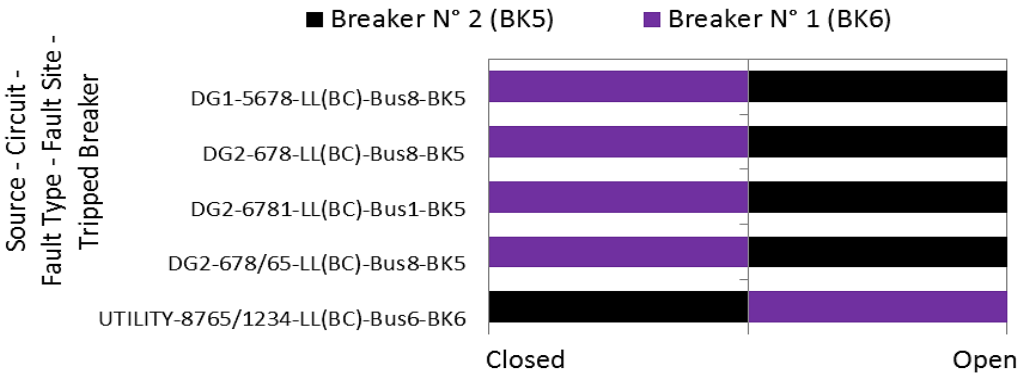

Figure 11.6: Minimum fault overcurrent, tripping tests for Relay 2

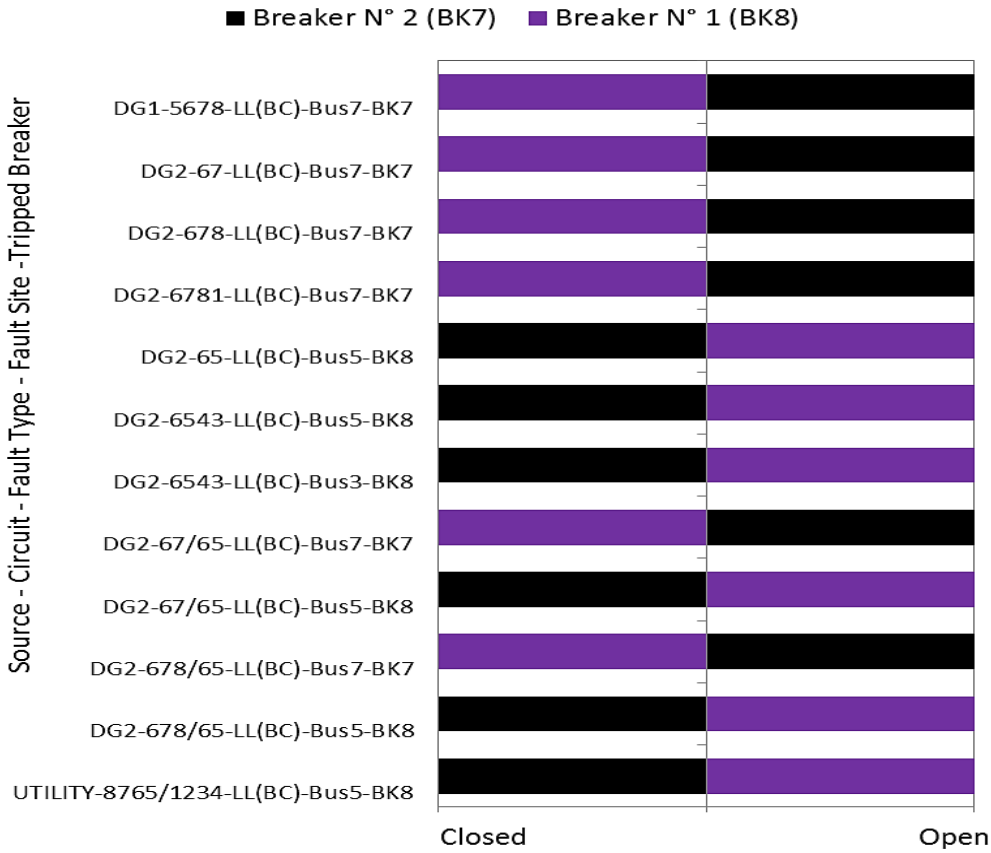

Figure 11.7: Minimum fault overcurrent, tripping tests for Relay 3

Figures 11.8 and 11.9 show the state (open or closed) of Breakers 1 and 2 for Relays 2 and 3, respectively, verifying that the desired breaker tripped during backup protection tests. In the backup protection tests, relay LLTI was disconnected in order to simulate a CT failure on the primary relay.

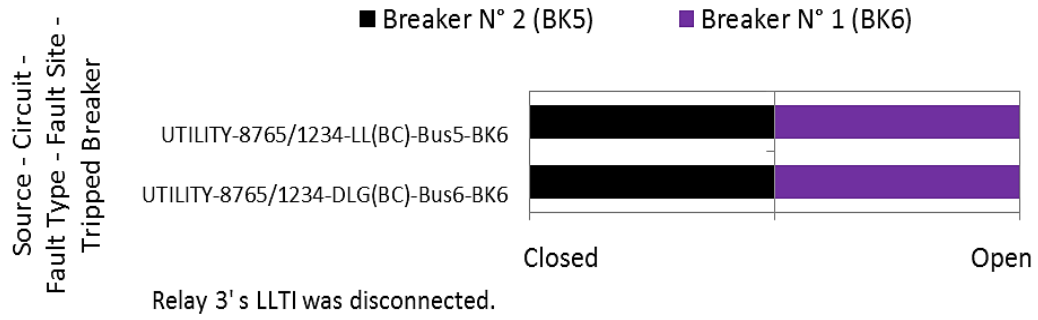

Figure 11.8: Backup protection tests for Relay 2

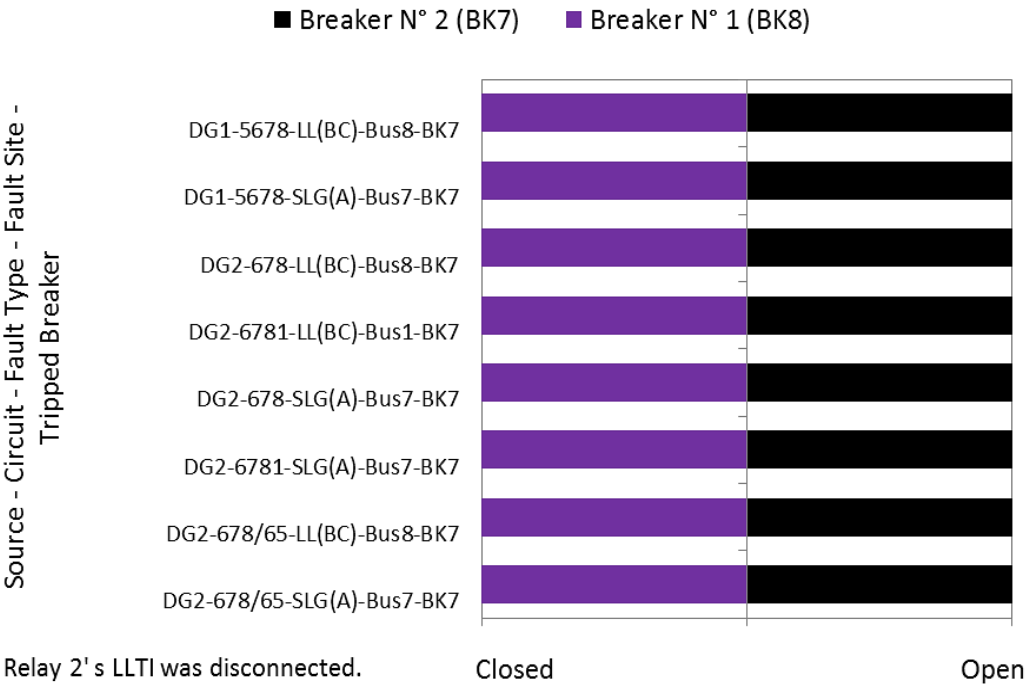

Figure 11.9: Backup protection tests for Relay 3

Additional tests indicated that Relays 2 and 3 did not trip because no overcurrent protection was needed. Additional tests were performed for circuits of Figures P.10 to P.12 of Appendix P. Table 11.6 describes additional tests for Relays 2 and 3. In additional tests were verified that relays did not trip by observing pushbutton LEDs from the relay's front panel. No record event files were collected for additional tests because trip events were not created by relays when relays did not trip.

Table 11.6: Additional tests for Relays 2 and 3

Relays	Setting Groups	Test N°	Circuit	Situation
2	SS3	3	DG3-2187	Relay 2 did not trip for the fault on Bus 7, because "BK4" breaker of Relay 1 protected "L78" line.
3	SS6	1	DG1-34/56	Relay 3 did not trip for the fault on Bus 6 because "BK10" breaker of Relay 4 protected "L56" line.
	SS6	2	DG2-6	Relay 3 did not trip for the fault on Bus 6 because "BK7" and "BK8" breakers of Relay 3 were opened.

Matlab® files generated after executing tripping tests were collected by setting a "stop time" of 5 sec. for "Executing Properties" of real-time simulation. Matlab® Simulink® software [14] was applied in order to plot tripping test results. Data collected from Matlab® file for "DG2-678/65-SLG(A)-BUS6-BK7" tripping test is shown in Figures 11.10 to 11.13. Figure 11.10 shows A-B-C line currents of breakers for Relays 2 and 3. Plot of A-B-C line currents of "BK7" breaker (C), shown as currents, were 0 amps at post-fault state because Relay 3 tripped "BK7" breaker. Plot of A-B-C line currents of "BK8" breaker (D), shown as currents, were not 0 amps at post-fault state, thereby maintaining loads fed by "BK8" breaker. However, plots of A-B-C line currents of "BK5" and "BK6" breakers (A and B), shown as currents, were 0 Amps at post-fault state because "BK7" was open. Figure 11.11 shows trip signals of breakers for Relays 2 and 3. Because the tripping circuit of relays for the RTS experiment had NC control outputs, the breaker opened when the trip signal fell from 14.3 to 0 Vdc. The trip signal plot for "BK7" breaker (C) shows the NC control output signal of Relay 3 that cleared the fault overcurrent. Trip signal plots for "BK5," "BK6," and "BK8" breakers (A, B, and D) indicate that the signals were always 14.3 Vdc without tripping"BK5," "BK6," and "BK8" breakers. Figure 11.12 shows breaker states, indicating "1" or "0" when breakers were closed or open, respectively. The plot of "BK7" breaker states (C) indicates when "BK7" breaker was opened at post-fault state. However, plots of "BK5", "BK6," and "BK8" breaker states (A, B, and D) indicate how "BK5," "BK6," and "BK8" breakers remained closed because relays did not trip those breakers.

Figure 11.13 shows active setting groups of Relays 2 (A) and 3 (B). Although Relays 2 and 3 had four (SS1, SS2, SS3, and SS4) and six (SS1, SS2, SS3, SS4, SS5, and SS6) setting groups available for adaptive overcurrent protection, “DG2-678/65-BUS6-BK7” tripping test had only setting group 2 (SS2) available for Relays 2 and 3.

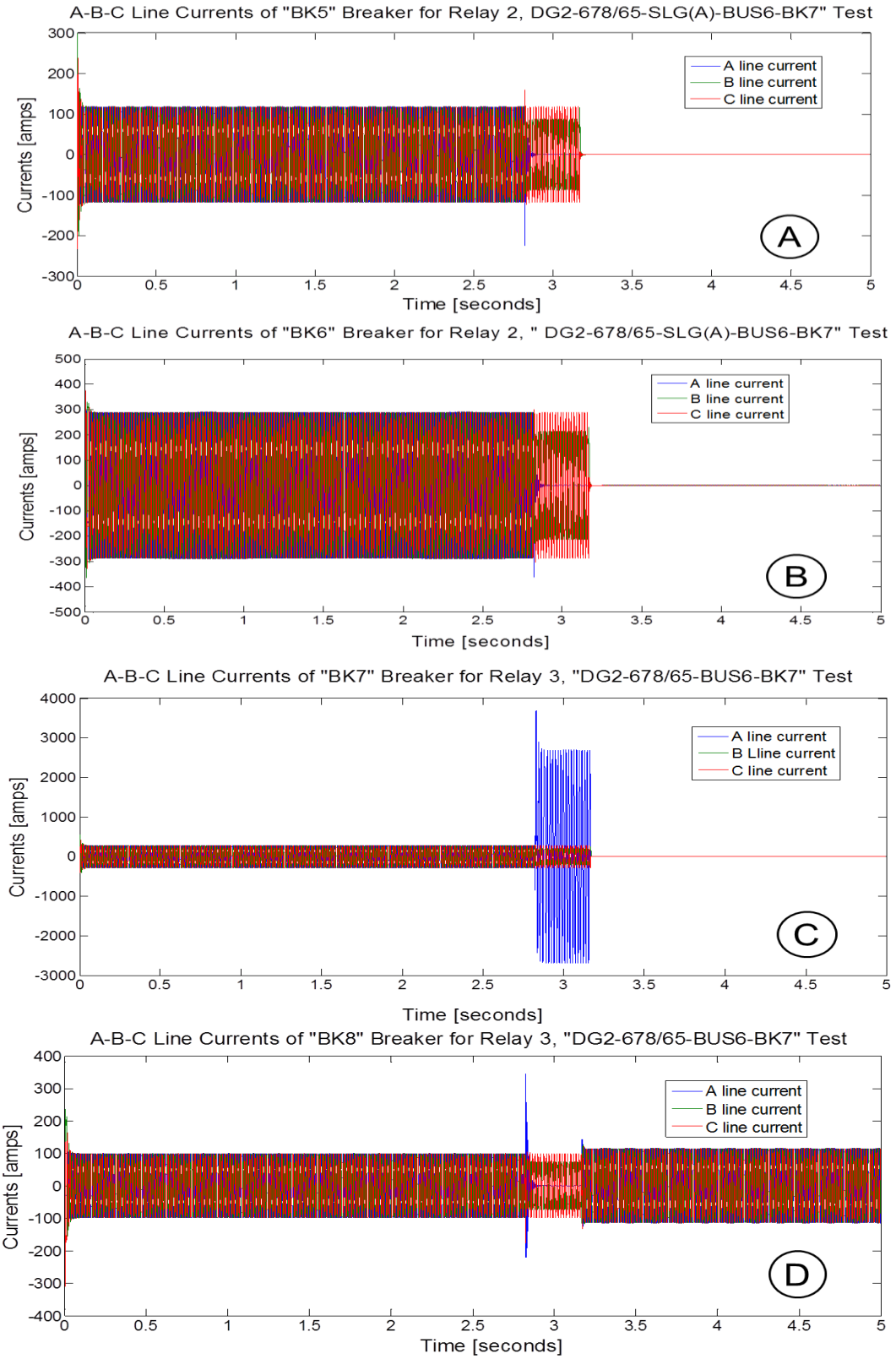

Figure 11.10: A-B-C line currents of breakers for Relays 2 and 3, "DG2-678/65-SLG(A)-BUS6-BK7" tripping test

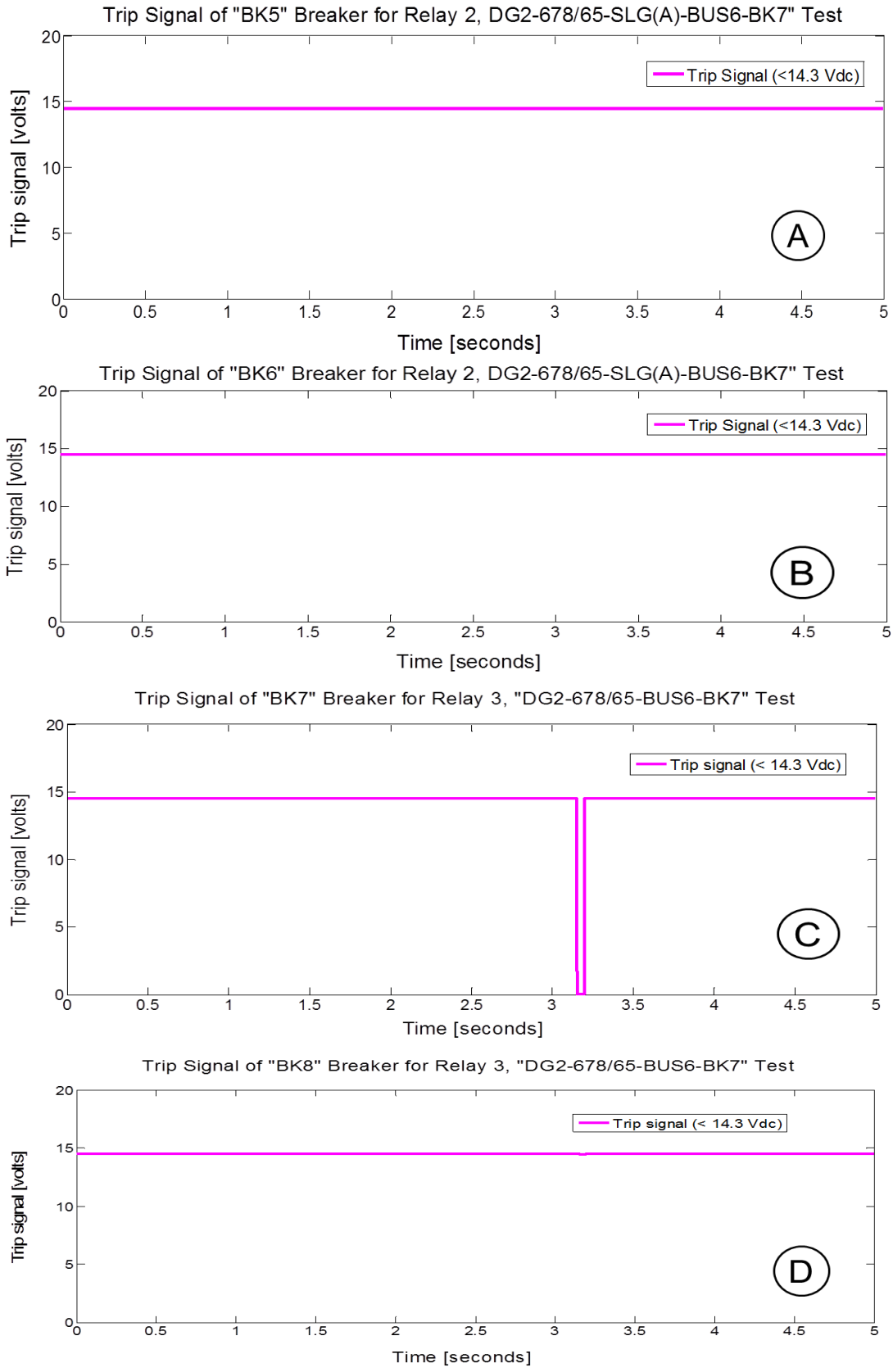

Figure 11.11: Trip signals of Relays 2 and 3, "DG2-678/65-SLG(A)-BUS6-BK7" tripping test

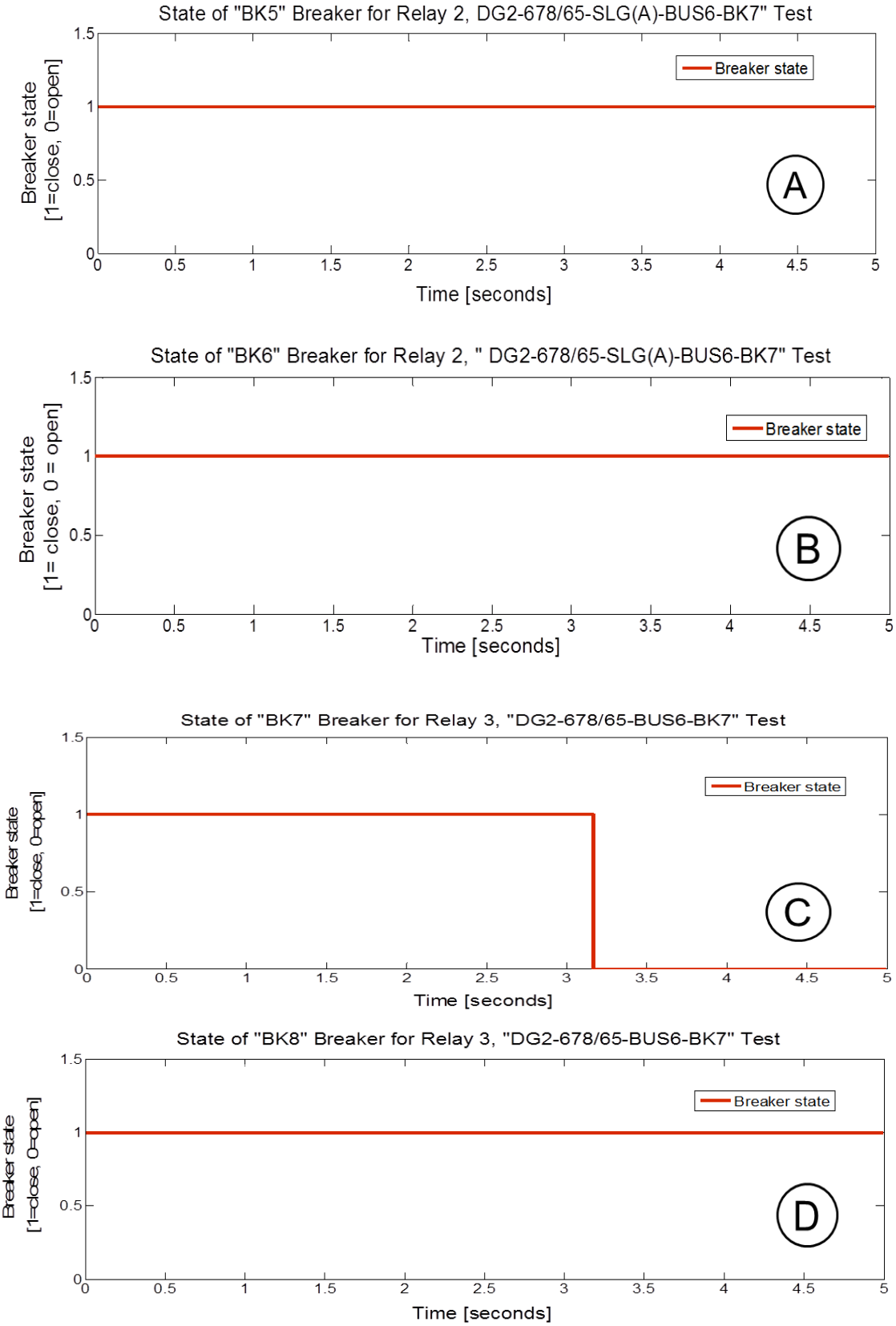

Figure 11.12: Breaker states of Relays 2 and 3, "DG2-678/65-SLG(A)-BUS6-BK7" tripping test

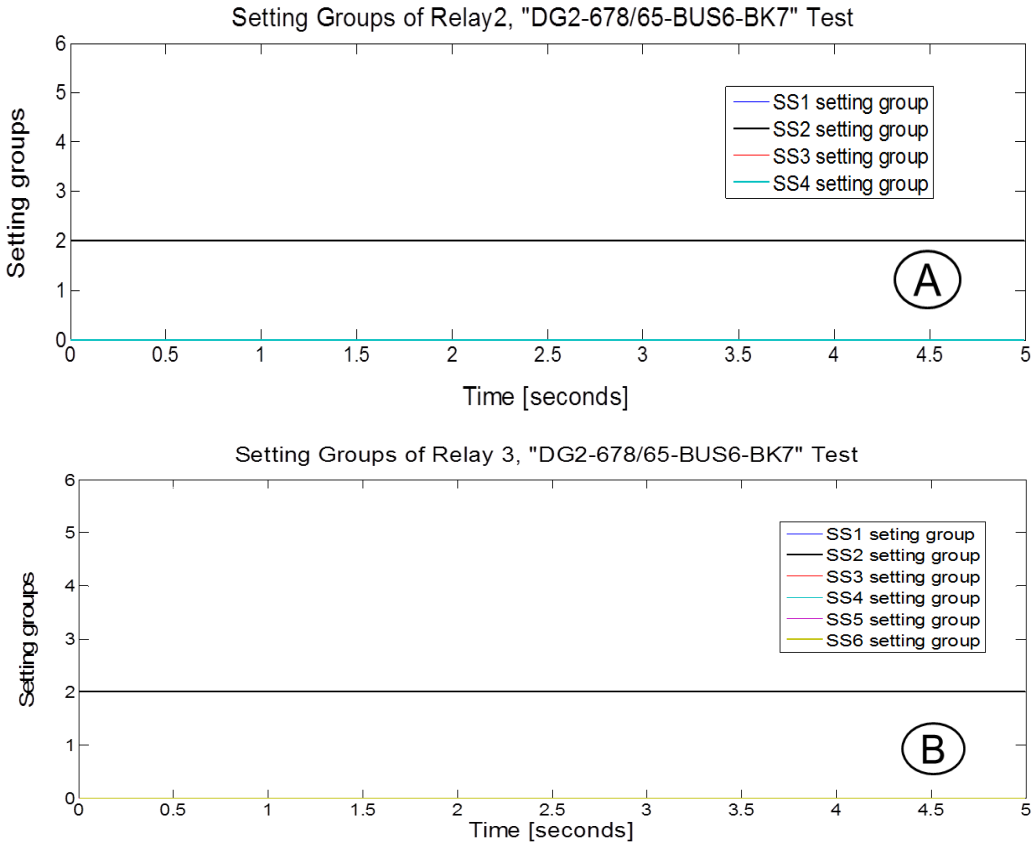

Figure 11.13: Setting groups of Relays 2 and 3, "DG2-678/65-SLG(A)-BUS6-BK7" tripping test

11.2 Non-tripping tests

Non-tripping tests made for maximum and minimum fault overcurrent were performed for RTS experiments for circuits of adaptive overcurrent protection of microgrid with distributed generators. RT-LAB® software [14] was applied in order to run non-tripping tests. Although "stop time" in the execution properties of RT-LAB® was set at 5 sec. for tripping tests, "stop time" was set as less than 5 sec. for non-tripping tests in order for relays to not trip during the fault state in real-time simulation. Therefore, for non-tripping tests, the fault state time must be less than the relay time, preventing relays from tripping for inverse time overcurrent protection curve setting.

Figure 11.14 shows RMS breaker current of tripping and non-tripping tests for minimum and maximum fault overcurrent. For tripping tests (A and C), relays tripped, thereby clearing overcurrent fault. However, for non-tripping tests (B and D), relays did not trip because real-time simulations were

stopped before relays could trip. The "stop time" of non-tripping tests for minimum (T_{S2}) and maximum (T_{S3}) fault overcurrent was estimated before executing real-time simulations and the fault clearing time collected from tripping tests was considered.

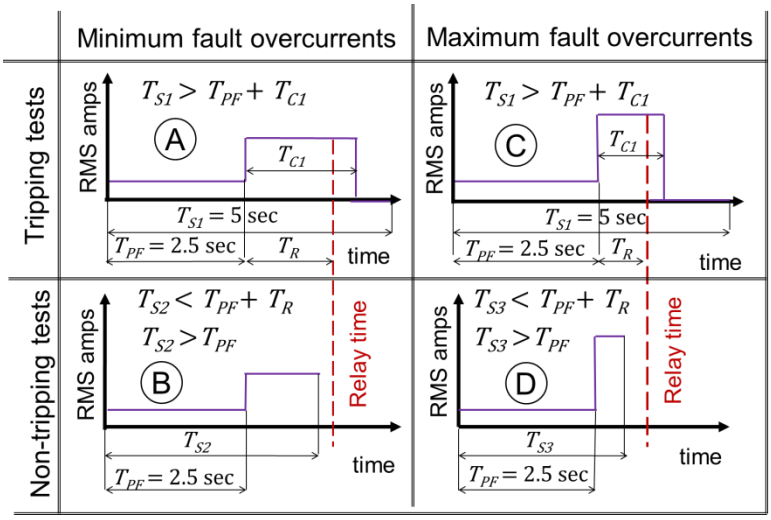

Figure 11.14: Tripping and non-tripping tests for minimum and maximum fault overcurrent

Using pre-fault state time (T_{PF}) of 2.5 sec. and Plots (A) and (B) in Figure 11.14, "stop time" of non-tripping tests for minimum fault overcurrent can be given by

$$T_{S2} = T_{PF} + (0.9 \times T_{C1}) = 2.5 + (0.9 \times T_{C1}) \tag{11.1}$$

where T_{S2} is the "stop time" of non-tripping tests for minimum fault overcurrent in seconds, T_{PF} is pre-fault time set at 2.5 sec. in RT-LAB® second console, and T_{C1} is fault clearing time in seconds from tripping tests. Fault clearing time of tripping tests can also be represented by

$$T_{C1} = \frac{T_{EF} - T_{IF}}{60} = \frac{T_{EF} - 150}{60} \tag{11.2}$$

where T_{EF} is the ending fault time for tripping test in cycles, and T_{IF} is initial fault time for tripping test set at 150 cycles. The ending fault time was measured from RT-LAB® second console after running tripping tests. When Equation (11.2) was placed into (11.1), "stop time" of non-tripping tests for minimum fault overcurrent was estimated by Equation (11.3).

$$T_{S2} = 2.5 + \left(0.9 \times \left[\frac{T_{EF} - 150}{60}\right]\right) . \tag{11.3}$$

"Stop time" of non-tripping tests for maximum fault overcurrent was based on Plots (C) and (D) in Figure 11.14. However, an expression similar to Equation (11.3) was not valid for maximum fault overcurrent of non-tripping tests and additional time had to be added to "stop time" in order to prevent relays from tripping during a fault state in real-time simulation. "Stop time" of non-tripping tests for maximum fault overcurrent was estimated by Equation (11.4).

$$T_{S3} = 2.5 + T_{AD} + \left(0.9 \times \left[\frac{T_{EF}-150}{60}\right]\right) \quad (11.4)$$

where T_{AD} is additional time factor set at 0.236 sec. and T_{S3} is "stop time" of non-tripping tests for maximum fault overcurrent in seconds. Based on Equations (11.3) and (11.4), tripping tests had to be performed before non-tripping tests in order to obtain ending fault time of RT-LAB® second console for tripping tests. Equations (11.4) and (11.3) then calculated "stop time" of non-tripping tests for maximum and minimum fault overcurrent, respectively. Table 11.7 shows ending fault time values collected from the RT-LAB® second console for tripping tests when Relay 2 tripped and "stop time" values of non-tripping tests for maximum and minimum fault overcurrent.

Table 11.7: "Stop Time" for non-tripping tests, Relay 2, RTS experiment

Fault Overcurrent	**Test Description**	**LLTI [on/off]**		**Tripping Tests (RT-LAB® Second Console)**		**Non-Tripping Tests**	
	Source - Circuit - Type of Fault - Fault Location - Opened Breaker	**Relay 2**	**Relay 3**	**Ending Fault Time, cycles [T_{EF}]**	**Measured Fault State Time, cycles [T_{FSm} =T_{EF} -150]**	**Stop Time, sec. [T_{S2}]**	**Stop Time, sec. [T_{S3}]**
Maximum	**UTILITY-8765/1234-DLG(BC)-Bus6-BK6**	**on**	**off**	**184.086**	**34.09**		**3.25**
	UTILITY-8765/1234-DLG(BC)-Bus7-BK6	on	on	177.060	27.06		3.14
	DG2-678/65-SLG(A)-Bus7-BK5	on	on	171.540	21.54		3.06
	DG2-6781-SLG(A)-Bus7-BK5	on	on	169.245	19.25		3.02
	DG2-678-SLG(A)-Bus7-BK5	on	on	168.525	18.53		3.01
	DG1-5678-SLG(A)-Bus7-BK5	on	on	169.539	19.54		3.03
Minimum	**UTILITY-8765/1234-LL(BC)-Bus5-BK6**	**on**	**off**	**203.760**	**53.76**	**3.31**	
	UTILITY-8765/1234-LL(BC)-Bus6-BK6	on	on	196.035	46.04	3.19	
	DG2-678/65-LL(BC)-Bus8-BK5	on	on	196.335	46.34	3.20	
	DG2-6781-LL(BC)-Bus8-BK5	on	on	194.100	44.10	3.16	
	DG2-678-LL(BC)-Bus8-BK5	on	on	192.261	42.26	3.13	
	DG1-5678-LL(BC)-Bus8-BK5	on	on	197.895	47.90	3.22	

Bold represents backup protection tests.

Table 11.8 shows ending fault time values collected from the RT-LAB® second console for tripping tests when Relay 3 tripped and "stop time" values of non-tripping tests for maximum and minimum fault overcurrent.

Table 11.8: "Stop Time" for non-tripping tests, Relay 3, RTS Experiment

Fault Overcurrent	Test Name	LLTI [on/off]		Tripping Tests (RT-LAB® Second Console)		Non-Tripping Tests	
	Source - Circuit - Type of Fault - Fault Location - Opened Breaker	Relay 2	Relay 3	Ending Fault Time, cycles [T_{EF}]	Measured Fault State Time, cycles [T_{FSm} =T_{EF} - 150]	Stop Time, sec. [T_{S2}]	Stop Time, sec. [T_{S3}]
Maximum	UTILITY-8765/1234-DLG(BC)-Bus6-BK8	on	on	169.650	19.65		3.03
	DG2-678/65-SLG(A)-Bus6-BK8	on	on	165.825	15.83		2.97
	DG2-678/65-SLG(A)-Bus6-BK7	on	on	173.355	23.36		3.09
	DG2-678/65-SLG(A)-Bus7-BK7	**off**	**on**	**181.095**	**31.10**		**3.20**
	DG2-67/65-SLG(A)-Bus6-BK8	on	on	165.315	15.32		2.97
	DG2-67/65-SLG(A)-Bus6-BK7	on	on	171.015	21.02		3.05
	DG2-6543-SLG(A)-Bus4-BK8	on	on	165.885	15.89		2.97
	DG2-6543-SLG(A)-Bus6-BK8	on	on	165.000	15.00		2.96
	DG2-65-SLG(A)-Bus6-BK8	on	on	165.345	15.35		2.97
	DG2-6781-SLG(A)-Bus6-BK7	on	on	172.425	22.43		3.07
	DG2-6781-SLG(A)-Bus7-BK7	**off**	**on**	**178.746**	**28.75**		**3.17**
	DG2-678-SLG(A)-Bus6-BK7	on	on	173.205	23.21		3.08
	DG2-678-SLG(A)-Bus7-BK7	**off**	**on**	**177.840**	**27.84**		**3.15**
	DG2-67-SLG(A)-Bus6-BK7	on	on	164.760	14.76		2.96
	DG1-5678-SLG(A)-Bus6-BK7	on	on	172.665	22.67		3.08
	DG1-5678-SLG(A)-Bus7-BK7	**off**	**on**	**180.750**	**30.75**		**3.20**
Minimum	UTILITY-8765/1234-LL(BC)-Bus5-BK8	on	on	177.750	27.75	2.92	
	DG2-678/65-LL(BC)-Bus5-BK8	on	on	185.955	35.96	3.04	
	DG2-678/65-LL(BC)-Bus7-BK7	on	on	201.885	51.89	3.28	
	DG2-678/65-LL(BC)-Bus8-BK7	**off**	**on**	**217.320**	**67.32**	**3.51**	
	DG2-67/65-LL(BC)-Bus5-BK8	on	on	186.375	36.38	3.05	
	DG2-67/65-LL(BC)-Bus7-BK7	on	on	204.528	54.53	3.32	
	DG2-6543-LL(BC)-Bus3-BK8	on	on	185.970	35.97	3.04	
	DG2-6543-LL(BC)-Bus5-BK8	on	on	181.335	31.34	2.97	
	DG2-65-LL(BC)-Bus5-BK8	on	on	185.220	35.22	3.03	
	DG2-6781-LL(BC)-Bus7-BK7	on	on	200.805	50.81	3.26	
	DG2-6781-LL(BC)-Bus8-BK7	**off**	**on**	**211.863**	**61.86**	**3.43**	
	DG2-678-LL(BC)-Bus7-BK7	on	on	201.663	51.66	3.27	
	DG2-678-LL(BC)-Bus8-BK7	**off**	**on**	**216.300**	**66.30**	**3.49**	
	DG2-67-LL(BC)-Bus7-BK7	on	on	187.380	37.38	3.06	
	DG1-5678-LL(BC)-Bus7-BK7	on	on	203.850	53.85	3.31	
	DG1-5678-LL(BC)-Bus8-BK7	**off**	**on**	**217.065**	**67.07**	**3.51**	

Bold represents the backup protection tests

In Tables 11.7 and 11.8, bold lines represent backup protection tests developed for minimum fault overcurrent. Primary relay LLTI was disconnected (off) instead of connected (on) throughout the

backup protection tests. “Stop time” values of non-tripping tests for maximum and minimum fault overcurrent were applied to set “Execution Properties” of RT-LAB® model from the host computer before loading the RT-LAB® model and running real-time simulation of non-tripping tests.

Matlab® files for non-tripping tests were generated after executing real-time simulation. Matlab® Simulink® software [14] was applied to plot tripping test results. As an example, Data collected from Matlab® file for “DG2-678/65-SLG(A)-BUS6-BK7” non-tripping test in which “stop time” of 3.09 sec. was set in “Execution Properties” based on Table 11.8 are shown in Figures 11.15 to 11.18. Figure 11.15 shows A-B-C line currents of breakers for Relays 2 and 3. The plot of A-B-C line currents of “BK7” breaker (C) shows that fault overcurrent was not cleared because “stop time” was less than the sum of pre-fault and relay times. Plots of A-B-C line currents of “BK5,” “BK6,” and “BK8” breakers (A, B, and D) show A-B-C line currents during pre-fault and fault state. Figure 11.16 shows breaker trip signals for Relays 2 and 3. Because tripping circuit of relays for RTS experiment had NC control outputs, the breaker opened when the trip signal fell from 14.3 to 0 Vdc. However, the plot of trip signals for “BK7” beaker (C) indicates that the signal was always 14.3 Vdc, without tripping “BK7” breaker. Figure 11.17 shows breaker states, indicating “1” or “0” when breakers were closed or open, respectively. The plot of “BK7”breaker states (C) indicates that “BK7” breaker remained closed because Relay 3 did not trip. Figure 11.18 shows active setting groups of Relays 2 (A) and 3 (B). Although Relays 2 and 3 had four (SS1, SS2, SS3, and SS4) and six (SS1, SS2, SS3, SS4, SS5, and SS6) setting groups available for adaptive overcurrent protection, “DG2-678/65-BUS6-BK7” non-tripping test had only setting group 2 (SS2) available for Relays 2 and 3.

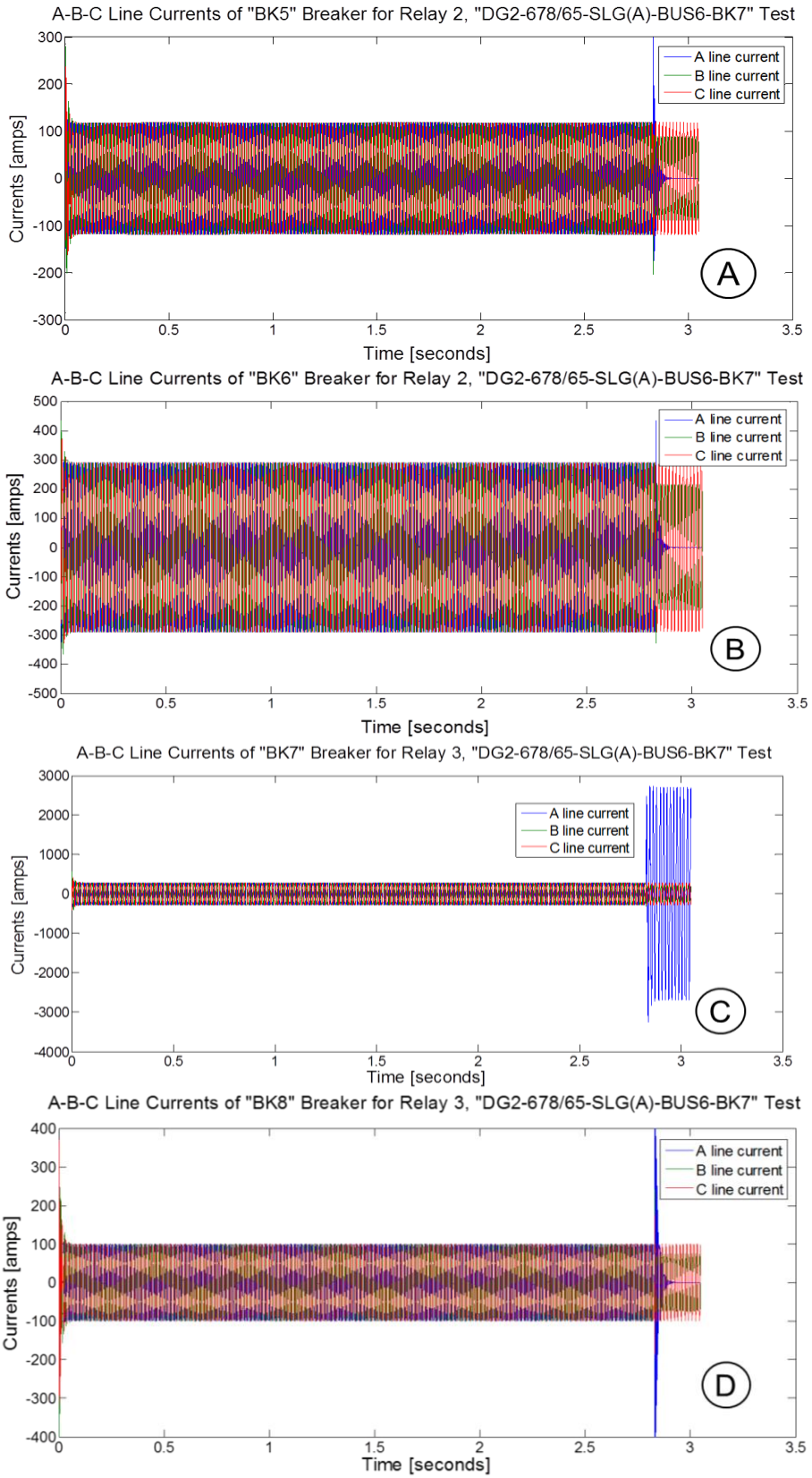

Figure 11.15: A-B-C line currents of breakers for Relays 2 and 3, "DG2-678/65-SLG(A)-BUS6-BK7" non-tripping test

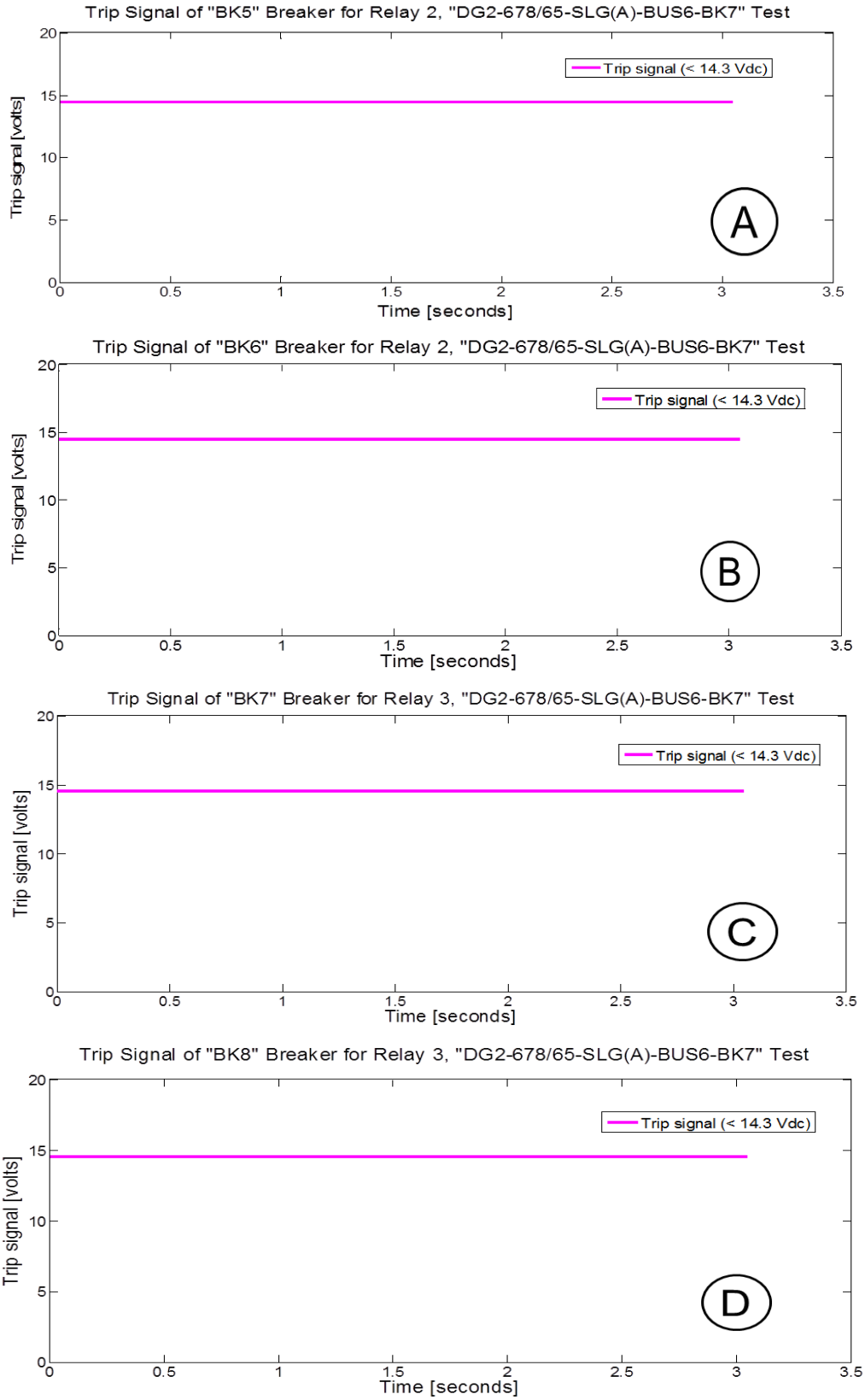

Figure 11.16: Trip signals of Relays 2 and 3, “DG2-678/65-SLG(A)-BUS6-BK7” non-tripping test

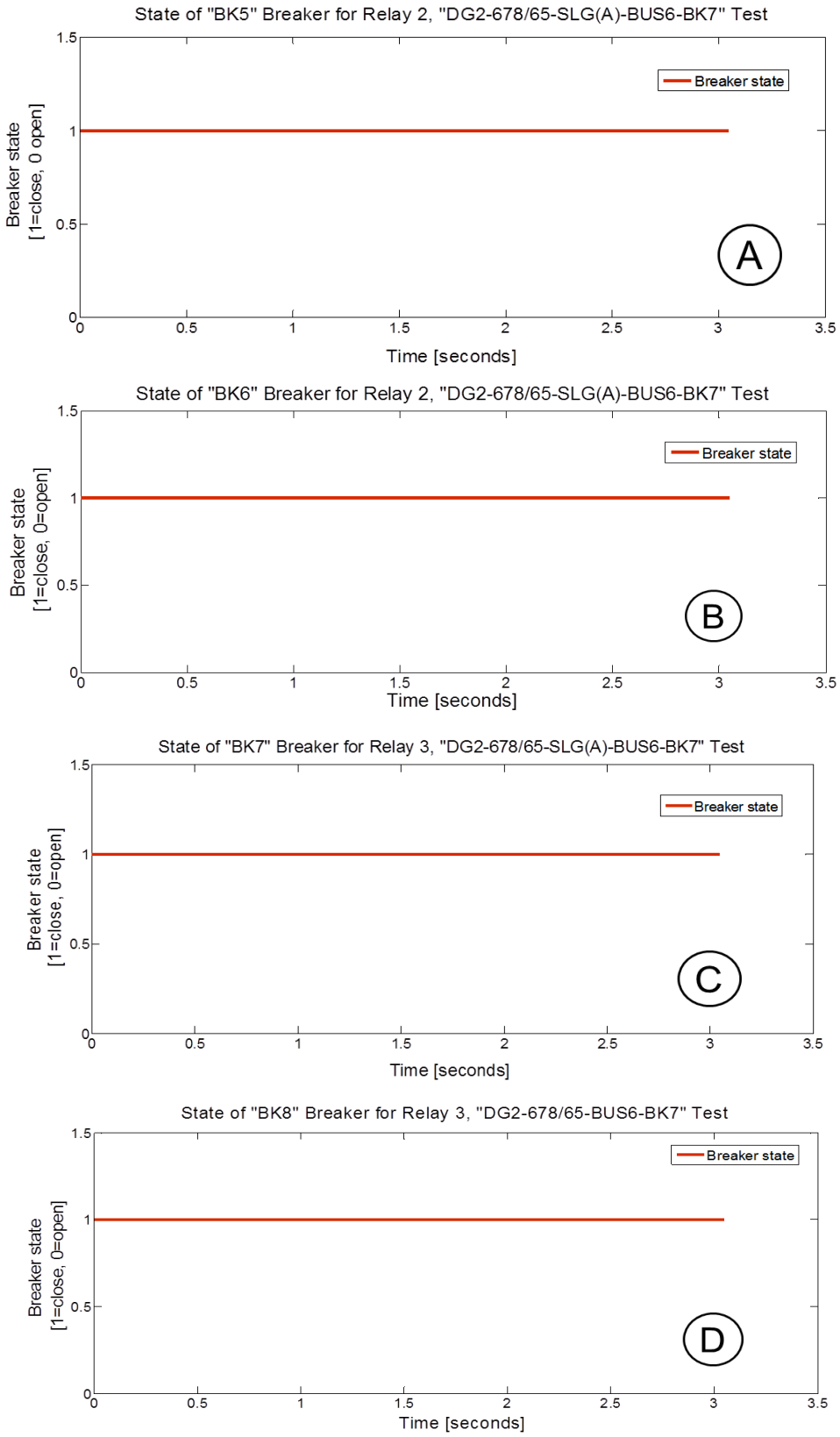

Figure 11.17: Breaker states of Relays 2 and 3, “DG2-678/65-SLG(A)-BUS6-BK7” non-tripping test

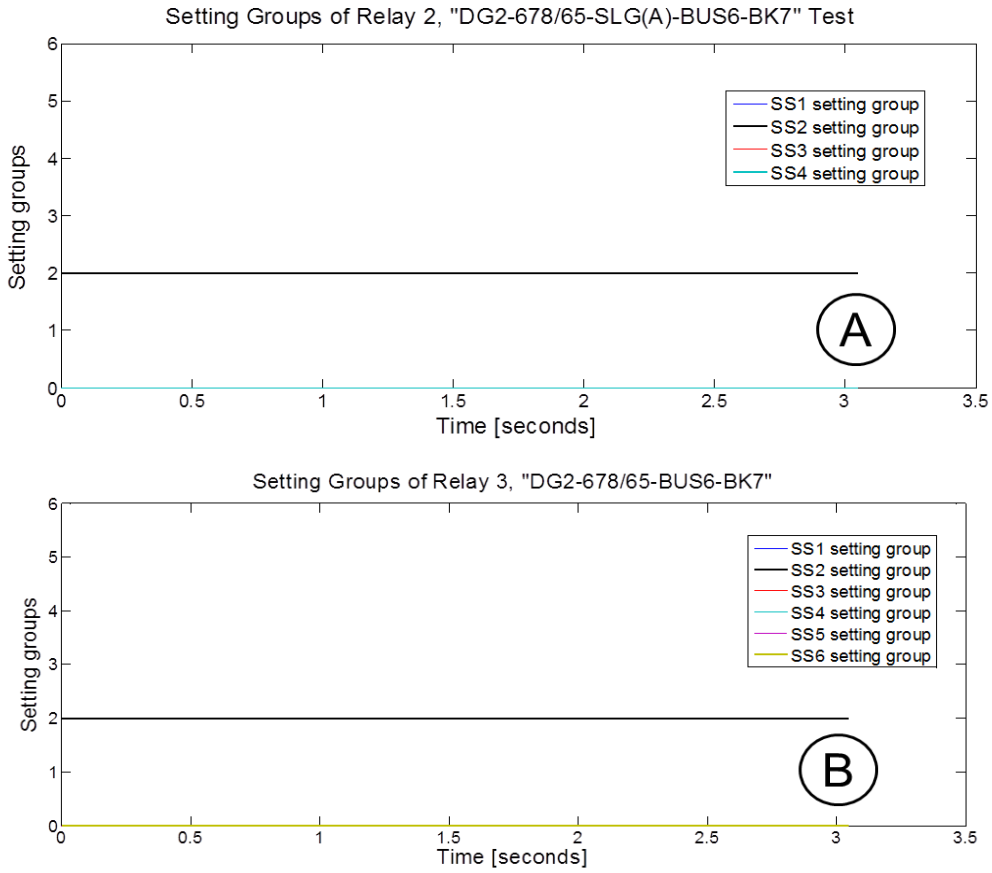

Figure 11.18: Setting groups of Relays 2 and 3, "DG2-678/65-SLG(A)-BUS6-BK7" non-tripping test

11.3 Tripping and non-tripping tests

Tripping and non-tripping tests were developed in the RTS experiment to observe whether or not relays tripped breakers. Tripping tests were set to a "stop time" greater than the sum of pre-fault and fault clearing times to observe if relays tripped. However, non-tripping tests were set at a "stop time" less than the sum of pre-fault and relay times to observe if relays not trip.

Matlab® files instead of record events were used to compare ending fault time for tripping and non-tripping tests because relay record events could not be recorded from relays when relays did not trip. Fault states of "A" line current for SLG(A) faults and "B" line currents for DLG(BC) and LL(BC) faults were collected from Matlab® files generated after executing real-time simulation for tripping and non-tripping tests. Fault states were plotted and Equation (11.5) counted cycles of fault state.

$$T_{FSm} = [(N-1)/2] + \delta \quad (11.5)$$

where T_{FSm} is measured fault state time in cycles, N is number of times the sinusoidal fault current passes through 0 amps, and δ is the sum of cycle fractions to each extreme of the fault state time in cycles. Figure 11.19 shows the fault state of "DG2-67-SLG(A)-Bus6-BK7" tripping test for maximum fault overcurrent with a plot of "A" line current of "BK7" breaker. Horizontal and vertical axes represent time in cycles and current in amps, respectively. Matlab® Simulink® software [14] was applied in order to plot Figure 11.19.

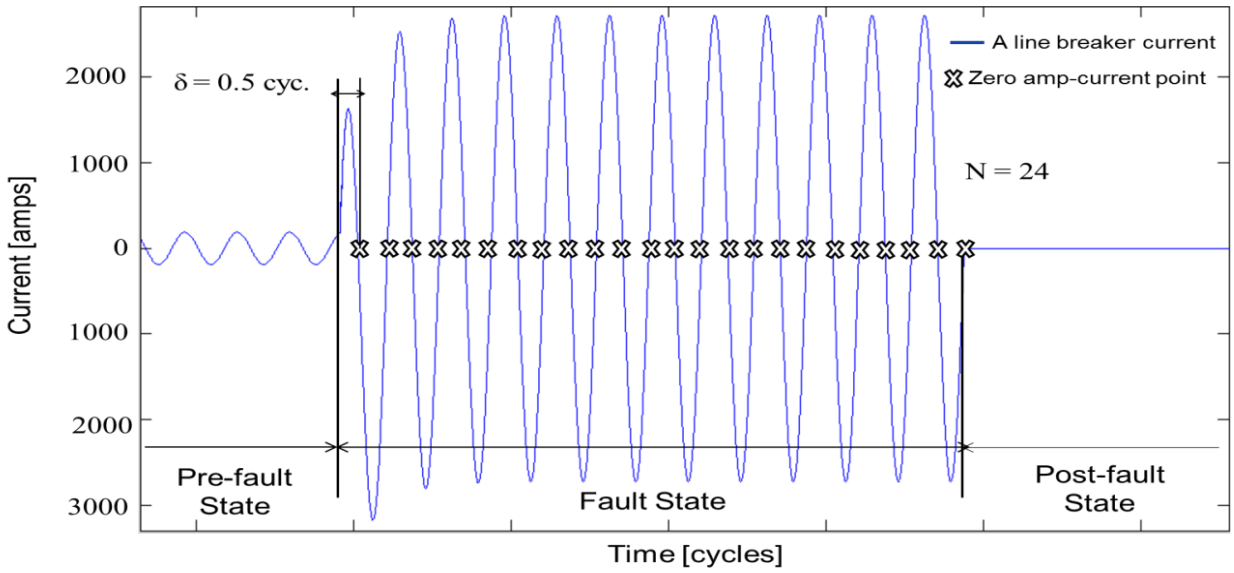

Figure 11.19: "DG2-67-SLG(A)-Bus6-BK7" tripping test for maximum fault overcurrent

Based on Figure 11.19 and Equation (11.5), the measured fault state time of the DG2-67-SLG(A)-Bus6-BK7" tripping test was 12 cycles. Primary pickup fault currents for tripping tests were collected from the "C8_13142" record event that corresponded to "DG2-67-SLG(A)-Bus6-BK7" tripping test for maximum fault overcurrent. Figure 11.20 shows primary pickup fault current collected from "Event Report Summary." AcSELerator Analytic Assistant® software [100] was applied to read "Event Report Summary." Adaptive overcurrent protection was analyzed for Relays 2 and 3 in the

microgrid with distributed generators by collecting primary pickup fault current for tripping tests and fault state time values for tripping and non-tripping tests.

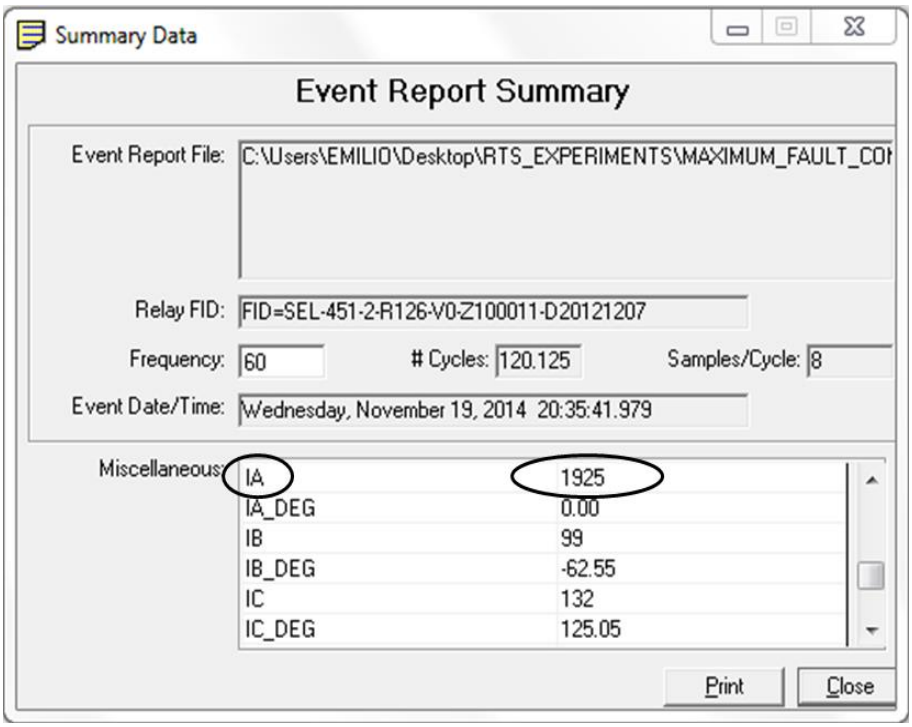

Figure 11.20: Primary pickup fault current from C8_13142 record event

Figure 11.21 shows tripping and non-tripping tests for Relays 2 (A) and 3 (B), respectively. Horizontal and vertical axes represent primary pickup fault currents and time in cycles, respectively. The red line represents the pre-fault state for tripping and non-tripping tests, and violet dots and green squares represent the ending fault time for tripping and non-tripping states, respectively. For the identical "source-circuit-fault type-fault site-tripped breaker" tripping and non-tripping tests, the ending fault time of the tripping test was greater than the ending fault time of non-tripping test. For non-tripping tests, fault overcurrents flowed along relay breakers, but the relay did not trip, verifying the non-trip condition. However, for tripping tests, fault currents flowed along relay breakers, and the relay tripped, verifying the tripping condition. Ending fault time and primary pickup fault current values of Figure 11.21 are presented in Appendix Q, Tables Q.1 and Q.2.

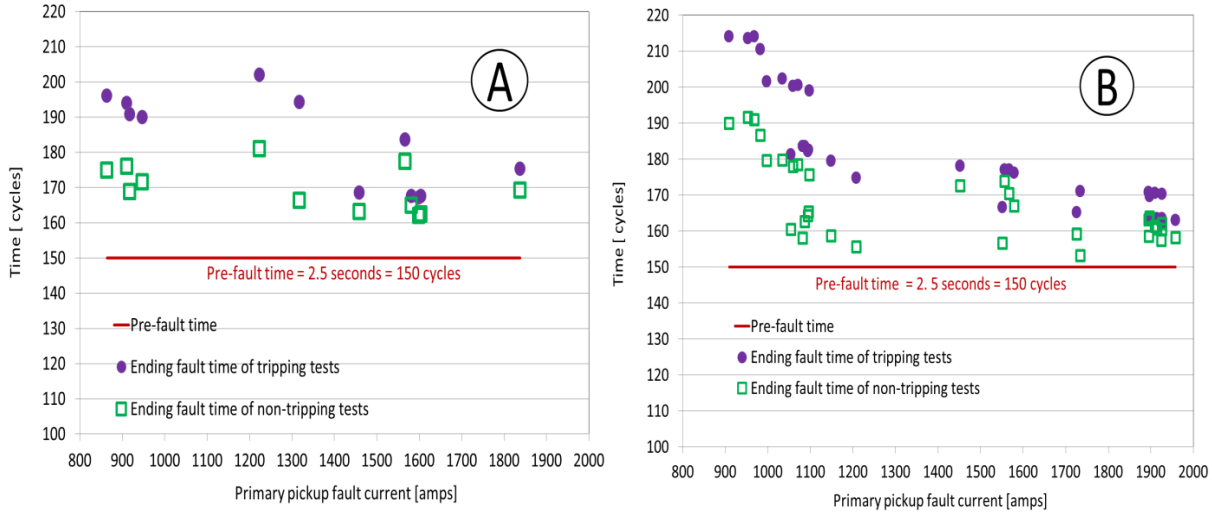

Figure 11.21: Ending fault time for tripping and non-tripping tests of Relays 2 (A) and 3 (B)

11.4 Validation of real-time simulation

Real-time simulation was validated by plotting relay and microgrid fault state time for the "DG2-678/65-SLG(A)-BUS7-BK5" tripping test. By analyzing Matlab® and HR event files from the microgrid and relay, respectively, real-time simulation was validated by plotting and visualizing the identical measured fault state time from the microgrid and relay.

The fault state collected from HR (High Resolution) record event (Relay 2) and Matlab® (microgrid) files for the identical tripping test were visually compared. The "HR_14169" record event and Matlab® files corresponding to "DG2-678/65-SLG(A)-BUS7-BK5" tripping test were analyzed by plotting A-B-C line currents. In this tripping test, DG2-678/65 circuit path and single line-to-ground fault located near Bus 7 were considered. Then "BK5" breaker of Relay 2 tripped by clearing fault overcurrent. Figure 111.22 shows A-B-C line currents of "BK5" breaker collected from Relay 2 (A) and microgrid (B), respectively. AcSELerator Analytic Assistant® software [100] was applied to obtain plots in Figure 11.22. Length of pre-fault time for the record event was set at 0.1 sec. for Relay 2. However, length of pre-fault time for the relay tests was greater than 2.5 sec. for real-time simulation. The pre-fault states were not defined with identical time scales for Plots (A and B) in Figure 11.22.

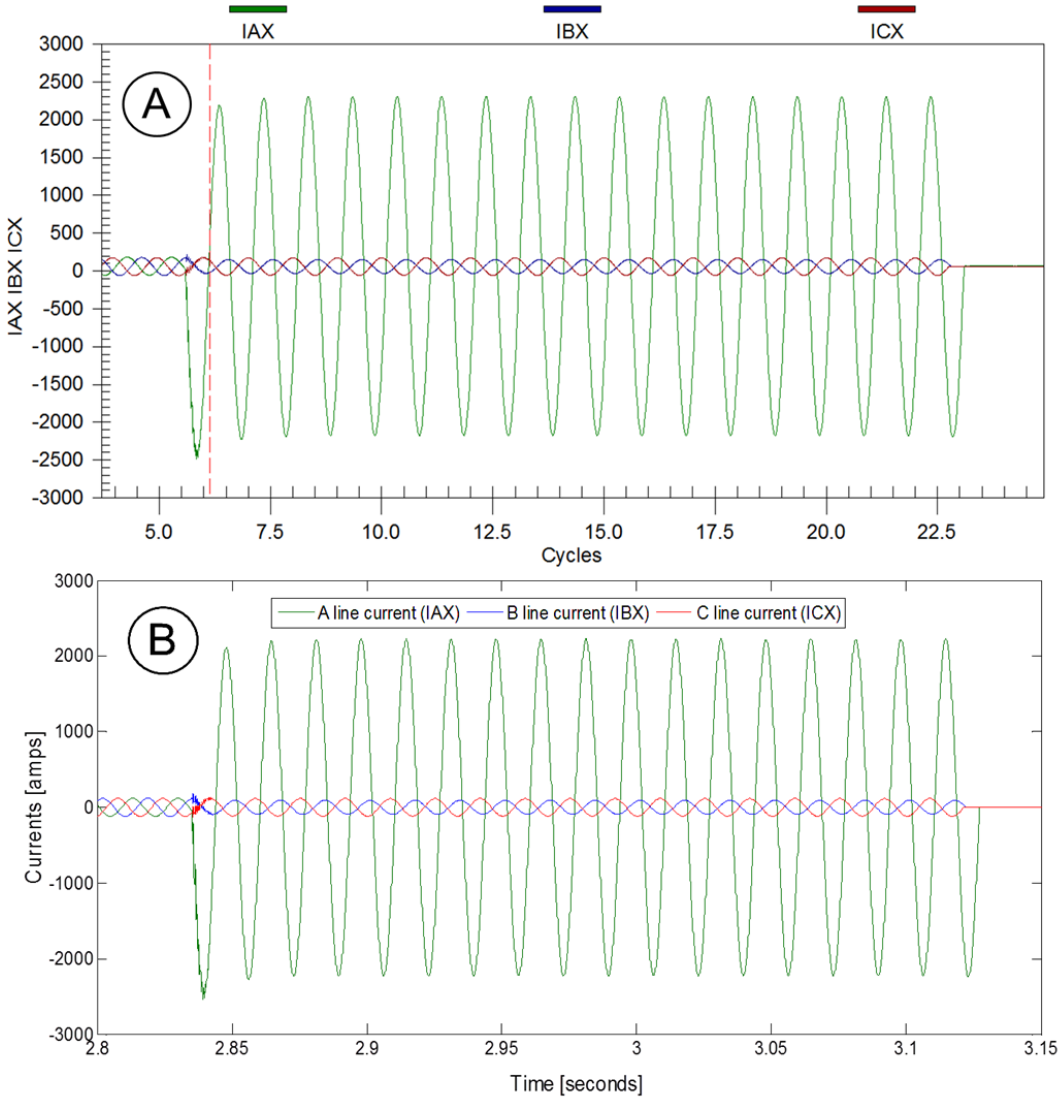

Figure 11.22: A-B-C line currents from Relay 2 (A) and microgrid (B)

In Figures 11.22 (A and B), A-B-C line currents of "BK5" breaker for fault state had similar shape and number of cycles, thereby validating real-time simulation for the tripping test. However, HR_14169 instead of the C8_14169 record event was applied because the HR_14169 record event measured the raw (not processed) instantaneous values of line currents and the C8 record event measured the digital filtered (processed) instantaneous values of currents. Therefore, the HR_14169

record event of the Relay 2 presented the same A-B-C line currents of the Matlab® file from the microgrid (real-time scenario) for the "DG2-678/65-SLG(A)-BUS7-BK5" tripping test.

11.5 Record events, RT-LAB® second console, and Matlab® files

In the RTS experiment, measured fault state time values of tripping tests were collected from relays, microgrid, and RT-LAB® second console. Fault state time values from relays, microgrid, and RT-LAB® second console were collected from C8 record event files, Matlab® files, and control fault timing circuit, respectively. Measured fault state time values from relays were collected from C8 record event files, including measurement of ending and initial fault time values and calculation of fault state time. Figure 11.23 shows initial (A) and ending (B) fault state time values from the "C8_13193" record event corresponding to "UTILITY-8765/1234-DLG(BC)-Bus6-BK8" tripping test. AcSELerator Analytic Assistant® software [100] was applied to plot Figure 11.23.

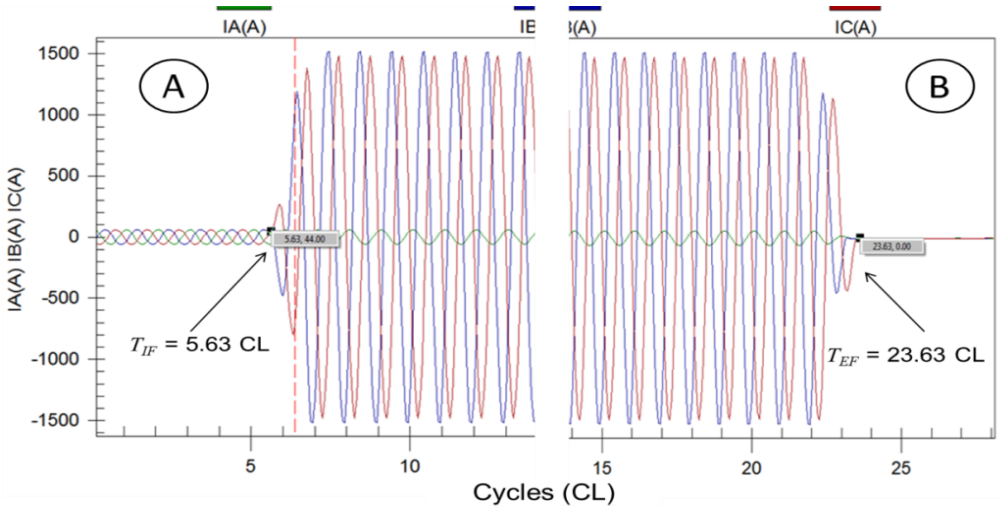

Figure 11.23: "C8_13193" record event file, "UTILITY-8765/1234-DLG(BC)-Bus6-BK8" tripping test

In Figure 11.23, initial and ending fault time values were referenced to length of pre-fault time set on Relay 3. In the "C8_13193" record event, initial and ending fault time values were 5.63 cycles and 23.63 cycles, respectively, and measured fault state time was 18 cycles, according to Equation (11.6).

$$T_{FSm} = T_{EF} - T_{IF} \tag{11.6}$$

where T_{FSm} is measured fault state time in cycles, T_{EF} is measured ending fault time in cycles, and T_{IF} is measured initial fault time in cycles.

Measured fault state time values from RT-LAB® second console were collected from the control fault timing circuit located in the RT-LAB® second console generated during execution of real-time simulation. Ending (TEF) and initial (TIF) fault state time values were measured from the TEF and TIF displays, respectively, and measured fault state time values were estimated using Equation (11.6). Figure 11.24 shows ending and initial fault time values of "UTILITY-8765/1234-DLG(BC)-Bus6-BK8" tripping test.

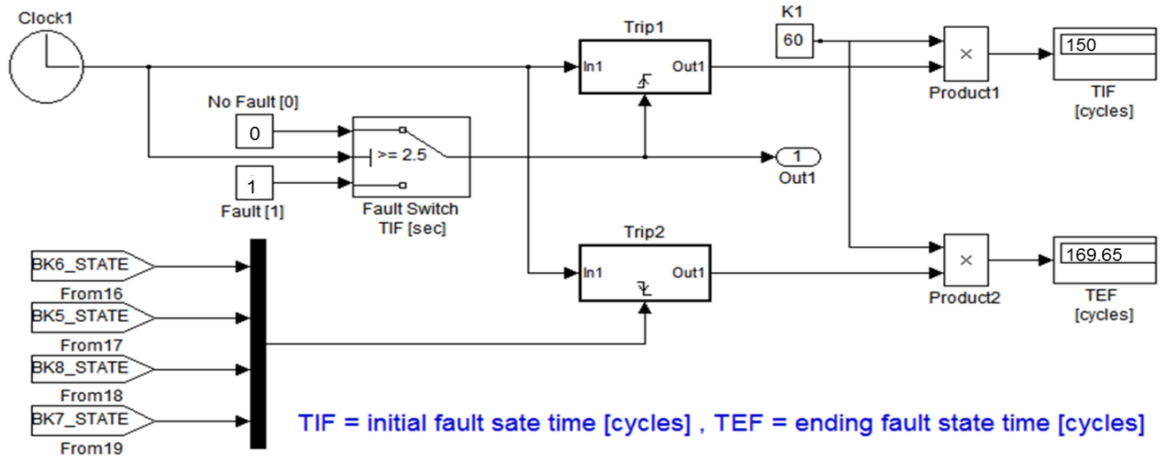

Figure 11.24: Control fault timing circuit, "UTILITY-8765/1234-DLG(BC)-Bus6-BK8" tripping test

Based on Figure 11.24, initial and ending fault time values were referenced to pre-fault time of 150 cycles on the control fault timing circuit of RT-LAB® second console. Initial and ending fault time values were 150.00 and 169.65 cycles, respectively, and Equation (11.6) determined measured fault state time to be 19.65 cycles.

Measured fault state time values from Matlab® files were generated by the "OpWriteFile" block in the "SM_Network" subsystem. The "OpWriteFile" block was configured to collect A-B-C

line currents, breaker states, trip signals, and relay setting groups. When the tripping test was executed in real-time, the "OpWriteFile" block created a Matlab® file that collected test results. The fault state from this plot was measured by plotting time and line currents in horizontal and vertical axes, respectively.

Measured fault state time values collected from record events, RT-LAB® second console, and Matlab® files were plotted in Figure 11.25, indicating measured fault state time for tripping tests of Relays 2 (A) and 3 (B). In tripping tests, fault state time also represented fault clearing time because breakers tripped.

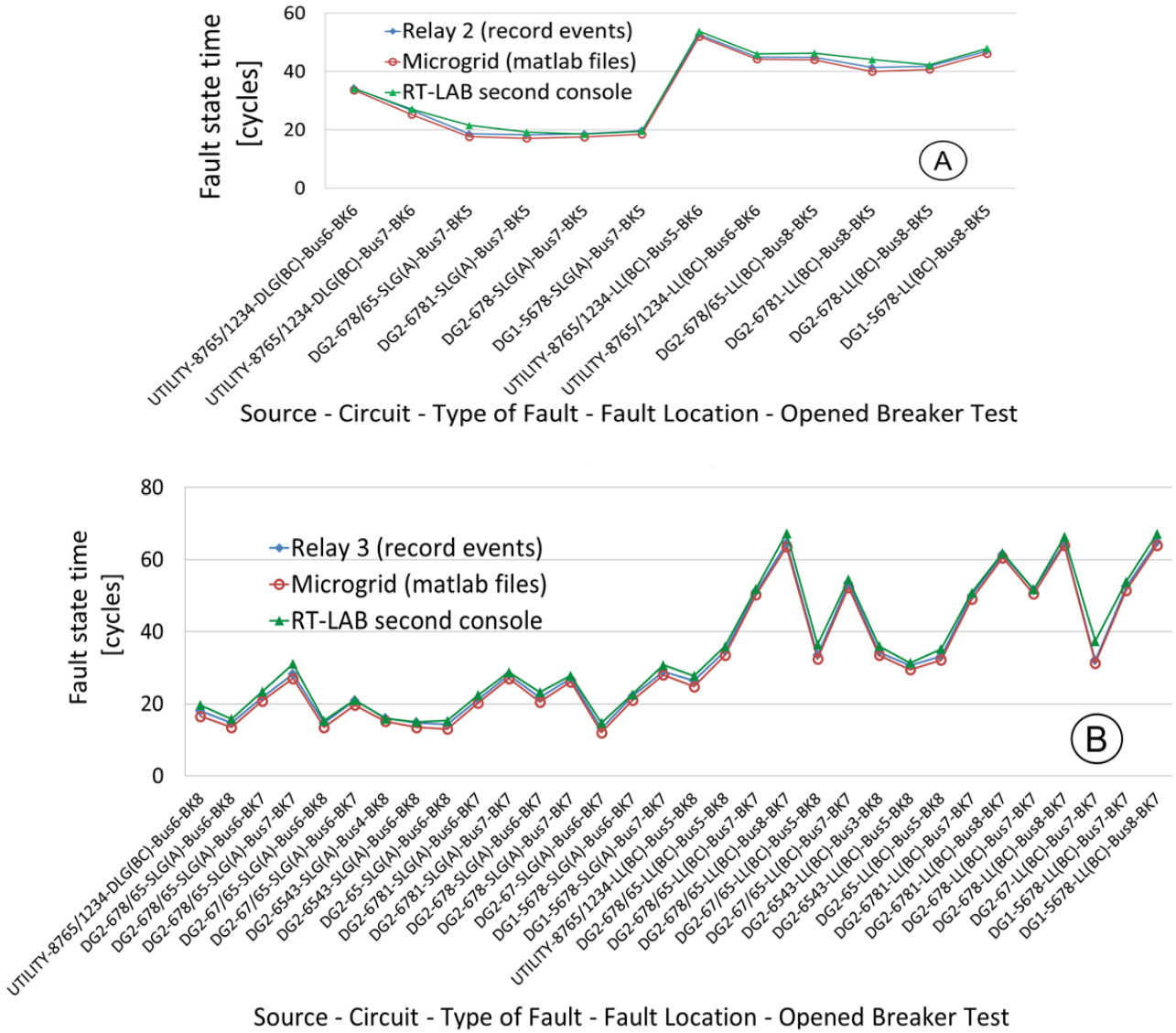

Figure 11.25: Measured fault state times from relay, microgrid, and RT-LAB® second console

Measured fault state time values from record events, RT-LAB® second console, and Matlab® files are indicated in Tables R.1 and R.2 of Appendix R. The mean ± SEM of measured fault state time values from Tables R.1 and R.2 were calculated for the three applied methods to collect tripping test results for Relays 2 and 3. SAS® software [97] was used for statistical analysis, and data distribution was evaluated using a Shapiro Wilk test. Differences in means between methods were compared. Differences were considered significant when $P < 0.05$. Figure 11.26 shows mean ± SEM of measured fault state time values collected with the event file, RT-LAB® second console, and Matlab® file methods.

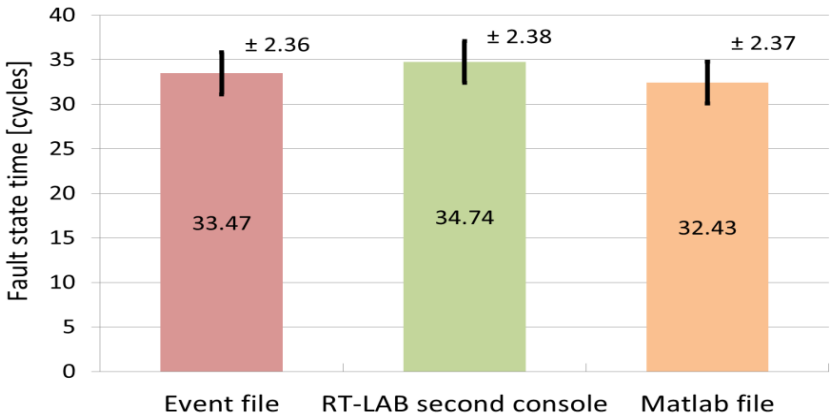

Figure 11.26: Measured fault state time values collected from event file, RT-LAB® second console, and Matlab® file (Mean ± SEM, P < 0.05)

Mean of measured fault state time values for event file (33.47 ± 2.36), RT-LAB® second console (34.74 ± 2.38), and Matlab® file (32.43 ± 2.37) methods did not differ ($P < 0.05$). Therefore, these three methods could be applied to collect fault state time for tripping tests.

11.6 Record event analysis

Analog and digital signals formed record events. Analog signals provided plots of A-B-C line breaker currents and A-B-C ground bus voltages. However, digital signals provided plots of trips, breaker states, setting groups, and control inputs and outputs. Analysis of record events allowed verification of adaptive overcurrent protection by measuring analog and digital signals from record

event plots. Therefore, record event files from tripping tests for Relays 2 and 3 were collected to plot and measure digital signals, delay, and relay times.

11.6.1 Measured digital signals

Analysis of record events allowed verification of adaptive overcurrent protection logic, trips, breaker states, setting groups, and control inputs and outputs. Having collected the "HR_14169" record event from Relay 2 that corresponded to the "DG2-678/65-SLG(A)-BUS7-BK5" tripping test, A-B-C line currents of "BK5" breaker and digital signals were plotted in Figure 11.27. AcSELerator Analytic Assistant® software [100] was applied in order to plot Figure 11.27 in which Relay 2 digital signals, SG2, IN202, PSV04, T3P2, 51S2, IN104, 52AA2, OUT107, and TRIP, are represented as bold blue lines when digital trip signals were active. Digital signals from Relay 2 are shown in Table 11.9, indicating functions, codes, names, and descriptions of digital signals.

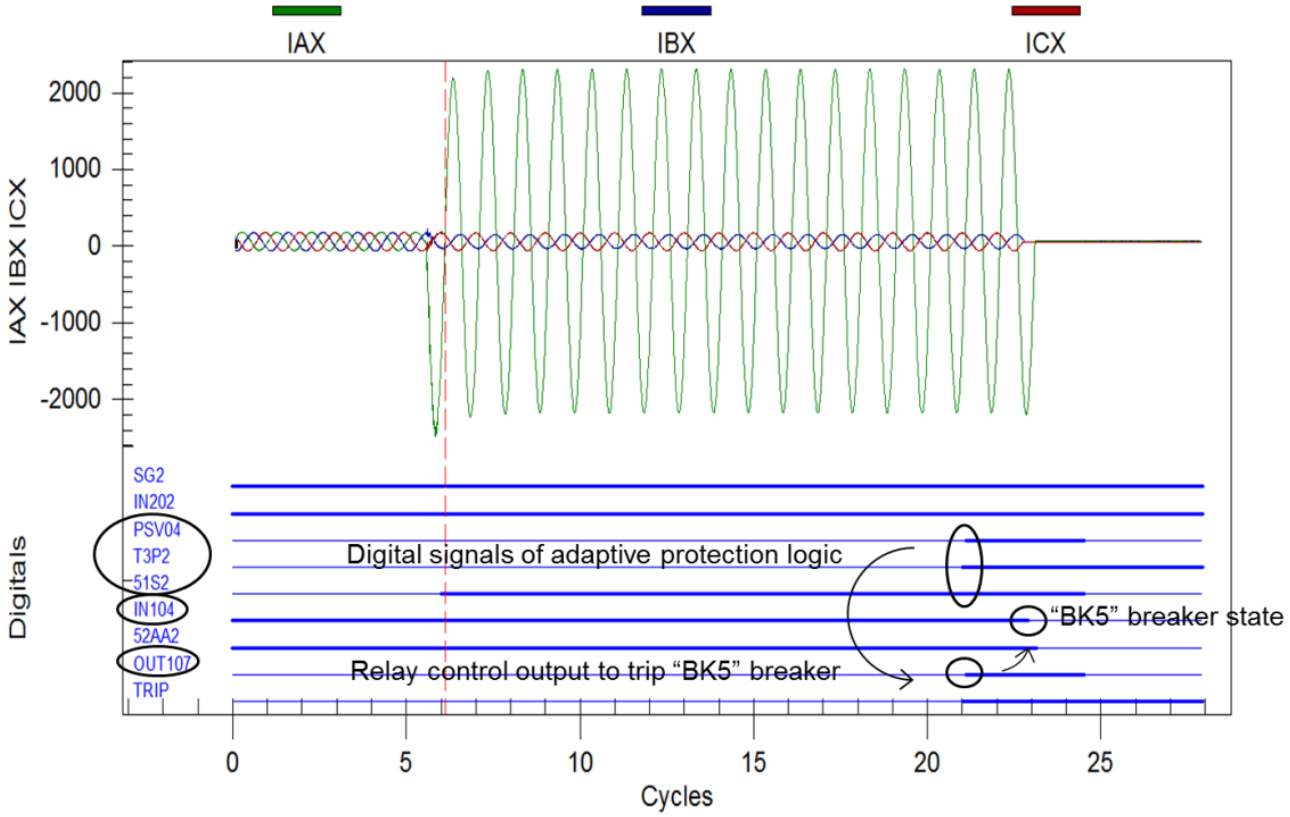

Figure 11.27: A-B-C line currents and digital signals, "DG2-678/65-SLG(A)-BUS7-BK5" tripping test.

Table 11.9: Functions, codes, names, and descriptions of digital signals

Functions	Digital Signals		Descriptions
	Codes	Names	
Setting group 2	SG2	Setting group 2	Control input turn on setting group 2
	IN102	Control input	
Adaptive protection logic	PSV04	SELogic variable	Based on protection logic, SELogic variable tripped "BK5" breaker when the inverse time overcurrent element pickup and trip circuit breaker digital signals were turned on.
	T3P2	Trip circuit breaker 2	
	51S2	Inverse time overcurrent pickup of element 2	
Breaker pole states	IN104	Control input	Control input sensed if breaker (52AAA) was open or closed
	52AA2	Breaker aux. contact	
Trip	OUT107-NC	Control output	The "PSV04" SELogic variable controlled the control output and after the trip signal, the control output tripped the "BK5" breaker.
	TRIP	Trip signal	

NC = normally closed

When the inverse time overcurrent element pickup "51S2" and trip breaker circuit "T3P2" digital signals were turned on, SELogic variable "PSV04" was active, as shown in Figure 11.27. The "PSV04" SELogic variable controlled the control output (OUT-107-NC), and the "BK5" breaker was tripped by protection logic of setting group 2 for Relay 2. This protection logic was represented by "AND" gate, as shown in Figure 11.28.

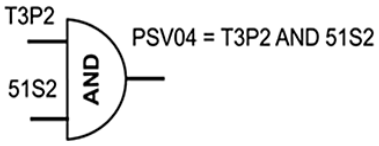

T3P2	51S2	PSV04
1	1	1
0	1	0
1	0	0
0	0	0

Figure 11.28: Protection logic of setting group 2 for Relay 2

Based on Figures 11.27 and 11.28, at "51S2" and "T3P2" digital signals were active, the "PSV04" SELogic variable was generated simultaneously with the "OUT107" NC control output signal validating the "AND" protection logic gate. In addition, "HR" record events were collected from tripping tests for Relays 2 and 3, plotting and verifying digital signals of adaptive protection logic for setting groups of Relays 2 and 3.

11.6.2 Measured delay time

In real-time simulation with relays in the loop, delay time of the tripping tests for Relays 2 and 3 were defined by the sum of relay-microgrid communication and tripping circuit delay time. In the tripping tests, C8 record events of Relays 2 and 3 were collected and delay and relay time values were measured.

As an example of how collecting the measured delay time for the "DG2-678/65-SLG(A)-BUS7-BK5" tripping test, AcSELerator Analytic Assistant® software [100] was applied to analyze the"C8_14169" record that corresponded to the "DG2-678/65-SLG(A)-BUS7-BK5" tripping test. The event report summary of "C8_14169" record event was opened in order to determine the magnitude of A-B-C line currents for the fault state, the "BK5" of Relay 2 was tripped in the "DG2-678/65-SLG(A)-BUS7-BK5" tripping test. Figure 11.29 presents the magnitude of A-B-C line currents for "C8_14169" record events. The primary pickup fault current for the "DG2-678/65-SLG(A)-BUS7-BK5" tripping test was 1582 amps.

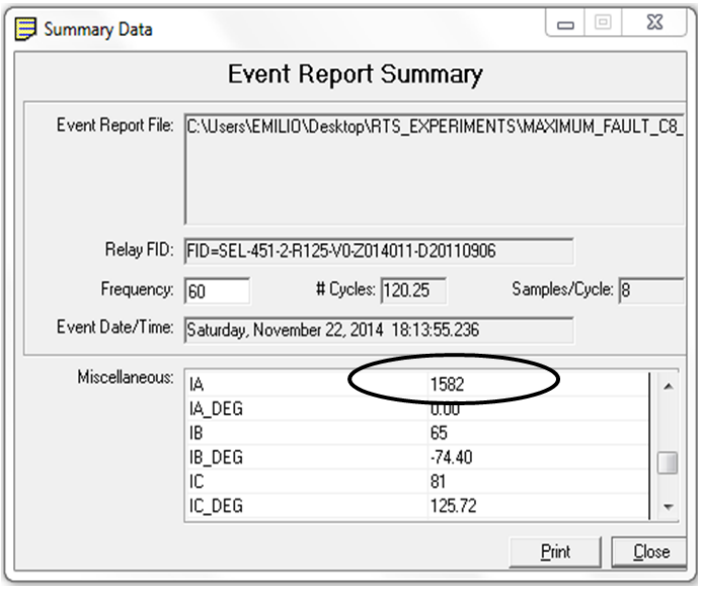

Figure 11.29: Event report summary from "C8_14169" record event

Figure 11.30 plots the magnitude of A-B-C line currents and "TRIP" digital signal from the "C8_14169" record event. The primary pickup fault current of 1582 amps was located at 7.63cycles,

and the magnitude of A-B-C line fault currents matched for record event plots and event report summary. In Figure 11.30, relays detected the primary pickup fault current after SLG(A) faults was initiated. Although relay time depended on primary pickup fault current, the relay started to count the relay time once the SLG(A) fault was initiated. As shown in Figure 11.30, the measured fault clearing time (T_{Cm}) was represented by the sum of measured relay (T_{Rm}) and delay (T_{Dm}) time. In addition, measured fault clearing time for the tripping tests was equal to the measured fault state time (T_{FSm}). Figure 11.30 shows the magnitude of A-B-C line currents of "BK5" breaker and "TRIP" digital signal for Relay 2. The relay time of Relay 2 was measured using Figure 11.30. The relay time was initiated and finished when the fault state and trip signals were initiated, respectively, relay time of Relay 2 was 15.25 cycles. The delay time of Relay 2 was also measured from Figure 11.30, and because delay time was initiated and finished when the trip signal and post-fault state were initiated, respectively, the measured delay time of Relay 2 was 3.37 cycles.Delay time values of Relays 2 and 3 were measured for tripping tests.

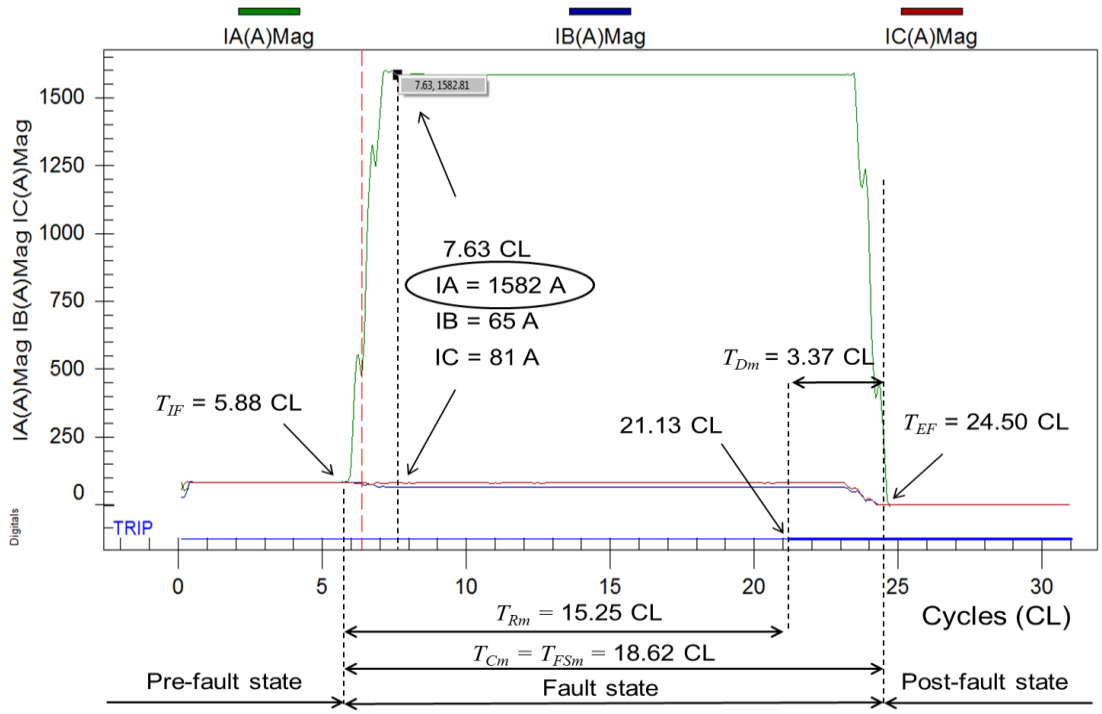

Figure 11.30: Magnitude of A-B-C line currents of "BK5" breaker, "DG2-678/65-SLG(A)-BUS7-BK5" tripping test for Relay 2, "C8_14169" record event

In Figure 11.31, red and blue dots represent the delay time of tripping tests for Relays 2 and 3, respectively. Maximum measured delay time for Relays 2 and 3 were 3.26 and 4.38 cycles, respectively. The measured delay time for each tripping test represents the sum of relay-microgrid communication and tripping circuit delay time. Measured delay time values are shown in Tables S.1 and S.2 of Appendix S.

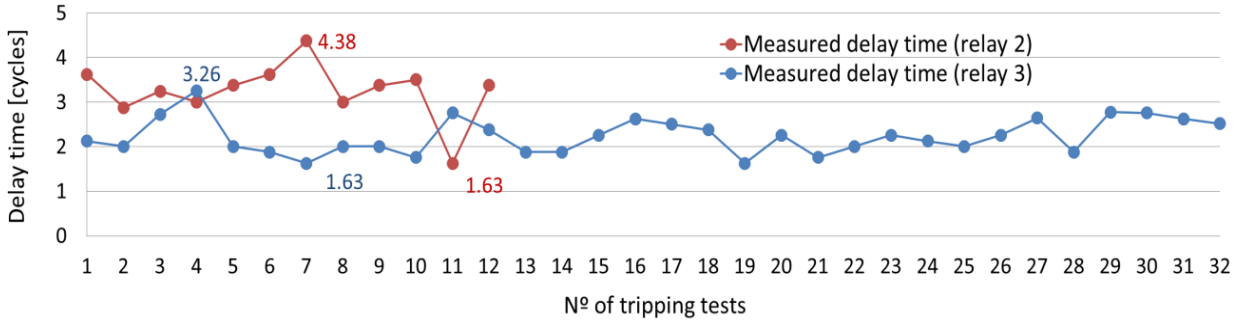

Figure 11.31: Measured delay time of tripping tests for Relays 2 and 3

11.7 Theoretical and measured relay time

Theoretical and measured relay time values were evaluated for the tripping tests. Although theoretical relay values were based on the inverse time overcurrent U3 curve from the relay instruction manual [5], measured relay time values were collected from relay record events. Theoretical and measured relay time values for tripping tests were evaluated in order to verify record events against the inverse time overcurrent setting groups of Relays 2 and 3. Theoretical relay time values were estimated by Equation (11.7).

$$T_R = TDS \times \left(0.0963 + \frac{3.88}{(I/CTR/\ I_P)^2 - 1}\right) \times 60 \qquad (11.7)$$

where T_R is theoretical relay time in cycles, *TDS* is the inverse time overcurrent time dial setting, *I* is the primary pickup fault current in amps, *CTR* is the current transformer ratio, and I_P is the secondary overcurrent pickup in amps. In order to calculate theoretical relay time values of tripping tests for

Relays 2 and 3 using Equation (11.7), primary pickup fault currents of Tables Q.1 and Q.2 in Appendix Q and inverse time overcurrent settings from Table 11.10 were collected.

Table 11.10: Inverse time overcurrent settings of active settings for Relays 2 and 3

Setting Groups	Element	Relay 2				Relay 3			
		Breakers	**Curve**	**Secondary Overcurrent Pickup, amps [I_P]**	**Time Dial Setting [TDS]**	**Breakers**	**Curve**	**Secondary Overcurrent Pickup, amps [I_P]**	**Time Dial Setting [TDS]**
SS1	1	BK6	U3	9.00	1.13	BK8	U3	8.04	0.68
	2	BK5				BK7			
SS2	1	BK6				BK8	U3	7.88	0.77
	2	BK5	U3	7.44	0.78	BK7	U3	7.80	1.18
SS3	1	BK6				BK8			
	2	BK5				BK7	U3	7.88	1.19
SS4	1	BK6				BK8			
	2	BK5	U3	7.56	0.71	BK7	U3	7.88	0.67
SS5	1					BK8			
	2					BK7	U3	7.60	1.12
SS6	1					BK8			
	2					BK7			

Current transformer ratio (CTR) = 50

However, measured relay time values for tripping tests of Relays 2 and 3 were estimated by Equation (11.8).

$$T_{Rm} = T_{FSm} - T_{Dm} \tag{11.8}$$

where T_{Rm} is measured relay time in cycles, T_{FSm} is measured fault state time in cycles, and T_{Dm} is measured delay time for relays in cycles. Measured relay time values for tripping tests were estimated by Equation (11.8) using measured fault state and delay time values from C8 record events files shown in Tables S.1 and S.2 of Appendix S.

Figure 11.32 presents measured and theoretical relay time values for tripping tests for Relays 2 (A) and 3 (B). Horizontal and vertical axes represent primary pickup fault currents and relay time

values, respectively. Green squares and orange dots are theoretical and measured relay time values, respectively.

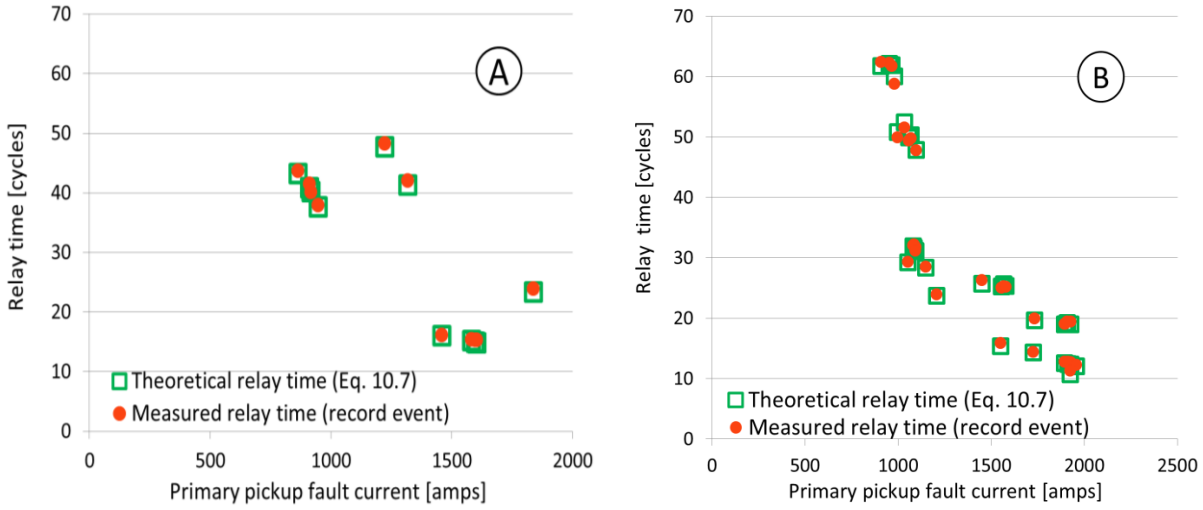

Figure 11.32: Theoretical and measured relay time values for Relays 2(A) and 3(B)

As shown in Figure 11.32, measured and theoretical relay time values represented by green square and orange dots, respectively, had matched visually, verifying the inverse time overcurrent setting groups of Relays 2 and 3 that were indicated in Table 11.10. Theoretical and measured relay time values shown in Figure 11.32 for Relays 2(A) and 3(B) were applied to estimate percent error of relay time values for tripping tests, calculated by Equation (11.9).

$$E_{TR\%} = \frac{T_{Rm} - T_R}{T_R} \times 100 \tag{11.9}$$

where $E_{TR\%}$ is percent error of relay time, T_{Rm} is measured relay time in cycles, and T_R is theoretical relay time in cycles. SAS® software [97] was used for correlation analysis. The correlation between primary pickup fault currents and relay time percent error values was evaluated for each relay using Pearson's analysis, significance was considered when $P < 0.05$. The correlation coefficient was high ($R = 0.7182$, $P = 0.0085$) and moderate ($R = 0.5279$, $P = 0.0019$) for Relays 2 and 3, respectively. Figure 11.33 presents percent error of relay time values for Relays 2 and 3 based on tripping tests. Horizontal and vertical axes represent primary pickup fault currents and percent error of relay time values,

respectively. Red diamonds and violet circles represent relay time percent error values for Relays 2 and 3, respectively.

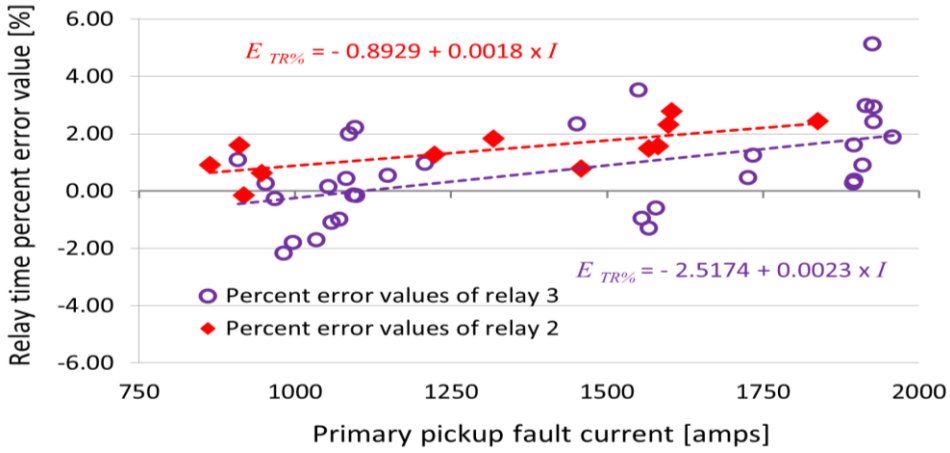

Figure 11.33: Percent error values of Relays 2 and 3

Trend line equations were estimated by correlation analysis with SAS® software application [97]. Based on these trend lines, the higher the primary pickup fault current, the higher the relay time percent error. Measured and theoretical relay time values and percent error values of tripping tests for Relays 2 and 3 are shown in Tables S.1 and S.2 of Appendix S.

11.8 Coordination time intervals

Coordination time intervals (CTIs) between the upstream (backup relay) and downstream (primary relay) protections were measured from C8 record events of Relays 2 and 3 for protection coordination scenarios in which Relays 2 and 3 were applied as backup and primary relays or vice versa, depending on the selected circuit of the microgrid and fault location. Table 11.11 shows protection coordination scenarios for Relays 2 and 3. Each protection coordination scenario consisted of a backup and tripping test that corresponded to the upstream (backup relay) and downstream (primary relay) protections, respectively. Bold font in Table 11.11 represents backup protection tests. Measured relay times for backup and primary relays were collected from Tables S.1 and S.2 in Appendix S. Measured CTIs between backup and primary relays were estimated by Equation (11.10).

$$CTI_m = T_{RBm} - T_{RPm} \quad (11.10)$$

where CTI_m is the measured CTI in cycles, T_{RBm} is the measured relay time of backup (upstream protection) relay in cycles, and T_{RPm} is the measured relay time of primary (downstream protection) relay in cycles

Table 11.11: Protection coordination scenarios for Relays 2 and 3

Fault Overcurrent	Scenarios	Protection Area	Tests	LLTI[1]		C8 Event Files			
			Source - Circuit - Type of Fault -Fault Location - Opened Breaker	Relay 2 [on / off]	Relay 3 [on / off]	Record Event File	Measured Relay Time[2] of Backup Protection, cycles [T_{RBm}]	Measured Relay Time[2] of Primary Protection, cycles [T_{RPm}]	Measured CTI, cycles [CTI_m]
Maximum	1	L56	**UTILITY-8765/1234-DLG(BC)-Bus6-BK6**	**on**	**off**	**C8_14156**	**30.62**		14.75
			UTILITY-8765/1234-DLG(BC)-Bus6-BK8	on	on	C8_13193		15.87	
	2	L78	**DG2-678/65-SLG(A)-Bus7-BK7**	**off**	**on**	**C8_13113**	**24.99**		9.62
			DG2-678/65-SLG(A)-Bus7-BK5	on	on	C8_14169		15.37	
	3	L78	**DG2-6781-SLG(A)-Bus7-BK7**	**off**	**on**	**C8_13157**	**25.24**		10.00
			DG2-6781-SLG(A)-Bus7-BK5	on	on	C8_14173		15.24	
	4	L78	**DG2-678-SLG(A)-Bus7-BK7**	**off**	**on**	**C8_13149**	**25.12**		9.88
			DG2-678-SLG(A)-Bus7-BK5	on	on	C8_14175		15.24	
	5	L78	**DG1-5678-SLG(A)-Bus7-BK7**	**off**	**on**	**C8_13138**	**26.24**		10.12
			DG1-5678-SLG(A)-Bus7-BK5	on	on	C8_14177		16.12	
Minimum	6	L56	**UTILITY-8765/1234-LL(BC)-Bus5-BK6**	**on**	**off**	**C8_14026**	**48.24**		24.37
			UTILITY-8765/1234-LL(BC)-Bus5-BK8	on	on	C8_13015		23.87	
	7	L78	**DG2-678/65-LL(BC)-Bus8-BK7**	**off**	**on**	**C8_12794**	**62.24**		20.75
			DG2-678/65-LL(BC)-Bus8-BK5	on	on	C8_13953		41.49	
	8	L78	**DG2-6781-LL(BC)-Bus8-BK7**	**off**	**on**	**C8_13000**	**58.72**		20.85
			DG2-6781-LL(BC)-Bus8-BK5	on	on	C8_14052		37.87	
	9	L78	**DG2-678-LL(BC)-Bus8-BK7**	**off**	**on**	**C8_12987**	**61.72**		21.60
			DG2-678-LL(BC)-Bus8-BK5	on	on	C8_14048		40.12	
	10	L78	**DG1-5678-LL(BC)-Bus8-BK7**	**off**	**on**	**C8_12980**	**62.36**		18.74
			DG1-5678-LL(BC)-Bus8-BK5	on	on	C8_14044		43.62	

CTI = Coordination time interval , Bold represents backup protection tests, [1] Low level test interface, [2] Values from Tables S.1-2 in Appendix S,

Measured CTIs for protection coordination scenarios for Relays 2 and 3 were plotted by Equation (11.10) and collecting relay times from Table 11.11, as shown in Figure 11.34. In the figure,

blue and green bars represent measured CTIs for minimum and maximum fault overcurrents, respectively.

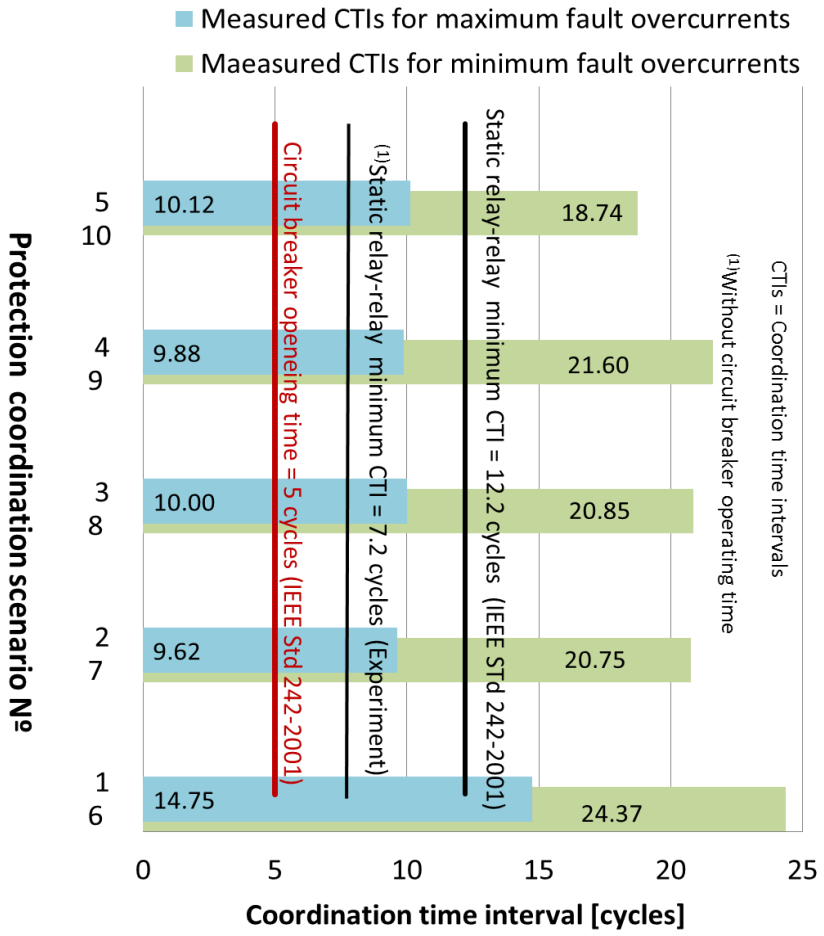

Figure 11.34: Measured CTIs for protection coordination scenarios

Based on the IEEE Std 242-2001 [7], the minimum CTI for "static relay- static relay" coordination was 0.20 sec. (12.2 cycles) for maximum fault current, based on the sum of the circuit breaker opening time (0.08 sec. = 5 cycles) and relay tolerance and setting error time (0.12 sec. = 7.2 cycles). However, since the circuit breaker operating time was not added in the RTS experiment, the minimum CTI between primary and backup relays was 0.12 sec. (7.2 cycles) instead of 0.20 sec. (12.2 cycles). In Figure 11.34, the measured CTIs for maximum fault current tests were not less than 7.2 cycles, verifying the inverse time overcurrent settings of relays 2 and 3.

The measured CTIs were acceptable because the primary relay tripped instead of backup relay for the“DG2-678/65-SLG(A)-Bus7-BK5,” “DG2-6781-SLG(A)-Bus7-BK5,” “DG2-678-SLG(A)-Bus7-BK5,” “ DG1-5678-SLG(A)-Bus7-BK5,” and “DG1-5678-SLG(A)-Bus7-BK5” tests. In the RTS experiment, relays 2 and 3 were tested with a real-time simulator in a loop at the same time (power system real-time simulation). Then, selectivity coordination between relays 2 and 3 was observed during the real-time tests, primary relay tripped faster than backup relay, validating the application of the minimum CTI of 0.12 sec. (7.2 cycles) instead of 0.2 sec. (12.2 cycles) between relays 2 and 3 for RTS experiment.

11.9 Chapter summary

This chapter presented RTS experiment results. The RTS experiment was divided into tripping and non-tripping tests, including backup protection tests in tripping tests. For tripping and non-tripping tests, setting groups of relays, A-B-C- line currents, trip signals, and states of breakers were collected. In tripping tests, real-time simulation was stopped at a time greater than the sum of pre-fault and fault clearing time, including observation that relays had tripped. However, non-tripping tests were stopped at a time less than the sum of pre-fault and relay time, including observation that relays did not trip. Plotting breaker states and trip signals for tripping tests verified that relays tripped breakers. However, for non-tripping tests, verification was made that relays did not trip breakers.

In order to validate real-time simulation with relays in the loop, results were collected as Matlab® and record event files from the microgrid and relays, respectively, observing that A-B-C- line currents for fault state matched. For non-tripping tests, results were collected from the microgrid instead of relays because relays did not record event files when relays did not trip.

SAS® software [97] evaluated methods for collecting test results in order to verify that measured fault state time values collected from RT-LAB® second console, microgrid, and relays were acceptable for testing relays in the loop with OP5600 as a relay test system. Results obtained with the

three methods did not differ, indicating that all these methods were validated. Analysis of relay record events was performed and A-B-C line currents of tripped breaker and digital variables were plotted to verify the protection logic of setting groups for relays.

Measured delay time of relays was defined by the sum of relay-microgrid communication and tripping circuit delay time. Delay time values for Relays 2 and 3 were measured from record events collected from tripping tests. Measured and theoretical relay time values were identical, verifying inverse time overcurrent protection settings for groups of Relays 2 and 3. Measured relay time values allowed percent error calculation and measured CTIs between backup and primary relays for protection coordination scenarios.

Conclusions of this chapter were based on collected results that demonstrated that the selectivity, speed, and reliability of the adaptive inverse time overcurrent protection were achieved and that OP-5600 with relays in the loop can be utilized as a real-time relay test system.

Selectivity: In adaptive inverse time overcurrent protection, each relay had two breakers. The protection logic of the setting groups allowed breakers to be tripped based on circuit paths. For maximum and minimum fault overcurrents of tripping and non-tripping tests, breaker state sequences were verified satisfactorily, breakers were open or remained closed for tripping and non-tripping tests, respectively. In addition, the protection logic of the setting groups validated the selectivity of the adaptive inverse time overcurrent protection, selecting breakers that tripped or remained closed for the circuit paths with distributed generators in the microgrid.

Speed: In adaptive inverse time overcurrent protection, setting groups were set with inverse time overcurrent settings based on upstream fuses and/or relays. Application of various inverse time overcurrent settings achieved the speed to clear a fault overcurrent because inverse time overcurrent settings were adequate for each circuit path. The inverse time overcurrent settings of Relays 2 and 3 were verified by evaluating measured and theoretical relay times. In addition, digital signals of the

protection logic gate of the setting groups generated the trip signal without delay, confirming non-delay in protection logic applied in adaptive inverse time overcurrent protection.

Reliability: Protection coordination was applied to achieve the reliability of adaptive inverse time overcurrent protection. When the primary relay did not trip because of a CT failure, the backup relay tripped the breaker, thereby clearing the fault overcurrent. Protection coordination scenarios were verified by observing that the primary relay tripped instead of the backup relay when the LLTI of both relays was connected. Backup protection tests were also performed in order to disconnect the LLTI of primary relays and observe whether or not the backup relays tripped. Measured CTIs between primary and backup relays were verified.

Real-time relay test system: The OP-5600 real-time simulator with Relays 2 and 3 in the loop was applied in the Burns & McDonnell - K-State Smart Grid Laboratory [8]. Setting groups of adaptive inverse time overcurrent protection for the microgrid with distributed generators were verified and real-time simulation was validated by evaluating the microgrid fault state and relays collected from Matlab® and record event files, respectively. Confirmation that OP-5600 with relays in the loop could be used as a relay test system was verified in this research. This experiment was the first application of a real-time simulator with relays in the loop at Kansas State University and they results will significantly contribute to other graduate students' research regarding techniques of real-time simulators with relays in the loop.

Chapter 12 - Conclusions

Adaptive overcurrent protection was developed in this research in order to integrate fuses and relays in a microgrid with distributed generators. The proposed adaptive overcurrent protection was tested with two relay in the loop techniques in order to verify adaptive overcurrent settings. This adaptive overcurrent protection was proven to achieve selectivity, speed, and reliability during the relay tests. In addition, application of NRTS and RTS with relays in the loop for testing Relays 2 and 3 setting groups for adaptive overcurrent protection were described.

12.1 Research contributions

Utilities have used fuses instead of protective relays in power distribution systems because fuses are less expensive than protective relays. However, cost of protective relays has decreased in the last years [73]. In this research, the proposed adaptive overcurrent protection significantly contributed to the improvement of protection and control systems for microdgrid with distributed generators that must integrate feeder fuses with relays. This adaptive overcurrent protection integrated technically and economically advantageous of relays and fuses, respectively, in order to achieve selectivity, reliability, and speed of protection systems in a microgrid with distributed generators.

In addition, this author was the first graduate student to implement real-time simulation with two relays in the loop at the Burns & McDonnell - K-State Smart Grid Laboratory [8] by integrating a relay's digital and analog signals with OP5600 [4]. The RTS experimental circuit and project are detailed in this dissertation so that other graduate students can apply this technique with relays in the loop to research areas such as phasor measurement units, adaptive protection systems, and communication and cyber security applications.

12.2 Conclusions of adaptive overcurrent protection

Adaptive overcurrent protection developed in this research was based on the relay setting group and protection logic methods. The adaptive overcurrent protection was designed to protect power lines and bus feeders of the microgrid with distributed generators by coordinating inverse time-current curves of fuses and relays in the microgrid. Based on relay test results collected for tripping and non-tripping tests, adaptive inverse time overcurrent protection achieved selectivity, speed, and reliability.

Selectivity: In adaptive inverse time overcurrent protection, each protective relay contained two breakers. The breaker adjacent to the overcurrent fault (primary protection) always tripped more quickly than the other breakers (backup protection) in order to clear the overcurrent fault at the protection area (power line) and keep the rest of the power lines in the circuit energized. In addition, determination of which breaker tripped or did not trip depended on the active circuit path in the microgrid. Selectivity of the adaptive overcurrent protection system was achieved by configuring relay setting groups for circuit paths in the microgrid and inverse time overcurrent elements and protection logics for each relay breaker. Setting groups of Relays 2 and 3 were selected by grouping similar circuit paths with identical protection logic gates and inverse time overcurrent settings. In adaptive overcurrent protection, relay breakers were controlled by “AND” or “ZERO” logic gates to trip or not trip, respectively. “AND” logic gate input was formed by the inverse time overcurrent element pickup (51S1 or 51S2) and the trip circuit breaker (T3P1 or T3P2) digital signals, but the “ZERO” gate was an open circuit. “AND” and “ZERO” gates were the relay control inputs for expected tripping and non-tripping breakers, respectively. Validation of selectivity for adaptive overcurrent protection was achieved by verifying the breaker state sequence of Relays 2 and 3. Based on selectivity, Relays 2 and 3 had to trip one breaker at fault states of tripping tests. NRTS and RTS with relay in the loop techniques, called NRTS and RTS experiments, respectively, were run for maximum and minimum

fault overcurrent tests, including backup protection tests. As shown in Figures 12.1 and 12.2, expected breaker state sequences were verified by the NRTS (A) and RTS (B) experiments for Relays 2 and 3, respectively, thereby validating selectivity of breaker state sequence for adaptive overcurrent protection.

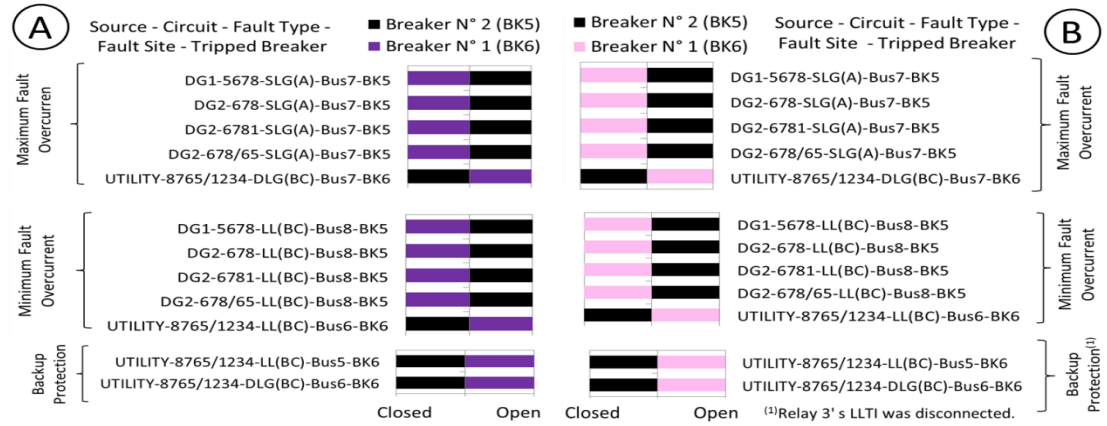

Figure 12.1: Breaker state sequence by (A) NRTS and (B) RTS experiments for Relay 2

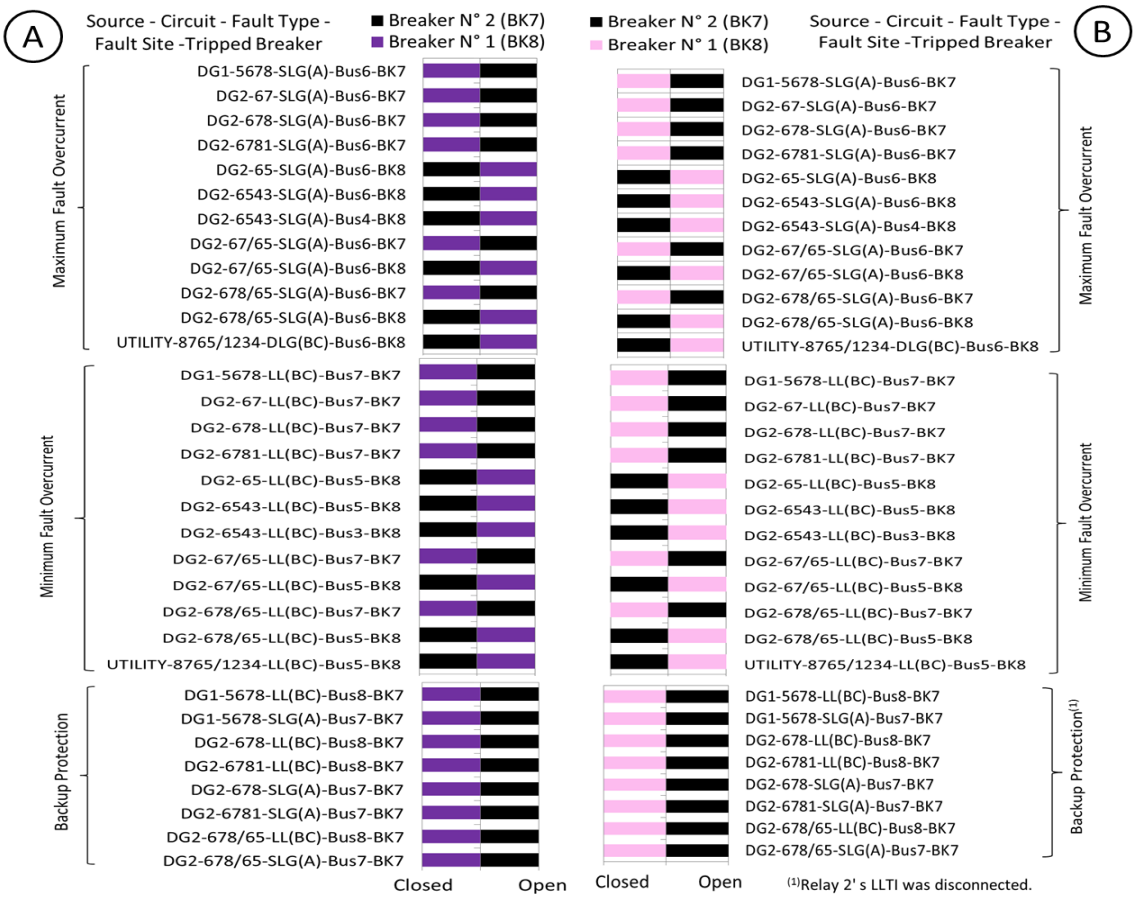

Figure 12.2: Breaker state sequence by (A) NRTS and (B) RTS experiments for Relay 3

Figures 12.1 and 12.2 show measured breakers states of tripping tests for Relays 2 and 3, respectively, based on NRTS (A) and RTS (B) experiments. As in the RTS experiment, Relays 2 and 3 were tested together and the LLTI of the primary relay was disconnected before running the backup protection test in order to observe tripping of backup relays. In addition, NRTS and RTS experiments for non-tripping tests were run for Relays 2 and 3, proving that the relays did not trip at fault overcurrent when fault state times were less than relay times.

Speed: In adaptive inverse time overcurrent protection, setting groups of Relays 2 and 3 were set with inverse time overcurrent settings based on upstream fuses and/or relays for circuit paths. Inverse time overcurrent elements of setting groups for Relays 2 and 3 tripped breakers at maximum fault overcurrents in less than 30 cycles (0.5 sec), thereby achieving speed in order to clear overcurrent faults. Validation of speed for adaptive overcurrent protection was verified by collecting measured fault clearing times of Relays 2 and 3 for tripping tests. Figure 12.3 shows measured fault clearing times for maximum fault overcurrents (excluding backup protections) of tripping tests for Relays 2 (A) and 3 (B) based on NRTS and RTS experiments.

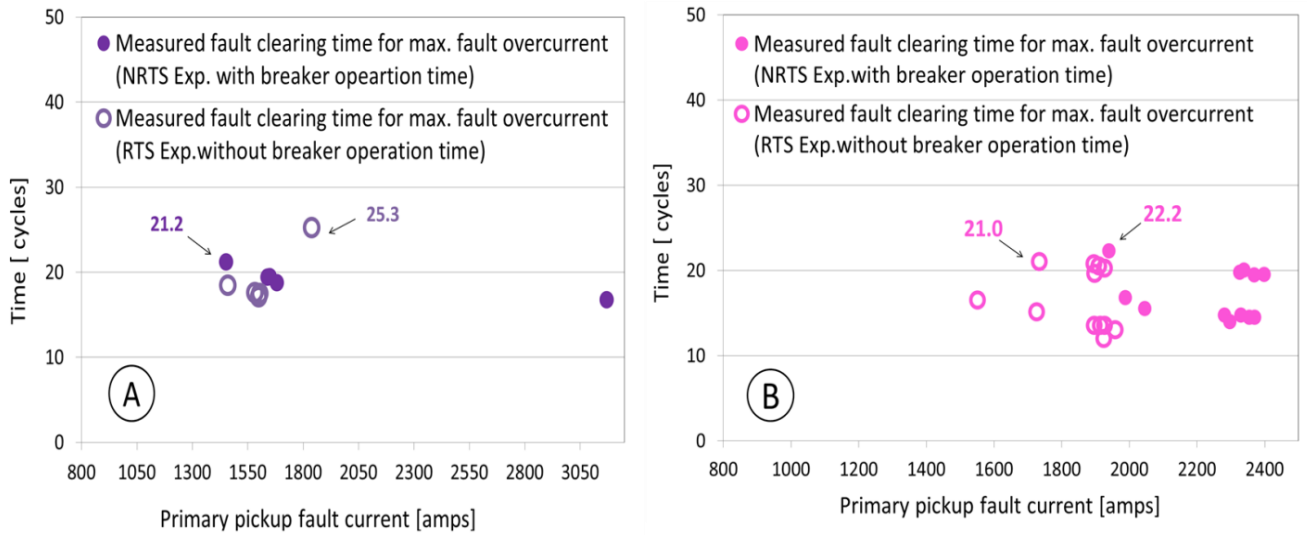

Figure 12.3: Measured fault clearing times for maximum fault overcurrents (excluding backup protections) for tripping tests of (A) Relays 2 and (B) 3 (B) based on NRTS and RTS experiments

In addition, speed of the protection logic gate (“AND”) to trip relay breakers generated the trip signal without delay, confirming non-delay in protection logic applied in adaptive inverse time overcurrent protection. For example, Figure 12.4 verifies that A-B-C line currents and digital signals corresponded to “DG2-678/65-SLG(A)-Bus6-BK7” tripping test from the RTS experiment. Relay 3 tripped the “BK7” breaker at SLG fault near Bus 6 (10% of L67 power line length). Based on “AND” logic gate, when the inverse time overcurrent element pickup (51S2) and trip circuit breaker (T3P2) digital signals were activated, the SELogic variable (PSV04) was turned on instantaneously, generating a trip signal at the relay’s NC control output (OUT107) in order to trip “BK7” breaker at fault overcurrent. The “BK7” breaker state changed from closed to open according to the relay’s control input (IN104).

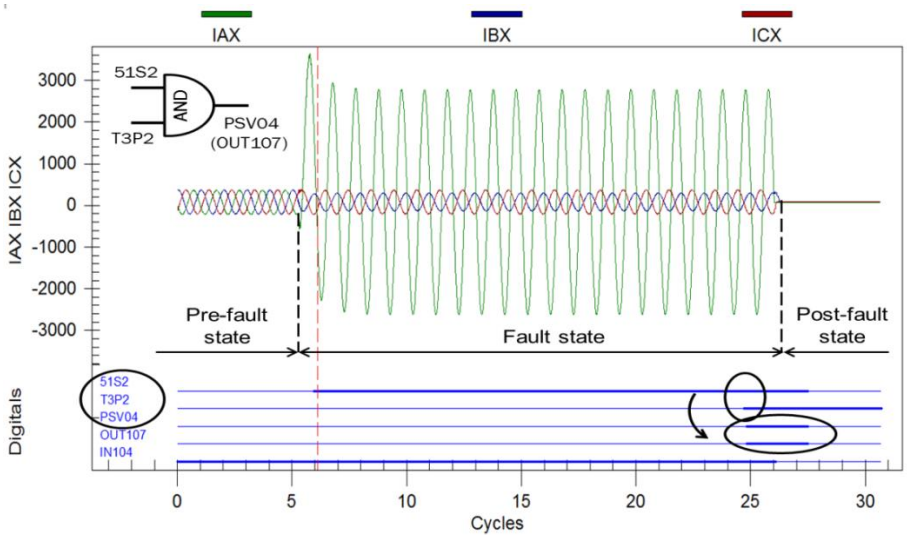

Figure 12.4: Trip logic digital signals of “AND” gate corresponding to “BK7” breaker of Relay 3 from collected HR_13115 event in RTS experiment

Reliability: Coordination between backup and primary protection devices was applied to adaptive inverse time overcurrent protection in order to achieve the protection system’s reliability. When the primary relay did not trip because of current transformer failure, the backup relay tripped the breaker, thereby clearing the fault overcurrent. In the RTS experiment, protection coordination scenarios were verified by observing that the primary relay tripped instead of the backup relay when

the LLTI of both relays was connected. Backup protection tests were also performed in order to disconnect the LLTI of primary relays and observe whether or not the backup relays tripped, thereby validating reliability of the protection system. In addition, application of distributed generators in the microgrid improved reliability of the power system in case of equipment (e.g., utility source, distributed generators, power lines, transformers, and breakers) failure or maintenance operation because the microgrid with distributed generators contained more than one circuit path in order to energize bus feeders.

12.3. Conclusions of relay in the loop techniques

In this research, adaptive overcurrent protection was verified by testing Relays 2 and 3 with NRTS and RTS experiments using SEL-AMS [3] and OP5600 [4] as NRTS and RTS, respectively. The following conclusions were made regarding application of these two relay in the loop techniques to test Relays 2 and 3:

Prior to running relay tests in the NRTS experiment, secondary currents and line-to-ground voltages of pre-fault, fault, and post-fault states had to be calculated with Power World® software [10] in order to run the power flow and fault analysis for circuit paths. The RTS did not require calculation of secondary currents and line-to-ground voltages because the power system and the pre-fault, fault, and post-fault states were simulated in real-time during the relay tests.

The RTS experiment represented secondary current variations at fault state in real-time. Sags, ramps, and frequency variations in fault overcurrents were represented with Matlab® software [14] in the RTS experiment, but ramps, and frequency variations in fault overcurrents could not be estimated with Power World® software [10] in the NRTS experiment.

Because Relays 2 and 3 were tested individually in the NRTS experiment, selectivity coordination between backup and primary relays could not be observed. However, in the RTS experiment, Relays 2 and 3 were tested together by connecting both relays to the microgrid simulated

in real-time with OP5600 [4]. The RTS experiment verified selectivity coordination between backup and primary relays, proving that primary relays tripped faster than backup relays.

In the NRTS experiment, setting groups of relays were selected manually from the front of the relays. However, in the RTS experiment, setting groups of the relays were selected automatically from the host computer, thereby activating relay control inputs (rear side of relays) for setting groups.

In the RTS and NRTS experiments, the relay's LLTI connections (front side of the relays) were connected in both experiments instead of current-voltage source connections (rear side of the relays). The LLTI connection allowed an analog signal of up to 5 volts (peak value) instead of 5 amps and 67 volts line-to-ground (current and voltage source connections). Because the NRTS and RTS experiments were performed with LLTI voltages, both experiments were performed in a low-voltage environment. However, application of the LLTI connection did not allow problems with the interface to be perceived between the LLTI (front side of relays) and current-voltage source (rear side of relays) connections.

External voltage sources were required for the RTS experiments. OP5600 [4] and SEL-AMS [3] were applied as RTS and NRTS, respectively. Although SEL-AMS included 14.3 and 125 Vdc sources in order to generate the trip signal and sense breaker states, OP5600 required 14.3 and 125 Vdc external sources to be connected at trip signal and breakers state circuits.

Analog outputs in the NRTS and RTS experiments represented measured secondary currents and line-to-ground voltages of current and potential transformers, respectively. Because SEL-AMS [3] and OP5600 [4] simulated secondary and primary values, respectively, SEL-AMS and OP5660 required one and two gains, respectively, to be connected to SEL 451 relay's LLTI. In the NRTS experiment, the gain of SEL-AMS was represented by scaling factors of SEL 451 relays [5]. However, in the RTS experiment, gains were represented by the measurement of transformer ratios and scaling factors of SEL451 relays.

Tripping circuits in the NRTS and RTS experiments were represented by NO and NC relay control inputs, respectively. NO and NC relay control inputs for tripping circuits were based on the SEL-AMS instruction manual [3] and IEEE publication [70].

Power lines of the microgrid were shorter than 15 km. In the RTS experiment, three-phase transmission line models with lumped (short lines) and distributed parameters (long lines) from the SimPowerSystems library were applied initially without success with real-time simulation because three-phase transmission line models with lumped and distributed parameters had length limitations. Based on an OPAL-RT website article [99], therefore, the stubline model from the ARTEMIS library was applied in order to model power lines with lengths less than 15 km in the microgrid circuit.

Measured relay time errors of Relays 2 and 3 were compared between the NRTS and RTS experiments. RTS and NRTS with relay in the loop techniques presented similar relay time percent error values of Relays 2 and 3. Figure 12.5 shows that a majority of relay time percent error values of tripping tests for NRTS and RTS experiments were concentrated inside the violet and pink dashed lines, respectively, indicating a relay time error percent range of 5.71 and 5.94 for the NRTS and RTS experiments, respectively, thus validating NRTS and RTS experiments for similar relay time error percent ranges.

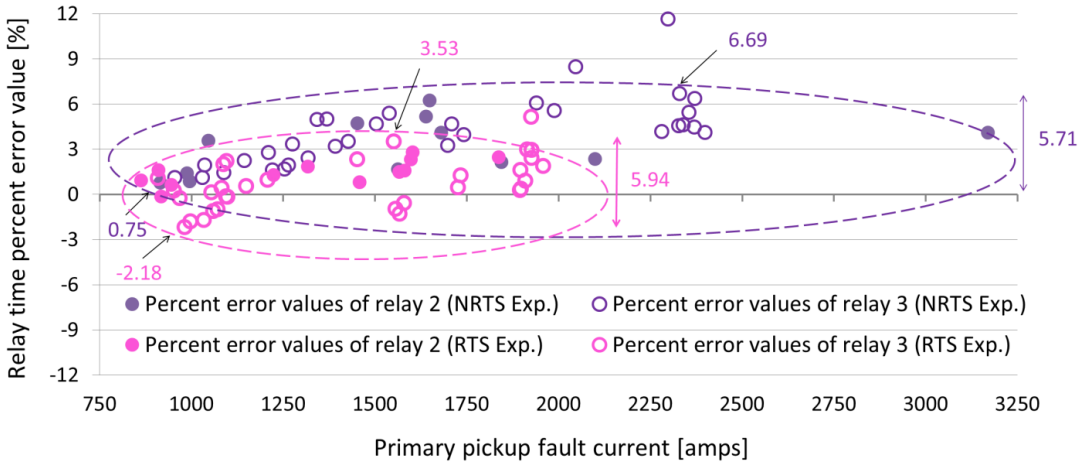

Figure 12.5: Relay time percent error values of Relays 2 and 3 for NRTS and RTS experiments

The RTS experiment was set without a breaker operation time in order to validate the RTS experiment with minimum CTI between backup and primary relays (without breaker operation time) based on IEEE Std. 242-2001 [7]. In addition, measured CTIs between backup and primary relays at maximum fault currents from NRTS and RTS experiments were compared to the calculated minimum CTIs. Figure 12.6 shows CTIs between backup and primary relays at maximum fault currents for NRTS and RTS experiments versus calculated minimum CTIs. For the RTS and NRTS experiments, measured CTIs for maximum fault currents were not less than 7.2 cycles, the relay-relay minimum CTIs based on RTS experiment (without breaker operating time).

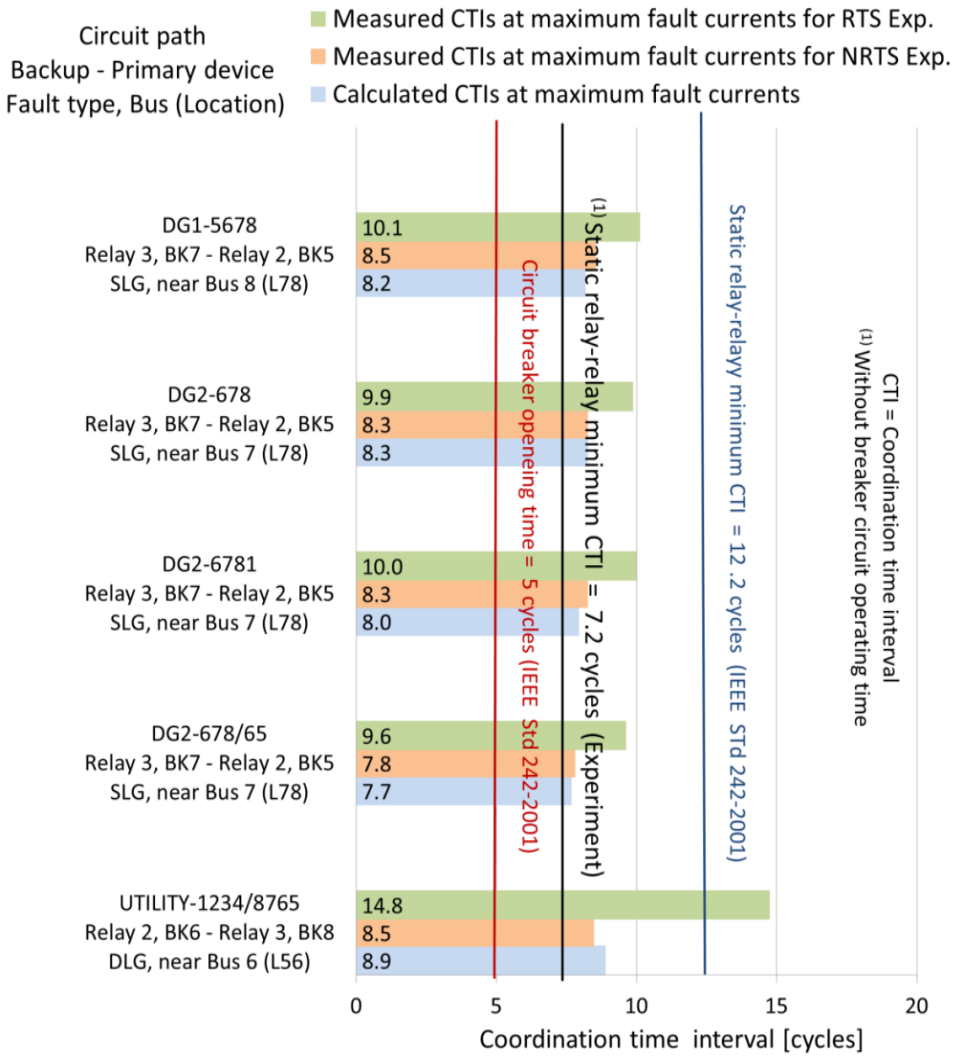

Figure 12.6: Measured CTIs between backup and primary relays for NRTS and RTS experiments versus calculated CTIs at maximum fault currents

As a validation of real-time simulation with OP5600 [4], Figure 12.7 shows that the HR_14169 record event (A) from Relay 2 presented identical A-B-C line currents of the Matlab® file (B) from the microgrid (host computer). The record event and Matlab® files were collected after running the "DG2-678/65-SLG (A)-BUS7-BK5" tripping test. The length of pre-fault time for the record event was set at 0.1 sec. for Relay 2. However, length of the pre-fault time for the tests was greater than 2.5 sec. for real-time simulation, observing no identical time scales for plots (A and B) in Figure 12.7.

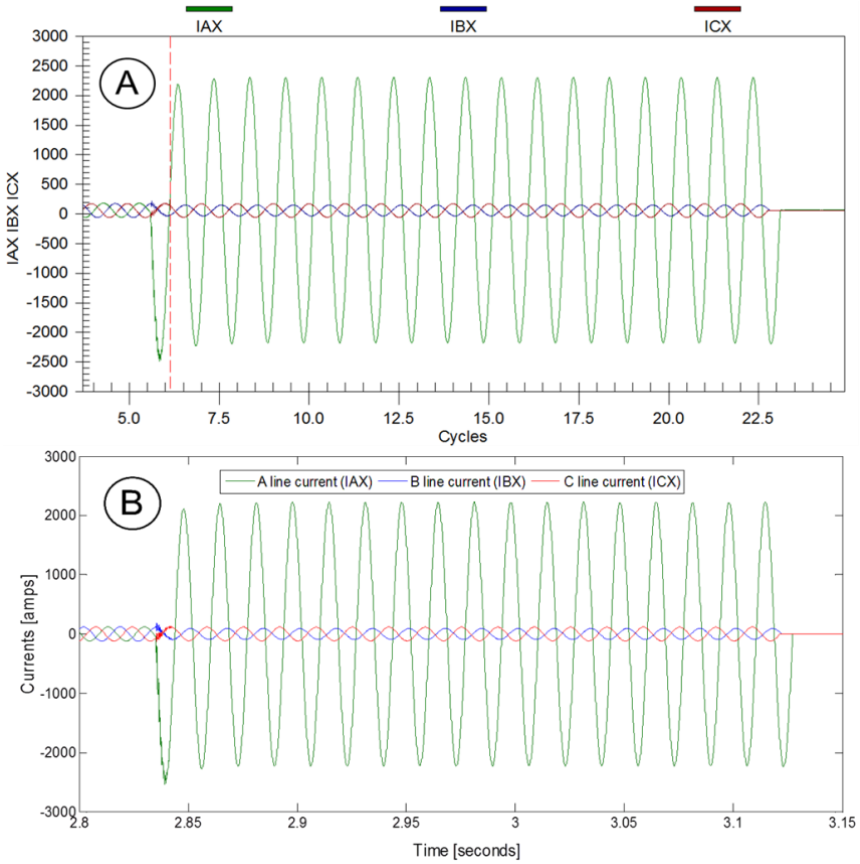

Figure 12.7: A-B-C line currents from (A) Relay 2 and (B) microgrid simulation for the "DG2-678/65-SLG (A)-BUS7-BK5" tripping test

This research details how to collect results from the relays and host computer and how to connect LLTI of SEL451 relays to analog outputs of OP5600, considering current and voltage scaling factors and maximum allowed peak voltages of LLTIs. The application of relays in the microgrid infrastructure was crucial in order to improve measurement, control, communication, and protection in

power systems. Other graduate students are encouraged to apply two or more relays in the loop with the OP5600 [4] because the installation of more than one relay in the loop with RTS allows measurements to be collected from relays and relay test results to be compared. In the RTS experiment of adaptive overcurrent protection in this research, Relays 2 and 3 allowed comparison of test results from both relays and verification of coordination between backup and primary protective relays, proving that the primary relays tripped more quickly than backup relays.

12.4 Future work

The adaptive inverse time overcurrent protection algorithm was based on selection of the inverse time overcurrent settings (*US* curve, *TDS*, *Ip*), creation of protection logic gates ("AND", "ZERO"), and groupings of identical inverse time overcurrent settings and protection logic gates for circuit paths of Relays 2 and 3 in the microgrid. In the adaptive inverse time overcurrent protection algorithm, inverse time overcurrent settings (*US* curve, *TDS*, *Ip*) were calculated by first collecting maximum ampere rating fuses on bus feeders for circuit paths. If fuse-relay and breaker-relay communications must be implemented in order to collect fuse ampere ratings on feeder busses and measure breaker states (open or closed) on power lines, respectively, then maximum ampere rating fuses on feeder buses and circuit paths of the microgrid should be calculated in order to determine inverse time overcurrent settings (*US* curve, *TDS*, *Ip*) of relays.

In the RTS experiment, setting groups of Relays 2 and 3 were selected automatically by the relay's control inputs according to circuit paths of the simulated microgrid in host computer. The communication system of adaptive overcurrent protection could be improved by adding power line wireless sensors in the loop. Because feeder fuses could communicate with relays by integrating modern power line wireless sensors with fuses, a hybrid smart fuse could be created to communicate fuse ampere ratings, currents, and on-off line states to relays. Future work could include integration of

power line sensors to the OP5600 [4] with relays in the loop in order to apply the algorithm of adaptive overcurrent protection system presented in this research.

In the adaptive overcurrent protection of this research, setting groups of relays were limited to six setting groups based on SEL 451 relay's instruction manual [5]. In case, more than three distributed generators were available in the microgrid located at different locations, more than six setting groups could be needed to perform the adaptive overcurrent protection. Fortunately, the SEL-451 relay is able to provide protection, control, and logic functions in one system. Programmable logic and math operators allow SEL 451 relays to implement new protection and control functions. Application of overvoltage elements with inverse-time characteristics for protection and control schemes of capacitor banks [101] could be adapted to inverse time overcurrent elements for adaptive overcurrent protection in microgrid with distributed generators. In that case, only one setting group is needed for all inverse time overcurrent settings of SEL-451 relay, and inverse time overcurrent settings are picked up automatically based on an external variable voltage level referenced to selected circuit paths in the microgrid.

References

[1] Bartel T., Butz L., Butz T., Dimberio T., and Stroess W., Costs of Utility Distributed Generators, 1-10 MW : Twenty-Four Case Studies, 1007760, EPRI, Palo Alto, CA, and Cooperative Research Network, Arlington, VA, pp.1-124, March 2003.

[2] Walling R. and Miller N., Distributed Generation-Impact on Distribution Systems, GE Power Systems Energy Consulting, One River Road, Schenectady, NY 12345, Distribution Systems Testing Application and Research Project 8-8, Final Report, pp. 1-56, July 9, 2002.

[3] SEL-Relay Test System, SEL- Adaptive Multichannel Source, Instruction Manual, Schweitzer Engineering Laboratories, Inc., February 3 1997.

[4] OP5600 HIL Box User Guide, Real-Time Simulator , ©Opal-RT Technologies, Inc. 1751 Richardson, suite 2525 Montreal, Quebec, Canada H3K 1G6, 2011.

[5] SEL-451-5, Protection, Automation, and Control System Instruction Manual, Date Code 20120220, Schweitzer Engineering Laboratories, Inc.

[6] Total Clearing Time-Current Characteristic Curves, SMU Fuse Standard Speed, SMU-40® Fuse Type, 4.8 kV, 3- 400E Ampere Rating, TCC Number 153-2-1-4 , S&C Electric Company, Chicago, IL, pp.1, 1991(http://www.sandc.com/support/publications/smu-tccs.asp).

[7] IEEE Std. 242- 2001, IEEE Recommended Practice for Protection and Coordination of Industrial and Commercial Power Systems, Book, Institute of Electrical and Electronics Engineers Inc., 25 October 2001.

[8] Piesciorovsky EC, Schulz NN. Burns & McDonnell - K-State Smart Grid Laboratory: Protection, Communication & Power Metering. IEEE Power & Energy Society General Meeting, Maryland, Washington, DC Metro Area, July 27 to 31, 2014.

[9] http://ewh.ieee.org/soc/pes/dsacom/testfeeders/index.html

[10] PowerWorld® Simulator, 12_GSO, Glover, Sarma, and Overbye Textbook Edition, 2007 PowerWorld Corporation.

[11] AcSELerator QuickSet®, SEL-5030 Software, Instruction Manual, Date Code 20140130, Schweitzer Engineering Laboratories, Inc.

[12] SEL-5401 Test System Software(Windows®95, Windows®NT), Schweitzer Engineering Laboratories, Inc.

[13] OPAL RT, RT-LAB® software, Version 10.4, User Guide, RTLAB-UG-104-00, 1751 Richardson, suite 2525, Montreal, QC, Canada, H3K 1G6.

[14] Matlab® Simulink® software and SimPower Systems Library, 64 bytes version, 2012.

[15] Che L., Khodayar M. E., and Shahidehpour M., Adaptive protection system for microgrids: protection practices of a functional microgrid system, Electrification Magazine, IEEE Journals & Magazines, 2014, Vol. 2, pp 66-80.

[16] Butler-Purry K. L. and Marotti M., Impact of distributed generators on protective devices in radial distribution systems, Transmission and Distribution Conference and Exhibition, IEEE PES, 2005-6, pp.87-88.

[17] Voima S., Laaksonen H., and Kauhaniemi K., Adaptive protection scheme for smart grids, Developments in Power System Protection, 12th IET International Conference, 2014, IET Conference Publications, pp. 1-6.

[18] Codling J. D., House S. A., Joice J. H., Labhart K. M., Richards J. R., Tenbusch J. E., Tullis M. D., Wilkerson T. D., and Rostamkolai N., Adaptive relaying: A new direction in power system protection, IEEE Potentials, 1996, Vol.15, pp. 28-33.

[19] Oudalov A., Degner T., Van Overbeeke F., and Yarza J. M., Microgrids: Architectures and Control, First Edition. Edited by Nikos Hatziargyriou, John Wiley & Sons, 2014, Chapter 4: Microgrid Protection, pp. 117-163.

[20] Gupta P., Bhatia R. S., and Jain D. K., Adaptive protection schemes for the microgrid in a smart grid scenario: Technical challenges, IEEE conference on Innovative Smart Grid Technologies-Asia, 2013, pp. 1-5.

[21] Ramaswamy P. C. and Deconinck G., Relevance of voltage control, grid reconfiguration and adaptive protection in smart grids and genetic algorithm as an optimization tool in achieving their control objectives, IEEE International Conference on Networking, Sensing and Control, 2011, pp. 26-31.

[22] Abdulhadi I., Coffele F., Dysko A., Booth C., and Burt G., Adaptive protection architecture for the smart grid, 2nd IEEE PES International Conference and Exhibition on Innovative Smart Grid Technologies - Europe, 2011, pp. 1-8.

[23] Sham M., Chethan K., and Vittal K., Development of adaptive distance relay for STATCOM connected transmission line, IEEE PES on Innovative Smart Grid Technologies - India, 2011, pp. 248-253.

[24] Islam M. R. and Gabbar H. A., Analysis of Microgrid protection strategies, IEEE International Conference on Smart Grid Engineering, 2012, pp. 27-29.

[25] Ojaghi M., Sudi Z., and Faiz J., Implementation of full adaptive technique to optimal coordination of overcurrent relays , IEEE Transactions on Power Delivery, 2013, Vol. 28, No. 1, pp. 235-244.

[26] Laaksonen H., Ishchenko D., and Oudalov A., Adaptive protection and microgrid control design for Hailuoto Island, Smart Grid, IEEE Transaction, IEEE Journals & Magazines, 2014, Vol. 5, pp. 1486-1493.

[27] Laway N. A. and Gupta H. O., A method for adaptive coordination of overcurrent relays in an interconnected power system, Proceedings of the Fifth International Conference on Developments in Power System Protection, 1993, pp. 240-243.

[28] Sachdev M. S., Sidhu T. S., and Talukdar B. K., Topology detection for adaptive protection of distribution networks, Proceedings of the International Conference on Energy Management and Power Delivery, 1995, Vol. 1, pp 445-450.

[29] Zhang Y., Bastos J. L., and Schulz N. N., Model-based design of a protection scheme for shipboard power systems, IEEE Power and Energy Society General Meeting - Conversion and Delivery of Electrical Energy in the 21st Century, 2008, pp. 1-9.

[30] Mahat P., Chen Z., Bak-Jensen B., and Bak C. L., A simple adaptive overcurrent protection of distribution systems with distributed generation, IEEE Transactions on Smart Grid, 2011, Vol. 2, pp. 428-437.

[31] Liu, C., Chen Z., and Liu Z., A communication-less overcurrent protection for distribution system with distributed generation integrated, 3rd IEEE International Symposium on Power Electronics for Distributed Generation Systems, 2012, pp. 140-147.

[32] Matic-Cuka B. and Kezunovic M., Improving smart grid operation with new hierarchically coordinated protection approach, 8th Mediterranean Conference on Power Generation, Transmission, Distribution and Energy Conversion, 2012, pp. 1-6.

[33] Khederzadeh M., Adaptive setting of protective relays in microgrids in grid-connected and autonomous operation, Developments in Power Systems Protection, 11th International Conference, IET Conference Publications, 2012, pp. 1-4.

[34] Buque C., Ipinnimo O., Chowdhury S., and Chowdhury S. P., Modeling and simulation of an adaptive relaying scheme for a microgrid, Power and Energy Society General Meeting, 2012, IEEE Conference Publication, pp. 1-8.

[35] Montoya L., Montenegro D., and Ramos G., Adaptive protection testbed using real time and hardware-in-the-loop simulation, IEEE conference on PowerTech, 2013, pp. 1-4.

[36] Rones A. S. and Vittal K. P., Adaptive protection schemes for feeders with the penetration of SEIG based wind farm, IEEE Conference on Innovative Smart Grid Technologies-Asia, 2013, pp. 1-6.

[37] Jafari R., Naderi M. S., Gharehpetian G. B., and Moaddabi N., Compensation of DGs impact on overcurrent protection system of smart micro-grids, 2013.

[38] Singh M., Protection coordination in grid connected & islanded modes of micro-grid operations, IEEE, Innovative Smart Grid Technologies, Asia, Banglore, 2013, pp. 1-6.

[39] Mishra C., Mohanta D. K., and Reddy M. J. B, Impact of adaptive relaying in smart grid, Environment and Electrical Engineering International Conference, 2014, pp.169 - 174.

[40] IEEE C37.2 -2008 Standard, “Standard for Electrical Power System Device Function Numbers Acronyms and Contact Designations”, IEEE Std., October 2008.

[41] Simulink® Control Design™ User's Guide, Matlab® Simulink®, 2014-15.

[42] DSpace ® Manual, Release 1.6.2, DuraSpace, 2010.

[43] SEL-351S Protection System Instruction Manual. Schweitzer Engineering Laboratories Inc., Date Code 20110429, 2011.

[44] Integrated Power System Analysis Software, DIgSILENT® PowerFactory 15 Flyer, DIgSILENT GmbH, Heinrich-Hertz-Straße 9, 72810 Gomaringen, Germany.

[45] Milano F., An open source power system analysis toolbox, IEEE Transaction on Power Systems, 2004, pp. 1-8.

[46] LabVIEW™ User Manual, National Instruments™, April 2003 Edition, Part Number 320999E-01.

[47] ETAP® 7.0.0, Demo, Getting Started, Operation Technology, Inc., 2009.

[48] User’s guide on the use of PSCAD®, Power Systems Computer Aided Design, Manitoba HVDC Research Centre, a division of Manitoba Hydro International Ltd., 2010.

[49] Mantawy A. H. and Al-Ghamdi M. S., A new reactive power optimization algorithm, Proc. IEEE Power Tech. Conf., 2003, Vol. 4, pp. 6-11.

[50] De Oliveira M. E., Ochoa L. F., Padilha-Feltrin A., and Mantovani J. R. S., Network reconfiguration and loss allocation for distribution systems with distributed generation, Proc. IEEE/PES Transmission and Distribution Conf. and Exposition: Latin America, 2004, pp. 206-11.

[51] Mendoza J., Lopez R., and Morales D., Minimal loss reconfiguration using genetic algorithms with restricted population and addressed operators: Real application, IEEE Transactions on Power Systems, 2006, Vol. 21, No. 2, pp. 948–54.

[52] Enacheanu B., Raison B., Caire R., Devaux O., Bienia W., and HadjSaid N., Radial network reconfiguration using genetic algorithm based on the Matroid theory, IEEE Transactions on Power Systems, 2008, Vol. 23, No. 1, pp. 186 – 195.

[53] Hong Y.Y. and Ho S.Y., Determination of network configuration considering multi objective in distribution systems using genetic algorithms, IEEE Transactions on Power Systems, 2005, Vol. 20, No. 2, pp. 1062-69.

[54] Damborg M. J., Kim M., Huang J., Venkata S. S., and Phadke A. G., Adaptive protection as preventive and emergency control, Power Engineering Society Summer Meeting, 2000, Vol. 2, pp. 1208-1212.

[55] Bittencourt A., Carvalho M. R., and Rolim J. G., Adaptive strategies in power systems protection using artificial intelligence techniques, Proc. 15th Int. Conf. on Intelligent System Applications to Power Systems, 2009, Brazil, pp.1-6.

[56] Chattopadhyay B., Sachdev M.S., and Sidhu T.S., Adaptive relaying for protecting a distribution system - a feasibility study, Proc. WESCANEX'91 IEEE Western Canada Conf. on Computer, Power and Comm. Systems in a Rural Environment, 1991, pp. 20-25.

[57] So C.W., Li K.K., Lai K.T., and Fung K.Y., Application of genetic algorithm for overcurrent relay coordination, Proc. 6th Int. Conf. on Developments in Power System Protection, 1997, pp. 66-69.

[58] Ghanbarian M. M., Havehnia F., and Kazerooni A., Setting directional over current relays as the backup of distance relays in power network, 15th National Power Systems Conference IIT Bombay, 2008, pp. 329-333.

[59] Nordman M. M. and Lehtonen M., A wireless sensor concept for managing electrical distribution networks, Power Systems Conference and Exposition, IEEE PES, 2004, IEEE Conference publication, Vol. 2, pp. 1198-1206.

[60] Parker, D.M. and McCollough N.D, Medium-voltage sensors for the smart grid: Lessons learned, Power and Energy Society General Meeting, IEEE Conference Publications, 2011, pp.1-7.

[61] Leon, R.A., Vittal, V., and Manimaran G., Application of sensor network for secure electric energy infrastructure, Power Delivery IEEE Transactions, IEEE Journals & Magazines, 2007, Vol. 22, pp. 1021-1028.

[62] Salvadori F., Gehrke C.S., De Oliveira A.C., De Campos M., and Sausen P. S., Smart grid infrastructure using a hybrid network architecture, Smart Grid, IEEE Transactions, IEEE Journals & Magazines, 2013, Vol. 4, pp. 1630-1639.

[63] Radhakrishnanand R. and Kalkstein E. W., Design, development and application of smart fuses - Part 1, IEEE Transactions on Industry Applications, 1994. Vol. 30, No. 1, pp. 164-169.

[64] LineWatchTM M for medium voltage applications (up to 36 kV), QinetiQ North America, Inc., Document name: 13-7-313.

[65] Sachdev M. S., Sidhu T. S., and McLaren P. G., Issues and opportunities for testing numerical relays, IEEE Power Engineering Society Summer Meeting, 2000, Vol. 2, pp. 1185-1190.

[66] Forsyth P. and Kuffel R., Utility applications of a RTDS® Simulator, 8th International Power Engineering Conference, 2007, pp. 112-117.

[67] FREJA 300 Relay Test System Flyer, 2009. Megger® Sweden AB Eldarvägen 4, Box 2970, SE-187 29 TÄBY, Art. No. ZI-CF01E, Doc. CF0284CE, pp. 1-10.

[68] Almas M. S. and Vanfretti L., Methodologies for power protection relay testing: from conventional to real-time hardware-in-the-loop (HIL) simulation approaches, International Conference on Power Systems Transients (IPST2013) in Vancouver, Canada July 18-20, 2013.

[69] SEL-487E Relay Current Differential and Voltage Protection Instruction Manual. Schweitzer Engineering Laboratories Inc., Date Code 20121126, 2012.

[70] Almas M. S., Leelaruji R., and Vanfretti L., Over-current relay model implementation for real time simulation & hardware-in-the-loop (HIL) validation, IECON 2012 - 38th Annual Conference on IEEE Industrial Electronics Society, IEEE Conference Publications, 2012, pp. 4789- 4796.

[71] Wang X., Woodford D. A., Kuffel R., and Wierckx R., A real-time transmission line model for a digital TNA, IEEE Trans. Power Delivery, 1996, Vol. 11, pp. 1092–1097.

[72] Smolarczyk A., Kowalik R., Bartosiewicz E., and Rasolomampionona D., A simple real-time simulator for protection devices testing, IEEE International Energy Conference, IEEE Conference Publications, 2014, pp.793-799.

[73] Kirby R. D. and Schwartz R., Microprocessor-based protective relays deliver more information and superior reliability with lower maintenance costs, IEEE Industrial and Commercial Power Systems Technical Conference, 2006, pp.1-6.

[74] IEEE Standard C37.100-1992, Definitions for Power Switchgear, Institute of Electrical and Electronics Engineers.

[75] An Introduction to Symmetrical Components, System Modeling and Fault Calculation , 30th Annual Hands-on Relay School, , Washington State University, Pullman, WA, pp. 1-64, March 11- 15, 2013

[76] Steady-State Power System Security Analysis with PowerWorld Simulator, S10: Integrated Topology Processing, Power World Corporation, Champaign, IL, pp. 56, 2012.

[77] Brand K., Volker L. and Wolfgang W., ABB Substation Handbook: Comprhensive description of Substation Automation and the coordination with Network Operation to obtain both performance and cost benefits by enabling enhanced Power System Mangement, Germany, 2003.

[78] Pad-Mounted, Small Power Transformers 75–20,000 kVA, 2.5–46 kV Primary Voltage, 120 V–25 kV Secondary Voltage, Class 7230, 7230DB0501R08/10 Data Bulletin, Schneider Electric USA Inc., Nashville, TN, pp. 1-10, August 2010.

[79] Application Information: Short Circuit Current Calculations For Industrial and Commercial Power Systems,GET-3550F 0489 BLC, General Electric Company, Plainville, CT, 06062, pp.1-59, 1989.

[80] DM7824 Caterpillar SR4B Generators (50-60 Hz), 825 Generator Frame, 1825 / 2281 kW/ kVA Genset Rating, 480 / 227 V Line/ Phase voltage, Prime Duty, pp.1-8.

[81] Fuseology - Fuse Application Guide, Littelfuse POWR-GARD®, pp. 170-198.

[82] National Electrical Code, 2011.

[83] Aluminum Conductor Steel Reinforced (ACSR) Bare, 11-4 ACSR, Southwire, Carrolton, GA, pp. 1-4, April 19, 2012.

[84] Power Quality Standards for Electric Service, Entergy®, DZ02-04, revision 00 June 1, 2008

[85] ANSI Std. C84.1-2006, American National Standard for Electric Power Systems and Equipment - Voltage Ratings (60 Hertz).

[86] Yang Ming-Ta and Jyh-Cherng Gu, Optimal Coordination of Automatic Line Switches for Distribution Systems, Energies 2012-5 article, ISSN 1996-1073, pp. 1150-74.

[87] Total Clearing Time-Current Characteristic Curves, SMU Fuse Standard Speed, SMU-20® Fuse Type, 25 and 34.5 kV, 5- 200E Ampere Rating, TCC Number 153-2, S&C Electric Company, Chicago, IL, pp.1, 1988 (http://www.sandc.com/support/publications/smu-tccs.asp).

[88] Red Hat® Enterprise Linux 5, Installation Guide, Installing Red Hat Enterprise Linux 5 for all architectures, Edition 3.1.

[89] National Instrument software, LabView Signal Express, Version 2.5.1, Tektronix Edition.

[90] OPAL-RT, Section E: High Voltage Interface Panel, OPAL-RT Connections to the High Voltage Interface Panel, Opal-RT Technologies, Inc. 1751 Richardson, suite 2525 Montréal (Québec) Canada H3K 1G6.

[91] TDS2000C and TDS1000C-EDU Series, Digital Storage Oscilloscopes, User Manual, Rev. A, Tektronix, Inc. 14150 SW Karl Braun Drive, P.O. Box 500, Beaverton, OR 97077, USA.

[92] OP5330 USER GUIDE, Digital to Analog Converter Module, Opal-RT Technologies, Inc. 1751 Richardson, suite 2525 Montréal (Québec) Canada H3K 1G6, 2010.

[93] OP5354 16/32 Digital Outputs User Guide, Opal-RT Technologies, Inc. 1751 Richardson, suite 2525 Montréal (Québec) Canada H3K 1G6, 2010.

[94] OP5340 USER GUIDE, Analog to Digital Converter Module, Opal-RT Technologies, Inc. 1751 Richardson, suite 2525 Montréal (Québec) Canada H3K 1G6, 2014.

[95] Gold Box “Infinity” Power Supplies Flyer, Linear Regulated (to 150 watts) AC-DC single output & wide adjust output, Acopian Power Supplies, P.O. Box 638, Easton, PA 18044.

[96] Metal-Clad Switchgear, VacClad W Medium Voltage Drawout Vacuum Breakers 5 kV, EATON & Cutler Hammer, Sheet 05012.

[97] SAS® software, Version 8.2, SAS Institute, Cary, NC, USA.

[98] http://www.opal-rt.com/kb-article/bin-bitstream-file-and-conf-configuration-file-explained.

[99] http://www.opal-rt.com/kb-article/distributed-parameters-line-length

[100] AcSELerator Analytic Assistant® Software, Schweitzer Engineering Laboratories, Inc.

[101] Hardister D., Reidt J., Fischer N., Implementation of inverse-time over- and undervoltage elements in SEL-451 and SEL-421 Relays, Schweitzer Engineering Laboratories, Inc., SEL Application Guide, 2005, Date Code 20050705.

Appendix A - Research impact questionnaire

Table A.1: Research impact questionnaire

Options	**Questions**	**Place** (X)
	1. Have you ever seen fuses that could communicate with relays in a real distribution system?	
a	Yes	
b	No	
	2. Do you think relays could be integrated to fuses with communication in a real distribution system?	
a	Yes	
b	No	
	3. How much does a fuse-relay adaptive protection improve selectivity in a distribution system with fuses?	
a	A lot	
b	Some	
c	Little	
d	Nothing	
	4. How much does a fuse-relay adaptive protection innovate a distribution system?	
a	A lot	
b	Some	
c	Little	
d	Nothing	

Appendix B - Data and per-unit results of equipment in microgrid

Table B.1: Data and per-unit results of equipment in microgrid (S_{base} = 100 MVA)

Phase	Parameters		Power Lines		Transfor`mers		Utility Source	Distribution Generators
			1-2, 2-3, 6-7, 7-8	3-4, 5-6	Utility Transformer	Distribution Transformer	UTILITY	DG1, DG2, and DG3
Data	Positive Sequence	Resistance, $R_{1\,pu}$ [Ω/mile]	0.3375	0.3375				
		Reactance, $j\,X_{1\,pu}$ [Ω/mile]	1.0478	1.0478				
	Negative Sequence	Resistance, $R_{2\,pu}$ [Ω/mile]	0.3414	0.3414				
		Reactance, $j\,X_{2\,pu}$ [Ω/mile]	1.0348	1.0348				
	Zero Sequence	Resistance, $R_{0\,pu}$ [Ω/mile]	0.3465	0.3465				
		Reactance, $j\,X_{0\,pu}$ [Ω/mile]	1.0179	1.0179				
	Line length, L [ft.]		6000	3000				
	Resistance in percent, $R_{T\%}$ [%]				1	0.66		
	Reactance in percent, $j\,X_{T\%}$ [%]				8	5.71		
	X/R ratio						15	
	Sub transient-direct axis reactance, $X''_{G\,d} = X_{G\,1}$ [Ω]							0.0143
	Negative sequence reactance, $X_{G\,2}$ [Ω]							0.0130
	Zero sequence reactance, $X_{G\,0}$ [Ω]							0.0008
	No of breakers per equipment		2	2	2	2	1	1
Per-Unit Method	Areas		1				2	3
	Line-to-line voltage of area, V_{area} [kV]		7.2				115	0.48
	Total power of area, S_{area} [MVA]		100		5	2.5	1500	2.281
	Old system impedance, $Z_{old} = V^2_{area} / S_{area}$ [Ω]		0.5184		10.368	20.736	1013.916	0.101
	New system impedance, $Z_{new} = V^2_{area} / S_{base}$ [Ω]		0.5184				132.25	0.002304
Results[(1)]	Positive Sequence	Resistance, $R_{1\,pu}$ [pu]	0.700	0.400	0.200	0.264	0.00443	
		Reactance, $j\,X_{1\,pu}$ [pu]	2.301	1.101	1.601	2.285	0.06702	6.2075
	Negative Sequence	Resistance, $R_{2\,pu}$ [pu]	0.700	0.400	0.200	0.264	0.00443	
		Reactance, $j\,X_{2\,pu}$ [pu]	2.301	1.101	1.601	2.285	0.06702	5.6425
	Zero Sequence	Resistance, $R_{0\,pu}$ [pu]	0.800	0.400	0.200	0.264	0.00443	
		Reactance, $j\,X_{0\,pu}$ [pu]	2.201	1.101	1.601	2.285	0.06702	0.3475

(1) In Results, reactances include breaker reactances (j 0.0005 pu / breaker)

Appendix C - Calculated real and reactive power of distributed generators and bus voltages in the microgrid

Table C.1: Calculated real and reactive power of distributed generators and bus voltages in the microgrid test modes (Tap ratio = 1.00)

Microgrid test modes		Utility		[(1)]Distributed generators						[(2)]Bus voltages [%]							
Test modes	Circuit paths			DG1		DG2		DG3		Bus 1	Bus 2	Bus 3	Bus 4	Bus 5	Bus 6	Bus 7	Bus 8
		kW	kVar	kW	kVar	kW	kVar	kW	kVar								
1	UTILITY-1234/5678	3201	2497							95.5	92.9	91.3	90.7	90.6	90.9	92.6	95.5
2	DG1-1234, DG2-65/678			1584	1235	1520	1300			92.1	93.3	95.5	96.8	96.3	96.7	94.4	93.4
3	DG1-432/5 , DG2-6781			1340	1052	1745	1565			89.9	95.7	96.6	97.3	97.3	96.0	92.3	89.9
4	DG1-5678, DG3-21/234			1530	1334			1565	1221	95.6	96.9	95.2	94.6	96.6	95.0	92.3	91.7
5	DG1-34/56, DG3-2187			1307	1092			1811	1407	93.0	96.4	96.9	97.2	97.2	96.7	91.7	93.0
6	DG2-65/678, DG3-21/234					1520	1300	1565	1221	95.6	96.9	95.2	94.6	96.3	96.7	94.4	93.5
7	DG2-6781, DG3-2345					1745	1565	1364	1070	89.9	97.2	94.8	93.9	93.9	96.0	92.3	89.9
8	DG2-6543, DG3-2187					1312	1109	1811	1407	93.0	96.4	95.6	95.9	95.9	97.2	91.7	93.0
9	DG1-4, DG2-5678			451	358	1520	1300	1081	844	96.6	97.8	97.3	99.1	96.3	96.7	94.4	93.5
10	DG1-4, DG2-65/67			451	358	1158	954	1461	1148	94.9	97.0	96.5	99.1	97.2	97.5	96.3	94.9
11	DG1-5, DG2678			302	231	1217	1033	1565	1221	95.6	96.9	95.2	94.6	99.4	97.4	95.4	94.2
12	DG1-5, DG2-6781, DG3-234			302	231	1745	1565	1001	851	89.9	97.8	96.1	95.5	99.4	96.0	92.3	89.9
13	DG1-45, DG2-67, DG3-218/23			752	601	856	698	1461	1148	94.9	97.0	96.5	98.8	98.4	98.2	96.9	94.9
14	DG1-45, DG2-678, DG3-21/23			752	601	1217	1033	1081	844	96.6	97.8	97.3	98.8	98.4	97.4	95.4	91.5
15	DG1-45, DG2-6781, DG3-23			752	601	1745	1565	557	446	89.9	98.8	98.3	98.8	98.4	96.0	92.3	89.9
16	DG1-45, DG2-678, DG3-23			652	527	1158	954	1249	978	95.3	97.5	98.4	98.6	97.2	97.6	96.3	95.3
17	DG1-45, DG2-56, DG3-2187			652	527	652	528	1811	1407	93.0	96.4	98.4	98.6	98.3	98.6	91.7	93.0
18	DG1-45, DG2-65/678, DG3-21			652	527	1520	1300	871	677	97.0	98.2	98.4	98.6	96.3	96.7	94.4	93.5
19	DG1-34/5, DG2-678, DG3-21			954	775	1217	1033	871	677	97.0	98.2	97.7	98.0	98.0	97.4	95.4	94.2
20	DG1-34/5, DG2-6781, DG3-2			954	775	1745	1565	353	282	89.9	99.3	97.7	98.0	98.0	96.0	92.3	89.9
21	DG1-34/5, DG2-67, DG3-218			954	775	856	698	1249	978	95.3	97.5	97.7	98.0	98.0	98.2	96.9	95.3
22	DG1-34/5, DG2-6, DG3-2187			954	775	350	285	1811	1407	93.0	96.4	97.7	98.0	98.0	99.3	91.7	93.0

[(1)]Prime real (1825 kW) and reactive (1368 kVar) power of DG1, DG2, and DG3 distributed generators [1], [(2)] Bus voltage limit range (95-105%) based on service voltage limits of ANSI Std.C84.1 [3]

Table C.2: Calculated real and reactive power of distributed generators and bus voltages in microgrid test modes (Tap ratio = 0.95)

Microgrid test modes		Utility		[(1)]Distributed generators						[(2)]Bus voltages [%]							
Test modes	Circuit paths			DG1		DG2		DG3		Bus 1	Bus 2	Bus 3	Bus 4	Bus 5	Bus 6	Bus 7	Bus 8
		kW	kVar	kW	kVar	kW	kVar	kW	kVar								
1	UTILITY-1234/5678	3071	2714							100.7	98.2	96.5	96.0	95.6	96.0	97.7	100.7
2	DG1-1234, DG2-65/678			1527	1309	1476	1209			97.3	98.6	100.7	102.1	102.0	102.3	100.3	99.5
3	DG1-432/5 , DG2-6781			1310	1310	1686	1367			96.8	101.0	101.9	102.6	102.6	101.9	98.7	96.8
4	DG1-5678, DG3-21/234			1477	1208			1517	1278	100.9	102.2	100.5	100.0	102.3	100.9	99.0	98.0
5	DG1-34/56, DG3-2187			1308	1082			1685	1368	98.7	101.9	102.4	102.6	102.6	102.2	97.6	98.7
6	DG2-65/678, DG3-21/234					1476	1209	1517	1278	100.9	102.2	100.5	100.0	102.0	102.3	100.3	99.5
7	DG2-6781, DG3-2345					1686	1367	1321	1126	96.8	102.5	100.1	99.2	99.2	101.9	98.7	96.8
8	DG2-6543, DG3-2187					1312	1096	1685	1368	98.7	101.9	101.2	101.4	101.4	102.6	97.6	98.7
9	DG1-4, DG2-5678			451	357	1476	1209	1057	868	101.9	103.1	102.6	104.4	102.0	102.3	100.3	99.5
10	DG1-4, DG2-65/67			451	357	1159	946	1375	1135	100.5	102.5	102.0	104.4	102.6	102.9	101.7	100.5
11	DG1-5, DG2678			300	233	1174	964	1517	1278	100.9	102.2	100.5	99.5	104.7	102.9	100.9	100.1
12	DG1-5, DG2-6781, DG3-234			300	233	1686	1367	1010	845	96.8	103.2	101.6	101.0	104.7	101.9	98.7	96.8
13	DG1-45, DG2-67, DG3-218/23			752	599	855	693	1375	1135	100.5	102.5	102.0	103.8	103.8	103.6	102.4	100.5
14	DG1-45, DG2-678, DG3-21/23			752	599	1174	964	1057	868	101.9	103.1	102.6	103.8	103.8	102.9	100.9	100.1
15	DG1-45, DG2-6781, DG3-23			752	599	1686	1367	552	452	96.8	104.2	103.7	103.8	103.8	101.9	98.7	96.8
16	DG1-45, DG2-678, DG3-23			652	525	1159	946	1174	965	100.9	102.9	103.7	104.0	102.6	102.9	101.7	100.9
17	DG1-45, DG2-56, DG3-2187			652	525	652	526	1685	1368	98.7	101.9	103.7	104.0	103.6	104.0	97.6	98.7
18	DG1-45, DG2-65/678, DG3-21			652	525	1476	1209	855	693	102.4	103.6	103.7	104.0	102.0	102.3	100.3	99.5
19	DG1-34/5, DG2-678, DG3-21			953	772	1174	964	855	693	102.4	103.6	103.1	103.4	103.4	102.9	100.9	100.1
20	DG1-34/5, DG2-6781, DG3-2			953	772	1686	1367	350	284	96.8	104.6	103.1	103.4	103.4	101.9	98.7	96.8
21	DG1-34/5, DG2-67, DG3-218			953	772	855	693	1174	965	100.9	102.9	103.1	103.4	103.4	103.6	102.4	100.9
22	DG1-34/5, DG2-6, DG3-2187			953	772	350	284	1685	1368	98.7	101.9	103.1	103.4	103.4	104.6	97.6	98.7

[(1)]Prime real (1825 kW) and reactive (1368 kVar) power of DG1, DG2, and DG3 distributed generators [1], [(2)] Bus voltage limit range (95-105%) based on service voltage limits of ANSI Std. C84.1 [3]

Appendix D - Circuits paths for Relays 2 and 3

Circuit paths for Relays 2 and 3 based on microgrid constraints are shown in Figure D.1-12.

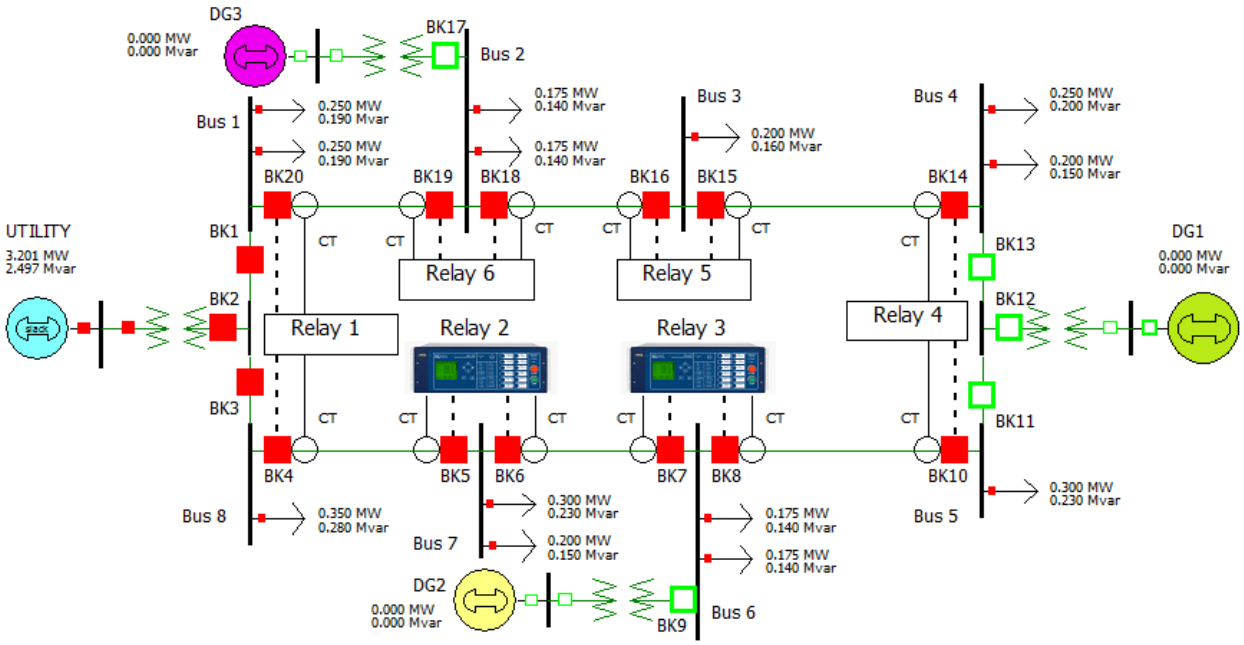

Figure D.1: UTILITY-8765/1234 (Test mode: 1)

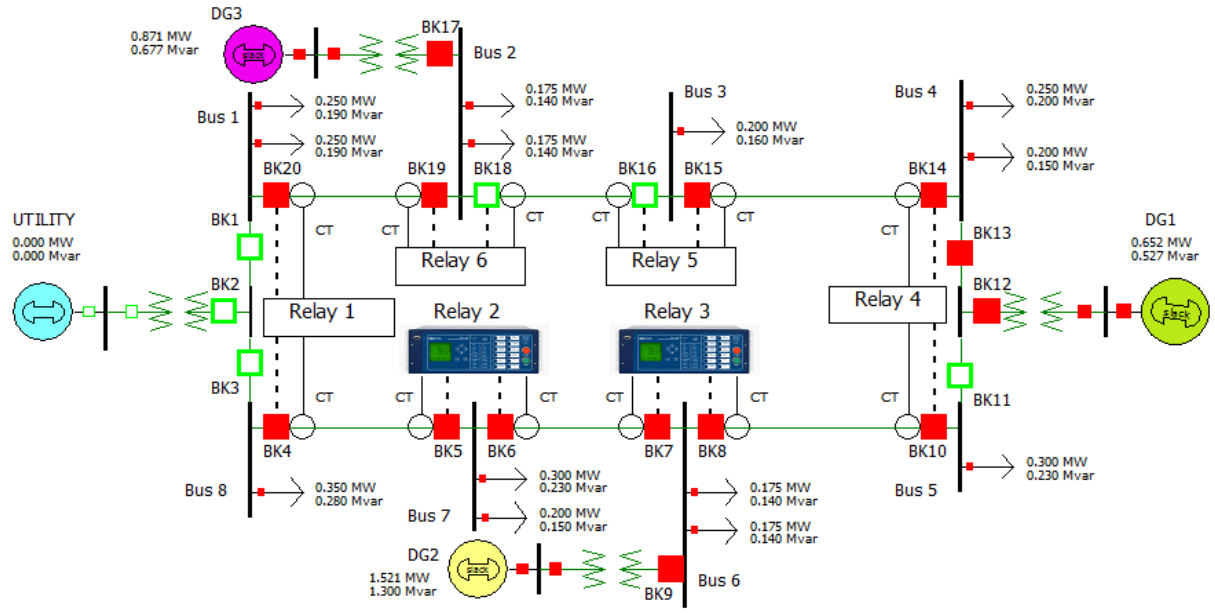

Figure D.2: DG2-678/65 (Test modes: 2, 6, 9, and 18)

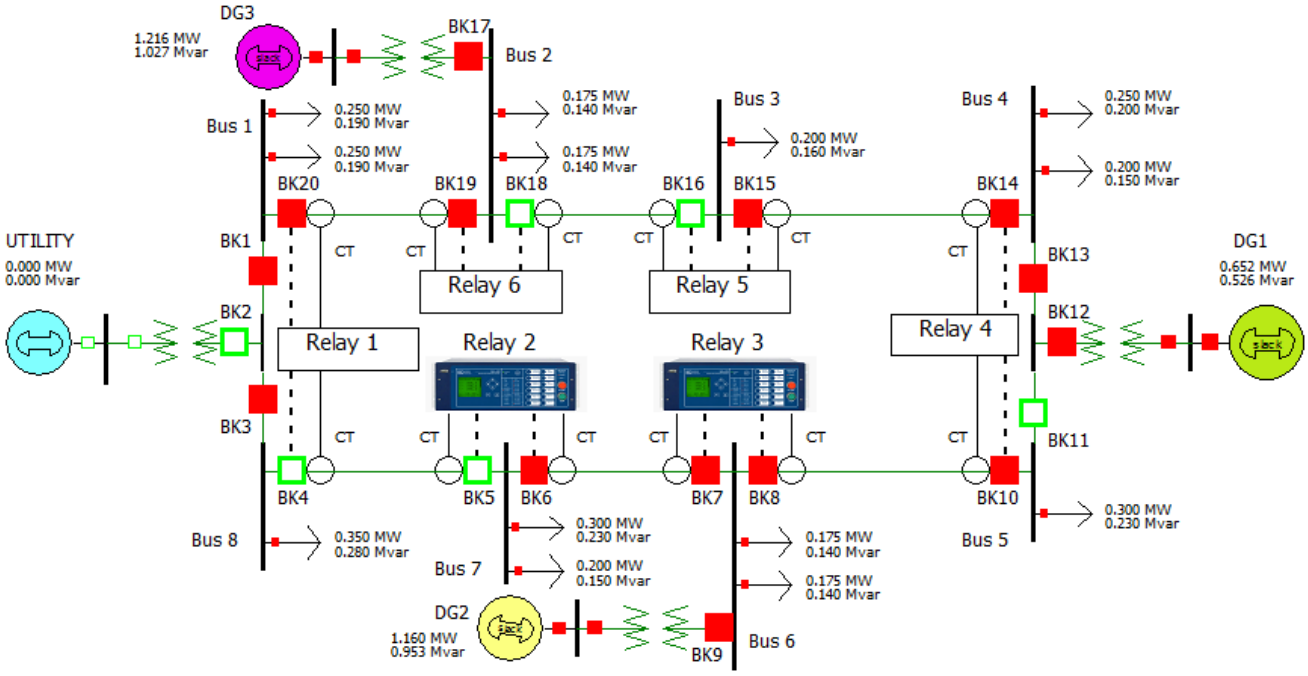

Figure D.3: DG2-67/65 (Test modes: 10 and 16)

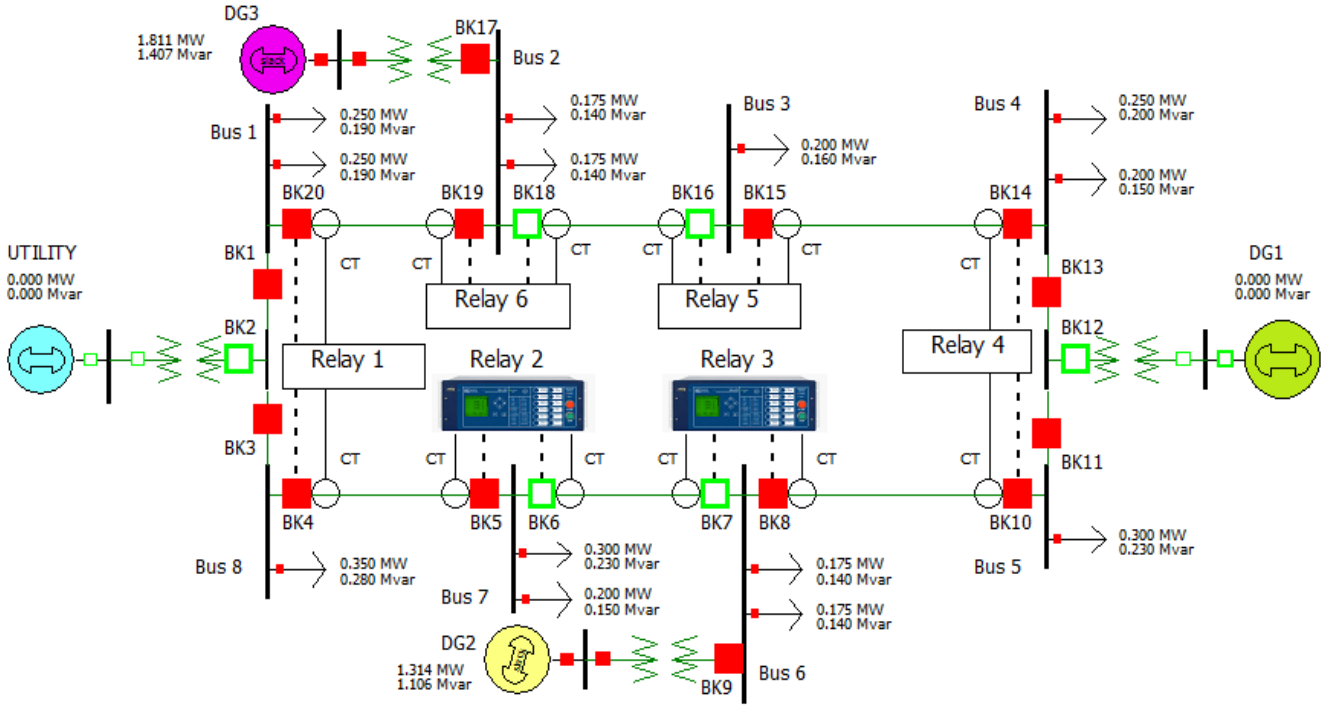

Figure D.4: DG2-6543 (Test mode: 8)

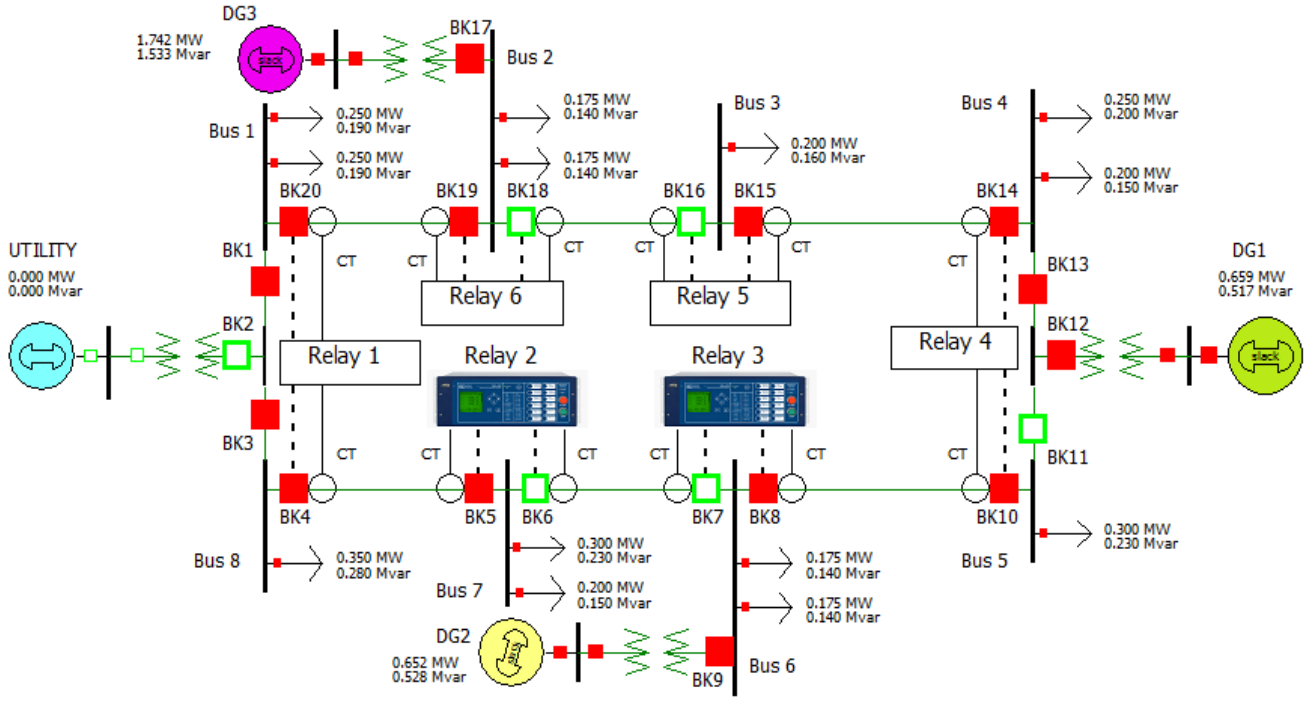

Figure D.5: DG2-65 (Test mode: 17)

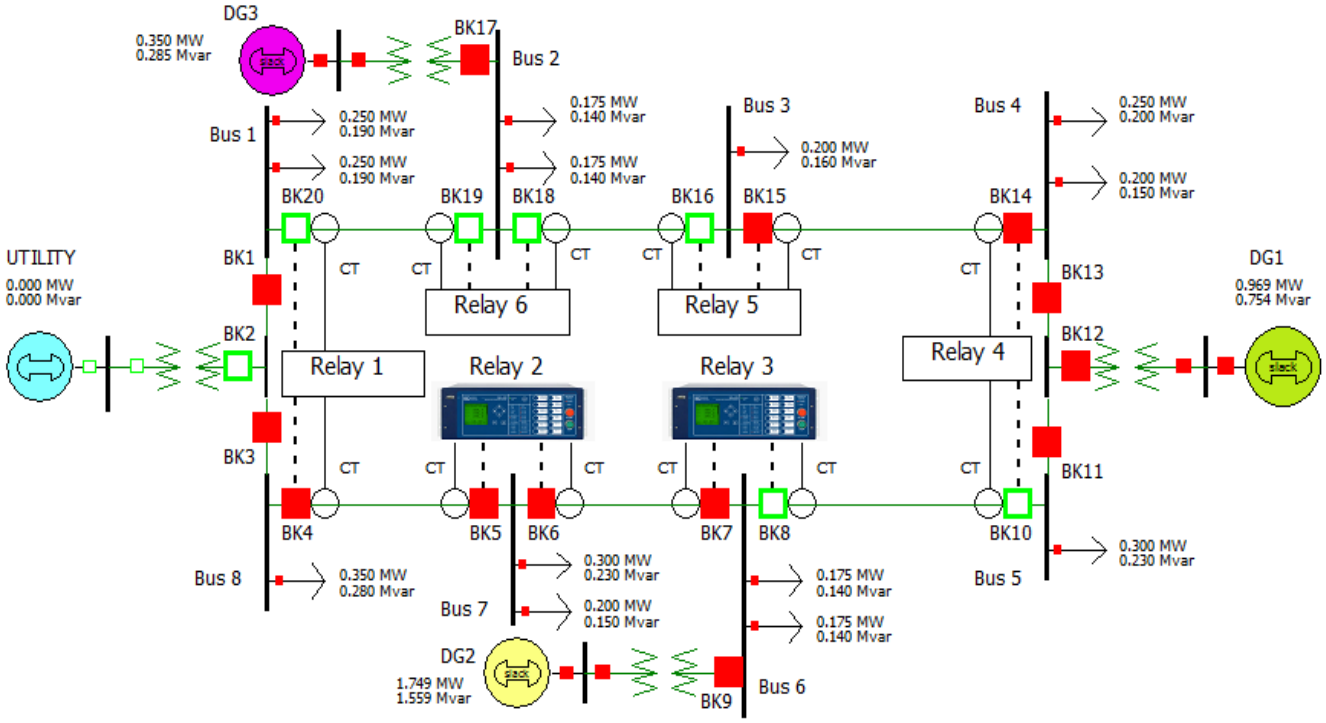

Figure D.6: DG2-6781 (Test modes: 3, 7, 12, 15, and 20)

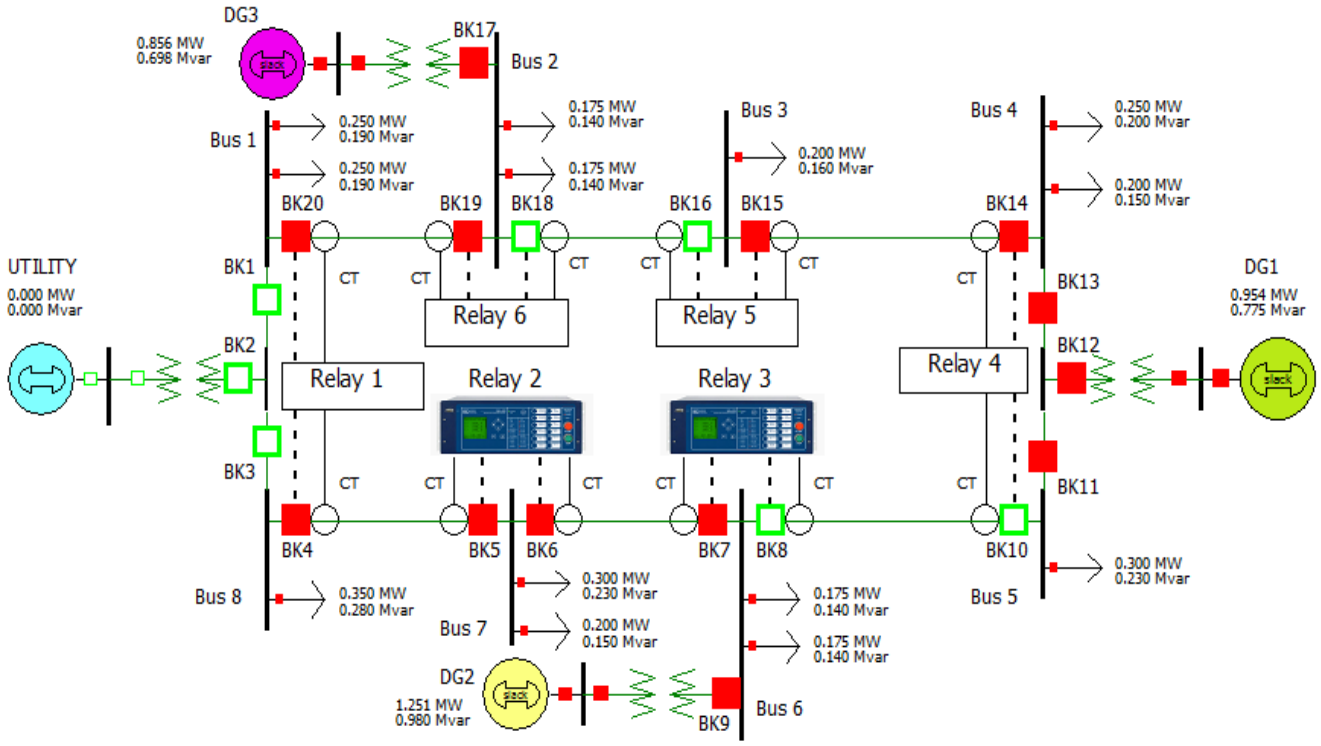

Figure D.7: DG2-678 (Test modes: 11, 14, and 19)

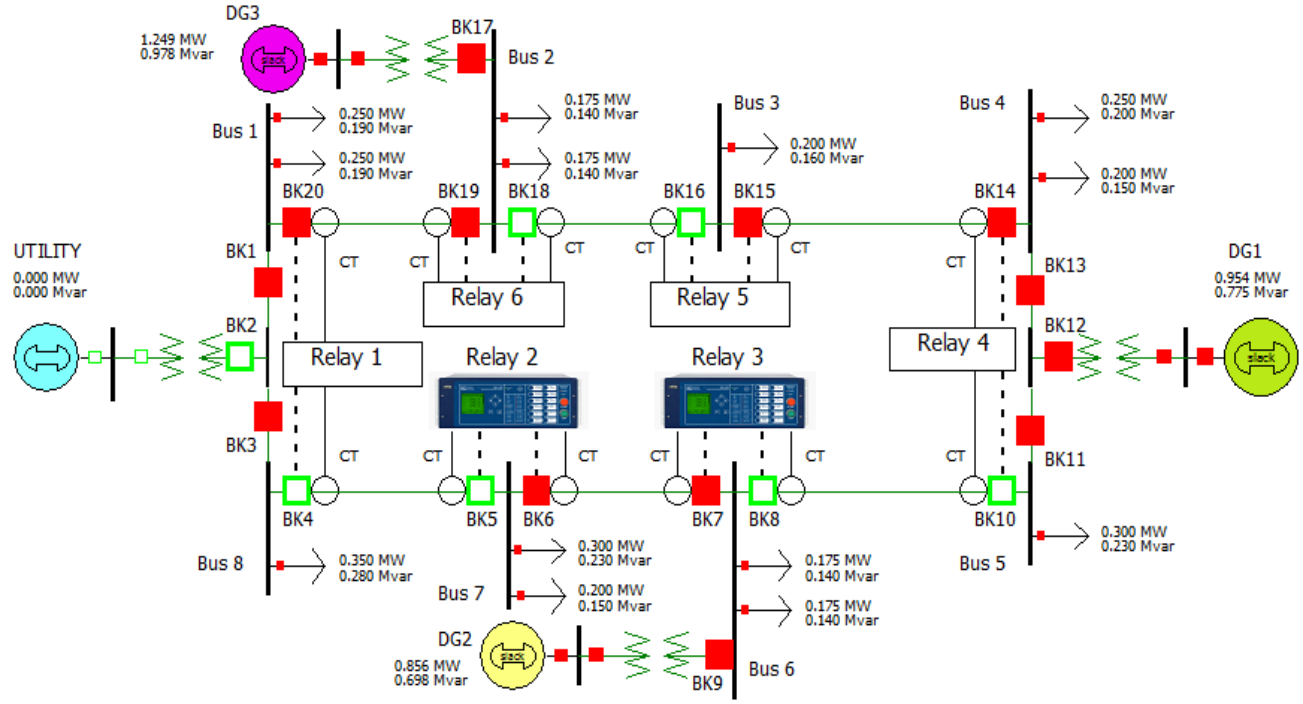

Figure D.8: DG2-67 (Test modes: 13 and 21)

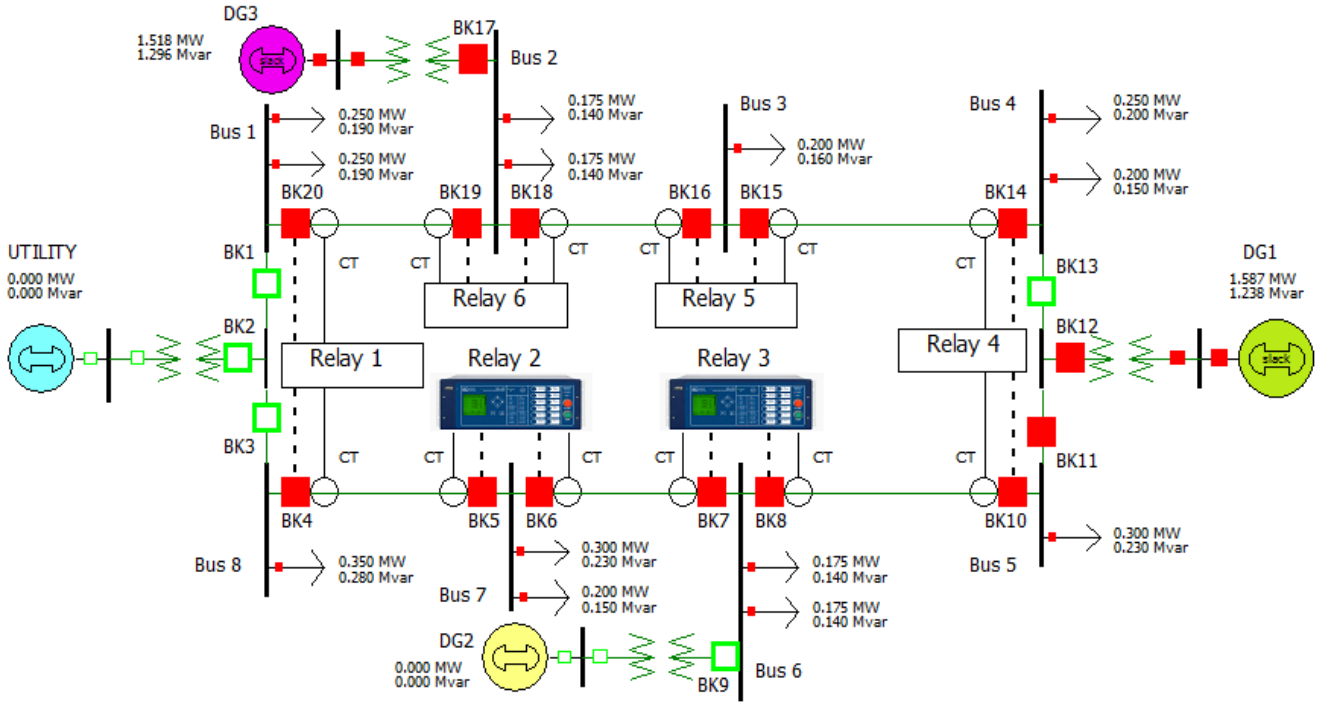

Figure D.9: DG1-5678 (Test mode: 4)

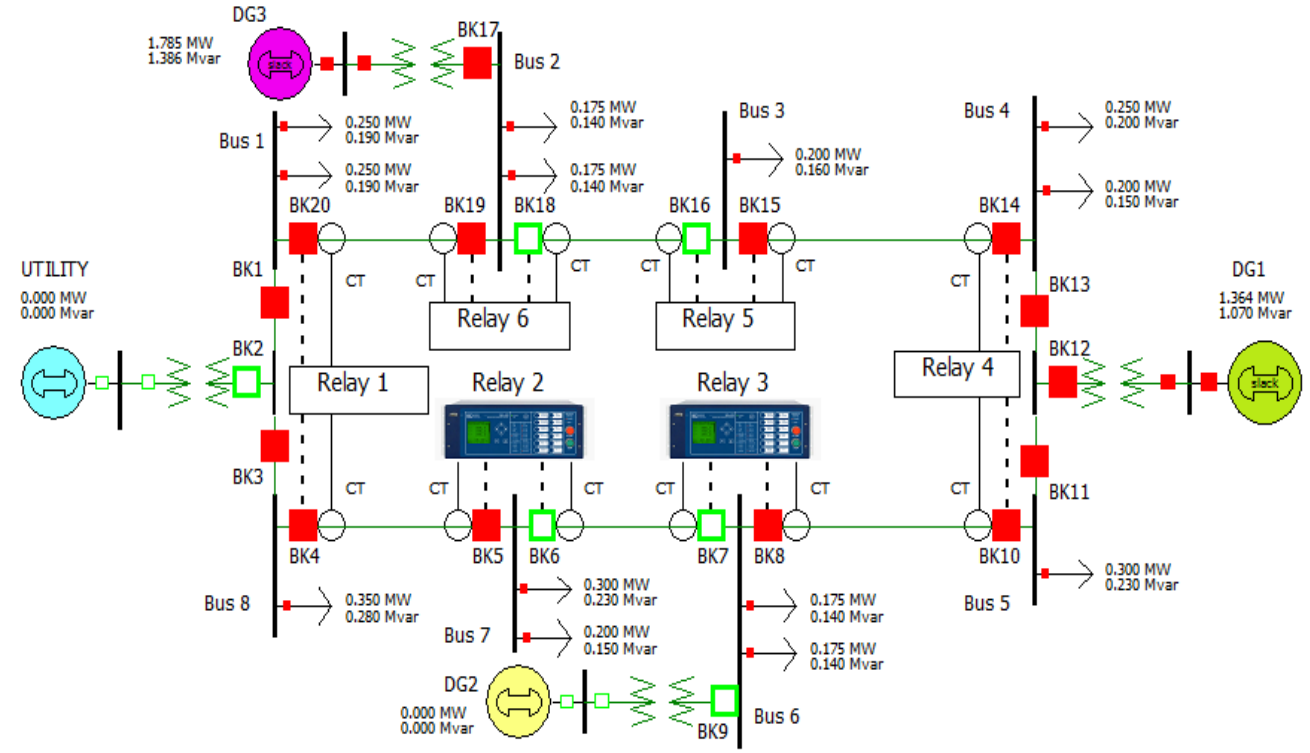

Figure D.10: DG1-34/56 (Test mode: 5)

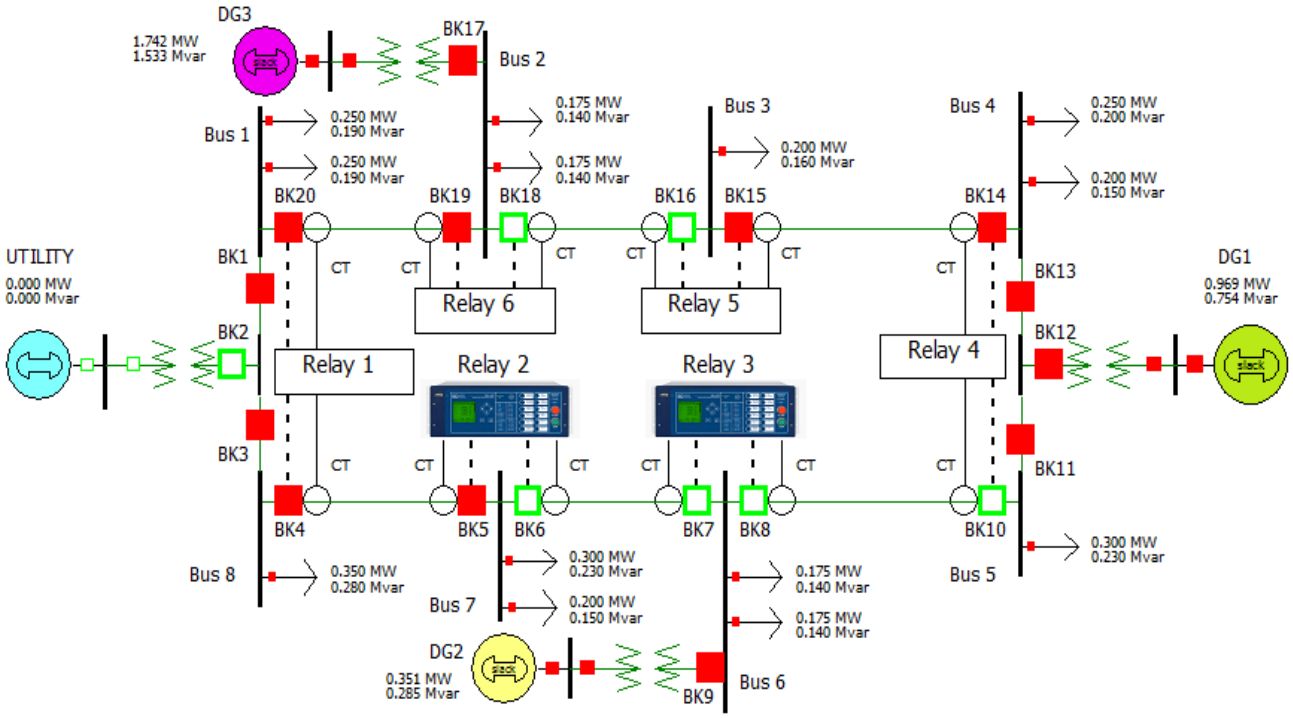

Figure D.11: DG2-6 (Test mode: 22)

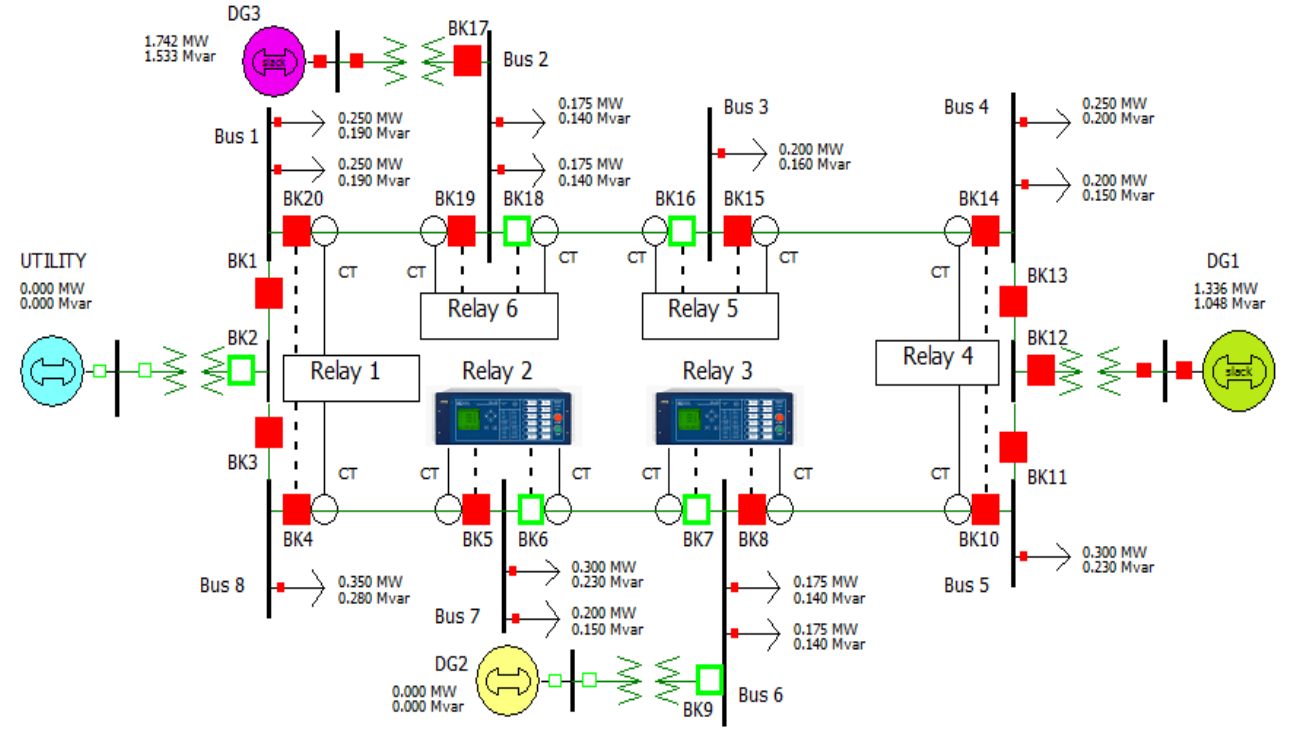

Figure D.12: DG3-2187 (Test modes: 5, 8, 17, and 22)

Appendix E - Calculated breaker fault current magnitudes of circuit paths for Relays 2 and 3 in the microgrid with distributed generators

Table E.1: Calculated breaker fault current magnitudes for UTILITY-8765/1234 (Test mode 1) circuit path

Protection Areas	Fault Location	Relays	Breakers	Magnitudes of breaker fault currents [Amps]											
				LL(BC) Fault			3PB Fault			SLG(A) Fault			DLG(BC) Fault		
				Phase A	Phase B	Phase C	Phase A	Phase B	Phase C	Phase A	Phase B	Phase C	Phase A	Phase B	Phase C
L56	Bus 5 (90% L56)	3	BK8	56	**1539**	1504	1775	1775	1775	1777	51	47	37	1781	1780
			BK7	122	1564	1488	1783	1783	1783	1797	112	105	85	1803	1783
		2	BK6	122	**1564**	1488	1783	1783	1783	1797	112	105	85	1803	1783
			BK5	215	1622	1490	1821	1821	1821	1843	199	189	162	1850	1814
		1	BK4	215	**1622**	1490	1821	1821	1821	1843	199	189	162	1850	1814
	Bus 6 (10% L56)	3	BK8	56	1794	1758	2039	2039	2039	2040	51	47	37	**2046**	2045
			BK7	122	1812	1735	2040	2040	2040	2055	112	104	82	2101	2093
		2	BK6	122	1812	1735	2040	2040	2040	2055	112	104	82	2101	2093
			BK5	215	1864	1730	2072	2072	2072	2097	198	187	156	2143	2100
		1	BK4	215	1864	1730	2072	2072	2072	2097	198	187	156	2143	2100
L67	Bus 6 (90%L67)	2	BK6	122	1845	1767	2167	2167	2167	2175	112	104	82	2182	2159
			BK5	215	1897	1761	2190	2190	2190	2214	198	187	155	2224	2180
		1	BK4	215	1897	1761	2190	2190	2190	2214	198	187	155	2224	2180
	Bus 7 (10%L67)	2	BK6	122	2781	2702	3165	3165	3165	3167	112	104	82	**3170**	3162
			BK5	215	2812	2673	3165	3165	3165	3191	196	184	146	3198	3159
		1	BK4	215	2812	2673	3165	3165	3165	3191	196	184	146	3198	3159
L78	Bus 7 (90%L78)	1	BK4	215	3160	3019	3567	3567	3567	3594	196	183	144	3597	3563
	Bus 8 (10%L78)	1	BK4	216	6336	6182	7227	7227	7227	7258	196	183	145	7205	**7279**

LL(BC): line-to-line fault at BC phases, 3PB: three phase balanced fault, SLG(A): single line-to-ground fault at A phase, DLG(BC): double line-to-ground fault at BC phases.
Bolds are current magnitudes at relays that tripped the three-pole breakers for maximum (DLG) and minimum (LL) faults

- Table E.1 continue in next page -

Table E.1 (Continue): Calculated breaker fault current magnitudes for UTILITY-8765/1234 (Test mode 1) circuit path

Protection Areas	Fault Location	Relays	Breaker	Magnitudes of breaker fault currents [Amps]											
				LL(BC) Fault			3PB Fault			SLG(A) Fault			DLG(BC) Fault		
				Phase A	Phase B	Phase C	Phase A	Phase B	Phase C	Phase A	Phase B	Phase C	Phase A	Phase B	Phase C
L34	Bus 4 (90% L34)	5	BK15	86	**1567**	1500	1780	1780	1780	1779	76	75	57	1785	1775
			BK16	124	1581	1511	1784	1784	1784	1793	111	109	85	1799	1778
		6	BK18	124	**1581**	1511	1784	1784	1784	1793	111	109	85	1799	1778
			BK19	191	1624	1517	1811	1811	1811	1830	172	171	141	1836	1804
		1	BK20	191	**1624**	1517	1811	1811	1811	1830	172	171	141	1836	1804
	Bus 3 (10% L34)	5	BK15	86	1793	1743	2041	2041	2041	2040	76	75	57	**2047**	2034
			BK16	124	1804	1733	2042	2042	2042	2051	110	109	83	2059	2033
		6	BK18	124	1804	1733	2042	2042	2042	2051	110	109	83	2059	2033
			BK19	191	1843	1734	2063	2063	2063	2084	172	170	137	2093	2054
		1	BK20	191	1843	1734	2063	2063	2063	2084	172	170	137	2093	2054
L23	Bus 3 (90%L23)	6	BK18	124	1908	1836	2160	2160	2160	2170	110	109	83	2179	2152
			BK19	191	1944	1835	2180	2180	2180	2202	171	170	136	2211	2171
		1	BK20	191	1944	1835	2180	2180	2180	2202	171	170	136	2211	2171
	Bus 2 (10%L23)	6	BK18	125	2766	2692	3151	3151	3151	3158	111	109	83	**3162**	3147
			BK19	191	2789	2676	3154	3154	3154	3178	170	168	129	3184	3148
		1	BK20	191	2789	2676	3154	3154	3154	3178	170	168	129	3184	3148
L12	Bus 2 (90%L12)	1	BK20	192	3136	3022	3554	3554	3554	3580	170	168	128	3583	3551
	Bus 1 (10%L12)	1	BK20	192	6309	6184	7212	7212	7212	7237	172	167	128	7183	**7266**

LL(BC): line-to-line fault at BC phases, 3PB: three phase balanced fault, SLG(A): single line-to-ground fault at A phase, DLG(BC): double line-to-ground fault at BC phases. Bolds are current magnitudes at relays that tripped the three-pole breakers for maximum (DLG) and minimum (LL) faults.

Table E.2: Calculated breaker fault current magnitudes of DG2-678/65 (Test modes 2, 6, 9, and 18) circuit path

Protection Areas	Fault Location	Relays	Breakers	Magnitudes of breaker fault currents [Amps]											
				LL(BC) Fault			3PB Fault			SLG(A) Fault			DLG(BC) Fault		
				Phase A	Phase B	Phase C	Phase A	Phase B	Phase C	Phase A	Phase B	Phase C	Phase A	Phase B	Phase C
L56	Bus 5 (90%L56)	4	BK10	53	1392	1354	1563	1563	1563	2013	46	46	24	1907	1885
		3	BK8	53	**1392**	1354	1563	1563	1563	2013	46	46	24	1907	1885
	Bus 6 (10%L56)	3	BK8	53	1576	1539	1746	1746	1746	**2371**	48	46	21	2206	2216
L78	Bus 8(90%L78)	2	BK5	64	**996**	954	1127	1127	1127	1340	57	55	35	1279	1243
			BK6	153	1036	936	1141	1141	1141	1368	137	138	92	1311	1259
		3	BK7	153	**1036**	936	1141	1141	1141	1368	137	138	92	1311	1259
	Bus 7(10%L78)	2	BK5	65	1206	1165	1339	1339	1339	**1650**	57	54	33	1564	1532
			BK6	153	1265	1161	1341	1341	1341	1709	137	137	79	1588	1534
		3	BK7	153	1265	1161	1341	1341	1341	1709	137	137	79	1588	1534
L67	Bus 7 (90%L67)	3	BK7	155	1295	1195	1403	1403	1403	1762	135	135	76	1678	1626
	Bus 6 (10%L67)	3	BK7	154	1588	1483	1721	1721	1721	**2369**	137	128	62	2182	2169

LL(BC): line-to-line fault at BC phases, 3PB: three phase balanced fault, SLG(A): single line-to-ground fault at A phase, DLG(BC): double line-to-ground fault at BC phases. Bolds are current magnitudes at relays that tripped the three-pole breakers for maximum (SLG) and minimum (LL) faults.

Table E.3: Calculated breaker fault current magnitudes of DG2-67/65 (Test modes 10 and 16) circuit path

Protection Areas	Fault Location	Relays	Breakers	Magnitudes of breaker fault currents [Amps]											
				LL(BC) Fault			3PB Fault			SLG(A) Fault			DLG(BC) Fault		
				Phase A	Phase B	Phase C	Phase A	Phase B	Phase C	Phase A	Phase B	Phase C	Phase A	Phase B	Phase C
L56	Bus 5(90%L56)	4	BK10	53	1369	1332	1517	1517	1517	1957	46	45	23	1863	1821
		3	BK8	53	**1369**	1332	1517	1517	1517	1957	46	45	23	1863	1821
	Bus 6(10%L56)	3	BK8	53	1566	1528	1732	1732	1732	**2330**	46	45	20	2223	2217
L67	Bus 7(90%L67)	3	BK7	88	**1221**	1159	1341	1341	1341	1680	78	76	42	1606	1542
			BK6	88	1221	1159	1341	1341	1341	1680	78	76	42	1606	1542
	Bus 6(10%L67)	3	BK7	87	1576	1511	1727	1727	1727	**2327**	78	74	33	2223	2211

LL(BC): line-to-line fault at BC phases, 3PB: three phase balanced fault, SLG(A): single line-to-ground fault at A phase, DLG(BC): double line-to-ground fault at BC phases. Bolds are current magnitudes at relays that tripped the three-pole breakers for maximum (SLG) and minimum (LL) faults.

Table E.4: Calculated breaker fault current magnitudes of DG2-6543 (Test mode 8) circuit path

Protection Areas	Fault Location	Relays	Breakers	Magnitudes of breaker fault currents [Amps]											
				LL(BC) Fault			3PB Fault			SLG(A) Fault			DLG(BC) Fault		
				Phase A	Phase B	Phase C	Phase A	Phase B	Phase C	Phase A	Phase B	Phase C	Phase A	Phase B	Phase C
L34	Bus 3 (90%L34)	5	BK15	37	1235	1210	1378	1378	1378	1715	33	32	18	1625	1593
		4	BK14	37	**1235**	1210	1378	1378	1378	1715	33	32	18	1625	1593
			BK10	169	1275	1162	1388	1388	1388	1744	153	150	92	1662	1607
		3	BK8	169	**1275**	1162	1388	1388	1388	1744	153	150	92	1662	1607
	Bus 4 (10%L34)	4	BK14	36	1365	1339	1520	1520	1520	**1942**	32	31	17	1838	1814
			BK10	168	1427	1310	1520	1520	1520	1989	150	145	80	1866	1816
		3	BK8	168	1427	1310	1520	1520	1520	1989	150	145	80	1866	1816
L56	Bus 5 (90%L56)	4	BK10	171	1447	1327	1557	1557	1557	2022	152	147	77	1926	1879
		3	BK8	171	1447	1327	1557	1557	1557	2022	152	147	77	1926	1879
	Bus 6(10%L56)	3	BK8	171	1602	1478	1724	1724	1724	**2355**	150	143	68	2213	2194

LL(BC): line-to-line fault at BC phases, 3PB: three phase balanced fault, SLG(A): single line-to-ground fault at A phase, DLG(BC): double line-to-ground fault at BC phases. Bolds are current magnitudes at relays that tripped the three-pole breakers for maximum (SLG) and minimum (LL) faults.

Table E.5: Calculated breaker fault current magnitudes of DG2-65 (Test mode 17) circuit path

Protection Areas	Fault Location	Relays	Breaker	Magnitudes of breaker fault currents [Amps]											
				LL(BC) Fault			3PB Fault			SLG(A) Fault			DLG(BC) Fault		
				Phase A	Phase B	Phase C	Phase A	Phase B	Phase C	Phase A	Phase B	Phase C	Phase A	Phase B	Phase C
L56	Bus 5(90%L56)	4	BK10	52	1342	1305	1485	1485	1485	1928	45	45	22	1850	1782
		3	BK8	52	**1342**	1305	1485	1485	1485	1928	45	45	22	1850	1782
	Bus 6(10%L56)	3	BK8	52	1527	1488	1685	1685	1685	**2282**	45	45	19	2195	2159

LL(BC): line-to-line fault at BC phases, 3PB: three phase balanced fault, SLG(A): single line-to-ground fault at A phase, DLG(BC): double line-to-ground fault at BC phases. Bolds are current magnitudes at relays that tripped the three-pole breakers for maximum (SLG) and minimum (LL) faults.

Table E.6: Calculated breaker fault current magnitudes of DG2-6781 (Test modes 3, 7, 12, 15, and 20) circuit path

Protection Areas	Fault Location	Relays	Breaker	Magnitudes of breaker fault currents [Amps]											
				LL(BC) Fault			3PB Fault			SLG(A) Fault			DLG(BC) Fault		
				Phase A	Phase B	Phase C	Phase A	Phase B	Phase C	Phase A	Phase B	Phase C	Phase A	Phase B	Phase C
L78	Bus 8 (90%L78)	1	BK4	157	1047	945	1155	1155	1155	1373	144	143	91	1307	1274
		2	BK5	157	**1047**	945	1155	1155	1155	1373	144	143	91	1307	1274
			BK6	249	1088	929	1170	1170	1170	1403	226	226	151	1340	1291
		3	BK7	249	**1088**	929	1170	1170	1170	1403	226	226	151	1340	1291
	Bus 7 (10%L78)	2	BK5	163	1262	1162	1368	1368	1368	**1681**	144	131	84	1595	1564
			BK6	255	1295	1139	1371	1371	1371	1742	225	209	132	1620	1568
		3	BK7	255	1295	1139	1371	1371	1371	1742	225	209	132	1620	1568
L67	Bus 7(90%L67)	3	BK7	248	1318	1152	1433	1433	1433	1801	224	223	127	1712	1661
	Bus 6(10%L67)	3	BK7	254	1645	1477	1748	1748	1748	**2400**	228	204	105	2218	2204

LL(BC): line-to-line fault at BC phases, 3PB: three phase balanced fault, SLG(A): single line-to-ground fault at A phase, DLG(BC): double line-to-ground fault at BC phases. Bolds are current magnitudes at relays that tripped the three-pole breakers for maximum (SLG) and minimum (LL) faults.

Table E.7: Calculated breaker fault current magnitudes of DG2-678 (Test modes 11, 14, and 19) circuit path

Protection Areas	Fault Location	Relays	Breaker	Magnitudes of breaker fault currents [Amps]											
				LL(BC) Fault			3PB Fault			SLG(A) Fault			DLG(BC) Fault		
				Phase A	Phase B	Phase C	Phase A	Phase B	Phase C	Phase A	Phase B	Phase C	Phase A	Phase B	Phase C
L78	Bus 8 (90%L78)	1	BK4	64	989	947	1119	1119	1119	1336	57	58	36	1279	1234
		2	BK5	64	**989**	947	1119	1119	1119	1336	57	58	36	1279	1234
			BK6	153	1031	930	1133	1133	1133	1364	136	138	92	1311	1249
		3	BK7	153	**1031**	930	1133	1133	1133	1364	136	138	92	1311	1249
	Bus 7 (10%L78)	2	BK5	65	1196	1154	1326	1326	1326	**1639**	57	54	33	1561	1516
			BK6	155	1228	1128	1328	1328	1328	1698	136	131	79	1584	1519
		3	BK7	155	1228	1128	1328	1328	1328	1698	136	131	79	1584	1519
L67	Bus 7(90%L67)	3	BK7	152	1253	1149	1388	1388	1388	1750	135	136	75	1673	1609
	Bus 6(10%L67)	3	BK7	154	1567	1459	1694	1694	1694	**2339**	136	128	62	2167	2136

LL(BC): line-to-line fault at BC phases, 3PB: three phase balanced fault, SLG(A): single line-to-ground fault at A phase, DLG(BC): double line-to-ground fault at BC phases. Bolds are current magnitudes at relays that tripped the three-pole breakers for maximum (SLG) and minimum (LL) faults.

Table E.8: Calculated breaker fault current magnitudes of DG2-67 (Test modes 13 and 21) circuit path

Protection Areas	Fault Location	Relays	Breaker	Magnitudes of breaker fault currents [Amps]											
				LL(BC) Fault			3PB Fault			SLG(A) Fault			DLG(BC) Fault		
				Phase A	Phase B	Phase C	Phase A	Phase B	Phase C	Phase A	Phase B	Phase C	Phase A	Phase B	Phase C
L67	Bus 7 (90%L67)	2	BK6	87	1209	1148	1328	1328	1328	1669	77	76	42	1602	1529
		3	BK7	87	**1209**	1148	1328	1328	1328	1669	77	76	42	1602	1529
	Bus 6 (10%L67)	3	BK7	87	1552	1487	1700	1700	1700	**2298**	77	74	32	2206	2176

LL(BC): line-to-line fault at BC phases, 3PB: three phase balanced fault, SLG(A): single line-to-ground fault at A phase, DLG(BC): double line-to-ground fault at BC phases.
Bolds are current magnitudes at relays that tripped the three-pole breakers for maximum (SLG) and minimum (LL) faults.

Table E.9: Calculated breaker fault current magnitudes of DG1-5678 (Test mode 4) circuit path

Protection Areas	Fault Location	Relays	Breaker	Magnitudes of breaker fault currents [Amps]											
				LL(BC) Fault			3PB Fault			SLG(A) Fault			DLG(BC) Fault		
				Phase A	Phase B	Phase C	Phase A	Phase B	Phase C	Phase A	Phase B	Phase C	Phase A	Phase B	Phase C
L78	Bus 8 (90%L78)	1	BK4	65	915	874	1034	1034	1034	1204	58	58	38	1150	1124
		2	BK5	65	**915**	874	1034	1034	1034	1204	58	58	38	1150	1124
			BK6	155	955	855	1047	1047	1047	1233	140	141	97	1182	1139
		3	BK7	155	**955**	855	1047	1047	1047	1233	140	141	97	1182	1139
			BK8	220	992	855	1067	1067	1067	1261	198	197	144	1211	1161
		4	BK10	220	**992**	855	1067	1067	1067	1261	198	197	144	1211	1161
	Bus 7 (10%L78)	2	BK5	66	1092	1052	1213	1213	1213	**1453**	59	55	36	1376	1353
			BK6	158	1123	1027	1215	1215	1215	1467	140	132	86	1402	1356
		3	BK7	158	1123	1027	1215	1215	1215	1503	140	132	86	1402	1356
			BK8	223	1156	1021	1228	1228	1228	1523	197	189	128	1426	1371
		4	BK10	223	1156	1021	1228	1228	1228	1523	197	189	128	1426	1371
L67	Bus 7 (90%L67)	3	BK7	155	1145	1042	1266	1266	1266	1545	139	139	83	1471	1426
			BK8	219	1176	1033	1278	1278	1278	1566	195	196	123	1494	1439
		4	BK10	219	1176	1033	1278	1278	1278	1566	195	196	123	1494	1439
	Bus 6 (10%L67)	3	BK7	158	1405	1302	1522	1522	1522	**1940**	140	130	74	1844	1808
			BK8	221	1428	1286	1525	1525	1525	1950	196	186	104	1861	1811
		4	BK10	221	1428	1286	1525	1525	1525	1950	196	186	104	1861	1811
L56	Bus 6 (90%L56)	3	BK8	221	1480	1338	1582	1582	1582	2051	194	193	100	1951	1906
		4	BK10	221	1480	1338	1582	1582	1582	2051	194	193	100	1951	1906
	Bus 5 (10%L56)	4	BK10	221	1638	1489	1750	1750	1750	**2350**	194	191	87	2241	2224

LL(BC): line-to-line fault at BC phases, 3PB: three phase balanced fault, SLG(A): single line-to-ground fault at A phase, DLG(BC): double line-to-ground fault at BC phases. Bolds are current magnitudes at relays that tripped the three-pole breakers for maximum (SLG) and minimum (LL) faults.

Table E.10: Calculated breaker fault current magnitudes of DG1-34/56 (Test mode 5) circuit path

Protection Areas	Fault Location	Relays	Breaker	Magnitudes of breaker fault currents [Amps]											
				LL(BC) Fault			3PB Fault			SLG(A) Fault			DLG(BC) Fault		
				Phase A	Phase B	Phase C	Phase A	Phase B	Phase C	Phase A	Phase B	Phase C	Phase A	Phase B	Phase C
L34	Bus 3(90%L34)	5	BK15	36	1387	1363	1546	1546	1546	1995	31	31	16	1895	1864
		4	BK14	36	**1387**	1363	1546	1546	1546	1995	31	31	16	1895	1864
	Bus 4(10%L34)	4	BK14	36	1551	1526	1724	1724	1724	**2303**	31	31	14	2189	2189
L56	Bus 6 (90%L56)	3	BK8	62	1399	1357	1548	1548	1548	2001	55	55	28	1901	1867
		4	BK10	62	**1399**	1357	1548	1548	1548	2001	55	55	28	1901	1867
	Bus 5 (10%L56)	4	BK10	62	1561	1518	1724	1724	1724	**2306**	54	54	24	2194	2190

LL(BC): line-to-line fault at BC phases, 3PB: three phase balanced fault, SLG(A): single line-to-ground fault at A phase, DLG(BC): double line-to-ground fault at BC phases. Bolds are current magnitudes at relays that tripped the three-pole breakers for maximum (SLG) and minimum (LL) faults.

Table E.11: Calculated breaker fault current magnitudes of DG2-6 (Test mode 4) circuit path

Protection Areas	Fault Location	Relays	Breaker	Magnitudes of breaker fault currents [Amps]											
				LL(BC) Fault			3PB Fault			SLG(A) Fault			DLG(BC) Fault		
				Phase A	Phase B	Phase C	Phase A	Phase B	Phase C	Phase A	Phase B	Phase C	Phase A	Phase B	Phase C
NA	NA	3	BK7	NA	NA	NA	NA	NA	NA	NA	NA	NA	NA	NA	NA
			BK8	NA	NA	NA	NA	NA	NA	NA	NA	NA	NA	NA	NA

NA (not available): The DG2-6 (Test mode 22) circuit path did not have protection areas limited by power lines, so calculated breaker fault current magnitudes were not available.
LL(BC): line-to-line fault at BC phases, 3PB: three phase balanced fault, SLG(A): single line-to-ground fault at A phase, DLG(BC): double line-to-ground fault at BC phases.

Table E.12: Calculated breaker fault current magnitudes of DG3-2187 (Test modes 5, 8, 17, and 22) circuit path

Protection Areas	Fault Location	Relays	Breaker	Magnitudes of breaker fault currents [Amps]											
				LL(BC) Fault			3PB Fault			SLG(A) Fault			DLG(BC) Fault		
				Phase A	Phase B	Phase C	Phase A	Phase B	Phase C	Phase A	Phase B	Phase C	Phase A	Phase B	Phase C
L78	Bus 7 (90%L78)	6	BK19	254	**1112**	962	1170	1170	1170	1405	224	225	155	1344	1293
		1	BK20	254	1112	962	1170	1170	1170	1405	224	225	155	1344	1293
			BK4	94	**1038**	981	1144	1144	1144	1353	82	82	52	1286	1262
		2	BK5	94	1038	981	1144	1144	1144	1353	82	82	52	1286	1262
	Bus 8 (10%L78)	6	BK19	253	1293	1138	1369	1369	1369	1702	222	222	132	1619	1567
		1	BK20	253	1293	1138	1369	1369	1369	1702	222	222	132	1619	1567
			BK4	94	1237	1179	1365	1365	1365	**1671**	82	82	48	1576	1560
L12	Bus 1 (90%L12)	6	BK19	252	1351	1193	1432	1432	1432	1799	222	221	127	1710	1659
		1	BK20	252	1351	1193	1432	1432	1432	1799	222	221	127	1710	1659
	Bus 2 (10%L12)	1	BK19	252	1644	1475	1747	1747	1747	**2330**	223	217	104	2216	2202

LL(BC): line-to-line fault at BC phases, 3PB: three phase balanced fault, SLG(A): single line-to-ground fault at A phase, DLG(BC): double line-to-ground fault at BC phases.
Bolds are current magnitudes at relays that tripped the three-pole breakers for maximum (SLG) and minimum (LL) faul

Appendix F - Primary currents and line-to-ground voltages of pre-fault states

Table F.1: Pre-fault states of tripping and non-tripping tests for maximum and minimum fault overcurrents of Relay 2

Setting Group	Test Mode	Protection Areas	Tests: Source - Circuit - Type of Fault - Fault Location -Opened Breaker	Breaker	Low Level Test Interface	Primary Currents and Line-to-ground Voltages											
						Pre-fault Currents						Bus 7 - Pre-fault Line-to-ground Voltages					
						IA		*IB*		*IC*		*VA*		*VB*		*VC*	
						Mag. [A]	β_A [°]	Mag. [A]	β_B [°]	Mag. [A]	β_C [°]	Mag. [V]	δ_A [°]	Mag. [V]	δ_B [°]	Mag. [V]	δ_C [°]
SS1	1	L56	**[1]UTILITY-8765/1234-DLG(BC)-Bus6-BK6** **[2]UTILITY-8765/1234-LL(BC)-Bus5-BK6**	BK6	IAW, IBW, ICW	122	-39.74	122	-159.74	122	80.26	3850	-4.20	3850	-124.20	3850	115.80
				BK5	IAX, IBX, ICX	215	-36.47	215	-156.47	215	83.53						
		L67	[1]UTILITY-8765/1234-DLG(BC)-Bus7-BK6 [2]UTILITY-8765/1234-LL(BC)-Bus6-BK6	BK6	IAW, IBW, ICW	122	-39.74	122	-159.74	122	80.26	3850	-4.20	3850	-124.20	3850	115.80
				BK5	IAX, IBX, ICX	215	-36.47	215	-156.47	215	83.53						
SS2	2, 6, 9, 18	L78	[1]DG2-678/65-SLG(A)-Bus7-BK5 [2]DG2-678/65-LL(BC)-Bus8-BK5	BK5	IAX, IBX, ICX	65	-39.79	65	-159.79	65	80.21	3940	-2.92	3940	-122.92	3940	117.08
				BK6	IAW, IBW, ICW	156	-35.62	156	204.38	156	84.38						
	3, 7, 12, 15, 20	L78	[1]DG2-6781-SLG(A)-Bus7-BK5 [2]DG2-6781-LL(BC)-Bus8-BK5	BK5	IAX, IBX, ICX	160	-37.60	160	-157.60	160	82.40	3870	-3.91	3870	-123.91	3870	116.09
				BK6	IAW, IBW, ICW	253	-37.79	253	-157.79	253	82.21						
	11, 14,19	L78	[1]DG2-678-SLG(A)-Bus7-BK5 [2]DG2-678-LL(BC)-Bus8-BK5	BK5	IAX, IBX, ICX	65	-39.37	65	-159.37	65	80.63	3970	-2.50	3970	-122.50	3970	117.50
				BK6	IAW, IBW, ICW	156	-35.22	156	-155.22	156	84.78						
SS4	4	L78	[1]DG1-5678-SLG(A)-Bus7-BK5 [2]DG1-5678-LL(BC)-Bus8-BK5	BK5	IAX, IBX, ICX	66	-40.49	66	-160.49	66	79.51	3870	-3.62	3870	-123.62	3870	116.38
				BK6	IAW, IBW, ICW	158	-36.28	158	-156.28	158	83.72						

[1] Maximum fault overcurrent tests, [2]Minimum fault overcurrent tests. Bold represents backup protection tests.

Table F.2: Pre-fault states of tripping and non-tripping tests for maximum and minimum fault overcurrents of Relay 3

Setting Group	Test Mode	Protection Areas	Tests: Source - Circuit - Type of Fault - Fault Location -Opened Breaker	Breaker	Low Level Test Interface	Primary Currents and Line-to-ground Voltages											
						Pre-fault Currents						Bus 6 - Pre-fault Line-to-ground Voltages					
						IA		*IB*		*IC*		*VA*		*VB*		*VC*	
						Mag. [A]	β_A [°]	Mag. [A]	β_B [°]	Mag. [A]	β_C [°]	Mag. [V]	δ_A [°]	Mag. [V]	δ_B [°]	Mag. [V]	δ_C [°]
SS1	1	L56	[1]UTILITY-8765/1234-DLG(BC)-Bus6-BK8	BK8	IAW, IBW, ICW	56	-38.74	56	-158.74	56	81.26	3780	-5.05	3780	-125.05	3780	114.95
			[2]UTILITY-8765/1234-LL(BC)-Bus5-BK8	BK7	IAX, IBX, ICX	122	-39.74	122	-159.74	122	80.26						
SS2	2, 6, 9, 18	L56	[1]DG2-678/65-SLG(A)-Bus6-BK8	BK8	IAW, IBW, ICW	55	-35.62	55	-155.62	55	84.38	4030	-1.93	4030	-121.93	4030	118.07
			[2]DG2-678/65-LL(BC)-Bus5-BK8	BK7	IAX, IBX, ICX	156	-35.62	156	-155.62	156	84.38						
		L67	[1]DG2-678/65-SLG(A)-Bus6-BK7	BK7	IAX, IBX, ICX	156	-35.62	156	-155.62	156	84.38	4030	-1.93	4030	-121.93	4030	118.07
			[2]DG2-678/65-LL(BC)-Bus7-BK7	BK8	IAW, IBW, ICW	55	-35.62	55	-155.62	55	84.38						
		L78	**[1]DG2-678/65-SLG(A)-Bus7-BK7**	BK7	IAX, IBX, ICX	156	-35.62	156	-155.62	156	84.38	4030	-1.93	4030	-121.93	4030	118.07
			[2]DG2-678/65-LL(BC)-Bus8-BK7	BK8	IAW, IBW, ICW	55	-35.62	55	-155.62	55	84.38						
	10, 16	L56	[1]DG2-67/65-SLG(A)-Bus6-BK8	BK8	IAW, IBW, ICW	54	-35.14	54	-155.14	54	84.86	4060	-1.45	4060	-121.45	4060	118.55
			[2]DG2-67/65-LL(BC)-Bus5-BK8	BK7	IAX, IBX, ICX	90	-40.11	90	-160.11	90	79.89						
		L67	[1]DG2-67/65-SLG(A)-Bus6-BK7	BK7	IAX, IBX, ICX	90	-40.11	90	-160.11	90	79.89	4060	-1.45	4060	-121.45	4060	118.55
			[2]DG2-67/65-LL(BC)-Bus7-BK7	BK8	IAW, IBW, ICW	54	-35.14	54	-155.14	54	84.86						
	8	L34	[1]DG2-6543-SLG(A)-Bus4-BK8	BK8	IAW, IBW, ICW	173	-36.64	173	-156.64	173	83.36	4050	-1.65	4050	-121.65	4050	118.35
			[2]DG2-6543-LL(BC)-Bus3-BK8	BK7	IAX, IBX, ICX	0	0.00	0	0.00	0	0.00						
		L56	[1]DG2-6543-SLG(A)-Bus6-BK8	BK8	IAW, IBW, ICW	173	-36.64	173	-156.64	173	83.36	4050	-1.65	4050	-121.65	4050	118.35
			[2]DG2-6543-LL(BC)-Bus5-BK8	BK7	IAX, IBX, ICX	0	0.00	0	0.00	0	0.00						
	17	L56	[1]DG2-65-SLG(A)-Bus6-BK8	BK8	IAW, IBW, ICW	53	-34.49	53	-154.49	53	85.51	4100	-0.80	4100	-120.80	4100	119.20
			[2]DG2-65-LL(BC)-Bus5-BK8	BK7	IAX, IBX, ICX	0	0.00	0	0.00	0	0.00						
SS3	3, 7, 12, 15, 20	L67	[1]DG2-6781-SLG(A)-Bus6-BK7	BK7	IAX, IBX, ICX	253	-37.79	253	-157.79	253	82.21	4010	-2.25	4010	-122.25	4010	117.75
			[2]DG2-6781-LL(BC)-Bus7-BK7	BK8	IAW, IBW, ICW	0	0.00	0	0.00	0	0.00						
		L78	**[1]DG2-6781-SLG(A)-Bus7-BK7**	BK7	IAX, IBX, ICX	253	-37.79	253	-157.79	253	82.21	4010	-2.25	4010	-122.25	4010	117.75
			[2]DG2-6781-LL(BC)-Bus8-BK7	BK8	IAW, IBW, ICW	0	0.00	0	0.00	0	0.00						
	11, 14, 19	L67	[1]DG2-678-SLG(A)-Bus6-BK7	BK7	IAX, IBX, ICX	156	-35.22	156	-155.22	156	84.78	4050	-1.53	4050	-121.53	4050	118.47
			[2]DG2-678-LL(BC)-Bus7-BK7	BK8	IAW, IBW, ICW	0	0.00	0	0.00	0	0.00						
		L78	**[1]DG2-678-SLG(A)-Bus7-BK7**	BK7	IAX, IBX, ICX	156	-35.22	156	-155.22	156	84.78	4050	-1.53	4050	-121.53	4050	118.47
			[2]DG2-678-LL(BC)-Bus8-BK7	BK8	IAW, IBW, ICW	0	0.00	0	0.00	0	0.00						
SS4	13, 21	L67	[1]DG2-67-SLG(A)-Bus6-BK7	BK7	IAX, IBX, ICX	89	-39.72	89	-159.72	89	80.28	4090	-1.06	4090	-121.06	4090	118.94
			[2]DG2-67-LL(BC)-Bus7-BK7	BK8	IAW, IBW, ICW	0	0.00	0	0.00	0	0.00						
SS5	4	L67	[1]DG1-5678-SLG(A)-Bus6-BK7	BK7	IAX, IBX, ICX	158	-36.28	158	-156.28	158	83.72	3960	-2.59	3960	-122.59	3960	117.41
			[2]DG1-5678-LL(BC)-Bus7-BK7	BK8	IAW, IBW, ICW	224	-36.65	224	-156.65	224	83.35						
		L78	**[1]DG1-5678-SLG(A)-Bus7-BK7**	BK7	IAX, IBX, ICX	158	-36.28	158	-156.28	158	83.72	3960	-2.59	3960	-122.59	3960	117.41
			[2]DG1-5678-LL(BC)-Bus8-BK7	BK8	IAW, IBW, ICW	224	-36.65	224	-156.65	224	83.35						

[1] Maximum fault overcurrent tests, [2]Minimum fault overcurrent tests. Bold represents backup protection tests.

Appendix G - Primary currents and line-to-ground voltages of post-fault states

Table G.1: Post-fault states of tripping and non-tripping tests for maximum and minimum fault overcurrents of Relay 2

Setting Group	Test Mode	Protection Areas	Tests: Source - Circuit - Type of Fault - Fault Location -Opened Breaker	Breaker	Low Level Test Interface	Primary Currents and Line-to-ground Voltages: Post-fault Currents IA Mag. [A]	IA β_A [°]	IB Mag. [A]	IB β_B [°]	IC Mag. [A]	IC β_C [°]	Bus 7 - Post-fault Line-to-ground Voltages: VA Mag. [V]	VA δ_A [°]	VB Mag. [V]	VB δ_B [°]	VC Mag. [V]	VC δ_C [°]
SS1	1	L56	**[1]UTILITY-8765/1234-DLG(BC)-Bus6-BK6** **[2]UTILITY-8765/1234-LL(BC)-Bus5-BK6**	BK6	IAW, IBW, ICW	0	0.00	0	0.00	0	0.00	3960	-2.71	3960	-122.71	3960	117.29
				BK5	IAX, IBX, ICX	92	-41.37	92	-161.37	92	78.63						
		L67	[1]UTILITY-8765/1234-DLG(BC)-Bus7-BK6 [2]UTILITY-8765/1234-LL(BC)-Bus6-BK6	BK6	IAW, IBW, ICW	0	0.00	0	0.00	0	0.00	3960	-2.71	3960	-122.71	3960	117.29
				BK5	IAX, IBX, ICX	92	-41.37	92	-161.37	92	78.63						
SS2	2, 6, 9, 18	L78	[1]DG2-678/65-SLG(A)-Bus7-BK5 [2]DG2-678/65-LL(BC)-Bus8-BK5	BK5	IAX, IBX, ICX	0	0.00	0	0.00	0	0.00	4010	-2.01	4010	-122.01	4010	117.99
				BK6	IAW, IBW, ICW	90	-40.67	90	-160.67	90	79.33						
	3, 7, 12, 15, 20	L78	[1]DG2-6781-SLG(A)-Bus7-BK5 [2]DG2-6781-LL(BC)-Bus8-BK5	BK5	IAX, IBX, ICX	0	0.00	0	0.00	0	0.00	4040	-1.61	4040	-121.61	4040	118.39
				BK6	IAW, IBW, ICW	89	-40.27	89	-160.27	89	79.73						
	11, 14,19	L78	[1]DG2-678-SLG(A)-Bus7-BK5 [2]DG2-678-LL(BC)-Bus8-BK5	BK5	IAX, IBX, ICX	0	0.00	0	0.00	0	0.00	4040	-1.61	4040	-121.61	4040	118.39
				BK6	IAW, IBW, ICW	89	-40.27	89	-160.27	89	79.73						
SS4	4	L78	[1]DG1-5678-SLG(A)-Bus7-BK5 [2]DG1-5678-LL(BC)-Bus8-BK5	BK5	IAX, IBX, ICX	0	0.00	0	0.00	0	0.00	3960	-2.47	3960	-122.47	3960	117.53
				BK6	IAW, IBW, ICW	91	-41.13	91	-161.13	91	78.87						

[1] Maximum fault overcurrent tests, [2]Minimum fault overcurrent tests. Bold represents backup protection tests.

Table G.2: Post-fault states of tripping and non-tripping tests for maximum and minimum fault overcurrents of Relay 3

Setting Group	Test Mode	Protection Areas	Tests: Source - Circuit - Type of Fault - Fault Location -Opened Breaker	Breaker	Low Level Test Interface	Primary Currents and Line-to-ground Voltages											
						Post-fault Currents						Bus 6 - Post-fault Line-to-ground Voltages					
						IA		*IB*		*IC*		*VA*		*VB*		*VC*	
						Mag. [A]	β_A [°]	Mag. [A]	β_B [°]	Mag. [A]	β_C [°]	Mag. [V]	δ_A [°]	Mag. [V]	δ_B [°]	Mag. [V]	δ_C [°]
SS1	1	L56	[1]UTILITY-8765/1234-DLG(BC)-Bus6-BK8	BK8	IAW, IBW, ICW	0	0.00	0	0.00	0	0.00	3860	-3.92	3860	-123.92	3860	116.08
			[2]UTILITY-8765/1234-LL(BC)-Bus5-BK8	BK7	IAX, IBX, ICX	66	-48.92	66	-168.92	66	71.08						
SS2	2, 6, 9, 18	L56	[1]DG2-678/65-SLG(A)-Bus6-BK8	BK8	IAW, IBW, ICW	0	0.00	0	0.00	0	0.00	4050	-1.48	4050	-121.48	4050	118.52
			[2]DG2-678/65-LL(BC)-Bus5-BK8	BK7	IAX, IBX, ICX	158	-39.35	158	-159.35	158	80.65						
		L67	[1]DG2-678/65-SLG(A)-Bus6-BK7	BK7	IAX, IBX, ICX	0	0.00	0	0.00	0	0.00	4100	-0.81	4100	-120.81	4100	119.19
			[2]DG2-678/65-LL(BC)-Bus7-BK7	BK8	IAW, IBW, ICW	53	-34.50	53	-154.50	53	85.50						
		L78	**[1]DG2-678/65-SLG(A)-Bus7-BK7**	BK7	IAX, IBX, ICX	0	0.00	0	0.00	0	0.00	4100	-0.81	4100	-120.81	4100	119.19
			[2]DG2-678/65-LL(BC)-Bus8-BK7	BK8	IAW, IBW, ICW	53	-34.50	53	-154.50	53	85.50						
	10, 16	L56	[1]DG2-67/65-SLG(A)-Bus6-BK8	BK8	IAW, IBW, ICW	0	0.00	0	0.00	0	0.00	4160	0.00	4160	-120.00	4160	120.00
			[2]DG2-67/65-LL(BC)-Bus5-BK8	BK7	IAX, IBX, ICX	88	-38.66	88	-158.66	88	81.34						
		L67	[1]DG2-67/65-SLG(A)-Bus6-BK7	BK7	IAX, IBX, ICX	0	0.00	0	0.00	0	0.00	4100	-0.81	4100	-120.81	4100	119.19
			[2]DG2-67/65-LL(BC)-Bus7-BK7	BK8	IAW, IBW, ICW	53	-34.50	53	-154.50	53	85.50						
	8	L34	[1]DG2-6543-SLG(A)-Bus4-BK8	BK8	IAW, IBW, ICW	0	0.00	0	0.00	0	0.00	4050	-1.65	4050	-121.65	4050	118.35
			[2]DG2-6543-LL(BC)-Bus3-BK8	BK7	IAX, IBX, ICX	0	0.00	0	0.00	0	0.00						
		L56	[1]DG2-6543-SLG(A)-Bus6-BK8	BK8	IAW, IBW, ICW	0	0.00	0	0.00	0	0.00	4050	-1.65	4050	-121.65	4050	118.35
			[2]DG2-6543-LL(BC)-Bus5-BK8	BK7	IAX, IBX, ICX	0	0.00	0	0.00	0	0.00						
	17	L56	[1]DG2-65-SLG(A)-Bus6-BK8	BK8	IAW, IBW, ICW	0	0.00	0	0.00	0	0.00	4050	-1.65	4050	-121.65	4050	118.35
			[2]DG2-65-LL(BC)-Bus5-BK8	BK7	IAX, IBX, ICX	0	0.00	0	0.00	0	0.00						
SS3	3, 7, 12, 15, 20	L67	[1]DG2-6781-SLG(A)-Bus6-BK7	BK7	IAX, IBX, ICX	0	0.00	0	0.00	0	0.00	4130	-0.42	4130	-120.42	4130	119.58
			[2]DG2-6781-LL(BC)-Bus7-BK7	BK8	IAW, IBW, ICW	0	0.00	0	0.00	0	0.00						
		L78	**[1]DG2-6781-SLG(A)-Bus7-BK7**	BK7	IAX, IBX, ICX	0	0.00	0	0.00	0	0.00	4130	-0.42	4130	-120.42	4130	119.58
			[2]DG2-6781-LL(BC)-Bus8-BK7	BK8	IAW, IBW, ICW	0	0.00	0	0.00	0	0.00						
	11, 14, 19	L67	[1]DG2-678-SLG(A)-Bus6-BK7	BK7	IAX, IBX, ICX	0	0.00	0	0.00	0	0.00	4130	-0.42	4130	-120.42	4130	119.58
			[2]DG2-678-LL(BC)-Bus7-BK7	BK8	IAW, IBW, ICW	0	0.00	0	0.00	0	0.00						
		L78	**[1]DG2-678-SLG(A)-Bus7-BK7**	BK7	IAX, IBX, ICX	0	0.00	0	0.00	0	0.00	4130	-0.42	4130	-120.42	4130	119.58
			[2]DG2-678-LL(BC)-Bus8-BK7	BK8	IAW, IBW, ICW	0	0.00	0	0.00	0	0.00						
SS4	13, 21	L67	[1]DG2-67-SLG(A)-Bus6-BK7	BK7	IAX, IBX, ICX	0	0.00	0	0.00	0	0.00	4130	-0.42	4130	-120.42	4130	119.58
			[2]DG2-67-LL(BC)-Bus7-BK7	BK8	IAW, IBW, ICW	0	0.00	0	0.00	0	0.00						
SS5	4	L67	[1]DG1-5678-SLG(A)-Bus6-BK7	BK7	IAX, IBX, ICX	0	0.00	0	0.00	0	0.00	4090	-0.96	4090	-120.96	4090	119.04
			[2]DG1-5678-LL(BC)-Bus7-BK7	BK8	IAW, IBW, ICW	63	-37.83	63	-157.83	63	82.17						
		L78	**[1]DG1-5678-SLG(A)-Bus7-BK7**	BK7	IAX, IBX, ICX	0	0.00	0	0.00	0	0.00	4090	-0.96	4090	-120.96	4090	119.04
			[2]DG1-5678-LL(BC)-Bus8-BK7	BK8	IAW, IBW, ICW	63	-37.83	63	-157.83	63	82.17						

[1] Maximum fault overcurrent tests, [2]Minimum fault overcurrent tests. Bold represents backup protection tests.

Appendix H - Primary currents and line-to-ground voltages of fault states

Table H.1: Fault states of tripping and non-tripping tests for maximum fault overcurrents of Relay 2

Setting Group	Test Mode	Protection Areas	Tests	Breaker	Low Level Test Interface	Primary Currents and Line-to-ground Voltages											
						Fault Currents						Bus 7 - Fault Line-to-ground Voltages					
						IA		*IB*		*IC*		*VA*		*VB*		*VC*	
			Source - Circuit - Type of Fault - Fault Location -Opened Breaker			Mag. [A]	β_A [°]	Mag. [A]	β_B [°]	Mag. [A]	β_C [°]	Mag. [V]	δ_A [°]	Mag. [V]	δ_B [°]	Mag. [V]	δ_C [°]
SS1	1	L56	**UTILITY-8765/1234-DLG(BC)-Bus6-BK6**	BK6	IAW, IBW, ICW	82	-35.26	2101	162.69	2093	43.06	3890	-3.81	1486	-124.25	1512	115.20
				BK5	IAX, IBX, ICX	156	-35.63	2143	163.18	2100	44.30						
		L67	UTILITY-8765/1234-DLG(BC)-Bus7-BK6	BK6	IAW, IBW, ICW	82	-34.30	3170	161.98	3162	42.05	3890	-3.82	224	-124.96	230	114.19
				BK5	IAX, IBX, ICX	146	-35.12	3198	161.89	3159	42.70						
SS2	2, 6, 9, 18	L78	DG2-678/65-SLG(A)-Bus7-BK5	BK5	IAX, IBX, ICX	1650	100.07	57	45.56	54	-121.69	118	-7.85	3538	-112.60	3576	106.63
				BK6	IAW, IBW, ICW	1709	100.34	137	46.11	137	-121.25						
	3, 7, 12, 15, 20	L78	DG2-6781-SLG(A)-Bus7-BK5	BK5	IAX, IBX, ICX	1681	101.12	144	46.85	131	119.96	120	-6.78	3514	-114.01	3499	106.43
				BK6	IAW, IBW, ICW	1742	101.65	225	45.92	209	-120.32						
	11, 14,19	L78	DG2-678-SLG(A)-Bus7-BK5	BK5	IAX, IBX, ICX	1639	99.68	57	45.51	54	-121.79	118	-8.23	3538	-112.06	3607	106.70
				BK6	IAW, IBW, ICW	1698	100.19	136	45.53	131	-120.82						
SS4	4	L78	DG1-5678-SLG(A)-Bus7-BK5	BK5	IAX, IBX, ICX	1453	101.27	59	45.00	55	-121.01	104	-6.64	3541	-115.18	3559	107.89
				BK6	IAW, IBW, ICW	1467	101.93	140	45.06	132	-120.10						

Bold represents backup protection tests.

Table H.2: Fault states of tripping and non-tripping tests for minimum fault overcurrents of Relay 2

Setting Group	Test Mode	Protection Areas	Tests: Source - Circuit - Type of Fault - Fault Location -Opened Breaker	Breaker	Low Level Test Interface	Primary Currents and Line-to-ground Voltages											
						Fault Currents						Bus 7 - Fault Line-to-ground Voltages					
						IA		*IB*		*IC*		*VA*		*VB*		*VC*	
						Mag. [A]	β_A [°]	Mag. [A]	β_B [°]	Mag. [A]	β_C [°]	Mag. [A]	δ_A [°]	Mag. [A]	δ_B [°]	Mag. [A]	δ_C [°]
SS1	1	L56	**UTILITY-8765/1234-LL(BC)-Bus5-BK6**	BK6	IAW, IBW, ICW	122	-38.12	1564	-168.34	1488	15.28	4090	-1.15	2689	-142.98	2582	138.77
				BK5	IAX, IBX, ICX	215	-37.74	1622	-168.59	1490	17.70						
		L67	UTILITY-8765/1234-LL(BC)-Bus6-BK6	BK6	IAW, IBW, ICW	122	-38.12	1845	-168.79	1767	14.23	4090	-1.15	2478	-149.54	2367	145.56
				BK5	IAX, IBX, ICX	215	-37.74	1897	-169.14	1761	16.13						
SS2	2, 6, 9, 18	L78	DG2-678/65-LL(BC)-Bus8-BK5	BK5	IAX, IBX, ICX	64	136.39	996	4.21	954	-172.92	3867	-2.88	2095	-163.34	2018	156.77
				BK6	IAW, IBW, ICW	153	137.22	1036	3.11	936	-170.12						
	3, 7, 12, 15, 20	L78	DG2-6781-LL(BC)-Bus8-BK5	BK5	IAX, IBX, ICX	157	137.50	1047	3.47	945	-169.67	3798	-3.84	2045	-163.33	2014	155.31
				BK6	IAW, IBW, ICW	249	137.63	1088	2.52	929	-166.59						
	11, 14,19	L78	DG2-678-LL(BC)-Bus8-BK5	BK5	IAX, IBX, ICX	64	136.35	989	3.80	947	-173.34	3882	-2.40	2110	-163.14	2013	157.37
				BK6	IAW, IBW, ICW	153	137.18	1031	2.68	930	-170.57						
SS4	4	L78	DG1-5678-LL(BC)-Bus8-BK5	BK5	IAX, IBX, ICX	65	141.44	915	9.98	874	-166.81	3809	-3.59	2029	-165.08	1991	157.52
				BK6	IAW, IBW, ICW	155	142.26	955	8.74	855	-163.66						

Bold represents backup protection tests.

Table H.3: Fault states of tripping and non-tripping tests for maximum fault overcurrents of Relay 3

Setting Group	Test Mode	Protection Areas	Tests: Source - Circuit - Type of Fault - Fault Location -Opened Breaker	Breaker	Low Level Test Interface	Primary Currents and Line-to-ground Voltages											
						Fault Currents						Bus 6 - Fault Line-to-ground Voltages					
						IA		*IB*		*IC*		*VA*		*VB*		*VC*	
						Mag. [A]	β_A [°]	Mag. [A]	β_B [°]	Mag. [A]	β_C [°]	Mag. [V]	δ_A [°]	Mag. [V]	δ_B [°]	Mag. [V]	δ_C [°]
SS1	1	L56	UTILITY-8765/1234-DLG(BC)-Bus6-BK8	BK8	IAW, IBW, ICW	37	-34.36	2046	162.93	2045	42.40	3832	-4.77	1	-127.04	1	112.43
				BK7	IAX, IBX, ICX	82	-35.31	2101	162.77	2093	43.15						
SS2	2, 6, 9, 18	L56	DG2-678/65-SLG(A)-Bus6-BK8	BK8	IAW, IBW, ICW	2371	-83.30	48	-132.10	46	57.95	0	0.00	3514	-105.24	3473	101.82
				BK7	IAX, IBX, ICX	21	159.83	136	47.64	128	-122.62						
		L67	DG2-678/65-SLG(A)-Bus6-BK7	BK7	IAX, IBX, ICX	2369	97.28	137	48.59	128	-122.03	0	0.00	3514	-105.24	3473	101.82
				BK8	IAW, IBW, ICW	8	0.00	47	-133.23	46	58.82						
		L78	**DG2-678/65-SLG(A)-Bus7-BK7**	BK7	IAX, IBX, ICX	1709	100.34	137	46.11	137	-121.25	2442	-7.56	3614	-111.08	3636	107.20
				BK8	IAW, IBW, ICW	22	-37.44	48	-140.72	48	65.94						
	10, 16	L56	DG2-67/65-SLG(A)-Bus6-BK8	BK8	IAW, IBW, ICW	2330	-84.10	46	-131.87	45	57.54	0	0.00	3517	-104.56	3510	101.88
				BK7	IAX, IBX, ICX	12	0.00	77	48.10	75	-122.14						
		L67	DG2-67/65-SLG(A)-Bus6-BK7	BK7	IAX, IBX, ICX	2327	96.22	78	48.78	74	-121.94	0	0.00	3517	-104.56	3510	101.88
				BK8	IAW, IBW, ICW	8	0.00	46	-132.98	45	58.39						
	8	L34	DG2-6543-SLG(A)-Bus4-BK8	BK8	IAW, IBW, ICW	1989	-81.14	150	-133.32	145	57.88	1398	-11.09	3556	-108.32	3594	104.94
				BK7	IAX, IBX, ICX	0	0.00	0	0.00	0	0.00						
		L56	DG2-6543-SLG(A)-Bus6-BK8	BK8	IAW, IBW, ICW	2355	-83.36	150	-131.87	143	57.32	0	0.00	3515	-104.85	3494	101.86
				BK7	IAX, IBX, ICX	0	0.00	0	0.00	0	0.00						
	17	L56	DG2-65-SLG(A)-Bus6-BK8	BK8	IAW, IBW, ICW	2282	-85.35	45	-131.71	45	57.13	0	0.00	3519	-103.68	3562	101.98
				BK7	IAX, IBX, ICX	0	0.00	0	0.00	0	0.00						
SS3	3, 7, 12, 15, 20	L67	DG2-6781-SLG(A)-Bus6-BK7	BK7	IAX, IBX, ICX	2400	98.17	228	49.26	204	-121.01	0	0.00	3512	-105.72	3451	101.78
				BK8	IAW, IBW, ICW	0	0.00	0	0.00	0	0.00						
		L78	**DG2-6781-SLG(A)-Bus7-BK7**	BK7	IAX, IBX, ICX	1742	101.38	225	46.31	209	-120.72	2488	-6.51	3627	-111.65	3609	107.40
				BK8	IAW, IBW, ICW	0	0.00	0	0.00	0	0.00						
	11, 14, 19	L67	DG2-678-SLG(A)-Bus6-BK7	BK7	IAX, IBX, ICX	2339	96.60	136	47.09	128	-123.25	0	0.00	3515	-104.70	3504	101.88
				BK8	IAW, IBW, ICW	0	0.00	0	0.00	0	0.00						
		L78	**DG2-678-SLG(A)-Bus7-BK7**	BK7	IAX, IBX, ICX	1698	99.92	136	44.59	131	-122.43	2426	-7.99	3615	-110.57	3667	107.27
				BK8	IAW, IBW, ICW	0	0.00	0	0.00	0	0.00						
SS4	13, 21	L67	DG2-67-SLG(A)-Bus6-BK7	BK7	IAX, IBX, ICX	2298	96.42	77	48.54	74	-122.06	0	0.00	3518	-104.03	3541	101.94
				BK8	IAW, IBW, ICW	0	0.00	0	0.00	0	0.00						
SS5	4	L67	DG1-5678-SLG(A)-Bus6-BK7	BK7	IAX, IBX, ICX	1940	99.63	140	47.53	130	-120.92	277	-8.28	3522	-110.14	3526	105.07
				BK8	IAW, IBW, ICW	1950	99.89	196	46.19	186	-121.72						
		L78	**DG1-5678-SLG(A)-Bus7-BK7**	BK7	IAX, IBX, ICX	1503	101.74	140	45.50	132	-120.56	2147	-6.15	3615	-113.68	3624	108.51
				BK8	IAW, IBW, ICW	1523	102.41	197	43.35	189	-118.91						

Bold represents backup protection tests.

Table H.4: Fault states of tripping and non-tripping tests for minimum fault overcurrents of Relay 3

Setting Group	Test Mode	Protection Areas	Tests: Source - Circuit - Type of Fault - Fault Location -Opened Breaker	Breaker	Low Level Test Interface	Primary Currents and Line-to-ground Voltages											
						Fault Currents						Bus 6 - Fault Line-to-ground Voltages					
						IA		*IB*		*IC*		*VA*		*VB*		*VC*	
						Mag. [A]	β_A [°]	Mag. [A]	β_B [°]	Mag. [A]	β_C [°]	Mag. [V]	δ_A [°]	Mag. [V]	δ_B [°]	Mag. [V]	δ_C [°]
SS1	1	L56	UTILITY-8765/1234-LL(BC)-Bus5-BK8	BK8	IAW, IBW, ICW	56	-37.48	1539	-167.69	1504	13.95	3783	-5.05	1981	-169.42	1970	159.05
				BK7	IAX, IBX, ICX	122	-38.12	1564	-168.34	1488	15.28						
SS2	2, 6, 9, 18	L56	DG2-678/65-LL(BC)-Bus5-BK8	BK8	IAW, IBW, ICW	53	-37.34	1392	-172.50	1354	9.11	3922	-1.84	2097	-168.76	1937	163.96
				BK7	IAX, IBX, ICX	152	142.34	75	-24.54	81	-49.81						
		L67	DG2-678/65-LL(BC)-Bus7-BK7	BK7	IAX, IBX, ICX	153	142.31	1265	6.95	1161	-167.73	3935	-1.86	2229	-158.91	2074	153.35
				BK8	IAW, IBW, ICW	54	-37.36	29	167.11	30	118.38						
		L78	**DG2-678/65-LL(BC)-Bus8-BK7**	BK7	IAX, IBX, ICX	153	142.26	1036	8.15	936	-165.07	3955	-1.89	2509	-147.73	2348	141.24
				BK8	IAW, IBW, ICW	54	-37.40	33	178.05	33	106.49						
	10, 16	L56	DG2-67/65-LL(BC)-Bus5-BK8	BK8	IAW, IBW, ICW	53	-37.39	1369	-173.36	1332	8.22	3949	-1.41	2118	-168.72	1940	164.72
				BK7	IAX, IBX, ICX	87	142.86	44	-24.36	45	-49.74						
		L67	DG2-67/65-LL(BC)-Bus7-BK7	BK7	IAX, IBX, ICX	88	142.84	1221	6.93	1159	-170.04	3961	-1.42	2254	-159.25	2060	154.17
				BK8	IAW, IBW, ICW	53	-37.42	29	165.58	28	118.91						
	8	L34	DG2-6543-LL(BC)-Bus3-BK8	BK8	IAW, IBW, ICW	169	-37.84	1275	-172.98	1162	12.93	3950	-1.62	2267	-159.82	2028	153.85
				BK7	IAX, IBX, ICX	0	0.00	0	0.00	0	0.00						
		L56	DG2-6543-LL(BC)-Bus5-BK8	BK8	IAW, IBW, ICW	168	-37.80	1427	-174.27	1310	10.83	3937	-1.59	2107	-168.63	1942	164.33
				BK7	IAX, IBX, ICX	0	0.00	0	0.00	0	0.00						
	17	L56	DG2-65-LL(BC)-Bus5-BK8	BK8	IAW, IBW, ICW	52	-37.48	1342	-174.69	1305	6.87	3986	-0.83	2146	-168.66	1942	165.69
				BK7	IAX, IBX, ICX	0	0.00	0	0.00	0	0.00						
SS3	3, 7, 12, 15, 20	L67	DG2-6781-LL(BC)-Bus7-BK7	BK7	IAX, IBX, ICX	248	142.58	1318	6.51	1152	-164.91	3919	-2.16	2210	-158.54	2090	152.78
				BK8	IAW, IBW, ICW	0	0.00	0	0.00	0	0.00						
		L78	**DG2-6781-LL(BC)-Bus8-BK7**	BK7	IAX, IBX, ICX	249	142.53	1088	7.55	929	-161.52	3938	-2.18	2491	-146.89	2387	140.73
				BK8	IAW, IBW, ICW	0	0.00	0	0.00	0	0.00						
	11, 14, 19	L67	DG2-678-LL(BC)-Bus7-BK7	BK7	IAX, IBX, ICX	152	142.27	1253	6.35	1149	-168.35	4060	0.02	2309	-157.59	2116	155.46
				BK8	IAW, IBW, ICW	0	0.00	0	0.00	0	0.00						
		L78	**DG2-678-LL(BC)-Bus8-BK7**	BK7	IAX, IBX, ICX	153	142.23	1031	7.73	930	-165.52	4080	0.00	2597	-146.56	2390	143.20
				BK8	IAW, IBW, ICW	0	0.00	0	0.00	0	0.00						
SS4	13, 21	L67	DG2-67-LL(BC)-Bus7-BK7	BK7	IAX, IBX, ICX	87	142.79	1210	6.28	1148	-170.71	4057	-0.02	2316	-158.36	2088	155.80
				BK8	IAW, IBW, ICW	0	0.00	0	0.00	0	0.00						
SS5	4	L67	DG1-5678-LL(BC)-Bus7-BK7	BK7	IAX, IBX, ICX	155	141.24	1145	6.89	1042	-167.00	3881	-2.54	2138	-160.99	2049	154.90
				BK8	IAW, IBW, ICW	219	140.99	1176	6.24	1033	-165.07						
		L78	**DG1-5678-LL(BC)-Bus8-BK7**	BK7	IAX, IBX, ICX	155	141.21	955	7.68	855	-164.72	3897	-2.56	2385	-149.69	2294	143.08
				BK8	IAW, IBW, ICW	220	140.95	992	7.19	855	-162.07						

Bold represents backup protection tests.

Appendix I - Secondary currents and line-to-ground voltages of pre-fault states

Table I.1: Pre-fault states of tripping and non-tripping tests for maximum and minimum fault overcurrents of Relay 2

Setting Group	Test Mode	Protection Areas	Tests: Source - Circuit - Type of Fault - Fault Location -Opened Breaker	Breaker	Low Level Test Interface	Secondary Currents and Line-to-ground Voltages (*CTR* = 200, *PTR* = 60)											
						Pre-fault Currents						Bus 7 - Pre-fault Line-to-ground Voltages					
						IAs		*IBs*		*ICs*		*VAs*		*VBs*		*VCs*	
						Mag. [A]	β_A [°]	Mag. [A]	β_B [°]	Mag. [A]	β_C [°]	Mag. [V]	δ_A [°]	Mag. [V]	δ_B [°]	Mag. [V]	δ_C [°]
SS1	1	L56	**[1]UTILITY-8765/1234-DLG(BC)-Bus6-BK6**	BK6	IAW, IBW, ICW	0.61	-39.74	0.61	-159.74	0.61	80.26	64.17	-4.20	64.17	-124.20	64.17	115.80
			[2]UTILITY-8765/1234-LL(BC)-Bus5-BK6	BK5	IAX, IBX, ICX	1.08	-36.47	1.08	-156.47	1.08	83.53						
		L67	[1]UTILITY-8765/1234-DLG(BC)-Bus7-BK6	BK6	IAW, IBW, ICW	0.61	-39.74	0.61	-159.74	0.61	80.26	64.17	-4.20	64.17	-124.20	64.17	115.80
			[2]UTILITY-8765/1234-LL(BC)-Bus6-BK6	BK5	IAX, IBX, ICX	1.08	-36.47	1.08	-156.47	1.08	83.53						
SS2	2, 6, 9, 18	L78	[1]DG2-678/65-SLG(A)-Bus7-BK5	BK5	IAX, IBX, ICX	0.33	-39.79	0.33	-159.79	0.33	80.21	65.67	-2.92	65.67	-122.92	65.67	117.08
			[2]DG2-678/65-LL(BC)-Bus8-BK5	BK6	IAW, IBW, ICW	0.78	-35.62	0.78	204.38	0.78	84.38						
	3, 7, 12, 15, 20	L78	[1]DG2-6781-SLG(A)-Bus7-BK5	BK5	IAX, IBX, ICX	0.80	-37.60	0.80	-157.60	0.80	82.40	64.50	-3.91	64.50	-123.91	64.50	116.09
			[2]DG2-6781-LL(BC)-Bus8-BK5	BK6	IAW, IBW, ICW	1.27	-37.79	1.27	-157.79	1.27	82.21						
	11, 14,19	L78	[1]DG2-678-SLG(A)-Bus7-BK5	BK5	IAX, IBX, ICX	0.32	-39.37	0.32	-159.37	0.32	80.63	66.17	-2.50	66.17	-122.50	66.17	117.50
			[2]DG2-678-LL(BC)-Bus8-BK5	BK6	IAW, IBW, ICW	0.78	-35.22	0.78	-155.22	0.78	84.78						
SS4	4	L78	[1]DG1-5678-SLG(A)-Bus7-BK5	BK5	IAX, IBX, ICX	0.33	-40.49	0.33	-160.49	0.33	79.51	64.50	-3.62	64.50	-123.62	64.50	116.38
			[2]DG1-5678-LL(BC)-Bus8-BK5	BK6	IAW, IBW, ICW	0.79	-36.28	0.79	-156.28	0.79	83.72						

[1] Maximum fault overcurrent tests, [2]Minimum fault overcurrent tests. Bold represents backup protection tests. *CTR* = current transformer ratio, *PTR* = potential transformer ratio.

Table I.2: Pre-fault states of tripping and non-tripping tests for maximum and minimum fault overcurrents of Relay 3

Setting Group	Test Mode	Protection Areas	Tests: Source - Circuit - Type of Fault - Fault Location -Opened Breaker	Breaker	Low Level Test Interface	Secondary Currents and Line-to-ground Voltages (*CTR* = 200, *PTR* = 60)											
						Pre-fault Currents						Bus 6 - Pre-fault Line-to-ground Voltages					
						IAs		*IBs*		*ICs*		*VAs*		*VBs*		*VCs*	
						Mag. [A]	β_A [°]	Mag. [A]	β_B [°]	Mag. [A]	β_C [°]	Mag. [V]	δ_A [°]	Mag. [V]	δ_B [°]	Mag. [V]	δ_C [°]
SS1	1	L56	[1]UTILITY-8765/1234-DLG(BC)-Bus6-BK8	BK8	IAW, IBW, ICW	0.28	-38.74	0.28	-158.74	0.28	81.26	64.50	-5.05	64.50	-125.05	64.50	114.95
			[2]UTILITY-8765/1234-LL(BC)-Bus5-BK8	BK7	IAX, IBX, ICX	0.61	-39.74	0.61	-159.74	0.61	80.26						
SS2	2, 6, 9, 18	L56	[1]DG2-678/65-SLG(A)-Bus6-BK8	BK8	IAW, IBW, ICW	0.27	-35.62	0.27	-155.62	0.27	84.38	67.17	-1.93	67.17	-121.93	67.17	118.07
			[2]DG2-678/65-LL(BC)-Bus5-BK8	BK7	IAX, IBX, ICX	0.78	-35.62	0.78	-155.62	0.78	84.38						
		L67	[1]DG2-678/65-SLG(A)-Bus6-BK7	BK7	IAX, IBX, ICX	0.78	-35.62	0.78	-155.62	0.78	84.38	67.17	-1.93	67.17	-121.93	67.17	118.07
			[2]DG2-678/65-LL(BC)-Bus7-BK7	BK8	IAW, IBW, ICW	0.27	-35.62	0.27	-155.62	0.27	84.38						
		L78	**[1]DG2-678/65-SLG(A)-Bus7-BK7**	BK7	IAX, IBX, ICX	0.78	-35.62	0.78	-155.62	0.78	84.38	67.17	-1.93	67.17	-121.93	67.17	118.07
			[2]DG2-678/65-LL(BC)-Bus8-BK7	BK8	IAW, IBW, ICW	0.27	-35.62	0.27	-155.62	0.27	84.38						
	10, 16	L56	[1]DG2-67/65-SLG(A)-Bus6-BK8	BK8	IAW, IBW, ICW	0.27	-35.14	0.27	-155.14	0.27	84.86	67.67	-1.45	67.67	-121.45	67.67	118.55
			[2]DG2-67/65-LL(BC)-Bus5-BK8	BK7	IAX, IBX, ICX	0.45	-40.11	0.45	-160.11	0.45	79.89						
		L67	[1]DG2-67/65-SLG(A)-Bus6-BK7	BK7	IAX, IBX, ICX	0.45	-40.11	0.45	-160.11	0.45	79.89	67.67	-1.45	67.67	-121.45	67.67	118.55
			[2]DG2-67/65-LL(BC)-Bus7-BK7	BK8	IAW, IBW, ICW	0.27	-35.14	0.27	-155.14	0.27	84.86						
	8	L34	[1]DG2-6543-SLG(A)-Bus4-BK8	BK8	IAW, IBW, ICW	0.87	-36.64	0.87	-156.64	0.87	83.36	67.50	-1.65	67.50	-121.65	67.50	118.35
			[2]DG2-6543-LL(BC)-Bus3-BK8	BK7	IAX, IBX, ICX	0.00	0.00	0.00	0.00	0.00	0.00						
		L56	[1]DG2-6543-SLG(A)-Bus6-BK8	BK8	IAW, IBW, ICW	0.87	-36.64	0.87	-156.64	0.87	83.36	67.50	-1.65	67.50	-121.65	67.50	118.35
			[2]DG2-6543-LL(BC)-Bus5-BK8	BK7	IAX, IBX, ICX	0.00	0.00	0.00	0.00	0.00	0.00						
	17	L56	[1]DG2-65-SLG(A)-Bus6-BK8	BK8	IAW, IBW, ICW	0.27	-34.49	0.27	-154.49	0.27	85.51	68.33	-0.80	68.33	-120.80	68.33	119.20
			[2]DG2-65-LL(BC)-Bus5-BK8	BK7	IAX, IBX, ICX	0.00	0.00	0.00	0.00	0.00	0.00						
SS3	3, 7, 12, 15, 20	L67	[1]DG2-6781-SLG(A)-Bus6-BK7	BK7	IAX, IBX, ICX	1.27	-37.79	1.27	-157.79	1.27	82.21	66.83	-2.25	66.83	-122.25	66.83	117.75
			[2]DG2-6781-LL(BC)-Bus7-BK7	BK8	IAW, IBW, ICW	0.00	0.00	0.00	0.00	0.00	0.00						
		L78	**[1]DG2-6781-SLG(A)-Bus7-BK7**	BK7	IAX, IBX, ICX	1.27	-37.79	1.27	-157.79	1.27	82.21	66.83	-2.25	66.83	-122.25	66.83	117.75
			[2]DG2-6781-LL(BC)-Bus8-BK7	BK8	IAW, IBW, ICW	0.00	0.00	0.00	0.00	0.00	0.00						
	11, 14, 19	L67	[1]DG2-678-SLG(A)-Bus6-BK7	BK7	IAX, IBX, ICX	0.78	-35.22	0.78	-155.22	0.78	84.78	67.50	-1.53	67.50	-121.53	67.50	118.47
			[2]DG2-678-LL(BC)-Bus7-BK7	BK8	IAW, IBW, ICW	0.00	0.00	0.00	0.00	0.00	0.00						
		L78	**[1]DG2-678-SLG(A)-Bus7-BK7**	BK7	IAX, IBX, ICX	0.78	-35.22	0.78	-155.22	0.78	84.78	67.50	-1.53	67.50	-121.53	67.50	118.47
			[2]DG2-678-LL(BC)-Bus8-BK7	BK8	IAW, IBW, ICW	0.00	0.00	0.00	0.00	0.00	0.00						
SS4	13, 21	L67	[1]DG2-67-SLG(A)-Bus6-BK7	BK7	IAX, IBX, ICX	0.45	-39.72	0.45	-159.72	0.45	80.28	68.17	-1.06	68.17	-121.06	68.17	118.94
			[2]DG2-67-LL(BC)-Bus7-BK7	BK8	IAW, IBW, ICW	0.00	0.00	0.00	0.00	0.00	0.00						
SS5	4	L67	[1]DG1-5678-SLG(A)-Bus6-BK7	BK7	IAX, IBX, ICX	0.79	-36.28	0.79	-156.28	0.79	83.72	66.00	-2.59	66.00	-122.59	66.00	117.41
			[2]DG1-5678-LL(BC)-Bus7-BK7	BK8	IAW, IBW, ICW	1.12	-36.65	1.12	-156.65	1.12	83.35						
		L78	**[1]DG1-5678-SLG(A)-Bus7-BK7**	BK7	IAX, IBX, ICX	0.79	-36.28	0.79	-156.28	0.79	83.72	66.00	-2.59	66.00	-122.59	66.00	117.41
			[2]DG1-5678-LL(BC)-Bus8-BK7	BK8	IAW, IBW, ICW	1.12	-36.65	1.12	-156.65	1.12	83.35						

[1] Maximum fault overcurrent tests, [2]Minimum fault overcurrent tests. Bold represents backup protection tests. *CTR* = current transformer ratio, *PTR* = potential transformer ratio.

Appendix J - Secondary currents and line-to-ground voltages of post-fault states

Table J.1: Post-fault states of tripping and non-tripping tests for maximum and minimum fault overcurrents of Relay 2

Setting Group	Test Mode	Protection Areas	Tests: Source - Circuit - Type of Fault - Fault Location -Opened Breaker	Breaker	Low Level Test Interface	Secondary Currents and Line-to-ground Voltages (*CTR* = 200, *PTR* = 60)											
						Post-fault Currents						Bus 7 - Post-fault Line-to-ground Voltages					
						IAs		*IBs*		*ICs*		*VAs*		*VBs*		*VCs*	
						Mag. [A]	β_A [°]	Mag. [A]	β_B [°]	Mag. [A]	β_C [°]	Mag. [V]	δ_A [°]	Mag. [V]	δ_B [°]	Mag. [V]	δ_C [°]
SS1	1	L56	**[1]UTILITY-8765/1234-DLG(BC)-Bus6-BK6** **[2]UTILITY-8765/1234-LL(BC)-Bus5-BK6**	BK6	IAW, IBW, ICW	0.00	0.00	0.00	0.00	0.00	0.00	66.00	-2.71	66.00	-122.71	66.00	117.29
				BK5	IAX, IBX, ICX	0.46	-41.37	0.46	-161.37	0.46	78.63						
		L67	[1]UTILITY-8765/1234-DLG(BC)-Bus7-BK6 [2]UTILITY-8765/1234-LL(BC)-Bus6-BK6	BK6	IAW, IBW, ICW	0.00	0.00	0.00	0.00	0.00	0.00	66.00	-2.71	66.00	-122.71	66.00	117.29
				BK5	IAX, IBX, ICX	0.46	-41.37	0.46	-161.37	0.46	78.63						
SS2	2, 6, 9, 18	L78	[1]DG2-678/65-SLG(A)-Bus7-BK5 [2]DG2-678/65-LL(BC)-Bus8-BK5	BK5	IAX, IBX, ICX	0.00	0.00	0.00	0.00	0.00	0.00	66.83	-2.01	66.83	-122.01	66.83	117.99
				BK6	IAW, IBW, ICW	0.45	-40.67	0.45	-160.67	0.45	79.33						
	3, 7, 12, 15, 20	L78	[1]DG2-6781-SLG(A)-Bus7-BK5 [2]DG2-6781-LL(BC)-Bus8-BK5	BK5	IAX, IBX, ICX	0.00	0.00	0.00	0.00	0.00	0.00	67.33	-1.61	67.33	-121.61	67.33	118.39
				BK6	IAW, IBW, ICW	0.45	-40.27	0.45	-160.27	0.45	79.73						
	11, 14,19	L78	[1]DG2-678-SLG(A)-Bus7-BK5 [2]DG2-678-LL(BC)-Bus8-BK5	BK5	IAX, IBX, ICX	0.00	0.00	0.00	0.00	0.00	0.00	67.33	-1.61	67.33	-121.61	67.33	118.39
				BK6	IAW, IBW, ICW	0.45	-40.27	0.45	-160.27	0.45	79.73						
SS4	4	L78	[1]DG1-5678-SLG(A)-Bus7-BK5 [2]DG1-5678-LL(BC)-Bus8-BK5	BK5	IAX, IBX, ICX	0.00	0.00	0.00	0.00	0.00	0.00	66.00	-2.47	66.00	-122.47	66.00	117.53
				BK6	IAW, IBW, ICW	0.45	-41.13	0.45	-161.13	0.45	78.87						

[1] Maximum fault overcurrent tests, [2]Minimum fault overcurrent tests. Bold represents backup protection tests. *CTR* = current transformer ratio, *PTR* = potential transformer ratio.

Table J.2: Post-fault states of tripping and non-tripping tests for maximum and minimum fault overcurrents of Relay 3

Setting Group	Test Mode	Protection Areas	Tests: Source - Circuit - Type of Fault - Fault Location -Opened Breaker	Breaker	Low Level Test Interface	Secondary Currents and Line-to-ground Voltages (*CTR* = 200, *PTR* = 60): Post-fault Currents *IAs* Mag. [A]	*IAs* β_A [°]	*IBs* Mag. [A]	*IBs* β_B [°]	*ICs* Mag. [A]	*ICs* β_C [°]	Bus 6 - Post-fault Line-to-ground Voltages: *VAs* Mag. [V]	*VAs* δ_A [°]	*VBs* Mag. [V]	*VBs* δ_B [°]	*VCs* Mag. [V]	*VCs* δ_C [°]
SS1	1	L56	[1]UTILITY-8765/1234-DLG(BC)-Bus6-BK8	BK8	IAW, IBW, ICW	0.00	0.00	0.00	0.00	0.00	0.00	64.33	-3.92	64.33	-123.92	64.33	116.08
			[2]UTILITY-8765/1234-LL(BC)-Bus5-BK8	BK7	IAX, IBX, ICX	0.33	-48.92	0.33	-168.92	0.33	71.08						
SS2	2, 6, 9, 18	L56	[1]DG2-678/65-SLG(A)-Bus6-BK8	BK8	IAW, IBW, ICW	0.00	0.00	0.00	0.00	0.00	0.00	67.50	-1.48	67.50	-121.48	67.50	118.52
			[2]DG2-678/65-LL(BC)-Bus5-BK8	BK7	IAX, IBX, ICX	0.79	-39.35	0.79	-159.35	0.79	80.65						
		L67	[1]DG2-678/65-SLG(A)-Bus6-BK7	BK7	IAX, IBX, ICX	0.00	0.00	0.00	0.00	0.00	0.00	68.33	-0.81	68.33	-120.81	68.33	119.19
			[2]DG2-678/65-LL(BC)-Bus7-BK7	BK8	IAW, IBW, ICW	0.27	-34.50	0.27	-154.50	0.27	85.50						
		L78	**[1]DG2-678/65-SLG(A)-Bus7-BK7**	BK7	IAX, IBX, ICX	0.00	0.00	0.00	0.00	0.00	0.00	68.33	-0.81	68.33	-120.81	68.33	119.19
			[2]DG2-678/65-LL(BC)-Bus8-BK7	BK8	IAW, IBW, ICW	0.27	-34.50	0.27	-154.50	0.27	85.50						
	10, 16	L56	[1]DG2-67/65-SLG(A)-Bus6-BK8	BK8	IAW, IBW, ICW	0.00	0.00	0.00	0.00	0.00	0.00	69.33	0.00	69.33	-120.00	69.33	120.00
			[2]DG2-67/65-LL(BC)-Bus5-BK8	BK7	IAX, IBX, ICX	0.44	-38.66	0.44	-158.66	0.44	81.34						
		L67	[1]DG2-67/65-SLG(A)-Bus6-BK7	BK7	IAX, IBX, ICX	0.00	0.00	0.00	0.00	0.00	0.00	68.33	-0.81	68.33	-120.81	68.33	119.19
			[2]DG2-67/65-LL(BC)-Bus7-BK7	BK8	IAW, IBW, ICW	0.27	-34.50	0.27	-154.50	0.27	85.50						
	8	L34	[1]DG2-6543-SLG(A)-Bus4-BK8	BK8	IAW, IBW, ICW	0.00	0.00	0.00	0.00	0.00	0.00	67.50	-1.65	67.50	-121.65	67.50	118.35
			[2]DG2-6543-LL(BC)-Bus3-BK8	BK7	IAX, IBX, ICX	0.00	0.00	0.00	0.00	0.00	0.00						
		L56	[1]DG2-6543-SLG(A)-Bus6-BK8	BK8	IAW, IBW, ICW	0.00	0.00	0.00	0.00	0.00	0.00	67.50	-1.65	67.50	-121.65	67.50	118.35
			[2]DG2-6543-LL(BC)-Bus5-BK8	BK7	IAX, IBX, ICX	0.00	0.00	0.00	0.00	0.00	0.00						
	17	L56	[1]DG2-65-SLG(A)-Bus6-BK8	BK8	IAW, IBW, ICW	0.00	0.00	0.00	0.00	0.00	0.00	67.50	-1.65	67.50	-121.65	67.50	118.35
			[2]DG2-65-LL(BC)-Bus5-BK8	BK7	IAX, IBX, ICX	0.00	0.00	0.00	0.00	0.00	0.00						
SS3	3, 7, 12, 15, 20	L67	[1]DG2-6781-SLG(A)-Bus6-BK7	BK7	IAX, IBX, ICX	0.00	0.00	0.00	0.00	0.00	0.00	68.83	-0.42	68.83	-120.42	68.83	119.58
			[2]DG2-6781-LL(BC)-Bus7-BK7	BK8	IAW, IBW, ICW	0.00	0.00	0.00	0.00	0.00	0.00						
		L78	**[1]DG2-6781-SLG(A)-Bus7-BK7**	BK7	IAX, IBX, ICX	0.00	0.00	0.00	0.00	0.00	0.00	68.83	-0.42	68.83	-120.42	68.83	119.58
			[2]DG2-6781-LL(BC)-Bus8-BK7	BK8	IAW, IBW, ICW	0.00	0.00	0.00	0.00	0.00	0.00						
	11, 14, 19	L67	[1]DG2-678-SLG(A)-Bus6-BK7	BK7	IAX, IBX, ICX	0.00	0.00	0.00	0.00	0.00	0.00	68.83	-0.42	68.83	-120.42	68.83	119.58
			[2]DG2-678-LL(BC)-Bus7-BK7	BK8	IAW, IBW, ICW	0.00	0.00	0.00	0.00	0.00	0.00						
		L78	**[1]DG2-678-SLG(A)-Bus7-BK7**	BK7	IAX, IBX, ICX	0.00	0.00	0.00	0.00	0.00	0.00	68.83	-0.42	68.83	-120.42	68.83	119.58
			[2]DG2-678-LL(BC)-Bus8-BK7	BK8	IAW, IBW, ICW	0.00	0.00	0.00	0.00	0.00	0.00						
SS4	13, 21	L67	[1]DG2-67-SLG(A)-Bus6-BK7	BK7	IAX, IBX, ICX	0.00	0.00	0.00	0.00	0.00	0.00	68.83	-0.42	68.83	-120.42	68.83	119.58
			[2]DG2-67-LL(BC)-Bus7-BK7	BK8	IAW, IBW, ICW	0.00	0.00	0.00	0.00	0.00	0.00						
SS5	4	L67	[1]DG1-5678-SLG(A)-Bus6-BK7	BK7	IAX, IBX, ICX	0.00	0.00	0.00	0.00	0.00	0.00	68.17	-0.96	68.17	-120.96	68.17	119.04
			[2]DG1-5678-LL(BC)-Bus7-BK7	BK8	IAW, IBW, ICW	0.32	-37.83	0.32	-157.83	0.32	82.17						
		L78	**[1]DG1-5678-SLG(A)-Bus7-BK7**	BK7	IAX, IBX, ICX	0.00	0.00	0.00	0.00	0.00	0.00	68.17	-0.96	68.17	-120.96	68.17	119.04
			[2]DG1-5678-LL(BC)-Bus8-BK7	BK8	IAW, IBW, ICW	0.32	-37.83	0.32	-157.83	0.32	82.17						

[1] Maximum fault overcurrent tests, [2]Minimum fault overcurrent tests. Bold represents backup protection tests. *CTR* = current transformer ratio, *PTR* = potential transformer ratio.

Appendix K - Secondary currents and line-to-ground voltages of fault states

Table K.1: Fault states of tripping and non-tripping tests for maximum fault overcurrents of Relay 2

Setting Group	Test Mode	Protection Areas	Tests: Source - Circuit - Type of Fault - Fault Location -Opened Breaker	Breaker	Low Level Test Interface	Secondary Currents and Line-to-ground Voltages (*CTR* = 200, *PTR* = 60)											
						Fault Currents						Bus 7 - Fault Line-to-ground Voltages					
						IAs		*IBs*		*ICs*		*VAs*		*VBs*		*VCs*	
						Mag. [A]	β_A [°]	Mag. [A]	β_B [°]	Mag. [A]	β_C [°]	Mag. [V]	δ_A [°]	Mag. [V]	δ_B [°]	Mag. [V]	δ_C [°]
SS1	1	L56	**UTILITY-8765/1234-DLG(BC)-Bus6-BK6**	BK6	IAW, IBW, ICW	0.41	-35.26	10.50	162.69	10.38	43.06	64.83	-3.81	24.76	-124.25	25.20	115.20
				BK5	IAX, IBX, ICX	0.78	-35.63	10.72	163.18	10.50	44.30						
		L67	UTILITY-8765/1234-DLG(BC)-Bus7-BK6	BK6	IAW, IBW, ICW	0.41	-34.30	15.85	161.98	15.81	42.05	64.83	-3.82	3.74	-124.96	3.84	114.19
				BK5	IAX, IBX, ICX	0.73	-35.12	15.99	161.89	15.79	42.70						
SS2	2, 6, 9, 18	L78	DG2-678/65-SLG(A)-Bus7-BK5	BK5	IAX, IBX, ICX	8.25	100.07	0.29	45.56	0.27	-121.69	1.96	-7.85	58.96	-112.60	59.60	106.63
				BK6	IAW, IBW, ICW	8.11	100.59	0.68	45.58	0.65	-120.73						
	3, 7, 12, 15, 20	L78	DG2-6781-SLG(A)-Bus7-BK5	BK5	IAX, IBX, ICX	8.41	101.12	0.72	46.85	0.66	119.96	2.00	-6.78	58.57	-114.01	58.32	106.43
				BK6	IAW, IBW, ICW	8.47	101.65	1.13	45.92	1.05	-120.32						
	11, 14,19	L78	DG2-678-SLG(A)-Bus7-BK5	BK5	IAX, IBX, ICX	8.20	99.68	0.28	45.51	0.27	-121.79	1.96	-8.23	58.97	-112.06	60.11	106.70
				BK6	IAW, IBW, ICW	8.26	100.19	0.68	45.53	0.65	-120.82						
SS4	4	L78	DG1-5678-SLG(A)-Bus7-BK5	BK5	IAX, IBX, ICX	7.27	101.27	0.29	45.00	0.27	-121.01	1.73	-6.64	59.02	-115.18	59.31	107.89
				BK6	IAW, IBW, ICW	7.33	101.93	0.70	45.06	0.66	-120.10						

Bold represents backup protection tests. *CTR* = current transformer ratio, *PTR* = potential transformer ratio.

Table K.2: Fault states of tripping and non-tripping tests for minimum fault overcurrents of Relay 2

Setting Group	**Test Mode**	**Protection Areas**	**Tests**	**Breaker**	**Low Level Test Interface**	**Secondary Currents and Line-to-ground Voltages (*CTR* = 200, *PTR* = 60)**											
						Fault Currents						**Bus 7 - Fault Line-to-ground Voltages**					
			Source - Circuit - Type of Fault - Fault Location -Opened Breaker			***IAs***		***IBs***		***ICs***		***VAs***		***VBs***		***VCs***	
						Mag. [A]	**β_A [°]**	**Mag. [A]**	**β_B [°]**	**Mag. [A]**	**β_C [°]**	**Mag. [A]**	**δ_A [°]**	**Mag. [A]**	**δ_B [°]**	**Mag. [A]**	**δ_C [°]**
SS1	1	L56	**UTILITY-8765/1234-LL(BC)-Bus5-BK6**	BK6	IAW, IBW, ICW	0.61	-38.12	7.82	-168.34	7.44	15.28	68.17	-1.15	44.82	-142.98	43.03	138.77
				BK5	IAX, IBX, ICX	1.08	-37.74	8.11	-168.59	7.45	17.70						
		L67	UTILITY-8765/1234-LL(BC)-Bus6-BK6	BK6	IAW, IBW, ICW	0.61	-38.12	9.22	-168.79	8.84	14.23	68.17	-1.15	41.31	-149.54	39.46	145.56
				BK5	IAX, IBX, ICX	1.08	-37.74	9.48	-169.14	8.81	16.13						
SS2	2, 6, 9, 18	L78	DG2-678/65-LL(BC)-Bus8-BK5	BK5	IAX, IBX, ICX	0.32	136.39	4.98	4.21	4.77	-172.92	64.45	-2.88	34.92	-163.34	33.63	156.77
				BK6	IAW, IBW, ICW	0.77	137.22	5.18	3.11	4.68	-170.12						
	3, 7, 12, 15, 20	L78	DG2-6781-LL(BC)-Bus8-BK5	BK5	IAX, IBX, ICX	0.79	137.50	5.23	3.47	4.72	-169.67	63.30	-3.84	34.08	-163.33	33.57	155.31
				BK6	IAW, IBW, ICW	1.24	137.63	5.44	2.52	4.65	-166.59						
	11, 14,19	L78	DG2-678-LL(BC)-Bus8-BK5	BK5	IAX, IBX, ICX	0.32	136.35	4.95	3.80	4.74	-173.34	64.70	-2.40	35.17	-163.14	33.56	157.37
				BK6	IAW, IBW, ICW	0.76	137.18	5.15	2.68	4.65	-170.57						
SS4	4	L78	DG1-5678-LL(BC)-Bus8-BK5	BK5	IAX, IBX, ICX	0.32	141.44	4.58	9.98	4.37	-166.81	63.48	-3.59	33.82	-165.08	33.19	157.52
				BK6	IAW, IBW, ICW	0.78	142.26	4.77	8.74	4.27	-163.66						

Bold represents backup protection tests. *CTR* = current transformer ratio, *PTR* = potential transformer ratio.

Table K.3: Fault states of tripping and non-tripping tests for maximum fault overcurrents of Relay 3

Setting Group	Test Mode	Protection Areas	Tests: Source - Circuit - Type of Fault - Fault Location -Opened Breaker	Breaker	Low Level Test Interface	Secondary Currents and Line-to-ground Voltages (*CTR* = 200, *PTR* = 60)											
						Fault Currents						Bus 6 - Fault Line-to-ground Voltages					
						IAs		*IBs*		*ICs*		*VAs*		*VBs*		*VCs*	
						Mag. [A]	β_A [°]	Mag. [A]	β_B [°]	Mag. [A]	β_C [°]	Mag. [V]	δ_A [°]	Mag. [V]	δ_B [°]	Mag. [V]	δ_C [°]
SS1	1	L56	UTILITY-8765/1234-DLG(BC)-Bus6-BK8	BK8	IAW, IBW, ICW	0.19	-34.36	10.23	162.93	10.22	42.40	63.86	-4.77	0.02	-127.04	0.02	112.43
				BK7	IAX, IBX, ICX	0.41	-35.31	10.31	162.77	10.47	43.15						
SS2	2, 6, 9, 18	L56	DG2-678/65-SLG(A)-Bus6-BK8	BK8	IAW, IBW, ICW	11.85	-83.30	0.24	-132.10	0.23	57.95	0.00	0.00	58.57	-105.24	57.88	101.82
				BK7	IAX, IBX, ICX	0.11	159.83	0.68	47.64	0.64	-122.62						
		L67	DG2-678/65-SLG(A)-Bus6-BK7	BK7	IAX, IBX, ICX	11.85	97.28	0.69	48.59	0.64	-122.03	0.00	0.00	58.57	-105.24	57.88	101.82
				BK8	IAW, IBW, ICW	0.04	0.00	0.24	-133.23	0.23	58.82						
		L78	**DG2-678/65-SLG(A)-Bus7-BK7**	BK7	IAX, IBX, ICX	8.55	100.34	0.68	46.11	0.65	-121.25	20.35	-7.56	60.23	-111.08	60.60	107.20
				BK8	IAW, IBW, ICW	0.11	-37.44	0.24	-140.72	0.24	65.94						
	10, 16	L56	DG2-67/65-SLG(A)-Bus6-BK8	BK8	IAW, IBW, ICW	11.65	-84.10	0.23	-131.87	0.23	57.54	0.00	0.00	58.61	-104.56	58.50	101.88
				BK7	IAX, IBX, ICX	0.06	0.00	0.39	48.10	0.37	-122.14						
		L67	DG2-67/65-SLG(A)-Bus6-BK7	BK7	IAX, IBX, ICX	11.64	96.22	0.39	48.78	0.37	-121.94	0.00	0.00	58.61	-104.56	58.50	101.88
				BK8	IAW, IBW, ICW	0.04	0.00	0.23	-132.98	0.23	58.39						
	8	L34	DG2-6543-SLG(A)-Bus4-BK8	BK8	IAW, IBW, ICW	9.94	-81.14	0.75	-133.32	0.72	57.88	11.65	-11.09	59.27	-108.32	59.90	104.94
				BK7	IAX, IBX, ICX	0.00	0.00	0.00	0.00	0.00	0.00						
		L56	DG2-6543-SLG(A)-Bus6-BK8	BK8	IAW, IBW, ICW	11.78	-83.36	0.75	-131.87	0.72	57.32	0.00	0.00	58.58	-104.85	58.23	101.86
				BK7	IAX, IBX, ICX	0.00	0.00	0.00	0.00	0.00	0.00						
	17	L56	DG2-65-SLG(A)-Bus6-BK8	BK8	IAW, IBW, ICW	11.41	-85.35	0.23	-131.71	0.22	57.13	0.00	0.00	58.65	-103.68	59.37	101.98
				BK7	IAX, IBX, ICX	0.00	0.00	0.00	0.00	0.00	0.00						
SS3	3, 7, 12, 15, 20	L67	DG2-6781-SLG(A)-Bus6-BK7	BK7	IAX, IBX, ICX	12.00	98.17	1.14	49.26	1.02	-121.01	0.00	0.00	58.54	-105.72	57.51	101.78
				BK8	IAW, IBW, ICW	0.00	0.00	0.00	0.00	0.00	0.00						
		L78	**DG2-6781-SLG(A)-Bus7-BK7**	BK7	IAX, IBX, ICX	8.71	101.38	1.13	46.31	1.04	-120.72	20.73	-6.51	60.45	-111.65	60.15	107.40
				BK8	IAW, IBW, ICW	0.00	0.00	0.00	0.00	0.00	0.00						
	11, 14, 19	L67	DG2-678-SLG(A)-Bus6-BK7	BK7	IAX, IBX, ICX	11.70	96.60	0.68	47.09	0.64	-123.25	0.00	0.00	58.59	-104.70	58.40	101.88
				BK8	IAW, IBW, ICW	0.00	0.00	0.00	0.00	0.00	0.00						
		L78	**DG2-678-SLG(A)-Bus7-BK7**	BK7	IAX, IBX, ICX	8.49	99.92	0.68	44.59	0.65	-122.43	20.22	-7.99	60.24	-110.57	61.12	107.27
				BK8	IAW, IBW, ICW	0.00	0.00	0.00	0.00	0.00	0.00						
SS4	13, 21	L67	DG2-67-SLG(A)-Bus6-BK7	BK7	IAX, IBX, ICX	11.49	96.42	0.38	48.54	0.37	-122.06	0.00	0.00	58.64	-104.03	59.02	101.94
				BK8	IAW, IBW, ICW	0.00	0.00	0.00	0.00	0.00	0.00						
SS5	4	L67	DG1-5678-SLG(A)-Bus6-BK7	BK7	IAX, IBX, ICX	9.70	99.63	0.70	47.53	0.65	-120.92	2.31	-8.28	58.70	-110.14	58.77	105.07
				BK8	IAW, IBW, ICW	9.75	99.89	0.98	46.19	0.93	-121.72						
		L78	**DG1-5678-SLG(A)-Bus7-BK7**	BK7	IAX, IBX, ICX	7.52	101.74	0.70	45.50	0.66	-120.56	17.90	-6.15	60.24	-113.68	60.40	108.51
				BK8	IAW, IBW, ICW	7.62	102.41	0.99	43.35	0.94	-118.91						

Bold represents backup protection tests. *CTR* = current transformer ratio, *PTR* = potential transformer ratio.

Table K.4: Fault states of tripping and non-tripping tests for minimum fault overcurrents of Relay 3

Setting Group	Test Mode	Protection Areas	Tests: Source - Circuit - Type of Fault - Fault Location -Opened Breaker	Breaker	Low Level Test Interface	Secondary Currents and Line-to-ground Voltages (*CTR* = 200, *PTR* = 60)											
						Fault Currents						Bus 6 - Fault Line-to-ground Voltages					
						IAs		*IBs*		*ICs*		*VAs*		*VBs*		*VCs*	
						Mag. [A]	β_A [°]	Mag. [A]	β_B [°]	Mag. [A]	β_C [°]	Mag. [V]	δ_A [°]	Mag. [V]	δ_B [°]	Mag. [V]	δ_C [°]
SS1	1	L56	UTILITY-8765/1234-LL(BC)-Bus5-BK8	BK8	IAW, IBW, ICW	0.28	-37.48	7.70	-167.69	7.52	13.95	63.05	-5.05	33.02	-169.42	32.84	159.05
				BK7	IAX, IBX, ICX	0.61	-38.12	7.82	-168.34	7.44	15.28						
SS2	2, 6, 9, 18	L56	DG2-678/65-LL(BC)-Bus5-BK8	BK8	IAW, IBW, ICW	0.27	-37.34	6.96	-172.50	6.77	9.11	65.36	-1.84	34.96	-168.76	32.29	163.96
				BK7	IAX, IBX, ICX	0.76	142.34	0.37	-24.54	0.40	-49.81						
		L67	DG2-678/65-LL(BC)-Bus7-BK7	BK7	IAX, IBX, ICX	0.76	142.31	6.32	6.95	5.80	-167.73	65.59	-1.86	37.15	-158.91	34.57	153.35
				BK8	IAW, IBW, ICW	0.27	-37.36	0.15	167.11	0.15	118.38						
		L78	**DG2-678/65-LL(BC)-Bus8-BK7**	BK7	IAX, IBX, ICX	0.77	142.26	5.18	8.15	4.68	-165.07	65.91	-1.89	41.81	-147.73	39.13	141.24
				BK8	IAW, IBW, ICW	0.27	-37.40	0.17	178.05	0.16	106.49						
	10, 16	L56	DG2-67/65-LL(BC)-Bus5-BK8	BK8	IAW, IBW, ICW	0.26	-37.39	6.85	-173.36	6.66	8.22	65.82	-1.41	35.30	-168.72	32.33	164.72
				BK7	IAX, IBX, ICX	0.44	142.86	0.22	-24.36	0.23	-49.74						
		L67	DG2-67/65-LL(BC)-Bus7-BK7	BK7	IAX, IBX, ICX	0.44	142.84	6.10	6.93	5.79	-170.04	66.02	-1.42	37.57	-159.25	34.33	154.17
				BK8	IAW, IBW, ICW	0.26	-37.42	0.15	165.58	0.14	118.91						
	8	L34	DG2-6543-LL(BC)-Bus3-BK8	BK8	IAW, IBW, ICW	0.84	-37.84	6.38	-172.98	5.81	12.93	65.83	-1.62	37.78	-159.82	33.81	153.85
				BK7	IAX, IBX, ICX	0.00	0.00	0.00	0.00	0.00	0.00						
		L56	DG2-6543-LL(BC)-Bus5-BK8	BK8	IAW, IBW, ICW	0.84	-37.80	7.14	-174.27	6.55	10.83	65.61	-1.59	35.12	-168.63	32.36	164.33
				BK7	IAX, IBX, ICX	0.00	0.00	0.00	0.00	0.00	0.00						
	17	L56	DG2-65-LL(BC)-Bus5-BK8	BK8	IAW, IBW, ICW	0.26	-37.48	6.71	-174.69	6.52	6.87	66.44	-0.83	35.77	-168.66	32.37	165.69
				BK7	IAX, IBX, ICX	0.00	0.00	0.00	0.00	0.00	0.00						
SS3	3, 7, 12, 15, 20	L67	DG2-6781-LL(BC)-Bus7-BK7	BK7	IAX, IBX, ICX	1.24	142.58	6.59	6.51	5.76	-164.91	65.31	-2.16	36.84	-158.54	34.84	152.78
				BK8	IAW, IBW, ICW	0.00	0.00	0.00	0.00	0.00	0.00						
		L78	**DG2-6781-LL(BC)-Bus8-BK7**	BK7	IAX, IBX, ICX	1.24	142.53	5.44	7.55	4.65	-161.52	65.63	-2.18	41.52	-146.89	39.79	140.73
				BK8	IAW, IBW, ICW	0.00	0.00	0.00	0.00	0.00	0.00						
	11, 14, 19	L67	DG2-678-LL(BC)-Bus7-BK7	BK7	IAX, IBX, ICX	0.76	142.27	6.27	6.35	5.74	-168.35	67.67	0.02	38.49	-157.59	35.27	155.46
				BK8	IAW, IBW, ICW	0.00	0.00	0.00	0.00	0.00	0.00						
		L78	**DG2-678-LL(BC)-Bus8-BK7**	BK7	IAX, IBX, ICX	0.76	142.23	5.15	7.73	4.65	-165.52	68.01	0.00	43.28	-146.56	39.83	143.20
				BK8	IAW, IBW, ICW	0.00	0.00	0.00	0.00	0.00	0.00						
SS4	13, 21	L67	DG2-67-LL(BC)-Bus7-BK7	BK7	IAX, IBX, ICX	0.44	142.79	6.05	6.28	5.74	-170.71	67.61	-0.02	38.59	-158.36	34.79	155.80
				BK8	IAW, IBW, ICW	0.00	0.00	0.00	0.00	0.00	0.00						
SS5	4	L67	DG1-5678-LL(BC)-Bus7-BK7	BK7	IAX, IBX, ICX	0.77	141.24	5.72	6.89	5.21	-167.00	64.69	-2.54	35.64	-160.99	34.15	154.90
				BK8	IAW, IBW, ICW	1.10	140.99	5.88	6.24	5.17	-165.07						
		L78	**DG1-5678-LL(BC)-Bus8-BK7**	BK7	IAX, IBX, ICX	0.78	141.21	4.77	7.68	4.27	-164.72	64.95	-2.56	39.74	-149.69	38.23	143.08
				BK8	IAW, IBW, ICW	1.10	140.95	4.96	7.19	4.27	-162.07						

Bold represents backup protection tests. *CTR* = current transformer ratio, *PTR* = potential transformer ratio.

Appendix L - Ending fault times of tripping and non-tripping tests for NRTS experiment

Table L.1: Ending fault times of tripping and non-tripping tests for Relay 2

Relay 2 - Tripping and Non-Tripping Tests - NRTS Experiment													
Fault Overcurrent	**Groups and Modes**		**Protection Area, Source, Circuit, Fault and Location**		**Pre-Fault State Time, [T_{PF}] cycles**	**Primary Pickup Fault Current, [I] Amps**	**Tripping Tests**				**Non-Tripping Tests**	
	Group Setting	**Test Mode**	**Protection Areas**	**Source - Circuit - Type of Fault - Fault Location - Opened Breaker**			**Fault State Time, cycles [T_{FS1}]**	**Measured Relay Time, cycles [T_{Rm}]**	**Measured Fault Clearing Time, cycles [T_{C1}]**	**Ending Fault Time, cycles [$T_{EF1} = T_{PF} + T_{C1}$]**	**Fault State Time, cycles [$T_{FS2} = 0.8\ T_{Rm}$]**	**Ending Fault Time, cycles [$T_{EF2} = T_{PF} + T_{FS2}$]**
Maximum	SS1	1	**L56**	**UTILITY-8765/1234-DLG(BC)-Bus6-BK6**	**600**	**2101**	**600**	**19.626**	**23.95**	**623.95**	**15.70**	**617.66**
			L67	UTILITY-8765/1234-DLG(BC)-Bus7-BK6	600	3170	600	12.426	16.75	616.75	9.94	611.18
	SS2	2, 6, 9, 18	L78	DG2-678/65-SLG(A)-Bus7-BK5	600	1650	600	15.114	19.44	619.44	12.09	613.60
		3, 7, 12, 15, 20	L78	DG2-6781-SLG(A)-Bus7-BK5	600	1681	600	14.418	18.73	618.73	11.53	612.98
		11, 14, 19	L78	DG2-678-SLG(A)-Bus7-BK5	600	1639	600	15.102	19.43	619.43	12.08	613.59
	SS4	4	L78	DG1-5678-SLG(A)-Bus7-BK5	600	1453	600	16.854	21.18	621.18	13.48	615.17
Minimum	SS1	1	**L56**	**UTILITY-8765/1234-LL(BC)-Bus5-BK6**	**600**	**1564**	**600**	**30.774**	**35.09**	**635.09**	**24.62**	**627.70**
			L67	UTILITY-8765/1234-LL(BC)-Bus6-BK6	600	1845	600	23.658	27.97	627.97	18.93	621.29
	SS2	2, 6, 9, 18	L78	DG2-678/65-LL(BC)-Bus8-BK5	600	996	600	34.254	38.57	638.57	27.40	630.83
		3, 7, 12, 15, 20	L78	DG2-6781-LL(BC)-Bus8-BK5	600	1047	600	31.842	36.17	636.17	25.47	628.66
		11, 14, 19	L78	DG2-678-LL(BC)-Bus8-BK5	600	989	600	34.878	39.19	639.19	27.90	631.39
	SS4	4	L78	DG1-5678-LL(BC)-Bus8-BK5	600	915	600	38.358	42.67	642.67	30.69	634.52

Bold represents backup protection tests

Table L.2: Ending fault times of tripping and non-tripping tests for Relay 3

Relay 3 - Tripping and Non-Tripping Tests - NRTS Experiment													
Fault Overcurrent	**Groups and Modes**		**Protection Area, Source, Circuit, Fault and Location**		**Pre-Fault State Time, [T_{PF}] cycles**	**Primary Pickup Fault Current, [I] Amps**	**Tripping Tests**				**Non-Tripping Tests**	
	Group Setting	**Test Mode**	**Protection Areas**	**Source - Circuit - Type of Fault - Fault Location - Opened Breaker**			**Fault State Time, cycles [T_{FS1}]**	**Measured Relay Time, cycles [T_{Rm}]**	**Measured Fault Clearing Time, cycles [T_{CI}]**	**Ending Fault Time, cycles [$T_{EF1} = T_{PF} + T_{CI}$]**	**Fault State Time, cycles [$T_{FS2} = 0.8\ T_{Rm}$]**	**Ending Fault Time, cycles [$T_{EF2} = T_{PF} + T_{FS2}$]**
Maximum	SS1	1	L56	UTILITY-8765/1234-DLG(BC)-Bus6-BK8	600	2046	600	11.154	15.47	615.47	8.92	610.04
	SS2	2, 6, 9, 18	L56	DG2-678/65-SLG(A)-Bus6-BK8	600	2371	600	10.146	14.46	614.46	8.12	609.13
			L67	DG2-678/65-SLG(A)-Bus6-BK7	600	2369	600	15.114	19.43	619.43	12.09	613.60
			L78	**DG2-678/65-SLG(A)-Bus7-BK7**	**600**	**1709**	**600**	**22.926**	**27.24**	**627.24**	**18.34**	**620.63**
		10, 16	L56	DG2-67/65-SLG(A)-Bus6-BK8	600	2330	600	10.374	14.70	614.70	8.30	609.34
			L67	DG2-67/65-SLG(A)-Bus6-BK7	600	2327	600	15.426	19.74	619.74	12.34	613.88
		8	L34	DG2-6543-SLG(A)-Bus4-BK8	600	1989	600	12.426	16.74	616.74	9.94	611.18
			L56	DG2-6543-SLG(A)-Bus6-BK8	600	2355	600	10.134	14.46	614.46	8.11	609.12
		17	L56	DG2-65-SLG(A)-Bus6-BK8	600	2282	600	10.374	14.69	614.69	8.30	609.34
	SS3	3, 7, 12, 15, 20	L67	DG2-6781-SLG(A)-Bus6-BK7	600	2400	600	15.150	19.46	619.46	12.12	613.64
			L78	**DG2-6781-SLG(A)-Bus7-BK7**	**600**	**1742**	**600**	**22.674**	**26.99**	**626.99**	**18.14**	**620.41**
		11, 14, 19	L67	DG2-678-SLG(A)-Bus6-BK7	600	2339	600	15.654	19.97	619.97	12.52	614.09
			L78	**DG2-678-SLG(A)-Bus7-BK7**	**600**	**1698**	**600**	**23.370**	**27.70**	**627.70**	**18.70**	**621.03**
	SS4	13, 21	L67	DG2-67-SLG(A)-Bus6-BK7	600	2298	600	9.594	13.91	613.91	7.68	608.63
	SS5	4	L67	DG1-5678-SLG(A)-Bus6-BK7	600	1940	600	17.898	22.21	622.21	14.32	616.11
			L78	**DG1-5678-SLG(A)-Bus7-BK7**	**600**	**1503**	**600**	**25.398**	**29.71**	**629.71**	**20.32**	**622.86**
Minimum	SS1	1	L56	UTILITY-8765/1234-LL(BC)-Bus5-BK8	600	1539	600	16.35	20.66	620.66	13.08	614.72
	SS2	2, 6, 9, 18	L56	DG2-678/65-LL(BC)-Bus5-BK8	600	1392	600	20.706	25.02	625.02	16.56	618.64
			L67	DG2-678/65-LL(BC)-Bus7-BK7	600	1265	600	36.378	40.70	640.70	29.10	632.74
			L78	**DG2-678/65-LL(BC)-Bus8-BK7**	**600**	**1036**	**600**	**53.142**	**57.47**	**657.47**	**42.51**	**647.83**
		10, 16	L56	DG2-67/65-LL(BC)-Bus5-BK8	600	1369	600	21.666	25.98	625.98	17.33	619.50
			L67	DG2-67/65-LL(BC)-Bus7-BK7	600	1221	600	38.67	42.98	642.98	30.94	634.80
		8	L34	DG2-6543-LL(BC)-Bus3-BK8	600	1275	600	24.138	28.46	628.46	19.31	621.72
			L56	DG2-6543-LL(BC)-Bus5-BK8	600	1427	600	19.914	24.24	624.24	15.93	617.92
		17	L56	DG2-65-LL(BC)-Bus5-BK8	600	1342	600	22.41	26.74	626.74	17.93	620.17
	SS3	3, 7, 12, 15, 20	L67	DG2-6781-LL(BC)-Bus7-BK7	600	1318	600	34.89	39.22	639.22	27.91	631.40
			L78	**DG2-6781-LL(BC)-Bus8-BK7**	**600**	**1088**	**600**	**49.35**	**53.66**	**653.66**	**39.48**	**644.42**
		11, 14, 19	L67	DG2-678-LL(BC)-Bus7-BK7	600	1253	600	37.878	42.20	642.20	30.30	634.09
			L78	**DG2-678-LL(BC)-Bus8-BK7**	**600**	**1031**	**600**	**54.894**	**59.22**	**659.22**	**43.92**	**649.40**
	SS4	13, 21	L67	DG2-67-LL(BC)-Bus7-BK7	600	1210	600	23.01	27.34	627.34	18.41	620.71
	SS5	4	L67	DG1-5678-LL(BC)-Bus7-BK7	600	1145	600	39.618	43.93	643.93	31.69	635.66
			L78	**DG1-5678-LL(BC)-Bus8-BK7**	**600**	**955**	**600**	**56.178**	**60.50**	**660.50**	**44.94**	**650.56**

Bold represents backup protection tests

Appendix M - Measured delay times of tripping tests for NRTS experiment

Table M.1: Measured delay times of tripping tests for Relay 2

Relay 2 - Tripping Tests - NRTS Experiment								
Fault Overcurrent	**Groups and Modes**		**Protection Area, Source, Circuit, Fault and Location**		**Primary Pickup Fault Current, [*I*] Amps**	**Tripping Tests**		
	Group Setting	**Test Mode**	**Protection Areas**	**Source - Circuit - Type of Fault - Fault Location - Opened Breaker**		**Measured Relay Time, cycles [T_{Rm}]**	**Measured Fault Clearing Time, cycles [T_{C1}]**	**Measured Delay Time, cycles [$T_D = T_{C1} - T_{Rm}$]**
Maximum	SS1	1	**L56**	**UTILITY-8765/1234-DLG(BC)-Bus6-BK6**	**2101**	**19.626**	**23.95**	**4.324**
			L67	UTILITY-8765/1234-DLG(BC)-Bus7-BK6	3170	12.426	16.75	4.324
	SS2	2, 6, 9, 18	L78	DG2-678/65-SLG(A)-Bus7-BK5	1650	15.114	19.44	4.326
		3, 7, 12, 15, 20	L78	DG2-6781-SLG(A)-Bus7-BK5	1681	14.418	18.73	4.312
		11, 14, 19	L78	DG2-678-SLG(A)-Bus7-BK5	1639	15.102	19.43	4.328
	SS4	4	L78	DG1-5678-SLG(A)-Bus7-BK5	1453	16.854	21.18	4.326
Minimum	SS1	1	**L56**	**UTILITY-8765/1234-LL(BC)-Bus5-BK6**	**1564**	**30.774**	**35.09**	**4.316**
			L67	UTILITY-8765/1234-LL(BC)-Bus6-BK6	1845	23.658	27.97	4.312
	SS2	2, 6, 9, 18	L78	DG2-678/65-LL(BC)-Bus8-BK5	996	34.254	38.57	4.316
		3, 7, 12, 15, 20	L78	DG2-6781-LL(BC)-Bus8-BK5	1047	31.842	36.17	4.328
		11, 14, 19	L78	DG2-678-LL(BC)-Bus8-BK5	989	34.878	39.19	4.312
	SS4	4	L78	DG1-5678-LL(BC)-Bus8-BK5	915	38.358	42.67	4.312

Bold represents backup protection tests

Table M.2: Measured delay times of tripping tests for Relay 3

Relay 3 - Tripping Tests - NRTS Experiment								
Fault Overcurrent	**Groups and Modes**		**Protection Area, Source, Circuit, Fault and Location**		**Primary Pickup Fault Current, [*I*] Amps**	**Tripping Tests**		
	Group Setting	**Test Mode**	**Protection Areas**	**Source - Circuit - Type of Fault - Fault Location - Opened Breaker**		**Measured Relay Time, cycles [T_{Rm}]**	**Measured Fault Clearing Time, cycles [T_{CI}]**	**Measured Delay Time, cycles [$T_D = T_{CI} - T_{Rm}$]**
Maximum	SS1	1	L56	UTILITY-8765/1234-DLG(BC)-Bus6-BK8	2046	11.154	15.47	4.316
	SS2	2, 6, 9, 18	L56	DG2-678/65-SLG(A)-Bus6-BK8	2371	10.146	14.46	4.314
			L67	DG2-678/65-SLG(A)-Bus6-BK7	2369	15.114	19.43	4.316
			L78	**DG2-678/65-SLG(A)-Bus7-BK7**	**1709**	**22.926**	**27.24**	**4.314**
		10, 16	L56	DG2-67/65-SLG(A)-Bus6-BK8	2330	10.374	14.70	4.326
			L67	DG2-67/65-SLG(A)-Bus6-BK7	2327	15.426	19.74	4.314
		8	L34	DG2-6543-SLG(A)-Bus4-BK8	1989	12.426	16.74	4.314
			L56	DG2-6543-SLG(A)-Bus6-BK8	2355	10.134	14.46	4.326
		17	L56	DG2-65-SLG(A)-Bus6-BK8	2282	10.374	14.69	4.316
	SS3	3, 7, 12, 15, 20	L67	DG2-6781-SLG(A)-Bus6-BK7	2400	15.150	19.46	4.310
			L78	**DG2-6781-SLG(A)-Bus7-BK7**	**1742**	**22.674**	**26.99**	**4.316**
		11, 14, 19	L67	DG2-678-SLG(A)-Bus6-BK7	2339	15.654	19.97	4.316
			L78	**DG2-678-SLG(A)-Bus7-BK7**	**1698**	**23.370**	**27.70**	**4.330**
	SS4	13, 21	L67	DG2-67-SLG(A)-Bus6-BK7	2298	9.594	13.91	4.316
	SS5	4	L67	DG1-5678-SLG(A)-Bus6-BK7	1940	17.898	22.21	4.312
			L78	**DG1-5678-SLG(A)-Bus7-BK7**	**1503**	**25.398**	**29.71**	**4.312**
Minimum	SS1	1	L56	UTILITY-8765/1234-LL(BC)-Bus5-BK8	1539	16.35	20.66	4.310
	SS2	2, 6, 9, 18	L56	DG2-678/65-LL(BC)-Bus5-BK8	1392	20.706	25.02	4.314
			L67	DG2-678/65-LL(BC)-Bus7-BK7	1265	36.378	40.70	4.322
			L78	**DG2-678/65-LL(BC)-Bus8-BK7**	**1036**	**53.142**	**57.47**	**4.328**
		10, 16	L56	DG2-67/65-LL(BC)-Bus5-BK8	1369	21.666	25.98	4.314
			L67	DG2-67/65-LL(BC)-Bus7-BK7	1221	38.67	42.98	4.310
		8	L34	DG2-6543-LL(BC)-Bus3-BK8	1275	24.138	28.46	4.322
			L56	DG2-6543-LL(BC)-Bus5-BK8	1427	19.914	24.24	4.326
		17	L56	DG2-65-LL(BC)-Bus5-BK8	1342	22.41	26.74	4.330
	SS3	3, 7, 12, 15, 20	L67	DG2-6781-LL(BC)-Bus7-BK7	1318	34.89	39.22	4.330
			L78	**DG2-6781-LL(BC)-Bus8-BK7**	**1088**	**49.35**	**53.66**	**4.310**
		11, 14, 19	L67	DG2-678-LL(BC)-Bus7-BK7	1253	37.878	42.20	4.322
			L78	**DG2-678-LL(BC)-Bus8-BK7**	**1031**	**54.894**	**59.22**	**4.326**
	SS4	13, 21	L67	DG2-67-LL(BC)-Bus7-BK7	1210	23.01	27.34	4.330
	SS5	4	L67	DG1-5678-LL(BC)-Bus7-BK7	1145	39.618	43.93	4.312
			L78	**DG1-5678-LL(BC)-Bus8-BK7**	**955**	**56.178**	**60.50**	**4.322**

Bold represents backup protection tests

Appendix N - Measured and theoretical relay times and relay time percent error values for NRTS experiment

Table N.1: Measured and theoretical relay times and relay time percent error values of Relay 2

Relay 2 - Tripping Tests - NRTS Experiment								
Fault Overcurrent	**Groups and Modes**		**Protection Area, Source, Circuit, Fault and Location**		**Primary Pickup Fault Current, [I] Amps**	**Tripping Tests**	**Calculations**	
	Group Setting	**Test Mode**	**Protection Areas**	**Source - Circuit - Type of Fault - Fault Location - Opened Breaker**		**Measured Relay Time, cycles [T_{Rm}]**	**Theoretical Relay Time, cycle [T_R]**	**Relay Time Percent Error, % [$E_{TR\%} = 100\ (T_{Rm} - T_R)/\ T_R$]**
Maximum	SS1	1	**L56**	**UTILITY-8765/1234-DLG(BC)-Bus6-BK6**	**2101**	**19.626**	**19.181**	**2.32**
			L67	UTILITY-8765/1234-DLG(BC)-Bus7-BK6	3170	12.426	11.938	4.08
	SS2	2, 6, 9, 18	L78	DG2-678/65-SLG(A)-Bus7-BK5	1650	15.114	14.231	6.20
		3, 7, 12, 15, 20	L78	DG2-6781-SLG(A)-Bus7-BK5	1681	14.418	13.855	4.06
		11, 14, 19	L78	DG2-678-SLG(A)-Bus7-BK5	1639	15.102	14.364	5.14
	SS4	4	L78	DG1-5678-SLG(A)-Bus7-BK5	1453	16.854	16.096	4.71
Minimum	SS1	1	**L56**	**UTILITY-8765/1234-LL(BC)-Bus5-BK6**	**1564**	**30.774**	**30.272**	**1.66**
			L67	UTILITY-8765/1234-LL(BC)-Bus6-BK6	1845	23.658	23.170	2.11
	SS2	2, 6, 9, 18	L78	DG2-678/65-LL(BC)-Bus8-BK5	996	34.254	33.968	0.84
		3, 7, 12, 15, 20	L78	DG2-6781-LL(BC)-Bus8-BK5	1047	31.842	30.753	3.54
		11, 14, 19	L78	DG2-678-LL(BC)-Bus8-BK5	989	34.878	34.405	1.38
	SS4	4	L78	DG1-5678-LL(BC)-Bus8-BK5	915	38.358	38.073	0.75

Bold represents backup protection tests

Table N.2: Measured and theoretical relay times and relay time percent error values of Relay 3

Relay 3 - Tripping Tests - NRTS Experiment								
Fault Overcurrent	**Groups and Modes**		**Protection Area, Source, Circuit, Fault and Location**		**Primary Pickup Fault Current, [*I*] Amps**	**Tripping Tests**	**Calculations**	
	Group Setting	**Test Mode**	**Protection Areas**	**Source - Circuit - Type of Fault - Fault Location - Opened Breaker**		**Measured Relay Time, cycles [T_{Rm}]**	**Theoretical Relay Time, cycle [T_R]**	**Relay Time Percent Error, % [$E_{TR\%} = 100\ (T_{Rm} - T_R)/\ T_R$]**
Maximum	SS1	1	L56	UTILITY-8765/1234-DLG(BC)-Bus6-BK8	2046	11.154	10.284	8.46
	SS2	2, 6, 9, 18	L56	DG2-678/65-SLG(A)-Bus6-BK8	2371	10.146	9.540	6.35
			L67	DG2-678/65-SLG(A)-Bus6-BK7	2369	15.114	14.468	4.47
			L78	**DG2-678/65-SLG(A)-Bus7-BK7**	**1709**	**22.926**	**21.901**	**4.68**
		10, 16	L56	DG2-67/65-SLG(A)-Bus6-BK8	2330	10.374	9.724	6.69
			L67	DG2-67/65-SLG(A)-Bus6-BK7	2327	15.426	14.756	4.54
		8	L34	DG2-6543-SLG(A)-Bus4-BK8	1989	12.426	11.770	5.57
			L56	DG2-6543-SLG(A)-Bus6-BK8	2355	10.134	9.611	5.45
		17	L56	DG2-65-SLG(A)-Bus6-BK8	2282	10.374	9.958	4.18
	SS3	3, 7, 12, 15, 20	L67	DG2-6781-SLG(A)-Bus6-BK7	2400	15.150	14.551	4.12
			L78	**DG2-6781-SLG(A)-Bus7-BK7**	**1742**	**22.674**	**21.811**	**3.96**
		11, 14, 19	L67	DG2-678-SLG(A)-Bus6-BK7	2339	15.654	14.964	4.61
			L78	**DG2-678-SLG(A)-Bus7-BK7**	**1698**	**23.370**	**22.637**	**3.24**
	SS4	13, 21	L67	DG2-67-SLG(A)-Bus6-BK7	2298	9.594	8.594	11.64
	SS5	4	L67	DG1-5678-SLG(A)-Bus6-BK7	1940	17.898	16.875	6.07
			L78	**DG1-5678-SLG(A)-Bus7-BK7**	**1503**	**25.398**	**24.266**	**4.66**
Minimum	SS1	1	L56	UTILITY-8765/1234-LL(BC)-Bus5-BK8	1539	16.35	15.516	5.38
	SS2	2, 6, 9, 18	L56	DG2-678/65-LL(BC)-Bus5-BK8	1392	20.706	20.067	3.18
			L67	DG2-678/65-LL(BC)-Bus7-BK7	1265	36.378	35.685	1.94
			L78	**DG2-678/65-LL(BC)-Bus8-BK7**	**1036**	**53.142**	**52.125**	**1.95**
		10, 16	L56	DG2-67/65-LL(BC)-Bus5-BK8	1369	21.666	20.634	5.00
			L67	DG2-67/65-LL(BC)-Bus7-BK7	1221	38.67	38.053	1.62
		8	L34	DG2-6543-LL(BC)-Bus3-BK8	1275	24.138	23.359	3.34
			L56	DG2-6543-LL(BC)-Bus5-BK8	1427	19.914	19.236	3.52
		17	L56	DG2-65-LL(BC)-Bus5-BK8	1342	22.41	21.349	4.97
	SS3	3, 7, 12, 15, 20	L67	DG2-6781-LL(BC)-Bus7-BK7	1318	34.89	34.065	2.42
			L78	**DG2-6781-LL(BC)-Bus8-BK7**	**1088**	**49.35**	**48.646**	**1.45**
		11, 14, 19	L67	DG2-678-LL(BC)-Bus7-BK7	1253	37.878	37.255	1.67
			L78	**DG2-678-LL(BC)-Bus8-BK7**	**1031**	**54.894**	**54.295**	**1.10**
	SS4	13, 21	L67	DG2-67-LL(BC)-Bus7-BK7	1210	23.01	22.388	2.78
	SS5	4	L67	DG1-5678-LL(BC)-Bus7-BK7	1145	39.618	38.752	2.24
			L78	**DG1-5678-LL(BC)-Bus8-BK7**	**955**	**56.178**	**55.558**	**1.12**

Bold represents backup protection tests

Appendix O - Setting parameters of elements in the microgrid circuit for real-time simulation

Table O.1: Setting parameters of elements in the microgrid circuit for real-time simulation with relays in the loop

Masks	Setting Parameters	Load 1	Load 2	Load 3	Load 4	Load 5	Load 6	Load 7	Load 8	Load 9	Load 10	Load 11	Load 12	Load 13
Three-Phase Series RLC Load	Configuration	Yg	Yg	Yg	Yg	Yg	Yg	Yg	Yg	Yg	Yg	Yg	Yg	Yg
	Nominal phase-to-phase voltage Vn (Vrms)	7200	7200	7200	7200	7200	7200	7200	7200	7200	7200	7200	7200	7200
	Nominal frequency fn (Hz)	60	60	60	60	60	60	60	60	60	60	60	60	60
	Active power P (W)	7.5e5	7.5e5	5.25e5	5.25e5	6e5	7.5e5	6e5	9e5	5.25e5	5.25e5	9e5	5.25e5	1.05e6
	Inductive reactive power QL (positive var)	5.7e5	5.7e5	4.2e5	4.2e5	4.8e5	6e5	4.5e5	6.9e5	4.2e5	4.2e5	6e5	4.5e5	8.4e5
	Capacitive reactive power Qc (negative var)	0	0	0	0	0	0	0	0	0	0	0	0	0
	Load type	Constant PQ												

Artemis Stubline	Setting Parameters	Line 1-2	Line 2-3	Line 3-4	Line 5-6	Line 6-7	Line 7-8
	Number of phases	3	3	3	3	3	3
	Inductance (pu)	2.2968	2.2968	1.1484	1.1484	2.2968	2.2968
	Resistance (pu)	0.7398	0.7398	0.3699	0.3699	0.7398	0.7398
	Nominal power (VA)	100e6	100e6	100e6	100e6	100e6	100e6
	Nominal voltage (V)	4160	4160	4160	4160	4160	4160
	Nominal frequency (Hz)	60	60	60	60	60	60
	Sample time (s)	50e-6	50e-6	50e-6	50e-6	50e-6	50e-6

Three-Phase Transformer (Two Windings)	Setting Parameters	Transformer	Transformer 1	Transformer 2	Transformer 3
	Winding 1 connection (ABC terminals)	Delta (D1)	Delta (D1)	Delta (D1)	Delta (D1)
	Winding 2 connection (ABC terminals)	Yg	Yg	Yg	Yg
	Nominal power Pn (VA)	5e6	2.5e6	2.5e6	2.5e6
	Frequency fn (Hz)	60	60	60	60
	Winding 1 phase-to-phase voltage V1 (Vrms)	115000	480	480	480
	Winding 1 resistance R1 (pu)	0.1	0.132	0.132	0.132
	Winding 1 inductance L1 (pu)	0.002123	0.003031	0.003031	0.003031
	Winding 2 phase-to-phase voltage V2 (Vrms)	7200	7200	7200	7200
	Winding 2 resistance R2 (pu)	0.1	0.132	0.132	0.132
	Winding 2 inductance L2 (pu)	0.002123	0.003031	0.003031	0.003031

Three-Phase Source	Setting Parameters	Utility	Dist. Generator 1	Dist. Generator 2	Dist. Generator 3
	Phase-to-phase rms voltage (V)	115000*1.05	480*1.05	480*1.05	480*1.05
	Phase angle of phase A (degrees)	0	0	0	0
	Frequency (Hz)	60	60	60	60
	Internal connection	Yg	Yg	Yg	Yg
	3-phase short-circuit level at base voltage (VA)	150332949	16111888	16111888	16111888
	Base phase-to-phase voltage (Vrms)	115000	480	480	480
	X/R ratio	15	83	83	83

Appendix P - Circuits for RTS experiment

Circuit paths based on the maximum generator power and loads constraints for the RTS experiment.

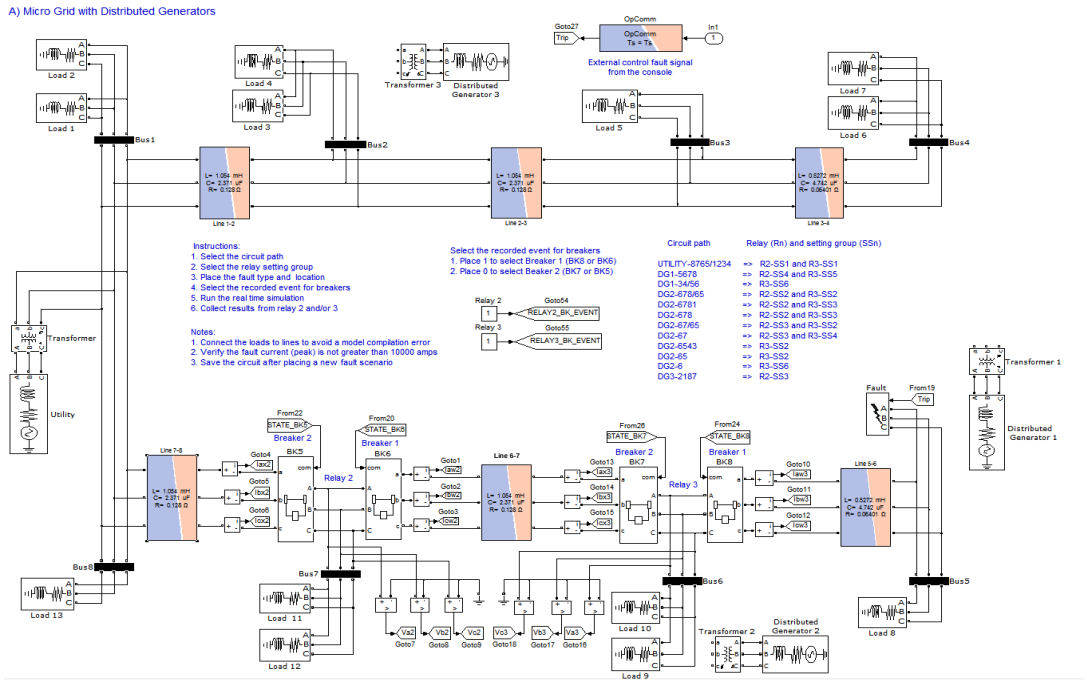

Figure P.1: UTILITY-8765/1234 circuit for the RTS experiment

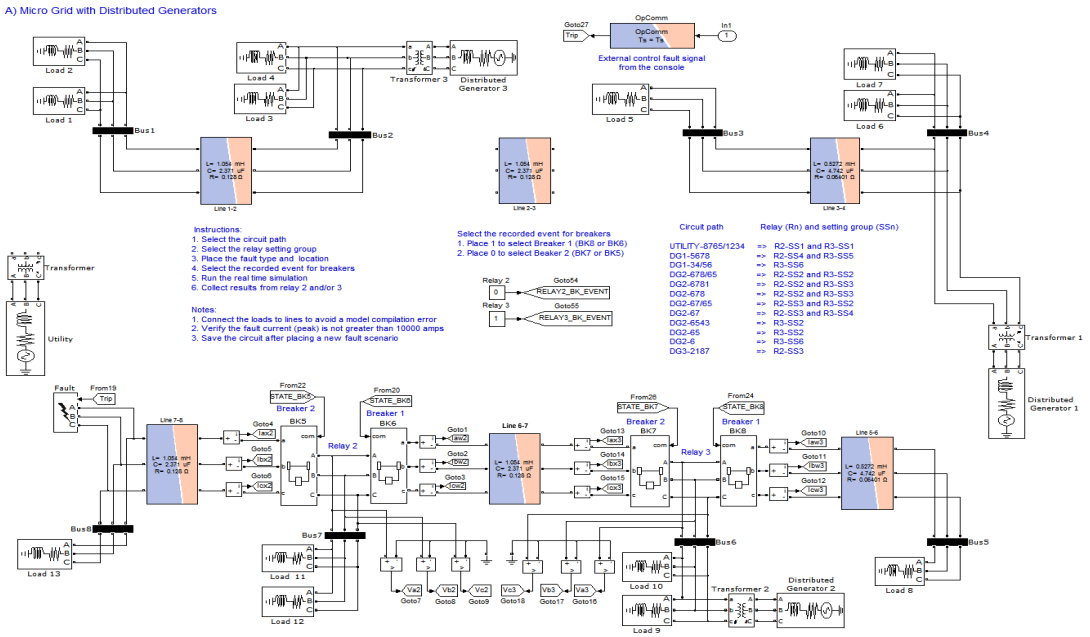

Figure P.2: DG2-678/65 circuit for the RTS experiment

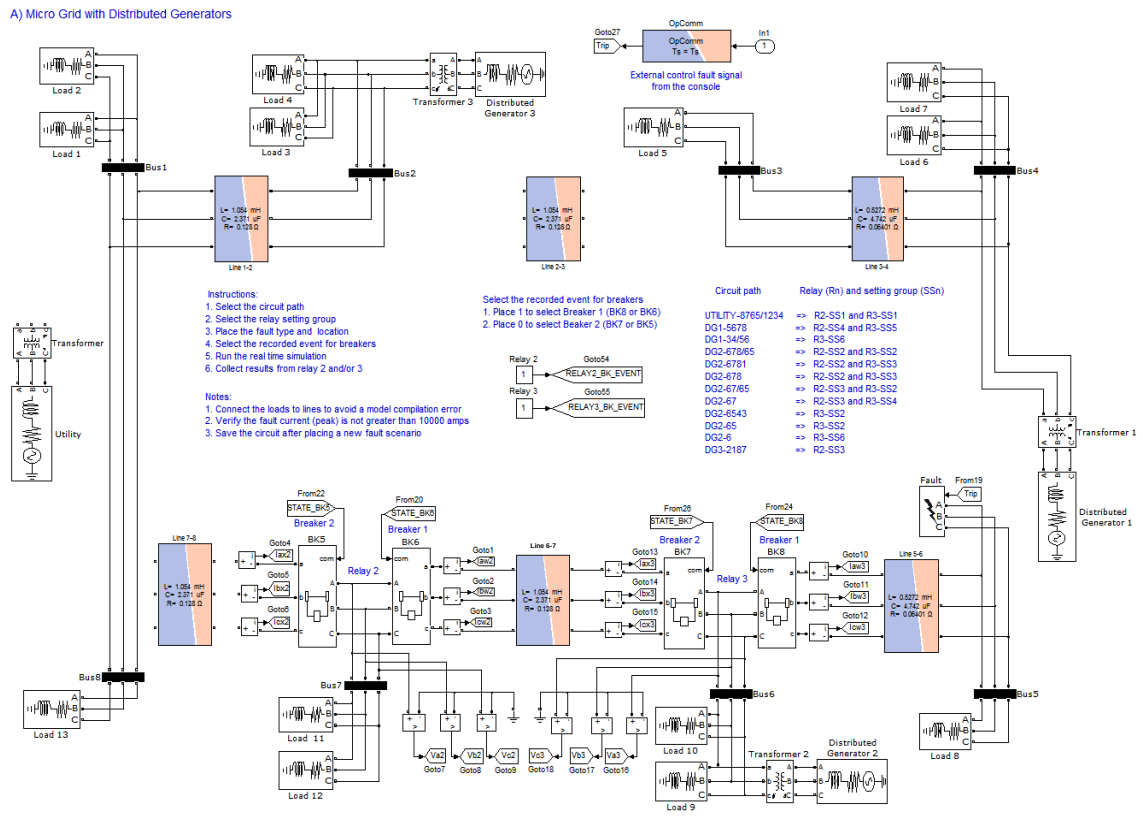

Figure P.3: DG2-67/65 circuit for the RTS experiment

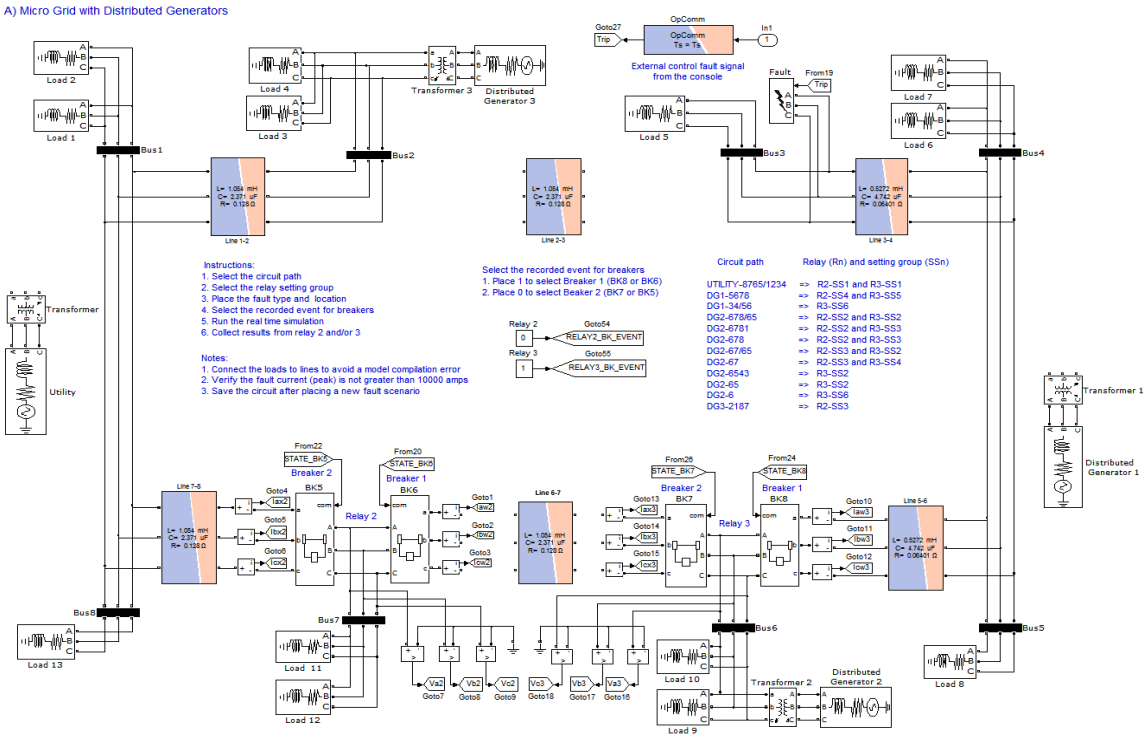

Figure P.4: DG2-6543 circuit for the RTS experiment

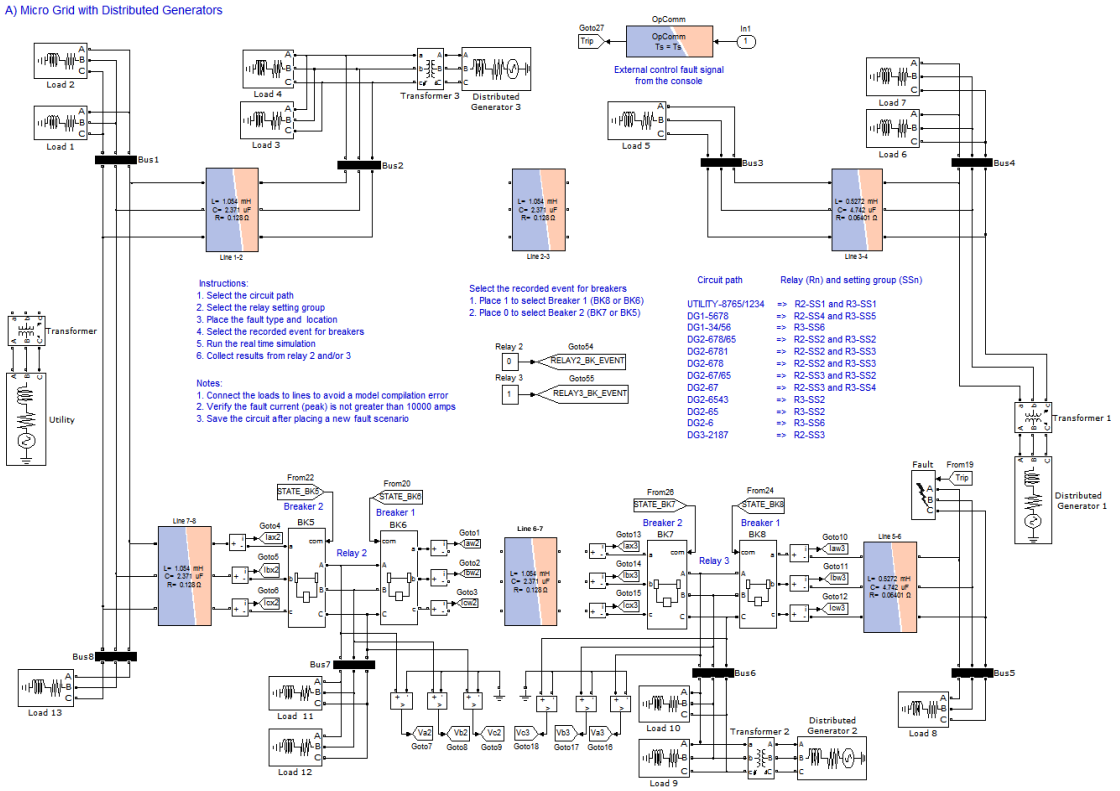

Figure P.5: DG2-65 circuit for the RTS experiment

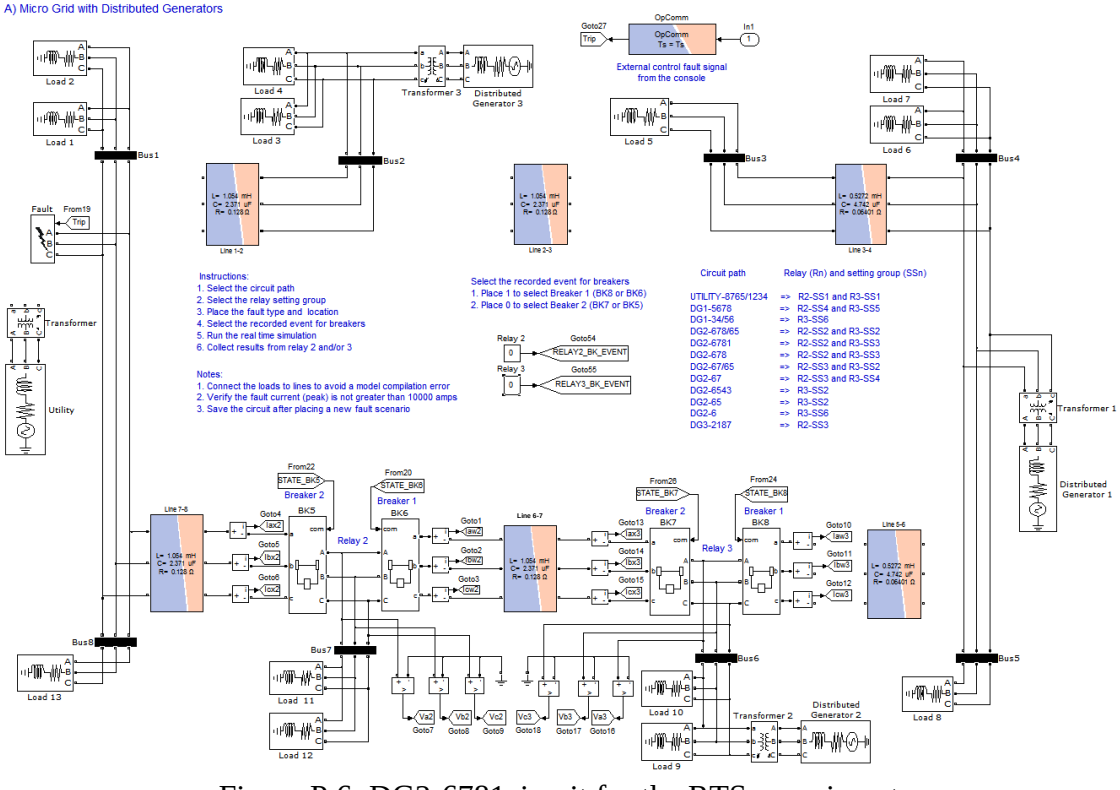

Figure P.6: DG2-6781circuit for the RTS experiment

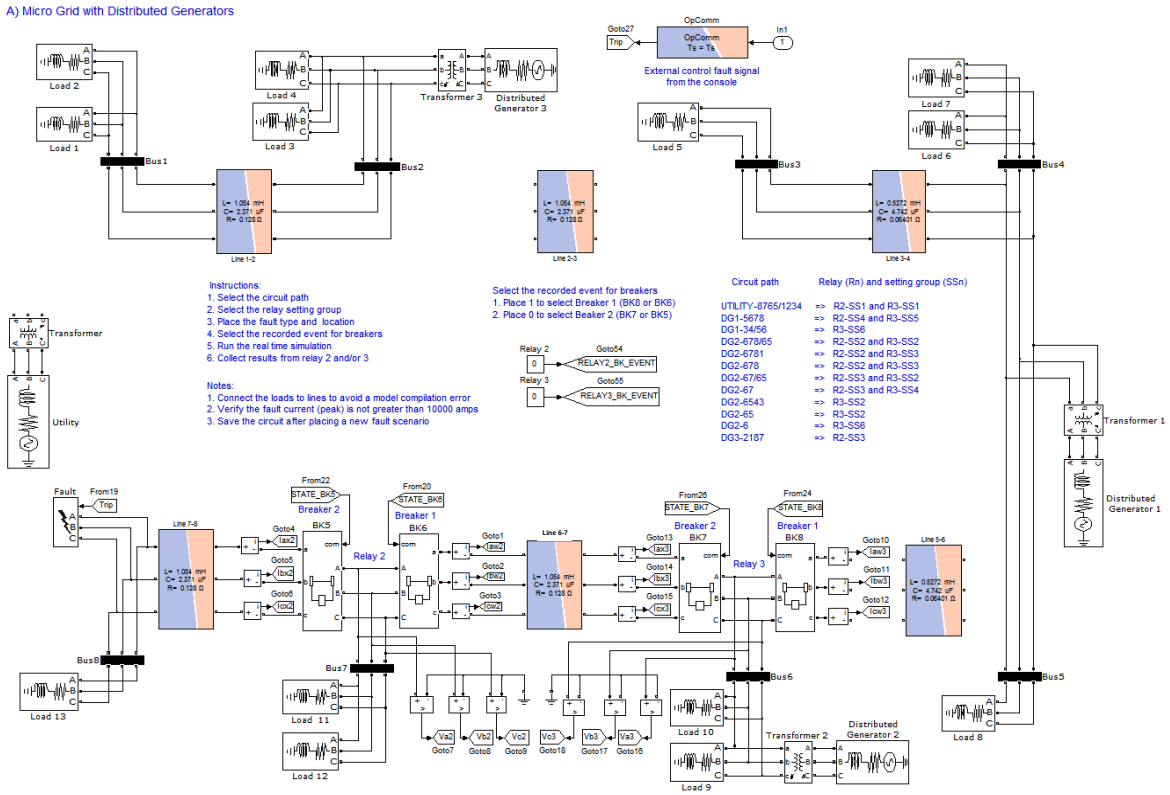

Figure P.7: DG2-678 circuit for the RTS experiment

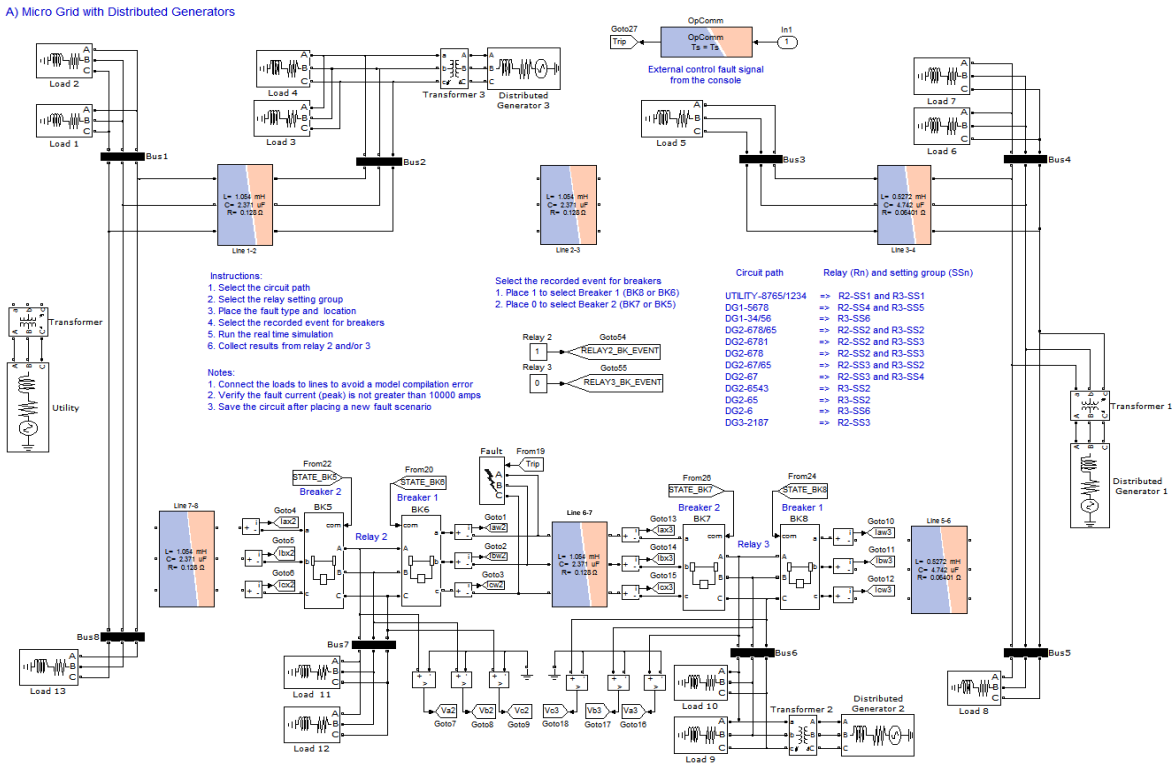

Figure P.8:DG2-67 circuit for the RTS experiment

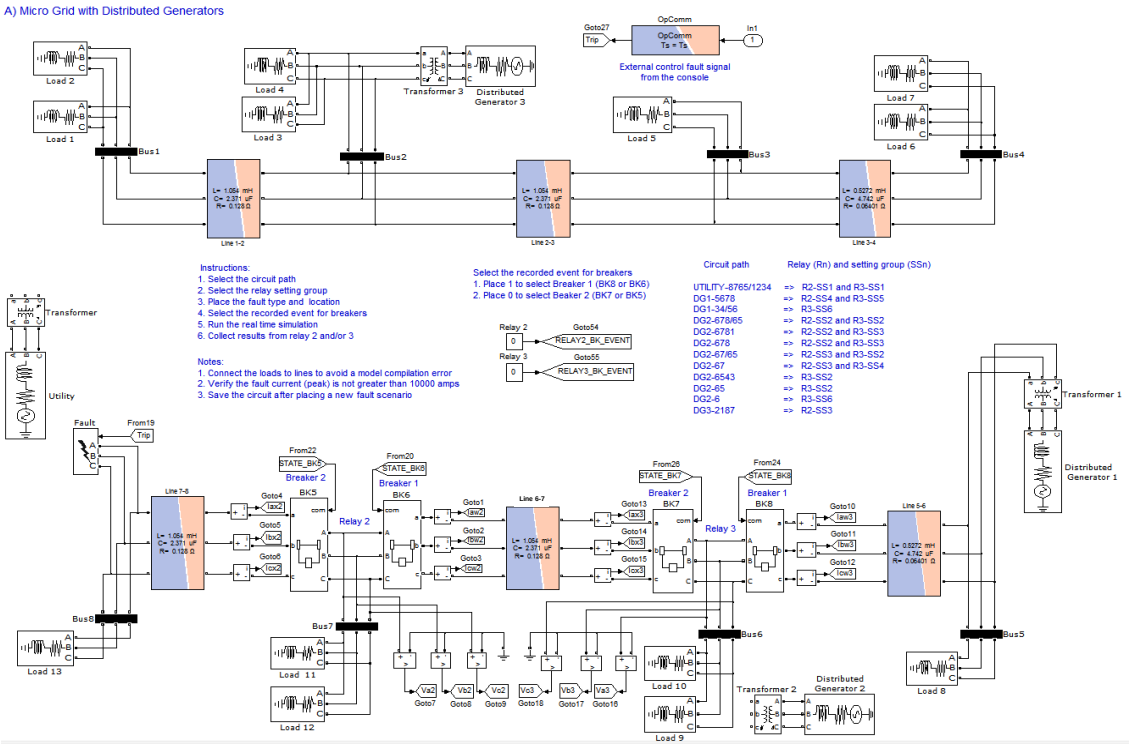

Figure P.9: DG1-5678 circuit for the RTS experiment

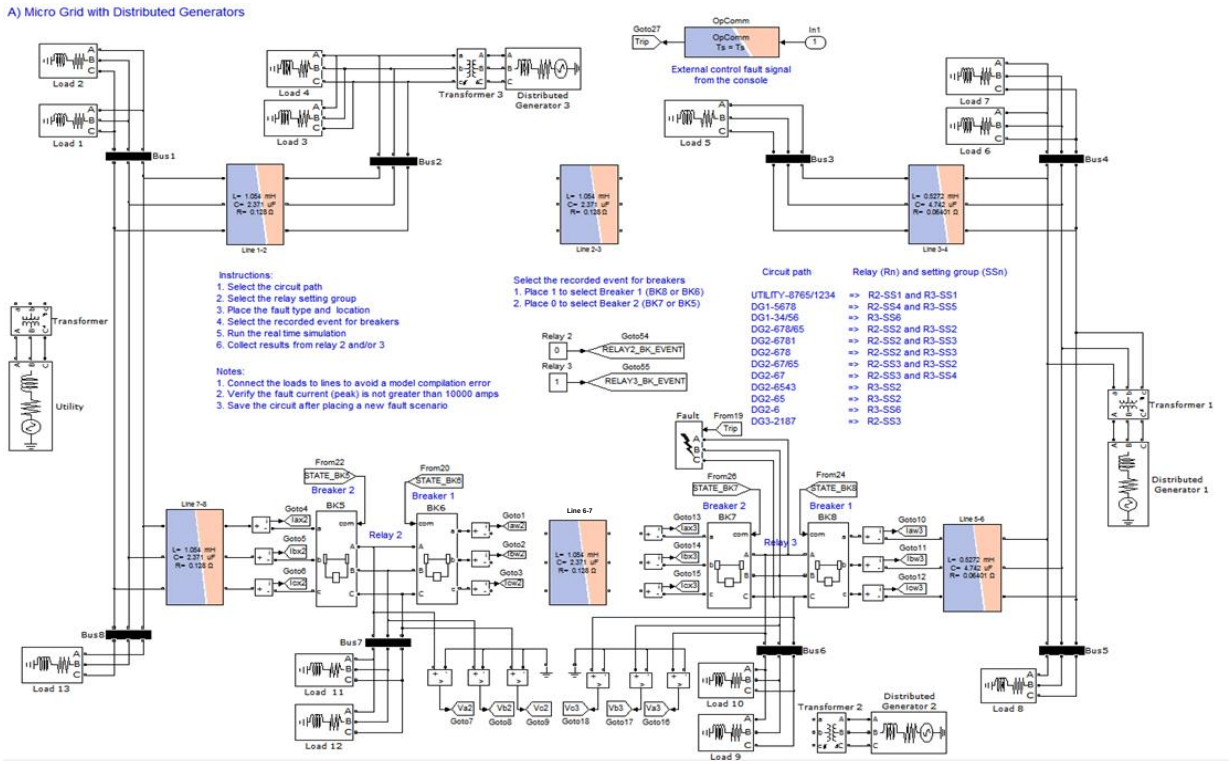

Figure P.10: DG1-34/56 circuit for the RTS experiment

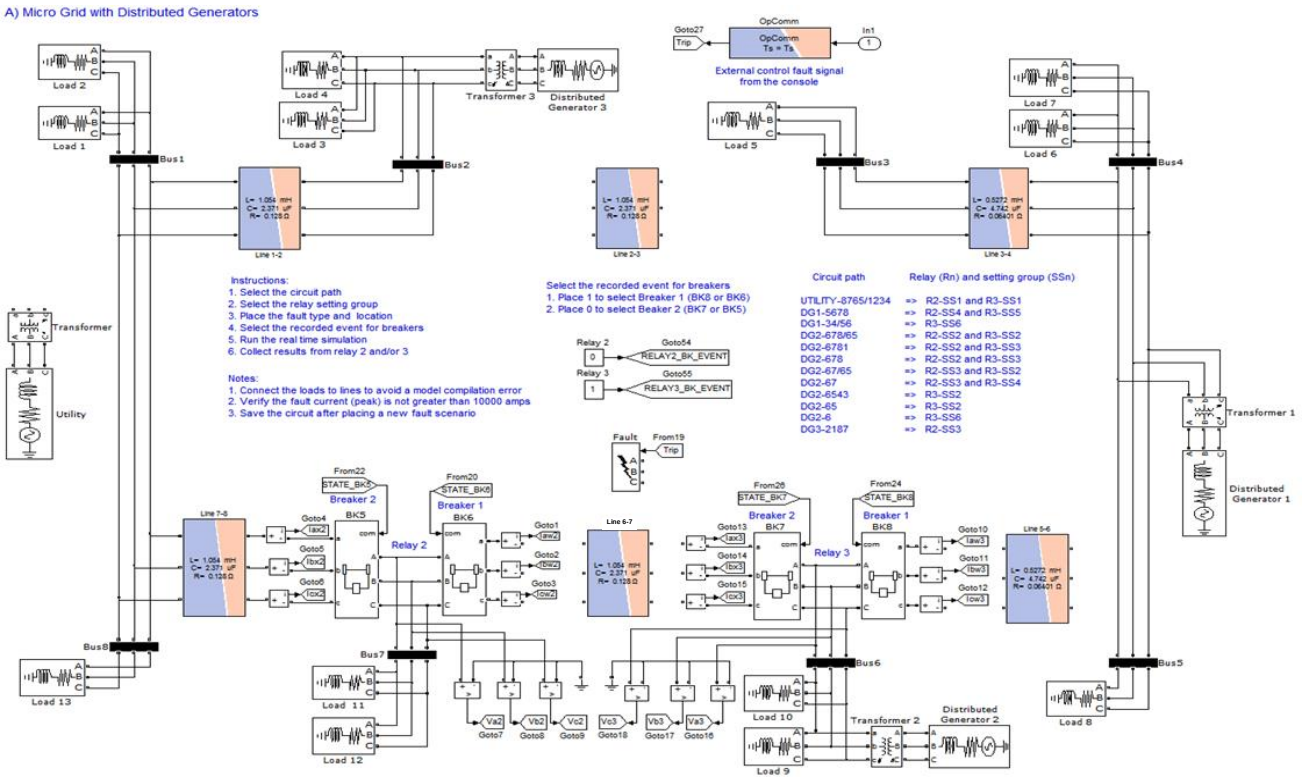

Figure P.11: DG2-6 circuit for the RTS experiment

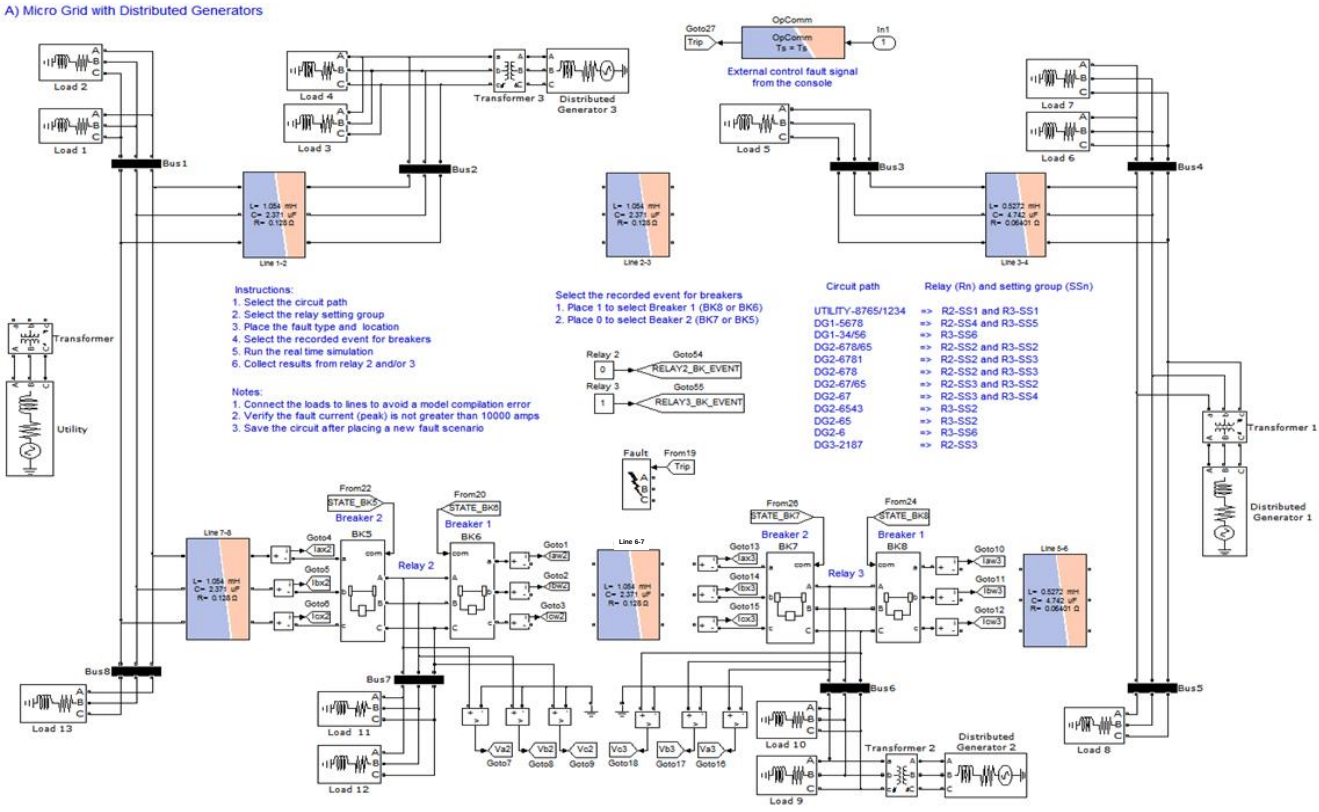

Figure P.12: DG3-2187 circuit for the RTS experiment

Appendix Q - Measured fault state and ending time values for tripping and non-tripping tests for RTS experiment

Table Q.1: Measured fault state and ending time values for tripping and non-tripping tests of Relay 2

Relay 2 - Tripping and Non-Tripping Tests - RTS Experiment													
Fault Overcurrent	**Groups and Modes**		**Protection Area, Source, Circuit, Fault and Location**		**LLTI[(1)]**		**C8 Event**		**Matlab® Files**				
										Tripping Tests		**Non-Tripping Tests**	
	Group Setting	**Test Mode**	**Protection Areas**	**Source - Circuit- Type of Fault - Fault Location - Opened Breaker**	**Relay 2 [on / off]**	**Relay 3 [on / off]**	**Record Event File**	**Primary Pickup Fault Current, amps [*I*]**	**Initial Fault Time, cycles [T_{IF}]**	**Measured Fault State Time, cycles [T_{FSm}]**	**Ending Fault Time, cycles [T_{EF}]**	**Measured Fault State Time, cycles [T_{FSm}]**	**Ending Fault Time, cycles [T_{EF}]**
Maximum	SS1	1	**L56**	**UTILITY-8765/1234-DLG(BC)-Bus6-BK6**	**on**	**off**	**C8_14156**	**1567**	**150.00**	**33.625**	**183.63**	**27.375**	**177.38**
			L67	UTILITY-8765/1234-DLG(BC)-Bus7-BK6	on	on	C8_14167	1838	150.00	25.250	175.25	19.250	169.25
	SS2	2, 6, 9, 18	L78	DG2-678/65-SLG(A)-Bus7-BK5	on	on	C8_14169	1582	150.00	17.625	167.63	15.000	165.00
		3, 7, 12, 15, 20	L78	DG2-6781-SLG(A)-Bus7-BK5	on	on	C8_14173	1599	150.00	17.125	167.13	12.000	162.00
		11, 14, 19	L78	DG2-678-SLG(A)-Bus7-BK5	on	on	C8_14175	1604	150.00	17.500	167.50	12.500	162.50
	SS4	4	L78	DG1-5678-SLG(A)-Bus7-BK5	on	on	C8_14177	1459	150.00	18.500	168.50	13.125	163.13
Minimum	SS1	1	**L56**	**UTILITY-8765/1234-LL(BC)-Bus5-BK6**	**on**	**off**	**C8_14026**	**1224**	**150.00**	**52.000**	**202.00**	**31.000**	**181.00**
			L67	UTILITY-8765/1234-LL(BC)-Bus6-BK6	on	on	C8_14042	1318	150.00	44.250	194.25	16.375	166.38
	SS2	2, 6, 9, 18	L78	DG2-678/65-LL(BC)-Bus8-BK5	on	on	C8_13953	911	150.00	44.000	194.00	26.000	176.13
		3, 7, 12, 15, 20	L78	DG2-6781-LL(BC)-Bus8-BK5	on	on	C8_14052	947	150.00	40.000	190.00	21.625	171.63
		11, 14, 19	L78	DG2-678-LL(BC)-Bus8-BK5	on	on	C8_14048	918	150.00	40.750	190.75	18.875	168.88
	SS4	4	L78	DG1-5678-LL(BC)-Bus8-BK5	on	on	C8_14044	864	150.00	46.125	196.13	24.875	174.88

Bold represents backup protection tests, [(1)] Low level test interface

Table Q.2: Measured fault state and ending fault time values for tripping and non-tripping tests of Relay 3

Relay 3 - Tripping and Non-Tripping Tests - RTS Experiment													
Fault Overcurrent	**Groups and Modes**		**Protection Area, Source, Circuit, Fault and Location**		**LLTI[(1)]**		**C8 Events**		**Matlab® Files**				
										Tripping Tests		**Non-Tripping Tests**	
	Group Setting	**Test Mode**	**Protection Areas**	**Source - Circuit - Type of Fault - Fault Location - Opened Breaker**	**Relay 2 [on / off]**	**Relay 3 [on / off]**	**Record Event File**	**Primary Pickup Fault Current, amps [I]**	**Initial Fault Time, cycles [T_{IF}]**	**Measured Fault State Time, cycles [T_{FSm}]**	**Ending Fault Time, cycles [T_{EF}]**	**Measured Fault State Time, cycles [T_{FSm}]**	**Ending Fault Time, cycles [T_{EF}]**
Maximum	SS1	1	L56	UTILITY-8765/1234-DLG(BC)-Bus6-BK8	on	on	C8_13193	1551	150.00	16.500	166.5	6.625	156.63
	SS2	2, 6, 9, 18	L56	DG2-678/65-SLG(A)-Bus6-BK8	on	on	C8_13106	1896	150.00	13.500	163.5	8.500	158.50
			L67	DG2-678/65-SLG(A)-Bus6-BK7	on	on	C8_13115	1895	150.00	20.750	170.8	13.125	163.13
			L78	**DG2-678/65-SLG(A)-Bus7-BK7**	**off**	**on**	**C8_13113**	**1556**	**150.00**	**27.000**	**177.0**	**23.875**	**173.88**
		10, 16	L56	DG2-67/65-SLG(A)-Bus6-BK8	on	on	C8_13127	1927	150.00	13.500	163.5	10.375	160.38
			L67	DG2-67/65-SLG(A)-Bus6-BK7	on	on	C8_13131	1897	150.00	19.625	169.6	13.875	163.88
		8	L34	DG2-6543-SLG(A)-Bus4-BK8	on	on	C8_13170	1726	150.00	15.125	165.1	9.125	159.13
			L56	DG2-6543-SLG(A)-Bus6-BK8	on	on	C8_13175	1915	150.00	13.500	163.5	10.500	160.50
		17	L56	DG2-65-SLG(A)-Bus6-BK8	on	on	C8_13120	1958	150.00	13.000	163.0	8.125	158.13
	SS3	3, 7, 12, 15, 20	L67	DG2-6781-SLG(A)-Bus6-BK7	on	on	C8_13161	1927	150.00	20.250	170.3	12.125	162.13
			L78	**DG2-6781-SLG(A)-Bus7-BK7**	**off**	**on**	**C8_13157**	**1567**	**150.00**	**27.000**	**177.0**	**20.375**	**170.38**
		11, 14, 19	L67	DG2-678-SLG(A)-Bus6-BK7	on	on	C8_13151	1910	150.00	20.500	170.5	11.375	161.38
			L78	**DG2-678-SLG(A)-Bus7-BK7**	**off**	**on**	**C8_13149**	**1579**	**150.00**	**26.125**	**176.1**	**16.875**	**166.88**
	SS4	13, 21	L67	DG2-67-SLG(A)-Bus6-BK7	on	on	C8_13142	1925	150.00	12.000	162.0	7.375	157.38
	SS5	4	L67	DG1-5678-SLG(A)-Bus6-BK7	on	on	C8_13207	1734	150.00	21.000	171.0	3.125	153.13
			L78	**DG1-5678-SLG(A)-Bus7-BK7**	**off**	**on**	**C8_13138**	**1452**	**150.00**	**28.000**	**178.0**	**22.500**	**172.50**
Minimum	SS1	1	L56	UTILITY-8765/1234-LL(BC)-Bus5-BK8	on	on	C8_13015	1208	150.00	24.750	174.8	5.520	155.52
	SS2	2, 6, 9, 18	L56	DG2-678/65-LL(BC)-Bus5-BK8	on	on	C8_12784	1087	150.00	33.500	183.5	12.625	162.63
			L67	DG2-678/65-LL(BC)-Bus7-BK7	on	on	C8_12796	1059	150.00	50.250	200.3	27.875	177.88
			L78	**DG2-678/65-LL(BC)-Bus8-BK7**	**off**	**on**	**C8_12794**	**953**	**150.00**	**63.500**	**213.5**	**41.625**	**191.63**
		10, 16	L56	DG2-67/65-LL(BC)-Bus5-BK8	on	on	C8_12862	1096	150.00	32.500	182.5	15.250	165.25
			L67	DG2-67/65-LL(BC)-Bus7-BK7	on	on	C8_12867	1034	150.00	52.250	202.3	29.750	179.75
		8	L34	DG2-6543-LL(BC)-Bus3-BK8	on	on	C8_12854	1082	150.00	33.500	183.5	8.000	158.00
			L56	DG2-6543-LL(BC)-Bus5-BK8	on	on	C8_12856	1149	150.00	29.500	179.5	8.625	158.63
		17	L56	DG2-65-LL(BC)-Bus5-BK8	on	on	C8_12850	1094	150.00	32.125	182.1	14.250	164.25
	SS3	3, 7, 12, 15, 20	L67	DG2-6781-LL(BC)-Bus7-BK7	on	on	C8_13002	1098	150.00	49.000	199.0	25.625	175.63
			L78	**DG2-6781-LL(BC)-Bus8-BK7**	**off**	**on**	**C8_13000**	**982**	**150.00**	**60.500**	**210.5**	**36.625**	**186.63**
		11, 14, 19	L67	DG2-678-LL(BC)-Bus7-BK7	on	on	C8_12990	1071	150.00	50.500	200.5	28.375	178.38
			L78	**DG2-678-LL(BC)-Bus8-BK7**	**off**	**on**	**C8_12987**	**968**	**150.00**	**64.000**	**214.0**	**40.875**	**190.88**
	SS4	13, 21	L67	DG2-67-LL(BC)-Bus7-BK7	on	on	C8_13012	1054	150.00	31.250	181.3	10.375	160.38
	SS5	4	L67	DG1-5678-LL(BC)-Bus7-BK7	on	on	C8_12978	997	150.00	51.500	201.5	29.625	179.63
			L78	**DG1-5678-LL(BC)-Bus8-BK7**	**off**	**on**	**C8_12980**	**909**	**150.00**	**64.000**	**214.0**	**39.875**	**189.88**

Bold represents backup protection tests, [(1)] Low level test interface

Appendix R - Measured fault state time values from event files, RT-LAB® second console, and Matlab® files for RTS experiment

Table R.1: Measured fault state times collected from event files, RT-LAB® second console, and Matlab® files for tripping tests of Relay 2

Fault Overcurrent	Test	LLTI[1]		C8 Event Files				RT-LAB® Second Console			Matlab® Files[2]
	Source – Circuit - Type of Fault - Fault Location - Opened Breaker	Relay 2 [on / off]	Relay 3 [on / off]	No Event	Ending Fault State Time, cycles [T_{EF}]	Initial Fault State Time, cycles [T_{IF}]	Measured Fault State Time, cycles [$T_{FSm} = T_{EF} - T_{IF}$]	Pre-fault State Time, cycles [T_{PR}]	Sum of Pre-Fault and Fault State Time, cycles [$S = T_{PR} + T_{FSm}$]	Measured Fault State Time, cycles [$T_{FSm} = S - T_{PR}$]	Measured Fault State Time, cycles [T_{FSm}]
Maximum	**UTILITY-8765/1234-DLG(BC)-Bus6-BK6**	**on**	**off**	**C8_14156**	**40.00**	**5.75**	**34.25**	**150.00**	**184.086**	**34.086**	**33.625**
	UTILITY-8765/1234-DLG(BC)-Bus7-BK6	on	on	C8_14167	32.25	5.50	26.75	150.00	177.060	27.060	25.250
	DG2-678/65-SLG(A)-Bus7-BK5	on	on	C8_14169	24.50	5.88	18.62	150.00	171.540	21.540	17.625
	DG2-6781-SLG(A)-Bus7-BK5	on	on	C8_14173	24.13	5.88	18.25	150.00	169.245	19.245	17.125
	DG2-678-SLG(A)-Bus7-BK5	on	on	C8_14175	24.50	5.88	18.62	150.00	168.525	18.525	17.500
	DG1-5678-SLG(A)-Bus7-BK5	on	on	C8_14177	25.50	5.75	19.75	150.00	169.539	19.539	18.500
Minimum	**UTILITY-8765/1234-LL(BC)-Bus5-BK6**	**on**	**off**	**C8_14026**	**58.00**	**5.38**	**52.62**	**150.00**	**203.760**	**53.760**	**52.000**
	UTILITY-8765/1234-LL(BC)-Bus6-BK6	on	on	C8_14042	50.38	5.38	45.00	150.00	196.035	46.035	44.250
	DG2-678/65-LL(BC)-Bus8-BK5	on	on	C8_13953	50.75	5.88	44.87	150.00	196.335	46.335	44.000
	DG2-6781-LL(BC)-Bus8-BK5	on	on	C8_14052	46.88	5.50	41.38	150.00	194.100	44.100	40.000
	DG2-678-LL(BC)-Bus8-BK5	on	on	C8_14048	47.25	5.50	41.75	150.00	192.261	42.261	40.750
	DG1-5678-LL(BC)-Bus8-BK5	on	on	C8_14044	52.75	5.75	47.00	**150.00**	197.895	47.895	46.125

Bold represents backup protection tests, [1] Low level test interface, [2] Values from Table Q.1 in Appendix Q

Table R.2: Measured fault state times collected from event files, RT-LAB® second console, and Matlab® files for tripping tests of Relay 3

Fault Overcurrent	Test	LLTI[1]		C8 Event Files				RT-LAB® Second Console			Matlab® Files[2]
	Source - Circuit - Type of Fault -Fault Location - Opened Breaker	Relay 2 [on / off]	Relay 3 [on / off]	No Event	Ending Fault State Time, cycles [T_{EF}]	Initial Fault State Time, cycles [T_{IF}]	Measured Fault State Time, cycles [$T_{FSm} = T_{EF} - T_{IF}$]	Pre-fault State Time, cycles [T_{PR}]	Sum of Pre-Fault and Fault State Time, cycles [$S = T_{PR} + T_{FSm}$]	Measured Fault State Time, cycles [$T_{FSm} = S - T_{PR}$]	Measured Fault State Time, cycles [T_{FSm}]
Maximum	UTILITY-8765/1234-DLG(BC)-Bus6-BK8	on	on	C8_13193	23.63	5.63	18.00	150.00	169.65	19.650	16.500
	DG2-678/65-SLG(A)-Bus6-BK8	on	on	C8_13106	20.38	5.63	14.75	150.00	165.825	15.825	13.500
	DG2-678/65-SLG(A)-Bus6-BK7	on	on	C8_13115	27.50	5.75	21.75	150.00	173.355	23.355	20.750
	DG2-678/65-SLG(A)-Bus7-BK7	**off**	**on**	**C8_13113**	**33.88**	**5.63**	**28.25**	**150.00**	**181.095**	**31.095**	**27.000**
	DG2-67/65-SLG(A)-Bus6-BK8	on	on	C8_13127	20.38	5.74	14.64	150.00	165.315	15.315	13.500
	DG2-67/65-SLG(A)-Bus6-BK7	on	on	C8_13131	26.50	5.61	20.89	150.00	171.015	21.015	19.625
	DG2-6543-SLG(A)-Bus4-BK8	on	on	C8_13170	21.75	5.75	16.00	150.00	165.885	15.885	15.125
	DG2-6543-SLG(A)-Bus6-BK8	on	on	C8_13175	20.38	5.63	14.75	150.00	165.000	15.000	13.500
	DG2-65-SLG(A)-Bus6-BK8	on	on	C8_13120	20.13	5.88	14.25	150.00	165.345	15.345	13.000
	DG2-6781-SLG(A)-Bus6-BK7	on	on	C8_13161	27.13	5.95	21.18	150.00	172.425	22.425	20.250
	DG2-6781-SLG(A)-Bus7-BK7	**off**	**on**	**C8_13157**	**33.88**	**5.88**	**28.00**	**150.00**	**178.746**	**28.746**	**27.000**
	DG2-678-SLG(A)-Bus6-BK7	on	on	C8_13151	27.50	5.76	21.74	150.00	173.205	23.205	20.500
	DG2-678-SLG(A)-Bus7-BK7	**off**	**on**	**C8_13149**	**32.75**	**5.75**	**27.00**	**150.00**	**177.840**	**27.840**	**26.125**
	DG2-67-SLG(A)-Bus6-BK7	on	on	C8_13142	18.50	5.38	13.12	150.00	164.76	14.760	12.000
	DG1-5678-SLG(A)-Bus6-BK7	on	on	C8_13207	27.88	5.75	22.13	150.00	172.665	22.665	21.000
	DG1-5678-SLG(A)-Bus7-BK7	**off**	**on**	**C8_13138**	**34.25**	**5.38**	**28.87**	**150.00**	**180.750**	**30.750**	**28.000**
Minimum	UTILITY-8765/1234-LL(BC)-Bus5-BK8	on	on	C8_13015	32.13	5.75	26.38	150.00	177.75	27.750	24.750
	DG2-678/65-LL(BC)-Bus5-BK8	on	on	C8_12784	39.75	5.18	34.57	150.00	185.955	35.955	33.500
	DG2-678/65-LL(BC)-Bus7-BK7	on	on	C8_12796	56.75	5.75	51.00	150.00	201.885	51.885	50.250
	DG2-678/65-LL(BC)-Bus8-BK7	**off**	**on**	**C8_12794**	**70.13**	**5.63**	**64.50**	**150.00**	**217.32**	**67.320**	**63.500**
	DG2-67/65-LL(BC)-Bus5-BK8	on	on	C8_12862	38.88	5.38	33.50	150.00	186.375	36.375	32.500
	DG2-67/65-LL(BC)-Bus7-BK7	on	on	C8_12867	59.13	5.63	53.50	150.00	204.528	54.528	52.250
	DG2-6543-LL(BC)-Bus3-BK8	on	on	C8_12854	40.13	5.88	34.25	150.00	185.97	35.970	33.500
	DG2-6543-LL(BC)-Bus5-BK8	on	on	C8_12856	36.50	5.88	30.62	150.00	181.335	31.335	29.500
	DG2-65-LL(BC)-Bus5-BK8	on	on	C8_12850	38.63	5.50	33.13	150.00	185.22	35.220	32.125
	DG2-6781-LL(BC)-Bus7-BK7	on	on	C8_13002	55.88	5.88	50.00	150.00	200.805	50.805	49.000
	DG2-6781-LL(BC)-Bus8-BK7	**off**	**on**	**C8_13000**	**67.25**	**5.88**	**61.37**	**150.00**	**211.863**	**61.863**	**60.500**
	DG2-678-LL(BC)-Bus7-BK7	on	on	C8_12990	57.50	5.88	51.62	150.00	201.663	51.663	50.500
	DG2-678-LL(BC)-Bus8-BK7	**off**	**on**	**C8_12987**	**70.38**	**5.88**	**64.50**	**150.00**	**216.3**	**66.300**	**64.000**
	DG2-67-LL(BC)-Bus7-BK7	on	on	C8_13012	37.88	5.87	32.01	150.00	187.38	37.380	31.250
	DG1-5678-LL(BC)-Bus7-BK7	on	on	C8_12978	58.25	5.75	52.50	150.00	203.85	53.850	51.500
	DG1-5678-LL(BC)-Bus8-BK7	**off**	**on**	**C8_12980**	**70.38**	**5.50**	**64.88**	**150.00**	**217.065**	**67.065**	**64.000**

Bold represents backup protection tests, [1] Low level test interface, [2] Values from Table Q.2 in Appendix Q

Appendix S - Measured and theoretical relay times and relay time percent error values for RTS experiment

Table S.1: Measured and theoretical relay times and relay time percent error values for Relay 2

Fault Overcurrent	Test		LLTI[1]		C8 Event Files					Calculations	
	N°	Source – Circuit - Type of Fault - Fault Location - Opened Breaker	Relay 2 [on / off]	Relay 3 [on / off]	No Event	Primary Pickup Fault Current , amps [I]	Measured Fault State Time, cycles [T_{FSm}]	Measured Delay Time, cycles [TD_m]	Measured Relay Time, cycles [$T_{Rm} = T_{FSm} - T_{Dm}$]	Theoretical Relay Time, cycle [T_R]	Relay Time Percent Error, % [$E_{TR\%} = 100 (T_{Rm} - T_R)/ T_R$]
Maximum	1	**UTILITY-8765/1234-DLG(BC)-Bus6-BK6**	**on**	**off**	**C8_14156**	**1567**	**34.25**	**3.63**	**30.62**	**30.17**	**1.48**
	2	UTILITY-8765/1234-DLG(BC)-Bus7-BK6	on	on	C8_14167	1838	26.75	2.88	23.38	23.30	0.33
	3	DG2-678/65-SLG(A)-Bus7-BK5	on	on	C8_14169	1582	18.62	3.25	15.25	15.13	0.76
	4	DG2-6781-SLG(A)-Bus7-BK5	on	on	C8_14173	1599	18.25	3.01	14.88	14.90	-0.12
	5	DG2-678-SLG(A)-Bus7-BK5	on	on	C8_14175	1604	18.62	3.38	15.25	14.83	2.84
	6	DG1-5678-SLG(A)-Bus7-BK5	on	on	C8_14177	1459	19.75	3.63	16.38	16.00	2.40
Minimum	**7**	**UTILITY-8765/1234-LL(BC)-Bus5-BK6**	**on**	**off**	**C8_14026**	**1224**	**52.62**	**4.38**	**49.25**	**47.64**	**3.37**
	8	UTILITY-8765/1234-LL(BC)-Bus6-BK6	on	on	C8_14042	1318	45.00	3.01	41.63	41.24	0.94
	9	DG2-678/65-LL(BC)-Bus8-BK5	on	on	C8_13953	911	44.87	3.38	41.50	40.84	1.61
	10	DG2-6781-LL(BC)-Bus8-BK5	on	on	C8_14052	947	41.38	3.51	38.01	37.64	0.99
	11	DG2-678-LL(BC)-Bus8-BK5	on	on	C8_14048	918	41.75	1.63	38.38	40.18	-4.49
	12	DG1-5678-LL(BC)-Bus8-BK5	on	on	C8_14044	864	47.00	3.38	43.63	43.23	0.93

Bold represents backup protection tests, [1] Low level test interface

Table S.2: Measured and theoretical relay times and relay time percent error values for Relay 3

Fault Overcurrent	Test		LLTI[1]		C8 Event Files					Calculations	
	N°	Source - Circuit - Type of Fault -Fault Location - Opened Breaker	Relay 2 [on / off]	Relay 3 [on / off]	No Event	Primary Pickup Fault Current, amps [I]	Measured Fault State Time, cycles [T_{FSm}]	Measured Delay Time, cycles [TD_m]	Measured Relay Time, cycles [$T_{Rm} = T_{FSm} - T_{Dm}$]	Theoretical Relay Time, cycle [T_R]	Relay Time Percent Error, % [$E_{TR\%} = 100 (T_{Rm} - T_R)/ T_R$]
Maximum	1	UTILITY-8765/1234-DLG(BC)-Bus6-BK8	on	on	C8_13193	1551	18.00	2.13	15.38	15.329	3.53
	2	DG2-678/65-SLG(A)-Bus6-BK8	on	on	C8_13106	1896	14.75	2.01	12.13	12.539	1.60
	3	DG2-678/65-SLG(A)-Bus6-BK7	on	on	C8_13115	1895	21.75	2.73	19.13	18.968	0.27
	4	**DG2-678/65-SLG(A)-Bus7-BK7**	**off**	**on**	**C8_13113**	**1556**	**28.25**	**3.26**	**24.99**	**25.232**	**-0.96**
	5	DG2-67/65-SLG(A)-Bus6-BK8	on	on	C8_13127	1927	14.64	2.01	12.02	12.270	2.94
	6	DG2-67/65-SLG(A)-Bus6-BK7	on	on	C8_13131	1897	20.89	1.88	18.27	18.941	0.36
	7	DG2-6543-SLG(A)-Bus4-BK8	on	on	C8_13170	1726	16.00	1.63	13.38	14.303	0.47
	8	DG2-6543-SLG(A)-Bus6-BK8	on	on	C8_13175	1915	14.75	2.01	12.13	12.372	2.97
	9	DG2-65-SLG(A)-Bus6-BK8	on	on	C8_13120	1958	14.25	2.01	11.63	12.014	1.88
	10	DG2-6781-SLG(A)-Bus6-BK7	on	on	C8_13161	1927	21.18	1.76	18.56	18.962	2.41
	11	**DG2-6781-SLG(A)-Bus7-BK7**	**off**	**on**	**C8_13157**	**1567**	**28.00**	**2.76**	**25.24**	**25.572**	**-1.30**
	12	DG2-678-SLG(A)-Bus6-BK7	on	on	C8_13151	1910	21.74	2.38	19.12	19.188	0.90
	13	**DG2-678-SLG(A)-Bus7-BK7**	**off**	**on**	**C8_13149**	**1579**	**27.00**	**1.88**	**25.12**	**25.270**	**-0.59**
	14	DG2-67-SLG(A)-Bus6-BK7	on	on	C8_13142	1925	13.12	1.88	10.50	10.691	5.13
	15	DG1-5678-SLG(A)-Bus6-BK7	on	on	C8_13207	1734	22.13	2.26	19.51	19.625	1.25
	16	**DG1-5678-SLG(A)-Bus7-BK7**	**off**	**on**	**C8_13138**	**1452**	**28.87**	**2.63**	**26.24**	**25.642**	**2.33**
Minimum	17	UTILITY-8765/1234-LL(BC)-Bus5-BK8	on	on	C8_13015	1208	26.38	2.51	23.76	23.643	0.96
	18	DG2-678/65-LL(BC)-Bus5-BK8	on	on	C8_12784	1087	34.57	2.38	31.95	31.562	1.99
	19	DG2-678/65-LL(BC)-Bus7-BK7	on	on	C8_12796	1059	51.00	1.63	48.38	49.920	-1.10
	20	**DG2-678/65-LL(BC)-Bus8-BK7**	**off**	**on**	**C8_12794**	**953**	**64.50**	**2.26**	**61.88**	**62.078**	**0.26**
	21	DG2-67/65-LL(BC)-Bus5-BK8	on	on	C8_12862	1096	33.50	1.76	30.88	31.053	2.21
	22	DG2-67/65-LL(BC)-Bus7-BK7	on	on	C8_12867	1034	53.50	2.01	50.88	52.380	-1.70
	23	DG2-6543-LL(BC)-Bus3-BK8	on	on	C8_12854	1082	34.25	2.26	31.63	31.852	0.43
	24	DG2-6543-LL(BC)-Bus5-BK8	on	on	C8_12856	1149	30.62	2.13	28.00	28.336	0.54
	25	DG2-65-LL(BC)-Bus5-BK8	on	on	C8_12850	1094	33.13	2.01	30.51	31.165	-0.14
	26	DG2-6781-LL(BC)-Bus7-BK7	on	on	C8_13002	1098	50.00	2.26	47.38	47.819	-0.17
	27	**DG2-6781-LL(BC)-Bus8-BK7**	**off**	**on**	**C8_13000**	**982**	**61.37**	**2.65**	**58.75**	**60.029**	**-2.18**
	28	DG2-678-LL(BC)-Bus7-BK7	on	on	C8_12990	1071	51.62	1.88	49.00	50.237	-0.99
	29	**DG2-678-LL(BC)-Bus8-BK7**	**off**	**on**	**C8_12987**	**968**	**64.50**	**2.78**	**61.88**	**61.885**	**-0.27**
	30	DG2-67-LL(BC)-Bus7-BK7	on	on	C8_13012	1054	32.01	2.76	29.39	29.207	0.15
	31	DG1-5678-LL(BC)-Bus7-BK7	on	on	C8_12978	997	52.50	2.63	49.88	50.786	-1.80
	32	**DG1-5678-LL(BC)-Bus8-BK7**	**off**	**on**	**C8_12980**	**909**	**64.88**	**2.52**	**62.26**	**61.687**	**1.09**

Bold represents backup protection tests, [1] Low level test interface